Stephan Ulmer
Olav Jansen *Editors*

fMRI

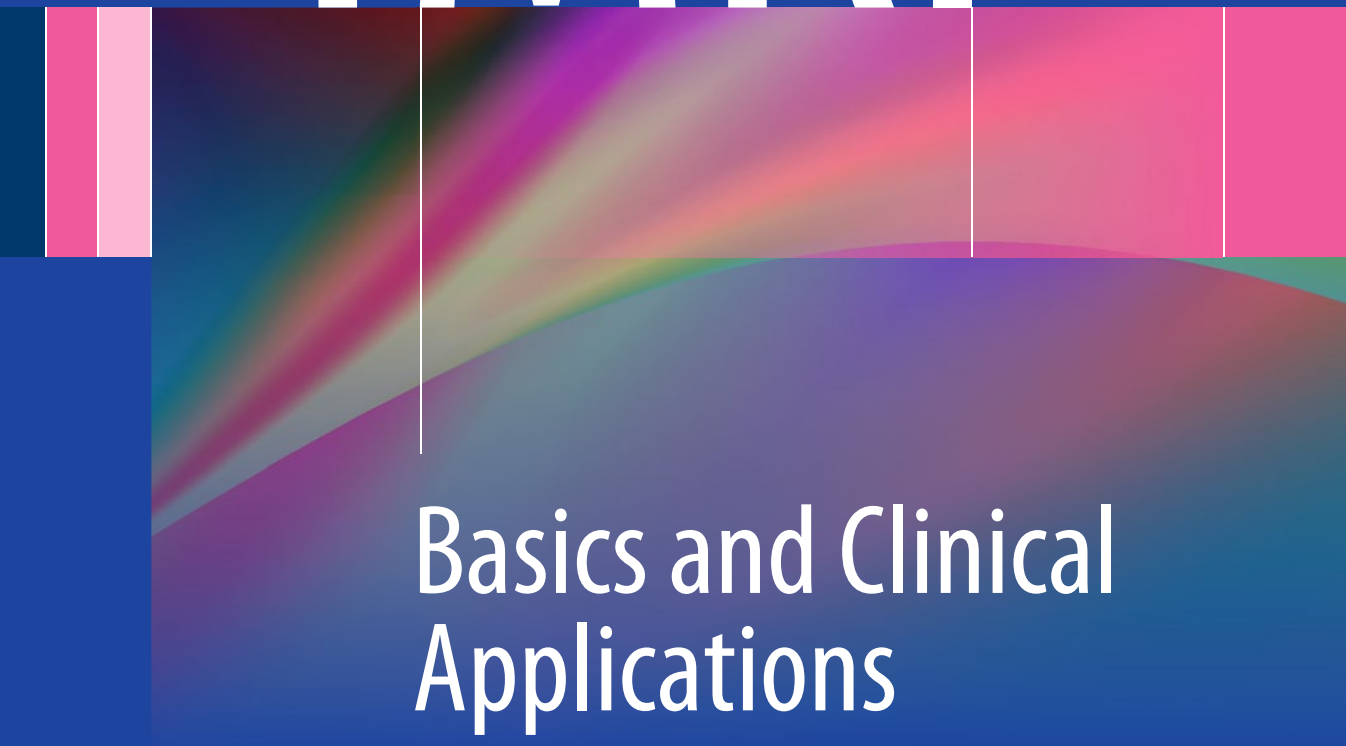

Basics and Clinical Applications

Second Edition

Springer

fMRI

Stephan Ulmer • Olav Jansen
Editors

fMRI

Basics and Clinical Applications

Second Edition

Springer

Editors
Stephan Ulmer
Medizinisch Radiologisches Institut
(MRI) Zürich
(Bahnhofsplatz/Bethanien/Stadelhofen)
Zürich
Switzerland

Olav Jansen
Institut für Neuroradiologie
Universitätsklinikum Schleswig-Holstein
Kiel
Germany

Institut für Neuroradiologie
Universitätsklinikum Schleswig-Holstein
Kiel
Germany

ISBN 978-3-642-34341-4 ISBN 978-3-642-34342-1 (eBook)
DOI 10.1007/978-3-642-34342-1
Springer Heidelberg New York Dordrecht London

Library of Congress Control Number: 2013935476

Contents

Part I

Basics

Introduction

1

Stephan Ulmer

Within the past two decades, functional magnetic resonance imaging (fMRI) has developed tremendously and continues to do so. From initial descriptions of changes in blood oxygenation that can be mapped with MRI using T2*-weighted images to very basic investigations performing studies of the visual and motor cortex, fMRI has further evolved into a very powerful research tool and has also become an imaging modality of daily clinical routine, especially for presurgical mapping. With the first edition of this book, we tried to give an overview of the basic concepts and their clinical applications. With increasing demands by you, the reader, as a researcher and/or clinical colleague, and due to increasing applications, we feel an update is due, with add-ons to the previous edition. We are delighted to present this second edition of *fMRI: Basics and Clinic Applications*.

Understanding brain function and localizing functional areas have ever since been a main goal of neuroscience, with fMRI being a very powerful tool to approach this aim. Studies on healthy volunteers usually take a different approach and often have a very complex study design, while clinical applications face other problems most commonly related to the limited compliance of the patients, even more so in the context of dementia, advanced-stage tumor patients, or with children. Therefore, the application of fMRI in a clinical setting is a different challenge, reflected in the study designs as well as in the analysis of the data algorithms. Analyzing data also has become increasingly complex due to sophisticated study designs in single-center studies, multicenter trials requiring meta-analysis, and for mapping connectivity. Analyzing fMRI data is a science of its own. Fortunately, there is a variety of software solutions available free of charge for the most part. Manufacturers also offer analyzing software.

Besides the classical definition of functional areas that might have been shifted through a lesion or could be present in a distorted anatomy prior to neurosurgical resection, further clinical applications include mapping of recovery from stroke or trauma, cortical reorganization (if these areas were affected), and changes during the development of the brain or during the course of a disease. For the understanding of psychiatric disorders, dementia, and Parkinson's disease, fMRI offers new horizons.

Knowledge of basic neuroanatomy, the associated physiology, and especially the possible pathophysiology that might affect the results to start with is mandatory. The results in volunteers are the requisite to understand the results in patients, and they can only be as good as the design itself. Monitoring the patient in the scanner is necessary to guarantee that the results obtained

S. Ulmer
Medizinisch Radiologisches Institut (MRI) Zürich, (Bahnhofsplatz/Bethanien/Stadelhofen), Bahnhofsplatz 3, Zürich 8001, Switzerland

Institut für Neuroradiologie, Universitätsklinikum Schleswig-Holstein, Schittenhelmstrasse 10, Kiel 24105, Germany
e-mail: ulmer@email.com

S. Ulmer, O. Jansen (eds.), *fMRI – Basics and Clinical Applications*,
DOI 10.1007/978-3-642-34342-1_1,

will reflect activation caused by the stimulation, or to understand that reduced or even missing activation could have hampered the results, and to analyze how they were generated. Obviously, we have to realize that while the patient is still in the scanner, a repetition of the measurement can be done or an unnecessary scan avoided if the patient is incapable of performing the task. Performing motor tasks seems relatively straightforward, as patient performance can be directly observed in the scanner. Cognitive and language tasks are more challenging. Also, a vascular stenosis or the steal effects of a brain tumor or an arteriovenous malformation (AVM) may corrupt the results. There are some sources resulting in disturbances that might depict no activation in a patient, e.g., in language tasks that usually depict reliable results in volunteers. It is essential to have a person with expertise in training and testing patients on the cognitive tasks involved, such as a neuropsychologist or a cognitive neurologist.

Task performance and paradigm development usually follow a graduated scheme. Initially, experiments are performed in healthy volunteers. This, however, has the disadvantage that the volunteers are most likely healthy students or staff who are used to the scanner environment and can therefore focus unrestrictedly on the task, whereas patients may be scared or too nervous concerning their disease and about what might happen in the near future (such as a brain tumor resection).

The same paradigm must be used in less affected patients first, to confirm the feasibility in this setting that might become more specific after some experience. Test-retest reliability finally enables clinical application to address specific questions. Passive or "covert" tasks might be helpful; however, at least in cognitive studies performance cannot be measured. Semantic and cognitive processes continue during passive situations, including rest and other passive baseline conditions. Regions involved will therefore be eliminated from the analysis when such conditions are used as a baseline.

Mapping children represents a twofold challenge. Normative data is not available and compliance is limited. In early childhood or in cognitively impaired children, or just simply during brain development, cognitive tasks need to be modified individually, and that again causes problems in analyzing the data and interpreting the results.

As already stated, absence of an expected activation represents a real challenge and raises the question of the reliability of the method per se. Suppression of activation or task-related signal intensity decrease has also not been fully understood. Missing activation in a language task could mislead the neurosurgeon to resect a low-grade lesion close to the inferior frontal lobe and still cause speech disturbance or memory loss after resection of a lesion close to the mesial temporal lobe, and therefore – depending on the close cooperation between the clinicians – healthy skepticism as well as combination with other modalities such as direct cortical stimulation may be advisory. Indeed, the combination of fMRI with further modalities such as electroencephalography (EEG), transcranial magnetic stimulation (TMS), magnetoencephalography (MEG), or positron emission tomography (PET) is very promising. Hemispheric (language) dominance is only the tip of the iceberg and we have to ask ourselves again how sensitive our methods and paradigms are to depict minor deficits. The same is true for clinical bedside testing and thus questions "silent" brain regions.

Sequence selection is important in terms of what we want to see and how to achieve it. Prior to the introduction of echo planar imaging, temporal resolution was restricted. Spatial resolution requirements are much more important in individual cases than in a healthy control group, especially in the presurgical definition of the so-called eloquent areas.

Higher field strengths might enable us to depict more signals but possibly more noise in the data as well. From a clinician's point of view, reliability of individual results is desired.

It is exciting to see how fMRI became a clinical application in recent years of which neurosurgeons were initially very suspicious during the first clinical experiments in presurgical mapping. Its current acceptance can be appreciated in the increasing numbers of studies performed on demand, not only in brain tumor mapping but also in epilepsy.

A completely new field has developed more recently, namely, ethical considerations arising from incidental imaging findings. For patients, incidental findings are often part of the daily routine, yet "healthy" volunteers are faced with completely unexpected consequences and so are researchers.

With the second edition of this book, we will try to answer new questions while giving an overview on how fMRI can be applied for clinical purposes. After the first edition we felt the need to add further fields and applications, this being an ongoing project that we try to keep alive. It is a great honor for me to have such a distinguished board of experts in the field involved in this project. I hope that you will enjoy this book as much as I have and that it will help you in your own daily work.

Neuroanatomy and Cortical Landmarks

2

Stephan Ulmer

2.1 Neuroanatomy and Cortical Landmarks of Functional Areas

Prior to any type of functional mapping, a profound knowledge of neuroanatomy is mandatory. Focusing on the clinical applications of fMRI, this chapter will present methods to identify characteristic anatomical landmarks and describe the course and shape of some gyri and sulci and how they can be recognized on MR imaging. As anatomy will be presented in neurofunctional systems, some redundancy is desired in order to course over cortical landmarks. If fMRI is not performed during clinical routine imaging, usually a 3D data set is acquired to overlay the results. Nowadays, fMRI is performed using echo planar imaging (EPI) with anisotropic distortion, whereas 3D T1-weighted data sets, such as MPRage (magnetization-prepared rapid acquisition gradient echo) or SPGR (spoiled gradient-recalled acquisition in steady state) sequences, are usually isotropic. Normalization of the fMRI data may reduce this systemic error to some extent that is more pronounced at the very frontal aspect of the frontal lobe and the very posterior aspect of the occipital lobe. However, for individual data, normalization and overlaying fMRI results on anatomy remain crucial. No two brains, not even the two hemispheres within one subject, are identical at a macroscopic level, and anatomical templates represent only a compromise (Devlin and Poldrack 2007). Usage of templates like the Talairach space (based on the anatomy of one brain) or the MNI template (based on 305 brains) can cause registration error as well as additional variation and reduce accuracy; indeed, it does not warrant the shammed anatomical precision in the individual case.

S. Ulmer
Medizinisch Radiologisches Institut (MRI) Zürich, (Bahnhofsplatz/Bethanien/Stadelhofen), Bahnhofsplatz 3, Zürich 8001, Switzerland

Institut für Neuroradiologie, Universitätsklinikum Schleswig-Holstein, Schittenhelmstrasse 10, Kiel 24105, Germany
e-mail: ulmer@email.com

2.1.1 Sensorimotor Cortex

2.1.1.1 Transverse Sections

There are various methods to identify the precentral gyrus (preCG; [3]), the central sulcus (CS) and the postcentral gyrus (postCG; [4]). From a craniocaudal point of view, the sensorimotor strip follows (from the apex to the Sylvian fissure [35b]) a medial-posterior-superior to lateral-anterior-inferior course. The precentral gyrus [3] fuses with the superior frontal gyrus (SFG; [1]) at the very upper convexity (Ebeling et al. 1986; Kido et al. 1980; Naidich et al. 1995; Ono et al. 1990). This can be well depicted on transverse sections (see Figs. 2.1 and 2.2). The precentral gyrus [3] is the most posterior part of the frontal lobe that extends inferiorly to the Sylvian fissure [35b]. The precentral gyrus [3] is thicker than the postcentral gyrus [4] in anterior-posterior (ap) dimension (Naidich et al. 1995) as is the grey

S. Ulmer, O. Jansen (eds.), *fMRI – Basics and Clinical Applications*,
DOI 10.1007/978-3-642-34342-1_2,

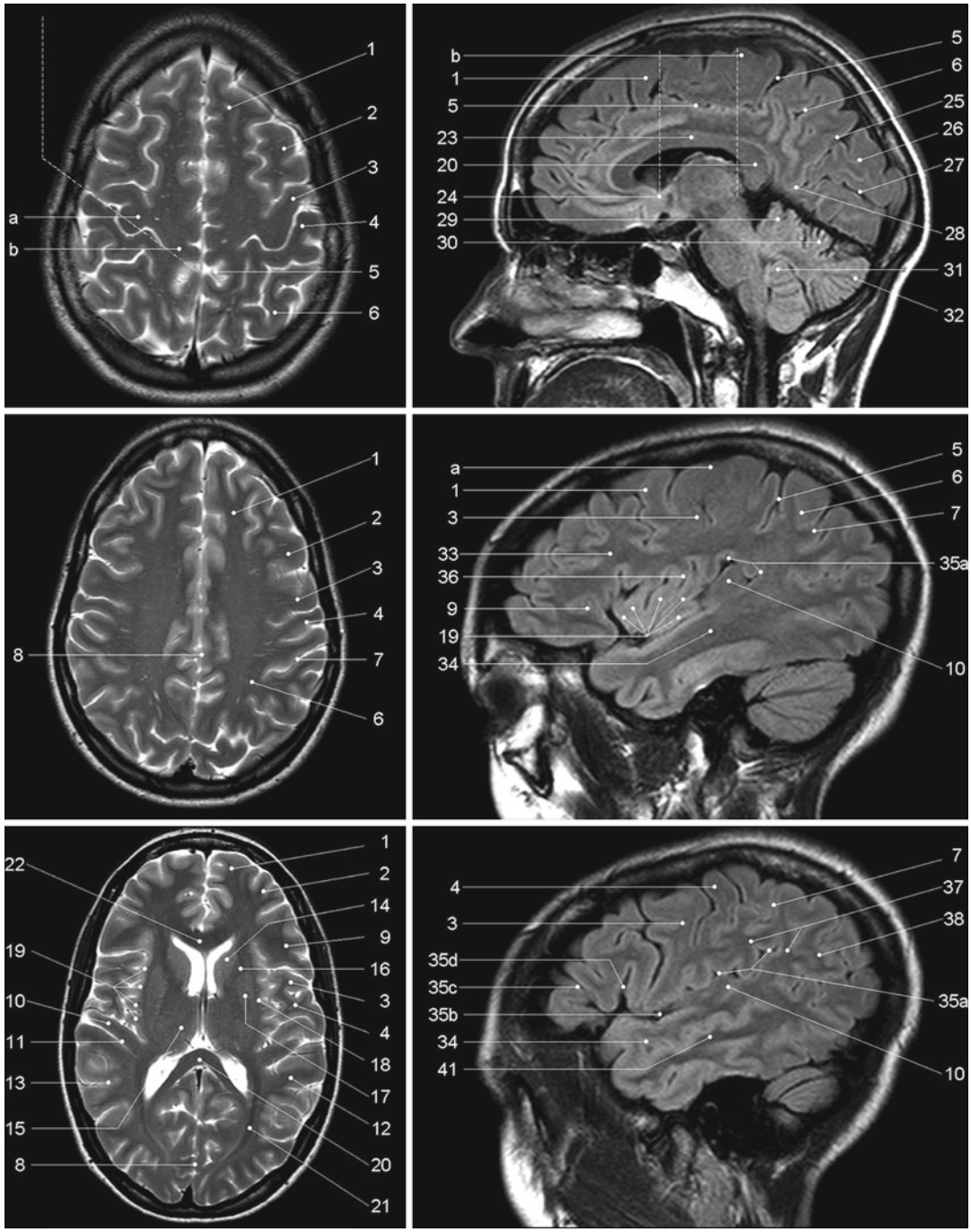

Fig. 2.1 Overview of the used sections. The numbers are explained within the text as well as in the other figure legends in detail

matter (Meyer et al. 1996). At the apex, the pre- [3] and postcentral gyri [4] form the paracentral lobule [b] as they fuse. Making a little detour to a lateral view (see Fig. 2.3), the cingulate sulcus [5] ascends at the medial interhemispheric surface dorsal to the paracentral lobule (pars marginalis)

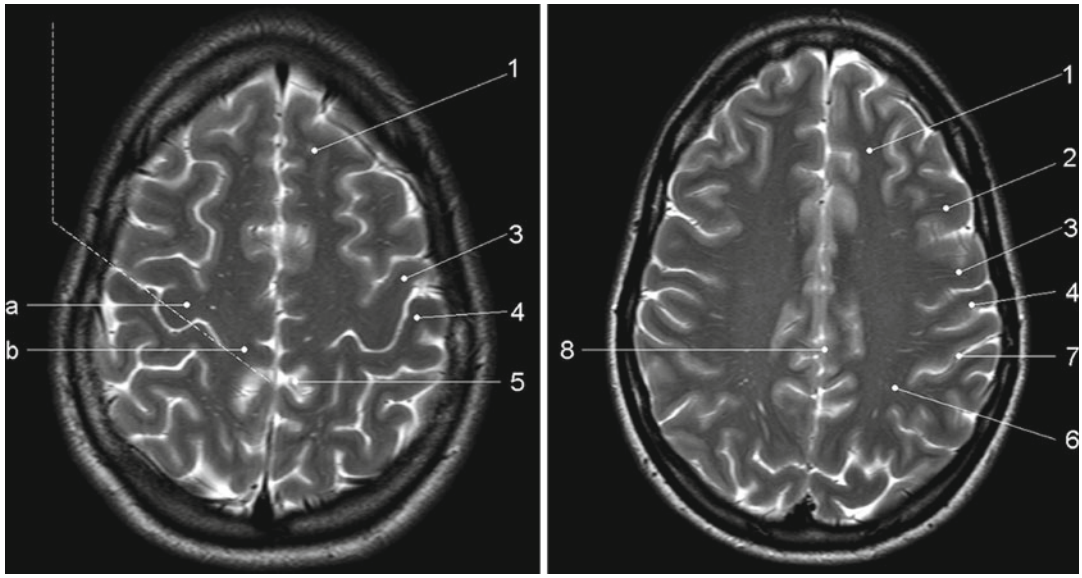

Fig. 2.2 Axial T2-weighted TSE MR images. *1* superior frontal gyrus, *2* medial frontal gyrus, *3* precentral gyrus, *4* postcentral gyrus, *5* "pars bracket", cingulated sulcus, *6* precuneus, parietal lobe, *7* intraparietal sulcus, *8* interhemispheric fissure, *a* hand knob, *b* paracentral lobule

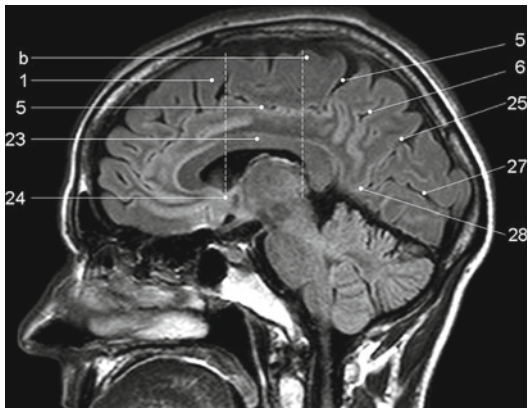

Fig. 2.3 Sagittal FLAIR image at the midline. *1* superior frontal gyrus, *5* "pars bracket", cingulate sulcus, *6* precuneus, parietal lobe, *23* body of the corpus callosum, *24* anterior commissure, *25* parietooccipital sulcus, *27* calcarine fissure, *b* paracentral lobule, *28* cuneal point

[b] and thus separates it from the precuneus [6]. This intersection can be appreciated on axial sections as the "bracket" sign (see Fig. 2.2; Naidich and Brightbill 1996) that borders the postcentral gyrus [4]. Somatotopographically, the apex harbours the cortical representation the lower extremity (Penfield and Rasmussen 1950). Following its course along the superficial convexity (from medial-posterior-superior to lateral-anterior-inferior), the cortical surface of the precentral gyrus increases at its posterior margin, building the omega-shaped motor hand knob ([a]; Yousry et al. 1995, 1997). Within this primary motor cortex (M1) of the hand, there is an additional somatotopic order of the individual digits (with interindividual overlap and variation). From medial to lateral, the hand is organized beginning with digit 5 (D5), to the thumb representation (D1) being the most lateral (Dechent and Frahm 2003). The motor hand knob [a] is another typical landmark of the precentral gyrus [3]; however, as the CS and the postcentral gyrus [4] follow this course, there is also an omega-shaped structure in the postcentral gyrus (harbouring the somatosensory hand area). However, as described above, the ap-dimension of the postcentral gyrus [4] is smaller compared to the precentral gyrus [3], thus often enabling a differentiation. Somatotopographically, the cortical somatosensory representation follows the distribution of the precentral gyrus [3] (Penfield and Rasmussen 1950; Overduin and Servos 2004). Lateral to the SFG [1], the medial frontal gyrus [2] zigzags posteriorly and points towards the motor

hand knob [a]. Beginning at this "junction" and lateral-inferior to this landmark, the ap-diameter of the preCG [3] decreases, but it increases again along the lower convexity. This has already been recognized by Eberstaller (1890). Using modern imaging techniques, the diameter had been measured and the previous findings validated that the biggest diameter of the preCG [3] is found at the lower portion of the gyrus adjacent to the Sylvian fissure [35b] (Ono et al. 1990). This is the primary motor cortex (M1) of lip representation and tongue movements. In the axial sections, there is neither a typical shape or landmark of the gyrus, nor does measuring from the motor hand area or the ac (anterior commissure) help us to describe the location precisely. This can be solved on sagittal sections (see below).

Previously, the anatomy of the frontal lobe has been described partially. As the course of the medial frontal gyrus [2] can be followed nicely on axial sections, the lateral inferior aspect of the frontal lobe represents the inferior frontal gyrus. Anterior to the preCG [3], the prefrontal motor areas can be found. The inferior frontal gyrus borders and overhangs the insula [19] anteriorly. This part is the frontal operculum [9] harbouring the motor speech area of Broca (see below sagittal sections).The lateral ventricles with its anterior and posterior horn can easily be depicted on axial sections due to its typical form and typical signal caused by corticospinal fluid (CSF, see Figs. 2.1, 2.5 and 2.6). Their shape is formed through the head of the caudate nucleus [10] lateral to the anterior horn, the thalamus [11] lateral at its waist (III. ventricle) and posteriorly by the fibres of the anterior-posteriorly running optic radiation [21] and left-right running fibres of the splenium [20] (see Figs. 2.5 and 2.6). Lateral to these structures, descending corticospinal fibres pass the internal capsule [16] and follow a certain somatotopic organization. The internal capsule is framed medial by the head of the caudate nucleus [10], the third ventricle and the thalamus [11] (at the posterior aspect of the third ventricle) and lateral by the globus pallidus [17]. From medial to lateral towards the insula [19], the globus pallidus, putamen and claustrum within the lentiform nucleus [17] can be differentiated. In the anterior limb and the genu of the internal capsule, [16] corticospinal fibres from the tongue, lip and face descend, whereas in the posterior limb, fibres from the upper extremity, body and finally lower extremity are found.

2.1.1.2 Sagittal Sections

Previously sagittal sections have been described at the interhemispheric surface (see Fig. 2.3). The corpus callosum [20, 22, 23] represents the biggest connection between the two hemispheres. The frontal aspect is the genu [22], the medial part is the body [23] and the most rostral part is the splenium [20]. The corpus callosum encases the lateral ventricles. At the base, the anterior commissure (ac; [24]) can be identified as a roundish structure. Sometimes, the posterior commissure (pc) can also be defined, which represents a bundle of white fibres crossing the midline, at the dorsal aspect of the upper end of the cerebral aqueduct. Previously slice orientation of most fMRI studies had been performed according to this ac-pc line in order to have a reference system.

From the base to the apex, the corpus callosum is abutted by the callosal sulcus and the cingulate gyrus. The gyrus abutting the cingulate sulcus [5] is the medial part of the SFG [1]. In the region (at the medial cortical surface) framed by vertical lines perpendicular to the ac (Vac) or pc (Vpc; see Fig. 2.3), the supplementary motor area (SMA) is harboured in the cingulate gyrus and superior frontal gyrus. As described above, the cingulate sulcus [5] ascends at the medial interhemispheric surface (see Fig. 2.3) dorsal to the paracentral lobule ([b]; pars marginalis) and thus separates it from the precuneus [6]. This intersection can be nicely appreciated on axial sections as the "bracket" sign (see Fig. 2.2; Naidich and Brightbill 1996) that borders the postcentral gyrus [4]. The postcentral gyrus is already a part of the parietal lobe. The precuneus [6] is located dorsal to the postcentral sulcus. There is another important landmark that separates the parietal lobe from the occipital lobe (cuneus [26]), the parietooccipital sulcus [25]. It can be easy recognized in sagittal views (see Fig. 2.3), as the dorsal sulcus that follows an inferior-anterior to superior-posterior course, posterior to the ascending

part of the cingulate sulcus [5]. It is advisable to follow one of these structures moving laterally through the brain in sagittal sections. Once the Sylvian fissure [35b] can be identified, anatomical landmarks are again easy to define.

In midsagittal sections (see Fig. 2.6), the motor hand knob [a] can again be recognized as a "hook" that rises out of the parenchyma and points dorsally. Further, laterally the sensorimotor cortex overhangs the insula [19]. The Sylvian fissure [35b] that separates the frontal lobe and the temporal lobe has an inferior-anterior to superior-posterior course. At its anterior margin, it ascends into the anterior horizontal ramus [35c] and more dorsally into the anterior ascending ramus [35d] of the frontal operculum [9] that also overhangs the anterior aspect of the insula [19]. The anterior horizontal ramus [35c] separates the pars orbitalis [40] from the pars triangularis [39], whereas the anterior ascending ramus [35d] separates the pars triangularis [39] from the pars opercularis [9] of the frontal operculum of the inferior frontal gyrus and thus forms an "M" (Naidich et al. 1995). The pars opercularis [9] of the frontal operculum of the inferior frontal lobe harbours Broca's area. At its posterior margin, the pars opercularis is delimited by the anterior subcentral sulcus. At the base of the sensorimotor strip, the precentral [3] and postcentral gyrus [4] fuse (Eberstaller 1890; Ono et al. 1990). This junction is delimited dorsally by the posterior subcentral sulcus. Movement of the lips or tongue induce an increase in BOLD signal at this portion (Fesl et al. 2003, own observations). The base of the sensorimotor area has, depending on anatomical variations, a "K" or an "N" shape that is built by the anterior subcentral sulcus and inferior precentral sulcus, the precentral gyrus, posterior subcentral sulcus, postcentral gyrus and postcentral sulcus that again borders the angular gyrus [38] (Eberstaller 1890; Ono et al. 1990, own observations; see Fig. 2.6). The posterior part of the Sylvian fissure separates – following its superior-posterior course – and ascends into the posterior ascending ramus [35a] flanked by the anterior and posterior aspect of the supramarginal gyrus [37] that has a horseshoe appearance.

2.1.2 The Insula

The insula [19] is covered by the superior temporal gyrus [34], the frontal operculum [9] and the base of the sensorimotor strip. Its anatomy is best depicted in sagittal sections (see Fig. 2.6).

2.1.2.1 Sagittal Sections

The insula [19] is separated by the CS [36] that runs from superior-posterior towards the inferior-anterior located apex of the insula into an anterior lobule and a posterior lobule (see Fig. 2.6). The anterior lobule consists of three gyri (anterior, medial and posterior short insular gyri); the posterior lobule consists of two gyri, the anterior long insular gyrus and the posterior long insular gyrus separated by the postcentral gyrus (Naidich et al. 2004).

From a neurofunctional point of view, the insula has various functional areas. The anterior lobule was found to cause word-finding difficulties during electrical stimulation in epilepsy surgery (Ojemann and Whitaker 1978a, b) and to be responsible for speech planning (Wise et al. 1999; Price 2000). Speech apraxia is induced through lesions in the left precentral gyrus of the insula (Dronkers 1996; Nagao et al. 1999), whereas the right anterior lobule becomes activated during vocal repetition of nonlyrical tunes (Riecker et al. 2000). Stimulation of the right insula increases sympathetic tone, and stimulation of the left insula increases parasympathetic tone (Oppenheimer 1993), possibly playing a role in cardiac mortality in left insular stroke. Finally visual-vestibular interactions have been found (Brandt et al. 1998) to name a few systems.

2.1.2.2 Transverse Sections

The insular cortex [19] is delimited medially by the globus pallidus, putamen and claustrum (lentiform nucleus [17]) and separated by a small border of white matter (extreme capsula [18]). The gyri can be differentiated by counting each knob starting ventrally at the anterior peri-insular sulcus that abuts the pars opercularis [9] of the frontal operculum of the inferior frontal gyrus (see Figs. 2.4 and 2.5). Five knobs can be defined (anterior, medial and posterior short insular gyri and anterior and posterior long insular gyri).

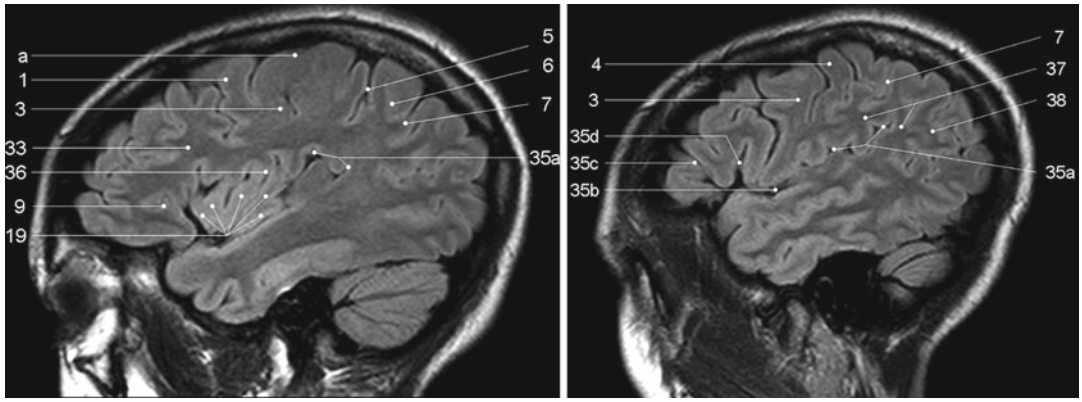

Fig. 2.4 Sagittal FLAIR images. *1* superior frontal gyrus, *3* precentral gyrus, *4* postcentral gyrus, *5* "pars bracket", cingulate sulcus, *6* precuneus, parietal lobe, *7* intraparietal sulcus, *9* pars opercularis, inferior frontal lobe, frontal operculum, *19* insula (anterior and posterior short insular gyri, anterior and posterior long insular gyri), *33* medial frontal gyrus, *35a* posterior ascending ramus of the Sylvian fissure, *35b* Sylvian fissure, *35c* anterior horizontal ramus of the Sylvian fissure, *35d* anterior ascending ramus of the Sylvian fissure, *36* central sulcus of the insula, *37* supramarginal gyrus, *38* angular gyrus, *a* hand knob

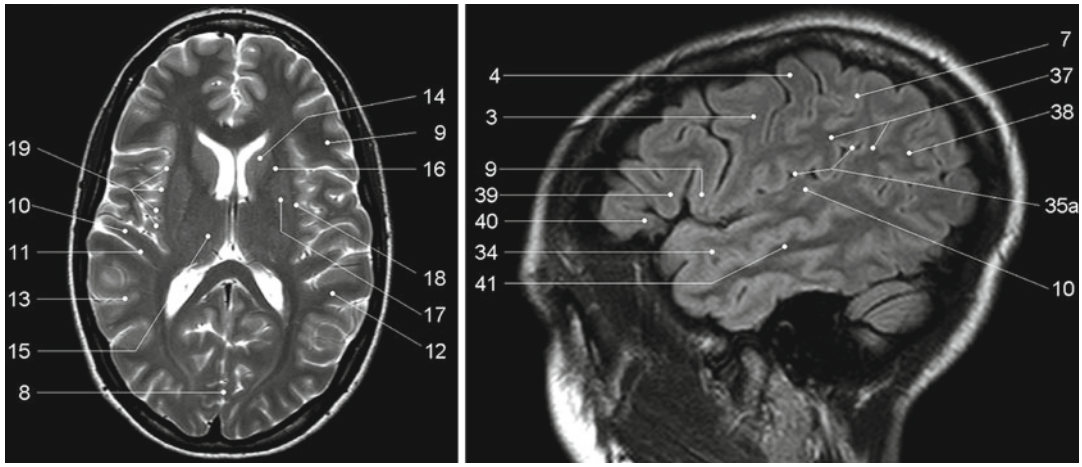

Fig. 2.5 Axial T2-weighted TSE MR and sagittal FLAIR images. *3* precentral gyrus, *4* postcentral gyrus, *7* intraparietal sulcus, *8* interhemispheric fissure, *9* pars opercularis, inferior frontal lobe, frontal operculum, *10* Heschl's gyrus, *11* Heschl's sulcus, *12* planum temporale, *13* superior temporal sulcus, *14* head of the caudate nucleus, *15* thalamus, *16* internal capsule, *17* globus pallidus, putamen, claustrum (lentiform nucleus), *18* extreme capsule, *19* insula (anterior and posterior short insular gyri, anterior and posterior long insular gyri), *34* superior temporal gyrus, *35a* posterior ascending ramus of the Sylvian fissure, *37* supramarginal gyrus, *38* angular gyrus, *39* pars triangularis, frontal operculum, inferior frontal gyrus, *40* pars orbitalis, frontal operculum, inferior frontal gyrus, *41* medial temporal gyrus

2.1.3 Speech-Associated Frontal Areas

2.1.3.1 Transverse Sections

In axial sections, the insula [19] can be found easily (see Figs. 2.5 and 2.6). From medial (ventricles) to lateral, the globus pallidus, putamen and claustrum, within the lentiform nucleus, [17] can be differentiated followed by the extreme capsula [18] and the cortex of the insula [19]. The Sylvian fissure [35b] separates the insula [19] from the temporal lobe. As stated above, the insula – taking anatomic variations into account – has 4–5 knobs

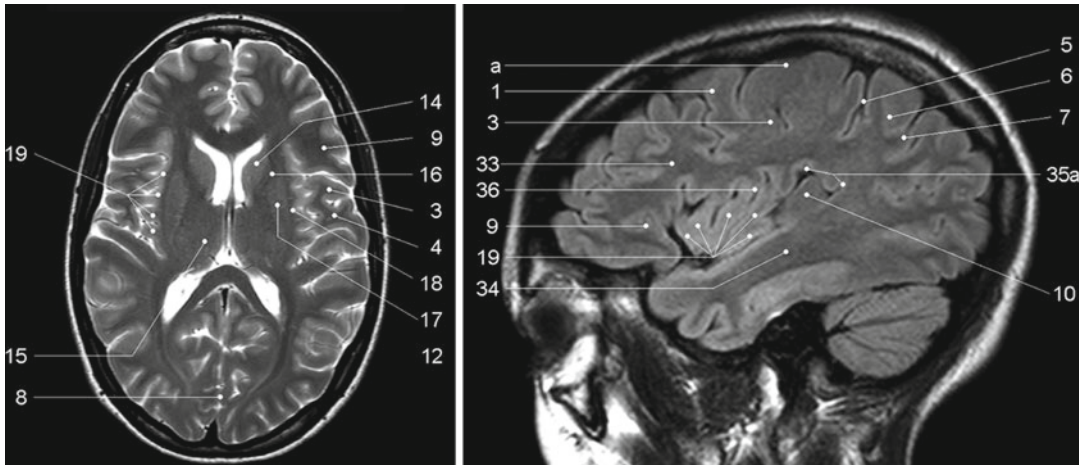

Fig. 2.6 Axial T2-weighted TSE MR and sagittal FLAIR images. *1* superior frontal gyrus, *3* precentral gyrus, *4* postcentral gyrus, *5* "pars bracket", cingulate sulcus, *6* precuneus, parietal lobe, *7* intraparietal sulcus, *8* interhemispheric fissure, *9* pars opercularis, inferior frontal lobe, frontal operculum, *10* Heschl's gyrus, *12* planum temporale, *14* head of the caudate nucleus, *15* thalamus, *16* internal capsule, *17* globus pallidus, putamen, claustrum (lentiform nucleus) *18* extreme capsule, *19* insula (anterior and posterior short insular gyri, anterior and posterior long insular gyri), *33* medial frontal gyrus, *34* superior temporal gyrus, *35*a posterior ascending ramus of the Sylvian fissure, *36* central sulcus of the insula

(anterior, medial and posterior short insular gyri divided, by the CS, from the anterior and posterior long insular gyri). The insula [19] is covered by the superior temporal gyrus [34], the frontal operculum [9] and the base of the sensorimotor strip. After identifying the anterior short gyrus of the anterior lobule of the insular cortex, on a transverse view, the anterior border between the insula and inferior frontal lobe is the anterior peri-insular sulcus. It abuts the insula [19], on one hand, and the pars opercularis [9] of the frontal operculum of the inferior frontal gyrus, on the other. The pars opercularis [9] has a triangular shape in axial sections and covers the anterior part of the insula [19]. It can be followed into the anterior cranial fossa where it abuts the gyrus orbitalis that runs parallel to the gyrus rectus. The convolution anterior to the pars opercularis [9] on the lateral surface is the pars triangularis [39], separated by the anterior ascending ramus [35d] of the Sylvian fissure.

2.1.3.2 Sagittal Sections

Beginning at the lateral border of the brain (in sagittal views, see Figs. 2.4 and 2.5) there is the Sylvian fissure [35b] that runs anterior-inferior to posterior-superior. Previously, the posterior margins have been described (see above). The Sylvian fissure separates the temporal lobe from the frontal lobe. At its anterior margin, it ascends into the anterior horizontal ramus [35c] and more dorsally into the anterior ascending ramus [35d] of the frontal operculum [9] that also overhangs the anterior aspect of the insula [19]. The anterior horizontal ramus [35c] separates the pars orbitalis [40] from the pars triangularis [39], whereas the anterior ascending ramus [35d] separates the pars triangularis [39] from the pars opercularis [9] of the frontal operculum of the inferior frontal gyrus that form an "M" (Naidich et al. 1995). The pars opercularis of the frontal operculum of the inferior frontal lobe harbours Broca's area. At its posterior margin, the pars opercularis is delimited by the anterior subcentral sulcus.

2.1.4 Auditory Cortex and Speech-Associated Temporoparietal Areas

2.1.4.1 Transverse Sections

From medial to lateral (see Figs. 2.5 and 2.6) towards the insula [19], the globus pallidus,

putamen and claustrum within the lentiform nucleus [17] can be differentiated. Between the lentiform nucleus [17] and the cortex of the insula [19] the extreme capsula [18] is depicted as a small rim of white matter. The Sylvian fissure [35b] separates the insula [19] from the temporal lobe. This is an easy definable landmark on axial views. The insula – taking anatomic variations into account – has 4–5 knobs (anterior, medial and posterior short insular gyri divided, by the CS [36], from the anterior and posterior long insular gyri). Posterior to the convolution that represents the section of the posterior long insular gyrus, a gyrus in the superior temporal lobe can be identified with a dorsomedial to anterior-lateral course, called the transverse temporal gyrus or Heschl's gyrus [10]. This is the primary auditory cortex (Mukamel et al. 2005; Devlin and Poldrack 2007). Number and size may vary (Penhune et al. 1996; Rademacher et al. 2001); however, this is another good landmark that is easy to define. Heschl's gyrus [10] might be interrupted by the sulcus intermedius of Beck. Two gyri on the right and only one on the left hemisphere can be found frequently (Shapleske et al. 1999). Heschl's sulcus [11], which borders Heschl's gyrus [10] posteriorly, is the anterior border of the planum temporale [12]. Although direct cortical stimulation intraoperatively may cause speech disturbances in this area (Sanai et al. 2008; Shapleske et al. 1999), the planum temporale [12] represents, more likely, the auditory association cortex. The planum temporale [12] extends on the superior surface of the temporal lobe and is delimited laterally by the superior temporal sulcus [13], posteriorly by the posterior ascending ramus and/or descending ramus of the Sylvian fissure and medially in the depth of the Sylvian fissure, which is less well defined (Shapleske et al. 1999). These borders are easier depicted in sagittal views; however, in transverse sections, remaining in the same plane in which Heschl's gyrus [10] can be found, the superior temporal sulcus [13] is the next biggest sulcus posterior to Heschl's sulcus [11]. Heschl's gyrus [10] bulges into the Sylvian fissure [35b]. The Sylvian fissure can therefore also be followed in ascending axial images. At the parietotemporal junction, sulci such as the Sylvian fissure or the superior temporal sulcus [13] ascend, whereas the sulcus intermedius primus descends. This hampers anatomical description in axial sections. Ascending in axial slice order, the superior temporal sulcus [13] diminishes. As Heschl's gyrus [10] bulges into the Sylvian fissure [35b], the Sylvian fissure can be followed on its course as posterior ascending ramus [35a] up to the level of the cella media of the lateral ventricles (in bicommissural orientation), as a big intersection posterior to Heschl's sulcus [11]. The posterior ascending ramus [35a] of the Sylvian fissure is imbedded in the supramarginal gyrus [37] which again is separated from the angular gyrus [38] by the sulcus intermedius primus. Descending in axial slice order, pre- and postcentral gyri can be identified as described above. The next sulcus dorsal to the postcentral sulcus is the intraparietal sulcus [7] which can be followed from the medial apical surface, laterally and dorsally in the parietal lobe [6]. Laterally, it ends above the sulcus intermedius primus and abuts the angular gyrus [38]. Size of the planum temporale [12] varies depending on sex, handedness and hemispherical dominance (Shapleske et al. 1999). Activation in functional imaging studies was found in verb generation tasks (Wise et al. 1991) and listening to tones, words and tone sequences (Binder et al. 1996, 1997, 2000).

2.1.4.2 Sagittal Sections

According to its dorsomedial to anterior-lateral course (see Fig. 2.6), the transverse temporal gyrus or Heschl's gyrus [10] abuts the base of the inferior sensorimotor strip (most likely the postcentral gyrus) at the lateral aspect and the posterior long gyrus of the insula [19] in more medially located sections. It is erected into the Sylvian fissure [35b]. Heschl's sulcus [11], which borders Heschl's gyrus [10] posteriorly, is the anterior border of the planum temporale [12]. The planum temporale [12] extends on the superior surface of the temporal lobe and is delimited laterally by the superior temporal sulcus [13], posteriorly by the posterior ascending ramus and/or descending ramus of the Sylvian fissure and medially in the depth of the Sylvian fissure, which is less well

defined (Shapleske et al. 1999). The Sylvian fissure can be followed from the anterior ascending [35d] and horizontal rami [35c] in the frontal operculum [9] of the inferior frontal gyrus, dorsally to the ascending [35a] and descending rami at the temporoparietal junction. Medially it is flanked by the insula [19], laterally by the superior temporal gyrus [34] and inferior parts of the pre- and postcentral gyri. Parallel to the Sylvian fissure [35b], the superior temporal gyrus [34] also demonstrates an anterior-posterior course. The posterior ascending ramus [35a] of the Sylvian fissure is imbedded in the supramarginal gyrus [37] which has a horseshoe appearance. Posterior to the supramarginal gyrus [37], the superior-inferior running sulcus intermedius primus separates it from the angular gyrus [38]. The superior temporal sulcus [13] ascends at its posterior end and diminishes.

2.1.4.3 Coronal Sections

In coronal views, the Sylvian fissure separating the temporal lobe from the insula and the frontal lobe can easily be seen. Originating from the temporal lobe, Heschl's gyrus points towards the insula (not shown).

2.1.5 Visual Cortex

2.1.5.1 Sagittal Sections

At the medial surface of the occipital lobe, there is a sulcus that zigzags anterior-posteriorly called the calcarine sulcus [27], along which the visual cortex is located. The calcarine sulcus [27] separates the superior lip from the inferior lip of the visual cortex.

References

Binder JR, Frost JA et al (1996) Function of the left planum temporale in auditory and linguistic processing. Brain 119:1239–1247

Binder JR, Frost JA et al (1997) Human brain language areas identified by functional imaging. J Neurosci 17:353–362

Binder JR, Frost JA et al (2000) Human temporal lobe activation by speech and nonspeech sounds. Cereb Cortex 10:512–528

Brandt T, Bartenstein P et al (1998) Reciprocal inhibitory visual-vestibular interactions: visual motion stimulation deactivates the parieto-insular vestibular cortex. Brain 121:1749–1758

Dechent P, Frahm J (2003) Functional somatotopy of finger representations in human primary motor cortex. Hum Brain Mapp 18:272–283

Devlin JT, Poldrack RA (2007) In praise of tedious anatomy. Neuroimage 37:1033–1041

Dronkers NF (1996) A new brain region for coordinating speech articulation. Nature 384:159–161

Ebeling U, Huber P et al (1986) Localization of the precentral gyrus in the computed tomogram and its clinical application. J Neurol 233(2):73–76

Eberstaller O (1890) Ein beitrag zur anatomie der oberfläche des grosshirns. Urban & Schwarzenberg, Wien/Leipzig

Fesl G, Moriggl B et al (2003) Inferior central sulcus: variations of anatomy and function on the example of the motor tongue area. Neuroimage 20(1):601–610

Kido DK, LeMay M et al (1980) Computed tomographic localization of the precentral gyrus. Radiology 135:373–377

Meyer JR, Roychowdhury S et al (1996) Location of the central sulcus via cor-tical thickness of the precentral and postcentral gyri on MR. AJNR Am J Neuroradiol 17(9):1699–1706

Mukamel R, Hagar G et al (2005) Coupling between neuronal firing, field potentials, and fMRI in human auditory cortex. Science 309:951–954

Nagao M, Takeda K et al (1999) Apraxia of speech associated with an infarct in the precentral gyrus of the insula. Neuroradiology 41:356–357

Naidich TP, Brightbill TC (1996) The pars marginalis: part I. A "bracket" sign for the central sulcus in axial plane CT and MRI. Int J Neuroradiol 2:3–19

Naidich TP, Valavanis AG et al (1995) Anatomic relationships along the low-middle convexity: part I – normal specimen and magnetic resonance imaging. Neurosurgery 36:517–532

Naidich TP, Kang E et al (2004) The insula: anatomic study and MR imaging display at 1.5 T. AJNR Am J Neuroradiol 25:222–232

Ojemann GA, Whitaker HA (1978a) The bilingual brain. Arch Neurol 35(7):409–412

Ojemann GA, Whitaker HA (1978b) Language localization and variability. Brain Lang 6(2):239–260

Ono M, Kubik S et al (eds) (1990) Atlas of the cerebral sulci. Georg Thieme, Stuttgart/New York

Oppenheimer S (1993) The anatomy and physiology of cortical mechanisms of cardiac control. Stroke 24:I3–I5

Overduin SA, Servos P (2004) Distributed digit somatotopy inprimary somatosensory cortex. Neuroimage 23(2):462–472

Penfield W, Rasmussen T (1950) The cerebral cortex in man. Macmillan, New York

Penhune VB, Zatorre RJ et al (1996) Interhemispheric anatomical differences in human primary auditory cortex: probabilistic mapping and volume measurement from magnetic resonance scans. Cereb Cortex 6:661–672

Price CJ (2000) The anatomy of language: contributions from functional neuroimaging. J Anat 197:335–359
Rademacher J, Galaburda AM et al (1992) Human cerebral cortex: localization, parcellation, and morphometry with magnetic resonance imaging. J Cogn Neurosci 4(4):352–374
Rademacher J, Morosan P et al (2001) Probabilistic mapping and volume measurement of human auditory cortex. Neuroimage 13:669–683
Riecker A, Ackermann H et al (2000) Opposite hemispheric lateralization effects during speaking and singing at motor cortex, insula and cerebellum. Neuroreport 11:1997–2000
Sanai N, Mirzadeh Z et al (2008) Functional outcome after language mapping for glioma resection. N Engl J Med 358(1):18–27
Shapleske J, Rossell SL et al (1999) The planum temporale: a systematic review of its structural, functional and clinical significance. Brain Res Rev 29:26–49
Wise R, Chollet U et al (1991) Distribution of cortical neuronal networks involved in word comprehension and word retrieval. Brain 114:1803–1817
Wise RJ, Greene J et al (1999) Brain regions involved in articulation. Lancet 353:1057–1061
Yousry TA, Schmid UD et al (1995) Topography of the cortical motor hand area: prospective study with functional MR imaging and direct motor mapping at surgery. Radiology 195(1):23–29
Yousry TA, Schmid UD et al (1997) Localization of the motor hand area to a knob on the precentral gyrus. A new landmark. Brain 120(Pt 1):141–157

Spatial Resolution of fMRI Techniques

3

Seong-Gi Kim, Tao Jin, and Mitsuhiro Fukuda

3.1 Introduction

Following its introduction over two decades ago, functional magnetic resonance imaging (fMRI) based on the blood oxygenation level-dependent (BOLD) contrast (Ogawa et al. 1990) has become the tool of choice for visualizing neural activity in the human brain. The conventional BOLD approach has been extensively used for pinpointing functional foci of vision, motor, language, and memory in normal and clinical patients. Intraoperative localization of functional foci will greatly improve surgical planning for epilepsy and tumor dissection, and potentially, for deep brain stimulation. Therefore, it is critical to understand the spatial resolution of fMRI relative to the actual neural active site (see review articles, (Kim and Ogawa 2002; Kim and Ugurbil 2003)).

In order to reliably determine the functional foci, high signal-to-noise ratio (SNR), which can be achieved using optimized imaging techniques, is critical. However, high SNR of fMRI techniques is not sufficient for high-resolution functional mapping if the signals that are being imaged do not have a high *specificity* to the local neural activity. Therefore, it is important to understand the signal source of BOLD fMRI and its fundamental limit of spatial resolution. Increased neural activity induces an increase in tissue metabolic demands. Thus, imaging the metabolic change (e.g., 2-fluorodeoxyglucose positron emission tomography) will yield high spatial specificity as metabolism will occur at the tissue at the site of the neuronal activity and not in the vasculature. Changes in neural activity and metabolism could directly or indirectly modulate the hemodynamic responses, including the cerebral blood flow (CBF), the cerebral blood volume (CBV), and the venous oxygenation levels. It has been well established that the magnitude of CBF change is well correlated with that of metabolic change. Thus, CBF mapping can pinpoint the most active spot of neural activity even if the exact spatial extent of the CBF response is controversial ((Malonek and Grinvald 1996) vs. (Duong et al. 2001)). The most commonly used BOLD technique is sensitive to paramagnetic deoxyhemoglobin (dHb), which is located at the capillaries and the venous draining vascular system (Ogawa et al. 1993), reducing spatial specificity of the gradient-echo BOLD signal. Often in fMRI studies, higher resolution BOLD images appear localized to large venous vessels because of larger contributions of venous signals due to the reduced volume fraction of tissue.

To understand the spatial resolution of hemodynamic responses, functional changes of different vascular origins should be carefully considered. In this chapter, we will discuss the intrinsic limitations and the improvements of spatial resolution.

S.-G. Kim (✉) • T. Jin • M. Fukuda
Department of Radiology, University of Pittsburgh,
3025 East Carson Street, Pittsburgh, PA 15203, USA
e-mail: kimsg@pitt.edu

S. Ulmer, O. Jansen (eds.), *fMRI – Basics and Clinical Applications*,
DOI 10.1007/978-3-642-34342-1_3,

3.2 Vascular Structure and Hemodynamic Response

As all fMRI signals originate from changes in hemodynamics, it is important to examine vascular structure. Detailed human brain vasculature was studied anatomically by Duvernoy et al. (1981). In short, vessels can be classified into pial and parenchymal vessels. Superficial pial arterial and venous vessels are numerous; arterial vessels with ~40–280-mm diameter have lesser branches than venous vessels with a ~130–380-mm diameter. These vessels can run a few centimeters and even longer. At the surface of the cortex, pial vessels connect to penetrating arteries and emerging veins at a right angle.

Parenchymal vessels can be divided into arteries, veins, and capillary network. Capillaries with ~5-μm average diameter and ~100-μm length are most abundant at the middle of the cortex (Pawlik et al. 1981). Intracortical arteries and veins can be further classified into their cortical depths (Duvernoy et al. 1981); group 1 and 2 vessels (with 10–20 μm diameter for arterial vessels and 20–30 μm for venous vessels) reach the upper cortical layers (layers 2–3), group 3 (with 15–30 μm for arterial vessels and 45 μm for venous vessels) the middle of the cortex (layers 3–5), group 4 (with 30–40 μm for arterial vessels and 65 μm for venous vessels) the lower cortical region (layer 6), and group 5 (with 30–75 μm for arterial vessels and 80–125 μm for venous vessels) the white matter. The number of intracortical arteries is ~4 times the number of intracortical veins (Duvernoy et al. 1981).

The intrinsic limit of spatial specificity of hemodynamic-based fMRI can be dependent on how finely CBF and CBV are regulated. Blood in each intracortical artery will supply a certain tissue volume, which is referred to as "the volume of arterial unit"; the volume of arterial unit is a volume with 0.33–0.5 mm diameter around a vessel for groups 2–3 and for 0.5–2 mm for group 5 (Duvernoy et al. 1981). If an individual intracortical artery can be independently regulated, spatial resolution can be 0.33–0.5 mm if arterial vessels or capillary changes are detected. Our fMRI studies suggest that intrinsic CBF and CBV changes are reasonably specific to submillimeter functional domains (Duong et al. 2001; Zhao et al. 2005), which are in the order of 0.5–0.7-mm diameter in cats. If the regulation point exists at precapillary arterioles or capillaries, then spatial resolution is even better. Recent papers indicate that precapillary arterioles indeed dilate during stimulation via astrocyte-capillary signaling (Zonta et al. 2003; Mulligan and MacVicar 2004; Metea and Newman 2006; Schummers et al. 2008; Petzold and Murthy 2011). In fact, the capillary network responds precisely in regions of neural activity in rat olfactory bulb, suggesting that spatial resolution of ~100 μm is achievable (Chaigneau et al. 2003).

When an imaging technique is sensitive to changes in intracortical veins, its spatial resolution is determined by the volume of tissue draining to each vein, which is considered to be "the volume of venous unit." The volume of venous units is a volume with 0.75–1 mm diameter around a vessel for groups 3–4 vessels and 1–4 mm diameter for group 5 (Duvernoy et al. 1981). Thus, spatial resolution cannot be better than 0.75 mm even if one single intracortical artery regulates precisely and downstream vessels respond. Intracortical venous vascular structures can be visualized with MRI. Figure 3.1 shows venographic images of cat brain, which were obtained using the BOLD contrast at 9.4 T. Venous vessels appear as dark lines or dots because venous blood has short T_2^* relative to tissue and arterial blood. Furthermore, blood susceptibility effect extends to tissue, enlarging apparent venous vessel size. Clearly, groups 3–5 intracortical veins can be easily visualized, and group 3 is most numerous. Typical distance between intercortical veins is ~0.5–1 mm (Fig. 3.1).

3.3 Spatial Resolution of BOLD fMRI

Since blood travels from capillaries to intracortical veins, and finally pial veins, a change in dHb concentration in blood can also occur far away from the actual gray matter region with increased neural activity, reducing effective spatial

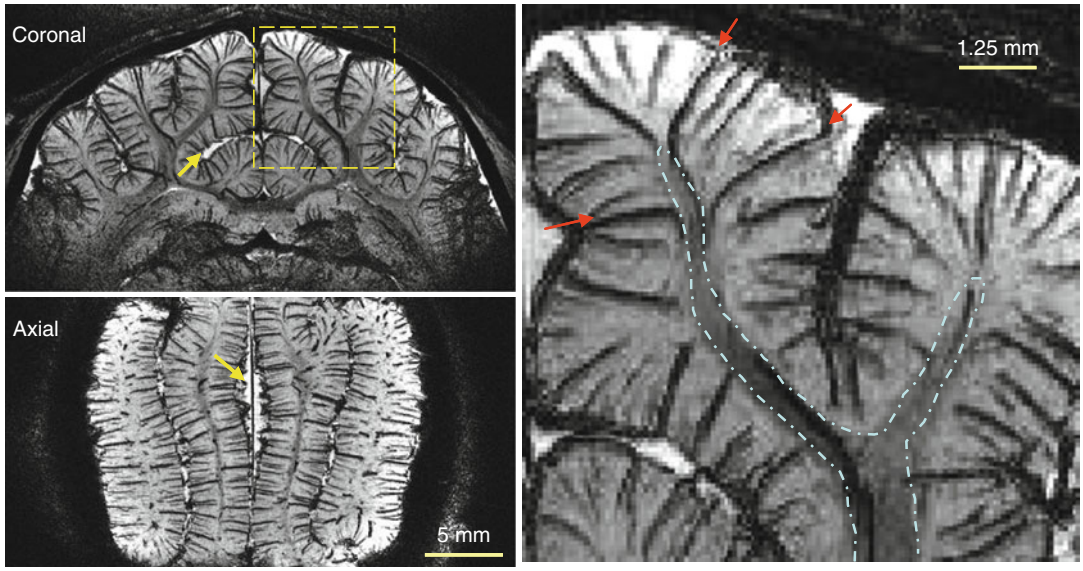

Fig. 3.1 Visualization of venous vessels in a cat brain. A 3-D T_2^*-weighted MR image was obtained at 9.4 T with 78 μm isotropic resolution and field of view of $2\times2\times4$ cm^3. A gradient-echo time of 20 ms was used to maximize the contrast between venous vessels and tissue. Data acquisition and processing methods were reported elsewhere (Park et al. 2008). 1.25-mm-thick slabs were selected, and minimum intensity projection was performed to enhance the contrast of venous vessels. As a surface coil was used, the ventral section in the coronal slice (*top left*) had poor signal-to-noise ratio (SNR), and thus, vessels could not be detected in that region. White matter areas (*contours in right*) can be distinguished from gray matter. *Dotted yellow box* in the coronal image was expanded 4 times into right. *Yellow arrows* cerebrospinal fluid (CSF) areas; *red arrows* venous vessels draining from white matter, which are "group 5." *Scale bar*, 5 mm for *left* and 1.25 mm for *right*

resolution. However, there is considerably more dilution of dHb change at farther downstream from the neuronally active region due to larger blood contribution from inactive regions. This dilution issue is also closely related to strength and spatial extent of neural activity. When the area of activation is small, this deoxygenated blood is diluted with blood from inactivated regions, effectively reducing the oxygenation level change. Thus BOLD fMRI is capable of differentiating small functional modules such as single whisker barrels (Yang et al. 1996). However, when the area of activation is large, blood drained from active regions can travel far away without much dilution.

Conventional BOLD response is related to a change in dHb contents within a voxel, thus directly correlated with (baseline dHb content) time (oxygenation change). Since a pixel with draining veins has high baseline dHb content, the BOLD response is particularly sensitive to large draining veins. Thus, spatial resolution of conventional BOLD signal can be much worse than that determined by the volume of venous unit. It is a reasonable assumption that conventional BOLD-based *high-resolution* fMRI may mostly detect the functionally less-specific large-vessel signals. To precisely localize functional foci, it is desirable to remove or minimize large-vessel contributions.

In order to understand which size of venous vessels can be detected by BOLD fMRI, we review the source of BOLD fMRI signals. Detailed biophysical models and explanations can be found in others (Ogawa et al. 1993; Weisskoff et al. 1994; Kim and Ugurbil 2003). The BOLD contrast induced by dHb arises from both intravascular (IV) and extravascular (EV) components. Since exchange of water between these two compartments (typical lifetime of the water in capillaries >500 ms) is relatively slow when compared with the imaging time (echo time <100 ms), MRI signals from these can be treated as separate pools.

The IV component is considered to be uniform within vessels because water rapidly exchanges between red blood cells (RBC) with paramagnetic dHb and plasma (average water residence time in RBCs = ~5 ms) and travels through space by exchange and diffusion. Thus, "dynamic" time averaging occurs over the many different fields induced by dHb. All water molecules inside the vessel will experience similar dynamic averaging, resulting in reduction of blood water T_2 in the venous pool. At high magnetic fields, venous blood T_2 can be shorter than tissue T_2 because R_2 ($=1/T_2$) of venous blood is quadratically dependent on magnetic field (Thulborn et al. 1982). Thus, at a higher magnetic field, IV contribution can be reduced by setting echo time much longer than blood T_2 (or T_2^*) (Lee et al. 1999; Jin et al. 2006). Alternatively, the IV signal can be reduced by applying bipolar gradients (as employed in diffusion-weighted images), which, with a "*b*" value of >30 s/mm^2, are expected to leave only the microvascular/extravascular contribution (Le Bihan et al. 1986).

The EV BOLD phenomenon has two biophysical sources (Ogawa et al. 1993; Weisskoff et al. 1994): one is due to intra-voxel dephasing of the magnetization in the presence of susceptibility-induced gradients, and the other is due to diffusion across the steep, susceptibility-induced gradients around small vessels (capillaries and venules). The first component induces high percentage signal changes around large venous vessels, regardless of magnetic field strength. Since field gradient decreases by $(r/a)^2$ where r is the distance from vessel to the region of interest and a is the vessel radius, the dephasing effect around a larger vessel is more spatially widespread. However, the dephasing effect of the static field can be refocused by the 180° radiofrequency (RF) pulse. Therefore, the EV contribution of large vessels can be reduced by using the spin-echo technique (which is similar to T_2-weighting in diagnostic imaging). The second component induces small signal changes in areas around capillaries and small venules. The reason is that tissue water around capillaries and small venules will be "dynamically" averaged over the many different fields during TE, similar to the IV component. This effect is larger at a higher magnetic field due to an increased susceptibility gradient within the water diffusion distance during TE. The dynamic diffusion-induced signals can be detected by either GE or SE approach. It is conceivable that the T_2-based BOLD technique is better localized to neuronal active region than T_2^*-based BOLD if the IV component of large vessels is removed (Zhao et al. 2004, 2006). However, the sensitivity of spin-echo techniques is less than gradient-echo BOLD signal.

To examine the spatial resolution of GE and SE BOLD fMRI, we used cortical layers as a model because layer 4 has the highest metabolic and CBF responses during neural activity as well as the highest synapse density and cytochrome oxidase activity (Woolsey et al. 1996). If the fMRI technique is highly specific to metabolic response and/or neural activity, the middle of the cortex should have the highest signal change. Figure 3.2 shows GE and SE BOLD fMRI maps of one isoflurane-anesthetized cat obtained during visual stimulation at 9.4 T (Zhao et al. 2006). To view the cortical cross section within a plane resolution of 156 × 156 μm^2, a 2-mm-thick imaging slice was selected perpendicular to the cortical surface. In both GE and SE BOLD maps, signal intensities increased during visual stimulation, indicating an increase in venous oxygenation. In conventional GE BOLD fMRI (Fig. 3.2), the highest percentage signal changes (yellow pixels) were seen in the CSF space (within the green contours), where pial veins are located. This large-vessel contribution to BOLD signals is reduced using the SE technique (Fig. 3.2) because the dephasing around large vessels refocuses. This result is consistent with high-field SE BOLD observations (Lee et al. 1999; Yacoub et al. 2003; Zhao et al. 2004).

SE BOLD fMRI is an excellent alternative approach if high spatial resolution is required and high magnetic field (such as 7 T) is available (Moon et al. 2007; Yacoub et al. 2008). Otherwise, conventional GE BOLD fMRI should be used with post-processing approaches to remove or minimize large-vessel contributions. Location of large pial venous vessels can be determined from

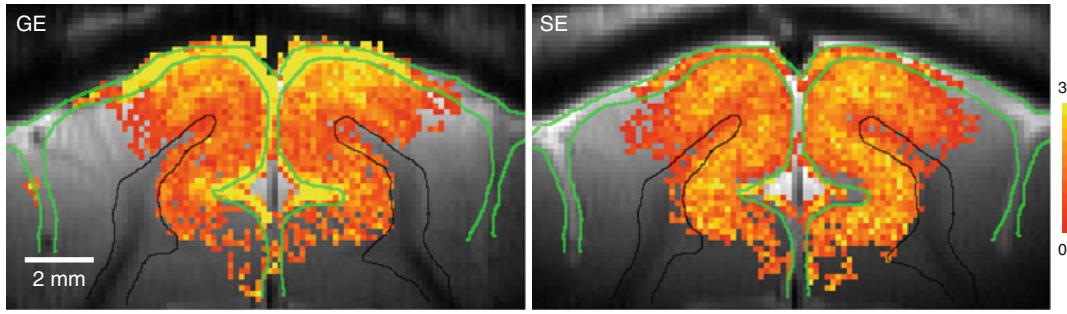

Fig. 3.2 High-resolution GE (*left*) and SE BOLD (*right*) fMRI maps of cat brain during visual stimulation overlaid on anatomical EPI images (Zhao et al. 2006). Coronal 2-mm-thick images with 156×156 μm² in-plane resolution were acquired using the four shot EPI technique at 9.4 T with gradient-echo time of 20 ms and spin-echo time of 40 ms. To determine statistically significant pixels, Student's *t* test was performed on a pixel-by-pixel basis with a t-value threshold of 2.0. Then, percentage signal changes were calculated for statistically active pixels. *Green contours* CSF area, *black contours* white matter, *scale bar* 2 mm, *color scale bar* 0.3–3 %

venographic images obtained with high-resolution T_2^*-weighted MR techniques (see Fig. 3.1) or from anatomical structures such as sulci and CSF. Large venous vessel areas tend to induce large BOLD percent change (see also Fig. 3.2) (Kim et al. 1994), delayed response (Lee et al. 1995), significant phase change (Menon 2002), and large baseline fluctuations (Kim et al. 1994). Although these criteria are subjective, they are effective in detecting and reducing large-vessel contamination.

3.4 Perfusion-Based fMRI Approaches

Alternative to the BOLD approach, CBF-weighted techniques which are sensitive mainly to parenchyma should be considered for mapping functional foci. CBF-weighted functional images can be obtained using MR by employing arterial blood water as an endogenous flow tracer. Arterial spin labeling (ASL) can be achieved by RF pulse(s). Then, labeled spins move into capillaries in the imaging slice and exchange with tissue water spins. To obtain only perfusion-related images, two images are acquired, one with ASL and the other without labeling. The difference between the two images is directly related to CBF, and relative CBF changes due to physiological perturbations can be measured. Most of the labeled water molecules extract into tissue and the remaining labeled water lose most of their labeling by the time they reach the draining veins due to its relatively short half-life (i.e., T_1 of blood). Thus, CBF-weighted MRI signals predominantly originate from tissue/capillary as well as arterial vessels (Ye et al. 1997; Lee et al. 2002; Kim and Kim 2005). Sensitivity of perfusion-weighted signals increases with magnetic field strength due to an increase in arterial blood T_1. ASL techniques include continuous ASL (Detre et al. 1992), flow-sensitive alternating inversion recovery (FAIR) (Kim 1995; Kwong et al. 1995), and various other techniques (Edelman et al. 1994; Wong et al. 1998).

Perfusion-based MR techniques have been used for fMRI studies. The spatial specificity of CBF-based fMRI is superior compared to GE BOLD techniques (Duong et al. 2001). Figure 3.3 shows BOLD and CBF functional maps during finger movements obtained at 4 T (Kim et al. 1997). The FAIR technique was used with inversion time of 1.4 s; the BOLD map was obtained from non-slice-selective inversion recovery images, while the CBF map was from subtraction of non-slice-selective from slice-selective inversion recovery images. Generally, activation areas are consistent between the maps measured by both techniques. However, pixel-wise comparison shows discrepancy between the two maps. Large signal changes in BOLD are located at draining veins indicated by arrows in the middle slice, while no signal change was observed in

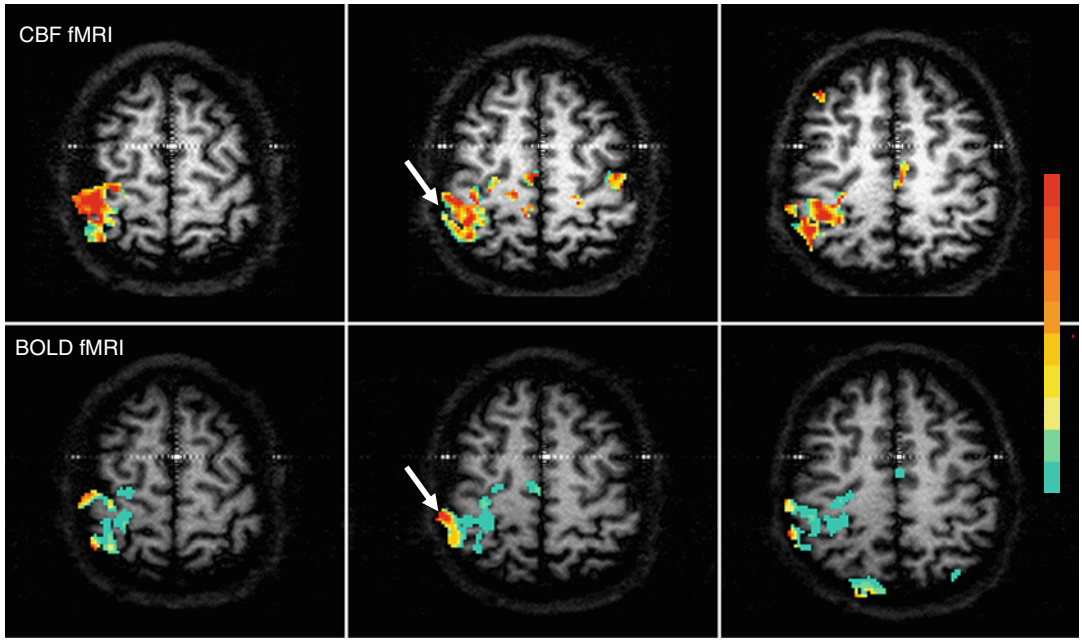

Fig. 3.3 BOLD and CBF functional maps of left-hand finger opposition, overlaid on T_1-weighted EPI (Kim et al. 1997). The flow-sensitive alternating inversion recovery (FAIR) technique was used to acquire BOLD (*bottom*) and CBF (*top*) contrast simultaneously at 4.0 T. BOLD maps were obtained from non-slice-selective inversion recovery (IR) images, while CBF maps were calculated from differences between slice-selective and non-slice-selective IR images. A cross-correlation value of 0.3 was used for threshold. For BOLD images, each color increment represents a 1 % increment starting from the bottom 1 %, while for CBF images, each color increment represents a 10 % increment starting from the bottom 10 %. The oblique arrow at the middle slice, indicating the right (contralateral) central sulcus, shows no activation in the CBF map, but large signal increase in the BOLD map, suggesting BOLD is sensitive to large draining veins

CBF. Tissue areas with high percent CBF changes have low BOLD signal changes. This indicates that the CBF approach is more specific to tissue than GE BOLD fMRI. To further confirm human fMRI results, BOLD and CBF fMRI were also compared in the cat's layer model. Figure 3.4 shows GE BOLD and CBF fMRI maps obtained during visual stimulation at 9.4 T (Jin and Kim 2008). CBF data were obtained using the FAIR technique with inversion time of 1.25 s, while gradient BOLD data were obtained with TE of 20 ms. The highest GE BOLD signal changes occur at the surface of the cortex, while the highest CBF changes occur at the middle of the cortex. This again demonstrates that perfusion-based fMRI technique is superior to GE BOLD for pinpointing functional foci precisely.

Proper CBF contrast is achieved only when enough time is allowed for the labeled arterial water to travel into the region of interest and exchange with tissue water. This makes it difficult to detect changes in CBF with a temporal resolution greater than T_1 of arterial blood water. Acquisition of a pair of images can further reduce temporal resolution and consequently SNR. Thus, it is difficult to obtain whole brain fMRI rapidly. However, baseline CBF value can be obtained, in addition to quantitative functional response. An additional advantage is less sensitivity to baseline signal drifts because slow non-activation-related signal changes can be removed by the pairwise subtraction (Kim 1995), and it is more stable to low-frequency stimulation compared to BOLD. Therefore, perfusion-based fMRI techniques are preferable for repetitive measurements over a long time period such as weeks and months, allowing investigations of functional reorganization and development. In

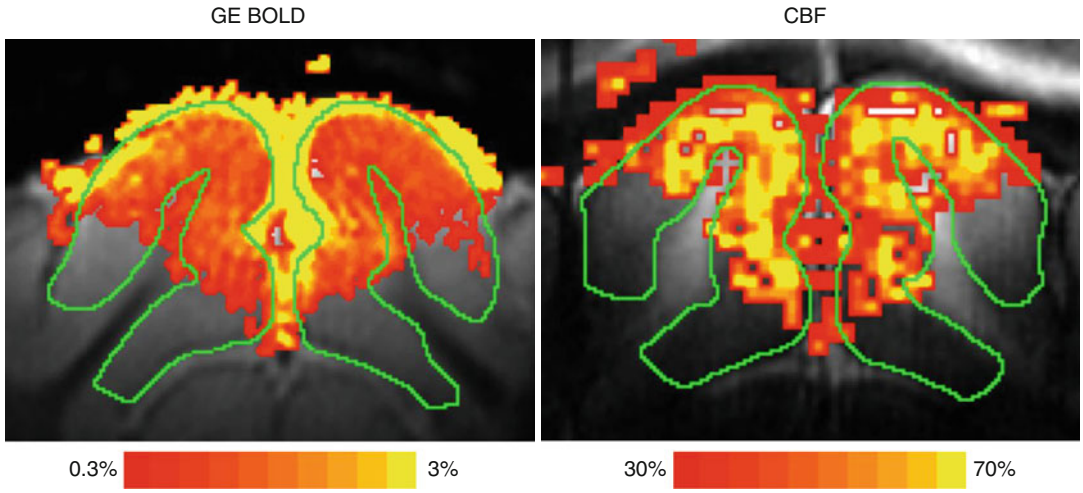

Fig. 3.4 BOLD and CBF fMRI maps of cat brain during visual stimulation overlaid on anatomical EPI images (Jin and Kim 2008). Coronal 2-mm-thick images with 312×312 μm^2 in-plane resolution were acquired at 9.4 T; BOLD fMRI (*left*) was obtained with TE of 20 ms, while CBF (*right*) was detected with the FAIR technique with inversion time of 1.25 s. Maps were obtained by thresholding with a P value <0.05 and number of contiguous active pixels ≥3. The gray matter areas are outlined by *green contours*. The highest BOLD signal changes are observed at the surface of the cortex, while the highest CBF changes occur at the middle of the cortex. *Color bar* 0.3–3.0 % for BOLD and 30–70 % for CBF

clinical applications of fMRI where precise mapping is required around abnormal regions, the CBF-based fMRI technique is most appropriate because parenchymal signals are dominant.

Acknowledgments This work was supported in part by NIH (EB003324, EB003375, and NS44589). The authors thank their colleagues in the Neuroimaging Laboratory for providing the figures and for the discussion.

References

Chaigneau E, Oheim M et al (2003) Two-photon imaging of capillary blood flow in olfactory bulb glomeruli. Proc Natl Acad Sci USA 100(22):13081–13086

Detre JA, Leigh JS et al (1992) Perfusion imaging. Magn Reson Med 23:37–45

Duong TQ, Kim D-S et al (2001) Localized cerebral blood flow response at submillimeter columnar resolution. Proc Natl Acad Sci USA 98:10904–10909

Duvernoy HM, Delon S et al (1981) Cortical blood vessels of the human brain. Brain Res Bull 7(5):519–579

Edelman RR, Siewert B et al (1994) Qualitative mapping of cerebral blood flow and functional localization with echo-planar MR imaging and signal targeting with alternating radio frequency. Radiology 192:513–520

Jin T, Kim SG (2008) Cortical layer-dependent dynamic blood oxygenation, cerebral blood flow and cerebral blood volume responses during visual stimulation. Neuroimage 43(1):1–9

Jin T, Wang P et al (2006) Source of nonlinearity in echo-time-dependent BOLD fMRI. Magn Reson Med 55:1281–1290

Kim S-G (1995) Quantification of relative cerebral blood flow change by flow-sensitive alternating inversion recovery (FAIR) technique: application to functional mapping. Magn Reson Med 34:293–301

Kim T, Kim S-G (2005) Quantification of cerebral arterial blood volume and cerebral blood flow using MRI with modulation of tissue and vessel (MOTIVE) signals. Magn Reson Med 54:333–342

Kim S-G, Ogawa S (2002) Insights into new techniques for high resolution functional MRI. Curr Opin Neurobiol 12:607–615

Kim S-G, Ugurbil K (2003) High-resolution functional magnetic resonance imaging of the animal brain. Methods 30:28–41

Kim SG, Hendrich K et al (1994) Potential pitfalls of functional MRI using conventional gradient-recalled echo techniques. NMR Biomed 7(1–2):69–74

Kim S-G, Tsekos NV et al (1997) Multi-slice perfusion-based functional MRI using the FAIR technique: comparison of CBF and BOLD effects. NMR Biomed 10:191–196

Kwong KK, Chesler DA et al (1995) MR perfusion studies with T1-weighted echo planar imaging. Magn Reson Med 34:878–887

Le Bihan D, Breton E et al (1986) MR imaging of intravoxel incoherent motions: application to diffusion

and perfusion in neurologic disorders. Radiology 161:401–407
Lee AT, Glover GH et al (1995) Discrimination of large venous vessels in time-course spiral blood-oxygen-level-dependent magnetic resonance functional neuroimaging. Magn Reson Med 33:745–754
Lee S-P, Silva AC et al (1999) Diffusion-weighted spin-echo fMRI at 9.4 T: microvascular/tissue contribution to BOLD signal change. Magn Reson Med 42: 919–928
Lee S-P, Silva AC et al (2002) Comparison of diffusion-weighted high-resolution CBF and spin-echo BOLD fMRI at 9.4 T. Magn Reson Med 47:736–741
Malonek D, Grinvald A (1996) Interactions between electrical activity and cortical microcirculation revealed by imaging spectroscopy: implication for functional brain mapping. Science 272:551–554
Menon RS (2002) Postacquisition suppression of large-vessel BOLD signals in high-resolution fMRI. Magn Reson Med 47:1–9
Metea M, Newman E (2006) Glial cells dilate and constrict blood vessels: a mechanism of neurovascular coupling. J Neurosci 26:2862–2870
Moon CH, Fukuda M et al (2007) Neural interpretation of blood oxygenation level-dependent fMRI maps at submillimeter columnar resolution. J Neurosci 27: 6892–6902
Mulligan S, MacVicar B (2004) Calcium transients in astrocyte endfeet cause cerebrovascular constrictions. Nature 431:195–199
Ogawa S, Lee T-M et al (1990) Oxygenation-sensitive contrast in magnetic resonance image of rodent brain at high magnetic fields. Magn Reson Med 14:68–78
Ogawa S, Menon RS et al (1993) Functional brain mapping by blood oxygenation level-dependent contrast magnetic resonance imaging. A comparison of signal characteristics with a biophysical model. Biophys J 64(3):803–812
Park SH, Masamoto K et al (2008) Imaging brain vasculature with BOLD microscopy: MR detection limits determined by in vivo two-photon microscopy. Magn Reson Med 59:855–865
Pawlik G, Rackl A et al (1981) Quantitative capillary topography and blood flow in the cerebral cortex of cats: an in vivo microscopic study. Brain Res 208:35–58
Petzold GC, Murthy VN (2011) Role of astrocytes in neurovascular coupling. Neuron 71:782–797
Schummers J, Yu H et al (2008) Tuned responses of astrocytes and their influence on hemodynamic signals in the visual cortex. Science 320:1638–1643
Thulborn KR, Waterton JC et al (1982) Oxygenation dependence of the transverse relaxation time of water protons in whole blood at high field. Biochim Biophys Acta 714:265–270
Weisskoff RM, Zuo CS et al (1994) Microscopic susceptibility variation and transverse relaxation: theory and experiment. Magn Reson Med 31:601–610
Wong E, Buxton R et al (1998) Quantitative imaging of perfusion using a single subtraction (QUIPSS anf QUIPSS II). Magn Reson Med 39:702–708
Woolsey TA, Rovainen CM et al (1996) Neuronal units linked to microvascular modules in cerebral cortex: response elements for imaging the brain. Cereb Cortex 6:647–660
Yacoub E, Duong TQ et al (2003) Spin-echo fMRI in humans using high spatial resolutions and high magnetic fields. Magn Reson Med 49:655–664
Yacoub E, Harel N et al (2008) High-field fMRI unveils orientation columns in humans. Proc Natl Acad Sci USA 105:10607–10612
Yang X, Hyder F et al (1996) Activation of single whisker barrel in rat brain localized by functional magnetic resonance imaging. Proc Natl Acad Sci USA 93: 475–478
Ye FQ, Mattay VS et al (1997) Correction for vascular artifacts in cerebral blood flow values by using arterial spin tagging techniques. Magn Reson Med 37:226–235
Zhao F, Wang P et al (2004) Cortical depth-dependent gradient-echo and spin-echo BOLD fMRI at 9.4 T. Magn Reson Med 51:518–524
Zhao F, Wang P et al (2005) Spatial specificity of cerebral blood volume-weighted fMRI responses at columnar resolution. Neuroimage 27:416–424
Zhao F, Wang P et al (2006) Cortical layer-dependent BOLD and CBV responses measured by spin-echo and gradient-echo fMRI: insights into hemodynamic regulation. Neuroimage 30:1149–1160
Zonta M, Angulo MC et al (2003) Neuron-to-astrocyte signaling is central to the dynamic control of brain microcirculation. Nat Neurosci 6:43–50

The Electrophysiological Background of the fMRI Signal

4

Christoph Kayser and Nikos K. Logothetis

4.1 Introduction

The ability to non-invasively study the architecture and function of the human brain constitutes one of the most exciting cornerstones for modern medicine, psychology and neuroscience. Current in vivo imaging techniques not only provide clinically essential information and allow new forms of treatment but also reveal insights into the mechanisms behind brain function and malfunction. This supremacy of modern imaging rests on its ability to study the structural properties of the nervous system simultaneously with the functional changes related to neuronal activity. As a result, imaging allows us to combine information about the spatial organization and connectivity of the nervous system with information about the underlying neuronal processes and provides the only means to link perception and cognition with the neural substrates in the human brain. Functional imaging techniques build on the interconnections of cerebral blood flow (CBF), the brain's energy demand and the neuronal activity (for reviews on this topic, see Heeger and Ress 2002; Logothetis 2002; Logothetis and Wandell 2004; Lauritzen 2005). Indeed, elaborate mechanisms exist to couple changes in CBF and blood oxygenation to the maintenance and restoration of ionic gradients and the synthesis, transport and reuptake of neurotransmitters. More than 125 years ago, Angelo Mosso had already realized that there must be a relation between energy demand and CBF when he observed increasing brain pulsations in a patient with a permanent skull defect performing a mental task (Mosso 1881). Similar observations on the coupling of blood flow to neuronal activity (from experiments on animals) led Roy and Sherrington to make the insightful statement that "… the chemical products of cerebral metabolism contained in the lymph that bathes the walls of the arterioles of the brain can cause variations of the caliber of the cerebral vessels: that is, in this reaction, the brain possesses an intrinsic mechanism by which its vascular supply can be varied locally in correspondence with local variations of functional activity" (Roy and Sherrington 1890).

Nowadays, there is little doubt about the usefulness of imaging to basic research and clinical diagnosis. In fact, with the wide availability of magnetic resonance imaging (MRI), functional imaging has become a self-sustaining branch of neuroscience research. Yet, and despite all this progress, it is still not clear how faithfully functional imaging replicates the patterns of neuronal activity underlying the changes in brain perfusion. Debating over the spatial and temporal precision of the imaging signal, researchers have compared it to more direct measurements of electrical neuronal activity from electrophysiological approaches. This holds especially true for the blood-oxygenation level-dependent signal (BOLD-fMRI), which is probably the most widely

C. Kayser (✉) • N.K. Logothetis
Department Physiology of Cognitive Processes,
Max Planck Institute for Biological Cybernetics,
Spemannstrasse 38, Tübingen 72076, Germany
e-mail: christoph.kayser@tuebingen.mpg.de

S. Ulmer, O. Jansen (eds.), *fMRI – Basics and Clinical Applications*,
DOI 10.1007/978-3-642-34342-1_4,

used functional imaging technique (Ogawa et al. 1998). As direct measurements of neuronal activity can be obtained from mesoscopic recordings of electrical potentials on the scalp (EEG) as well as from spatially localized recordings using fine microelectrodes, they offer a wide variety of signals that characterize neuronal processes. Hence, before reviewing the neurophysiological basis of the functional imaging signal, it is worth considering the properties of the signals recorded using electrophysiological methods.

4.2 The Compound Neural Signal

Electrophysiological studies at the systems level typically record extracellular signals, defined by the superposition of local currents. In contrast to the intracellular recordings that directly assess the membrane potential of individual neurons, extracellular signals can arise from a number of sources and are more difficult to interpret. Neurons are embedded in the extracellular medium, which acts as a volume conductor, allowing the passive spread of electrical signals across considerable spatial distances. For an extracellular recording point, the inflow of positively charged ions into the active sites of a neuron appears as a current sink (inward currents), while inactive membrane sites act as a source (outward currents) for the active regions. Given the resistive nature of the extracellular medium, these currents generate so-called extracellular field potentials (EFP) (Freeman 1975). The signal measured by an electrode placed at a neural site represents the mean EFP from the spatially weighted sum of sinks and sources along multiple cells at this particular site. In addition, by the superposition principle, the EFPs from multiple cells add up linearly throughout the volume conductor. Thus, for cells, or cell compartments, with diametrically opposite orientations, currents of equal magnitude but opposite polarity will generate potentials that tend to cancel each other, while for well-aligned and elongated processes of neural elements, the currents add, resulting in a strongly oriented electric field. Despite these difficulties in interpreting the measured signals, EFP remains the most important tool for the systems neurophysiologist, as they convey a great deal of information about the underlying brain function.

If a small-tipped microelectrode is placed sufficiently close to the soma or axon of a neuron, then the measured EFP directly reports the spike (action potentials) of that neuron, and possibly also of its immediate neighbours. The firing rates of such well-isolated neurons have been the critical measure for comparing neural activity with sensory processing or behaviour ever since the early development of microelectrodes (Adrian and Zotterman 1929). Indeed, measuring firing rates has been the mainstay of systems neuroscience for decades. Although a great deal has been learned from this measure of neuronal activity, the single-unit technique has the drawback of not providing information about subthreshold integrative processes or associational operations taking place at a given site. In addition, this recording technique suffers from a bias toward certain cell types and sizes (Towe and Harding 1970; Stone 1973). For large neurons, the active and passive regions are further apart, resulting in a substantially greater flow of membrane current and a larger extracellular spike than for a small cell. As a result, spikes generated by large neurons will remain above noise level over a greater distance from the cell than spikes from small neurons. It follows that typically measured spiking activity mostly represents the small population of large cells, which are the pyramidal cells in the neocortex . This bias is particularly pronounced in experiments with alert-behaving animals or humans, in which even slight movements of the subjects make it extremely difficult to record from smaller neurons for a sufficiently long time (Fried et al. 1997; Kreiman et al. 2000). As a result, most of the experiments using single-unit extracellular recordings report on the activity of large principal cells, which represent the output of the cortical area under study.

If the impedance of the microelectrode is sufficiently low, or when no clear signal from individual neurons can be isolated, then the

electrode can be used to monitor the totality of the action potentials in that region. Often, the multiunit activity (MUA) is characterized as compound electrical signal in a frequency range above 300–500 Hz. This signal has been shown to be site specific (Buchwald and Grover 1970) and to vary systematically with stimulus properties in the same way as the activity of single neurons (e.g. Kayser et al. (2007a)). There is good evidence that MUA activity reflects variations in the magnitude of extracellular spike potentials, with large-amplitude signal variations in the MUA reflecting large-amplitude extracellular potentials. Overall, the MUA seems to incorporate signals from a sphere with a radius of 150–300 mm, depending on the detailed electrode properties (Buchwald and Grover 1970; Legatt et al. 1980; Gray et al. 1989). Typically, such a region will contain thousands of neurons, suggesting that the MUA is especially sensitive to the synchronous firings of many cells, which is further enhanced by the principle of superposition mentioned above.

While the fast, high-frequency components of the aggregate field potentials mostly reflect the spiking activity of neighbouring neurons, the slower components of the EFP seem to reflect a different kind of activity. The so-called local field potential (LFP) is defined as the low-frequency component of the EFP and represents mostly slow events reflecting cooperative activity in neural populations. In contrast to the MUA, the magnitude of the LFP does not correlate with cell size but instead reflects the extent and geometry of local dendrites (Fromm and Bond 1964, 1967; Buchwald et al. 1966). A prominent geometric arrangement is formed by the pyramidal neurons with their apical dendrites running parallel to each other and perpendicular to the pial surface. They form a so-called open field arrangement, in which dendrites face in one direction and somata in another, producing strong dendrite-to-soma dipoles when they are activated by synchronous synaptic input. The spatial summation of the LFP has been suggested to reflect a weighted average of synchronized den-drosomatic components of the synaptic signals of a neural population within 0.5–3 mm of the electrode tip (Mitzdorf 1985, 1987; Juergens et al. 1999). The upper limits of the spatial extent of LFP summation were indirectly calculated by computing the phase coherence as a function of interelectrode distance in experiments with simultaneous multiple-electrode recordings (e.g. see Fig. 4.1). Combined intracellular and field potential recordings also suggest a synaptic/dendritic origin of the LFPs, representing locally averaged excitatory and inhibitory postsynaptic potentials, which are considerably slower than the spiking activity (Steriade and Amzica 1994; Steriade et al. 1998). In addition, the LFP can also include other types of slow activity unrelated to synaptic events, including voltage-dependent membrane oscillations (Juergens et al. 1999) and spike after potentials (Buzsaki et al. 1988).

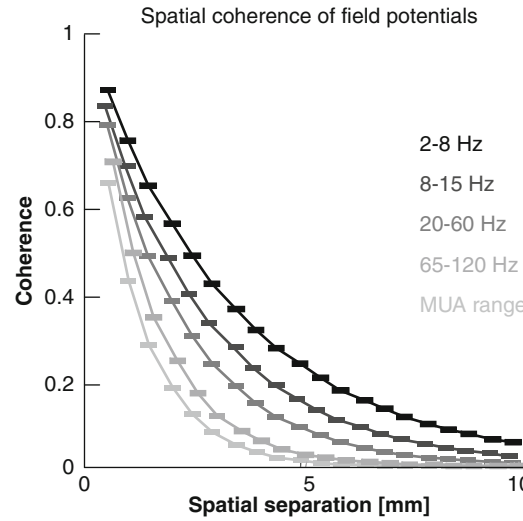

Fig. 4.1 Spatial coherence of the local field potential in primary visual cortex. Each graph displays the average coherence of the field potentials recorded from two electrodes as a function of the electrodes' spatial separation. Each *line* indicates a different frequency band

In summary, three different signals can commonly be extracted from extracellular microelectrode recordings, each partially covering a different frequency regime of the acquired signal. Representing fast events, the MUA reflects the averaged spiking activity of populations of neurons, with a bias for the larger, principal (projection) neurons. Covering the same frequency

range, the single-unit activity reports mainly on the activity of the principal neurons that form the major output of a cortical area. In contrast, and representing slower events, the LFP reflects slow waveforms such as synaptic potentials, afterpotentials and voltage-gated membrane oscillations that mostly reflect the input of a given cortical area as well as its local intracortical processing.

4.3 The Passive Electric Properties of the Brain

To better understand how the signal picked up by a microelectrode emerges from the underlying neuronal processes, especially with regard to the distinction of the different frequency regimes, it is important to know the basic electrical properties of brain tissue. The extracellular microenvironment consists of narrow gaps between cellular processes, probably not more than 200-Å wide on average. These spaces form a complex three-dimensional mosaic filled with extracellular fluid. Theoretical considerations suggest that currents and ions spread within this fluid but not through the cells (Robinson 1968). As a result, the resistance to electrical currents of this space depends on the detailed spatial layout of neuronal tissue, possibly resulting in an un-isotropic current flow that does not necessarily behave like that in a simple saline bath (Ranck 1963a, b; Mitzdorf 1985). Especially, from these considerations, it is unclear whether cortical tissue behaves like an ohmic resistor or whether signals of different frequencies experience frequency-dependent attenuation, that is, whether the tissue behaves like a capacitive filter.

A frequency-dependent behaviour was suggested by the fact that the activity of the slow wave measured by the EEG is largely independent of spiking responses, suggesting strong frequency-filtering properties of the tissue overlying the sources of the activity (Ajmone-Marsan 1965; Bedard et al. 2004, 2006). In addition, in extracellular unit recordings, the shape and amplitude of recorded spikes depend on the spatial position of the electrode relative to the neuron (Gold et al. 2006), while slow potentials show much less sensitivity to position and correlate over large spatial distances. Since the lower frequencies of the field potentials typically correlate over larger spatial distances than the higher frequencies of the same signal (Fig. 4.1), this can be interpreted as strong evidence for the cortical tissue to behave as a capacitive filter (Destexhe et al. 1999). Such a frequency-dependent impedance spectrum could selectively attenuate electric signals of some frequencies more than those of others, for example, high-frequency spiking events more than low-frequency potentials.

To clarify whether the brain's tissue behaves like an ohmic or a capacitive medium, we recently quantified the passive electrical spread of different signals in the brain in vivo. These measurements were conducted in the primary visual cortex, a typical model system for sensory processing, and on the scale of hundreds of micrometres to several millimetres, that is, the scale relevant to the typical functional imaging techniques such as fMRI-BOLD (Logothetis et al. 2007). At this scale, theoretical considerations suggest that the extracellular medium can be considered as largely homogenous and mostly isotropic (within the grey matter). Our results confirmed this and, more importantly, demonstrated that the cortical tissue does not behave like a capacitive filter but acts like an ohmic resistor, attenuating signals of different frequencies in the same manner.

In detail, we measured the voltage drop across two neighbouring electrodes induced by an injected current of predefined frequency (Fig. 4.2). Our measurements employed a four-point electrode system, allowing highly accurate and unperturbed measurements of resistance of cortical tissue in vivo. Over a wide range of current frequencies and for all tested spatial arrangements of the electrodes, the brain's grey matter tissue behaved like an isotropic and ohmic resistor. The white matter, in contrast, showed directional anisotropies, with lower resistance in one and higher resistance in the orthogonal direction. Yet, as for the grey matter, the white matter also behaved like an ohmic resistor. Altogether, our measurements clearly rejected the notion that the cortical tissue behaves like a frequency-dependent

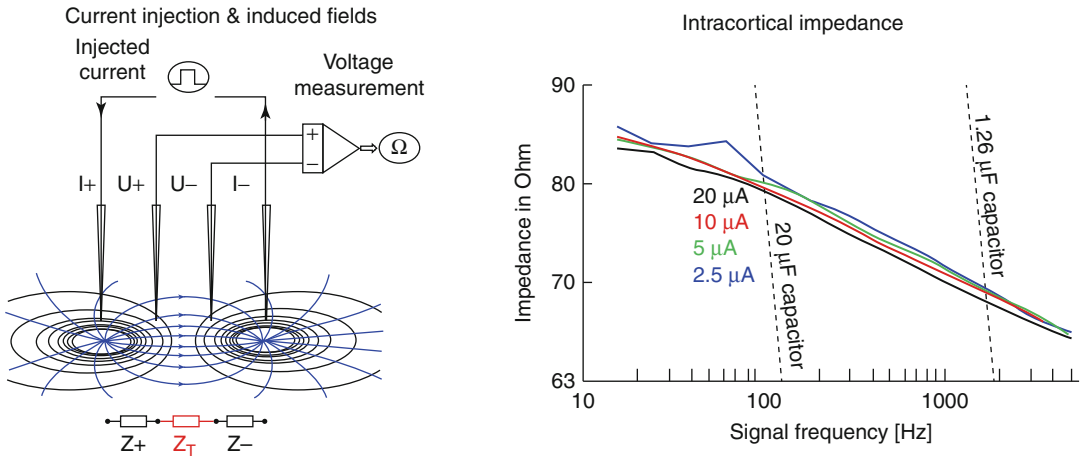

Fig. 4.2 Impedance spectrum of cortical tissue. The *left panel* displays the schematic representation of the impedance measurement. A current of a predefined frequency was injected (via electrodes I+ and I–), and the voltage difference was measured across electrodes U+ and U–. From this voltage difference, one can infer the cortical resistance (Z_T) as a function of current frequency, that is, the frequency-dependent impedance spectrum. The field *lines* indicate the current flow in a homogenous tissue. The *right panel* displays the measured impedance values for different current strengths in cortex (*solid lines*) and for electronic capacitances. Clearly, the impedance spectrum of the cortex is nearly flat compared to that of the capacitance, suggesting that the cortex does not behave like a frequency-dependent filter but rather like an ohmic resistor. For details, see Logothetis et al. (2007)

filter, at least on the spatial scale relevant to the typical functional imaging applications.

As a consequence of this finding, one has to conclude that some of the properties of the field potentials noted above, such as the different degree of spatial correlations in different frequency bands, are not the result of passive electrical spread in the tissue. In contrast, our findings suggest that the long-range correlations of the low-frequency signals, such as the theta or beta rhythms, result from properties of the generators of these signals, that is, from the spatial patterning of the connections mediating these oscillations, and hence might be a property that is also reflected in the functional imaging signal.

4.4 The Neural Correlate of the BOLD Signal

Given the distinction of the different signals that can be obtained from extracellular recordings, one can ask which signal best explains the activity patterns seen in functional imaging experiments? Or stated otherwise, which signal correlates best with the functional imaging signal? A growing body of work addresses this important question with two complementary approaches. An indirect approach asks whether both methodologies yield similar answers to a typical neuroscientific question, such as whether a certain region in the brain responds to a given stimulus. A direct approach, on the other hand, measures both signals at the same time to directly correlate the functional imaging activation with the different signals of neuronal activity.

A typical example for an indirect comparison was provided by Rees et al. who compared human fMRI measurements with electrophysiological data from single-unit recordings in monkeys (Rees et al. 2000). Both data sets were obtained from the motion-specific areas of the respective species and reflected how much the respective signal changed as a function of the stimulus' motion coherence. Comparing the slope of both signals, the authors concluded that the BOLD signal was directly proportional to the average firing rate, with a constant of proportionality of approximately nine spikes per second per percentage BOLD increase. Using the same strategy, but focusing on the signal increase in primary visual cortex as a function of stimulus contrast,

Heeger et al. confirmed such a linear relation of spiking activity and the BOLD signal, albeit with a smaller proportionality constant of 0.4 spikes per percentage BOLD increase (Heeger et al. 2000). While these results suggest a good correlation of the BOLD signal and firing rates in the same cortical region, they already indicate that the details of this relation, here the constant or proportionality, depend on detailed characteristics of each area.

While the above studies focused only on firing rates, another study on primary visual cortex extended this approach to a wider range of stimuli and physiological signals (Kayser et al. 2004). Studying the cat visual system, the BOLD signal was obtained from one group of animals, while MUA and field potential responses were recorded in a second group of animals. As a metric of comparison, the authors asked which of the different electrophysiological signals would yield similar relative responses to different stimuli as found in the BOLD signal. Stated otherwise, if stimulus A elicits a stronger BOLD response than stimulus B, which of the electrophysiological signal obeys the same relation across a large fraction of recording sites sampled in the same region of interest from which the BOLD signal is sampled (Fig. 4.3)? Overall, the MUA provided a worse match to the BOLD signal than did the LFP, although the latter showed strong frequency dependence. The best match between LFP and BOLD was obtained in the frequency range of 20–50 Hz, while slower oscillations generally showed a poor concordance with the imaging data. Noteworthy, this study also showed that the precise results of an indirect comparison can depend strongly on the specific stimuli employed: when the contrast involved grating stimuli, which elicit strong gamma band responses, a good match between the gamma band of the LFP and the BOLD was obtained. However, when the contrast involved only stimuli with less distinct activation patterns in the LFP, the correlation of LFP and BOLD also showed less frequency dependence.

While these studies only compared the average response strength of each signal, another extended the comparison to the temporal dimension and correlated the average time course obtained from fMRI with that obtained from neuronal responses (Mukamel et al. 2005). Using the human auditory cortex as a model system, these authors correlated the average fMRI responses obtained in a group of healthy subjects with intracortical recordings obtained from a group of epilepsy patients monitored for surgical treatment. While the BOLD signal again correlated well with the LFP, it showed an even stronger correlation with neuronal firing rates, contrasting the above result from visual cortex.

As these examples demonstrate, the results of an indirect comparison between the BOLD signal and neuronal responses may vary depending on the particular experimental paradigm and stimuli involved. In fact, an indirect comparison can only be conducted after the responses in the two measurements have each been highly averaged over trials. While such averaging will result in a robust estimate of the stimulus-related response, it will also remove the trial to trial variability of neuronal responses, the influence of the mental state and other brain state fluctuations that are not locked to the stimulus used to align the responses. As a result, one compares two "artificial" signals that do not necessarily resemble the pattern of neuronal activity seen during normal brain function. In addition, the temporal resolution of the imaging signal is often quite low, especially in human studies, resulting in a blurred signal which cannot be adequately compared to the fast changes of neuronal activity (see also below). An indirect comparison of functional imaging and neuronal activity can hence only speak about a certain, stimulus-driven aspect of the signals, but does not generalize the complex interactions of feedforward and feedback processing that occur during normal conditions, where each activity pattern might be unique and non-repeatable.

To overcome the limitations of these indirect comparisons, our lab examined the relationship of the BOLD signal to neural activity directly by simultaneously acquiring electrophysiological and fMRI data from the same animals. To this end, we developed a 4.7 T vertical scanner environment specifically for combined neurophysiology and imaging experiments, including novel methods for interference compensation, microelectrodes and data denoising (Logothetis et al. 2001). Our

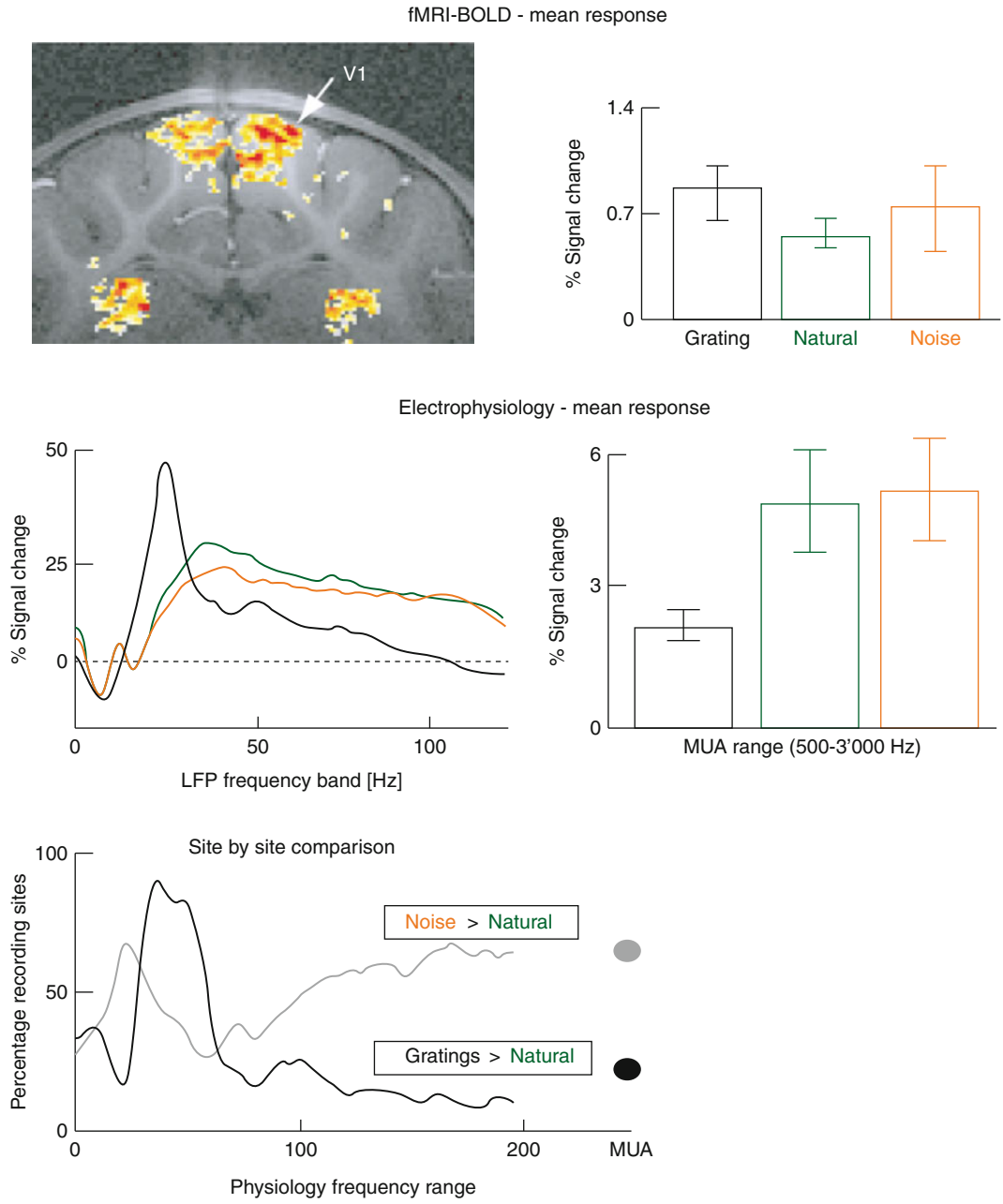

Fig. 4.3 Indirect comparison of BOLD and neurophysiological signals in cat primary visual cortex. The *upper panel* displays the average BOLD responses to the three kinds of stimuli used in this study, while the *middle panel* displays the average responses in the LFP and MUA. The *lower panel* displays the comparison between signals. This was done by counting the fraction of neurophysiological recording sites where the activity obeyed the same relations as found in the BOLD signal (noise > natural and gratings > natural). This comparison was performed separately for each LFP frequency band and MUA. For details, see Kayser et al. (2004)

measurements showed that the fMRI-BOLD response directly reflects a local increase in neural activity as assessed by the EFP signal. For the majority of recording sites, the BOLD signal was found to be a linear but not time-invariant function of LFPs, MUA and the firing rate of individual neurons (Fig. 4.4, upper panel). After stimulus presentation, a transient increase in power was

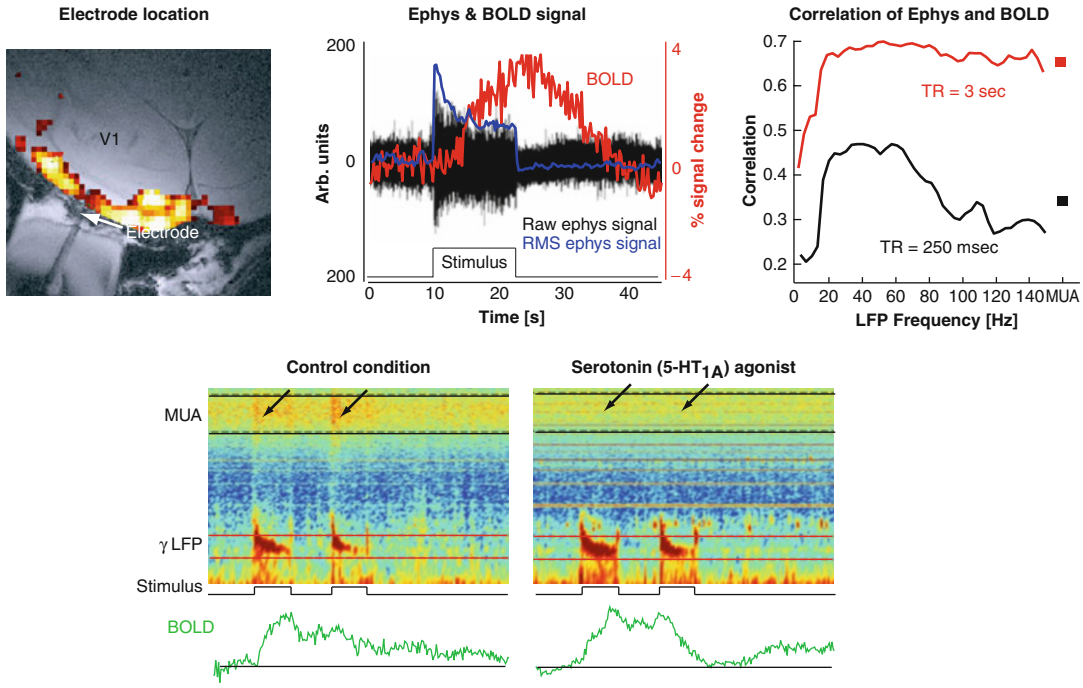

Fig. 4.4 Simultaneous measurement of BOLD and neurophysiological signals in the monkey primary visual cortex. In the *upper row*, the *left panel* displays the electrode location in V1, together with the functional response near the electrode (*red-yellow* colour code). The *middle panel* displays the simultaneously recorded BOLD and neuronal signals. The *right panel*, finally, displays the temporal correlation of both signals, once at high-temporal resolution (TR = 250 ms) and once using a smoothed, low-resolution signal (TR = 3 s). The *lower row* displays a dissociation of BOLD, MUA and LFP induced by the application of a serotonin agonist, which suppresses the firing of pyramidal neurons. During drug application, BOLD and LFP responses persist, while the MUA response ceases. For details, see Logothetis et al. (2001); Goense and Logothetis (2008); Rauch et al. (2008)

typically observed across all LFP frequencies, followed by a lower level of activation that was maintained for the entire duration of stimulus presentation. The MUA, in contrast, often showed a more transient response, suggesting a lower correlation to the BOLD response. This hypothesis was confirmed using system identification techniques: while in general both LFPs and MUA served as good predictors for the BOLD, LFPs on average accounted for 7.6 % more of the variance in the fMRI response than the MUA. This difference, albeit small, was statistically significant across experiments. In further experiments, we confirmed the same findings in alert animals, demonstrating that the correlation of BOLD and LFP holds good also during more complex, natural situations (Goense and Logothetis 2008). On the one hand, these findings confirm and extend the previous studies suggesting an analogy between spiking responses and the BOLD signal, while on the other hand, they reveal the strong contribution of field potentials to the BOLD signal, thereby suggesting that a direct translation of changes in the BOLD signal into changes in firing rates is misleading. Rather, we suggested on the basis of these observations that the BOLD signal reflects the input to a local region and its local processing, as reflected by the aggregate synaptic activity, more than its output, as reflected in the spiking activity of the principal cells.

A recent study in the cat visual cortex confirmed these findings by combining optical imaging to measure hemodynamic responses with simultaneous microelectrode recordings (Niessing et al. 2005). Along the lines of previous results, they found a frequency-dependent match between the imaging signal and LFPs. Especially, frequency bands below 10 Hz showed negative correlations with the imaging signal, that is, reduced field potential during increased blood flow response.

Higher frequencies, especially between 50 and 90 Hz, showed good correlation with the imaging signal and, importantly, stronger correlations than observed for the MUA.

It is worth noting that the exact strength of the correlation between LFP, MUA and BOLD depends on the detailed properties of the paradigm and data acquisition. Especially, the different acquisition rates for functional imaging signals and neuronal responses can have profound influences, as can easily be demonstrated (Fig. 4.4, middle panel). Starting from a BOLD signal which was acquired using a temporal resolution of 250 ms, we subsequently decimated all signals to an effective temporal resolution of 3 s, the typical temporal resolution of human imaging studies. While the "fast" BOLD signal exhibits the well-established differential correlation of LFP and MUA with the BOLD, the "slow" signal shows an overall stronger correlation and less of a difference between LFP and MUA. Decreasing the temporal resolution effectively smoothes a signal and increases the coherence between LFP frequency bands hence the increased correlation. Not surprisingly, the correlation coefficients did not increase uniformly across frequency bands; the filtering particularly affected the high-frequency bands (>60 Hz), which are typically modulated on faster timescales. As a result, the smoothing unavoidably increases the correlation of MUA to the BOLD response as well. Such simple differences of the temporal resolution of the acquired signals can explain the different degree of correlations found in ours and in indirect human studies, since the latter heavily relied on temporally smoothed signals and subject-averaged signals (Mukamel et al. 2005). To conclude, care must be taken when interpreting correlations of hemodynamic and neuronal signals, as apparent conflicts can simply arise from methodological artefacts rather than true differences.

4.5 The Coupling of Synaptic Activity and CBF

A reason for the more gradual differences between LFP and MUA in their relation to the BOLD signal is that under many conditions, MUA and LFPs will vary together. In other words, in many stimulation conditions, the output of any processing station in subcortical and early cortical structures is likely to reflect the changes of the input, and the LFP-MUA relationship will be "tight" and both will be well correlated with BOLD. Yet, this scenario might be an "exception" when generating cognitive maps during complex tasks; as in such cases, the subject's "mental" state might be instantiated in diverse feedforward and feedback processes that do not necessarily increase the net output of cortical microcircuits. Hence, conditions might exist during which there is a dissociation of these signals, for example, a condition in which an increase in local input (LFP) results in a reduction in local output activity (MUA). Clearly, such situations could reveal important insights into the different processes underlying the different signals and their mutual relations. A powerful example of such a dissociation was provided by Mathiesen et al. (1998, 2000; Thomsen et al. 2004). These authors nicely exploited the synaptic organization of the cerebellar cortex, where electrical stimulation of the parallel fibres causes monosynaptic excitation of the Purkinje cells and disynaptic inhibition of the same neurons through the basket cells. This results in inhibition of the spiking activity in the Purkinje cells while at the same time increasing the synaptic input to these cells. Combining electrophysiological recordings with laser Doppler flowmetry to measure changes in CBF, Mathiesen et al. demonstrated a powerful dissociation of the spiking activity and the CBF. Both LFPs and CBF increased while spiking activity ceased, clearly demonstrating that increases in CBF or BOLD do not allow to make inferences about potential increases or decreases in the spiking activity of the stimulated region (Lauritzen and Gold 2003).

A similar dissociation of the imaging signal and neuronal firing rates could be seen in our studies (Logothetis et al. 2001). Often, the single- or multiunit activity showed strong response adaptation during the first few seconds, with a subsequent decay of the firing rates to baseline. In contrast to this, the BOLD signal and the LFP did persist above baseline throughout the stimulation period. As a result,

during the sustained period of the stimulus, only the field potential can be associated with the imaging signal, but not the spiking activity. Importantly, there was no condition or observation period during which the opposite was observed. In addition to this naturally occurring dissociation, similar situations can be induced pharmacologically. For example, the application of a serotonin receptor agonist, which causes persistent hyperpolarization of pyramidal neurons, leads to a ceasing of the MUA responses (Fig. 4.4, lower panel). However, at the very same time, both the LFP and the BOLD signal still respond to visual stimulation, again demonstrating that the BOLD signal is not necessarily coupled to neuronal spiking responses (see Rauch et al. (2008) for further results along this line).

Is the CBF signal then linearly coupled to synaptic activity? While this indeed seems to hold good under some conditions, other conditions produce a nonlinear relation between afferent input and the hemodynamic response (Mathiesen et al. 1998; Norup Nielsen and Lauritzen 2001). Especially for very low or high levels of synaptic input, the CBF response can be decoupled from the input. For example, inducing deactivation of neuronal responses by either functional deactivation or application of TTX resulted in only a small reduction in baseline CBF (Gold and Lauritzen 2002). During such instances of neurovascular decoupling, the imaging data does not reflect all the changes in synaptic afferents, clearly highlighting the limited dynamic range of functional imaging. Such nonlinear relation between synaptic activity and CBF might, for example, arise from the unequal contribution of different receptors and channels to synaptic potentials and blood flow. For example, glutamatergic NMDA channels contribute to CBF but only little to the LFP (Hoffmeyer et al. 2007). As a result, blood flow responses might also exist in the absence of large changes in the LFP, providing strong evidence that it is not the extracellular current that causes increase in CBF but the intracellular signalling cascades related to neurotransmitter release, uptake and recycling. Indeed, while the hemodynamic response provides supplies of glucose and oxygen, it is not the processes that require the energy that call for an increase in CBF but rather the processes triggered in a feedforward manner by neurotransmitter-related signalling (Lauritzen 2005).

The notion that functional imaging measures the aggregate synaptic input to a local area also resolves a number of apparently conflicting results from imaging and electrophysiological experiments. Being sensitive to the synaptic input, functional imaging "sees" modulatory lateral and feedback projections, which might not be strong enough to induce significant changes in neuronal firing rates, but nevertheless provides a larger proportion of the total synaptic input. For example, human imaging revealed influences of spatial attention in many visual areas, including primary visual cortex. At the same time, such attentional influences have been persistently difficult to demonstrate using single-neuron recordings or turned out to be much weaker than expected from human imaging (Luck et al. 1997; Kastner and Ungerleider 2000; Heeger and Ress 2002). Given that attentional influences are supposedly mediated by feedback projections from higher visual and frontoparietal regions, they might provide exactly this kind of input that is visible only using functional imaging. Along the same lines, it has been much easier to see cross-modal interactions, that is, influences of one sensory modality on another, using functional imaging than using electrophysiology (Calvert 2001; Kayser and Logothetis 2007). For example, functional imaging demonstrated that auditory cortex can be modulated and even activated by visual or somatosensory stimuli (Kayser et al. 2007b), while the same effects are only weakly present at the level of single-neuron firing rates. However, in full agreement with the above, visual modulation was well evident at the level of field potentials recorded in auditory cortex, again demonstrating a closer correspondence of the BOLD signal with field potentials than with firing rates (Kayser et al. 2008).

4.6 Conclusions

The hemodynamic responses characterized by functional imaging better reflect the aggregate synaptic activity and local processing that is characterized by the LFPs rather than providing

information about the typical firing rates in the same region. This partly results from the mechanisms that drive increases in blood flow, which reside upstream from the axosomatic level and near the synaptic-dendritic level.

The collective findings of many studies provide good evidence for the notion that functional imaging reflects the input into a local region but not necessarily the output of the same. Under many normal conditions, the input and output of a local region will be related, and hence functional imaging will provide information about the typical neuronal firing rates in the same region. As a result of this sensitivity to synaptic input, functional imaging signals are more susceptible to modulatory feedback input, which often might provide only a minor contribution to the response strength of large principal neurons. However, for a priori and most experimental conditions, it is unclear what relationship to expect between in- and output, and hence feedforward- and feedback-related activations cannot be distinguished. As a result, it can sometimes be misleading, if not dangerous, to make direct inferences from imaging results about the underlying neuronal processes. Especially for applications with immediate consequences, such as clinical diagnostics and surgical planning, it seems prudent to establish well-defined paradigms in which the neural correlates of the imaging signal have been validated using combined electrophysiological and imaging approaches.

References

Adrian ED, Zotterman Y (1929) The impulses produced by sensory nerve endings, part 2. The response of a single end-organ. J Physiol 61:151–171

Ajmone-Marsan C (1965) Electrical activity of the brain: slow waves and neuronal activity. Isr J Med Sci 1: 104–117

Bedard C, Kroger H et al (2004) Modeling extracellular field potentials and the frequency-filtering properties of extracellular space. Biophys J 86:1829–1842

Bedard C, Kroger H et al (2006) Model of low-pass filtering of local field potentials in brain tissue. Phys Rev E Stat Nonlin Soft Matter Phys 73:051911

Buchwald JS, Grover FS (1970) Amplitudes of background fast activity characteristic of specific brain sites. J Neurophysiol 33:148–159

Buchwald JS, Halas ES et al (1966) Relationships of neuronal spike populations and EEG activity in chronic cats. Electroencephalogr Clin Neurophysiol 21: 227–238

Buzsaki G, Bickford RG et al (1988) Nucleus basalis and thalamic control of neocortical activity in the freely moving rat. J Neurosci 8:4007–4026

Calvert GA (2001) Crossmodal processing in the human brain: insights from functional neuroimaging studies. Cereb Cortex 11:1110–1123

Destexhe A, Contreras D et al (1999) Spatiotemporal analysis of local field potentials and unit discharges in cat cerebral cortex during natural wake and sleep states. J Neurosci 19:4595–4608

Freeman W (1975) Mass action in the nervous system. Academic, New York

Fried I, MacDonald KA et al (1997) Single neuron activity in human hippocampus and amygdala during recognition of faces and objects. Neuron 18: 753–765

Fromm GH, Bond HW (1964) Slow changes in the electrocorticogram and the activity of cortical neurons. Electroencephalogr Clin Neurophysiol 17:520–523

Fromm GH, Bond HW (1967) The relationship between neuron activity and cortical steady potentials. Electroencephalogr Clin Neurophysiol 22:159–166

Goense J, Logothetis N (2008) Neurophysiology of the BOLD fMRI signal in awake monkeys. Curr Biol 18:631–640

Gold L, Lauritzen M (2002) Neuronal deactivation explains decreased cerebellar blood flow in response to focal cerebral ischemia or suppressed neocortical function. Proc Natl Acad Sci USA 99: 7699–7704

Gold C, Henze DA et al (2006) On the origin of the extracellular action potential waveform: a modeling study. J Neurophysiol 95:3113–3128

Gray CM, Konig P et al (1989) Oscillatory responses in cat visual cortex exhibit inter-columnar synchronization which reflects global stimulus properties. Nature 338:334–337

Heeger DJ, Ress D (2002) What does fMRI tell us about neuronal activity? Nat Rev Neurosci 3:142–151

Heeger DJ, Huk AC et al (2000) Spikes versus BOLD: what does neuroimaging tell us about neuronal activity? Nat Neurosci 3:631–633

Hoffmeyer HW, Enager P et al (2007) Nonlinear neurovascular coupling in rat sensory cortex by activation of transcallosal fibers. J Cereb Blood Flow Metab 27: 575–587

Juergens E, Guettler A et al (1999) Visual stimulation elicits locked and induced gamma oscillations in monkey intracortical- and EEG-potentials, but not in human EEG. Exp Brain Res 129:247–259

Kastner S, Ungerleider LG (2000) Mechanisms of visual attention in the human cortex. Annu Rev Neurosci 23:315–341

Kayser C, Logothetis NK (2007) Do early sensory cortices integrate cross-modal information? Brain Struct Funct 212:121–132

Kayser C, Kim M et al (2004) A comparison of hemodynamic and neural responses in cat visual cortex using complex stimuli. Cereb Cortex 14:881–891

Kayser C, Petkov CI et al (2007a) Tuning to sound frequency in auditory field potentials. J Neurophysiol 98:1806–1809

Kayser C, Petkov CI et al (2007b) Functional imaging reveals visual modulation of specific fields in auditory cortex. J Neurosci 27:1824–1835

Kayser C, Petkov CI et al (2008) Visual modulation of neurons in auditory cortex. Cereb Cortex 18:1560–1574. doi:10.1093/cercor/bhm187

Kreiman G, Koch C et al (2000) Category-specific visual responses of single neurons in the human medial temporal lobe. Nat Neurosci 3:946–953

Lauritzen M (2005) Reading vascular changes in brain imaging: is dendritic calcium the key? Nat Rev Neurosci 6:77–85

Lauritzen M, Gold L (2003) Brain function and neurophysiological correlates of signals used in functional neuroimaging. J Neurosci 23:3972–3980

Legatt AD, Arezzo J et al (1980) Averaged multiple unit activity as an estimate of phasic changes in local neuronal activity: effects of volume-conducted potentials. J Neurosci Methods 2:203–217

Logothetis NK (2002) The neural basis of the blood-oxygen-level-dependent functional magnetic resonance imaging signal. Philos Trans R Soc Lond B Biol Sci 357:1003–1037

Logothetis NK, Wandell BA (2004) Interpreting the BOLD signal. Annu Rev Physiol 66:735–769

Logothetis NK, Pauls J et al (2001) Neurophysiological investigation of the basis of the fMRI signal. Nature 412:150–157

Logothetis NK, Kayser C et al (2007) In vivo measurement of cortical impedance spectrum in monkeys: implications for signal propagation. Neuron 55:809–823

Luck SJ, Chelazzi L et al (1997) Neural mechanisms of spatial selective attention in areas V1, V2, and V4 of macaque visual cortex. J Neurophysiol 77:24–42

Mathiesen C, Caesar K et al (1998) Modification of activity-dependent increases of cerebral blood flow by excitatory synaptic activity and spikes in rat cerebellar cortex. J Physiol 512(Pt 2):555–566

Mathiesen C, Caesar K et al (2000) Temporal coupling between neuronal activity and blood flow in rat cerebellar cortex as indicated by field potential analysis. J Physiol 523(Pt 1):235–246

Mitzdorf U (1985) Current source-density method and application in cat cerebral cortex: investigation of evoked potentials and EEG phenomena. Physiol Rev 65:37–100

Mitzdorf U (1987) Properties of the evoked potential generators: current source-density analysis of visually evoked potentials in the cat cortex. Int J Neurosci 33:33–59

Mosso A (1881) Ueber den Kreislauf des Blutes im Menschlichen Gehirn. von Veit, Leipzig

Mukamel R, Gelbard H et al (2005) Coupling between neuronal firing, field potentials, and FMRI in human auditory cortex. Science 309:951–954

Niessing J, Ebisch B et al (2005) Hemodynamic signals correlate tightly with synchronized gamma oscillations. Science 309:948–951

Norup Nielsen A, Lauritzen M (2001) Coupling and uncoupling of activity-dependent increases of neuronal activity and blood flow in rat somatosensory cortex. J Physiol 533:773–785

Ogawa S, Menon RS et al (1998) On the characteristics of functional magnetic resonance imaging of the brain. Annu Rev Biophys Biomol Struct 27:447–474

Ranck JB (1963a) Analysis of specific impedance or rabbit cerebral cortex. Exp Neurol 7:153–174

Ranck JB (1963b) Specific impedance of rabbit cerebral cortex. Exp Neurol 7:144–152

Rauch A, Rainer G et al (2008) The effect of a serotonin induced dissociation between spiking and perisynaptic activity on BOLD functional MRI. Proc Natl Acad Sci 108:6759–6764

Rees G, Friston K et al (2000) A direct quantitative relationship between the functional properties of human and macaque V5. Nat Neurosci 3:716–723

Robinson DA (1968) The electrical properties of metal microelectrodes. Proc IEEE 56:1065–1071

Roy CS, Sherrington CS (1890) On the regulation of the blood supply of the brain. J Physiol 11:85–108

Steriade M, Amzica F (1994) Dynamic coupling among neocortical neurons during evoked and spontaneous spike-wave seizure activity. J Neurophysiol 72:2051–2069

Steriade M, Amzica F et al (1998) Spike-wave complexes and fast components of cortically generated seizures. II. Extra- and intracellular patterns. J Neurophysiol 80:1456–1479

Stone J (1973) Sampling properties of microelectrodes assessed in the cat's retina. J Neurophysiol 36:1071–1079

Thomsen K, Offenhauser N et al (2004) Principal neuron spiking: neither necessary nor sufficient for cerebral blood flow in rat cerebellum. J Physiol 560:181–189

Towe AL, Harding GW (1970) Extracellular microelectrode sampling bias. Exp Neurol 29:366–381

High-Field fMRI

5

Elke R. Gizewski

5.1 Introduction

In recent years, functional magnetic resonance imaging (fMRI) has become a widely used approach for neuroscience. However, this method has the potential to be improved with regard to both spatial and temporal resolution. The blood-oxygenation level-dependent contrast (BOLD) represents signal changes in T2- or T2*-weighted images. These sequences are presumed to be well suited to high magnetic field strength, as fMRI sequences benefit from higher signal-to-noise ratio (SNR) and higher signal in BOLD contrast images (Vaughan et al. 2001). However, their sensitivity to susceptibility also causes problems, e.g. in-plane dephasing and signal dropouts near tissue-air boundaries.

To achieve greater insights into brain function, ultra-high-field fMRI has been applied in some studies to attain higher spatial resolutions (Duong et al. 2003; Pfeuffer et al. 2002a). These studies focused on high-resolution images which can be acquired rapidly and with good temporal and special resolution. Additionally, the signal increase advantage in high-field MRI has been studied (Pfeuffer et al. 2002b). Nearly all of these early studies, therefore, accepted restrictions in the field of view and the number of slices for 7-T imaging and avoided areas near tissue-air boundaries. For broader application including pre-surgical fMRI and for analysing cognitive functions, however, a more extended coverage of the brain is needed to reveal network activation involving multiple areas. This chapter will give insights into the pros and cons of high- and ultra-high-field fMRI and into ongoing developments to overcome the restrictions referred to and improve the benefits.

5.2 Benefits and Limitations of High- and Ultra-High-Field MRI

The introduction of ultra-high-field MRI systems has brought MRI technology closer to the physical limitations, and greater development effort is required to achieve appropriate sequences and images. 3-T MRI systems are high-field systems maintaining a relatively high-comfort level for the user similar to 1.5-T MRI systems (Alvarez-Linera 2008; Norris 2003). Theoretically, the SNR at high-field MRI should, according to the Boltzmann equation, show a linear increase with increasing magnetic field strength. But, the interactions of the magnetic field and other influencing factors, e.g. relaxation times, radio frequency (RF) pulses and coils performance during image acquisition, are very complex. One important factor is the change in RF pulses in higher magnetic field strengths. Changing the field strength from 1.5 to 3 T results in a fourfold increase in the required energy, resulting in an increase in

E.R. Gizewski, MHBA
University Clinic for Neuroradiology,
Department for Radiology,
Medical University Innsbruck,
Anichstr 35, Innsbruck 6020, Austria
e-mail: elke.gizewski@i-med.ac.at

S. Ulmer, O. Jansen (eds.), *fMRI – Basics and Clinical Applications*,
DOI 10.1007/978-3-642-34342-1_5,

specific absorption rate (SAR) (Ladd 2007). The increase in SAR leads to limitations in image acquisition, as the absorption of energy in the tissue cannot be allowed to exceed certain thresholds. Therefore, restrictions in the number of slices and achieving homogenous excitation of the nuclei increase with higher field strength.

Current 3-T scanners have been significantly improved since their introduction, especially with regard to coil developments; therefore, today the advantages, such as faster acquisition time and/or higher resolution, are greater than the disadvantages, such as higher costs and in some cases instability in running the systems (Scheef et al. 2007). For higher field strength, e.g. 7 T, the developments have also improved in the recent time but are still in the process of improvement.

Another important point is the magnet design. Especially at 7-T whole body systems, the magnet is very long compared to a typical 1.5-T magnet. The bore is 60 cm as for a long time at common 1.5 T but due to the length gives a narrow impression (Fig. 5.1). Therefore, anxiety is again a problem for imaging. However, newer studies could demonstrate that the acceptance of 7-T imaging procedures in subjects and patients was acceptable (Theysohn et al. 2008). A final important point is the contraindication of every metal implant at 7 T. Even non-ferromagnetic material can be influenced due to induced electrical currents. When located in the centre of imaging, such material, e.g. a surgical calotte fixation, would lead to disturbing artefacts.

Some recent studies addressed the possible side effects of ultra-high-field MRI as increasing spread of high-field and ultra-high-field scanners has encouraged new discussion of the safety aspects of MRI. Studies on possible cognitive effects of MRI examinations could not reveal any significant influence of high field strength and the application of HF impulses during and after normal scanning procedures (Schlamann et al. 2010a). However, one study showed that immediately after MRI exposure, the cortical silent period during transcranial magnetic stimulation was highly significantly prolonged in normal subjects (Schlamann et al. 2010b). Interestingly this was found for 1.5 and 7 T with no significant difference or dependency on the field strength.

5.3 Special Aspects of High-Field fMRI

BOLD contrast images are normally acquired using a gradient echo-planar technique (EPI). Optimal sequence design has to take into account echo times and sampling period; the variation in sensitivity between tissues with different baseline T2*, the effects of physiological noise, and non-exponential signal decay are relevant influencing factors (Gowland and Bowtell 2007). In high-field fMRI, the optimal TE is shorter than at 1.5 T. The shortening of T2* is proportional to the magnetic field (Okada et al. 2005). The TE used in optimized 3-T fMRI imaging is between 30 and 35 ms (Preibisch et al. 2008). The optimum TE for 7 T has been reported to be around 25 ms in focused fMRI in the occipital cortex (Yacoub et al. 2001).

As mentioned above, the SNR should increase with the magnetic field strength. Some studies have revealed a BOLD signal increase up to fivefold in 7-T fMRI compared to 1.5-T BOLD signals. Studies focusing on an increase in resolution and small field of view (Pfeuffer et al. 2002c) could reveal a higher signal increase at 7 T than studies with whole-brain coverage (Gizewski et al. 2007). This variability can be explained taking into account the above-mentioned factors influencing the SNR. Additionally, the impact of these factors increases with higher field strength, resulting in a greater variability of BOLD signal between different measurements and subjects at 7 T compared to 1.5 T. The relatively wide range of relative BOLD signal changes compared to 1.5 T and even 3 T may also be explained by the difficulty in achieving a uniform static magnetic field shim and a uniform RF excitation field at 7 T. The fMRI experiments at 7 T are therefore more dependent on field inhomogeneities, and these have to be taken into account during image analysis.

The BOLD effect at higher field strength increases less in vessels larger than the voxel

Fig. 5.1 7-T MR scanner with a bore of 60 cm and a length of 3.50 m. The MR is surrounded by 425 tonnes of steel. The *upper figure* shows a person before positioned feet first into the scanner. The *lower figure* shows a person head first in the scanner with the head in the isocentre, the feet covered with a sheet. The scanner used here is located at the Erwin L. Hahn Institut, Essen, Germany

size and is thus more pronounced in vessels smaller than the voxel size. By using smaller voxels at higher field strength compared to 1.5 T, the BOLD signal can become more specific and reliable (Shimada et al. 2008; Zou et al. 2005). Therefore, the signal changes should be more closely linked to the cortical activity. With the increasing signal and enhanced stability of the BOLD signal at higher field strength, the repetition of events can be reduced. At ultra-high fields, even single events can give reliable BOLD signal as discussed in more detail below (Sect. 5.5).

Recent studies have addressed further aspects of SNR and BOLD signal improvement: Newton et al. (2012) evaluated the potential benefits of higher fields for detecting and analysing functional connectivity. The authors measured the influence of spatial resolution (from 1 mm up to 3-mm slice thickness) during a motor task at 7 T on estimates of functional connectivity through decreased partial volume averaging. They could show that resting state correlations within the sensorimotor system increase as voxel dimensions decreased from $3\times3\times2$ to $1\times1\times2$ mm. These results suggest that the true representation of

sensorimotor network is more focal than could be resolved with larger voxels. The authors conclude that the described increase may be due to decreased partial volume averaging and that functional connectivity within the primary seed region might be heterogeneous on the scale of single voxels.

A main problem at high field strength is the achievement of good response functions even in areas suffering from in-plane dephasing and signal dropouts near tissue-air boundaries. A further central problem is the increasing chemical shift, proportional to the magnetic field strength. All these limitations lead to errors when reading the echo. Therefore, the optimization of scanning parameters and coil construction is of much greater importance than in routine 1.5-T scanners. Today, many improvements are achieved and lead to increased use of 7 T for fMRI studies as discussed below. The following paragraphs will give some examples of these developments in ultra-high-field BOLD imaging.

The shimming, especially at 7 T, should be performed manually by the user. Although the standard shimming algorithm may be used, multiple repetitions should be performed with close verification of the result before starting the EPI sequence. At higher field strengths, a per slice shimming may be necessary to account for increased B0 distortions. Additionally, the phase correction parameters can be calculated slice by slice using three non-phase-encoded navigator echoes before the EPI readout (Heid 1997).

Nevertheless, there are increased susceptibility artefacts at 3 and 7 T compared to 1.5 T. Significant improvement can be reached by using more advanced head coils than circularly polarized (CP) coils. Multichannel coils allow application of parallel acquisition techniques (Mirrashed et al. 2004). Multiple channels provide further increases in SNR and, coupled with parallel imaging, reduce artefacts, e.g. due to susceptibility differences near tissue-air boundaries as is known from experience at 1.5 T. It has been demonstrated that the use of parallel imaging at 3 T results in an increase of BOLD signal depending on the employed parallel imaging method and its implementation (Preibisch et al. 2008). At 7 T, the coil equipment has to be newly developed, as the 7-T MRI systems require combined transmit and receive (t/r) coils. The first t/r coils were CP designs which did not enable parallel imaging techniques, but multichannel designs with up to 32 receiver channels are now available. Some groups also design their own coils in respect to higher resolution using more than 32 channels. As multichannel t/r coils for 7 T are now available more easily, nearly all experimental groups switched from CP to multichannel coils.

A further disadvantage at high field could be a restriction in the number of slices due to SAR restrictions and inhomogeneous resolution over the brain (Wiggins et al. 2005). Therefore, the coils and sequences have to be chosen depending on the paradigms to be applied. Again, parallel imaging can be useful for reducing the RF load on the tissue and enabling more slices. It was shown that at 3 T, a reduction factor of 2 in parallel imaging can be used with only little penalty with regard to sensitivity (Preibisch et al. 2008).

Some problems in image distortion can be solved using spin-echo instead of gradient-echo EPI sequences, but they are, so far, not routinely used. The blood contribution that dominates Hahn spin-echo (HSE)-based BOLD contrast at low magnetic fields and degrades specificity is highly attenuated at high fields because the apparent T2 of venous blood in an HSE experiment decreases quadratically with increasing magnetic field. In contrast, the HSE BOLD contrast increases supralinearly with the magnetic field strength. Yacoub et al. report the results of detailed quantitative evaluations of HSE BOLD signal changes for functional imaging in the human visual cortex at 4 and 7 T (Yacoub et al. 2003). They used the increased SNR of higher field strengths and surface coils to avoid partial volume effects. Furthermore, they could show that high-resolution acquisitions lead to a CNR increase with voxel sizes <1 mm^3. It was concluded that the high-field HSE fMRI signals originated largely from the capillaries and that the magnitude of the signal changes associated with brain function reached sufficiently high levels at 7 T to make it a useful approach for mapping on the millimetre to submillimetre spatial scale.

The problem that thermal and physiological noise dominates the SNR of the fMRI time course

at high spatial resolutions at high field strengths can be a prominent issue if a high-resolution matrix and a thin slice thickness are used. The problem is acquiring data at lower resolution, which is then dominated by physiological noise. A solution would be to acquire data at high resolution and smooth the data back to the desired lower resolution. In such cases, the physiological noise can limit some benefits of high-field acquisition, since increases in image SNR produce only small increases in time-course SNR if the 1.5-T resolution is used (Triantafyllou et al. 2006). But, some problems even at 3 T remain; low-frequency periodic fluctuations were found to have increased as well as the time-dependent increase in noise, especially in long EPI sessions (Shimada et al. 2008).

The Nyquist ghost also increases at higher field strength and is an important factor in BOLD imaging at 7 T. There are strategies to improve the traditional Nyquist ghost correction approach in EPI at high fields. One group describes schemes based on the reversal of the EPI readout gradient polarity for every other volume throughout a fMRI acquisition train as one improvement. The authors concluded that at high B(0) fields, substantial gains in Nyquist ghost correction of echo-planar time series are possible by this alternating method (van der Zwaag et al. 2009).

The gradient-echo EPI sequences are mostly used for fMRI, especially for clinical applications. Therefore, the optimization of EPI sequences and reduction in artefacts is of great importance. Multichannel coils are basically an array of surface coils with higher signal in the periphery than in the centre. At higher field strength, the signal even in the centre of multichannel coils is higher compared to 1.5 T. Results obtained at 3 T using a combination of multichannel coil and parallel imaging showed that BOLD sensitivity improved by 11 % in all brain regions, with larger gains in areas typically affected by strong susceptibility artefacts. The use of parallel imaging markedly reduces image distortion, and hence, the method should find widespread application in functional brain imaging (Poser et al. 2006).

A further interesting approach for BOLD imaging might be the three-dimensional segmented echo-planar imaging (3D-EPI). Single-shot EPI at 7 T often suffers from significant geometric distortions partly due to low bandwidth in the phase-encoded direction and amplified physiological noise. The 3D sequence could further improve high-resolution fMRI as it provides an increased SNR at similar temporal resolution to traditional multislice 2D-EPI readouts, in total, leading to increased volume coverage and decreased geometric distortions. The study of van der Zwaag et al. (2012) could reveal that during fMRI experiments at 7 T with a motor task, the 3D EPI outperforms the 2D-EPI in terms of temporal SNR and sensitivity to detect activated brain regions. Similar results were reported in a further study using a 3D PRESTO sequence (Barry and Strother 2011).

In summary, an extended optimization of sequences and new coil developments, especially new transmit-receive coils, was done in the recent years and, however, still will be necessary to exploit all of the outstanding possibilities and advantages of ultra-high-field MRI (Scheef et al. 2007).

5.4 Ultra-High-Field fMRI: Recent Neurocognitive Studies

Early experiments have, besides motor paradigms, addressed retinotopic maps at 7 T. An identification of visual areas in the occipitoparietal cortex was found (Hoffmann et al. 2009). It was demonstrated that the mean coherence increased with magnetic field strength and with voxel size. At 7 T, the occipital cortex could be sampled with high sensitivity in a single short session at high resolution. Therefore, retinotopic mapping at 7 T opens the possibility of detailed understanding of the cortical visual field representations and of their plasticity in visual system pathologies. A further study analysed the use of spin-echo BOLD with 1.8 mm resolution at 3 and 7-T imaging for retinotopic mapping in comparison to gradient sequences (Olman et al. 2010). As mentioned above, some early studies could demonstrate the use of spin-echo sequences for fMRI. Olman et al. could now

show that GE BOLD and at 7-T SE BOLD had no systematic differences in either the area or the boundary locations for V1, V2 and V3. Therefore, the feasibility of high-resolution spin-echo BOLD experiments with good sensitivity throughout multiple visual areas was demonstrated. However, the highest resolution at ultra-high-field fMRI is restricted due to biological point-spread of the hemodynamic signal. The extent of this spread is described to be determined by the local vascular distribution and by the spatial specificity of blood flow regulation. Apart from this, there is influence from the measurement parameters. A recent study introduced a laminar surface-based analysis method and studied the relationship between spatial localization and activation strength as a function of laminar depth by acquiring an isotropic, single-shot EPI at 7 T (Polimeni et al. 2010). The BOLD signal was sampled exclusively from the superficial, middle or deep cortical laminae. This group could show that avoiding surface laminae improved spatial localization. They conclude that optimal spatial resolution in functional imaging of the cortex can be achieved using anatomically informed spatial sampling to avoid large pial vessels.

Apart from analyses of direct motor tasks as described in the clinical application discussion below, the sensorimotor network has recently been the focus on 7-T fMRI studies. Hale et al. used resting state fMRI at 3 and 7 T to assess connectivity in the sensorimotor network and default mode network at different spatial smoothing levels (Hale and Brookes 2010). The authors found higher temporal correlation coefficients for both sensorimotor network and default mode network at 7 T compared to 3 T for all smoothing levels. The maximum physiological noise contribution was higher at 7 T. However, no significant difference in the spatial correlation of maps following physiological correction was found. Whole-brain high-resolution (down to 1-mm isotropic voxels) resting state fMRI at 7 T using parallel imaging technology could be performed without restrictions in temporal resolution or brain coverage (De Martino and Esposito 2011).

Up to now, some studies have and further studies will have to also address cognitive functions involving more challenging brain areas. One study evaluated BOLD responses due to visual sexual stimuli at 7 T (Walter et al. 2008). This study could demonstrate that fMRI at high fields provides an ideal tool to investigate functional anatomy of subcortical structures. Furthermore, due to an increased SNR, functional scans of short duration can be acquired at high resolution. Coming back to experiments involving areas with high sensitivity to susceptibility artefacts first results revealed acceptable image quality using a 8-channel head coil at 7 T compared to 3 T (Fig. 5.2). Additionally, in these preliminary results, the hippocampal activation during a memory-encoding task improved from 3 to 7 T. However, the dropout of volunteers due to image inhomogeneities was higher at 7 T.

5.5 Ultra-High-Field fMRI and Possible Clinical Applications

3-T fMRI is increasingly used in clinical and experimental studies in most countries. In addition to developments in coil technology, 3-T MRI provides an excellent solution for higher resolution and/or signal changes with an acceptable increase in susceptibility artefacts (Alvarez-Linera 2008).

3-T fMRI has been used in a variety of experiments so far. The initial dip in the motor and visual areas was examined simultaneously using a visually guided finger-tapping paradigm (Yacoub and Hu 2001). Other experiments could show that fMRI measurements quantifying the strength of activity and centres of mass in response to tasks offer sensitive measurements of change over repeated imaging sessions. Therefore, fMRI at high field strength can be used for serial investigations of individual participants using simple motor and cognitive tasks in a simple block design (Goodyear and Douglas 2008). These results are very promising in respect to advanced clinical use of high-field fMRI. At 1.5 T, one main problem is the restriction in obtaining individual activation maps due to lack of sensitivity and specificity. This can be overcome with the more stable hemodynamic response function and higher BOLD signal at 3 T and even more at higher field strength, e.g. 7 T.

Within the recent years, the number of fMRI studies using 3-T scanners has much grown as

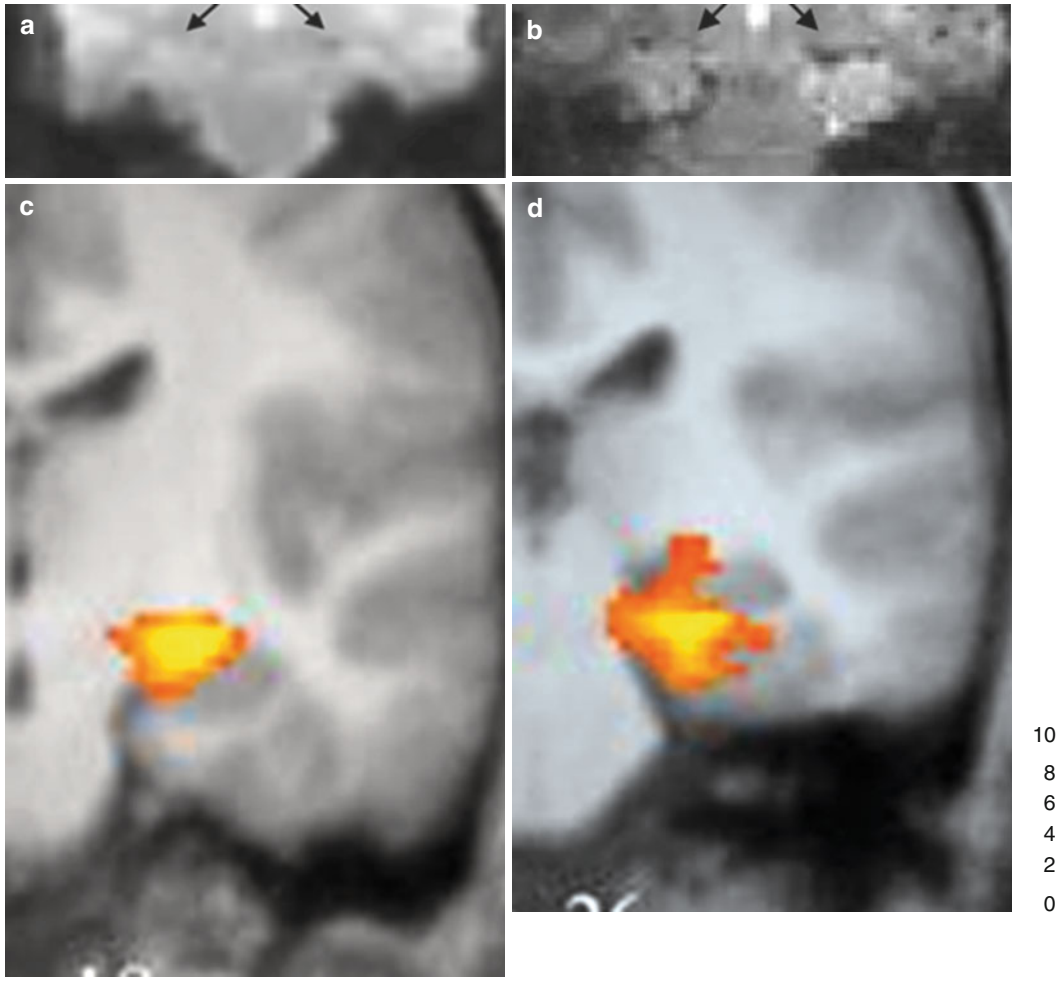

Fig. 5.2 EPI images with its sensitivity for susceptibility artefacts are compared at 3 T (**a**) and 7 T (**b**) imaging. Parallel acquisition techniques for reduction of these artefacts were used at both scanners (matrix 92×92 m^2 in this case at both scanners with 8-channel head coil). (**c** and **d**) The images show that the improvement of 7-T imaging techniques leads to acceptable image quality, allowing fMRI studies of the hippocampal region

those scanners become more and more available. Besides experimental studies like evaluation of gender differences encoding and recognition of pseudowords (Banks et al. 2012) or differences in humour (Kohn et al. 2011), also clinical studies revealed improvement of activation at 3 T compared to 1.5 T (Blatow et al. 2011). Figure 5.3 gives a typical clinical example of the use of 3-T (f)MRI in tumour patients. In the everyday setting, such significant activation during a finger-tapping task can be achieved robustly in a short block design and a scanner-associated postprocessing with overlay on structural 3D T1 image after contrast application (MPRAGE).

The first 7-T studies were performed to demonstrate the feasibility of BOLD fMRI using EPI and to characterize the BOLD response in humans at 7 T using visual stimulation. These results indicate that fMRI can be reliably performed at 7 T and that at this field strength, both the sensitivity and spatial specificity of the BOLD response are increased. These studies suggest that ultra-high-field MR systems are advantageous for functional mapping in humans (Yacoub et al. 2001).

Decreasing the voxel size at high field strength and simultaneously obtaining high temporal resolution is a major challenge and is mainly limited by gradient performance. Pfeuffer et al. used an

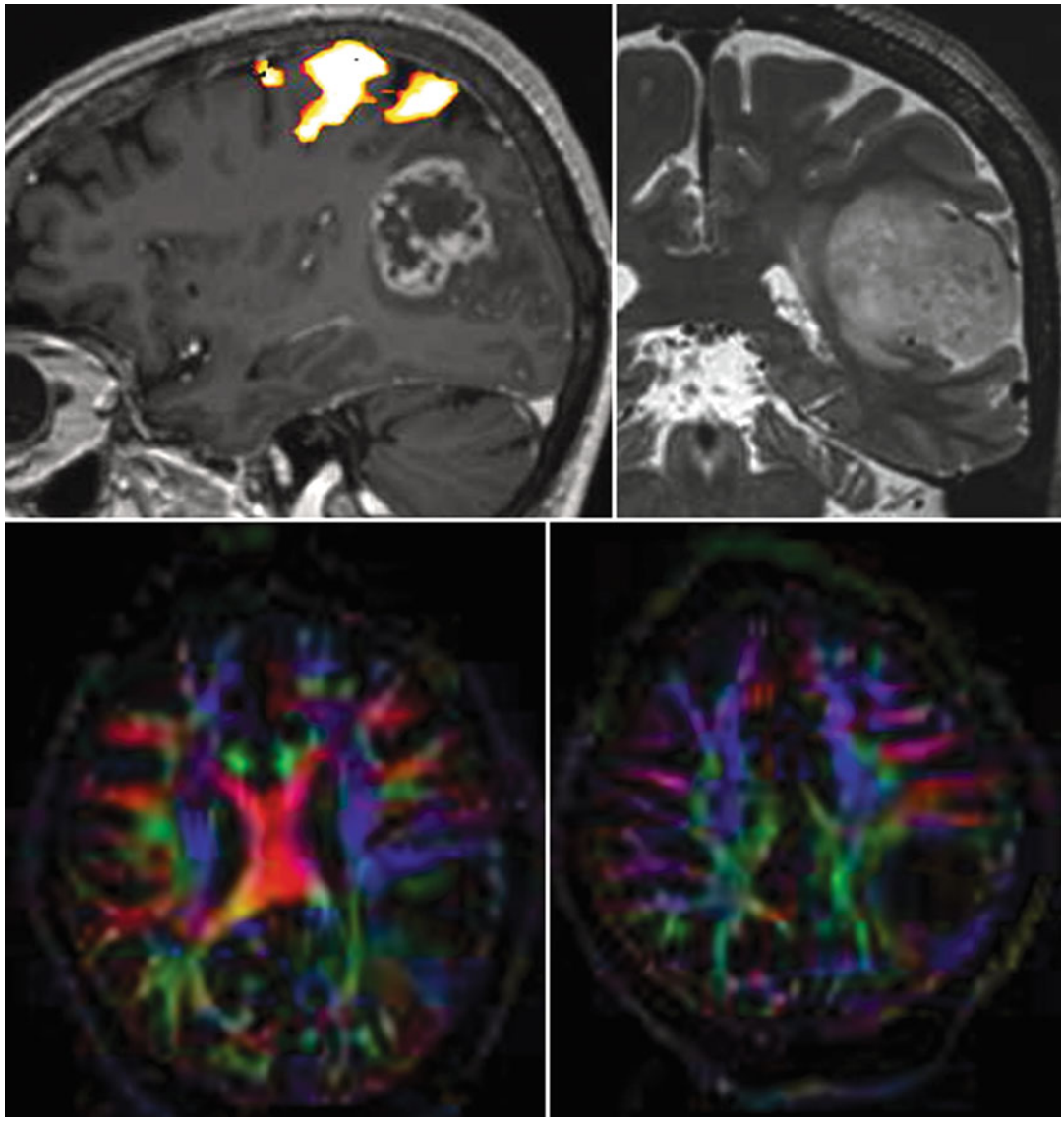

Fig. 5.3 Clinical application of 3 T: Significant activation during a finger-tapping task performed by a patient with a brain tumour near the central area in a short block design. Results are presented after scanner-associated postprocessing with overlay on structural 3D T1 image after contrast application (MPRAGE). In the same session, normally T2-weighted 3D images and a DTI are added to the fMRI task

optimized surface coil setup for zoomed functional imaging in the visual cortex (Pfeuffer et al. 2002c). With a single-shot acquisition at submillimetre resolution (500×500 mm^2) in the human brain and a high temporal resolution of 125 ms, activation of single-trial BOLD responses was obtained. Therefore, the possibilities of event-related functional imaging in the human brain were expanded. One recent study in relation to brain-computer-interface (BCI) technology research used a real-time fMRI at 7 T to evaluate the potential benefit of this method for BCI interactions (Andersson et al. 2010).

For clinical use, the activation in eloquent areas such as the sensorimotor areas and coverage of larger brain volumes are of great importance. One study at 7 T revealed activation in all sensorimotor motor areas at 7 T: SI, MI, SII, SMA, thalamus and contralateral cerebellar areas involved in sensorimotor processing (Gizewski et al. 2007). Even when using a t/r CP coil, the signal change was a factor of

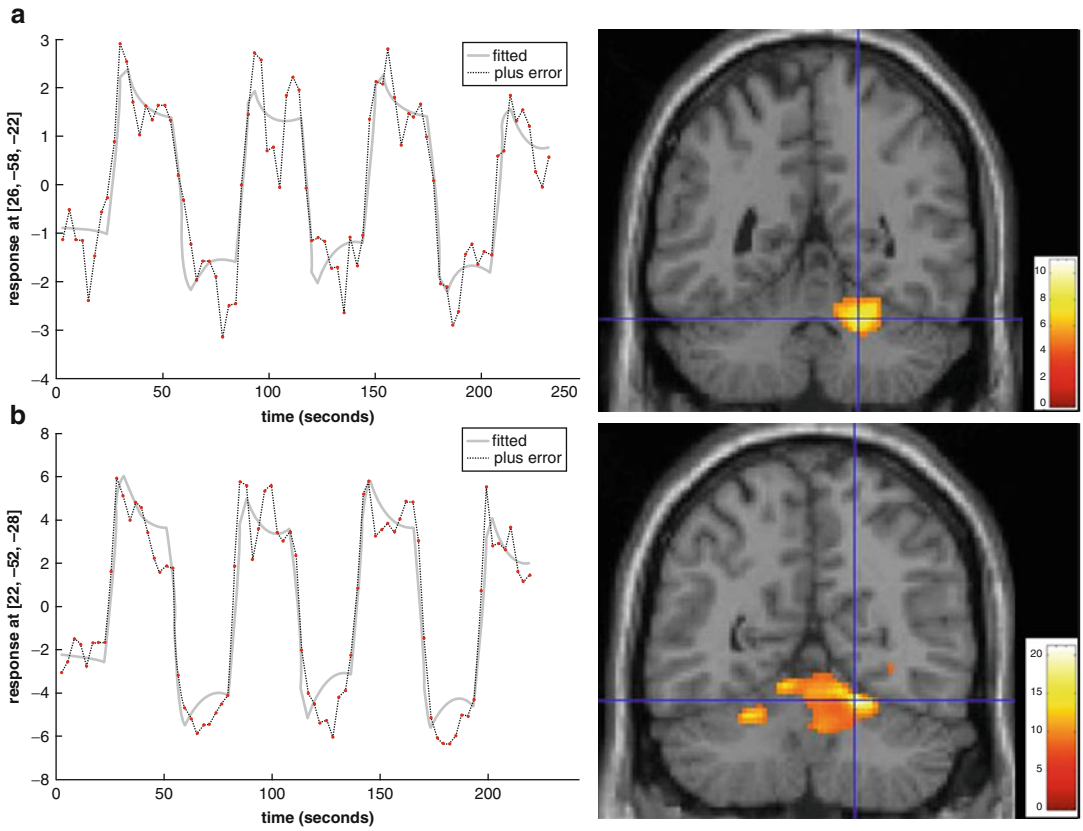

Fig. 5.4 (**a**) Plot of fitted response function at the main cluster in the cerebellar sensorimotor areas at 1.5 T (representative subject). Statistical parametric maps of activation within all subjects performing the finger-tapping task compared with rest period at 1.5 T. Task-related increase in MR signal is superimposed on coronal section of a 3D T1-weighted standard brain. Statistically corrected threshold is $p<0.05$. Results show main activation in cerebellum. (**b**) Plot of fitted response function at the main cluster in the cerebellar sensorimotor areas at 7 T (representative subject). Statistical parametric maps of activation within all subjects performing the finger-tapping task compared with rest period at 7 T. Statistically corrected threshold is $p<0.005$. Results show main activation in cerebellum

2–5 higher at 7 T than at 1.5 T. At 7 T, susceptibility artefacts were present especially in the basal brain structures, but a well-fitted response curve could be detected in all sensorimotor areas at 7 T, even in areas suffering from susceptibility such as the cerebellum (Fig. 5.4). In contrast to the results at 1.5 T, thalamic activation was found in all subjects and revealed an excellent response function. Even single-block analyses at 7 T revealed similar or even higher response strength than multi-block measurements at 1.5 T. These results indicate that fMRI can be robustly performed at 7 T, covering the whole brain using a t/r CP head coil with higher signal and increased stability of the hemodynamic response curve. The excellent response functions and signal change elevations shown in this study using a well-established, simple sensorimotor paradigm indicate that even in susceptibility problematic brain regions, ultra-high-field fMRI is possible. A further study used a 16-channel head coil at 7 T to measure the topographic representation of the digits in human somatosensory cortex at 1-mm isotropic resolution in individual subjects (Sanchez-Panchuelo and Schluppeck 2010). This study using a tactile stimulation of each finger could show an orderly map of the digits on the postcentral gyrus. Those activations were robust and could be made in individual subjects, leading to a wide use of this method in clinical and experimental settings. These results are very interesting in relation to a similar study performed at 3 T (Olman et al. 2012). This group found strong evidence of BOLD selectivity

in the hemisphere contralateral to the cued digit; however, they found no evidence for an orderly spatial topography. One can discuss the differences in respect to slight differing settings but also in respect to the influence of higher field strength.

As mentioned above the signal increase in ultra-high-field fMRI depends on many factors, not only on the magnetic field strength. Some studies have revealed a signal increase of up to fivefold using imaging parameters focused on increased spatial resolution and small field of view (Pfeuffer et al. 2002a, b). The sensitivity is somewhat constrained by the SNR characteristics if a CP head coil is used in conjunction with standard voxel sizes from 1.5 T. It has been shown that a reduction in voxel size leads to an improvement in time series SNR through a decrease in physiological noise (Triantafyllou et al. 2005). The relatively small BOLD changes in certain brain areas in the CP study might be explained by this effect, but the use of larger voxels allows whole-brain coverage.

It is likely that future studies will not strive for exceptional resolution in one area of the brain but be targeted at analysing complex networks. Especially cognitive functions but also clinical applications require more slices and coverage of extended brain areas. Furthermore, some interesting structures such as the hippocampal region can, as in the cerebellum, suffer from signal dropouts near tissue-air boundaries. The recent developments in coils technique and sequences as well as post processing have much improved the use of ultra-high field even in the mentioned problematic areas. Some examples were described in the cognitive section above. Figure 5.5 shows a further example with possible use not only in experimental settings but also in clinical applications: a representative activation of the dentate nucleus during a finger-tapping task. With such technique, even examination of activation of the dentate nucleus in a verb-generation task in normal volunteers was possible using the increase in signal-to-noise ratio (Thürling et al. 2011). For image processing, a newly developed region of interest-driven normalization method of the dentate nuclei was applied. This experiment suggests that the human dentate nucleus can be subdivided into a rostral and more dorsal motor domain and a ventrocaudal non-motor

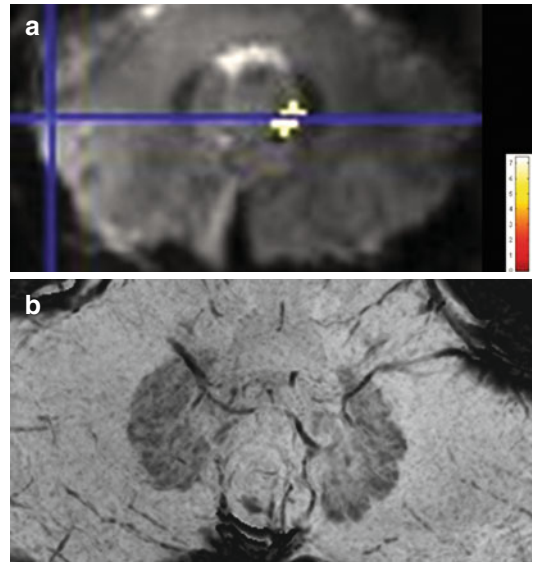

Fig. 5.5 Statistical parametric maps of activation of a single subject performing finger-tapping task compared with rest period at 7 T superimposed on EPI transverse orientation (**a**) and the high-resolution SWI imaging of dentate nucleus at 7 T (**b**). Statistically corrected threshold is $p < 0.001$

domain. Such findings represent the benefit of high-field fMRI with its higher SNR and possibility to reveal deep brain structures more reliable.

In respect to more direct clinical application, first experiments with a speech paradigm could reveal the advantages of 7-T fMRI combined with an eight-channel head coil and a parallel acquisition technique (Fig. 5.6). Even using the parallel acquisition technique, an increase in BOLD signal could be obtained, and a more extended activation and detection of lateralization could be found. Furthermore, the application of parallel imaging led to a significant reduction of artefacts (Fig. 5.2). Therefore, a reliable co-registration of high-resolution structural images with the EPI images could be performed. Figure 5.7 shows a patient with a cavernoma scanned pre-surgically at 1.5 T (a) and 7 T (b). The speech paradigm was a verb-generation task in both measurements in a block design. The activation maps are superimposed on susceptibility-weighted images (SWI) at 1.5 and 7 T. In addition to the higher BOLD signal and the more extended activation at 7 T, the higher spatial resolution of the structural images confers further

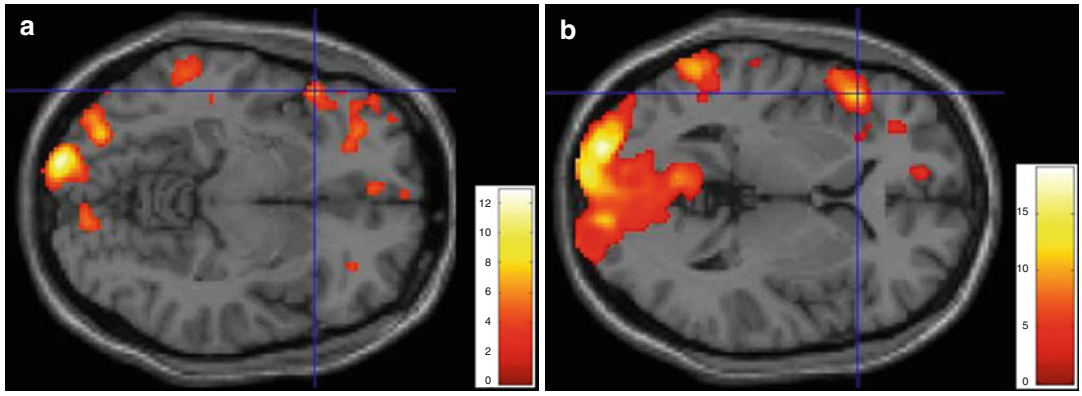

Fig. 5.6 Statistical parametric maps of activation within all subjects performing the verb-generation task compared with rest period at 1.5 T (**a**) and 7 T (**b**) superimposed on a standard brain in transverse orientation. Statistically corrected threshold is $p<0.005$. Activated areas of Broca and Wernicke regions are shown at both field strengths but with more extended clusters and higher signal change at 7 T

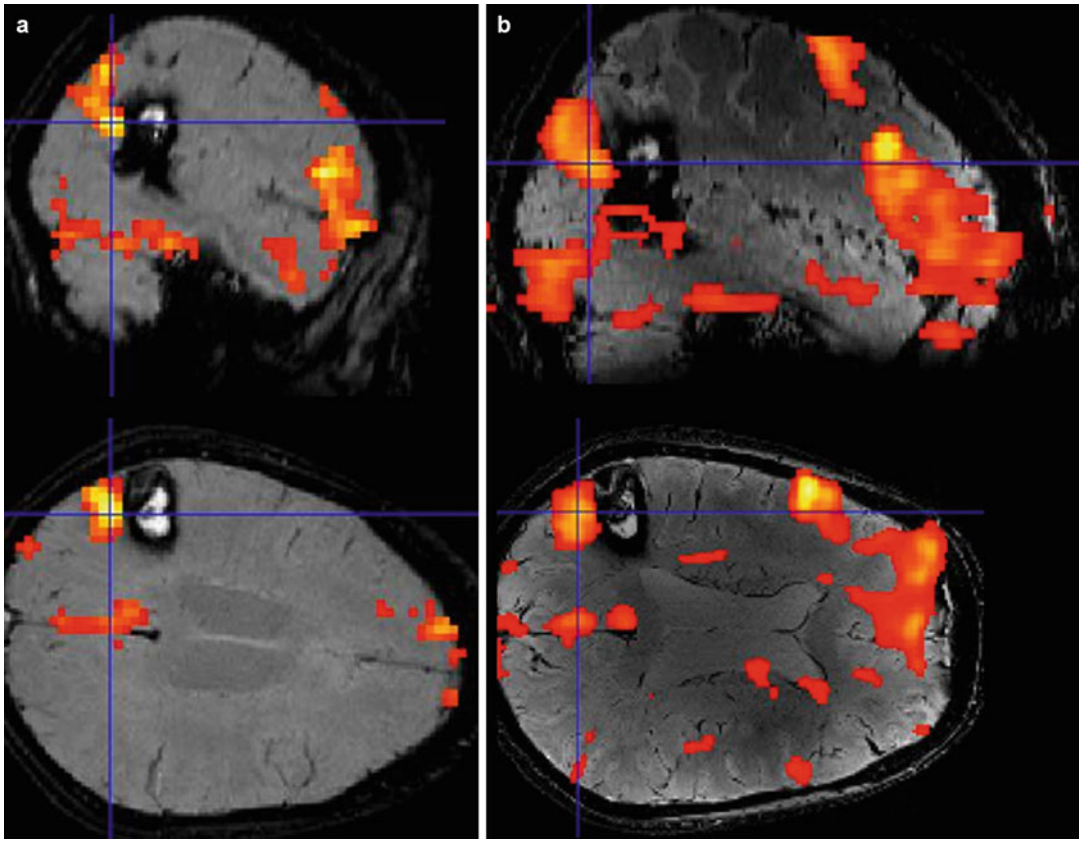

Fig. 5.7 Statistical parametric maps of activation within one patient performing the verb-generation task compared with rest period at 1.5 T (**a**) and 7 T (**b**) superimposed on SWI images. Statistically corrected threshold is $p<0.005$. Activated areas of Broca and Wernicke regions are shown at both field strengths but with more extended clusters and higher signal change at 7 T. Furthermore, the structural images have a higher in-plane resolution at 7 T with enhanced tumour-brain differentiation and superior depiction of the inner structure of the cavernoma

benefit for surgical planning. One recent study could demonstrate the clinical benefit of 7-T fMRI. The primary motor hand area was analysed at 3 and 7 T in 17 patients (Beisteiner and Robinson 2011). However, as in former studies, 7-T data suffered from significant increase of artefacts (ghosting, head motion).

Besides fundamental experimental interests, e.g. for cognitive studies, clinical indications of 7-T fMRI can be imagined. Pre-surgical fMRI in patients with brain tumours could benefit from either higher resolution or faster imaging. Even patients impaired with respect to motor function are for the most part able to perform a short-finger movement sufficient for a single-block examination.

References

Alvarez-Linera J (2008) 3 T MRI: advances in brain imaging. Eur J Radiol 67(3):415–426

Andersson P, Ramsey NF et al (2010) BCI control using 4 direction spatial visual attention and real-time fMRI at 7 T. Conf Proc IEEE Eng Med Biol Soc 2010:4221–4225

Banks SJ, Jones-Gotman M et al (2012) Sex differences in the medial temporal lobe during encoding and recognition of pseudowords and abstract designs. Neuroimage 59(2):1888–1895

Barry RL, Strother SC (2011) Data-driven optimization and evaluation of 2D EPI and 3D PRESTO for BOLD fMRI at 7 Tesla: I. Focal coverage. Neuroimage 55(3): 1034–1043

Beisteiner R, Robinson S (2011) Clinical fMRI: evidence for a 7T benefit over 3T. Neuroimage 57(3):1015–1021

Blatow M, Reinhardt J et al (2011) Clinical functional MRI of sensorimotor cortex using passive motor and sensory stimulation at 3 Tesla. J Magn Reson Imaging 34(2):429–437

De Martino F, Esposito F (2011) Whole brain high-resolution functional imaging at ultra high magnetic fields: an application to the analysis of resting state networks. Neuroimage 57(3):1031–1044

Duong TQ, Yacoub E et al (2003) Microvascular BOLD contribution at 4 and 7 T in the human brain: gradient-echo and spin-echo fMRI with suppression of blood effects. Magn Reson Med 49(6):1019–1027

Gizewski ER, de Greiff A et al (2007) FMRI at 7 T: whole-brain coverage and signal advantages even infratentorially? Neuroimage 37(3):761–768

Goodyear BG, Douglas EA (2008) Minimum detectable change in motor and prefrontal cortex activity over repeated sessions using 3 T functional MRI and a block design. J Magn Reson Imaging 28(5):1055–1060

Gowland PA, Bowtell R (2007) Theoretical optimization of multi-echo fMRI data acquisition. Phys Med Biol 52(7):1801–1813

Hale JR, Brookes MJ (2010) Comparison of functional connectivity in default mode and sensorimotor networks at 3 and 7 T. MAGMA 23(5–6):339–349

Heid O (1997) Robust EPI phase correction. In: Proceedings of the ISMRM, Vancouver, 1997

Hoffmann MB, Stadler J et al (2009) Retinotopic mapping of the human visual cortex at a magnetic field strength of 7 T. Clin Neurophysiol 120(1):108–116

Kohn N, Kellermann T et al (2011) Gender differences in the neural correlates of humor processing: implications for different processing modes. Neuropsychologia 49(5):888–897

Ladd ME (2007) High-field-strength magnetic resonance: potential and limits. Top Magn Reson Imaging 18(2):139–152

Mirrashed F, Sharp JC et al (2004) High-resolution imaging at 3 T and 7 T with multiring local volume coils. MAGMA 16(4):167–173

Newton AT, Rogers BP et al (2012) Improving measurement of functional connectivity through decreasing partial volume effects at 7 T. Neuroimage 59(3):2511–2517

Norris DG (2003) High field human imaging. J Magn Reson Imaging 18(5):519–529

Okada T, Yamada H et al (2005) Magnetic field strength increase yields significantly greater contrast-to-noise ratio increase: measured using BOLD contrast in the primary visual area. Acad Radiol 12(2):142–147

Olman CA, Van de Moortele PF et al (2010) Retinotopic mapping with spin echo BOLD at 7 T. Magn Reson Imaging 28(9):1258–1269

Olman CA, Pickett KA et al (2012) Selective BOLD responses to individual finger movement measured with fMRI at 3 T. Hum Brain Mapp 33(7):1594–1606

Pfeuffer J, Adriany G et al (2002a) Perfusion-based high-resolution functional imaging in the human brain at 7 Tesla. Magn Reson Med 47(5):903–911

Pfeuffer J, Van de Moortele PF et al (2002b) Correction of physiologically induced global off-resonance effects in dynamic echo-planar and spiral functional imaging. Magn Reson Med 47(2):344–353

Pfeuffer J, Van de Moortele PF et al (2002c) Zoomed functional imaging in the human brain at 7 Tesla with simultaneous high spatial and high temporal resolution. Neuroimage 17(1):272–282

Polimeni JR, Fischl B et al (2010) Laminar analysis of 7 T BOLD using an imposed spatial activation pattern in human V1. Neuroimage 52(4):1334–1346

Poser BA, Versluis MJ et al (2006) BOLD contrast sensitivity enhancement and artifact reduction with multiecho EPI: parallel-acquired inhomogeneity-desensitized fMRI. Magn Reson Med 55(6):1227–1235

Preibisch C, Wallenhorst T et al (2008) Comparison of parallel acquisition techniques generalized autocalibrating partially parallel acquisitions (GRAPPA) and

modified sensitivity encoding (mSENSE) in functional MRI (fMRI) at 3 T. J Magn Reson Imaging 27(3):590–598
Sanchez-Panchuelo RM, Schluppeck D (2010) Mapping human somatosensory cortex in individual subjects with 7T functional MRI. J Neurophysiol 103(5): 2544–2556. doi: 10.1152/jn.01017.2009. Epub 2010 Feb 17
Scheef L, Landsberg MW et al (2007) Methodological aspects of functional neuroimaging at high field strength: a critical review. Rofo 179(9):925–931
Schlamann M, Voigt MA et al (2010a) Exposure to high-field MRI does not affect cognitive function. J Magn Reson Imaging 31(5):1061–1066
Schlamann M, Yoon MS et al (2010b) Short term effects of magnetic resonance imaging on excitability of the motor cortex at 1.5 T and 7 T. Acad Radiol 17(3): 277–281, Epub 2009 Dec 29
Shimada Y, Kochiyama T et al (2008) System stability of a 3 T-MRI during continuous EPI scan. Nippon Hoshasen Gijutsu Gakkai Zasshi 64(12): 1504–1512
Theysohn JM, Maderwald S et al (2008) Subjective acceptance of 7 Tesla MRI for human imaging. MAGMA 21(1–2):63–72
Thürling M, Küper M et al (2011) Activation of the dentate nucleus in a verb generation task: a 7 T MRI study. Neuroimage 57(3):1184–1191
Triantafyllou C, Hoge RD et al (2005) Comparison of physiological noise at 1.5 T, 3 T and 7 T and optimization of fMRI acquisition parameters. Neuroimage 26(1):243–250
Triantafyllou C, Hoge RD et al (2006) Effect of spatial smoothing on physiological noise in high-resolution fMRI. Neuroimage 32(2):551–557
van der Zwaag W, Marques JP et al (2009) Minimization of Nyquist ghosting for echo-planar imaging at ultra-high fields based on a "negative readout gradient" strategy. J Magn Reson Imaging 30(5):1171–1178
van der Zwaag W, Marques JP et al (2012) Temporal SNR characteristics in segmented 3D-EPI at 7 T. Magn Reson Med 67(2):344–352
Vaughan JT, Garwood M et al (2001) 7 T vs. 4 T: RF power, homogeneity, and signal-to-noise comparison in head images. Magn Reson Med 46(1):24–30
Walter M, Stadler J et al (2008) High resolution fMRI of subcortical regions during visual erotic stimulation at 7 T. MAGMA 21(1–2):103–111
Wiggins GC, Potthast A et al (2005) Eight-channel phased array coil and detunable TEM volume coil for 7 T brain imaging. Magn Reson Med 54(1):235–240
Yacoub E, Hu X (2001) Detection of the early decrease in fMRI signal in the motor area. Magn Reson Med 45(2):184–190
Yacoub E, Shmuel A et al (2001) Imaging brain function in humans at 7 Tesla. Magn Reson Med 45(4):588–594
Yacoub E, Duong TQ et al (2003) Spin-echo fMRI in humans using high spatial resolutions and high magnetic fields. Magn Reson Med 49(4):655–664
Zou KH, Greve DN et al (2005) Reproducibility of functional MR imaging: preliminary results of prospective multi-institutional study performed by biomedical informatics research network. Radiology 237(3):781–789

fMRI Data Analysis Using SPM

6

Guillaume Flandin and Marianne J.U. Novak

Abbreviations

DCM	Dynamic causal model
EPI	Echo planar imaging
fMRI	Functional magnetic resonance imaging
FFX	Fixed-effects analysis
FPR	False-positive rate
FWE	Family-wise error
FWHM	Full width at half maximum
GLM	General linear model
HRF	Haemodynamic response function
MIP	Maximum intensity projection
PET	Positron emission tomography
RFT	Random field theory
RFX	Random-effects analysis
SPM	Statistical parametric map(ping)
SVC	Small volume correction
TR	Time to repeat
VBM	Voxel-based morphometry

G. Flandin (✉) • M.J.U. Novak
Wellcome Trust Centre for NeuroImaging,
UCL Institute of Neurology,
Queen Square, London WC1N 3BG, UK
e-mail: g.flandin@ucl.ac.uk; m.novak@ucl.ac.uk

6.1 Introduction

Statistical parametric mapping (SPM) is an established statistical data analysis framework through which regionally specific effects in structural and functional neuroimaging data can be characterised. SPM is also the name of a free and open source academic software package through which this framework (amongst other things) can be implemented. In this chapter, we will give an overview of the underlying concepts of the SPM framework and will illustrate this by describing how to analyse a typical block-design functional MRI (fMRI) data set using the SPM software. An exhaustive description of SPM would be beyond the scope of this introductory chapter; for more information, we refer interested readers to *Statistical Parametric Mapping: The Analysis of Functional Brain Images* (Friston et al. 2007).

The aim of the SPM software[1] is to communicate and disseminate neuroimaging data analysis methods to the scientific community. It is developed by the SPM co-authors, who are associated with the Wellcome Trust Centre for Neuroimaging, including the Functional Imaging Laboratory, UCL Institute of Neurology. For those interested, a history of SPM can be found in a special issue of the NeuroImage journal, produced to mark 20 years of fMRI (Ashburner 2011). In brief, SPM was created by Karl Friston in approximately 1991 to carry out statistical analysis of positron emission tomography (PET) data. Since then, the SPM project has evolved to

[1] http://www.fil.ion.ucl.ac.uk/spm/

S. Ulmer, O. Jansen (eds.), *fMRI – Basics and Clinical Applications*,
DOI 10.1007/978-3-642-34342-1_6, © Springer-Verlag Berlin Heidelberg 2013

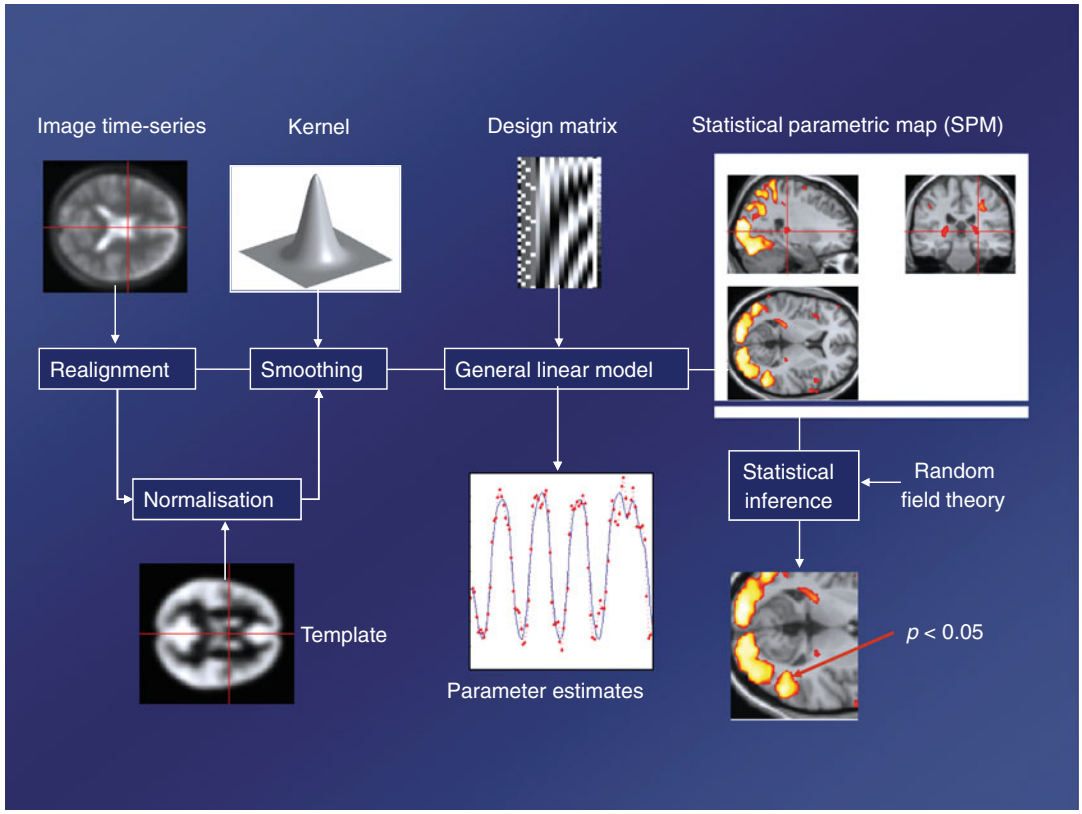

Fig. 6.1 Flowchart of the SPM processing pipeline, starting with raw imaging data and ending with a statistical parametric map (*SPM*). The raw images are motion-corrected, then subject to non-linear warping so that they match a template that conforms to a standard anatomical space. After smoothing, the general linear model is employed to estimate the parameters of a model encoded by a design matrix containing all possible predictors of the data. These parameters are then used to derive univariate test statistics at every voxel; these constitute the SPM. Finally, statistical inference is performed by assigning p values to unexpected features of the SPM, such as high peaks or large clusters, through the use of the random field theory

support newer imaging modalities such as functional magnetic resonance imaging (fMRI) and to incorporate constant development and improvement of existing methods. The second half of the last decade saw an emphasis on the development of methods for the analysis of MEG and EEG (M/EEG) data, giving rise to the current version of SPM, SPM8.

The SPM framework is summarised in Fig. 6.1. The analysis pipeline starts with a raw imaging data sequence at the top left corner of the figure and ends with a statistical parametric map (also abbreviated to SPM) showing the significance of regional effects in the bottom right corner. The SPM framework can be partitioned into three key components, all of which will be described in this chapter:

- Preprocessing, or spatially transforming data: images are spatially aligned to each another to correct for the effect of subject movement during scanning (realignment/motion correction), then spatially normalised into a standard space and smoothed.
- Modelling the preprocessed data: parametric statistical models are applied at each voxel (a *vo*lume *el*ement, the three-dimensional extension of a pixel in 2D) of the data, using a general linear model (GLM) to describe the data in terms of experimental effects, confounding effects and residual variability.
- Statistical inference on the modelled data: classical statistical inference is used to test hypotheses that are expressed in terms of

GLM parameters. This results in an image in which the voxel values are statistics: this is a statistical parametric map (SPM). For such classical inferences, a multiple comparisons problem arises from the application of mass-univariate tests to images with many voxels. This is solved through the use of random field theory (RFT), resulting in inference based on corrected p values.

In this chapter, we will illustrate the concepts underpinning SPM through the analysis of an actual fMRI data set. The data set we will use was the first ever fMRI data set collected and analysed at the Functional Imaging Laboratory (by Geraint Rees, under the direction of Karl Friston) and is locally known as the Mother of All Experiments. The data set can be downloaded from the SPM website,[2] allowing readers to reproduce the analysis pipeline that we will describe on their own computers. (For more detailed step-by-step instructions to this analysis, we refer readers to the SPM manual.[3]) The purpose of the experiment was to explore equipment and techniques in the early days of fMRI. The experiment consisted of a single session in a single subject; the subject was presented with alternating blocks of rest and auditory stimulation, starting with a rest block. The auditory stimulation consisted of binaurally, bi-syllabic words presented at a rate of 60 words/min. Ninety-six whole brain echo planar imaging (EPI) scans were acquired on a modified 2 T Siemens MAGNETOM Vision System, with a repetition time (TR) of 7 s. Each block lasted for six scans, and there were 16 blocks in total, each lasting for 42 s. Each scan consisted of 64 contiguous slices ($64\times64\times64$, $3\times3\times3$ mm^3 voxels). A structural scan was also acquired prior to the experiment ($256\times256\times54$, $1\times1\times3$ mm^3 voxels).

Acquisition techniques have tremendously improved since this data set was acquired – a TR of 7 s seems very slow in comparison with today's standards – but the analysis pipeline is identical to that of more recent data sets and fits nicely with the purpose of illustration in this chapter. While analysing this block, or epoch, designed experiment, we will point out the few steps that differ in the analysis of event-related data sets.

After an overview of the SPM software, we will describe in the next sections the three key components of an SPM analysis, namely, (i) spatial transformations, (ii) modelling and (iii) statistical inference.

6.2 SPM Software Overview

6.2.1 Requirements

The SPM software is written in MATLAB[4] (The MathWorks, Inc.), a high-level technical computing language and interactive environment. SPM is distributed under the terms of the GNU General Public Licence. The software consists of a library of MATLAB M-files and a small number of C-files (which perform some of the most computationally intensive operations) and will run on any platform supported by MATLAB: 32- and 64-bit Microsoft Windows, Mac OS and Linux. This means that a prospective SPM user must first install commercially available software MATLAB. More specifically, SPM8 requires either MATLAB version 7.1 (R14SP3, released in 2005) or any more recent version (up to 7.13 (R2011b) at time of writing). Only core MATLAB software is required; no extra MATLAB toolboxes are needed.

A standalone version of SPM8, compiled using the MATLAB Compiler, is also available from the SPM development team upon request. This allows the use of most of the SPM functions without the need for a MATLAB licence (although this comes at the expense of being able to modify the software).

6.2.2 Installation

The installation of SPM simply consists of unpacking a ZIP archive from the SPM website on the user computer and then adding the root

[2] http://www.fil.ion.ucl.ac.uk/spm/data/auditory/

[3] http://www.fil.ion.ucl.ac.uk/spm/doc/manual.pdf

[4] http://www.mathworks.com/

SPM directory to the MATLAB path. If needed, more details on the installation can be found on the SPM wiki on Wikibooks.[5]

SPM updates (which include bug fixes and improvements to the software) take place regularly (approximately every 6 months) and are advertised on the SPM mailing list.[6] SPM is a constantly evolving software package, and we therefore recommend that users either subscribe to the mailing list or check the SPM website so that they can benefit from ongoing developments. Updates can be easily installed by unpacking the update ZIP archive on top of the existing installation so that newer files overwrite existing ones. We would, however, advise users not to install updates mid-analysis (unless a specific update is needed), to ensure consistency within an analysis.

6.2.3 Interface

To start up SPM, simply type *spm* in the MATLAB command line and choose the modality in which you wish to use SPM in the new window that opens. A shortcut is to directly type *spm fmri*. The SPM interface consists of three main windows, as shown in Fig. 6.2. The Menu window (1) contains entry points to the various functions contained in SPM. The Interactive window (2) is used either when SPM functions require additional information from the user or when an additional function-specific interface is available. The Graphics window (3) is the window in which results and figures are shown. Additional windows can appear, such as the Satellite Graphics window (4), in which extra results can be displayed, or the Batch Editor window (5). SPM can run in batch mode (in which several SPM functions can be set up to run consecutively through a single analysis pipeline), and the Batch Editor window is the dedicated interface for this. The window can be accessed through the 'Batch' button in the Menu window.

The Menu window is subdivided into three sections, which reflect the key components of an SPM analysis: spatial preprocessing, modelling and inference.

6.2.4 File Formats

In general, the first step when using SPM is to convert the raw data into a format that the software can read. Most MRI scanners produce image data that conform to the DICOM (Digital Imaging and Communications in Medicine) standard.[7] The DICOM format is very flexible and powerful, but this comes at the expense of simplicity. As a consequence, the neuroimaging community agreed in 2004 to use a simpler image data format, the NIfTI (Neuroimaging Informatics Technology Initiative)[8] format, to facilitate interoperability between fMRI data analysis software. The Mayo Clinic Analyze format was used prior to this but had several shortcomings which the NIfTI format overcame (including variability in the format versions used by different software packages which caused uncertainty about the laterality of the brain).

A NIfTI image file can consist either of two files, with the extensions *.hdr* and *.img*, or a single file, with the extension *.nii*. The two versions can be used in SPM interchangeably (note that you can also come across a compressed version of these files with a *.gz* extension; these are not supported in SPM and will need to be uncompressed outside the software before use). The *header* (*.hdr*) file contains meta-information about the data, such as the voxel size, the number of voxels in each direction and the data type used to store values. The *image* (*.img*) file contains the raw 3D array of voxel values. A file with the *.nii* extension contains all of this information in one file. A key piece of information stored in the header is the *voxel-to-world mapping*: this is a spatial transformation that maps from the stored data coordinates (voxel column i, row j, slice k) into a real-world

[5] http://en.wikibooks.org/wiki/SPM/
[6] http://www.fil.ion.ucl.ac.uk/spm/support/
[7] http://dicom.nema.org/
[8] http://nifti.nimh.nih.gov/

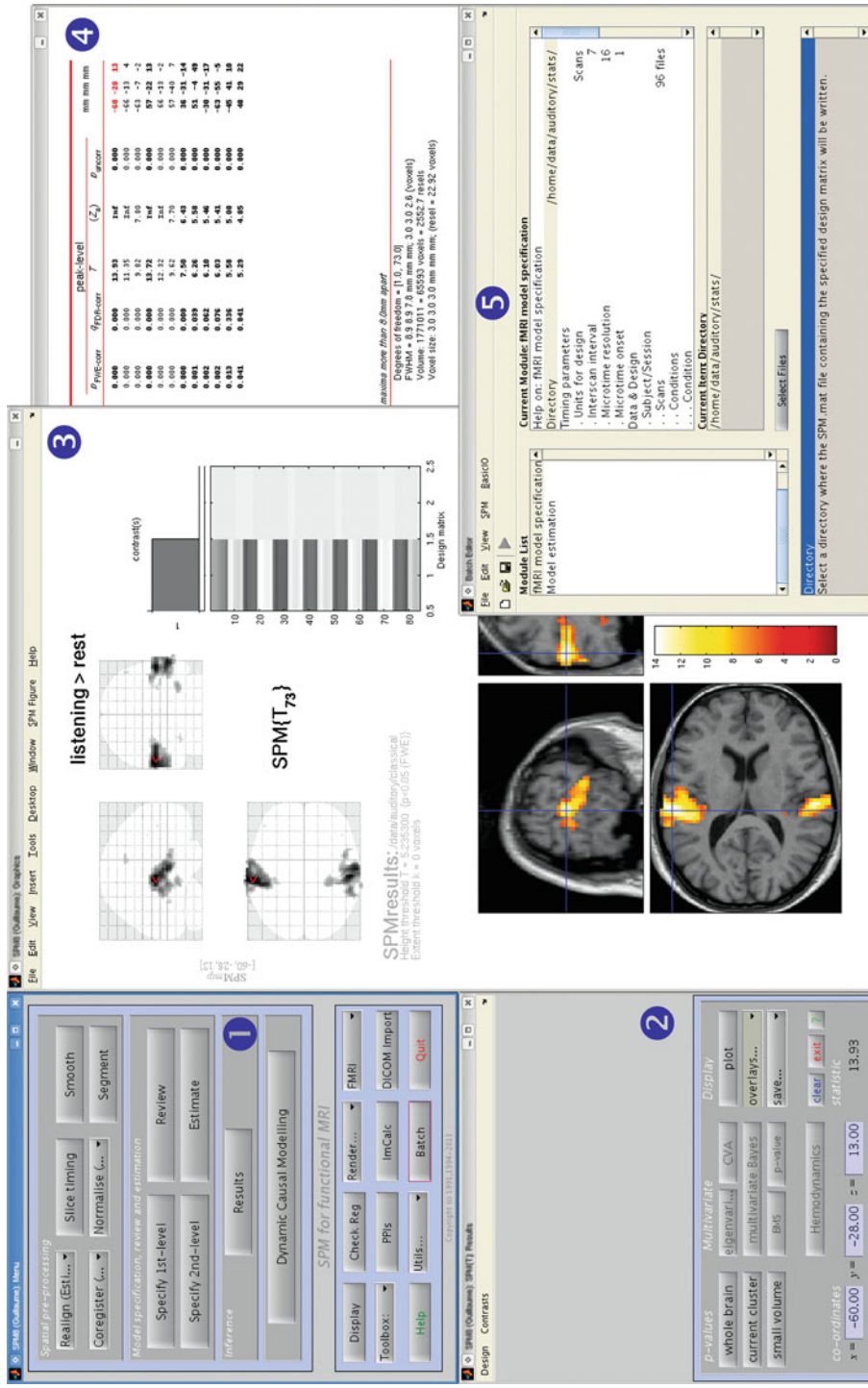

Fig. 6.2 Interface of the SPM8 software for the fMRI modality: (*1*) Menu window, (*2*) Interactive window, (*3*) Graphics window, (*4*) Satellite Results window and (*5*) Batch editor interface

position (x, y, z *mm*) in space. The real-world position can be in either a standardised space such as Talairach and Tournoux space or Montreal Neurological Institute (MNI) space or a subject-specific space based on scanner coordinates.

FMRI data can be considered as 4D data – a time series of 3D data – and can therefore be stored as a single file in the NIfTI format where the first three dimensions are in space and the fourth is in time. However, use of multiple 3D (spatial) files rather than a single 4D file is recommended with SPM for the time being because the software handles them more efficiently.

DICOM image data can be converted into NIfTI files in SPM using the 'DICOM Import' button in the Menu window. This is usually a straightforward process. If needed, however, NIfTI data obtained from the file converter of any other software package (such as the LONI Debabeler[9] or dcm2nii[10]) can also be used in SPM; the output NIfTI images are interoperable between software packages.

The auditory data set used in this chapter has already been converted from the DICOM format. We have 96 pairs of fMRI files, namely *fM00223_*.{hdr,img}*, and one pair of structural files, namely *sM00223_002.{hdr,img}*. These images are actually stored in the Analyze format because they were acquired prior to 2004; SPM8 can read Analyze format as well as NIfTI format but will save new images in the NIfTI format.

Images can be displayed in SPM using the 'Display' and 'Check Reg' buttons from the Menu window. The first function displays a single image and some information from its header, while the second displays up to 15 images at the same time. This can be used to check the accuracy of alignment, for example.

6.3 Spatial Transformations

A number of preprocessing steps must be applied to the fMRI data to transform them into a form suitable for statistical analysis. Most of these steps correspond to some form of image registration, and Fig. 6.3 illustrates a typical preprocessing pipeline. There is no universal pipeline to use in all circumstances – options depend on the data themselves and the aim of the analysis – but the one presented here is fairly standard.

The first preprocessing step is to apply a motion correction algorithm to the fMRI data (this is the *realignment function*). This may eventually include some form of distortion correction. A structural MRI of the same subject is often acquired and should be brought into alignment with the fMRI data in a second step (*coregister function*). The warps needed to spatially normalise the structural image into some standard space should then be estimated (*normalise function*) and applied to the motion-corrected functional images to normalise them into the same standard space (*write normalise function*). The final step will typically be to smooth the functional data spatially by applying a Gaussian kernel to them (*smooth function*).

The type of spatial *transformations* that should be applied to data depends on whether the data to be transformed all come from the same subject (*within-subject* transformations) or from multiple different subjects (*between-subject* transformations). The choice of *objective function* (the criterion to assess the quality of the registration) used to estimate the deformation also depends on the modality of data in question. Realignment is a *within-subject*, *within-modality* registration, while coregistration is a *within-subject*, *between-modality* registration. Normalisation is a *between-subject* registration. Within-subject registration will generally involve a *rigid body* transformation, while a between-subject registration will need estimation of affine or non-linear warps; this is because a more complex transformation is required to warp together the anatomically variable brains of different subjects than to warp together different images of the same brain. A criterion to compare two images of the same modality can be the sum of squares of the differences of the two images, while the comparison between two images of different modalities will involve more advanced criteria. An *optimisation algorithm* is then used in the registration step to

[9] http://loni.ucla.edu/Software/Debabeler

[10] http://www.cabiatl.com/mricro/mricron/dcm2nii.html

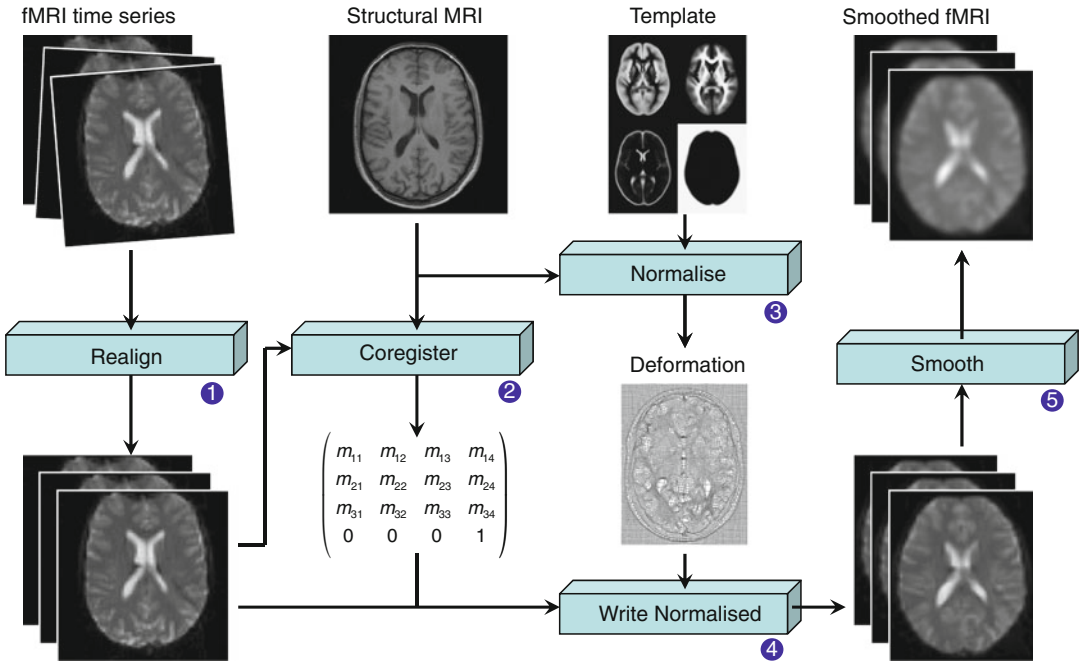

Fig. 6.3 Flowchart of a standard pipeline to preprocess fMRI data. After realignment (*1*) to correct for movement, structural and functional images are coregistered (*2*) then normalised (*3*, *4*) to conform to a standard anatomical space (e.g. MNI space) before being spatially smoothed using a Gaussian kernel (*5*)

maximise (or minimise) the objective function. Once the parameters have been estimated, the target image can be transformed to match the source image by resampling the data using an *interpolation* scheme. This step is referred to as *reslicing* when dealing with rigid transformations.

6.3.1 Data Preparation

Before preprocessing an fMRI data set, the first images acquired in a session should be discarded. This is because much of the very large signal change that they contain is due to the time it takes for magnetisation to reach equilibrium. This can be easily seen by looking at the first few images at the beginning of the time series using the display function. Some scanners might handle these '*dummy scans*' automatically by acquiring a few scans before the real start of the acquisition, but this should be checked. In our example data set, we are going to discard the first 12 scans, leaving us with 84 scans. This is more than necessary here but it preserves the simplicity of the experimental design as it corresponds to one complete cycle of auditory stimulation and rest.

It is good practice to manually reorient the images next so that they roughly match the normalised space that SPM uses (MNI space). This will help the convergence of the registration algorithms used in preprocessing; the algorithms use a local optimisation procedure and can fail if the initial images are not in rough alignment. In practice, the origin (*0*, *0*, *0* mm) should be within 5 cm of the anterior commissure (a white matter track which connects the two hemispheres across the midline), and the orientation of the images should be within about 20° of the SPM template. To check the orientation of images, display one image of the time series using the 'Display' button and manually adjust their orientation using the translation (right, forward, up) and rotation (pitch, roll, yaw) parameters in the bottom left panel until the prerequisites are met. To actually apply the transformation to the data, you need to press the 'Reorient images' button and select all the images to reorient. With the auditory data set, the structural image is already correctly orientated,

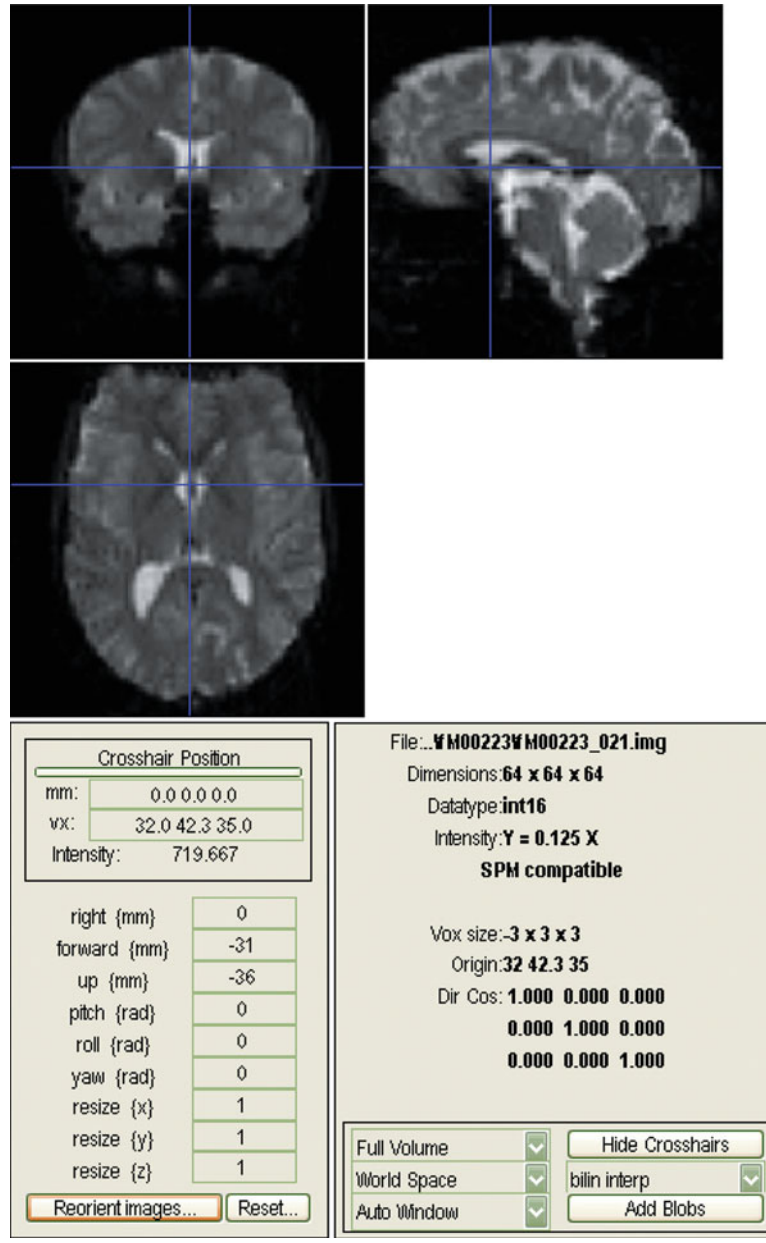

Fig. 6.4 Interface of the 'Display' option. The location of the crosshair, in *blue*, is indicated in the *bottom left panel*, both in mm and voxel. Here, a translation of [0, −31, −36] mm allows to set the origin of the image ([0, 0, 0] mm) near the anterior commissure

but the functional scans should be translated by about [*0*, *−31*, *−36*] mm. See Fig. 6.4 for a screenshot of the 'Display' interface illustrating how to change the origin of a series of images.

6.3.2 Realignment

As described above, the first preprocessing step is to realign the data to correct for the effects of subject movement during the scanning session. Despite restraints on head movement, cooperative subjects still show displacements of up to several millimetres, and these can have a large impact on the significance of the ensuing inference; in the unfortunate situation where a subject's movements are correlated with the experimental task, spurious activations can be observed if no correction was performed prior to statistical analysis. Alternatively, movements correlated with responses to an experimental task can inflate unwanted variance components

in the voxel time series and reduce statistical power.

The objective of realignment is to determine the rigid body transformation that best maps the series of functional image volumes into a common space. A rigid body transformation can be parameterised by six parameters in 3D: three translations and three rotations. The realignment process involves the estimation of the six parameters that minimise the mean squared difference between each successive scan and a reference scan (usually the first or the average of all scans in the time series) (Friston et al. 1995).

Unfortunately, even after realignment, there may still be some motion-related artefacts remaining in the functional data (Friston et al. 1996b); this is mainly because the linear, rigid body realignment transformation cannot capture non-linear effects. These non-linear effects can be the consequence of subject movement between slice acquisition, interpolation artefacts, magnetic field inhomogeneities or spin-excitation history effects. One solution is to use the movement parameter estimates as covariates of no interest during the modelling of the data. This will effectively remove any signal that is correlated with functions of the movement parameters but can still be problematic if the movement effects are correlated with the experimental design. An alternative option is to use the 'Realign and Unwarp' function (Andersson et al. 2001). The assumption in this function is that the residual movement variance can be largely explained by susceptibility-by-movement interaction: the non-uniformity of the magnetic field is the source of geometric distortions during magnetic resonance acquisition, and the amount of distortion depends partly on the position of the head of the subject within the magnetic field; hence, large movements will result in changes in the shape of the brain in the images which cannot be captured by a rigid body transformation. The 'Realign and Unwarp' function uses a generative model that combines a model of geometric distortions and a model of subject motion to correct images. The 'Realign and Unwarp' function can be combined with the use of field maps (see the FieldMap toolbox), to further correct those geometric distortions introduced during the echo planar imaging (EPI) acquisition (Jezzard and Balaban 1995). The resulting corrected images will have less movement-related residual variance and better matching between functional and structural images than will the uncorrected images.

For the auditory data set, functional data are motion-corrected using 'Realign: Estimate and Reslice'. Data have to be entered session by session to account for large subject movements between sessions that the algorithm is not expecting. With regard to the reslicing, it is sufficient to write out only the mean image. The output of the estimation will be encoded in the header of each image through modification of the original voxel-to-world mapping. It is best to reslice the data just once at the end of all the preprocessing steps; this ensures that all the affine transformations are taken into account in one step, preventing unnecessary interpolation of the data. The estimated movement parameters (see Fig. 6.5) are saved in a text file in the same folder as the data with an '*rp_*' prefix and will be used later in the analysis.

6.3.3 Coregistration

Coregistration is the process of registering two images of the same or different modalities from the same subject; the intensity pattern might differ between the two images, but the overall shape remains constant. Coregistration of single subject structural and functional data firstly allows functional results to be superimposed on an anatomical scan for clear visualisation. Secondly, spatial normalisation is more precise when warps are estimated from a detailed anatomical image than from functional images; if the functional and structural images are in alignment, warps estimated from the structural image can then be applied to the functional data.

As with realignment, coregistration is performed by optimising the six parameters of a rigid body transformation; however, the objective function is different as image intensities cannot be compared directly as they were with the sum of squared differences. Instead, the similarity measures that are used rely on a branch of applied mathematics called *information theory* (Collignon et al. 1995; Wells et al. 1996). The

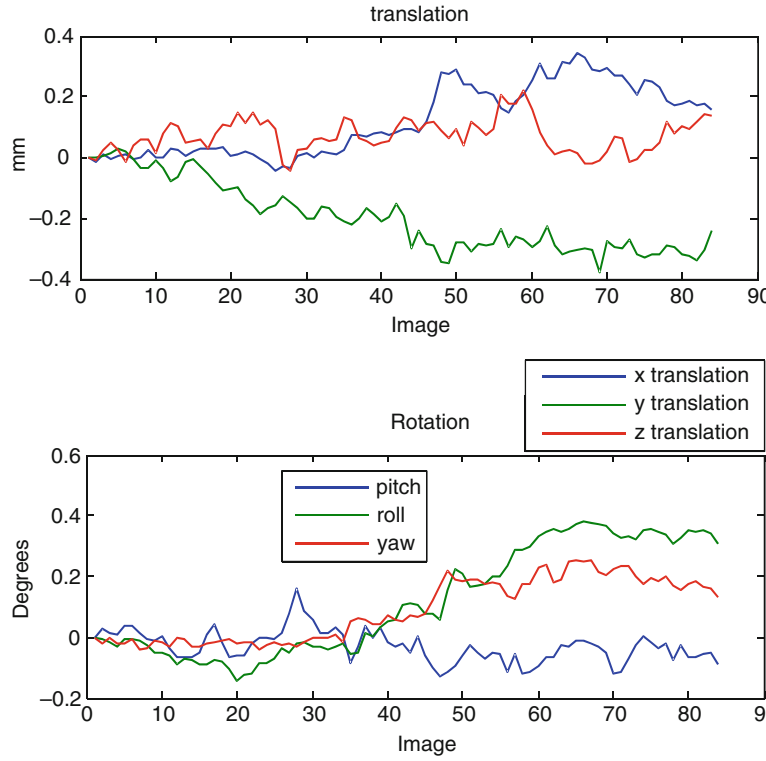

Fig. 6.5 Plot of the estimated movement parameters (three translations and three rotations) for the auditory data set as a function of time (or scan). Movements are small for this subject but we can still observe some slow drifts over time

most commonly used similarity measure is called *mutual information*; this is a measurement of shared information between data sets, based on joint probability distributions of the intensities of the images. The mutual information is assumed to be maximal when the two images are perfectly aligned and will serve here as the objective function to maximise.

For the auditory data set, the structural image should be coregistered to the mean functional image (computed during realignment) using 'Coregister: Estimate'. Once again, there is no need to reslice at this stage; reslicing can be postponed until later to minimise interpolation steps. In the interface, the *reference* image (the target) is the mean functional image, while the *source* image is the structural image. Default parameters can be left as they are; they have been optimised over years and should satisfy most situations. The output of the algorithm will be stored in the header of the structural image by adjusting its voxel-to-world mapping. Figure 6.6 shows the alignment of the two images after registration.

6.3.4 Spatial Normalisation

Spatial normalisation is the process of warping images from a number of individuals into a common space. This allows signals to be compared and averaged across subjects so that common activation patterns can be identified: the goal of most functional imaging studies. Even single subject analyses usually proceed in a standard anatomical space so that regionally specific effects can be reported within a frame of reference that can be related to other studies (Fox 1995). The most commonly used coordinate system within the brain imaging community is the one described by Talairach and Tournoux (1988), although new standards based on digital atlases (such as the Montreal Neurological Institute (MNI) space) are nowadays widespread (Mazziotta et al. 1995).

The rigid body approach used previously when registering brain images from the same subject is not appropriate for matching brain images from different subjects; it is insufficiently complex to deal with interindividual differences

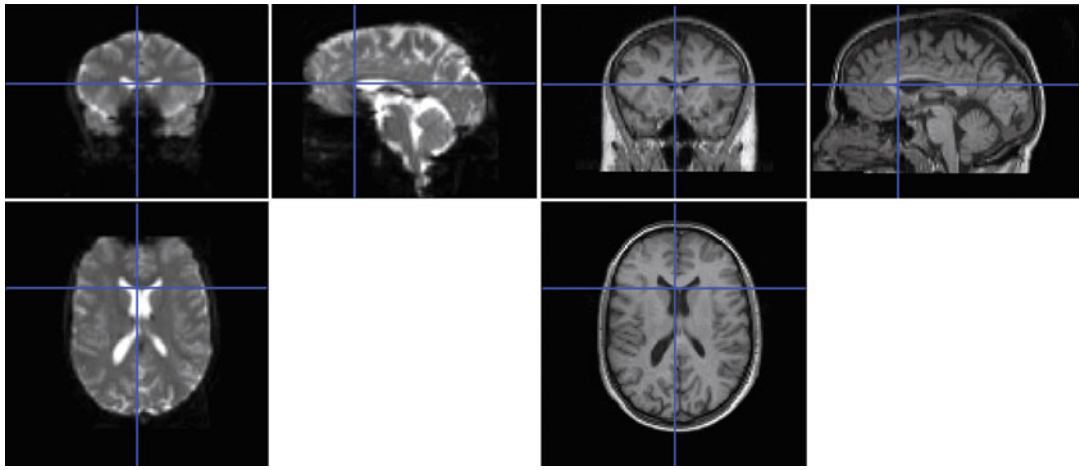

Fig. 6.6 Coregistered mean functional and structural images using mutual information. Some important dropouts in the functional data can be observed

in anatomy. More complex transformations (i.e. with more degrees of freedom) such as affine or *non-linear transformations* are used instead. (Non-linear registration is also used when characterising change in a subject's brain anatomy over time, such as those due to growth, ageing, disease or surgical intervention.)

The normalisation deformation model has to be flexible enough to capture most changes in shape but must also be sufficiently constrained that realistic brain warps are generated; *a priori*, we expect the deformation to be spatially smooth. This can be nicely framed in a Bayesian setting by adding a prior term to the objective function to incorporate prior information or add constraints to the warp. For instance, consider a deformation model in which each voxel is allowed to move independently in three dimensions. There would be three times as many parameters in this model than there are voxels. To deal with this, the deformation parameters need to be regularised; the prior term enables this. Priors become more important as the number of parameters specifying the mapping increases, and they are central to high-dimensional non-linear warping schemes. The approach taken in SPM is to parameterise the deformations by a linear combination of smooth, continuous basis functions, such as low-frequency cosine transform basis functions (see Fig. 6.7) (Ashburner and Friston 1999). These models have a relatively small number of parameters, about 1,000 (although this is of course large in comparison with 6 parameters for a rigid body transformation and 12 for an affine transformation), and allow a better description of the observed structural changes whilst providing reasonably smoothed deformations. The optimisation procedure relies on an iterative local optimisation algorithm and needs reasonable starting estimates (hence the reorientation of the images at the very beginning of the analysis pipeline). This is the model underlying the 'Normalise' button in SPM. For this function, the user should select a template image (in MNI space) in the same modality as the experimental image to be normalised.

In practice, better alignment can be achieved by matching grey matter with grey matter and white matter with white matter. The process of classifying voxels into different tissue types is called *segmentation*, and an approach combining segmentation and normalisation will provide better results than normalisation alone. This is the strategy implemented via the 'Segment' button in SPM; it is referred to as *Unified segmentation* (Ashburner and Friston 2005). Unified segmentation uses a generative model which involves (i) a mixture of Gaussians to model intensity distributions, (ii) a bias correction component to model smooth intensity variations in

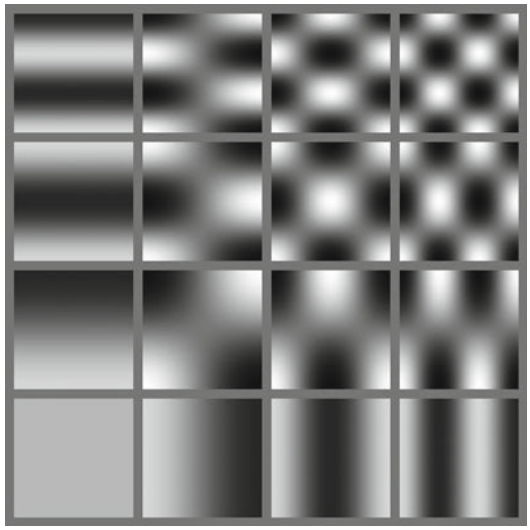

Fig. 6.7 Cosine transformation basis functions (in 2D) used by normalisation and unified segmentation. They allow deformations to be modelled with a relatively small number of parameters. The basis function registration estimates the global shapes of the brains, but is not able to account for high spatial frequency warps

space and (iii) a non-linear registration with tissue probability maps, parameterised using the low-dimension approach described in the previous paragraph.

We will use the unified segmentation approach on the auditory data set. The segmentation of the structural image (using, by default, tissue probability maps of grey matter, white matter and cerebrospinal fluid that can be found in the '*tpm*' folder of the SPM installation) will generate a few files: images with prefixes '*c1*' and '*c2*' are estimated maps of grey and white matter, respectively, while the image with an '*m*' prefix is the bias-corrected version of the structural image. Importantly, the estimated parameters of the deformation are saved in a MATLAB file ending with '*seg_sn.mat*'. This file can be used to apply the deformation, that is, to normalise the functional images (as they are in the same space as the structural scan thanks to the coregistration step) with the 'Normalise: Write' button. A new set of 84 images will be written to disk with a '*w*' prefix (for warp). The same procedure can be applied to the bias-corrected structural scan in order to later superimpose the functional activations on the anatomy of the subject. In both instances, some parameters have to be updated: the voxel size of the new set of images is preferably chosen in relation to the initial resolution of the images, for example, to the nearest integer. Here we used [*3*, *3*, *3*] for the functional data and [*1*, *1*, *3*] for the structural scan. Also, the interpolation scheme can be changed to use higher-order interpolation (the default is trilinear), such as a fourth-degree B-spline (Unser et al. 1993). The coordinates of locations within a normalised brain can now be reported as MNI coordinates in publications (Brett et al. 2002).

On a final note, spatial normalisation may require some extra care when dealing with patient populations with gross anatomical pathology, such as stroke lesions. This can generate a bias in the normalisation as the generative model is based on anatomically 'normal' data. Solving this usually involves imposing constraints on the warping to ensure that the pathology does not bias the deformation of undamaged tissue, for example, by decreasing the precision of the data in the region of pathology so that more importance is afforded to the anatomically normal priors. This is the principle of lesion masking (Brett et al. 2001). There is evidence, however, that the Unified Segmentation approach is actually quite robust in the presence of focal lesions (Crinion et al. 2007; Andersen et al. 2010).

6.3.5 Spatial Smoothing

Spatial smoothing consists of applying a spatial low-pass filter to the data. Typically, this takes the form of a 3D Gaussian kernel, parameterised by its full width at half maximum (FWHM) along the three directions. In other words, the intensity at each voxel is replaced by a weighted average of itself and its neighbouring voxels, where the weights follow a Gaussian shape centred on the given voxel. The underlying mathematical operation is a convolution, and the effect of smoothing with different kernel sizes is illustrated in Fig. 6.8.

It might seem counterintuitive to reduce the resolution of fMRI data through smoothing, but there are four reasons for doing this. Firstly,

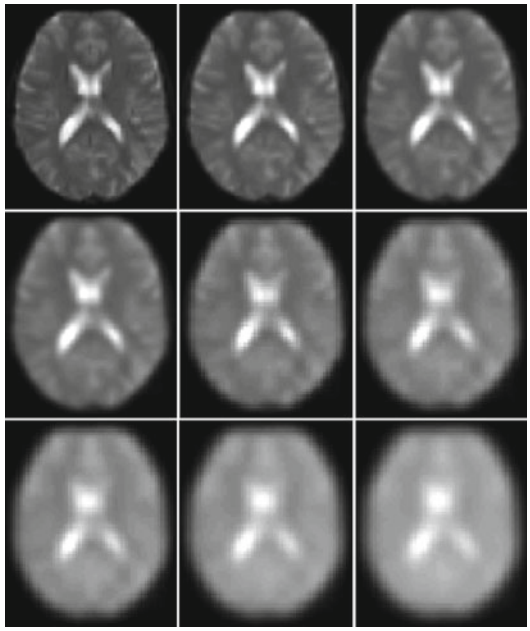

Fig. 6.8 Axial slice of a functional MRI scan smoothed with 3D Gaussian kernels of different isotropic FHWMs. From *top to bottom* and *left to right*, these show the effects of smoothing with kernels of the following FWHMs: 0, 2, 4, 6, 8, 10, 12, 14 and 16 mm

smoothing increases the signal-to-noise ratio in the data. The matched filter theorem stipulates that the optimal smoothing kernel corresponds to the size of the effect that one anticipates. A kernel similar in size to the anatomical extent of the expected haemodynamic response should therefore be chosen. Secondly, thanks to the central limit theorem, smoothing the data will render errors, or noise, more normally distributed, and will validate the use of inference based on parametric statistics. Thirdly, as we shall see later, when using the random field theory to make inference about regionally specific effects, there are specific assumptions that require smoothness in the data to be substantially greater than the voxel size (typically, as a rule of thumb, about three times the voxel size). Fourthly, small misregistration errors are inevitable in group studies; smoothing increases the degree of anatomical and functional overlap across subjects, reduces the effects of misregistration and thereby increases the significance of ensuing statistical tests.

In practice, there is no definitive amount of smoothing that should be applied to any data set; choice of smoothing kernel depends on the resolution of the data, the regions under investigation and single subject versus group analysis amongst other things. Commonly used FWHMs are between 6- and 12-mm isotropic.

For the auditory data set, we will smooth the 84 normalised scans with a [*6*, *6*, *6*]-mm FWHM kernel to produce a new set of 84 images with an '*s*' prefix.

6.4 Modelling and Statistical Inference

Statistical parametric mapping is a voxel by voxel hypothesis testing approach through which regions that show a significant experimental effect of interest are identified (Friston et al. 1991). It relies upon the construction of statistical parametric maps (SPMs), which are images with values at each voxel that are, under the null hypothesis, distributed according to a known probability density function (usually the Student's *t*- or *F*-distributions). The parameters used to compute a standard univariate statistical test at each and every voxel in the brain are obtained from the estimation of a *general linear model* which partitions observed responses into components of interest (such as the experimental effect of interest), confounding factors (examples of such will be given later) and error (or 'noise') (Friston et al. 1994a). Hence, SPM is a *mass-univariate* approach: statistics are calculated independently at each voxel. The *random field theory* is then used to characterise the SPM and resolve the multiple comparisons problem induced by making inferences over a volume of the brain containing multiple voxels (Worsley et al. 1992, 1996; Friston et al. 1994b). 'Unlikely' topological features of the SPM, like activation peaks, are interpreted as regionally specific effects attributable to the experimental manipulation.

In this section, we will describe the general linear model in the context of fMRI time series. We will then estimate its parameters using the

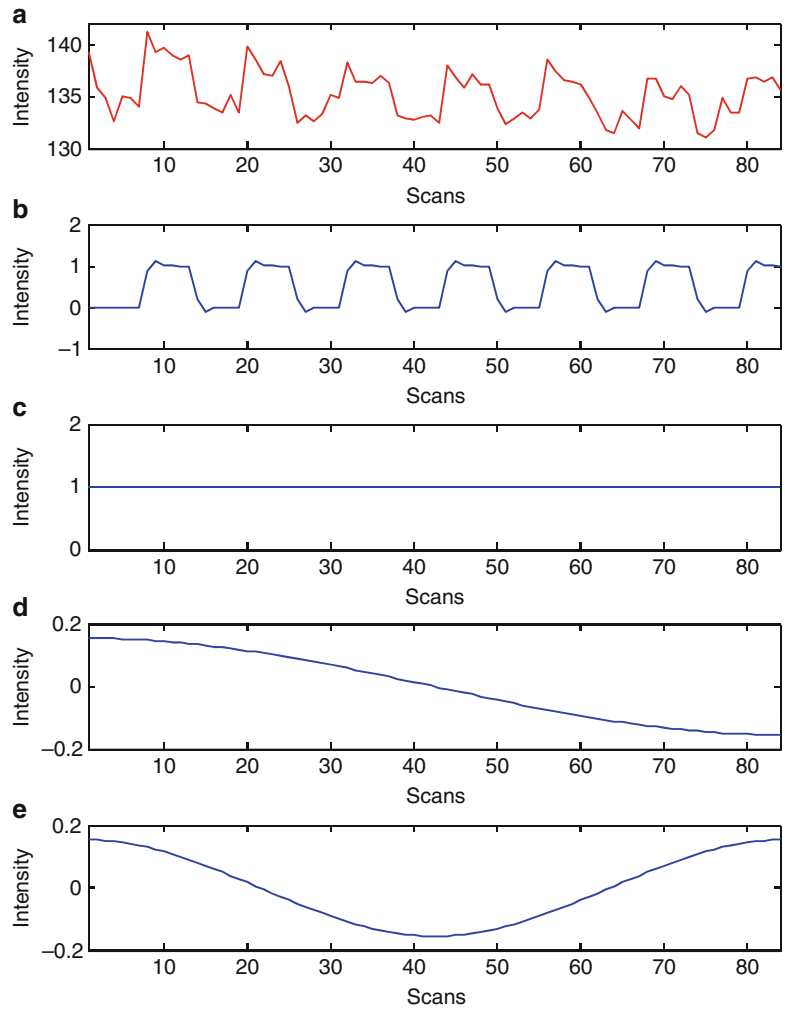

Fig. 6.9 Predictors of an fMRI time series: (**a**) raw time series at a given voxel in the brain, (**b**) stimulus function convolved with the canonical haemodynamic response function, (**c**) constant term modelling the mean whole brain activity, (**d**, **e**) the first two components of a discrete cosine basis set modelling slow fluctuations

maximum likelihood method and describe how to test hypotheses by making statistical inferences on some of the parameter estimates by using *contrast*. The resulting statistical parameters are assembled into an image: this is the SPM. The random field theory provides adjusted p values to control false-positive rate for the search volume.

6.4.1 The General Linear Model

After the spatial preprocessing of the fMRI data, we can assume that all data from one particular voxel are derived from the same part of the brain, and that in any single subject, the data from that voxel form a sequential time series. A time series selected from a (carefully chosen) voxel in the auditory data set is shown in Fig. 6.9a: variation in the response over time can be seen. There are 84 values, or data points, or observations. The aim is now to define a generative model of these data. This involves defining a prediction of what we might expect to observe in the measured BOLD signal given our knowledge of the acquisition apparatus and the experimental design. Here, the paradigm consisted of alternating periods (or 'blocks') of rest and auditory stimulation, with each block lasting for six scans. We expect that a voxel in a brain region sensitive to auditory stimuli will show a response that alternates with the same pattern and would thus, in the absence of noise, look like the plot in Fig. 6.10a.

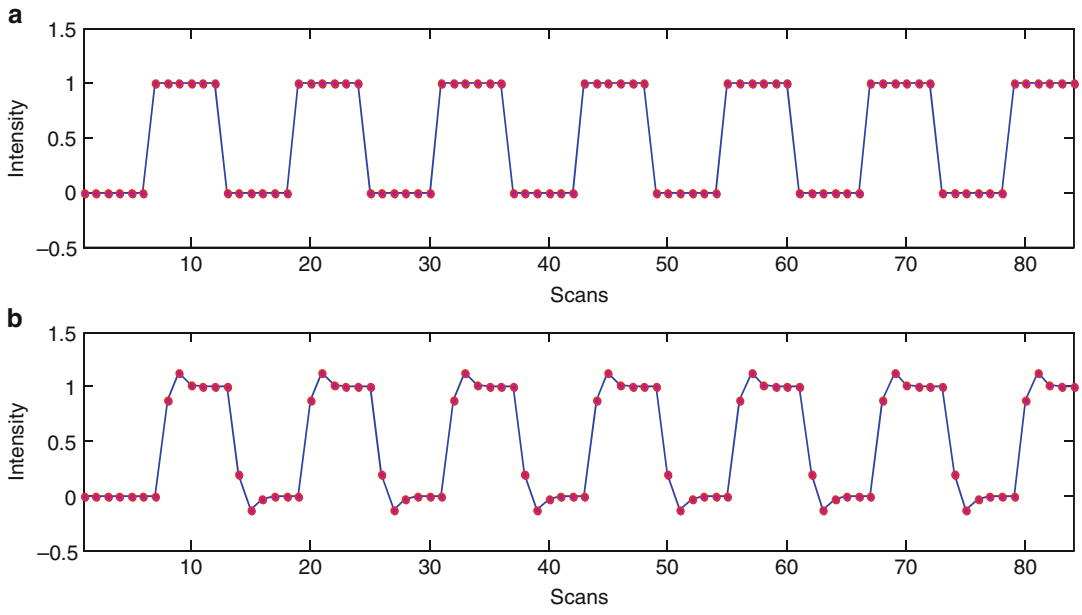

Fig. 6.10 Effect of convolution by the haemodynamic response function: (**a**) stimulus function constructed as a boxcar function and (**b**) after convolution with the canonical HRF

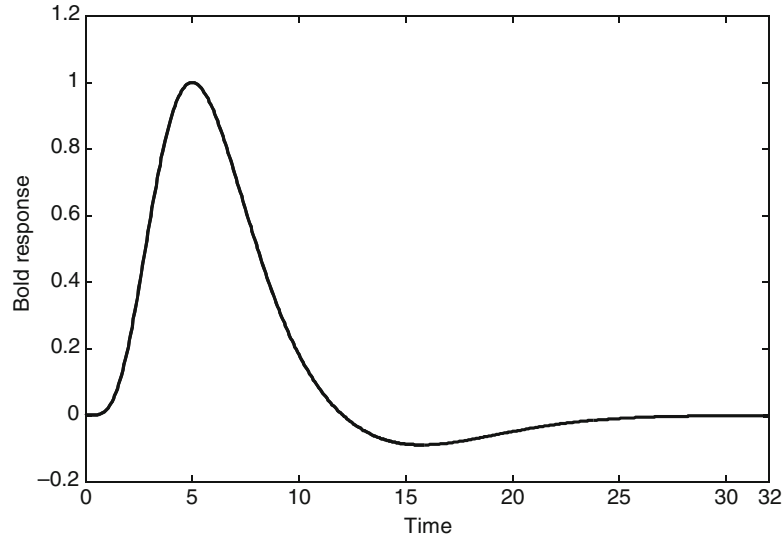

Fig. 6.11 Canonical haemodynamic response function (HRF) as used by SPM. This is the typical BOLD response to a single, impulse stimulation

However, we also know that with fMRI we are not directly measuring the neuronal activity, but the brain oxygen level-dependent (BOLD) signal with which it is associated. The observed BOLD signal corresponds to neuronally mediated haemodynamic change which can be modelled as a convolution of the underlying neuronal process by a *haemodynamic response function* (HRF). This function is called the *impulse response function*: it is the response that would be observed in the BOLD signal in the presence of a brief neuronal stimulation at $t = 0$. The *canonical HRF* used in SPM is depicted in Fig. 6.11. The HRF models the fact that the BOLD response peaks about 5 s after the neuronal stimulation and takes about 32 s to go back to baseline, in a slow and smooth fashion, undershooting towards the end before reaching baseline.

We can thus improve our prediction by modifying the box car stimulus function of Fig. 6.10a to take into account the shape of the HRF. This is done through convolution, by assuming a linear time-invariant model. This convolution operation is conceptually the same as the one that was used in the smoothing preprocessing step; that was a convolution in space with a Gaussian kernel, whilst here it is a convolution in time with the canonical HRF. The output of this mathematical operation is displayed in Fig. 6.10b.

Looking at the raw time series of Fig. 6.9a, we can also directly observe that the mean of the signal is not zero; this should also be part of our prediction model. We model the (non-zero) mean of the signal with a predictor that is held constant over time, as shown in Fig. 6.9c.

Furthermore, we can also observe some slow fluctuations in the measured signal: what seems to be the response to the first block of stimulation has a higher amplitude than the response to the last one shown. There are indeed some low-frequency components in fMRI signals; these can be attributed to scanner drift (small changes in the magnetic field of the scanner over time) and/or to the effect of cardiac and respiratory cycles. As slow fluctuations are something that we expect in the data, we should also define predictors for them. A solution is to model the fluctuations through a discrete cosine transform basis set: a linear combination of cosine waves at several frequencies can accommodate a range of fluctuations. In order to remove any function with a cycle longer than 128 s (the default in SPM) and given the sampling rate and the number of scans, nine components are here required in the basis set. The first two components are displayed in Fig. 6.9d, e. Together, the set of cosine waves will effectively act as a high-pass filter with a 128-s cutoff.

Our best prediction of the observed data in Fig. 6.9a will then be a linear superposition of all the effects and confounds defined above and displayed in Fig. 6.9b–e. This is the assumption underlying the general linear model (GLM): the observed response (BOLD signal) y is expressed in terms of a linear combination of explanatory variables plus a well-behaved error term ε (Friston et al. 1994a):

$$y = X\beta + \varepsilon$$

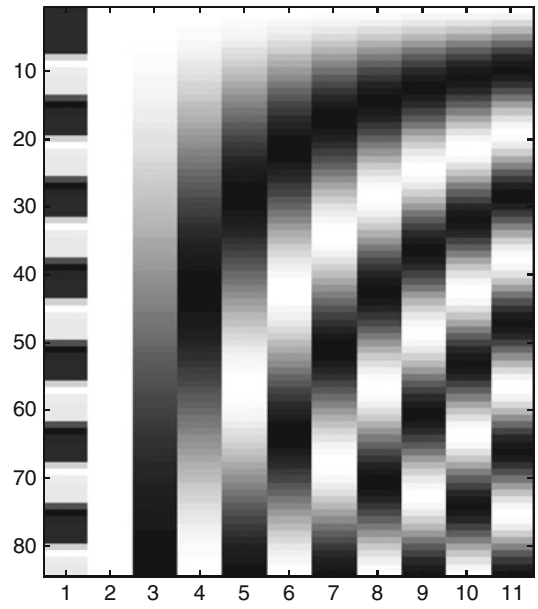

Fig. 6.12 Design matrix for the auditory data set: the first column models the condition-specific effect (boxcar function convolved with the HRF); the next column is a constant term, while the last nine columns are the components of a discrete cosine basis set modelling signal drifts over time. Note that a design matrix as displayed in SPM will not show the last nine terms

The matrix X contains column-wise all the predictors that we have defined: everything we know about the experimental design and all potential confounds. This matrix is referred to as the *design matrix*. The one described so far is depicted in Fig. 6.12: it has 84 rows and 11 columns, each representing a predictor (or explanatory variable, covariate, regressor). This is just another way of representing conjointly the time series of Fig. 6.9 as an image where white represents a high value and black a low one.

The relative contribution of each of these columns to the response is controlled by the parameters β. These are the weights or regression coefficients of the GLM and will correspond to the size of the effects that we are measuring. β is

a vector whose length is the number of regressors in the design matrix, that is, its number of columns. The β-parameters are the unknown factor in this model.

Finally, the error term ε contains everything that cannot be explained by the model; these values are also known as the residuals, that is, the difference between the data y and the model prediction $X\beta$. In the simplest case, ε is assumed to follow a Gaussian distribution with a mean of zero and a standard deviation σ.

The general linear model is a very generic framework that encompasses many standard statistical analysis approaches: multiple regression, analysis of variance (ANOVA), analysis of covariance (ANCOVA) and t tests can all be framed in the context of a GLM and correspond to a particular form of the design matrix.

Fitting the GLM, or inverting the generative model, is the process of estimating its parameters given the data that we observed. This corresponds to adjusting the β-parameters of the model in order to obtain the best fit of the model to the data. Another way of thinking of this is that we need to find the β-parameters that minimise the error term ε. It can be shown that under the assumption that the errors are normally distributed, the parameters can be estimated using the following equation:

$$\hat{\beta} = \left(X^{\mathrm{T}} X\right)^{-1} X^{\mathrm{T}} y$$

This is the ordinary least squares (OLS) equation that relates the estimated parameters $\hat{\beta}$ to the design matrix X and the observed time series y.

Figure 6.13 shows how the GLM with the design matrix shown in Fig. 6.12 fits the time series shown in Fig. 6.9a and reproduced in Fig. 6.13a in blue. The predicted time series is overlaid in red; it is a linear combination of the stimulus function (Fig. 6.13b), the mean whole brain activity (Fig. 6.13c) and the low-frequency drifts (Fig. 6.13d). The residuals are displayed in Fig. 6.13e; they are the difference between the observed time series and its model prediction.

This procedure is repeated for all voxels within the brain, generating maps of the estimated regression coefficients $\hat{\beta}$. The variance of the noise $\hat{\sigma}^2$ is also estimated voxel-wise. As mentioned above, this is essentially a mass-univariate approach: the same model (design matrix X) is fitted independently to the time series at every voxel, providing local estimates of the effect sizes.

Following on from this description of how data are modelled, there are a few more considerations that need to be taken into account:

- In practice, the low-frequency components from the discrete cosine transform (DCT) basis set are not added to the design matrix, but the data and design are instead temporally filtered before the model is estimated. This is mathematically identical but computationally more efficient as drift effects will always be confounds of no interest that are not tested. Hence, in practice they do not appear in the design matrix as in Fig. 6.12, but they are still dealt within the background (and the degrees of freedom of the model are adjusted accordingly).
- When using the canonical HRF to model the transfer function from neuronal activity to BOLD response, we assumed that it was known and fixed. However, in practice this is not actually the case; the HRF varies across brain regions and across individuals. A solution is to use a set of basis functions rather than a single function in order to add some flexibility to the modelling of the response. The HRF will then be modelled as a linear combination of these basis functions. A popular choice, providing flexibility and parsimony, is to use the *informed* basis set: this consists of the canonical HRF and its temporal and dispersion derivatives, as shown in Fig. 6.14. According to the weight given to each of the components, the informed basis set allows us to model a shift in the latency of the response (with the temporal derivative) and changes in the width of the response (with the dispersion derivative). When using the informed basis set, each experimental condition is modelled

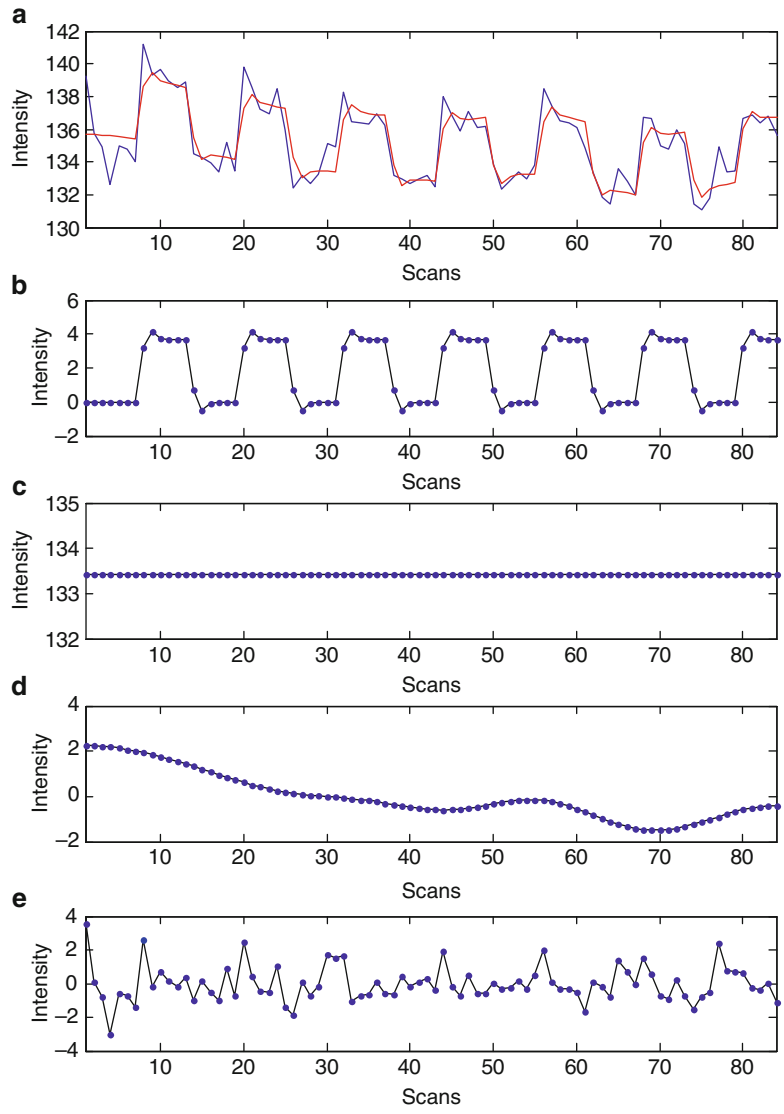

Fig. 6.13 Fit of the GLM defined earlier on the fMRI time series of Fig. 6.9: (**a**) observed fMRI time series in *blue* and model prediction in *red*, fitted predictors for the (**b**) condition-specific effect, (**c**) constant term, (**d**) slow frequency fluctuations and (**e**) residuals

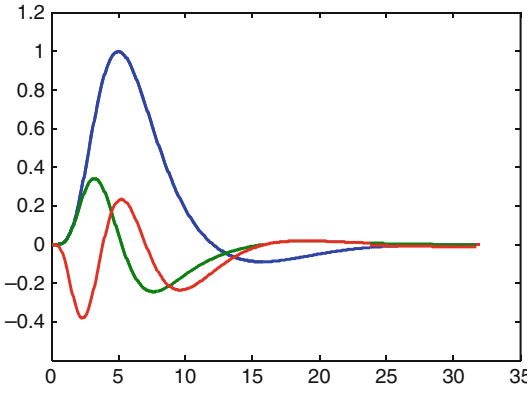

Fig. 6.14 The 'informed' basis set: the canonical HRF (*blue*) and its temporal (*green*) and dispersion (*red*) derivatives

by a set of three regressors, each of which is the neuronal activity stimulus function convolved separately with one of the three components. The predicted response for that condition will be a linear condition of these three regressors. The temporal derivative is also useful to model slice-timing issues. In multislice acquisitions, different slices are acquired at different times. A solution is to temporally realign the data as if they were acquired at the same time through interpolation. This is called slice-timing correction and is a possible option during the preprocessing of the data. Using the informed basis set is an

alternative way to correct for the same effect (please see (Sladky et al. 2011) for a recent comparison of the two approaches).

- fMRI data exhibit short-range serial or temporal correlations. This means that the error at time t is correlated with the error at previous time points. This has to be modelled, because ignoring these correlations may lead to invalid statistical testing. An error covariance matrix must therefore be estimated by assuming some kind of non-sphericity, a departure from the independent and identically distributed assumptions of the noise (Worsley and Friston 1995). A popular model used to capture the typical form of serial correlation in fMRI data is the autoregressive model of order 1, AR(1), relating the error at time t to the error at time $t-1$ with a single parameter. It can be estimated efficiently and precisely by pooling its estimate over voxels. Once the error covariance matrix is estimated, the GLM can be inverted using weighted least squares (WLS) instead of OLS; alternatively, the estimated error covariance matrix can be used to whiten data and design, that is, to *undo* the serial correlation, so that OLS can be applied again. This is the approach implemented in SPM.
- It is also possible to add regressors to the design matrix without going through the convolution process described above. An important example is the modelling of residual movement-related effects. Because movement expresses itself in the data directly and not through any haemodynamic convolution, it can be added directly as a set of explanatory variables. Similarly, in the presence of an abrupt artefact in the data corrupting one scan, a strategy is to model it as a regressor that is zero everywhere but one at that scan. This will effectively covary out that artefactual value in the time series, reducing the inflated variance that it was contributing to. This is better than manually removing that scan prior to analysis as it preserves the temporal process.
- An important distinction in experimental design for fMRI is that between event- and epoch-related designs. Event-related fMRI is simply the use of fMRI to detect responses to individual trials (Josephs et al. 1997). The neuronal activity is usually modelled as a delta function – an *event* – at the trial onset. Practically speaking, in SPM we assume that the duration of a trial is zero. In an epoch-related design, however, we assume that the duration of the trial is greater than zero. This is the case in block-design studies, in which the responses to a sequence of trials (which all evoke the same experimental effect of interest) are modelled together (as an epoch). There are otherwise no conceptual changes in the statistical analysis of event-related and epoch-related (block) designs. One of the advantages of event-related designs is that trials of different types can be intermixed instead of blocking events of the same type together, allowing the measurement of a greater range of psychological effects. There are a number of considerations which impact on the choice of an experimental design, including the constraints imposed by high-pass filtering and haemodynamic convolution of the data affecting its efficiency. We refer interested readers to Chapter 15 of (Friston et al. 2007) or its online version[11] for a thorough examination of design efficiency.

For the auditory data set, the first step is to specify the design matrix; this is done through the 'Specify first-level' button. After specifying a directory in which the results will be stored, the inputs to specify are the units in which the onsets and duration of each trial will be entered (these can be either 'scans' or 'seconds'; we will use 'scans' in this example), the TR (7 s) and the actual preprocessed data to be analysed (the 84 files with an '*sw*' prefix). In this data set, there is just one condition to specify: the onsets are [6 18 30 42 54 66 78], corresponding to the scan number at the beginning of each auditory stimulation block, and the durations are [*6*], indicating that each auditory stimulation block lasts for six scans (with a rest block in between each one). The movement parameters can be added as extra regressors using the 'Multiple regressors' entry by selecting the *'rp_*.txt'* file that was saved during the realignment. Other parameters can be left as default, especially the high-pass filter cut-off

[11] http://imaging.mrc-cbu.cam.ac.uk/imaging/DesignEfficiency

(128 s), the use of the canonical HRF only and the modelling of serial correlation using an AR(1) model. The output is an *SPM.mat* file; this contains all the information about the data and the model design. The design matrix is also displayed for review. As expected, it has eight columns: the first column is the block stimulus function convolved by the HRF, the following six columns are the movement parameters (three translations and three rotations, see Fig. 6.5) and the last column is a constant term modelling the whole brain activity. The 'Estimate' button then allows us to invert this GLM and estimate its parameters. A number of image files will be created, including eight maps of the estimated regression coefficients, one for each column of the design matrix (*beta_*.{hdr,img}*) and one mask image (*mask.{hdr,img}*), which contains a binary volume indicating which voxels were included in the analysis.

6.4.2 Contrasts

Having specified and estimated parameters of the general linear model, the next step is to make a statistical inference about those parameters. This is done by using their estimated variance. Some of the parameters will be of interest (those pertaining to the experimental conditions), while others will be of no interest (those pertaining to confounding effects). Inference allows one to test the null hypothesis that all the estimates are zero, using the *F*-statistic to give an *SPM{F}*, or that some particular linear combination (e.g. a subtraction) of the estimates is zero, using the *t*-statistic to give an *SPM{t}*. A linear combination of regression coefficients is called a *contrast*, and its corresponding vector of weights *c* is called a contrast vector.

The *t*-statistic is obtained by dividing a contrast (specified by contrast weights) of the associated parameter estimates by the standard error of that contrast. The latter is estimated using the variance of the residuals $\hat{\sigma}^2$.

$$T = \frac{c^{\mathrm{T}}\hat{\beta}}{\sqrt{\hat{\sigma}^2 c^{\mathrm{T}}(X^{\mathrm{T}}X)^{-1}c}}$$

This is essentially a signal-to-noise ratio, comparing an effect size with its precision.

An example of a contrast vector would be $c^{\mathrm{T}} = [1 \quad -1 \quad 0 \ldots]$ to compare the difference in responses evoked by two conditions, modelled by the first two condition-specific regressors in the design matrix. In SPM, a *t* test is signed, in the sense that a contrast vector $c^{\mathrm{T}} = [1 \quad -1 \quad 0 \ldots]$ is looking for a greater response in the first condition than in the second condition, while a contrast $c^{\mathrm{T}} = [-1 \quad 1 \quad 0 \ldots]$ is looking for the opposite effect. In other words, it means that a *t*-contrast tests the null hypothesis $c^{\mathrm{T}}\beta = 0$ against the one-sided alternative $c^{\mathrm{T}}\beta > 0$. The resulting *SPM{t}* is a statistic image, with each voxel value being the value of the *t*-statistic for the specified contrast at that location. Areas of the *SPM{t}* with high voxel values (higher than one might expect by chance) indicate evidence for 'neural activations'.

Similarly, if you have a design where the third column in the design matrix is a covariate, then the corresponding parameter is essentially a regression slope, and a contrast with weights $c^{\mathrm{T}} = [0 \quad 0 \quad 1 \quad 0 \ldots]$ tests the hypothesis of zero regression slope, against the alternative of a positive slope. This is equivalent to a test of no correlation, against the alternative of positive correlation. If there are other terms in the model beyond a constant term and the covariate, then this correlation is a partial correlation, the correlation between the data and the covariate after accounting for the other effects (Andrade et al. 1999).

Sometimes, several contrasts of parameter estimates are jointly interesting. In these instances, an *SPM{F}* is used and is specified with a matrix of contrast weights which can be thought of as a collection of *t*-contrasts. An *F*-contrast might look like this

$$c^{\mathrm{T}} = \begin{bmatrix} 1 & 0 & 0 & 0 & \ldots \\ 0 & -1 & 0 & 0 & \ldots \end{bmatrix}$$

This would test for the significance of the first or the second parameter estimates. The fact that the second weight is negative has no effect on the test because the *F*-statistic is blind to sign as it is based on sums of squares. The *F*-statistic can

also be interpreted as a model comparison device, comparing two nested models using the extra sum-of-squares principle. For the *F*-contrast above, this corresponds to comparing the specified full model with a reduced model where the first two columns would have been removed. *F*-contrasts are mainly used either as two-sided tests (the *SPM{F}* then being the square of the corresponding *SPM{t}*) or to test the significance of effects modelled by several columns. Effects modelled by several columns might include the use of a multiple basis set to model the HRF, a polynomial expansion of a parametric modulated response or a contrast testing more than two levels in a factorial design.

As with the *SPM{t}*, the resulting *SPM{F}* is a statistic image, with voxel values the value of the *F*-statistic for the specified contrast at that location. Areas of the *SPM{F}* with high voxel values indicate evidence for 'neural activations'.

6.4.3 Topological Inference

Having computed the statistic, we need to decide whether it represents convincing evidence of the effect in which we are interested; this decision is the process of making a statistical inference. This is done by testing the statistic against the null hypothesis that there is no effect. Here, the null hypothesis is distributed according to a known parametric probability density function, a Student's *t*- or *F*-distribution. Then, by choosing a significance level (which is the level of control over the false-positive error rate, usually chosen as *0.05*), we can derive a critical threshold above which we will reject the null hypothesis and accept the alternative hypothesis that there is convincing evidence of an effect. If the observed statistic is lower than the critical threshold, we fail to reject the null hypothesis and we must conclude that there is no convincing evidence of an effect. A *p* value can also be computed to measure the evidence against the null hypothesis: this is the probability of observing a statistic at least as large as the one observed under the null hypothesis (i.e. by chance).

The problem we face in functional imaging is that we are not dealing with a single statistic value, but with an image that comprises many thousands of voxels and their associated statistical values. This gives rise to the multiple comparisons problem, which is a consequence of the use of a mass-univariate approach: as a general rule, without using an appropriate method of correction, the greater the number of voxels tested, the greater the number of false positives. This is clearly unacceptable and requires the definition of a new null hypothesis which takes into account the whole volume, or family, of statistics contained in an image: the *family-wise* null hypothesis that there is no effect *anywhere* in the entire search volume (e.g. the brain). We then aim to control the family-wise error rate (FWER) – the probability of making one or more false positives over the entire search volume. This results in adjusted *p* values, *corrected* for the search volume.

A traditional statistical method for controlling FWER is to use the Bonferroni correction, in which a voxel-wise significance level simply corresponds to the family-wise significance level (e.g. 0.05) divided by the number of tests (i.e. voxels). However, this approach assumes that every test (voxel statistic) is independent and is too conservative to use in the presence of correlation between tests, such as the case with functional imaging data. Functional imaging data are intrinsically smoothed due to the acquisition process and have also been smoothed as part of the spatial preprocessing; neighbouring voxel statistics are therefore not independent. The random field theory (RFT) provides a way of adjusting the *p* value to take this into account (Worsley et al. 1992; (Friston et al. 1994b; Worsley et al. 1996). Providing that data are smooth, the RFT adjustment is less severe (i.e. more sensitive) than a Bonferroni correction for the number of voxels. The *p* value is a function of the search volume and *smoothness* (parameterised as the FWHM of the Gaussian kernel required to simulate images with the same apparent spatial smoothness as the one we observe). A description of the random field theory is well beyond the scope of this chapter, but it is worth mentioning that one of the

assumptions for its application on discrete data fields is that the observed fields are smooth. This was one of the motivations for smoothing the fMRI data as a preprocessing step. In practice, smoothness will be estimated from the data themselves (to take into account both intrinsic and explicit smoothness) (Kiebel et al. 1999). The RFT correction discounts voxel sizes by expressing the search volume in terms of smoothness or resolution elements (*resels*).

To make inferences about regionally specific effects, the SPM is thresholded using height and spatial extent thresholds that are specified by the user. Corrected *p* values can then be derived that pertain to topological features of the thresholded map (Friston et al. 1996a):

- The number of activated regions (i.e. the number of clusters above the height and volume threshold). These are *set-level* inferences.
- The number of activated voxels (i.e. the volume or extent) comprising a particular cluster. These are *cluster-level* inferences.
- The height of each local maxima, or peak, within that cluster. These are *peak-level* inferences.

Set-level inferences are generally more powerful than cluster-level inferences, which are themselves generally more powerful than peak-level inferences. The price paid for this increased sensitivity is a reduced localising power. Peak-level tests permit individual maxima to be identified as significant, whereas cluster and set-level inferences only allow clusters or a set of clusters to be declared significant. In some cases, however, focal activation might actually be detected with greater sensitivity using tests based on peak height (with a spatial extent threshold of zero). In practice, this is the most commonly used level of inference, reflecting the fact that characterisation of functional anatomy is generally more useful when specified with a high degree of anatomical precision.

When making inferences about regional effects in SPMs, one often has some idea *a priori* about where the activation should be. In this instance, a correction for the entire search volume is inappropriately stringent. Instead, a small search volume within which analyses will be carried out can be specified beforehand, and an RFT correction applied restricted to that region only (Worsley et al. 1996). This is often referred to as a small volume correction (SVC).

For the auditory data set, inference is performed through the 'Results' button by selecting the *SPM.mat* file from the previous step. To test for the positive effect of passive listening to words versus rest, the *t*-contrast to enter is $c^{\mathrm{T}} = [1 \quad 0 \quad 0 \quad 0 \quad 0 \quad 0 \quad 0 \quad 0]$. Two files will be created on disk at this stage: a *con_0001.{hdr,img}* file of the contrast image (here identical to *beta_0001.{hdr,img}*) and the corresponding *SPM{T} spmT_0001.{hdr,img}*. Choosing a 0.05 FWE-corrected threshold yields the results displayed in Fig. 6.15. The maximum intensity projection (MIP) image gives an overview of the activated regions, the auditory cortices. This can be overlaid on the anatomy of the subject (the normalised '*wm*.img*' image file) using the menu entry 'Overlays > Sections' of the Interactive window. The button 'whole brain' will display the results table (see Fig. 6.16) listing the *p* values adjusted for the search volume (the whole brain here) for all topological features of the excursion set: local maxima height for peak-level inference, cluster extent for cluster-level inference and number of clusters for set-level inference. The footnote of the results table lists some numbers pertaining to the RFT: the estimated FWHM smoothness is [*10.9*, *10.9*, *9.2*] in mm and the number of resels is 1,450 here. These are the values reflecting the size and smoothness of the search volume that are used to control for the FWER.

Guidelines for reporting an fMRI study in a publication are given in Poldrack et al. (2008).

6.4.4 Population-Level Inference

Neuroimaging data from multiple subjects can be analysed using fixed-effects (FFX) or random-effects (RFX) analyses (Holmes and Friston 1998). FFX analysis is used for reporting case studies, while RFX is used to make inferences about the population from which the subjects were drawn. In the former, the error variance is estimated on a scan-by-scan basis and contains contributions from within-subject variance only. We are therefore not

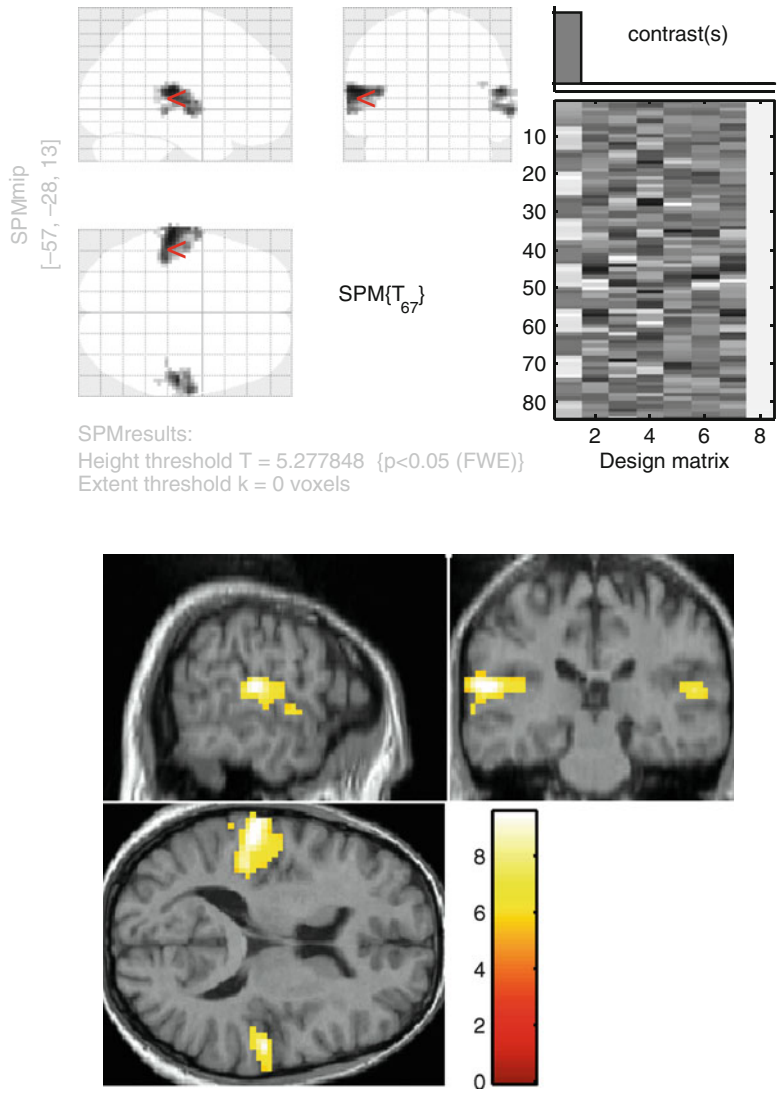

Fig. 6.15 Results of the statistical inference for the auditory data set when looking for regions showing an increased activity when words are passively listened to in comparison with rest. *Top right*: design matrix and contrast $c^{\mathrm{T}} = [1 \quad 0 \quad 0 \quad 0 \quad 0 \quad 0 \quad 0 \quad 0]$. *Top left*: *SPM{t}* displayed as a maximum intensity projection over three orthogonal planes. To control for $p < 0.05$ corrected, the applied threshold was $T = 5.28$. *Lower panel*: Thresholded *SPM{t}* overlaid on the normalised structural scan of that subject, highlighting the bilateral activation

making formal inference about population effects using FFX, but are restricted to informal inferences based on separate case studies or summary images showing the average group effect. (This is implemented in SPM by concatenating data from all subjects into the same GLM, simply modelling subjects as coming from separate sessions.) Conversely, random-effects analyses take into account both sources of variance (within- and between-subject). The term '*random effect*' indicates that we have accommodated the randomness of different responses from subject to subject.

Both analyses are perfectly valid but only in relation to the inferences that are being made: inferences based on fixed-effect analyses are about the particular subjects studied. Random-effects

Statistics: p-values adjusted for search volume

set-level		cluster-level				peak-level					mm mm mm		
p	c	$p_{FWE\text{-}corr}$	$q_{FDR\text{-}corr}$	k_E	p_{uncorr}	$p_{FWE\text{-}corr}$	$q_{FDR\text{-}corr}$	T	$(Z_{\equiv})$	p_{uncorr}			
0.000	5	0.000	0.000	328	0.000	0.000	0.000	9.58	7.58	0.000	–57	–28	13
						0.000	0.000	8.34	6.88	0.000	–42	–31	13
						0.000	0.000	8.31	6.87	0.000	–66	–13	4
		0.000	0.000	151	0.000	0.000	0.000	8.97	7.25	0.000	57	–22	13
						0.000	0.000	8.26	6.84	0.000	66	–13	–2
						0.000	0.001	7.38	6.29	0.000	54	–13	1
		0.002	0.072	4	0.043	0.003	0.106	6.02	5.36	0.000	42	–31	19
		0.015	0.288	1	0.288	0.034	0.757	5.38	4.89	0.000	69	–25	–2
		0.015	0.288	1	0.288	0.039	0.800	5.35	4.86	0.000	72	–34	–8

table shows 3 local maxima more than 8.0mm apart

Height threshold: T = 5.28, p = 0.000 (0.050)
Extent threshold: k = 0 voxels, p = 1.000 (0.050)
Expected voxels per cluster, <k> = 0.957
Expected number of clusters, <c> = 0.05

Degrees of freedom = [1.0, 67.0]
FWHM = 10.9 10.9 9.2 mm mm mm; 3.6 3.6 3.1 {voxels}
Volume: 1778922 = 65886 voxels = 1449.9 resels
Voxel size: 3.0 3.0 3.0 mm mm mm; (resel = 40.60 voxels)

Fig. 6.16 Results table summarising the inferences made with the *t*-contrast $c^{T} = [1 \quad 0 \quad 0 \quad 0 \quad 0 \quad 0 \quad 0 \quad 0]$, adjusted for the search volume (the whole brain in this case). See text for description of the key elements

analyses are usually more conservative but allow the inference to be generalised to the population from which the subjects were drawn.

In practice, RFX analyses can be implemented using the computationally efficient '*summary-statistic*' approach. Contrasts of parameters estimated from a *first-level* (within-subject) analysis are entered into a *second-level* (between-subject) analysis. The second-level design matrix then simply tests the null hypothesis that the contrasts are zero (and is usually a column of ones, implementing a one-sample *t* test). The validity of the approach rests upon the use of balanced designs (all subjects have identical design matrices and error variances) but has been shown to be remarkably robust to violations of this assumption (Mumford and Nichols 2009).

For our auditory data set, if we had scanned 12 subjects, for example, each of whom performed the same task, the group analysis would entail (i) applying the same spatial preprocessings to each of the 12 subjects, (ii) fitting a first-level GLM independently to each of the 12 subjects, (iii) defining the effect of interest for each subject with a contrast vector $c^{T} = [1 \quad 0 \quad 0 \quad 0 \quad 0 \quad 0 \quad 0 \quad 0]$ and producing a contrast image containing the contrast of the parameter estimates at each voxel and (iv) feeding each of the 12 contrast images into a second-level GLM, through which a one-sample *t* test could be carried out across all 12 subjects to find the activations that show significant evidence of a population effect.

6.5 Conclusions

In this chapter we have described how statistical parametric mapping can be used to identify and characterise regionally specific effects in functional MRI data. We have also illustrated the principles of SPM through the analysis of a block-design data set using the SPM software. After preprocessing the data to correct them for movement and normalise them into a standard space, the general linear model and random field theory are used to analyse and make classical inferences. The GLM is used to model BOLD responses to given experimental manipulations. The estimated parameters of the GLM are used to compute a standard univariate statistical test at each and every voxel, leading to the construction of statistical parametric maps. The random field theory is then used to resolve the multiple comparisons problem induced by inferences over a

volume of the brain containing many voxels. RFT provides a method for adjusting p values for the search volume of a statistical parametric map to control false-positive rates.

We have here described the fundamental methods used to carry out fMRI analyses in SPM. There are, however, many additional approaches and tools that can be used to refine and extend analyses, such as voxel-based morphometry (VBM) to analyse structural data sets (Ashburner and Friston 2000; Ridgway et al. 2008) and dynamic causal modelling (DCM) to study effective connectivity (Friston et al. 2003; Seghier et al. 2010; Stephan et al. 2010). While the key steps of the SPM approach we describe above remain broadly constant, SPM software (along with many other software analysis packages) is constantly evolving to incorporate advances in neuroimaging analysis; we encourage readers to explore these exciting new developments.

References

Andersen SM, Rapcsak SZ et al (2010) Cost function masking during normalization of brains with focal lesions: still a necessity? Neuroimage 53:78–84. doi:10.1016/j.neuroimage.2010.06.003

Andersson JLR, Hutton C et al (2001) Modeling geometric deformations in EPI time series. Neuroimage 13:903–919. doi:10.1006/nimg.2001.0746

Andrade A, Paradis AL et al (1999) Ambiguous results in functional neuroimaging data analysis due to covariate correlation. Neuroimage 10:483–486. doi:10.1006/nimg.1999.0479

Ashburner J (2011) SPM: a history. Neuroimage. doi:10.1016/j.neuroimage.2011.10.025

Ashburner J, Friston KJ (1999) Nonlinear spatial normalization using basis functions. Hum Brain Mapp 7:254–266

Ashburner J, Friston KJ (2000) Voxel-based morphometry – the methods. Neuroimage 11:805–821. doi:10.1006/nimg.2000.0582

AshburnerJ,FristonKJ(2005)Unifiedsegmentation.Neuroimage 26:839–851. doi:10.1016/j.neuroimage.2005.02.018

Brett M, Leff AP et al (2001) Spatial normalization of brain images with focal lesions using cost function masking. Neuroimage 14:486–500. doi:10.1006/nimg.2001.0845

Brett M, Johnsrude IS et al (2002) The problem of functional localization in the human brain. Nat Rev Neurosci 3:243–249. doi:10.1038/nrn756

Collignon A, Maes F et al (1995) Automated multimodality image registration based on information theory. In: Proceedings of information processing in medical imaging (IPMI), Ile de Berder, 1995

Crinion J, Ashburner J et al (2007) Spatial normalization of lesioned brains: performance evaluation and impact on fMRI analyses. Neuroimage 37:866–875. doi:10.1016/j.neuroimage.2007.04.065

Fox PT (1995) Spatial normalization origins: objectives, applications, and alternatives. Hum Brain Mapp 3:161–164. doi:10.1002/hbm.460030302

Friston KJ, Frith CD et al (1991) Comparing functional (PET) images: the assessment of significant change. J Cereb Blood Flow Metab 11:690–699. doi:10.1038/jcbfm.1991.122

Friston KJ, Holmes AP et al (1994a) Statistical parametric maps in functional imaging: a general linear approach. Hum Brain Mapp 2:189–210. doi:10.1002/hbm.460020402

Friston KJ, Worsley KJ et al (1994b) Assessing the significance of focal activations using their spatial extent. Hum Brain Mapp 1:210–220. doi:10.1002/hbm.460010306

Friston KJ, Ashburner J et al (1995) Spatial registration and normalization of images. Hum Brain Mapp 3:165–189. doi:10.1002/hbm.460030303

Friston KJ, Holmes A et al (1996a) Detecting activations in PET and fMRI: levels of inference and power. Neuroimage 4:223–235. doi:10.1006/nimg.1996.0074

Friston KJ, Williams S et al (1996b) Movement-related effects in fMRI time-series. Magn Reson Med 35:346–355

Friston KJ, Harrison L et al (2003) Dynamic causal modelling. Neuroimage 19:1273–1302

Friston K, Ashburner J et al (2007) Statistical parametric mapping: the analysis of functional brain images. Elsevier/Academic, Amsterdam/Boston

Holmes A, Friston K (1998) Generalisability, random effects and population inference. Neuroimage 7:S754

Jezzard P, Balaban RS (1995) Correction for geometric distortion in echo planar images from B0 field variations. Magn Reson Med 34:65–73

Josephs O, Turner R et al (1997) Event-related fMRI. Hum Brain Mapp 5:243–248

Kiebel SJ, Poline JB et al (1999) Robust smoothness estimation in statistical parametric maps using standardized residuals from the general linear model. Neuroimage 10:756–766. doi:10.1006/nimg.1999.0508

Mazziotta JC, Toga AW et al (1995) A probabilistic atlas of the human brain: theory and rationale for its development. The international consortium for brain mapping (ICBM). Neuroimage 2:89–101

Mumford JA, Nichols T (2009) Simple group fMRI modeling and inference. Neuroimage 47:1469–1475. doi:10.1016/j.neuroimage.2009.05.034

Poldrack RA, Fletcher PC et al (2008) Guidelines for reporting an fMRI study. Neuroimage 40:409–414. doi:10.1016/j.neuroimage.2007.11.048

Ridgway GR, Henley SMD et al (2008) Ten simple rules for reporting voxel-based morphometry studies.

Neuroimage 40:1429–1435. doi:10.1016/j.neuroimage.2008.01.003

Seghier ML, Zeidman P et al (2010) Identifying abnormal connectivity in patients using dynamic causal modeling of FMRI responses. Front Syst Neurosci. doi:10.3389/fnsys.2010.00142

Sladky R, Friston KJ et al (2011) Slice-timing effects and their correction in functional MRI. Neuroimage 58:588–594. doi:10.1016/j.neuroimage.2011.06.078

Stephan KE, Penny WD et al (2010) Ten simple rules for dynamic causal modeling. Neuroimage 49:3099–3109. doi:10.1016/j.neuroimage.2009.11.015

Talairach J, Tournoux P (1988) Co-planar stereotaxic atlas of the human brain: an approach to medical cerebral imaging. Thieme Medical, New York

Unser M, Aldroubi A et al (1993) B-spline signal processing. I. Theory. IEEE Trans Signal Process 41:821–833. doi:10.1109/78.193220

Wells WM 3rd, Viola P et al (1996) Multi-modal volume registration by maximization of mutual information. Med Image Anal 1:35–51

Worsley KJ, Friston KJ (1995) Analysis of fMRI time-series revisited – again. Neuroimage 2:173–181. doi:10.1006/nimg.1995.1023

Worsley K, Evans A et al (1992) A three-dimensional statistical analysis for CBF activation studies in human brain. J Cereb Blood Flow Metab 12:900–918

Worsley KJ, Marrett S et al (1996) A unified statistical approach for determining significant signals in images of cerebral activation. Hum Brain Mapp 4:58–73

Meta-Analyses in Basic and Clinical Neuroscience: State of the Art and Perspective

7

Simon B. Eickhoff and Danilo Bzdok

7.1 An Introduction to Quantitative Meta-Analysis in Neuroimaging Science

While a major overarching goal of systems neuroscience research is to unveil the dysfunctional neural mechanisms that underlie neurological and psychiatric disorders, such endeavor will be futile without a profound understanding of the physiological organization of brain functions. That is, to appreciate the relationship between localized changes in brain structure or function and pathological mental states or functional impairments, we have to elucidate the regionally specific localization of mental processes. Until about 20 years ago, the most common approaches to localize human brain functions consisted in lesion studies and direct brain stimulation during neurosurgical interventions. The beginning of the functional neuroimaging era by positron emission tomography (PET) and functional magnetic resonance imaging (fMRI) then enabled the noninvasive, in vivo investigation of functional specialization in the human brain. Based on local changes in cerebral blood flow, glucose or oxygen metabolism, these techniques allow the identification of regional increases in neural activation during the performance of specific tasks. Usually, the neural correlates of a given task (reflecting a mental process of interest) are isolated by subtraction of the activation measured during a closely related task (i.e., control task) that is supposed not to evoke the psychological process of interest. Evidently, the spectrum of neuroimaging-compatible tasks is practically only limited by the scanner surroundings and the interdiction of head movements. In fact, the constantly increasing publication rate currently counts more than 1,000 new neuroimaging articles per year (Derrfuss and Mar 2009). Functional neuroimaging has hence provided a wealth of information on the cerebral localization of sensory processing, motor actions, as well as cognitive and affective functions.

In spite of its success in revealing the location of regionally specific effects in health and disease, however, functional neuroimaging using PET or fMRI suffers from several limitations that restrict the amount of knowledge that may be gained from each individual imaging experiment:

First, there is the small sample size. Usually, between 15 and 30 subjects participate in a neuroimaging study. Although this denotes a remarkable increase since the beginnings of neuroimaging science, it is still a rather small sample

S.B. Eickhoff (✉)
Institut für Klinische Neurowissenschaften und Medizinische Psychologie, Heinrich-Heine Universität Düsseldorf, Düsseldorf, Germany

Institut für Neurowissenschaften und Medizin (INM-2), Forschungszentrum Jülich GmbH, Jülich 52425, Germany
e-mail: s.eickhoff@fz-juelich.de

D. Bzdok
Institut für Neurowissenschaften und Medizin (INM-2), Forschungszentrum Jülich GmbH, Jülich 52425, Germany
e-mail: danilo.bzdok@rwth-aachen.de

S. Ulmer, O. Jansen (eds.), *fMRI – Basics and Clinical Applications*,
DOI 10.1007/978-3-642-34342-1_7,

size comparing to other scientific disciplines, such as social sciences, population genetics, or clinical trials. Moreover, in contrast to, for example, experimental psychology, the considerable logistical and financial efforts of each neuroimaging study discourage replication studies as well as the combination of several studies into one paper, leading at times to the publication of isolated findings. It must be remembered that both PET and fMRI scanners measure neuronal activity in an indirect way by the triggered regional increases of metabolic respectively hemodynamic brain activity. On the one hand, the recorded signals are thus potentially confounded by a vast range of biological, technical, and methodological factors, which reduce the reliability of the obtained results. In fact, the underlying relationship between neuronal activity and measured signals is currently not exhaustively understood. On the other hand, PET and fMRI yield relative, rather than absolute, signals related to neuronal activity. The neural correlates underlying a given psychological task thus need to be derived by subtraction between two experimental conditions rendering the resulting activation pattern context dependent. In fact, it has repeatedly been questioned that conclusions on general physiological or pathological mechanisms can be drawn if relying on the neuroimaging-inherent subtraction logic (Stark and Squire 2001). In other words, even though frequently discussed in terms of general mechanisms, the results of a particular neuroimaging study actually just impart the difference of the two specifically chosen conditions.

These diverse limitations of any neuroimaging study thus severely lessen the amount of knowledge that may be gained from each individual neuroimaging study. This consideration has consequently prompted a need for synthesizing and integrating existing research. By judging concordance and variability across a high number of studies, the limitation of each individual PET or fMRI experiment may be overcome, and a synoptic view on published isolated findings can be acquired. Therefore, the sheer abundance of available neuroimaging studies encouraged the development of quantitative meta-analysis approaches. Such model-based neuroinformatic methods allow statistically summarizing hundreds of neuroimaging studies across a large number of participants and diverse experimental settings, which considerably strengthens ensuing conclusions on the organizational principles of the healthy and diseased brain.

In the course of the last years, the field of quantitative meta-analysis has been increasingly dominated by methods for coordinate-based meta-analysis (CBMA). Image-based meta-analysis (Schilbach et al. 2008), on the other hand, draws on the full statistic images and, thus, acknowledges the entirety of the spatial information of each neuroimaging experiment. Yet, these approaches usually rely on a much smaller experiment samples, as the original data is often considerably more difficult to obtain than activation coordinates and only comparable contrast images are eligible. Rather than pooling raw data or complete activation maps of previous neuroimaging experiments, CBMA only assesses convergence of the reported peak coordinates. As algorithms for CBMA hence rest on the model-based integration of published activation coordinates, they can potentially be applied to the entirety of the available literature. Applying CBMA to the published neuroimaging experiments on a specific topic (e.g., the brain areas related to grammar processing) thus permits to identify the quintessence of emergent knowledge in that entire field in an unbiased fashion without being skewed by experimental idiosyncrasies or neuroanatomical variability.

To this end, CBMA tries to answer the following question: where in the brain do the included activation foci cluster more tightly than it would be expected if they were randomly distributed? In statistical terms, the assumption of random distribution of the considered activation foci will be rejected in those voxels where the amount of convergence between reported foci is greater than expected by chance, yielding statistically defensible inference on the integration of previous findings. Taken together, CBMA is able to objectively synthesize large amounts of neuroimaging data and overcome the limitations of each individual experiment raised above.

7.2 Preconditions and Preliminaries of Quantitative Meta-Analysis

The feasibility and potential of quantitative integration for functional neuroimaging results is greatly aided by the high standardization for the reporting of neuroimaging data, which is brought upon by two important preconditions that thus paved the way for the emergence of meta-analyses. First, almost from the beginning of neuroimaging research, investigators adopted common stereotactic coordinate systems for specifying localization information, rather than relying purely on neuroanatomical nomenclatures. That is, most neuroimaging articles report significant activation foci according to either the Talairach-Tournoux (1988) or Montreal Neurological Institute [MNI; (Evans et al. 1992)] 3D reference space, which can be easily converted into each other (Lancaster et al. 2007). A common coordinate system is crucial because neuroimaging data is formally processed by cubical "voxels" and not by brain regions. The variably sized and shaped "native" brains of the participants therefore need to be warped to a "standard" brain space to enable comparison within and across neuroimaging studies. Second, results of functional imaging experiments are conventionally reported as coordinates for local maxima in standard coordinates provided in tables grouped by the contrast experiment from which they were derived. That is, tables usually provide all peak coordinates of significant differences in brain activity for each comparison between two conditions. These early established standards for spatial normalization to common reference systems and for communicating activation results as coordinates in these reference spaces greatly contributed to the accessibility of existing neuroimaging studies.

Any meta-analysis starts out by a thorough literature search for relevant publications pertaining to the research question. Literature databases, such as PubMed (www.ncbi.nlm.nih.gov), ISI Web of Knowledge (apps.webofknowledge.com), and PsycINFO (www.apa.org/pubs/databases/psycinfo), are powerful tools to find relevant papers by means of keywords search. Such a database search should be complemented by means of tracing the citations in the thus retrieved papers and review articles. Moreover, coordinate databases, BrainMap currently being the most comprehensive one (www.brainmap.org), allow searching relevant papers by means of brain locations or paradigm classes.

As for any meta-analysis, the thoughtful choice of judicious inclusion criteria is a crucial step of the analysis, given their obvious impact on the outcome of the analysis. Absolute inclusion criteria embrace considering only either neurotypicals (i.e., healthy subjects) or a specific clinical population (but not mixing these two), either focusing on or completely excluding pharmacological manipulation, exclusive consideration of studies that report coordinates provided in a standard reference space (Talairach/Tournoux, MNI), and reliance on full-brain coverage (versus analyses based on ROIs or functional localizers). Relative inclusion criteria, however, depend on the actual research question and may embrace specific contrast analyses, paradigms, stimulus material, or experimental instructions. For instance, only including target-versus-baseline contrasts would aim at identifying *all* the neural correlates underlying a given psychological process, while only including target-versus-control contrasts would aim at identifying only the *specific* neural correlates underlying a given psychological process.

Please note that within the realms of coordinate-based meta-analysis (CBMA), the term "experiment" usually refers to any single analysis on imaging data yielding localization information, while the term "study" usually refers to a scientific publication reporting one or more "experiments." Following this definition, a contrast analysis between two conditions and a correlation of brain activity with participants' reaction times would, for instance, make up two "experiments" whose activation coordinates are summarized in the tables of the one "study" publishing these results. The coordinates collected from all the eligible studies on a given topic are then to be summarized in a table, which forms the input for the CBMA algorithm.

7.3 Activation Likelihood Estimation

The most important algorithm for coordinate-based meta-analysis is activation likelihood estimation (ALE), proposed by Peter Turkeltaub et al. (2002). The key idea behind ALE resides in considering each included activation focus as a center of probability distribution instead of a dimensionless point in the voxel-scaled brain (Fig. 7.1a). This accounts for the spatial uncertainty associated with neuroimaging results, as it assumes that the true location of an activation is most likely at the reported coordinate but it may also be with finite possibility in its vicinity. Hence, the unit reflecting activation information in that 3D space is not binary (i.e., activated or not) but dimensional (i.e., more or less probable activation). In other words, the probability of "true" activation is regarded to diminish gradually with increasing distance from a reported activation peak.

As a first step, ALE therefore models foci as centers for 3D Gaussian probability distributions that capture the spatial uncertainty associated with each focus. This probability distribution acknowledges the uncertainty that arises mainly from between-subject variances, attributable in large extent to neuroanatomical variability and small sample sizes, as well as between-laboratory variances, attributable in large extent to different normalization strategies and brain templates across laboratories. These two sources of uncertainty used to be gauged subjectively by the investigator, which has recently been replaced by empirical estimates (Eickhoff et al. 2009). Moreover, the width of the spatial uncertainty of any focus is adjusted by the number of subjects that participated in the corresponding experiment. Put concretely, the more participants contributed to a study, the bigger the likelihood of "true" activation near the foci reported in that study; hence, the modeled spatial uncertainty around this studies' foci becomes smaller and the influence of those foci on the outcome of the meta-analysis larger.

In a second step, the probability distributions of all activation foci in a given experiment are combined for each voxel, yielding a so-called modeled activation map (MA map). The MA map can hence be thought of as a 3D summary of the results reported in that experiment, taking into account the spatial uncertainty associated with the reported coordinates. The final ALE map, comprising the voxel-wise ALE scores, then results from the union across these MA maps (Fig. 7.1b). The ALE map thus indicates the convergence across experiments at each particular location, which is subsequently assessed for statistical significance. More specifically, the original implementation of the ALE approach (Turkeltaub et al. 2002) was designed to test for above-chance clustering of individual *foci* instead of results from different *experiments*, invoking a fixed-effects analysis. In the current implementation (Eickhoff et al. 2009), the within-experiment distribution of foci is regarded to be fixed, hence testing for above-chance clustering of *experiments*, rather than *foci*, invoking a random-effects analysis. Importantly, only random-effects analyses allow extrapolation of the findings beyond the considered data set (Penny and Holmes 2004). Put differently, obsolete testing for convergence between *foci* only allowed conclusions about the very neuroimaging studies included in the meta-analysis, while testing for convergence between *experiments* allows conclusions about studies not included in the meta-analysis as well as about the investigated psychological state per se. Taken together, the ALE approach represents each included experiment as a modeled activation probability map (i.e., MA map) that was derived from the union of the Gaussian probabilities of that experiment's activation foci. These MA maps are then combined voxel-wise to yield the final ALE maps that indicate the likelihood of convergence between the considered experiments.

The third and last step distinguishes between random and "true" convergence by comparing the computed ALE map against a null distribution that reflects a random spatial association between the experiments' MA maps. That is, the null distribution indicates the voxel-wise ALE values that would be observed if the considered

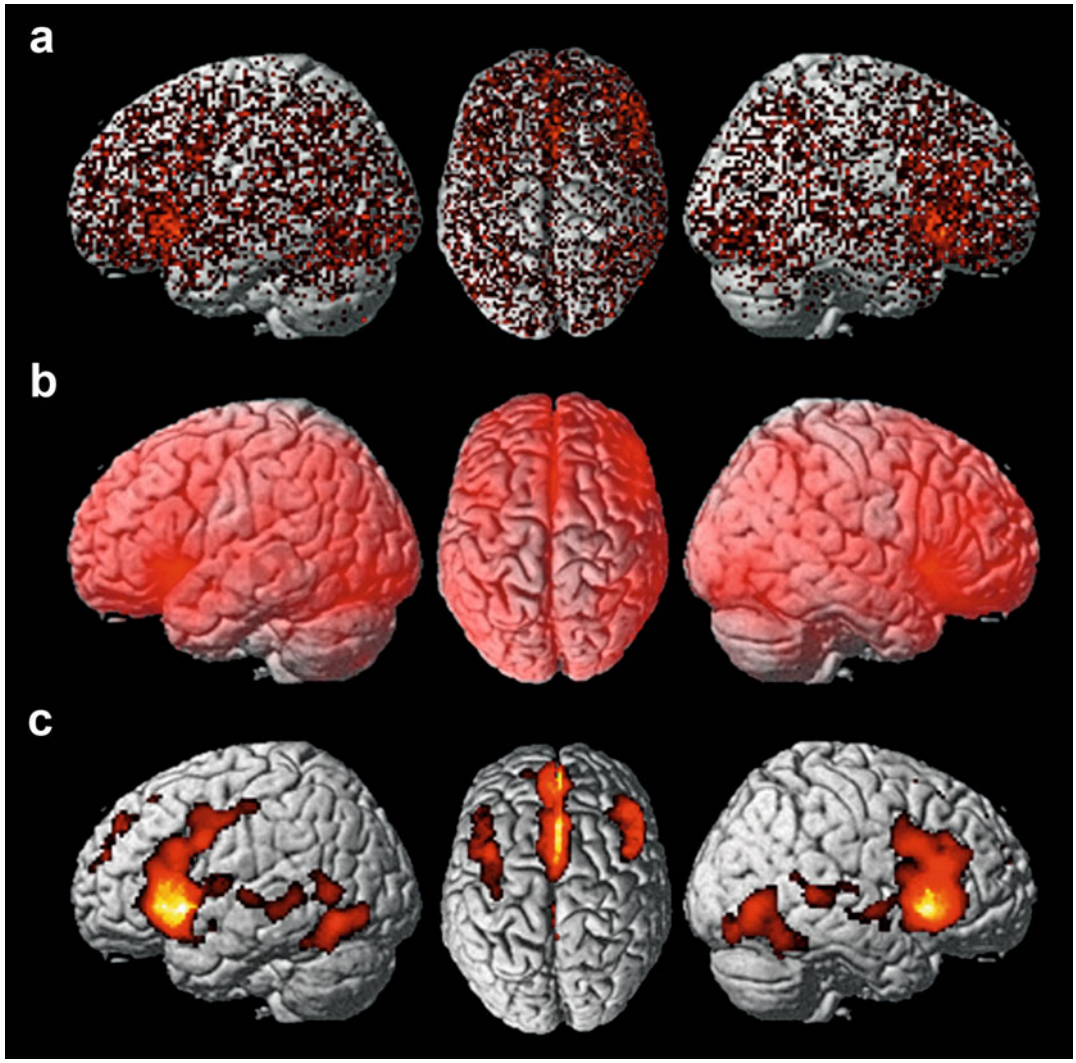

Fig. 7.1 (**a**) Reported peak locations of 2,393 individual neuroimaging experiments in 35,386 healthy participants related to the neural correlates involved in various paradigms on emotion processing (experiments provided by the BrainMap database). (**b**) Shows the unified "activation likelihood estimations" (i.e., union of modeled probability distributions) which describes the local convergence across the included neuroimaging experiments. (**c**) Significant voxels are determined as a function of whether the corresponding ALE score is higher than it would be expected if all included neuroimaging experiments converged completely by chance. This panel shows the significant convergence across experiments after correction for multiple comparisons

experiments converged entirely by chance. While most CBMA approaches proposed so far rely on a computationally expensive permutation procedure to obtain the null distribution (Wager et al. 2007), ALE recently adopted a faster and more accurate analytical solution to the problem (Eickhoff et al. 2011). Rather than considering each voxel individually, all voxels showing the same MA value in a particular experiment are joined into and represented as a single bin in a histogram. The entire histogram thus holds the occurrences of all possible MA values disregarding spatial information. The null distribution is then computed from successive integration of the probabilities stored in the histograms across the possible combinations. Finally, spatial inference

is drawn by identifying those voxels where the experiments (i.e., MA maps) converged more robustly (reflected by the ALE scores) than expected if the results were independently distributed (reflected by the null distribution) (Fig. 7.1c).

Importantly, the ALE algorithm is readily available to the neuroimaging community in form of the operation-system-independent GingerALE desktop application (http://brainmap.org/ale). GingerALE is part of the BrainMap project devoted to create tools for large-scale data mining and meta-analysis of the neuroimaging literature (Laird et al. 2009, 2011). The GingerALE software allows performing a quantitative meta-analysis based on the most recent version of the ALE algorithm on either the coordinates retrieved from automated queries to the BrainMap database or tabular-formatted list of coordinates retrieved by manual search of the literature.

7.4 Applying Quantitative Meta-Analysis

The ALE procedure has been illustrated above by depicting the three major steps of the analysis on a pool of neuroimaging experiments pertaining to emotion processing tasks in healthy participants (Fig. 7.1a–c). Converging brain activity across various emotional tasks included the bilateral amygdala, fusiform gyrus, posterior superior temporal sulcus, basal ganglia, dorsal anterior cingulate cortex/supplementary motor cortex (dACC/SMA), and the anterior insula/inferior frontal gyrus (AI/IFG) (Fig. 7.2, left column). Concurrently, the amygdala has been linked with processing various aspects of emotional and social environmental information as well as the shaping of respondent behavior. The fusiform gyrus is consistently accredited importance in processing mainly stable properties of facial stimuli, while the posterior superior temporal sulcus is consistently discussed as processing mainly variable properties of facial stimuli. The convergence in these two areas is meaningful in that most considered neuroimaging experiments employed facial pictures as stimulus material. The robust engagement of the basal ganglia in appraising emotional faces is believed to reflect the representation of motor programs for the facial musculature, which plays a crucial role in realizing emotional and social gestures. Similarly, the dACC/SMA and AI/IFG form a network that is believed to represent both one's own and others' emotional states regardless of the actual affective or sensory modality. This functional concept usually serves to explain the concomitant involvement of the dACC/SMA and AI/IFG in neuroimaging experiments on empathy. Taken together, the observed neural activation pattern underlying emotion processing is in line with the notion that similar brain regions are recruited in experiencing own and recognizing others' emotional states.

Another research question that can be addressed using ALE meta-analysis is the quantitative juxtaposition of the neural correlates that pertain to different psychological entities. This is exemplified here by computing the overlap between the coherent brain activity during emotion processing and the Stroop task. The latter refers to a classical paradigm in psychology for inducing cognitive conflict by asking participants to read aloud single words of colors whose letters are, however, colored incongruently. Put differently, we here compared the neural networks that subserve emotion processing and cognitive interference (Fig. 7.2, left and middle column), hence, two a priori rather unrelated psychological constructs. The conjunction analysis across the ALE meta-analysis on emotional tasks and Stroop tasks yielded robust convergence in the bilateral dACC/SMA and AI/IFG (Fig. 7.2, right column). In fact, increased brain activity in the bilateral dACC/SMA and AI/IFG in tandem is considered to be typical in the neuroscientific literature on both empathy (Lamm et al. 2011) and switching between cognitive sets (Dosenbach et al. 2006), notwithstanding they seldom cross-reference each other. The observed neural overlap across these two heterogeneous tasks epitomizes the urgent need for impartial integration of knowledge from intuitively unconnected, yet neurobiologically related, research areas in neuroimaging science.

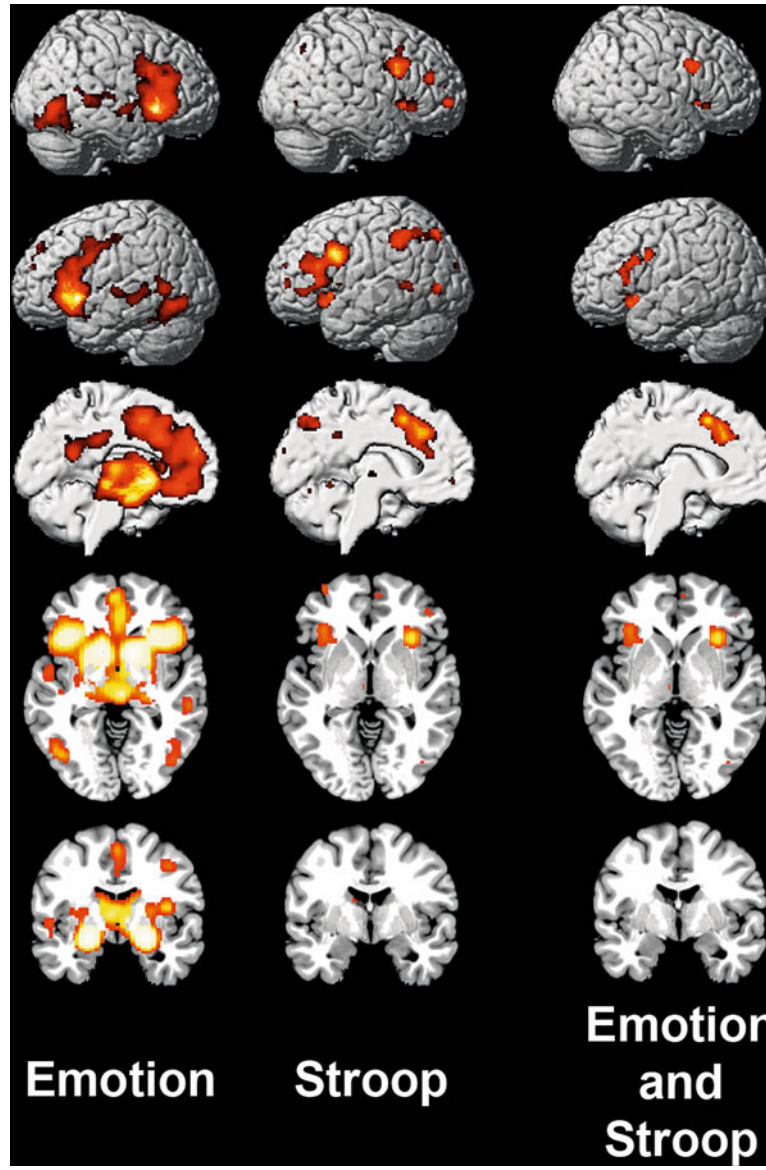

Fig. 7.2 Whole-brain renderings as well as sagittal, axial, and coronal slices depicting the results of the ALE meta-analyses on neuroimaging experiments related to emotion tasks in the *left column* (cf. Fig. 7.1) and related to the Stroop tasks in the *middle column* (219 individual neuroimaging experiments in 2,850 healthy participants). The *right column* shows significant convergence across both these individual ALE meta-analyses by performing an AND conjunction (all experiments provided by the BrainMap database)

The biggest potential of ALE might however rely in quantitatively summarizing neuroimaging data from clinical populations. That is because the above mentioned downsides of neuroimaging methods show the biggest effect for diagnosed participants, considering recruiting difficulties, the clinical exclusion/inclusion criteria, and the frequent occurrence of aborted measurements due to noncompliance, as well as often incongruent treatment within the clinical sample and inter-individual variability of a same disease. As a consequence, clinical neuroimaging research tends to be based on rather small sample sizes.

The aptitude of ALE to determine the neural substrates related to pathological brain function is exemplified here by a quantitative meta-analysis on differential brain activity in depressive patients during emotion processing (Fig. 7.3). Any ALE meta-analysis based on data from clinical populations necessarily rests on neuroimaging experiments that compare a group of patients versus a parallel group of healthy control

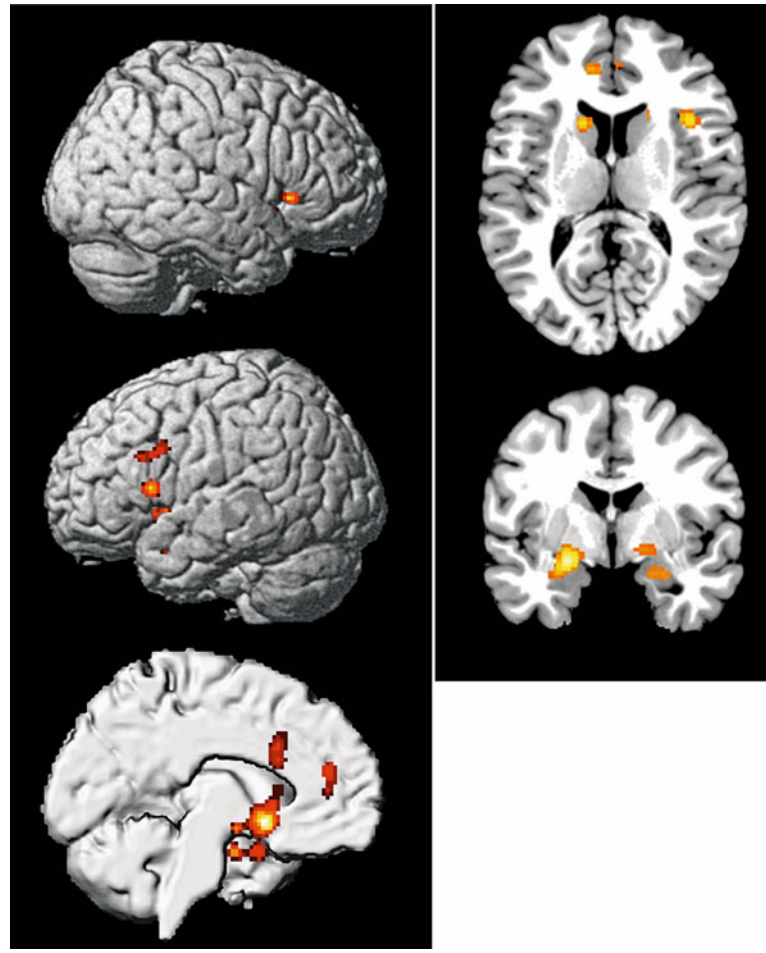

Fig. 7.3 Whole-brain renderings as well as sagittal, axial, and coronal slices depicting the results of the ALE meta-analysis of 131 individual neuroimaging experiments in 1,893 depressive patients that reported differential brain activity during various paradigms on emotion processing in comparison to healthy controls (experiments provided by the BrainMap database)

subjects. This approach yields consistent convergence between cerebral hypo- or hyperactivity in patients comparing to normal subjects. Figure 7.3 thus depicts the localization of deviant brain activity in depressed patients across a vast variety of subjects, paradigms, and experimental circumstances. Please appreciate that all the brain areas found to differ in brain metabolism during emotion processing in depression (Fig. 7.3) have also been determined to be part of the normal neural network engaged in emotion processing in a separate pool of subjects and experiment (Figs. 7.1c, 7.2, left column). This emphasizes the ability of ALE meta-analysis to identify the aberrant network nodes associated with a given mental condition within the neural network related to a given psychological process in healthy individuals.

Differences in brain metabolism in diseased populations cannot always be interpreted straightforwardly. For instance, more activity in the patient group could be read as reflecting an increased effort that is needed to compensate for deficient processing. Contrarily, less activity in the patient group could also be read as reflecting deficient processing due to lowered neural recruitment. This dilemma can be addressed by integrating the observed altered brain activity with prior evidence that was preferentially obtained using a different methodological modality, such as behavioral data or lesion studies. Furthermore, aberrant brain activity evidently raises the question of the underlying pathological process. One should be cautious to claim regional metabolic aberration as causal for the dysfunction of a specific psychological process. This line of

thought implicitly assumes that psychological processes can be identified from mere topography of brain activity, termed "reverse inference" (Poldrack 2006). This type of induction might, however, be limited in that one-to-one mapping between a certain brain region and a given psychological process is probably rare, if not inexistent.

7.5 Perspectives and Future Directions

Coordinate-based meta-analysis enables the quantitative localization of above-chance convergence across multiple neuroimaging experiments in a 3D reference space. This integration and synthesis of neuroimaging data thus permits statistically defensible generalizations on the neural basis of psychological processes in health and disease, which far exceeds the knowledge that may be gained from a single neuroimaging study. It also allows relating different tasks or processes to each other by performing meta-analyses on different neuropsychological phenomena, such as inhibition, attention, or working memory, which is often not feasible in a single experiment due to logistic expenses and the natural time limits of any scanner session. Moreover, CBMA offers a unique opportunity to weigh concordance between neuroimaging results without the implicit assumptions of neuroanatomical terminologies, which are frequently used in an inconsistent, if not competitive, manner. For instance, the temporoparietal junction is commonly referenced as angular gyrus, inferior parietal lobule, posterior superior temporal sulcus, supramarginal gyrus, BA 39, PGa/PGp, as well as "pli courbe" ("curved gyrus" in French). Another example is the long-standing debate about the constituent nodes of the limbic system. Consequently, conveying verbalized localization information may entail confusion by the same brain area being associated with discrepant neuroanatomical terms respectively the same neuroanatomical term being associated with discrepant groups of brain areas. Therefore, impartial comparison between neuroimaging studies using CBMA can possibly resolve conflicting views by reliance on location probabilities instead of neuroanatomical nomenclature.

Descriptive review articles are a commonly and eagerly employed mean to juxtapose and integrate distributed neuroimaging findings. However, those critical verbal analyses tend to focus on a limited number of preselected aspects and tend to be biased by the authors' own adherence to a specific research area. In contrast to classical review articles, CBMA is hypothesis-free, data-driven, and, hence, objective by algorithmically weighing all results equally. As the CBMA method is not skewed by subjectivity, it precludes overinterpretation of expected, easily interpretable findings and neglect of unexpected, barely reconcilable findings in neuroimaging research. CBMA might therefore help to point out consistent yet frequently ignored findings. For instance, cerebellar activation is typically overlooked in neuroimaging studies on non-motor topics, although cerebellar lesion does entail a variety of cognitive deficits, including language, visual-spatial, affective, and executive dysfunction (Stoodley and Schmahmann 2009). In this way, CBMA might be valuable in identifying previously unidentified brain regions or network nodes, respectively.

Moreover, it is increasingly acknowledged that the relationship between brain areas and psychological processes is best explained by a many-to-many rather than a one-to-one mapping (Price and Friston 2005). Said differently, a single brain region can be involved in several cognitive processes, and a single cognitive process may increase activity in several brain regions. These circumstances typically favor the development of parallel yet independent research trends that interpret activity in a same brain region according to completely diverging sets of theories and references. For instance, brain activity in the (left) inferior frontal gyrus is often read as specific for language processing by many authors yet specific for representation of (observed) motor action by others. By performing a rigorous summary of existing neuroimaging evidence, CBMA allows to unveil neurotopographical co-occurrences of a priori unrelated psychological processes and to,

thereby, potentially reconcile domain-centered research niches in an unbiased fashion. The ensuing meta-analytic convergence, in turn, might help to generate testable hypotheses for targeted neuroimaging studies to come.

CBMA can, however, not only be used for retrospective purposes, but also as a preliminary step to guide analysis in newly acquired experimental data. In particular, formal meta-analysis on a prespecified psychological state may yield reliable regions of interest (ROIs) that can be employed as a cornerstone for a variety of consecutive neuroimaging analyses. Functional ROIs constrained by prior meta-analysis can, for instance, readily inform seed-based structural and functional connectivity analyses. On the one hand, diffusion-weighted imaging (DWI) in concert with tractography algorithms has become popular as a measure of structural connectivity that delineates white-matter tracts in the human brain in vivo. On the other hand, resting-state neuroimaging data (rsMRI) is currently widely employed as a measure of functional connectivity based on correlations between spontaneous fluctuations of brain activity in the absence of an externally structured task. In both approaches, meta-analysis-derived ROIs can serve as a starting point for structural and functional connectivity analyses to reveal the whole-brain connectivity pattern of such functionally constrained seed regions (Eickhoff and Grefkes 2011). In a similar vein, approaches for effective connectivity aim at modeling the interactions within a predefined set of ROIs based on explicit a priori assumptions about their mutually related functional relationships. Such effective connectivity analyses, including psychophysiological interactions (PPI), structural equation models (SEM), dynamic causal modeling (DCM), and Granger causality mapping (GCM), infer the directionality in the information flow between the designated network nodes based on the ROI-defined fMRI signals (Eickhoff and Grefkes 2011). Evidently, the validity of the emerging interaction patterns critically hinges on the proper fit of the initially defined ROIs. Approaches for effective connectivity can thus take advantage of meta-analysis-defined ROIs that constitute a topographical consensus across numerous previous experiments. From a broader perspective, any neuroimaging technique reliant on preselected ROIs (e.g., even including transient brain lesion by transcranial magnetic stimulation) may enhance their potency by introducing coordinate-based meta-analysis as a complementary methodological step.

Summing up, CBMA represents a powerful utility to gain a synoptic view of distributed neuroimaging findings in a quantitative and impartial fashion. Retrospectively, CBMA might thus potentially remedy conflicting views that arose from inconsistent neuroanatomical labeling or domain-centered interpretation conventions. Prospectively, meta-analysis-derived regions of interest can serve as a solid basis for a variety of neuroimaging methods, including functional and effective connectivity analyses.

References

Derrfuss J, Mar RA (2009) Lost in localization: the need for a universal coordinate database. Neuroimage 48: 1–7

Dosenbach NU, Visscher KM et al (2006) A core system for the implementation of task sets. Neuron 50: 799–812

Eickhoff SB, Grefkes C (2011) Approaches for the integrated analysis of structure, function and connectivity of the human brain. Clin EEG Neurosci 42:107–121

Eickhoff SB, Laird AR et al (2009) Coordinate-based activation likelihood estimation meta-analysis of neuroimaging data: a random-effects approach based on empirical estimates of spatial uncertainty. Hum Brain Mapp 30:2907–2926

Eickhoff SB, Bzdok D et al (2011) Activation likelihood estimation meta-analysis revisited. Neuroimage 59(3): 2349–2361

Evans AC, Collins DL et al (1992) An MRI-based stereotactic atlas from 250 young normal subjects. Soc Neurosci Abstr 18:408

Laird AR, Eickhoff SB et al (2009) ALE meta-analysis workflows via the brainmap database: progress towards a probabilistic functional brain atlas. Front Neuroinform 3:23

Laird AR, Eickhoff SB et al (2011) The BrainMap strategy for standardization, sharing, and meta-analysis of neuroimaging data. BMC Res Notes 4:349

Lamm C, Decety J et al (2011) Meta-analytic evidence for common and distinct neural networks associated with directly experienced pain and empathy for pain. Neuroimage 54:2492–2502

Lancaster JL, Tordesillas-Gutierrez D et al (2007) Bias between MNI and Talairach coordinates analyzed using the ICBM-152 brain template. Hum Brain Mapp 28:1194–1205

Penny WD, Holmes AP (2004) Random effects analysis. In: Frackowiak RSJ, Friston KJ, Frith R, Dolan KJ, Price CJ, Zeki S, Ashburner J, Penny WD (eds) Human brain function. Academic, San Diego, pp 843–850

Poldrack RA (2006) Can cognitive processes be inferred from neuroimaging data? Trends Cogn Sci 10:59–63

Price C, Friston K (2005) Functional ontologies for cognition: the systematic definition of structure and function. Cogn Neuropsychol 22:262–275

Schilbach L, Eickhoff SB et al (2008) Minds at rest? Social cognition as the default mode of cognizing and its putative relationship to the "default system" of the brain. Conscious Cogn 17:457–467

Stark CE, Squire LR (2001) When zero is not zero: the problem of ambiguous baseline conditions in fMRI. Proc Natl Acad Sci USA 98:12760–12766

Stoodley CJ, Schmahmann JD (2009) Functional topography in the human cerebellum: a meta-analysis of neuroimaging studies. Neuroimage 44:489–501

Talairach J, Tournoux P (1988) Co-planar stereotaxic atlas of the human brain. Thieme, New York

Turkeltaub PE, Eden GF et al (2002) Meta-analysis of the functional neuroanatomy of single-word reading: method and validation. Neuroimage 16:765–780

Wager TD, Lindquist M et al (2007) Meta-analysis of functional neuroimaging data: current and future directions. Soc Cogn Affect Neurosci 2:150–158

Part II

Clinical Applications

8 Preoperative Blood Oxygen Level-Dependent (BOLD) Functional Magnetic Resonance Imaging (fMRI) of Motor and Somatosensory Function

Christoph Stippich

8.1 Rationale for fMRI in Rolandic Neurosurgery

Surgery in or around the "central region" entails a high risk for intraprocedural damage of the precentral and postcentral gyrus with consecutive motor and sensory deficits that can impact the patient's quality of life considerably. By noninvasively providing a precise localization of the different representations of the human body in relation to the surgical target, BOLD-fMRI facilitates the selection of candidates for surgery as well as the planning and performance of more aggressive but safe and function-preserving resections (Petrella et al. 2006). This also implies that fMRI plays a role in identifying those patients who are not the ideal candidates for surgery and who may profit more from less invasive therapeutic options like radiation or chemotherapy. Such patients often present with diffusely infiltrating or recurrent malignancies of the brain, and a complete resection and a surgical cure cannot be achieved. In this situation, deficits associated with the treatment should be kept to a minimum. Prior to treatment, fMRI provides important diagnostic information to evaluate the risks and chances on an individual basis and to optimize the therapeutic strategy accordingly. In addition, functional landmarks are helpful to plan partial resections or biopsies. This also applies for awake craniotomies or epilepsy surgery. Hence, the majority of preoperative fMRI studies are performed in patients with brain tumors and epilepsies to preserve the adjacent eloquent brain areas. In nonresective neurosurgery, also fMRI can be applied, for example, in patients with medically intractable chronic pain. Here, it has been demonstrated that fMRI facilitates the placement of stimulation electrodes over the motor cortex (Pirotte et al. 2005a, b). Ideally, preoperative fMRI studies are conducted for functional neuronavigation and in combination with diffusion tensor imaging (DTI), to also visualize important fiber bundles during surgery, for example, the pyramidal tract (Nimsky et al. 2006).

It is important to note that the central region can be localized easily and reliably on the basis of morphological images of the brain using different anatomical structures as landmarks (for details, see Chap. 2; Fig. 8.1). The most robust anatomical landmark is the "hand knob" of the precentral gyrus, representing the structural correlate of the motor hand area on transverse cross-sectional images (Yousry et al. 1997), which also corresponds to the "precentral hook" on sagittal images. The existence of these morphological landmarks substantiates the controversy whether functional imaging is necessary at all for rolandic neurosurgery. This view, however, does not account for the important limitations of morphological brain imaging in the presence of anatomical variants or under pathological conditions

C. Stippich, M.D.
Division of Diagnostic and Interventional Neuroradiology, University Hospitals Basel, Petersgraben 4, Basel 4031, Switzerland
e-mail: cstippich@usb.ch

S. Ulmer, O. Jansen (eds.), *fMRI – Basics and Clinical Applications*,
DOI 10.1007/978-3-642-34342-1_8, © Springer-Verlag Berlin Heidelberg 2013

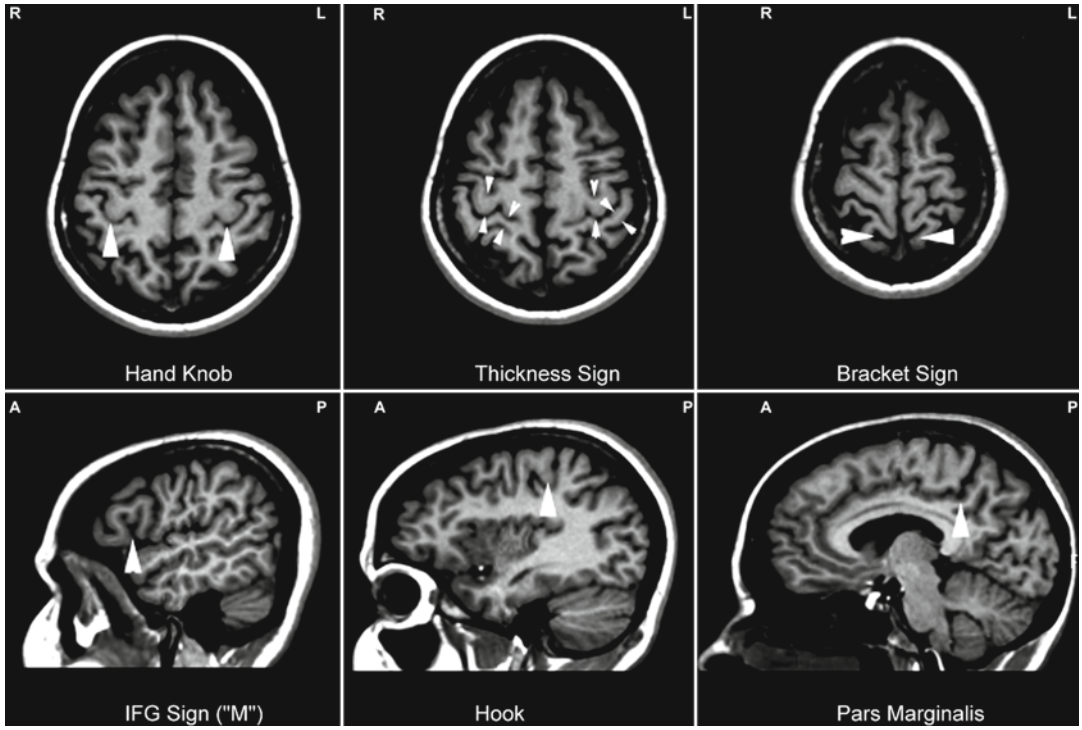

Fig. 8.1 Anatomical landmarks on morphological MRI according to Naidich and Yousry in transverse (*upper row*) and sagittal (*lower row*) views. *White arrowheads* indicate the relevant anatomical structures. The "hand knob" and "hook" are synonyms for the "precentral knob" (Reprinted from Stippich (2007, p. 90), with permission)

(e.g., mass effects, infiltration, destruction, postoperative state in recurrent malignancies), both precluding proper identification of the different gyri and sulci. More importantly, the motor hand area is the only functional area that can be identified reliably using anatomical criteria alone. All other representations of the human body can be identified only by using functional neuroimaging (Fesl et al. 2003), both in the primary motor cortex (M1) and in the primary somatosensory cortex (S1). A substantial body of research supports the role of fMRI as a valid and valuable preoperative imaging modality (Stippich et al. 2007). Hence, the rationale for preoperative fMRI results largely from the limitations of structural brain imaging (Rolls et al. 2007). Furthermore, neuroplasticity and functional reorganization induced by the lesion or by the treatment can be assessed using fMRI (Shinoura et al. 2006), for example, in patients with motor and somatosensory deficits that are not explained conclusively by anatomical consideration and in patients who are candidates for repeated neurosurgery because of recurrent malignancies.

Taken together, the rationale for carrying out presurgical fMRI is often based on the limitations of imaging morphology, clinical and electrophysiological diagnostics, and the need to include data on physiological and neuroplastic changes or pathologic (e.g., epileptic) activation of the brain in treatment planning. This diagnostic information may be generated by fMRI in a single investigation before treatment by means of a combined visualization of anatomy, pathology, and function. Combination of other modern methods of MRI, for example, by mapping fractional anisotropy (FA) or DTI, may be helpful in depicting important fiber pathways such as the pyramidal tract (Schonberg et al. 2006; Fig. 8.2).

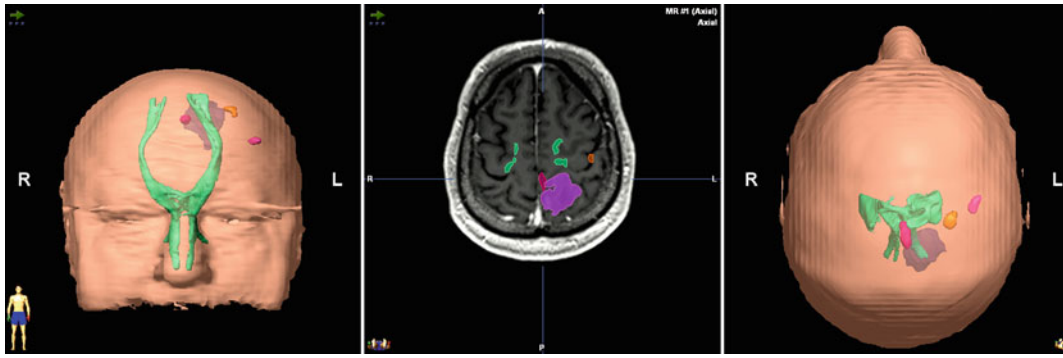

Fig. 8.2 Integration of BOLD-fMRI and DTI-tractography for functional neuronavigation. 3D-surface projections (*left*: anterior – posterior, *right*: top – down) and 2D-navigation view (*middle*). The spatial relationship of the cortical toe (*red*), finger (*orange*), and tongue (*pink*) motor representations and of the pyramidal tract (*green*) to the segmented brain tumor (*purple*) is clearly depicted. The tumor affects the superior parietal lobule and invades the postcentral gyrus extending toward the cortical motor representation of the lower extremity

8.2 Review of Literature

Mapping the primary motor cortex in patients with rolandic brain tumors has been the first clinical application of fMRI (Jack et al 1994). Shortly after the first reports on BOLD-fMRI in healthy subjects (Belliveau et al. 1991; Bandettini et al. 1992; Kwong et al. 1992; Ogawa et al. 1993), the potential usefulness of functional imaging techniques in clinical context and particularly in presurgical identification of motor and somatosensory cortices was postulated. The first description of presurgical fMRI as a clinically useful application dates from 1994, when Jack et al. provided proof of principle in two patients with brain tumors in the sensorimotor cortex, validating their preliminary results with established electrophysiological techniques (Jack et al. 1994). Soon after, several case studies (Baumann et al. 1995; Cosgrove et al. 1996) and reports with small numbers of patients (Puce et al. 1995; Pujol et al. 1996; Mueller et al. 1996; Krings et al. 1998), harboring glial tumors or arteriovenous malformations (AVM), confirmed technical and practical feasibility of fMRI using motor and sensory tasks in the clinical context and stressed the high potential value of this new upcoming technique for preoperative risk assessment, therapeutic decision making, and surgical planning.

During the following years, investigations with larger numbers of tumor patients (up to 50) were carried out, claiming their results to represent an important factor for surgical decision (Schlosser et al. 1997; Pujol et al. 1998). Comparisons of presurgical fMRI data with the established reference procedure intracortical stimulation (ICS) were numerous, and only those specifically dealing with brain tumor patients will be mentioned here, since a detailed description of validation studies is offered in Chapters 11, 12, 13, 21 and 22. Virtually all studies report highly concordant data of presurgical fMRI and ICS in patients with lesions around the central sulcus (Dymarkowski et al. 1998; Achten et al. 1999; Roux et al. 1999a, b) with agreement between fMRI and ICS data ranging from 83 % in 33 patients (Majos et al. 2005) to 92 % in 60 patients (Lehericy et al. 2000). Task sensitivity for identification of the sensorimotor region estimated in large groups of tumor patients was 85 % in 103 patients (Krings et al. 2001) or 97 % in 125 patients (Hirsch et al. 2000). Furthermore, it should be briefly noted that various groups focused on the correlation of fMRI results in patients with central lesions with those of other functional imaging procedures, for example, PET (Bittar et al. 1999).

One of the first attempts to evaluate the impact of fMRI on neurosurgical planning was published by Lee et al. The authors applied preoperative fMRI sensorimotor mapping in 32 tumor patients and reported that the results were used to determine feasibility of surgical

resection in 55 %, to aid in surgical planning in 22 %, and to select patients for invasive surgical functional mapping in 78 %. Overall, the fMRI results were useful in one or more of these surgical decision-making categories in 89 % of all examined tumor patients (Lee et al. 1999). A similar range was documented by Ternovoi et al., who found that presurgical fMRI results had an influence on therapeutic tactics in 69 % of 16 tumor patients (Ternovoi et al. 2004). Other investigators tried to establish a functional risk predictor for postoperative clinical outcome. Haberg et al. examined 25 patients with primary brain tumors near sensorimotor regions. In 80 % of the patients, successful fMRI measurements were obtained, out of which 75 % were used in preoperative planning. The risk of postoperative loss of function was significantly lower, when the distance between tumor periphery and BOLD activation was 10 mm or more (Haberg et al. 2004). Similarly, Krishnan et al., who evaluated BOLD activation in 54 patients, found that a lesion-to-activation distance of less than 5 mm and incomplete resection were predictors of new postoperative neurological deficits and recommended cortical stimulation within a 10-mm range (Krishnan et al. 2004). In patients with medial frontal lesions, preoperative fMRI was used to establish the area at risk for resection of specific parts of the supplementary motor area, associated with transient postoperative motor deficits and speech disorders (Krainik et al. 2001, 2003, 2004). In a recent study, the authors used fMRI-guided resection in 16 patients with low-grade gliomas. Since these tumors are generally not contrast enhancing, resection borders are particularly difficult to establish based on morphological imaging alone. Using fMRI for the determination of resection borders, no permanent neurological deficits and no radiographic tumor progression, within a median follow-up time of 25 months, were observed (Hall et al. 2005). However, the data available to quantify a safe distance between functional activation and resection borders with respect to surgically induced neurological deficits are still very limited and do not justify any general conclusion or recommendation.

Overall, although the above mentioned studies clearly demonstrated feasibility of presurgical fMRI in clinical environment and postulated a contribution of the obtained additional clinical information to pretherapeutic decision making, an effect on the decrease in posttherapeutic morbidity was not corroborated. In order to achieve this, controlled clinical trials using optimized and standardized protocols would be required. Although most investigators agree on the necessity of a standardized routine, and several methodological studies presenting optimized protocols for clinical use were published (Hirsch et al. 2000; Ramsey et al. 2001; Rutten et al. 2002; Stippich et al. 1999, 2000, 2002a, b, 2004; Stippich 2005), no large-scale clinical trials addressing actual benefit for the patient, in terms of decrease in morbidity, have been undertaken so far.

Although sensorimotor areas are identified with high success rates using fMRI in patients with central lesions by most investigators, a frequently encountered phenomenon is an altered pattern of activation as compared to the normal brain function, currently denominated as lesion-induced reorganization or plasticity. In an early study in seven patients with intracerebral gliomas of the primary sensorimotor cortex, activation was found to be displaced or reduced (Atlas et al. 1996). Roux et al. correlated the type of activation with histologic tumor characteristics in 17 patients. In infiltrating tumors, intratumoral activation was detected, which was displaced and scattered correlated with the degree of infiltration, whereas in noninfiltrating tumors, activation showed extra-tumoral shift. In tumors at a distance from the motor cortex, no intratumoral activation was measured (Roux et al. 1997). Likewise, a PET study with 51 patients describes that central lesions are more frequently associated with altered patterns of activation than lesions in non-central locations (Bittar et al. 2000). Other studies found significant BOLD-signal decrease in areas adjacent to tumor tissue in motor and sensory cortices as compared to the contralateral side. This effect was present in glial tumors, most pronounced in glioblastoma, and presumably related to tumor-induced changes in local cerebral

hemodynamics (Holodny et al. 1999, 2000; Krings et al. 2002a, b), while in nonglial tumors (metastasis, cavernoma, abscess, AVM, meningioma), no BOLD-signal decrease was found (Schreiber et al. 2000). A recent report on 33 patients, with different intra-and extra-axial tumors, established the influence of tumor type and distance from eloquent cortex on activation volumes in fMRI (Liu et al. 2005). In addition to displacement or reduction of activation in the primary sensorimotor cortex harboring the tumor, other patterns of lesion-induced reorganization encompass activation of solely the contralesional cortex or an enhanced activation of nonprimary sensorimotor areas with increasing degree of paresis (Alkadhi et al. 2000; Carpentier et al. 2001; Krings et al. 2002a, b). Also in patients with prior surgery (Kim et al. 2005) or newly acquired central paresis after resection (Reinges et al. 2005), significant decreases in BOLD activation are observed. One possible explanation for this tumor-induced BOLD-signal loss was lately proposed by an fMRI study where tumor blood volume and perfusion were measured. The authors concluded that the BOLD amplitude correlates with total intratumoral blood volume and, thus, reduced peritumoral perfusion due to a tumor-aspirating perfusion (steal phenomenon) goes along with reduced BOLD activation (Ludemann et al. 2006). Of note is, however, that resection of glioma with preoperative edema may cause transient increase of BOLD activation ipsilateral to the tumor, presumably by a decrease of pressure on the brain (Kokkonen et al. 2005). Lesion-induced functional reorganization may reflect the recruitment of plastic neuronal networks to compensate for sensory or motor impairment. On the level of a functional diagnosis in presurgical fMRI, these reorganization phenomena are of major clinical significance for the planning of resections, since they can potentially cause false-negative results.

During the past few years, the use of combined presurgical fMRI and DTI techniques for tractography was suggested to provide a better estimate of proximity of tumor borders to eloquent cortex than fMRI measurements alone. In particular, for space-occupying lesions affecting the central region, visualization of the origin, direction, and functionality of large white matter tracts, allowing imaging of functional connectivity, was put forward to improve surgical outcome and to promise a decrease in patient morbidity (Krings et al. 2001; Parmar et al. 2004; Ulmer et al. 2004; Shinoura et al. 2005; Stippich et al. 2003; Holodny et al. 2001).

Very recently, first reports on the application of real-time fMRI in clinical environment were published. This novel technique enables quick preliminary online analysis of fMRI data, which is particularly useful in surgical diagnostics, considering that fMRI data acquisition and processing are very time consuming. Möller et al. demonstrated the technical feasibility of presurgical real-time fMRI examination in ten patients with central area tumors immediately prior to surgery (Moller et al. 2005). In another study, motor and language tasks were used for real-time fMRI in 11 tumor patients. The authors reported satisfactory activation for hand motor tasks, weaker activation for foot motor tasks, and no useful activation for language tasks at the chosen threshold, concluding that the procedure needed to be optimized but was generally feasible in clinical routine (Schwindack et al. 2005). Furthermore, Gasser et al. lately achieved the recording of intraoperative fMRI in four anesthetized patients with lesions in the vicinity of the central region. Using a passive stimulation paradigm and analyzing the data during acquisition by online statistical evaluation, they obtained intraoperative identification of eloquent brain areas taking brain shift into account (Gasser et al. 2005).

Finally, with the introduction of higher magnetic field scanners to clinical diagnostics, practicability of presurgical fMRI at 3 T was established in patients with brain tumors (Roessler et al. 2005; Van Westen et al. 2005; Feigl et al. 2008). Today the clinical implementation of preoperative fMRI is possible also in regional hospitals (Geerts et al. 2007). For a general review on the role of imaging in disease management and the development of improved image-guided therapies in neurooncology, see also the latest article by Jacobs et al. (Jacobs et al. 2005).

Note: Very recently the American Medical Association (www.ama-assn.org) has released CPT-codes (Current Procedural Terminology) for clinical fMRI applications. General instructions for clinical fMRI can be found in the Current Protocols for Magnetic Resonance Imaging (Thulborn 2006).

8.3 General Considerations

Motor cortex mapping is the predominant preoperative application of fMRI because of its easy implementation in a clinical setting and the robust and valid functional localizations. Typically, a simple block design consisting of three to five stimulation-baseline cycles is applied while the patients perform self-paced movements with the tongue or lips, hand or fingers, and foot or toes to investigate the motor cortex somatotopy.

Essentials for the success of clinical fMRI examinations are (1) motor tasks that are feasible also in patients with paresis, (2) reduction of motion to a minimum, and (3) short scanning times. Under these conditions, BOLD activations in the primary motor cortex are generally very reliable. This can be achieved when the "most feasible" motor tasks have been selected from clinical testing, when patient positioning and head fixation is optimal during the fMRI scans, when appropriate motion correction is applied for data processing, and when the fMRI scanning protocols have been evaluated in volunteers for robust functional localization, high BOLD-signal yield, and low scanning time. For the diagnostic interpretation of clinical fMRI data, it is indispensable that the whole fMRI procedure is fully standardized (scanning, data processing, and evaluation) and that normative data are available for all applied fMRI scanning protocols (ideally including data for important influencing factors like handedness) as well as a precise assessment of each patient's neurological deficits at the time of the preoperative fMRI measurement. For the latter, the importance of the individual training of the investigator with each patient before the actual fMRI measurement cannot be overestimated. To control for incorrect task performance, a video monitoring during the fMRI measurements is highly recommended. In uncooperative patients, it may even be necessary that the investigator is inside the scanner room to give instructions directly (e.g., by tapping the hand when the movement is started and stopped). All erroneous measurements must be excluded from evaluation and repeat measurements must be performed.

The investigation of patients with pareses can be challenging, however. Dedicated paradigms based on somatosensory stimulation (Stippich et al. 1999, 2004; Stippich 2005) or complex finger movements of the unimpaired hand (Stippich et al. 2000) may help to overcome the problem. A somatosensory stimulation can also be useful in uncooperative or sedated patients and in children. Automated devices deliver reproducible stimuli and are ideal for follow-up measurements under standardized conditions (Golaszewski et al. 2002; Kurth et al. 1998; Stippich et al. 1999). For more details, see paragraphs in Sects. 8.6 and 8.7. A review of literature regarding the various fMRI paradigms for motor and somatosensory function is beyond the scope of this chapter. We refer the reader to the extensive database available. It is of note that most manufacturers offer online data processing software for functional BOLD imaging with their MR imagers today, providing easy access to the method.

8.4 Diagnostic Aims

The primary diagnostic aim of preoperative fMRI is to localize the primary motor cortex and/or the primary somatosensory cortex in relation to the surgical target and the different cortical representations of the human body of the precentral gyrus and/or postcentral gyrus. The secondary aims include the detection of neuroplastic changes and functional reorganization prior to treatment in patients with neurological deficits and in patients scheduled for repeated neurosurgery, investigating the natural course of brain activation in patients with rolandic pathologies, or the effects of a specific (surgical or alternative) treatment on brain function, which may represent further diagnostic aims of follow-up measurements.

8.5 Selection of Candidates for Preoperative fMRI

Most patients referred to preoperative motor and somatosensory fMRI present with rolandic brain tumors, metastases, AVMs, and epileptogenic lesions. In general, patients with meningiomas and other (non-infiltrative) extra-axial masses should not be considered for fMRI, except for difficult cases on request of the surgeon. fMRI is also not necessary for patients with frontal or parietal pathologies that do not involve the central region directly.

As a basic principle, candidates for preoperative fMRI should be selected by anatomical consideration first using morphological MR images and on the basis of clinical findings (motor and/or sensory deficit), both clearly indicating an involvement of the primary motor and/or somatosensory cortex. The appropriate examination protocol should be selected accordingly. Depending on the site and extent of the lesion, a single fMRI reading can suffice; however, it is often necessary to examine the entire motor and, where appropriate, somatosensory somatotopy.

Preoperative fMRI studies are justified when the following anatomical criteria apply: (1) complete destruction of the rolandic anatomy precluding identification of the precentral gyrus, central sulcus, and postcentral gyrus. (2) Compression or displacement of the precentral gyrus precluding reliable localization of the hand knob – the MR – morphologic reference of the motor hand area is absent as an orientation point for the somatotopic organization of the precentral gyrus. (3) The surgical target lies below or above the hand knob and a precise localization of the cortical face or lower extremity representations is warranted. (4) The surgical target is postcentral – a somatosensory stimulation may be applied. Other (nonanatomical) criteria include (5) suspected neuroplastic changes/functional reorganization with respect to neurological signs and symptoms and (6) repeated neurosurgery.

Note: The size of the BOLD-clusters and the center of gravity varies with the statistical threshold applied for data evaluation. As a consequence, fMRI studies should not be performed to determine resection borders or a "safe" distance between lesion and functional area. In a strict sense, this is not possible to date on the basis of fMRI data as the material published on that topic is very limited (Haberg et al. 2004; Krishnan et al. 2004; Hall et al. 2005). Furthermore, non-standardized measurements in "interesting cases" are not feasible for clinical decision making and should be avoided. However, such patients may be enrolled in research trials.

8.6 Paradigms for Clinical Motor and Somatosensory fMRI

When designing motor paradigms in a block design, it is of principal importance to establish whether only the primary motor cortex activation needs to be measured or secondary areas should also be considered. In the case where only the primary motor cortex is the target, paradigms can also include movements in both sides of the body (e.g., right hand vs. left hand). Since unilateral movements lead to activation of secondary areas in both hemispheres, secondary areas are active during alternating movements of the right and left body side throughout the entire measurement, but continuous activation is not shown in the statistical evaluation of fMRI data, acquired using conventional block designs, due to the lack of "contrast" between the various stimulation blocks. If information needs to be obtained regarding secondary motor activation, paradigms with strictly unilateral movements of a single body part should be applied, with "resting" as the control condition. Alternatively, three different stimulation conditions could be integrated in the paradigm, that is, right movement – rest – left movement. However, the number of blocks per paradigm is then increased, and consequently, the examination time and susceptibility to motion artifacts also increases. In addition, it should be borne in mind that information on brain activation in the tumor-unaffected hemisphere is largely insignificant for treatment. Also, paradigms enabling the examination of several cortical body representations are problematic in brain tumor patients (e.g., foot – hand – face). Although scan

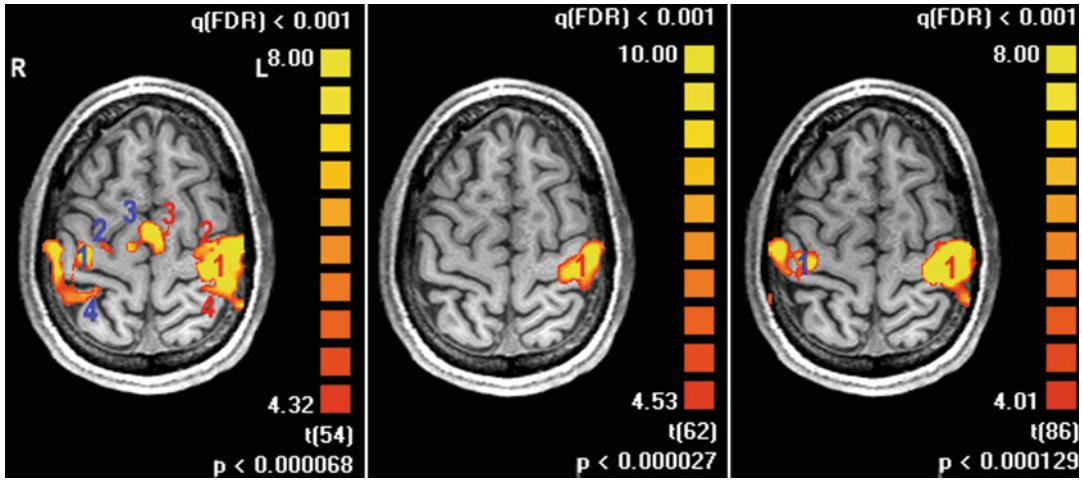

Fig. 8.3 Variation of paradigms to localize the motor hand area results in different activation patterns. *Left*: complex finger opposition of the right hand vs. rest; strong activation of cortical motor network in both hemispheres. The large contralateral cluster (*left*) covers the primary sensorimotor cortex (*1*), premotor cortex (*2*), and parietal cortex (*4*). Bilateral supplementary motor activation (*3*, *3*) is displayed in the midline as well as ipsilateral (*right*) premotor activation (*2*), primary sensorimotor coactivation (*1*), and parietal activation (*4*). *Middle*: complex finger opposition of the right vs. left hand; strong contralateral (*left*) primary sensorimotor activation (*1*), but no activation of secondary areas. *Right*: complex finger opposition of the right hand vs. right toe movements and tongue movements; strong contralateral (*left*) primary sensorimotor activation (*1*) and ipsilateral primary sensorimotor coactivation (*1*), but no activation of secondary areas (Reprinted from Stippich (2007, p. 106), with permission)

time could be reduced compared to three individual measurements, the time needed is still substantially longer than for each individual measurement alone. Particularly in the case of agitated patients or patients with paresis, the likelihood of motion artifacts increases, subsequently affecting all functional localizations. Only secondary functional areas which are exclusive to the respective movement can be localized. All jointly recruited areas escape detection on diagnostic fMRI. In conclusion, paradigms with movements of a single part of the body alternating with true rest that provide short scan times are most appropriate for preoperative fMRI (Fig. 8.3).

Clinical feasibility tests, carried out on neurosurgical patients with and without tumor-related pareses or sensory disturbances, showed that self-triggered movement tasks are better suited to preoperative fMRI than controlled paradigms, since only in this way each patient can perform within his or her ability. To keep the likelihood of motion artifacts to a minimum (Hoeller et al. 2002; Krings et al. 2001), the following movement tasks were chosen each with "rest" as control condition: repetitive tongue movements with the mouth closed, opposition of fingers D2–D5 to D1 with free choice of sequence, and repetitive flexion and extension of all five toes without moving the ankle (Stippich et al. 2002a, b) (Fig. 8.4). Alternatively, in the case of mild paresis of the upper extremity, fist clenching/releasing can be tested. Face, arm, and leg movements, or movement of the feet, can often lead to poor diagnostic evaluation of data due to strong motion artifacts; therefore, they are not recommended for clinical fMRI. A paradigm with a block duration of 20 s and three repeat cycles (four rest conditions alternating with three stimulation conditions), adding to an examination time of 140 s, is a suitable compromise between robust functional localization of the primary motor cortex, high BOLD signals, and short scan time (Fig. 8.5).

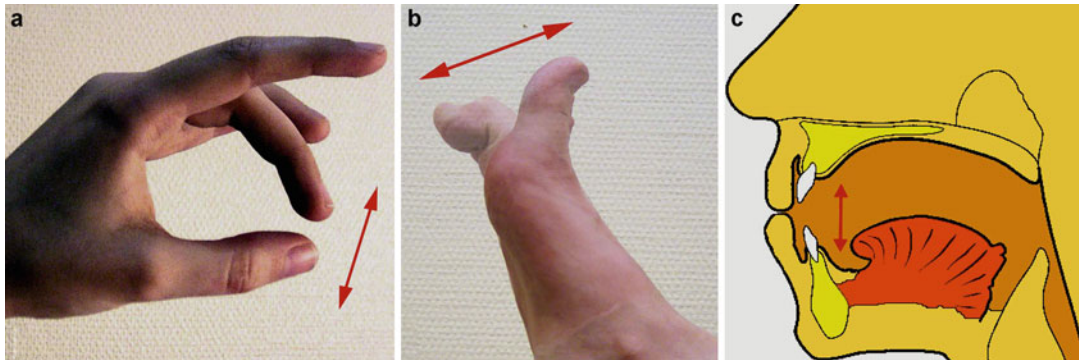

Fig. 8.4 (**a**–**c**) Recommended self-paced movements to investigate sensorimotor somatotopy in clinical fMRI. (**a**) Complex finger opposition of digits 2–5 against the thumb in a random order. Movement frequency ~3 Hz. (**b**) Toe up and down movements, frequency >1 Hz. (**c**) Tongue up and down movements with the mouth closed. Movement frequency ~3 Hz (Reprinted from Stippich (2007, p. 106), with permission)

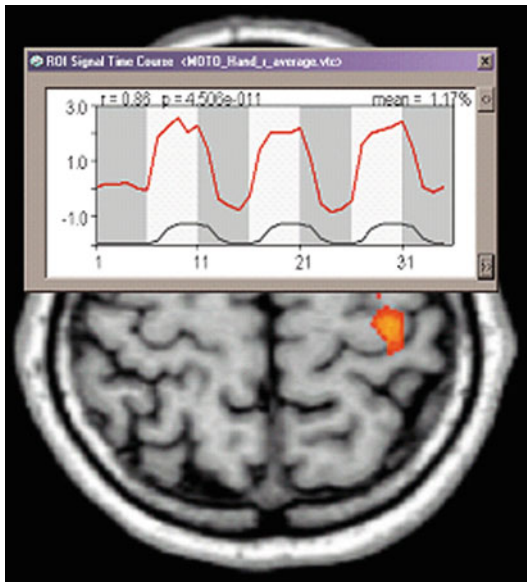

Fig. 8.5 Clinical standard protocol for motor paradigms. The block-designed paradigm consists of four rest periods (*light gray*) alternating with three stimulation periods (*white*), each 20 s in duration. The BOLD-signal time course of the motor hand area activation (*red line*) shows task-related increases in regional hemodynamics. The *black line* indicates the hemodynamic reference function (hrf) (Reprinted from Stippich (2007, p. 107), with permission)

Determination of motor function with preoperative fMRI is limited in patients with high-grade paresis (Pujol et al. 1998; Krings et al. 2002a, b). In the case where the fMRI protocol is based solely on self-triggered movements contralateral to the tumor, a reliable preoperative fMRI diagnosis is not guaranteed – the pareses are results of insufficient residual function of the primary motor cortex, which can lead to weak, or even absent, BOLD signals. Nevertheless, many patients with tumor-related paresis can be successfully examined by activating the primary somatosensory lip, finger, and toe representations of the postcentral gyrus (Stippich et al. 1999). While most investigators apply somatosensory stimuli manually (e.g., brushing the palm), automated devices provide reproducible and standardized stimulation conditions. Electric (Kurth et al. 1998; Kampe et al. 2000; Golaszewski et al. 2004), tactile (Stippich et al. 1999; Wienbruch et al. 2006), or vibrotactile (Golaszewski et al. 2002, 2006) stimulators are in use. The fully automatic pneumatically driven 24-channel tactile stimulation used in our institution works artifact-free and produces reproducible stimuli and consistent examination conditions for comparative and outcome studies. The whole unit can be set up and removed within 5 min (Fig. 8.6). Scan times per measurement are 66 s for S1 (Stippich et al. 2004) or 105 s for S2 (Stippich 2005). The S1-paradigm consists of five repeat cycles (six rest conditions alternating with five stimulation conditions, duration 6 s each), the S2-paradigm of three repeat cycles (four rest conditions alternating with three stimulation

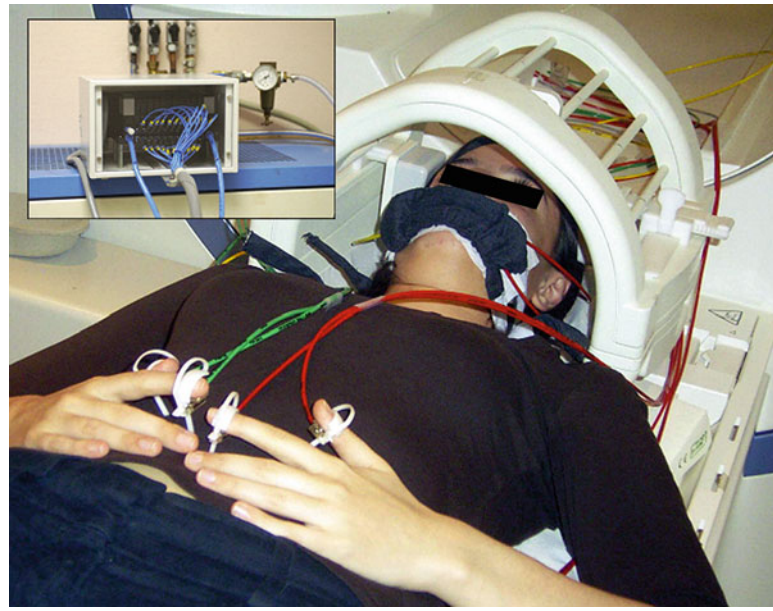

Fig. 8.6 Fully automated pneumatically driven tactile stimulation. Flexible membranes (4D Neuroimaging, Aachen, Germany) connected to pressure-resistant pneumatic tubes transmit the stimuli to the lips, fingers, or toes (not shown). *Upper left*: the 24-channel high-precision electromagnetic valve system was designed to investigate somatosensory somatotopy (Reprinted from Stippich (2007, p. 94), with permission)

conditions, duration 15 s each). For the latter paradigm, S1 activation is also robust.

As a further adjunct to investigate paretic patients, complex finger opposition of the nonparetic hand (ipsilateral to the pathology) can be used for the standard motor paradigm (140 s) to elicit robust premotor activation as an additional functional landmark for the precentral gyrus on the lesion side (Stippich et al. 2000; Fig. 8.7).

8.7 Preoperative fMRI in Patients with Rolandic Brain Tumors

8.7.1 Somatotopic Mapping of the Primary Motor Cortex (Standard Protocol)

Somatotopic mapping of the motor cortex is the most frequently used preoperative fMRI protocol in patients with rolandic lesions (Stippich et al. 2002a, b). The protocol contains three different fMRI measurements with a scanning time of 140 s each. Typical paradigms include tongue movements and finger and toe movements contralateral to the lesion to localize the motor homunculus in relation to the surgical target (Fig. 8.8). Even in case of complete destruction of the rolandic anatomy, fMRI provides three functional landmarks for different body representations (face, upper, and lower extremities). This diagnostic information is relevant to confirm the indication to operate and to plan and implement safer surgery. The same holds true for lesions that preclude proper identification of the hand knob as the anatomical reference for the motor hand area by compression or displacement (Fig. 8.9). In patients with small lesions that are – by anatomical consideration – not critical for all body representations, it seems appropriate to shorten the protocol by leaving the least relevant body representations unexamined (Fig. 8.10). However, the examination of a single body representation alone, for example, the motor hand representation, is often not sufficient to provide the required diagnostic information. Somatotopic mapping enables also to assess plastic changes of cortical motor activation, for example, in patients with recurrent malignancies prior to repeated surgical treatment (Fig. 8.11).

8.7.2 Somatotopic Mapping of the Primary Somatosensory Cortex

This fMRI protocol was designed to localize the different somatosensory body representations

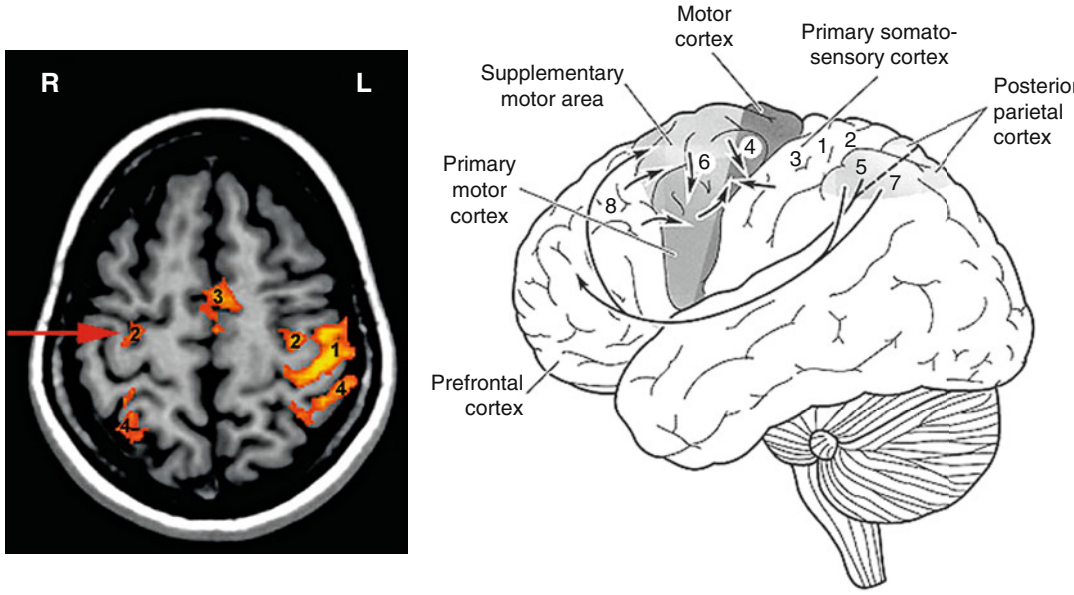

Fig. 8.7 Typical cortical activation pattern of complex finger opposition (right hand). Premotor activation ipsilateral to the moving hand (*red arrow*) serves as a functional landmark for the precentral gyrus in hemiparetic patients (a clinical case is presented in Fig. 8.13). Premotor activation is typically localized at the anterior wall of the precentral gyrus directly adjacent to the junction of the precentral sulcus with the superior frontal sulcus. It is important to note that this functional landmark does not localize the motor hand area! In the drawing of the cortical motor and somatosensory network (*right*), numbers indicate Brodmann areas (Reprinted from Stippich (2007, p. 113), with permission)

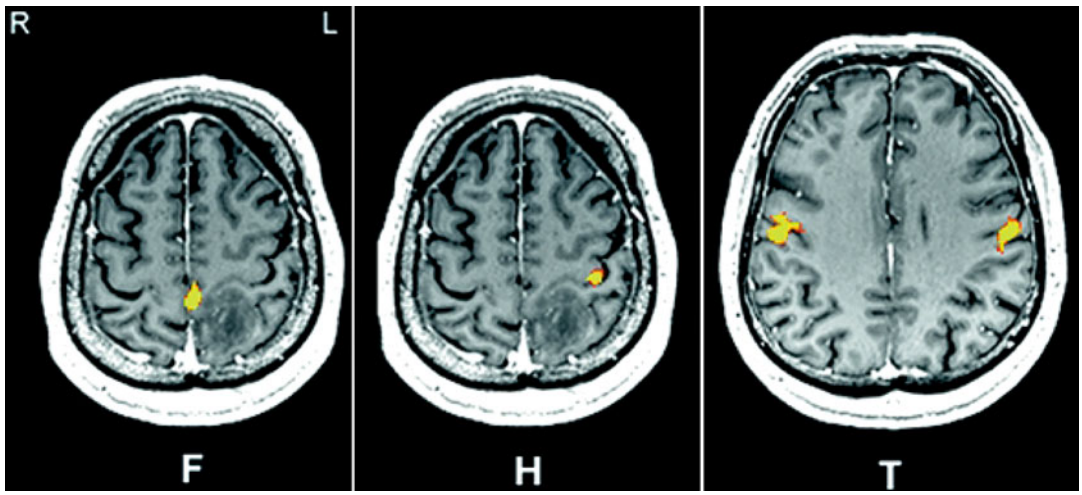

Fig. 8.8 Standard presurgical fMRI protocol: Somatotopic mapping of the motor cortex (same patient as in Fig. 8.2). The cortical foot representation (*F*) is closely related to the left parieto-postcentral anaplastic glioma. BOLD activation of the motor hand area (*H*) is localized at the hand knob and the bilateral tongue representations (*T*) at the level of the ventricular roof

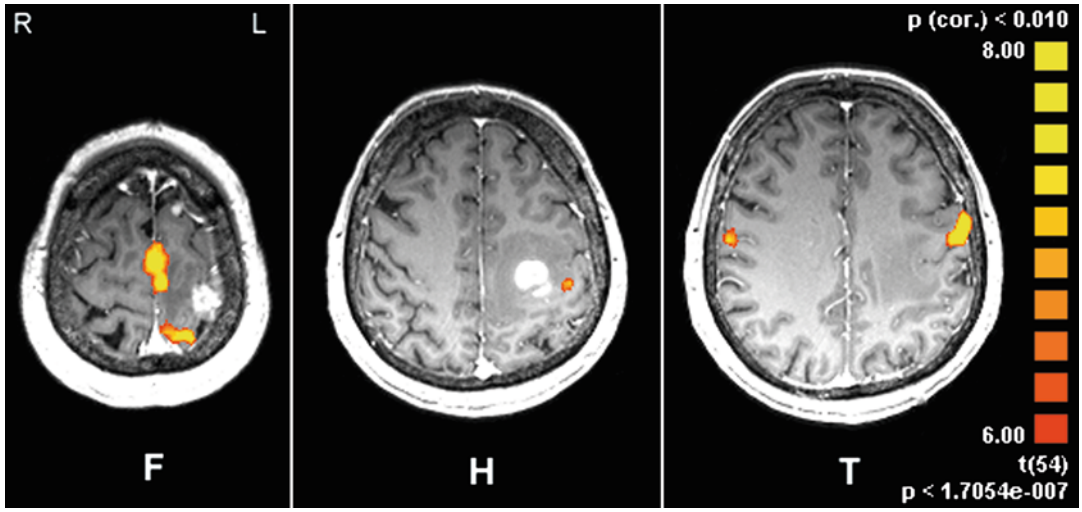

Fig. 8.9 Somatotopic fMRI mapping of the motor cortex in a patient with a left precentral glioblastoma precluding identification of the motor hand area using morphological landmarks. fMRI clearly indicates the position of the motor hand area during contralateral hand movements (*H*) as well as the cortical foot (*F*) and tongue representations (*T*)

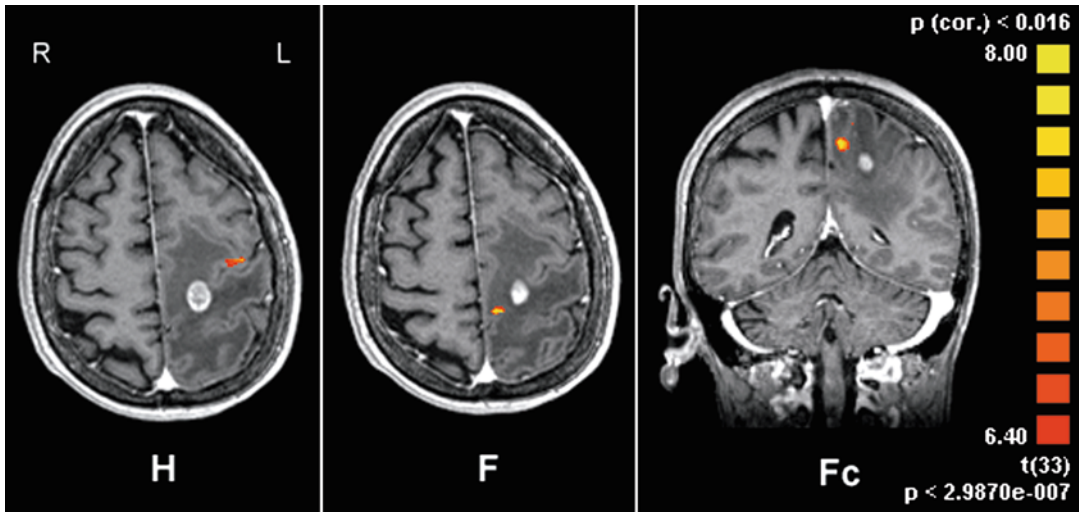

Fig. 8.10 Somatotopic fMRI mapping of the upper motor cortex in a patient with a left central metastasis indicating the spatial relationship to the cortical hand (*H*) and foot (*F*) representation. The latter is also displayed in coronal view (*Fc*). Additional fMRI localization of the motor tongue representations was not necessary by anatomical consideration

of the postcentral gyrus (Stippich et al. 1999). The somatosensory stimuli are transmitted to the lips, fingers, and toes contralateral to the brain lesion. In presurgical fMRI, somatotopic somatosensory mapping is mostly used as diagnostic adjunct, when motor paradigms are difficult to apply – for example, in uncooperative, sedated, or hemiparetic patients or in children – but there is also potential for standardized follow-up measurements on neuroplastic changes of the somatosensory system. This presurgical fMRI protocol enables a fully automated assessment of the spatial relationship between brain tumors and the postcentral gyrus, facilitating the estimation of possible postoperative sensory deficits (Fig. 8.12).

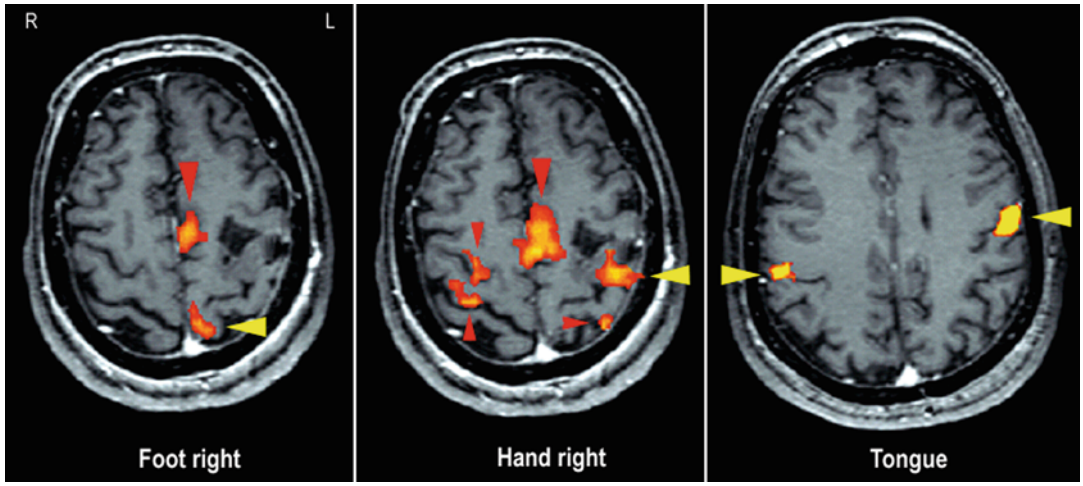

Fig. 8.11 Presurgical fMRI somatotopic mapping of the motor cortex in a hemiparetic patient with a recurrent left rolandic astrocytoma prior to repeated surgery. Foot, hand, and tongue movements revealed robust fMRI activation of the respective primary motor cortex body representations (*yellow arrowheads*). Note the increased activation in secondary areas (*red arrowheads*): in the supplementary motor area during toe and finger movements and in the whole cortical motor network in both hemispheres during finger movements (Reprinted from Stippich (2007, p. 111), with permission)

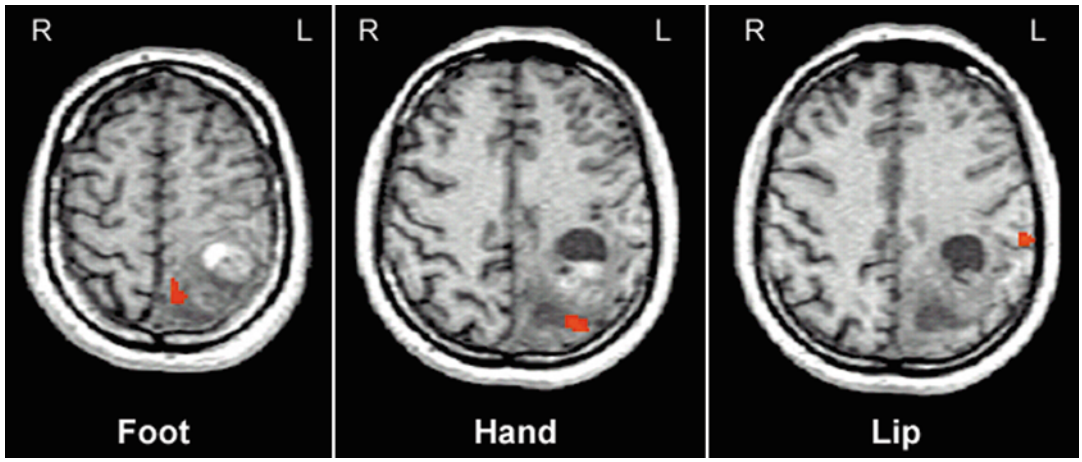

Fig. 8.12 Presurgical fMRI somatotopic mapping of the primary somatosensory cortex (S1) in a left parietal malignant glioma indicated compression of the upper postcentral gyrus at the level of the foot representation and tumor growth into the lower postcentral gyrus with dorsal displacement of the S1 hand representation (Reprinted from Stippich (2007, p. 112), with permission)

Diagnostic information about the spatial relationship between the central sulcus or precentral gyrus and precentral or frontal brain tumors can be obtained rather indirectly as both anatomical structures are directly adjacent to the postcentral gyrus in the anterior direction.

8.7.3 Localization of the Precentral Gyrus in Patients with Paresis

This special protocol was designed in volunteers to help localize the precentral gyrus in patients with contralateral paresis (Stippich et al. 2000). The clinical application is still experimental and

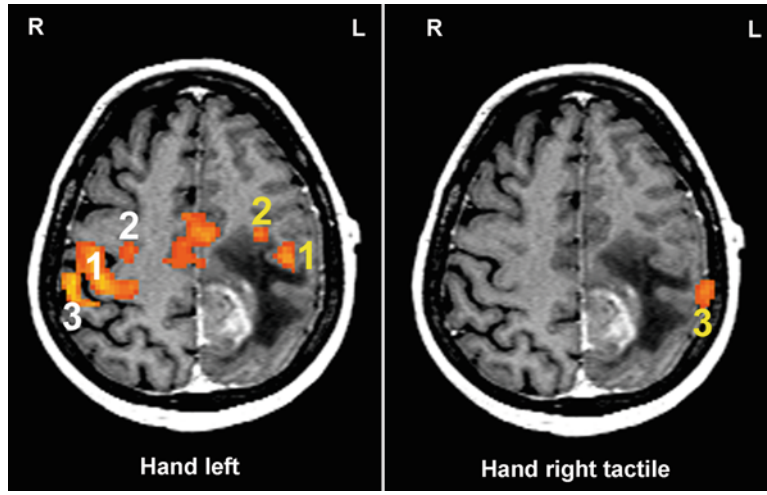

Fig. 8.13 Presurgical fMRI protocol for patients with preexisting paresis. This protocol may serve as an adjunct to the standard protocol using movements contralateral to the brain tumor. The application is still experimental and requires own validation. In this hemiparetic patient (grade 3/5) with a left malignant glioma, only weak BOLD activation was available from contralateral (*right*) hand movements precluding reliable localization of the motor hand area (not shown). By using complex finger opposition of the unimpaired hand ipsilateral to the tumor (*left*) and fully automated tactile stimulation of the right digits, BOLD activation is achievable in the motor hand area (*1*), premotor cortex (*2*), and primary somatosensory cortex (*3*) on the tumor's side. Note the corresponding activations in the unimpaired hemisphere (*right*) associated with the left finger movements (*white numbers*). Bilateral supplementary motor activation is in the midline

requires own validation. In these patients the primary motor cortex is commonly infiltrated by the tumor or severely compressed precluding both reliable identification of the rolandic anatomy on morphological images and proper performance of contralateral movements for presurgical fMRI. However, as a basic principle, residual contralateral motor function and passive somatosensory stimulation should be used first for the functional localization of the pre- and postcentral gyrus. As a further adjunct, complex finger opposition of the nonparetic hand ipsilateral to the brain tumor can be used to activate the whole cortical motor network in both hemispheres. The premotor activation on the tumors side may serve as an additional functional landmark for the precentral gyrus, by localizing the anterior wall of the precentral gyrus near the junction of the precentral sulcus with the posterior part of the superior frontal sulcus (Fig. 8.13). It is important to note that the risk of surgery-related motor deficits cannot be estimated using premotor activation as a functional landmark! However, in healthy volunteers, primary motor coactivation can be observed frequently localizing the motor hand area ipsilateral to the moving hand (Stippich et al. 2007). Our initial clinical experience indicates that ipsilateral primary motor coactivation may be supportive to localize the motor hand area on the tumor side in hemiparetic patients.

Note: For all preoperative fMRI protocols presented here, the combination with anisotropic diffusion-weighted MRI or DTI (FA-mapping, DTI-tractography) is highly recommended to also delineate the effects of the rolandic pathologies on the pyramidal tract (Stippich et al. 2003).

8.8 Limitations and Pitfalls

Traditionally, functional areas are electrophysiologically mapped intraoperatively to reliably assess the spatial relationship between brain tumor and functional cortex (Ojemann et al. 1989; Duffau et al. 1999). Intraoperative EcoG is considered

very reliable, but the sensitivity to detect motor function in the proximity of rolandic brain tumors can be low (Shinoura et al. 2005) and the method comprises several disadvantages. Surgery time can be substantially prolonged or patients need to be subjected to awake craniotomy. Furthermore, it is possible to derive activations only from the brain surface, while the by far larger portion of the cortex deep in the cerebral convolutions remains inaccessible (Cosgrove et al. 1996). Another significant disadvantage of EcoG is that the information is not available preoperatively and cannot be implemented in the assessment of the indication to operate and the planning of function-preserving surgery. After all, morphological imaging provides very detailed information about intracranial pathologies (Osborn 2004), but not about brain function. fMRI is capable of overcoming these disadvantages of the "traditional diagnostic procedures" by visualizing anatomy, pathology, and function noninvasively in a single examination even prior to surgery.

When carried out in a standard way, fMRI is basically capable of providing a clinical "functional diagnosis" for individual patients (Thulborn 2006). Functional landmarks help to estimate possible therapy-related deficits and are thus particularly useful in providing patient information, verifying the indication, and selecting a sparing therapeutic procedure. Once the operation has been decided upon, careful planning and appropriate selection of incision, trepanation, surgical access, and resection margins are essential to function-preserving surgery. Intraoperatively, functional localizations facilitate surgical orientation, although inaccuracies resulting from displaced brain tissue need to be taken into consideration (Stippich et al. 2002a, b, 2003). All these factors increase patient safety and reduce the risk of postoperative deficits which additionally reduce quality of life.

According to current knowledge, one can assume that presurgical fMRI is able to contribute to a reduction of invasive diagnostic procedures both before and during neurosurgical interventions in patients with brain tumors. Whether fMRI can have a positive effect on surgery-related morbidity and disease-related mortality remains to be determined in prospective studies. Prerequisites for this include a consensus on performance, analysis and medical appraisal of presurgical fMRI, as well as the delineation of recommendations and guidelines by the assigned medical societies.

Preoperative fMRI has limitations imposed by patient-specific and methodological factors. Despite intensive patient training, optimized examination protocols, and appropriate head fixation, some patients cannot be examined due to poor cooperation or marked restlessness. When motor paradigms are used, undesirable continuation of movement during resting periods, mostly uncontrolled and interspersed accompanying movements in other parts of the body, can significantly compromise the quality of the examination, even if individually adjusted evaluation is used to register the error precisely. In the end, after this time-consuming process, examination results often need to be discarded. The same holds true for strong motion artifacts which cannot be corrected at later data processing stages. Stimulus-related motion artifacts can simulate activations, leading to false high BOLD signals or even to incorrect localization (Hajnal et al. 1994; Krings et al. 2001; Hoeller et al. 2002; Steger and Jackson 2004). With regard to the appearance of motion artifacts, tongue and toe movements as well as finger opposition tasks are less critical than hand, foot, and lip movements.

The problems associated with investigating motor function in patients with tumor-related hemipareses have already been addressed (see Sect. 4.4). In most cases, functional localization of the pre- and postcentral gyrus can be achieved by using residual motor function in the affected extremities and applying special paradigms (Stippich et al. 2003). Compared to motor fMRI, BOLD signals are significantly weaker on tactile stimulation. Particularly in the lower extremities, tactile stimulation does not always achieve sufficient activation. This is accounted for by the lower number of receptors in toe tips, the comparatively small cortical toe representation, and ill-defined compressed air pulses when long pneumatic tubes are used.

The BOLD signals based on fMRI originate mainly in the capillary bed of the activated brain area and downstream veins (Frahm et al. 1994; Menon et al. 1995). Thus, fMRI measures a hemodynamic secondary phenomenon and not neuronal activity directly. Possible localization errors due to BOLD signals from draining veins can be identified by superimposing functional image data onto contrast-enhanced anatomical T1-weighted image sequences (Krings et al. 1999). Careful analysis of the signal-time curves of functional raw data helps to distinguish between parenchymatous and venous activation, since these rise at different rates (Krings et al. 2001). By causing vessel compression and pathological changes in vascular autoregulation, brain tumors can affect the localization and intensity of the BOLD signals measured (Holodny et al. 1999, 2000; Krings et al. 2002a, b; Ulmer et al. 2003, 2004; Kim et al. 2005; Liu et al. 2005; Hou et al. 2006; Ludemann et al. 2006). Whether artificial activations can occur due to their neovascularization remains to be clarified. For this reason, activations within contrast-enhanced tumor portions should be assessed as artifacts until reliable study results are available. Such activations should not be used for risk assessment, surgery planning, or functional neuronavigation. The same is true for BOLD signals in strongly vascularized cerebral metastases AVM (Lazar et al. 1997; Alkadhi et al. 2000; Lehericy et al. 2002; Ozdoba et al. 2002).

Investigator-dependent inaccuracies occur in manual superposition of EPI data, distorted by the method, onto anatomical 3D data sets. As a precaution, a possible localization error of approximately 0.5 cm should always be assumed (Stippich et al. 2003). Improvements are expected in the future when distortion corrections for EPI data sets are available for clinical application (Weiskopf et al. 2005; Liu and Ogawa 2006; Priest et al. 2006), enabling superposition routines to be automated. We consider defining resection margins in presurgical diagnostics on the basis of fMRI data as unreliable, since the spatial extent of activated areas depends on the evaluation parameters chosen and can therefore vary. In addition, the position of brain structures can change intraoperatively ("brain shift"), with the result that data obtained preoperatively no longer accurately reflect the intraoperative situation (Wirtz et al. 1997; Wittek et al. 2005; Nimsky et al. 2006). Effluent cerebrospinal fluid alone can lead to shifts of several millimeters after opening of the dura. Moreover, there is often a sharp shift in the position of the brain due to tissue resection. For these reasons, preoperative fMRI cannot replace intraoperative mapping of brain function completely. Irrespective of functional imaging, additional technical inaccuracies must be taken into consideration in neuronavigation and referencing.

Acknowledgment Text and figures have been reproduced in part from Stippich 2007 with permission.

References

Achten E, Jackson GD et al (1999) Presurgical evaluation of the motor hand area with functional MR imaging in patients with tumors and dysplastic lesions. Radiology 210(2):529–538

Alkadhi H, Kollias SS et al (2000) Plasticity of the human motor cortex in patients with arteriovenous malformations: a functional MR imaging study. AJNR Am J Neuroradiol 21(8):1423–1433

Atlas SW, Howard RS II et al (1996) Functional magnetic resonance imaging of regional brain activity in patients with intracerebral gliomas: findings and implications for clinical management. Neurosurgery 38(2): 329–338

Bandettini PA, Wong EC et al (1992) Time course EPI of human brain function during task activation. Magn Reson Med 25(2):390–397

Baumann SB, Noll DC et al (1995) Comparison of functional magnetic resonance imaging with positron emission tomography and magnetoencephalography to identify the motor cortex in a patient with an arteriovenous malformation. J Image Guid Surg 1(4):191–197

Belliveau JW, Kennedy DN et al (1991) Functional mapping of the human visual cortex by magnetic resonance imaging. Science 254(5032):716–719

Bittar RG, Olivier A et al (1999) Presurgical motor and somatosensory cortex mapping with functional magnetic resonance imaging and positron emission tomography. J Neurosurg 91(6):915–921

Bittar RG, Olivier A et al (2000) Cortical motor and somatosensory representation: effect of cerebral lesions. J Neurosurg 92(2):242–248

Carpentier AC, Constable RT et al (2001) Patterns of functional magnetic resonance imaging activation

in association with structural lesions in the rolandic region: a classification system. J Neurosurg 94(6):946–954

Cosgrove GR, Buchbinder BR et al (1996) Functional magnetic resonance imaging for intracranial navigation. Neurosurg Clin N Am 7(2):313–322

Duffau H, Capelle L et al (1999) Intra-operative direct electrical stimulations of the central nervous system: the Salpetriere experience with 60 patients. Acta Neurochir (Wien) 141(11):1157–1167

Dymarkowski S, Sunaert S et al (1998) Functional MRI of the brain: localisation of eloquent cortex in focal brain lesion therapy. Eur Radiol 8(9):1573–1580

Feigl GC, Safavi-Abbasi S et al (2008) Real-time 3 T fMRI data of brain tumour patients for intra-operative localization of primary motor areas. Eur J Surg Oncol 34(6):708–715

Fesl G, Moriggl B et al (2003) Inferior central sulcus: variations of anatomy and function on the example of the motor tongue area. Neuroimage 20(1):601–610

Frahm J, Merboldt KD et al (1994) Brain or vein – oxygenation or flow? On signal physiology in functional MRI of human brain activation. NMR Biomed 7(1–2):45–53

Gasser T, Ganslandt O et al (2005) Intraoperative functional MRI: implementation and preliminary experience. Neuroimage 26(3):685–693

Geerts J, Martens M et al (2007) Functional magnetic resonance imaging for preoperative localisation of eloquent brain areas relative to brain tumours: clinical implementation in a regional hospital. JBR-BTR 90(4):258–263

Golaszewski SM, Zschiegner F et al (2002) A new pneumatic vibrator for functional magnetic resonance imaging of the human sensorimotor cortex. Neurosci Lett 324(2):125–128

Golaszewski SM, Siedentopf CM et al (2004) Modulatory effects on human sensorimotor cortex by whole-hand afferent electrical stimulation. Neurology 62(12):2262–2269

Golaszewski SM, Siedentopf CM et al (2006) Human brain structures related to plantar vibrotactile stimulation: a functional magnetic resonance imaging study. Neuroimage 29(3):923–929

Haberg A, Kvistad KA et al (2004) Preoperative blood oxygen level-dependent functional magnetic resonance imaging in patients with primary brain tumors: clinical application and outcome. Neurosurgery 54(4):902–914; discussion 914–915

Hajnal JV, Myers R et al (1994) Artifacts due to stimulus correlated motion in functional imaging of the brain. Magn Reson Med 31(3):283–291

Hall WA, Liu H et al (2005) Functional magnetic resonance imaging-guided resection of low-grade gliomas. Surg Neurol 64(1):20–27; discussion 27

Hirsch J, Ruge MI et al (2000) An integrated functional magnetic resonance imaging procedure for preoperative mapping of cortical areas associated with tactile, motor, language, and visual functions. Neurosurgery 47(3):711–721; discussion 721–722

Hoeller M, Krings T et al (2002) Movement artefacts and MR BOLD signal increase during different paradigms for mapping the sensorimotor cortex. Acta Neurochir (Wien) 144(3):279–284; discussion 284

Holodny AI, Schulder M et al (1999) Decreased BOLD functional MR activation of the motor and sensory cortices adjacent to a glioblastoma multiforme: implications for image-guided neurosurgery. AJNR Am J Neuroradiol 20(4):609–612

Holodny AI, Schulder M et al (2000) The effect of brain tumors on BOLD functional MR imaging activation in the adjacent motor cortex: implications for image-guided neurosurgery. AJNR Am J Neuroradiol 21(8):1415–1422

Holodny AI, Schwartz TH et al (2001) Tumor involvement of the corticospinal tract: diffusion magnetic resonance tractography with intraoperative correlation. J Neurosurg 95(6):1082

Hou BL, Bradbury M et al (2006) Effect of brain tumor neovasculature defined by rCBV on BOLD fMRI activation volume in the primary motor cortex. Neuroimage 32(2):489–497

Jack CR, Thompson PM et al (1994) Sensory motor cortex: correlation of presurgical mapping with functional MR imaging and invasive cortical mapping. Radiology 190(1):85–92

Jacobs AH, Kracht LW et al (2005) Imaging in neurooncology. NeuroRx 2(2):333–347

Kampe KK, Jones RA et al (2000) Frequency dependence of the functional MRI response after electrical median nerve stimulation. Hum Brain Mapp 9(2):106–114

Kim MJ, Holodny AI et al (2005) The effect of prior surgery on blood oxygen level-dependent functional MR imaging in the preoperative assessment of brain tumors. AJNR Am J Neuroradiol 26(8):1980–1985

Kokkonen SM, Kiviniemi V et al (2005) Effect of brain surgery on auditory and motor cortex activation: a preliminary functional magnetic resonance imaging study. Neurosurgery 57(2):249–256; discussion 249–256

Krainik A, Lehericy S et al (2001) Role of the supplementary motor area in motor deficit following medial frontal lobe surgery. Neurology 57(5):871–878

Krainik A, Lehericy S et al (2003) Postoperative speech disorder after medial frontal surgery: role of the supplementary motor area. Neurology 60(4):587–594

Krainik A, Duffau H et al (2004) Role of the healthy hemisphere in recovery after resection of the supplementary motor area. Neurology 62(8):1323–1332

Krings T, Reul J et al (1998) Functional magnetic resonance mapping of sensory motor cortex for image-guided neurosurgical intervention. Acta Neurochir (Wien) 140(3):215–222

Krings T, Erberich SG et al (1999) MR blood oxygenation level-dependent signal differences in parenchymal and large draining vessels: implications for functional MR imaging. AJNR Am J Neuroradiol 20(10):1907–1914

Krings T, Reinges MH et al (2001) Functional MRI for presurgical planning: problems, artefacts, and solution strategies. J Neurol Neurosurg Psychiatry 70(6):749–760

Krings T, Reinges MH et al (2002a) Factors related to the magnitude of T2* MR signal changes during functional imaging. Neuroradiology 44(6):459–466

Krings T, Topper R et al (2002b) Activation in primary and secondary motor areas in patients with CNS neoplasms and weakness. Neurology 58(3):381–390

Krishnan R, Raabe A et al (2004) Functional magnetic resonance imaging-integrated neuronavigation: correlation between lesion-to-motor cortex distance and outcome. Neurosurgery 55(4):904–914; discussion 914–915

Kurth R, Villringer K et al (1998) FMRI assessment of somatotopy in human Brodmann area 3b by electrical finger stimulation. Neuroreport 9(2):207–212

Kwong KK, Belliveau JW et al (1992) Dynamic magnetic resonance imaging of human brain activity during primary sensory stimulation. Proc Natl Acad Sci USA 89(12):5675–5679

Lazar RM, Marshall RS et al (1997) Anterior translocation of language in patients with left cerebral arteriovenous malformation. Neurology 49(3):802–808

Lee CC, Ward HA et al (1999) Assessment of functional MR imaging in neurosurgical planning. AJNR Am J Neuroradiol 20(8):1511–1519

Lehericy S, Duffau H et al (2000) Correspondence between functional magnetic resonance imaging somatotopy and individual brain anatomy of the central region: comparison with intraoperative stimulation in patients with brain tumors. J Neurosurg 92(4): 589–598

Lehericy S, Biondi A et al (2002) Arteriovenous brain malformations: is functional MR imaging reliable for studying language reorganization in patients? Initial observations. Radiology 223(3):672–682

Liu G, Ogawa S (2006) EPI image reconstruction with correction of distortion and signal losses. J Magn Reson Imaging 24(3):683–689

Liu WC, Feldman SC et al (2005) The effect of tumour type and distance on activation in the motor cortex. Neuroradiology 47(11):813–819

Ludemann L, Forschler A et al (2006) BOLD signal in the motor cortex shows a correlation with the blood volume of brain tumors. J Magn Reson Imaging 23(4):435–443

Majos A, Tybor K et al (2005) Cortical mapping by functional magnetic resonance imaging in patients with brain tumors. Eur Radiol 15(6):1148–1158

Menon RS, Ogawa S et al (1995) BOLD based functional MRI at 4 Tesla includes a capillary bed contribution: echo-planar imaging correlates with previous optical imaging using intrinsic signals. Magn Reson Med 33(3):453–459

Moller M, Freund M et al (2005) Real time fMRI: a tool for the routine presurgical localisation of the motor cortex. Eur Radiol 15(2):292–295

Mueller WM, Yetkin FZ et al (1996) Functional magnetic resonance imaging mapping of the motor cortex in patients with cerebral tumors. Neurosurgery 39(3):515–520; discussion 520–521

Nimsky C, Ganslandt O et al (2006) Intraoperative visualization for resection of gliomas: the role of functional neuronavigation and intraoperative 1.5 T MRI. Neurol Res 28(5):482–487

Ogawa S, Menon RS et al (1993) Functional brain mapping by blood oxygenation level-dependent contrast magnetic resonance imaging. A comparison of signal characteristics with a biophysical model. Biophys J 64(3):803–812

Ojemann G, Ojemann J et al (1989) Cortical language localization in left, dominant hemisphere. An electrical stimulation mapping investigation in 117 patients. J Neurosurg 71(3):316–326

Osborn A (2004) Diagnostic imaging: brain. Amirsys, Salt Lake City

Ozdoba C, Nirkko AC et al (2002) Whole-brain functional magnetic resonance imaging of cerebral arteriovenous malformations involving the motor pathways. Neuroradiology 44(1):1–10

Parmar H, Sitoh YY et al (2004) Combined magnetic resonance tractography and functional magnetic resonance imaging in evaluation of brain tumors involving the motor system. J Comput Assist Tomogr 28(4):551–556

Petrella JR, Shah LM et al (2006) Preoperative functional MR imaging localization of language and motor areas: effect on therapeutic decision making in patients with potentially resectable brain tumors. Radiology 240(3): 793–802

Pirotte B, Goldman S et al (2005a) Integration of [11C] methionine-positron emission tomographic and magnetic resonance imaging for image-guided surgical resection of infiltrative low-grade brain tumors in children. Neurosurgery 57(1 Suppl):128–139

Pirotte B, Voordecker P et al (2005b) Combination of functional magnetic resonance imaging-guided neuronavigation and intraoperative cortical brain mapping improves targeting of motor cortex stimulation in neuropathic pain. Neurosurgery 56(2 Suppl):344–359; discussion 344–359

Priest AN, De Vita E et al (2006) EPI distortion correction from a simultaneously acquired distortion map using TRAIL. J Magn Reson Imaging 23(4):597–603

Puce A, Constable RT et al (1995) Functional magnetic resonance imaging of sensory and motor cortex: comparison with electrophysiological localization. J Neurosurg 83(2):262–270

Pujol J, Conesa G et al (1996) Presurgical identification of the primary sensorimotor cortex by functional magnetic resonance imaging. J Neurosurg 84(1):7–13

Pujol J, Conesa G et al (1998) Clinical application of functional magnetic resonance imaging in presurgical identification of the central sulcus. J Neurosurg 88(5):863–869

Ramsey NF, Sommer IE et al (2001) Combined analysis of language tasks in fMRI improves assessment of hemispheric dominance for language functions in individual subjects. Neuroimage 13(4):719–733

Reinges MH, Krings T et al (2005) Prospective demonstration of short-term motor plasticity following acquired central pareses. Neuroimage 24(4):1248–1255

Roessler K, Donat M et al (2005) Evaluation of preoperative high magnetic field motor functional MRI (3 Tesla) in glioma patients by navigated electrocortical stimulation and postoperative outcome. J Neurol Neurosurg Psychiatry 76(8):1152–1157

Rolls HK, Yoo SS et al (2007) Rater-dependent accuracy in predicting the spatial location of functional centers on anatomical MR images. Clin Neurol Neurosurg 109(3):225–235

Roux FE, Ranjeva JP et al (1997) Motor functional MRI for presurgical evaluation of cerebral tumors. Stereotact Funct Neurosurg 68(1–4 Pt 1):106–111

Roux FE, Boulanouar K et al (1999a) Cortical intraoperative stimulation in brain tumors as a tool to evaluate spatial data from motor functional MRI. Invest Radiol 34(3):225–229

Roux FE, Boulanouar K et al (1999b) Usefulness of motor functional MRI correlated to cortical mapping in rolandic low grade astrocytomas. Acta Neurochir (Wien) 141(1):71–79

Rutten GJ, Ramsey NF et al (2002) Interhemispheric reorganization of motor hand function to the primary motor cortex predicted with functional magnetic resonance imaging and transcranial magnetic stimulation. J Child Neurol 17(4):292–297

Schlosser MJ, McCarthy G et al (1997) Cerebral vascular malformations adjacent to sensorimotor and visual cortex. Functional magnetic resonance imaging studies before and after therapeutic intervention. Stroke 28(6):1130–1137

Schonberg T, Pianka P et al (2006) Characterization of displaced white matter by brain tumors using combined DTI and fMRI. Neuroimage 30(4): 1100–1111

Schreiber A, Hubbe U et al (2000) The influence of gliomas and nonglial space-occupying lesions on blood-oxygen-level-dependent contrast enhancement. AJNR Am J Neuroradiol 21(6):1055–1063

Schwindack C, Siminotto E et al (2005) Real-time functional magnetic resonance imaging (rt-fMRI) in patients with brain tumours: preliminary findings using motor and language paradigms. Br J Neurosurg 19(1):25–32

Shinoura N, Yamada R et al (2005) Preoperative fMRI, tractography and continuous task during awake surgery for maintenance of motor function following surgical resection of metastatic tumor spread to the primary motor area. Minim Invasive Neurosurg 48(2):85–90

Shinoura N, Suzuki Y et al (2006) Restored activation of primary motor area from motor reorganization and improved motor function after brain tumor resection. AJNR Am J Neuroradiol 27(6):1275–1282

Steger TR, Jackson EF (2004) Real-time motion detection of functional MRI data. J Appl Clin Med Phys 5(2):64–70

Stippich C (2005) Clinical functional magnetic resonance imaging: basic principles and clinical applications. Radiol up2date 5:317–336

Stippich C (ed) (2007) Clinical functional MRI: presurgical functional neuroimaging. Springer, New York. ISBN 978-3-540-24469-1

Stippich C, Hofmann R et al (1999) Somatotopic mapping of the human primary somatosensory cortex by fully automated tactile stimulation using functional magnetic resonance imaging. Neurosci Lett 277(1): 25–28

Stippich C, Kapfer D et al (2000) Robust localization of the contralateral precentral gyrus in hemiparetic patients using the unimpaired ipsilateral hand: a clinical functional magnetic resonance imaging protocol. Neurosci Lett 285(2):155–159

Stippich C, Heiland S et al (2002a) Functional magnetic resonance imaging: physiological background, technical aspects and prerequisites for clinical use. Rofo 174(1):43–49

Stippich C, Ochmann H et al (2002b) Somatotopic mapping of the human primary sensorimotor cortex during motor imagery and motor execution by functional magnetic resonance imaging. Neurosci Lett 331(1): 50–54

Stippich C, Kress B et al (2003) Preoperative functional magnetic resonance tomography (FMRI) in patients with rolandic brain tumors: indication, investigation strategy, possibilities and limitations of clinical application. Rofo 175(8):1042–1050

Stippich C, Romanowski A et al (2004) Fully automated localization of the human primary somatosensory cortex in one minute by functional magnetic resonance imaging. Neurosci Lett 364(2):90–93

Stippich C, Blatow M et al (2007) Global activation of primary motor cortex during voluntary movements in man. Neuroimage 34:1227–1237

Ternovoi SK, Sinitsyn VE et al (2004) Localization of the motor and speech zones of the cerebral cortex by functional magnetic resonance tomography. Neurosci Behav Physiol 34(5):431–437

Thulborn K (2006) Clinical functional magnetic resonance imaging. In: Haacke EM et al (eds) Current protocols in magnetic resonance imaging. Wiley, New York

Ulmer JL, Krouwer HG et al (2003) Pseudo-reorganization of language cortical function at fMR imaging: a consequence of tumor-induced neurovascular uncoupling. AJNR Am J Neuroradiol 24(2):213–217

Ulmer JL, Salvan CV et al (2004) The role of diffusion tensor imaging in establishing the proximity of tumor borders to functional brain systems: implications for preoperative risk assessments and postoperative outcomes. Technol Cancer Res Treat 3(6):567–576

Van Westen D, Skagerberg G et al (2005) Functional magnetic resonance imaging at 3 T as a clinical tool in patients with intracranial tumors. Acta Radiol 46(6):599–609

Weiskopf N, Klose U et al (2005) Single-shot compensation of image distortions and BOLD contrast optimization using multi-echo EPI for real-time fMRI. Neuroimage 24(4):1068–1079

Wienbruch C, Candia V et al (2006) A portable and low-cost fMRI compatible pneumatic system for the investigation of the somatosensensory system in clinical and research environments. Neurosci Lett 398(3):183–188

Wirtz CR, Tronnier VM et al (1997) Image-guided neurosurgery with intraoperative MRI: update of frameless stereotaxy and radicality control. Stereotact Funct Neurosurg 68(1–4 Pt 1):39–43

Wittek A, Kikinis R et al (2005) Brain shift computation using a fully nonlinear biomechanical model. Med Image Comput Comput Assist Interv Int Conf Med Image Comput Comput Assist Interv 8(Pt 2): 583–590

Yousry TA, Schmid UD et al (1997) Localization of the motor hand area to a knob on the precentral gyrus. A new landmark. Brain 120(Pt 1):141–157

9 The Functional Anatomy of Speech Processing: From Auditory Cortex to Speech Recognition and Speech Production

Gregory Hickok

9.1 Introduction

Lesion-based research has been successful in providing a broad outline of the neuroanatomy of speech/language processes (Dronkers et al. 2000; Hillis 2007) and continues to play a crucial role in the development of functional anatomic models of cognitive processes (Fellows et al. 2005). However, lesion studies lack the spatial resolution to assess more detailed functional anatomical hypotheses. Functional imaging methods such as fMRI, when appropriately guided and constrained by lesion and other methods, can provide much needed information.

In this chapter, we will review evidence regarding the functional anatomy of the human auditory cortex as it relates to speech recognition and speech production. Figure 9.1 displays an organizational framework for this discussion.

9.2 Hierarchical Organization of Auditory Cortex

The monkey auditory cortex is organized hierarchically with a core region at the center, a belt region surrounding the core, and a parabelt region surrounding the belt area, each containing subdivisions. The core corresponds to the primary auditory cortex, showing a distinct primary-type cytoarchitecture and robust single-unit responses to pure tones, with sharp tuning curves relative to belt regions. Both the core and the belt areas receive inputs from the medial geniculate nucleus (MGN), although from different subregions, MGv and MGd, respectively. The parabelt also receives direct ascending auditory input from MGd but is distinguished from the belt area in that it does not receive direct input from the core. Instead, information reaching the parabelt from the core appears to be mediated by the belt region which projects heavily to the parabelt (Kaas and Hackett 2000; Kaas et al. 1999).

The human auditory cortex appears to be similar in its hierarchical organization. Simple acoustic stimulation, such as noise bursts or tones, activates the auditory cortex in and around Heschl's gyrus. In addition, more complex stimuli, such as speech, activate a broader region, including the superior temporal sulcus (STS) (Binder et al. 2000).

In both human and nonhuman primates, there is evidence for two broad projection streams, sometimes referred to as the ventral and dorsal pathways (Hickok and Poeppel 2000, 2007; Rauschecker 1998; Romanski et al. 1999; Scott 2005). There is a general agreement that the ventral stream supports recognition of the content of auditory information (a "what" pathway), but there is disagreement regarding the nature of the dorsal stream, with some authors promoting a location-based function ("where"

G. Hickok
Department of Cognitive Sciences,
Center for Cognitive Neuroscience,
University of California, Irvine, CA, USA
e-mail: gshickok@uci.edu

S. Ulmer, O. Jansen (eds.), *fMRI – Basics and Clinical Applications*,
DOI 10.1007/978-3-642-34342-1_9,

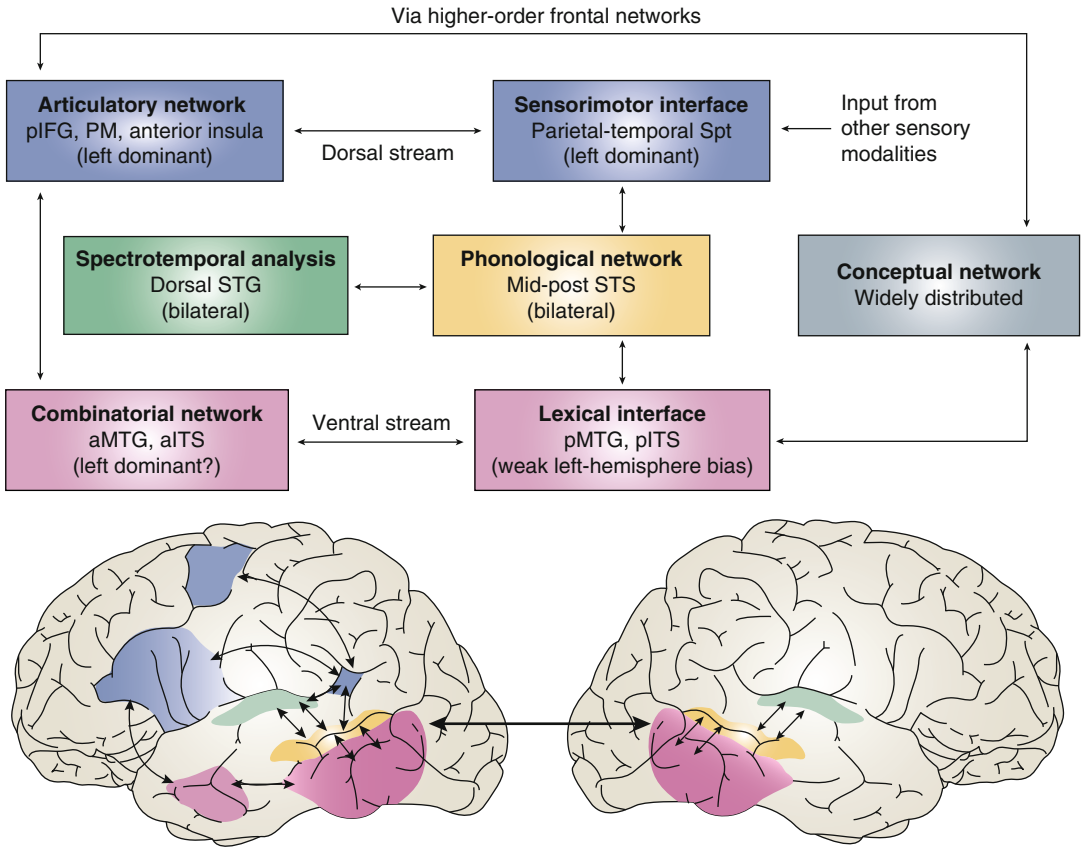

Fig. 9.1 The dual-stream model of the functional anatomy of language. (**a**) Schematic diagram of the dual-stream model. The earliest stage of cortical speech processing involves some form of spectrotemporal analysis, which is carried out in auditory cortices bilaterally in the supratemporal plane. These spectrotemporal computations appear to differ between the two hemispheres. Phonological-level processing and representation involves the middle to posterior portions of the superior temporal sulcus (STS) bilaterally, although there may be a weak left-hemisphere bias at this level of processing. Subsequently, the system diverges into two broad streams, a dorsal pathway (*blue*) that maps sensory or phonological representations onto articulatory motor representations and a ventral pathway (*pink*) that maps sensory or phonological representations onto lexical conceptual representations. (**b**) Approximate anatomical locations of the dual-stream model components, specified as precisely as available evidence allows. Regions shaded *green* depict areas on the dorsal surface of the superior temporal gyrus (STG) that are proposed to be involved in spectrotemporal analysis. Regions shaded *yellow* in the posterior half of the STS are implicated in phonological-level processes. Regions shaded *pink* represent the ventral stream, which is bilaterally organized with a weak left-hemisphere bias. The more posterior regions of the ventral stream, posterior middle, and inferior portions of the temporal lobes correspond to the lexical interface, which links phonological and semantic information, whereas the more anterior locations correspond to the proposed combinatorial network. Regions shaded *blue* represent the dorsal stream, which is strongly left dominant. The posterior region of the dorsal stream corresponds to an area in the Sylvian fissure at the parietotemporal boundary (area Spt), which is proposed to be a sensorimotor interface, whereas the more anterior locations in the frontal lobe, probably involving Broca's region and a more dorsal premotor site, correspond to portions of the articulatory network. *Arrows* indicate reciprocal connections. *aITS* anterior inferior temporal sulcus, *aMTG* anterior middle temporal gyrus, *pIFG* posterior inferior frontal gyrus, *PM* premotor cortex (Reprinted with permission from Hickok and Poeppel (2007))

pathway) (Rauschecker 1998) and others an auditory-motor integration function (Hickok et al. 2003; Hickok and Poeppel 2000, 2007; Warren et al. 2005). These hypotheses are not necessarily incompatible.

9.3 STS Supports Phonological Aspects of Speech Recognition

A number of studies have found that portions of the STS are important for representing and/or processing phonological information (Fig. 9.1, yellow; Binder et al. 2000; Hickok and Poeppel 2004, 2007; Indefrey and Levelt 2004; Liebenthal et al. 2005; Price et al. 1996). The STS is activated by several tasks that tap phonological information such as speech perception, speech production (Indefrey and Levelt 2004), and the active short-term maintenance of phonemic information (Buchsbaum et al. 2001; Hickok et al. 2003). Functional activation studies that have used subtraction methodologies to isolate phonological processes have found activation along the STS (Liebenthal et al. 2005; Narain et al. 2003; Obleser et al. 2006; Scott et al. 2000; Spitsyna et al. 2006; Vouloumanos et al. 2001), as have studies that manipulate psycholinguistic variables that tap phonological networks (Okada and Hickok 2006). Although a common view is that the phonological system is strongly left dominant, both lesion and imaging evidence (Hickok and Poeppel 2007) suggest a bilateral organization.

One currently unresolved question is the relative contribution of anterior vs. posterior STS regions in phonological processing. A majority of functional imaging studies targeting phonological processing in perception have highlighted regions in the posterior half of the STS (Hickok and Poeppel 2007). Other studies, however, have reported *anterior* STS activation in perceptual speech tasks (Mazoyer et al. 1993; Narain et al. 2003; Scott et al. 2000; Spitsyna et al. 2006). These studies involved sentence-level stimuli raising the possibility that anterior STS regions may be responding to some other aspect of the stimuli such as its syntactic or prosodic organization (Friederici et al. 2000; Humphries et al. 2001, 2005, 2006; Vandenberghe et al. 2002). Lesion evidence indicates that damage to posterior temporal lobe areas is most predictive of auditory comprehension deficits (Bates et al. 2003). The weight of the available evidence, therefore, suggests that the critical portion of the STS that is involved in phonological-level processes is bounded anteriorly by the anterolateral-most aspect of Heschl's gyrus and posteriorly by the posterior-most extent of the Sylvian fissure (Hickok and Poeppel 2007).

9.4 Access to Conceptual-Semantic Information May Involve Middle Temporal Regions

Comprehension of speech involves more than just processing and recognizing phonological information in speech. It crucially involves using speech sound information to access conceptual-semantic representations. Although the organization of semantic knowledge in the brain is far from understood, a common view is that conceptual-semantic information is widely distributed throughout the cortex (Damasio and Damasio 1994; Gage and Hickok 2005; Hickok and Poeppel 2000, 2004, 2007; Martin 1998; Martin and Chao 2001; Mesulam 1998; Squire 1986). Access to this system via auditory-linguistic channels, however, may be more focal. The posterior, middle, and ventral temporal lobe (~BA 37) appears to be an important node in the interface between auditory/speech systems and conceptual-semantic knowledge (Fig. 9.1, posterior pink-shaded area). This conclusion is supported by lesion evidence showing that damage to this region results in semantic-level deficits in both comprehension and production (Chertkow et al. 1997; Hart and Gordon 1990; Hickok and Poeppel 2004, 2007).

Functional imaging studies have implicated these same regions in lexical-semantic processing. For example, Binder and colleagues asked subjects to make semantic decisions about auditorily presented words (Binder et al. 1997). In comparison to a tone-decision control task,

semantic decisions strongly activated portions of the STS and middle temporal and inferior temporal gyri (in additional to frontal and parietal regions), but did not activate the superior temporal gyrus (STG). In the context of studies on phonological-level processes discussed above, a reasonable interpretation is that the STS activation reflects phonological aspects of word processing, whereas the more ventral activations, which do not show up reliably in studies of phonological processing, reflect postphonemic mechanisms involved in processing or accessing lexical-semantic information.

Similar conclusions are derived from studies of lexical-semantic processing that use different approaches. Some studies have found greater activation in inferior posterior temporal regions for words compared to nonwords (Binder et al. 2005; Rissman et al. 2003). This contrast should emphasize lexical-semantic processes as nonwords have minimal lexical-semantic associations. Posterior middle temporal regions have also been implicated in processing semantically ambiguous words. Rodd et al. found that listening to sentences that contained high levels of lexical ambiguity produced more activation in the left posterior MTG (Rodd et al. 2005).

Imaging studies of semantic priming, which also should highlight regions involved in lexical-semantic processing, have, however, led to a different conclusion. These studies (Copland et al. 2003; Rissman et al. 2003) have found a more anterior middle temporal site that shows a reduction in activation for semantically related, compared to semantically unrelated, word pairs (priming is typically reflected as a reduction of brain activity (Henson 2003)). The implication of anterior temporal regions is not consistent with stroke-based lesion studies, as noted above. However, it is consistent with recent claims derived from studies of semantic dementia that the anterior temporal lobes play a critical role in the representation of conceptual knowledge (Hodges and Patterson 2007; Patterson et al. 2007).

Much work remains to be done in understanding the functional anatomy of semantic-related processes, particularly the relation between the posterior and anterior regions which have been implicated. It is possible to make the generalization that while phonemic-level processes involve auditory-responsive regions in the STS, higher-level lexical- and conceptual-semantic processes involve regions surrounding the STS both ventrally and posteriorly.

9.5 Sensory Systems Participate in Speech Production

There is unequivocal evidence that posterior sensory-related cortex in the left, but not right, hemisphere participates in speech production. For example, damage to the left posterior temporal lobe often results not only in comprehension deficits but also in speech *production* deficits (Damasio 1991, 1992; Geschwind 1971; Goodglass 1993; Goodglass et al. 2001). Disruption to phonological systems appears to account for some of these production deficits. Damage to the left dorsal STG and/or the supramarginal gyrus/temporal-parietal junction is associated with conduction aphasia, a syndrome that is characterized by good comprehension but with frequent phonemic errors in speech production, naming difficulties that often involve tip-of-the-tongue states (implicating a breakdown in phonological encoding) and difficulty with verbatim repetition (Damasio and Damasio 1980; Goodglass 1992).[1] Conduction aphasia has classically been considered to be a disconnection syndrome involving damage to the arcuate fasciculus (Geschwind 1965). However, there is now good evidence that this syndrome results from cortical dysfunction (Anderson et al. 1999;

[1]Although conduction aphasia is often characterized as a disorder of repetition, it is clear that the deficit extends well beyond this one task (Hickok et al. 2000). In fact, Wernicke first identified conduction aphasia as a disorder of speech production in the face of preserved comprehension (Wernicke 1874/1969). It was only later that Lichtheim introduced repetition as a convenient diagnostic tool for assessing the integrity of the link between sensory and motor speech systems (Lichtheim 1885).

Hickok et al. 2000). Thus, conduction aphasia provides evidence for the involvement of left posterior auditory-related brain regions in phonological aspects of speech production (Hickok 2000; Hickok et al. 2000).

Functional imaging evidence also implicates left superior posterior temporal regions in speech production generally (Hickok et al. 2000; Price et al. 1996) and phonological stages of the process in particular (Indefrey and Levelt 2000, 2004). With respect to the latter, the posterior portion of the left planum temporale region, which is within the distribution of lesions associated with conduction aphasia, activates during picture naming and exhibits length effects (Okada et al. 2003) and frequency effects (Graves et al. 2007) and has a time course of activation, measured electromagnetically, that is consistent with the phonological encoding stage of naming (Levelt et al. 1998).

Taken together, the lesion and physiological evidence reviewed in this section make a compelling argument for the involvement of left posterior superior temporal regions in phonological aspects of speech production.

9.6 The Posterior Planum Temporale Supports Sensorimotor Integration

If left posterior superior temporal regions are involved in phonological aspects of speech *production*, there must be a mechanism for interfacing posterior and anterior brain regions. The need for such a mechanism has long been acknowledged and, in classical models, was instantiated as a simple white matter pathway, the arcuate fasciculus (Geschwind 1971). More recent proposals have argued, instead, for a *cortical* system that serves to integrate sensory and motor aspects of speech (Hickok et al. 2000, 2003; Hickok and Poeppel 2000, 2004, 2007; Warren et al. 2005), which is consistent with much research on sensorimotor integration systems studied in the context of the monkey visual system (Andersen 1997; Colby and Goldberg 1999; Milner and Goodale 1995).

A series of studies over the last several years has identified a cortical network for speech and related abilities (e.g., music), which has many of the properties exhibited by sensorimotor networks studied in other domains. These properties include sensorimotor responses, connectivity with frontal motor systems, motor effector specificity, and multisensory responses (Andersen 1997; Colby and Goldberg 1999). The speech-related network with these response properties includes an area (termed Spt) in the left posterior planum temporal (Okada and Hickok 2009) region (Fig. 9.1, posterior blue-shaded region) that has been argued to support sensorimotor integration for speech (Hickok et al. 2003). We will review the evidence for this claim below.

9.6.1 Spt Exhibits Sensorimotor Response Properties

A number of studies have demonstrated the existence of an area in the left posterior planum temporale that responds both during the perception and production of speech, even when speech is produced covertly (subvocally) so that there is no overt auditory feedback (Buchsbaum et al. 2001, 2005a, b; Hickok et al. 2003). Spt is not speech-specific, however. It responds equally well to the perception and (covert) production via humming of melodic stimuli (Hickok et al. 2003; Pa and Hickok 2008).

9.6.2 Spt Is Functionally Connected to Motor Speech Areas

Spt activity is tightly correlated with activity in frontal speech production-related areas, such as the pars opercularis (BA 44; Buchsbaum et al. 2001), suggesting that the two regions are functionally connected. Furthermore, cortex in the posterior portion of the planum temporale (area Tpt) has a cytoarchitectonic structure that is similar to BA44. Galaburda writes, "area Tpt … exhibits a degree of specialization like that of Area 44 in Broca's region. It contains prominent pyramids in layer IIIc and a broad lamina IV….

the intimate relationship and similar evolutionary status of Areas 44 and Tpt allows for a certain functional overlap" (Galaburda 1982).

9.6.3 Spt Activity Is Modulated by Motor Effector Manipulations

In monkey, parietal cortex sensorimotor integration areas are organized around motor effector systems (e.g., ocular vs. manual actions in LIP and AIP; (Andersen 1997; Colby and Goldberg 1999)). Recent evidence suggests that Spt may be organized around the vocal tract effector system: Spt was less active when skilled pianists listened to and then imagined playing a novel melody than when they listened to and covertly hummed the same melody (Pa and Hickok 2008).

9.6.4 Spt Is Sensitive to Speech-Related Visual Stimuli

Many neurons in sensorimotor integration areas of the monkey parietal cortex are sensitive to inputs from more than one sensory modality (Andersen 1997). The planum temporale, while often thought to be an auditory area, also activates in response to sensory input from other modalities. For example, silent lip-reading has been shown to activate auditory cortex in the vicinity of the planum temporale (Calvert et al. 1997; Calvert and Campbell 2003). Although these studies typically report the location as "auditory cortex" including primary regions, group-based localizations in this region can be unreliable. Indeed, a recent fMRI study using individual subject analyses has found that activation to visual speech and activation using the standard Spt-defining auditory-motor task (listen then covertly produce) are found in the same regions of the left posterior planum temporale. Thus, Spt appears to be sensitive also to visual input that is relevant to vocal tract actions.

In summary, Spt exhibits all the features of sensorimotor integration areas as identified in the parietal cortex of the monkey. This suggests that Spt is a sensorimotor integration area for vocal tract actions (Pa and Hickok 2008), placing it in the context of a network of sensorimotor integration areas in the posterior parietal and temporal/parietal cortex, which receive multisensory input and are organized around motor effector systems (Andersen 1997). Although area Spt is not language-specific, it counts sensorimotor integration for phonological information as a prominent function.

9.7 Summary

Data from functional imaging studies has augmented a long history of language-brain research based on traditional neuropsychological methods. This work converges on several broad conclusions that are particularly relevant to an understanding of the neural organization of speech processing. Human auditory cortex is hierarchically organized with early areas primarily involved in the spectrotemporal analysis of acoustic signals. Higher-order representations/processes, such as those involved in the analysis of phonological information, involve auditory-related regions in the STS, which are probably several steps downstream from primary auditory cortex. Beyond these high-level auditory-related systems in the STS, portions of the middle and inferior temporal gyri are important for mapping auditory-related representations onto conceptual-semantic systems. These systems, involved in mapping acoustic input onto conceptual-semantic representations, comprise the ventral stream and is bilaterally organized in its early stages, becoming somewhat left dominant at the level of conceptual-semantic access. A dorsal stream connects portions of the auditory system to articulatory motor systems, thus enabling speech production and related functions. This circuit involves the posterior planum temporale (area Spt), which may function as a sensorimotor interface system for the vocal tract.

References

Andersen R (1997) Multimodal integration for the representation of space in the posterior parietal cortex. Philos Trans R Soc Lond B Biol Sci 352:1421–1428

Anderson JM, Gilmore R et al (1999) Conduction aphasia and the arcuate fasciculus: a reexamination of the Wernicke-Geschwind model. Brain Lang 70:1–12

Bates E, Wilson SM et al (2003) Voxel-based lesion-symptom mapping. Nat Neurosci 6(5):448–450

Binder JR, Frost JA et al (1997) Human brain language areas identified by functional magnetic resonance imaging. J Neurosci 17:353–362

Binder JR, Frost JA et al (2000) Human temporal lobe activation by speech and nonspeech sounds. Cereb Cortex 10:512–528

Binder JR, Westbury CF et al (2005) Distinct brain systems for processing concrete and abstract concepts. J Cogn Neurosci 17(6):905–917

Buchsbaum B, Hickok G et al (2001) Role of left posterior superior temporal gyrus in phonological processing for speech perception and production. Cogn Sci 25:663–678

Buchsbaum BR, Olsen RK et al (2005a) Human dorsal and ventral auditory streams subserve rehearsal-based and echoic processes during verbal working memory. Neuron 48(4):687–697

Buchsbaum BR, Olsen RK et al (2005b) Reading, hearing, and the planum temporale. Neuroimage 24(2):444–454

Calvert GA, Campbell R (2003) Reading speech from still and moving faces: the neural substrates of visible speech. J Cogn Neurosci 15:57–70

Calvert GA, Bullmore ET et al (1997) Activation of auditory cortex during silent lipreading. Science 276: 593–596

Chertkow H, Bub D et al (1997) On the status of object concepts in aphasia. Brain Lang 58(2):203–232

Colby CL, Goldberg ME (1999) Space and attention in parietal cortex. Annu Rev Neurosci 22:319–349

Copland DA, de Zubicaray GI et al (2003) Brain activity during automatic semantic priming revealed by event-related functional magnetic resonance imaging. Neuroimage 20(1):302–310

Damasio H (1991) Neuroanatomical correlates of the aphasias. In: Sarno M (ed) Acquired aphasia, 2nd edn. Academic, San Diego, pp 45–71

Damasio AR (1992) Aphasia. N Engl J Med 326:531–539

Damasio H, Damasio AR (1980) The anatomical basis of conduction aphasia. Brain 103:337–350

Damasio AR, Damasio H (1994) Cortical systems for retrieval of concrete knowledge: the convergence zone framework. In: Koch C, Davis JL (eds) Large-scale neuronal theories of the brain. MIT Press, Cambridge, pp 61–74

Dronkers NF, Redfern BB et al (2000) The neural architecture of language disorders. In: Gazzaniga MS (ed) The new cognitive neurosciences. MIT Press, Cambridge, pp 949–958

Fellows LK, Heberlein AS et al (2005) Method matters: an empirical study of impact in cognitive neuroscience. J Cogn Neurosci 17(6):850–858

Friederici AD, Meyer M et al (2000) Auditory language comprehension: an event-related fMRI study on the processing of syntactic and lexical information. Brain Lang 74:289–300

Gage N, Hickok G (2005) Multiregional cell assemblies, temporal binding, and the representation of conceptual knowledge in cortex: a modern theory by a "classical" neurologist, Carl Wernicke. Cortex 41:823–832

Galaburda AM (1982) Histology, architectonics, and asymmetry of language areas. In: Arbib MA, Caplan D, Marshall JC (eds) Neural models of language processes. Academic, San Diego, pp 435–445

Geschwind N (1965) Disconnexion syndromes in animals and man. Brain 88(237–294):585–644

Geschwind N (1971) Aphasia. N Engl J Med 284:654–656

Goodglass H (1992) Diagnosis of conduction aphasia. In: Kohn SE (ed) Conduction aphasia. Lawrence Erlbaum, Hillsdale, pp 39–49

Goodglass H (1993) Understanding aphasia. Academic, San Diego

Goodglass H, Kaplan E et al (2001) The assessment of aphasia and related disorders, 3rd edn. Lippincott Williams and Wilkins, Philadelphia

Graves WW, Grabowski TJ et al (2007) A neural signature of phonological access: distinguishing the effects of word frequency from familiarity and length in overt picture naming. J Cogn Neurosci 19:617–631

Hart JJ, Gordon B (1990) Delineation of single-word semantic comprehension deficits in aphasia, with anatomical correlation. Ann Neurol 27:226–231

Henson RNA (2003) Neuroimaging studies of priming. Prog Neurobiol 70:53–81

Hickok G (2000) Speech perception, conduction aphasia, and the functional neuroanatomy of language. In: Grodzinsky Y, Shapiro L, Swinney D (eds) Language and the brain. Academic, San Diego, pp 87–104

Hickok G, Poeppel D (2000) Towards a functional neuroanatomy of speech perception. Trends Cogn Sci 4: 131–138

Hickok G, Poeppel D (2004) Dorsal and ventral streams: a framework for understanding aspects of the functional anatomy of language. Cognition 92:67–99

Hickok G, Poeppel D (2007) The cortical organization of speech processing. Nat Rev Neurosci 8(5):393–402

Hickok G, Erhard P et al (2000) A functional magnetic resonance imaging study of the role of left posterior superior temporal gyrus in speech production: implications for the explanation of conduction aphasia. Neurosci Lett 287:156–160

Hickok G, Buchsbaum B et al (2003) Auditory-motor interaction revealed by fMRI: speech, music, and working memory in area Spt. J Cogn Neurosci 15:673–682

Hillis AE (2007) Aphasia: progress in the last quarter of a century. Neurology 69(2):200–213

Hodges JR, Patterson K (2007) Semantic dementia: a unique clinicopathological syndrome. Lancet Neurol 6(11):1004–1014

Humphries C, Willard K et al (2001) Role of anterior temporal cortex in auditory sentence comprehension: an fMRI study. Neuroreport 12:1749–1752

Humphries C, Love T et al (2005) Response of anterior temporal cortex to syntactic and prosodic manipulations during sentence processing. Hum Brain Mapp 26:128–138

Humphries C, Binder JR et al (2006) Syntactic and semantic modulation of neural activity during auditory sentence comprehension. J Cogn Neurosci 18(4): 665–679

Indefrey P, Levelt WJM (2000) The neural correlates of language production. In: Gazzaniga MS (ed) The new cognitive neurosciences. MIT Press, Cambridge, pp 845–865

Indefrey P, Levelt WJ (2004) The spatial and temporal signatures of word production components. Cognition 92(1–2):101–144

Kaas JH, Hackett TA (2000) Subdivisions of auditory cortex and processing streams in primates. Proc Natl Acad Sci USA 97(22):11793–11799

Kaas JH, Hackett TA et al (1999) Auditory processing in primate cerebral cortex. Curr Opin Neurobiol 9(2): 164–170

Levelt WJM, Praamstra P et al (1998) An MEG study of picture naming. J Cogn Neurosci 10:553–567

Lichtheim L (1885) On aphasia. Brain 7:433–484

Liebenthal E, Binder JR et al (2005) Neural substrates of phonemic perception. Cereb Cortex 15(10): 1621–1631

Martin A (1998) The organization of semantic knowledge and the origin of words in the brain. In: Jablonski NG, Aiello LC (eds) The origins and diversification of language. California Academy of Sciences, San Francisco, pp 69–88

Martin A, Chao LL (2001) Semantic memory and the brain: structure and processes. Curr Opin Neurobiol 11(2):194–201

Mazoyer BM, Tzourio N et al (1993) The cortical representation of speech. J Cogn Neurosci 5:467–479

Mesulam M-M (1998) From sensation to cognition. Brain 121:1013–1052

Milner AD, Goodale MA (1995) The visual brain in action. Oxford University Press, Oxford

Narain C, Scott SK et al (2003) Defining a left-lateralized response specific to intelligible speech using fMRI. Cereb Cortex 13(12):1362–1368

Obleser J, Zimmermann J et al (2006) Multiple stages of auditory speech perception reflected in event-related fMRI. Cereb Cortex 17:2251–2257

Okada K, Hickok G (2006) Identification of lexical-phonological networks in the superior temporal sulcus using fMRI. Neuroreport 17:1293–1296

Okada K, Hickok G (2009) Two cortical mechanisms support the integration of visual and auditory speech: a hypothesis and preliminary data. Neurosci Lett 452(3):219–223

Okada K, Smith KR et al (2003) Word length modulates neural activity in auditory cortex during covert object naming. Neuroreport 14:2323–2326

Pa J, Hickok G (2008) A parietal-temporal sensory-motor integration area for the human vocal tract: evidence from an fMRI study of skilled musicians. Neuropsychologia 46:362–368

Patterson K, Nestor PJ et al (2007) Where do you know what you know? The representation of semantic knowledge in the human brain. Nat Rev Neurosci 8(12):976–987

Price CJ, Wise RJS et al (1996) Hearing and saying: the functional neuro-anatomy of auditory word processing. Brain 119:919–931

Rauschecker JP (1998) Cortical processing of complex sounds. Curr Opin Neurobiol 8(4):516–521

Rissman J, Eliassen JC et al (2003) An event-related FMRI investigation of implicit semantic priming. J Cogn Neurosci 15(8):1160–1175

Rodd JM, Davis MH et al (2005) The neural mechanisms of speech comprehension: fMRI studies of semantic ambiguity. Cereb Cortex 15:1261–1269

Romanski LM, Tian B et al (1999) Dual streams of auditory afferents target multiple domains in the primate prefrontal cortex. Nat Neurosci 2:1131–1136

Scott SK (2005) Auditory processing - speech, space and auditory objects. Curr Opin Neurobiol 15(2):197–201

Scott SK, Blank CC et al (2000) Identification of a pathway for intelligible speech in the left temporal lobe. Brain 123:2400–2406

Spitsyna G, Warren JE et al (2006) Converging language streams in the human temporal lobe. J Neurosci 26(28):7328–7336

Squire LR (1986) Mechanisms of memory. Science 232:1612–1619

Vandenberghe R, Nobre AC et al (2002) The response of left temporal cortex to sentences. J Cogn Neurosci 14(4):550–560

Vouloumanos A, Kiehl KA et al (2001) Detection of sounds in the auditory stream: event-related fMRI evidence for differential activation to speech and non-speech. J Cogn Neurosci 13(7):994–1005

Warren JE, Wise RJ et al (2005) Sounds do-able: auditory-motor transformations and the posterior temporal plane. Trends Neurosci 28(12):636–643

Wernicke C (1874/1969) The symptom complex of aphasia: a psychological study on an anatomical basis. In: Cohen RS, Wartofsky MW (eds) Boston studies in the philosophy of science. D. Reidel, Dordrecht, pp 34–97

10 Use of fMRI Language Lateralization for Quantitative Prediction of Naming and Verbal Memory Outcome in Left Temporal Lobe Epilepsy Surgery

Jeffrey R. Binder

Partial removal of the anterior temporal lobe (ATL) is the most commonly performed surgical procedure for intractable epilepsy. ATL resection is highly effective for seizure control, resulting in long-term cure rates of 60–80 % (Jeong et al. 2005; McIntosh et al. 2001; Tellez-Zenteno et al. 2005). The undeniable benefit of ATL surgery is partially offset by the occurrence of neuropsychological morbidity in some patients receiving this treatment. Evidence suggests a 30–60 % incidence of anomic aphasia (Bell et al. 2000b; Hermann et al. 1994, 1999a, b; Langfitt and Rausch 1996; Sabsevitz et al. 2003) and a similar risk for decline in verbal memory ability (Baxendale et al. 2006; Binder et al. 2008a; Chelune et al. 1993; Gleissner et al. 2004; Helmstaedter and Elger 1996; Lineweaver et al. 2006; Martin et al. 1998; Sabsevitz et al. 2001; Stroup et al. 2003) after left ATL surgery. Patients are generally aware of these deficits, which adversely affect quality of life and employability (Helmstaedter et al. 2003; Langfitt et al. 2007; Lineweaver et al. 2004; Perrine et al. 1995; Stroup et al. 2003). Cognitive deficits from right ATL resection have been much less consistently observed (Binder et al. 2008a; Lee et al. 2002; Loring et al. 1990a, 1995b; Pigot and Milner 1993; Pillon et al. 1999). Though the first priority in treating intractable epilepsy is seizure control, the importance of cognitive side effects for some patients undergoing left ATL surgery should not be underestimated or denied. Indeed, considerable resources have been devoted to developing methods for predicting and preventing cognitive morbidity, and many such methods are used routinely in the evaluation of surgical candidates despite ongoing controversy regarding their effectiveness.

This chapter focuses on recent advances in the prediction of postoperative language and verbal memory deficits using preoperative fMRI. The clinical value of such risk assessment is that it provides the patient and physician with additional information that can be useful in deciding whether to proceed with treatment in elective situations. The use of fMRI activation maps intraoperatively for defining surgical resection boundaries is a separate issue that will not be addressed in detail here.

10.1 Use of fMRI for Predicting Naming Outcome

10.1.1 Measuring Language Lateralization

The intracarotid amobarbital (Wada) test was developed to assess the risk of language decline in patients undergoing resective brain surgery (Wada and Rasmussen 1960), based on the assumption that operating on the language-dominant

J.R. Binder
Department of Neurology,
Medical College of Wisconsin,
Milwaukee, WI, USA
e-mail: jbinder@mcw.edu

S. Ulmer, O. Jansen (eds.), *fMRI – Basics and Clinical Applications*,
DOI 10.1007/978-3-642-34342-1_10,

hemisphere entailed increased risk. Though the Wada test has been in use for over 50 years, until recently the relationship between Wada language asymmetry and postoperative language outcome had never been quantified. The historical reasons for this relate to the fact that language lateralization was traditionally viewed as dichotomous (left or right) or trichotomous (left, right, or "bilateral"). Under this schema, it was obvious that operating on a nondominant hemisphere would be safer than operating on a language-dominant hemisphere. Several aspects of this formulation have changed in recent decades. First, language lateralization has come to be seen as a continuously graded rather than an all-or-none phenomenon, with relative *degrees* of dominance rather than distinct categories (Binder et al. 1996; Chlebus et al. 2007; Knecht et al. 2000b, 2002; Loring et al. 1990b; Seghier 2008; Springer et al. 1999). Thus, while the vast majority (~80 %) of patients who undergo left-hemisphere surgery for epilepsy are left dominant for language, there is variation within this group in terms of the degree of left dominance. This variability raises the question of whether graded degrees of language dominance are reflected in graded levels of risk. Second, neuropsychological methods for identifying postoperative language deficits have steadily improved and become more widespread, resulting in a shift of the clinical focus, particularly in left ATL cases, away from prediction of severe aphasia (which is very rare after standard left ATL resection) and toward prediction of more moderate degrees of language decline.

The effort to develop fMRI methods for predicting language outcome in ATL epilepsy surgery is therefore motivated by two critical assumptions. First, it is assumed that patients show varying degrees of language (mainly naming) deficit after surgery and that it is desirable to know before surgery what degree of decline can be expected. Second, it is assumed that the degree of decline will be related to the degree of language lateralization toward the surgical hemisphere. The goal of fMRI in this context is thus to provide a reliable and valid measure of language lateralization. A wide variety of fMRI language activation paradigms have been described, differing in the type of language stimuli, stimulus modality, language task, control stimuli, and control task used, raising the question of which of these paradigms, if any, is optimal. Though different paradigms have seldom been compared quantitatively, it is well known that they can produce very different, in some cases entirely nonoverlapping, activation patterns. This variation is related primarily to the cognitive, sensory, and motor processes engaged by the tasks, and the degree to which the language and control conditions differ in engaging these specific processes (Binder 2006).

Several simple criteria can be applied in assessing the usefulness of different language paradigms. First, the pattern of activation obtained in healthy, right-handed adults should be lateralized strongly to the left hemisphere, as it is known that almost all such individuals are left-hemisphere dominant for language (Knecht et al. 2000a; Loring et al. 1990b; Springer et al. 1999). Second, the activation should be robust, that is, it should be reliably obtained across individuals and in the same general brain regions from person to person. Third, there should be concordance between language lateralization measured with the fMRI paradigm and lateralization measured with other techniques, such as the Wada test, in the same individuals. Finally, in some cases it may be desirable that the paradigm produces activation in particular target brain regions. In the case of ATL surgery, for example, activation asymmetry in the temporal lobe might be more predictive of outcome than activation in the frontal lobe; thus, a paradigm that activates the temporal lobe would have advantages over one that does not.

Figure 10.1 illustrates some of these issues. The figure shows average activation maps obtained while 26 right-handed subjects listened to spoken words and performed a semantic decision task (Binder et al. 1997, 2008b). In the top panel, BOLD signal during this task is compared to a "resting" baseline. The activated regions are largely bilateral, including bilateral auditory, working memory, general executive, and attention networks. In the lower panel of the figure, the semantic decision task is compared to

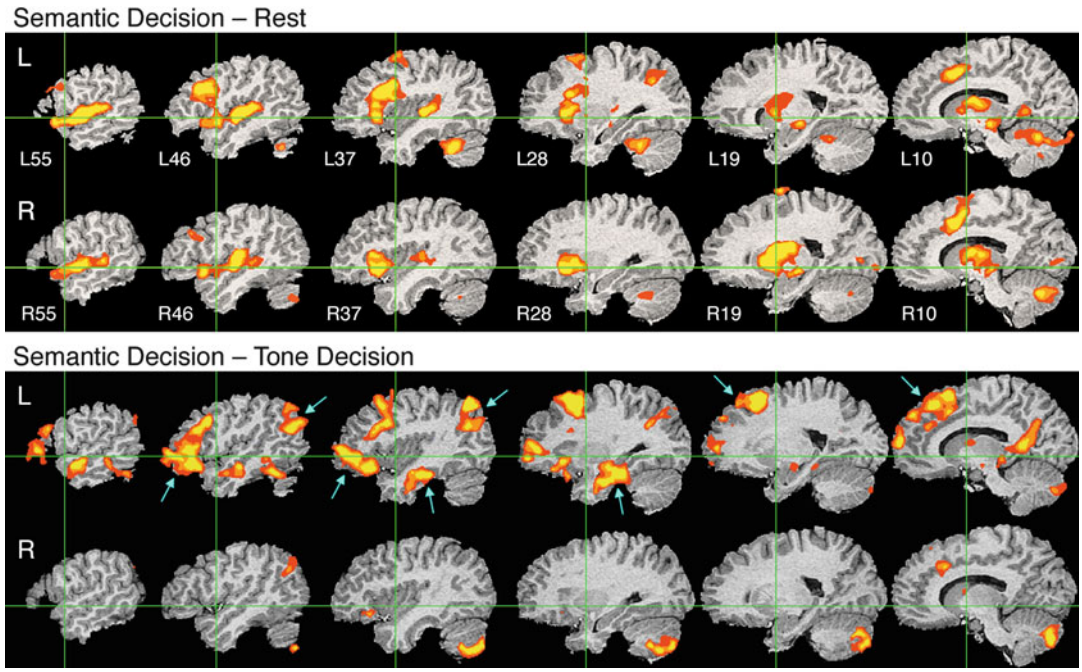

Fig. 10.1 Group fMRI activation maps from two auditory word comprehension experiments. *Top*: semantic decision relative to resting. *Bottom*: semantic decision relative to tone decision. Data are displayed as serial sagittal sections through the brain at 9-mm intervals. *X*-axis locations for each slice are given in the *top panel*. Both maps are thresholded at a whole-brain corrected $p < 0.05$ using voxel-wise $p < 0.0001$ and cluster extent > 200 mm^3. The three steps in each color continuum represent voxel-wise p thresholds of 10^{-4}, 10^{-5}, and 10^{-6}. *Blue arrows* in the lower image indicate left-hemisphere language areas that are active during the resting state and thus visible only when an active nonlinguistic task is used as the baseline (Adapted from Binder et al. (2008b))

a nonlinguistic auditory control task. In this case the activated regions are strongly left-lateralized, including several left temporal, parietal, and prefrontal regions (indicated by blue arrows) that were not observed when the resting baseline was used. These data illustrate in dramatic fashion how activation patterns depend on the choice of control condition. In the lower panel, the use of an active nonlinguistic control task "subtracts out" bilateral activation in early auditory, general executive, and attention networks, leaving activation in left-lateralized language networks. These results also demonstrate that certain high-level language processing regions are active during the "resting" state and can only be observed when an active nonlinguistic control condition is employed (Binder et al. 1999, 2008b).

Many fMRI language paradigms have been compared to Wada language testing (Adcock et al. 2003; Arora et al. 2009; Bahn et al. 1997; Benke et al. 2006; Benson et al. 1999; Binder et al. 1996; Carpentier et al. 2001; Chlebus et al. 2007; Deblaere et al. 2004; Desmond et al. 1995; Gaillard et al. 2004; Hertz-Pannier et al. 1997; Lehéricy et al. 2000; Rutten et al. 2002; Sabbah et al. 2003; Spreer et al. 2002; Szaflarski et al. 2008; Woermann et al. 2003; Worthington et al. 1997; Yetkin et al. 1998). These studies generally report high concordance rates, typically in the range of 80–100 % (for reviews, see Binder and Raghavan 2006; Swanson et al. 2007). In assessing the rate of concordance, patients are usually assigned to categories such as "left dominant," "right dominant," or "mixed" on each test. The proportion of concordant cases depends on how these arbitrary categories are defined as well as other factors. Another method for comparing fMRI and Wada results is to calculate the correlation between continuous measures of lateralization on both tests. In the case of fMRI,

a standard approach is to calculate a laterality index (LI) expressing the asymmetry of activation in numerical form. The first such LI was based on a simple count of the voxels that survived thresholding in each hemisphere (Binder et al. 1996). The formula $(L - R)/(L+R)$, where L and R refer to the voxel counts in each hemisphere, yields a number that varies from +1 when all activated voxels are on the left side to −1 when all activated voxels are on the right. LI values obtained with this method vary as a function of the threshold used for defining activated voxels; thus, several authors have explored alternative asymmetry measures that do not require thresholding (Adcock et al. 2003; Chlebus et al. 2007; Jones et al. 2011; Nagata et al. 2001; Seghier 2008; Wilke and Schmithorst 2006). No consensus regarding the optimal method for calculating activation asymmetry has yet emerged from these studies.

10.1.2 Predicting Outcome

With so many studies focusing on fMRI/Wada correlations, it is easy to forget that the actual aim of measuring language lateralization prior to brain surgery is prediction of language outcome. In the case of left ATL resection, an fMRI procedure that reliably identifies patients at risk for postoperative naming deficits would be a valuable clinical tool, especially if the fMRI results added information over and above other available tests. Previous behavioral studies have identified demographic and behavioral variables that may predict outcome. For example, left ATL patients who develop seizures at an earlier age generally have a lower risk for postoperative language decline (Hermann et al. 1999b; Saykin et al. 1995; Stafiniak et al. 1990), presumably because earlier age at onset is associated with a higher probability of language shift to the right hemisphere (Springer et al. 1999). Better preoperative naming performance is associated with a higher risk for decline (Hermann et al. 1994). As noted above, Wada language testing has always been assumed to be predictive of language outcome, though, apart from a few case reports of patients with right language dominance who did not decline (Langfitt and Rausch 1996; Wada and Rasmussen 1960), this assumption went untested for many years.

To date, only one study has examined the value of fMRI language lateralization as a predictor of language outcome. Sabsevitz et al. (2003) studied 24 consecutively encountered patients undergoing left ATL resection. The fMRI paradigm used a contrast between an auditory semantic decision task and a nonlinguistic tone decision task (Fig. 10.1, lower panel). A previous study had shown that asymmetry of activation with this task paradigm is correlated with language lateralization on the Wada test (Binder et al. 1996). For the Sabsevitz et al. study, separate LIs were computed for the whole hemisphere, frontal lobe, temporal lobe, and angular gyrus. All patients also underwent Wada testing and preoperative assessment of confrontation naming using the 60-item Boston Naming Test (BNT). The BNT was administered again at 6 months after surgery, and a change score was calculated as the difference between post-op and pre-op BNT scores. Surgeries were performed blind to the fMRI data.

Compared to a control group of 32 right ATL patients, the left ATL group declined postoperatively on the BNT ($p<.001$), with an average change score of −9. Within the left ATL group, however, there was considerable variability, with 13 patients (54 %) showing variable degrees of decline relative to the control group. The temporal lobe fMRI LI was the strongest predictor of outcome ($r=-.64$, $p<.001$), indicating that language lateralization toward the left (surgical) temporal lobe was related to poorer naming outcome, whereas lateralization toward the right temporal lobe was associated with little or no decline. This fMRI measure showed 100 % sensitivity, 73 % specificity, and a positive predictive value of 81 % in predicting significant decline. By comparison, the Wada language LI showed a somewhat weaker correlation with outcome ($r=-.50$, $p<.05$), 92 % sensitivity, 43 % specificity, and a positive predictive value of 67 %. Notably, the frontal lobe fMRI LI was also less predictive ($r=-.47$, $p<.05$), suggesting that an optimal LI is one that indexes lateralization near the surgical resection area.

Sabsevitz et al. also created multivariate models to determine the contribution of fMRI relative to other noninvasive predictors. Both age at epilepsy onset ($r = -.35$, $p = .09$) and preoperative performance ($r = -.39$, $p = .06$) showed strong trends toward a correlation with outcome, and together these variables predicted about 27 % of the variance in outcome. Adding the temporal lobe fMRI LI to this model accounted for an additional 23 % of the variance ($p < .01$), indicating a significant increase in predictive power. Addition of the Wada language asymmetry score did not improve the model (R^2 change = .01).

Though based on a relatively small sample, these results show how preoperative fMRI can be used to stratify patients in terms of risk for language decline in the setting of left ATL resection, allowing patients and physicians to more accurately weigh the risks and benefits of the surgery. It is crucial to note, however, that these results hold only for the particular methods used in the study and may not generalize to other fMRI protocols, analysis methods, patient populations, or surgical procedures. Future studies should not only confirm these results using larger patient samples but also test whether other fMRI protocols in current widespread use have similar predictive capability.

10.2 "Tailoring" Temporal Lobe Resections

It remains to be seen how useful fMRI language activation maps will be for planning resection boundaries in temporal lobe surgery. At least three significant problems complicate progress: (i) variation in language maps produced by different activation protocols; (ii) generally poor activation of the ATL, where the majority of temporal lobe surgeries are performed; and (iii) an inadequate understanding of the specificity of fMRI activations.

As indicated earlier, different fMRI language activation protocols in current clinical use produce markedly different patterns of activation (Binder 2006; Binder et al. 2008b). These findings suggest that activation maps are strongly dependent on the specific composition of cognitive processes engaged during the scan, and how these differ between the language and control tasks used (see discussion above). Most language activation protocols currently used in clinical studies do not elicit robust ATL activation, especially in inferior portions of the ATL. Because the dominant ATL is known to contribute to language processing (Damasio et al. 1996; Hamberger et al. 2001; Humphries et al. 2005; Mazoyer et al. 1993; Rogers et al. 2006), and left ATL resection not infrequently results in language decline (Bell et al. 2000b; Davies et al. 1998a; Hermann et al. 1994; Langfitt and Rausch 1996; Sabsevitz et al. 2003), it follows that these protocols are not detecting crucial language areas.

Considerable evidence suggests that the ATL plays a role in semantic processing, that is, storage and retrieval of conceptual knowledge that underlies word and sentence meaning (Binder et al. 2009; Mummery et al. 2000; Patterson et al. 2007; Rosen et al. 2002; Visser et al. 2010). Damage to this semantic system has been proposed as a major cause of the naming deficits observed in patients with ATL lesions (Bell et al. 2001; Lambon Ralph et al. 2001). Several methodological factors appear to influence the sensitivity of fMRI in detecting these ATL semantic networks. First, the ATL is more strongly activated by sentences than by single words or strings of unrelated words (Friederici et al. 2000; Humphries et al. 2005, 2006; Mazoyer et al. 1993; Vandenberghe et al. 2002; Xu et al. 2005). This observation suggests that the ATL is particularly necessary for integrating meaning across multiple words. Other studies have implicated the ATL specifically in processing semantic knowledge related to social interactions, as in stories depicting agents, actions, emotional states, motives, and so on (Olson et al. 2007; Ross and Olson 2010; Zahn et al. 2007). Finally, ATL activation is more likely to be observed when an active control task is used as a baseline rather than a resting state (Binder et al. 2008b; Spitsyna et al. 2006; Stark and Squire 2001; Visser et al. 2010). For example, Stark and Squire (2001) observed activation in medial ATL regions during a picture-encoding task when an active

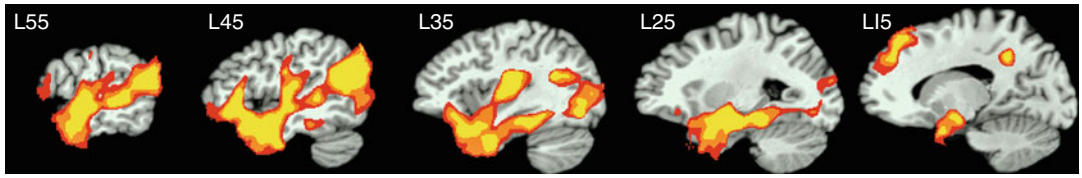

Fig. 10.2 Areas of greater activation for the Story condition relative to the Math condition (thresholded at whole-brain corrected $p < .05$), shown in serial sagittal sections through the left hemisphere. Stereotaxic locations are given in the *upper left corner* of each slice (Adapted from Binder et al. (2010a))

decision task was used as a baseline but not when a "rest" baseline was used. Similarly, Spitsyna et al. (2006) observed activation in the anterior fusiform gyrus and ITG during a story comprehension task when an active decision task was used as a baseline but not when a "passive" baseline was used. This observation suggests that semantic processes carried out by the ATL occur even during resting or passive states, perhaps comprising a component of normal consciousness that supports planning, problem solving, daydreaming, and other high-level integrative processes that depend on semantic knowledge (Binder et al. 1999, 2009). Active, attentionally demanding control tasks disrupt these ongoing "default" processes, which would otherwise mask ATL activation.

Based on these considerations, Binder et al. designed an fMRI protocol aimed specifically at eliciting reliable ATL activation (Binder et al. 2010a). An auditory story comprehension task ("Story") was selected to engage rapid integration of semantic information, including social concepts. This task was contrasted with an active, attentionally demanding arithmetic task ("Math") involving auditorily presented addition and subtraction problems. Prior evidence indicates that arithmetic, particularly addition and subtraction operations, does not engage the temporal lobe (Baldo and Dronkers 2007; Cappelletti et al. 2001; Crutch and Warrington 2002; Diesfeldt 1993); thus, this task was expected to interrupt ongoing "default mode" processing in the ATL and to cause minimal ATL activation. An additional feature of the arithmetic task is that it used verbal, sentence-like stimuli that could be matched to the stories on low-level features like auditory and phonological input. A second aim of this study was to test whether comparable results could be achieved across different centers using a variety of imaging hardware and software platforms.

The Story > Math contrast elicited strong activation throughout the ATL, lateral temporal lobe, and medial temporal lobe bilaterally in an initial cohort of 18 healthy participants (Fig. 10.2). The task protocol was then implemented at six other imaging centers using identical methods. Data from a second cohort of participants scanned at these centers closely replicated the results from the initial cohort. Compared to other fMRI protocols commonly used to elicit temporal lobe activation, the Story-Math protocol activated a much larger extent of the region typically removed in a standard ATL resection (Fig. 10.3).

In addition to these problems concerning sensitivity of the activation protocol, the problem of activation specificity is critical to address before language fMRI maps are used to tailor temporal lobe resections. Some regions activated during fMRI tasks may play a minor or nonspecific role rather than a critical role in language. Resection of these "active" foci may not necessarily produce clinically relevant or persisting deficits. Thus, using fMRI activation maps to decide which brain regions can be resected involves two potential risks: (i) resection of critical language zones that are "not activated" due to insensitivity of the particular

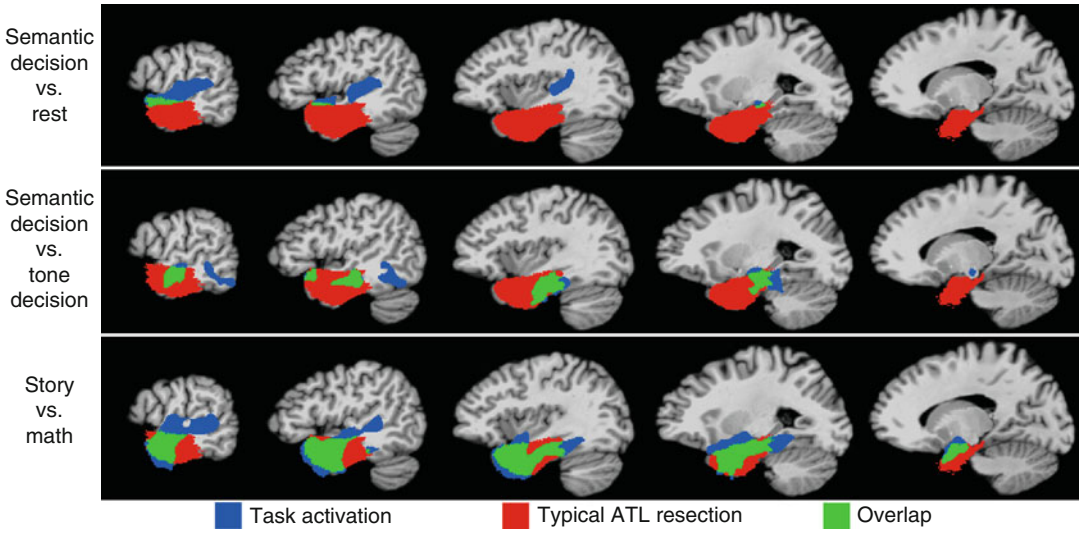

Fig. 10.3 Overlap between activated areas in three fMRI language comprehension paradigms and regions typically resected in left ATL surgery. *Red* indicates areas of lesion overlap in 23 left ATL surgery patients, based on spatially normalized postoperative MRI scans. *Blue* indicates temporal lobe regions activated with each paradigm (all thresholded at whole-brain corrected $p < .05$) that do not fall within this typical resection zone (see Fig. 10.1. and Binder et al. (2008a) for details regarding the semantic decision vs. rest and the semantic decision vs. tone decision paradigms). *Green* indicates activated regions that overlap with the typical resection zone. Overlap with the targeted surgical zone differs markedly between the language paradigms and is greatest for the Story-Math contrast (Adapted from Binder et al. (2010b))

language activation protocol employed, resulting in postoperative language decline, and (ii) sparing of "activated" regions that are in fact not critical for language, resulting in suboptimal seizure control. Only through very carefully designed studies – in which resections are performed blind to the fMRI data, standardized procedures are used for assessing outcome, and quantitative measures are made of the anatomical and functional lesion – will the usefulness of fMRI language maps for "tailoring" surgical resections be determined. One such study, the FMRI in Anterior Temporal Epilepsy Surgery (FATES) study, is currently underway. This prospective, multicenter study funded by the NINDS will evaluate whether language outcome after left ATL resection is related to the amount of "activated" brain tissue removed, as defined by preoperative fMRI.

10.3 Prediction of Verbal Memory Outcome

ATL resection typically involves removal of much of the anterior medial temporal lobe (MTL), including portions of the hippocampus and parahippocampus, which are known to be critical for encoding and retrieval of long-term episodic memories (Squire 1992). Verbal memory decline after left ATL resection is a consistent finding in group studies and is observed in 30–60 % of such patients (Baxendale et al. 2006; Binder et al. 2008a; Chelune et al. 1991, 1993; Chiaravalloti and Glosser 2001; Gleissner et al. 2004; Helmstaedter and Elger 1996; Hermann et al. 1995; Kneebone et al. 1995; Lee et al. 2002; Lineweaver et al. 2006; Loring et al. 1995b; Martin et al. 1998; Sabsevitz et al. 2001; Stroup et al. 2003). In contrast, nonverbal

memory decline after right ATL resection is less consistently observed in groups and individuals (Binder et al. 2008a; Lee et al. 2002; Lineweaver et al. 2006; Stroup et al. 2003). A main focus of the preoperative evaluation in ATL surgery candidates is, therefore, to estimate the risk of verbal memory decline in patients undergoing left ATL resection.

The Wada memory test was originally developed for the purpose of predicting global amnesia after ATL resection (Milner et al. 1962). Studies of its ability to predict relative verbal memory decline have been inconsistent, with several suggesting good predictive value (Bell et al. 2000a; Chiaravalloti and Glosser 2001; Kneebone et al. 1995; Loring et al. 1995b; Sabsevitz et al. 2001) and others showing little or none, particularly when used in combination with noninvasive tests (Binder et al. 2008a; Chelune and Najm 2000; Kirsch et al. 2005; Lacruz et al. 2004; Lineweaver et al. 2006; Stroup et al. 2003). Some authors have questioned the general validity and reliability of Wada memory results (Kubu et al. 2000; Lee et al. 1995; Loddenkemper et al. 2007; Loring et al. 1990a; Martin and Grote 2002; Novelly and Williamson 1989; Simkins-Bullock 2000). Others have emphasized the sensitivity of the test to certain details of the stimulus presentation, procedures used for recall, and other methodological factors (Alpherts et al. 2000; Carpenter et al. 1996; Loring et al. 1994, 1995a). Other presurgical tests of MTL functional or anatomical asymmetry are also modestly predictive of memory outcome, including structural MRI of the hippocampus (Cohen-Gadol et al. 2004; Lineweaver et al. 2006; Stroup et al. 2003; Trenerry et al. 1993; Wendel et al. 2001) and interictal positron emission tomography (Griffith et al. 2000). Preoperative neuropsychological testing also has predictive value, in that patients with good memory abilities prior to surgery are more likely to decline than patients with poor preoperative memory (Baxendale et al. 2006, 2007; Binder et al. 2008a; Chelune et al. 1991; Davies et al. 1998b; Gleissner et al. 2004; Helmstaedter and Elger 1996; Hermann et al. 1995; Jokeit et al. 1997; Lineweaver et al. 2006; Stroup et al. 2003).

10.3.1 FMRI of the Medial Temporal Lobe

MTL activation during memory encoding and retrieval tasks has been a subject of intense research with fMRI (for reviews, see Gabrieli 2001; Hwang and Golby 2006; Paller and Wagner 2002; Rugg et al. 2002; Schacter and Addis 2007; Schacter and Wagner 1999; Vilberg and Rugg 2008). Hippocampal activation has been demonstrated using a variety of task paradigms (e.g., Binder et al. 1997, 2005; Constable et al. 2000; Davachi and Wagner 2002; Eldridge et al. 2000; Fernandez et al. 1998; Greene et al. 2006; Hassabis et al. 2007; Henke et al. 1997; Kensinger et al. 2003; Killgore et al. 2002; Martin 1999; Otten et al. 2001; Parsons et al. 2006; Prince et al. 2007; Small et al. 2001; Sperling et al. 2001; Stark and Squire 2001; Vincent et al. 2006; Weis et al. 2004; Zeinah et al. 2003), although fMRI of this region is not without technical challenges. The hippocampal formation is small relative to typical voxel sizes used in fMRI. Within-voxel averaging of signals from active and inactive structures may thus impair detection of hippocampal activity. Loss of MRI signal in the medial ATL due to macroscopic field inhomogeneity can affect the amygdala and occasionally the anterior hippocampus (Constable et al. 2000; Fransson et al. 2001; Morawetz et al. 2008). Finally, the "baseline" state employed in subtraction analyses is probably of critical importance. Hippocampal encoding processes probably continue beyond the duration of the stimulus or event (Alvarez and Squire 1994), and human imaging evidence suggests that the hippocampus is relatively activated in the "resting" state (Andreasen et al. 1995; Binder et al. 1999; Martin 1999; Stark and Squire 2001).

Hippocampal fMRI paradigms generally employ one of three approaches. The first of these involves a contrast between encoding novel and repeated stimuli, based on earlier electrophysiological studies showing that the hippocampus responds more strongly to novel than to repeated stimuli (Grunwald et al. 1998; Knight 1996; Li et al. 1993; Riches et al. 1991). The encoding task might involve explicit memorization for later retrieval testing or a decision task designed to

produce implicit encoding. Such novelty contrasts mainly activate the posterior parahippocampus and adjacent fusiform gyrus, with involvement of the posterior hippocampus in some but not all studies (Binder et al. 2005; Fransson et al. 2001; Gabrieli et al. 1997; Hunkin et al. 2002; Kirchhoff et al. 2000; Stern et al. 1996; Tulving et al. 1996). The second approach involves manipulating the degree of associative/semantic processing that occurs during encoding. Hippocampal encoding is thought to involve the creation of "relational" representations that tie together sensory, semantic, affective, and other codes activated by an event (Cohen and Eichenbaum 1993; McClelland et al. 1995; O'Reilly and Rudy 2001). External events that are meaningful and activate semantic and emotional associations engage the hippocampus more robustly and are thus more effectively recorded (Craik and Lockhart 1972). Thus many fMRI studies have demonstrated hippocampal activation using contrasts between a stimulus (e.g., a word or picture) or task that engages associative/semantic processing and a stimulus (e.g., a nonword or unrecognizable visual form) or task that engages only sensory processing (Bartha et al. 2003; Binder et al. 1997, 2005; Davachi and Wagner 2002; Henke et al. 1997, 1999; Kensinger et al. 2003; Killgore et al. 2002; Martin 1999; Otten et al. 2001; Small et al. 2001; Sperling et al. 2001; Wagner et al. 1998; Zeinah et al. 2003). Finally, a third approach uses subsequent recognition performance as a direct index of MTL activity during encoding. Items encoded during the fMRI scan are sorted according to whether they were later remembered, and a contrast is made between successfully and unsuccessfully encoded items. These studies consistently show greater MTL activation during subsequently remembered compared to subsequently forgotten stimuli, though the precise MTL regions showing this effect have varied considerably (Brewer et al. 1998; Buckner et al. 2001; Constable et al. 2000; Davachi and Wagner 2002; Fernandez et al. 1998; Kirchhoff et al. 2000; Otten et al. 2001; Prince et al. 2005, 2007; Uncapher and Rugg 2005; Wagner et al. 1998; Weis et al. 2004).

Finally, the location of MTL activation detected by fMRI depends on the type of stimulus material encoded. MTL activation is left-lateralized for verbal stimuli and generally symmetric for pictorial stimuli (Binder et al. 1997, 2005; Golby et al. 2001; Kelley et al. 1998; Martin 1999; Otten et al. 2001; Powell et al. 2005; Reber et al. 2002).

10.3.2 Medial Temporal Lobe FMRI as a Predictor of Memory Outcome

Several fMRI studies have examined the relationship between preoperative MTL activation and memory outcome after ATL surgery (Table 10.1). Rabin et al. (2004) studied 23 patients undergoing ATL resection (10 left, 13 right) using a scene-encoding task that activates the posterior MTL bilaterally (Detre et al. 1998). Patients were tested for delayed recognition of the same pictures immediately after scanning. Delayed picture recognition was then tested again after surgery, and the change on this recognition task was used as the primary memory outcome variable. About half of the patients in both surgery groups declined on this measure. Preoperative fMRI activation lateralization toward the side of surgery was correlated with decline as was the extent of activation on the side of surgery. These results were the first to demonstrate a relationship between preoperative fMRI activation asymmetry and outcome, yet they are of limited relevance to the problem of predicting verbal memory outcome. In the left ATL patients studied by Rabin et al., neither Wada memory nor fMRI activation asymmetry predicted verbal memory decline as measured by standard psychometric tests.

Richardson, Powell, and colleagues studied correlations between hippocampal activation and verbal memory outcome in three small studies (Powell et al. 2008; Richardson et al. 2006, 2004). Patients performed a semantic decision task with words during the fMRI scan and then took a recognition test after scanning. Words that were subsequently recognized were contrasted with words that were judged to be familiar but not recognized. In the first of these studies (Richardson

Table 10.1 fMRI studies of verbal memory outcome prediction in ATL surgery

Author	Year	*N*	fMRI contrast	Memory measure	Summary
Rabin et al.	2004	10 L 13 R	Indoor/outdoor decision on visual scenes vs. passive viewing of scrambled scenes	Recognition of scenes encoded during fMRI	MTL LI predicts outcome on scene recognition task in both surgery groups
Richardson et al.	2004	10 L	Subsequently recognized vs. familiar but not recognized words encoded during a semantic decision task	Word-list learning and story recall (Adult Memory and Information Processing Battery)	Activation asymmetry in a hippocampus ROI predicts verbal memory outcome
Richardson et al.	2006	12 L	Same as Richardson et al. (2004)	Same as Richardson et al. (2004)	Unilateral activation in ether left or right hippocampus ROI predicts verbal memory outcome
Binder et al.	2008a	60 L	Semantic decision on auditory words vs. sensory decision on tones	Word-list learning and delayed recall (Selective Reminding Test)	LI predicts verbal memory outcome, adds value beyond other predictors
Frings et al.	2008	9 L 10 R	Memorizing and recognizing object locations vs. comparing size of two objects	Word-list learning (Verbaler Lern- and Merkfaehigkeitstest)	Hippocampal LI predicts verbal memory outcome, mainly in left group
Köylü et al.	2008	14 L 12 R	Semantic decision on auditory words vs. sensory decision on tones	Word-list learning and delayed recall (Münchner Gedächtnistest)	MTL activation correlates with pre- and postoperative memory
Powell et al.	2008	7 L 8 R	Subsequently recognized vs. forgotten words and faces encoded during a	Word-list learning and visual design learning	Unilateral activation in dominant-side hippocampus ROI predicts verbal memory
Binder et al.	2010b	30 L 37 R	Indoor/outdoor decision on visual scenes vs. perceptual matching of scrambled	Word-list learning and delayed recall (Selective Reminding Test)	Hippocampal LI for scenes does not predict verbal memory outcome
Bonelli et al.	2010	29 L 25 R	Same paradigm as in Powell (2008)	Same as Powell et al. (2008)	Anterior and posterior MTL LIs from the word-encoding condition predict verbal memory outcome

et al. 2004), the authors observed a focus in the anterior hippocampus where *asymmetry* of activation (i.e., left-right) predicted verbal memory outcome on a standardized word-list learning test after left ATL resection. Greater activation in this region on the left side relative to the right side predicted greater decline. The second study by the same authors, however, showed correlations between outcome and hippocampal activation on either side (Richardson et al. 2006). That is, greater activation unilaterally on the left or the right was associated with poorer outcome. The correlation between verbal memory decline after *left* ATL resection and activation in the *right* hippocampus is difficult to explain, as patients with greater activation in the right hippocampus preoperatively would be expected to have a better outcome, not a worse outcome (Chelune 1995). This finding was not replicated in the third study (Powell et al. 2008), which reported a correlation between left hippocampus activation and poor outcome but no correlation between right hippocampus activation and outcome. A methodological limitation in all of these studies is that they are based on fMRI activation values extracted from a small region of interest defined by searching the volume for voxels that show a correlation with outcome across a group of patients. As the coordinates of these correlated voxels have varied across the studies, it is not clear how this method of extracting activation values would be applied to a newly encountered patient.

Frings et al. studied the relationship between preoperative hippocampal activation asymmetry and verbal memory outcome in a small sample of patients undergoing left or right ATL resection (Frings et al. 2008). The fMRI protocol used a task in which patients viewed a virtual-reality environment containing colored geometric shapes and either memorized the location of these objects or performed a recognition decision following memorization. These "memory tasks" were contrasted with a control task in which patients saw two versions of a geometric object and indicated which one was larger. This fMRI contrast had been shown previously to activate posterior MTL regions (mainly posterior parahippocampus) bilaterally. An LI was computed over the entire hippocampus, defined using a stereotaxic atlas. Verbal memory change was marginally correlated (1-tailed $p = .077$) with preoperative LI in the left ATL surgery group, but not in the right surgery group. A significant correlation (1-tailed $p < .05$) was obtained when the groups were combined, indicating greater verbal memory decline when preoperative hippocampal activation was lateralized more toward the side of surgery.

Köylü et al. examined correlations between preoperative MTL activation and verbal memory performance before and after ATL surgery (Koylu et al. 2008). Average fMRI activation produced by a semantic decision-tone decision contrast was measured in left and right MTL regions of interest including the hippocampus and parahippocampus. The authors observed correlations between MTL activation and both preoperative and postoperative verbal memory. In the left ATL surgery group, postoperative memory was positively correlated with preoperative activation in the right MTL. Unfortunately, the analyses examined only pre- and postoperative scores in isolation and not pre- to postoperative change, which is the primary issue of clinical interest.

Binder et al. (2010b) measured hippocampal activation asymmetry in 30 left and 37 right ATL surgery patients using a scene-encoding task. An anterior hippocampal ROI was defined using a probabilistic atlas in standard stereotaxic space. When contrasted with a perceptual matching task, this paradigm activates the anterior hippocampus bilaterally (Binder et al. 2005). Activation asymmetry was correlated with side of seizure focus ($p = .004$) and with Wada memory testing performed in the same patients ($p = .009$). This activation asymmetry, however, did not predict verbal memory outcome.

In the most significant study on this topic to date, Bonelli et al. (2010) examined verbal and nonverbal memory outcome in 54 patients undergoing left or right ATL surgery. The fMRI paradigm used the subsequent recognition contrast with words and faces developed by Powell et al. (2005, 2008). The authors operationally defined ROIs in each individual as the location where activation asymmetry was highest. An "asymmetry image" was created in each individual by contrasting activation levels in mirror-symmetric voxels in the left and right temporal lobe. A small

sphere around the voxel with the highest asymmetry value was used as the ROI. Two such ROIs were created in each patient, one in the anterior MTL and one in the posterior MTL. The main finding was a strong correlation ($R^2 = 0.23$, $p = .008$) between anterior MTL ROI asymmetry during word encoding and verbal memory change scores in the left ATL surgery, such that the greater the asymmetry toward the left, the greater the decline in verbal memory. Interestingly, there was a significant correlation ($R^2 = 0.14$, $p = .04$) in the opposite direction for the posterior MTL ROI, such that greater asymmetry toward the left was associated with *less* verbal memory decline. Given that the posterior hippocampus is typically spared in ATL resections, the authors interpreted the latter finding as evidence that intrahemispheric recruitment of the posterior left hippocampus in left TLE is important for preservation of verbal memory processes.

These studies are informative in several ways. Three studies (Binder et al. 2010b; Frings et al. 2008; Rabin et al. 2004) used scene-encoding tasks that activate the MTL bilaterally on fMRI, a pattern that suggests activation of both verbal and nonverbal memory encoding systems. Prediction of verbal memory outcome using these paradigms appears to be weak at best. In contrast, the verbal memory fMRI paradigms used by Richardson, Powell, and Bonelli et al. provide better predictive information regarding verbal memory outcome. These results provide further support for the long-standing concept of material-specific encoding in the episodic memory system. The results of Bonelli et al., though based on a relatively small sample of 29 left ATL surgery patients, are particularly promising and should be confirmed prospectively in a larger group of patients.

10.3.3 Language Lateralization as a Predictor of Verbal Memory Outcome

Binder et al. studied the relationship between preoperative language lateralization and verbal memory outcome (Binder et al. 2008a). The premise underlying this approach is that the verbal episodic memory encoding system is likely to be co-lateralized with language. More generally, the authors proposed that the type of material preferentially encoded by the left or right episodic memory system depends on the type of information it receives from the ipsilateral neocortex. If this model is correct, then the MTL in the language-dominant hemisphere is likely to be more critical for supporting verbal episodic memory, and language lateralization should be a reliable indicator of verbal memory lateralization.

The study included 60 patients who underwent left ATL resection and a control group of 63 patients who underwent right ATL resection. The fMRI paradigm used a contrast between an auditory semantic decision task and a nonlinguistic tone decision task (Fig. 10.1, lower panel). Verbal memory was measured preoperatively and 6 months after surgery using the Selective Reminding Test, a word-list learning and retention test (Buschke and Fuld 1974). Other neuropsychological testing included the story recall and visual reproduction subtests from Wechsler Memory Scale (Wechsler 1997). Language LIs were computed from the fMRI data using a large region of interest covering the lateral two-thirds of each hemisphere (Springer et al. 1999). All patients also underwent preoperative Wada language and object memory testing.

The left ATL surgery group showed substantial changes in verbal memory, with an average raw score decline of 43 % on word-list learning and 45 % on delayed recall of the word list. Of the individual patients in this group, 33 % declined significantly on the learning measure and 55 % on the delayed recall measure. In contrast, the right ATL surgery group improved slightly on both measures. Neither groups showed significant changes on any nonverbal memory tests. Preoperative measures that predicted verbal memory decline in the left surgery group included the preoperative score, the fMRI language LI, the Wada language asymmetry score, the age at onset of epilepsy, and the Wada memory asymmetry score (Table 10.2, Fig. 10.4).

In applying these results to real clinical situations, the main questions to resolve are the following: which tests make a significant

Table 10.2 Preoperative predictors of verbal memory outcome in 60 left ATL surgery patients

Predictor variable	List Learning	*p*	Delayed Recall	*p*
Preoperative score	−.662	<.0001	−.654	<.0001
fMRI language LI	−.432	<.001	−.316	<.05
Wada language asymmetry	−.398	<.01	−.363	<.01
Age at epilepsy onset	−.341	<.01	−.390	<.01
Wada memory asymmetry	−.331	<.05	−.135	ns

List Learning and Delayed Recall refer to the Consistent Long-Term Recall and Delayed Recall subtests of the Selective Reminding Test. Simple correlation values and *p* values for each correlation are shown

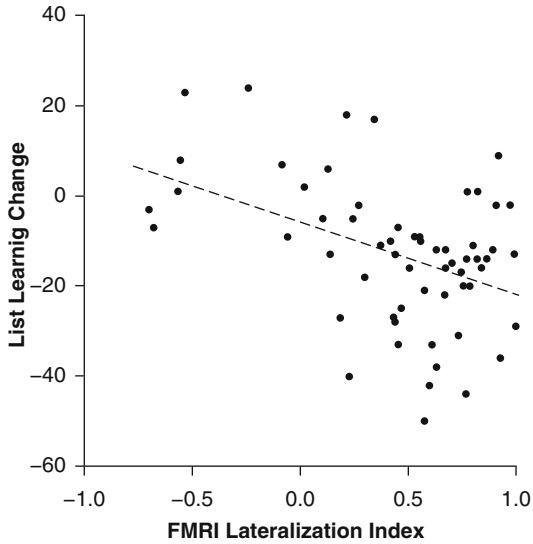

Fig. 10.4 Relationship between fMRI lateralization indexes and individual change scores on a word-list learning verbal memory test (Continuous Long-Term Recall from the Selective Reminding Test) in 60 left ATL surgery patients ($r = -.432$, $p < .001$) (Adapted from Binder et al. (2008a))

independent contribution to predicting outcome and how should results from these tests be optimally combined? Binder et al. addressed these questions in a series of stepwise multiple regression analyses. The first variables entered in all analyses were preoperative test performance and age at onset of epilepsy. The rationale for including these variables first is that they can be obtained with relatively little expense and at no risk to the patient. Next, the fMRI language LI was added, followed by simultaneous addition of both the Wada memory and Wada language asymmetry scores. The rationale for adding fMRI in the second step is that fMRI is noninvasive and carries less risk than the Wada test. The two Wada scores were added together in the final step because these measures are typically obtained together.

Preoperative score and age at onset of epilepsy together accounted for 49 % of the variance in List Learning outcome and 54 % of the variance in Delayed Recall outcome. The fMRI LI accounted for an additional 10 % of the variance in List Learning outcome ($p = .001$) and 7 % of the variance in Delayed Recall outcome ($p = .003$). Addition of the Wada language and memory data did not significantly improve the predictive power of either model (R^2 change for List Learning = .025, R^2 change for Delayed Recall = .017, both $p > .1$). When patients were categorized as showing decline or no decline based on a negative change score 1.5 standard deviations or more from the mean change score in the right ATL surgery group, the List Learning outcome model showed sensitivity of 90 % and specificity of 80 % for predicting decline on List Learning. The delayed recall outcome model showed sensitivity of 81 % and specificity of 100 % for predicting decline on Delayed Recall.

These results are interesting for several reasons. Most intriguing is the finding that *language* lateralization, whether measured by fMRI or the Wada test, was a better predictor of verbal *memory* outcome than Wada memory testing. The explanation for this paradox rests on two hypotheses. One, mentioned above, is that verbal memory encoding processes tend to co-lateralize with language processes. The second hypothesis is that many tests of memory lateralization do not specifically assess verbal memory encoding. That is, visual stimuli such as objects and pictures can be dually encoded using both verbal and visual codes. Wada memory procedures that use such stimuli (including the

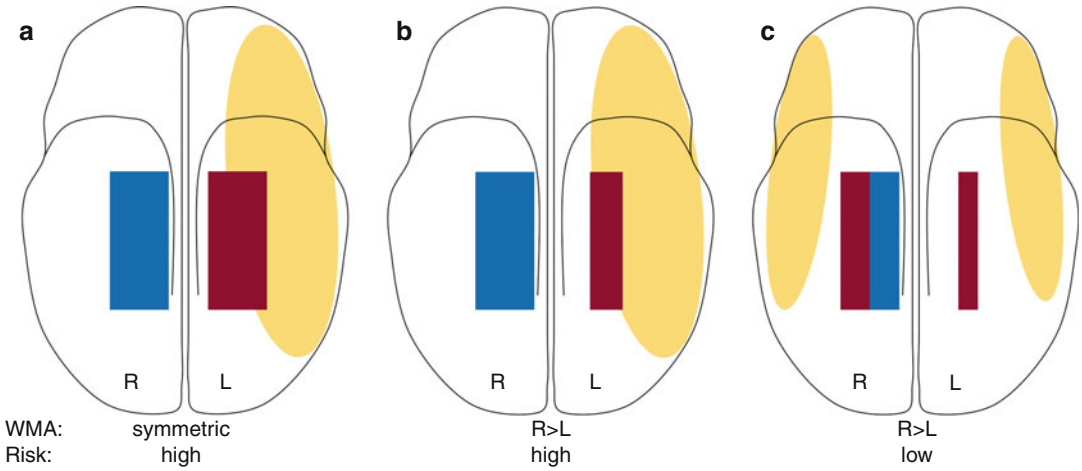

Fig. 10.5 Schematic diagram of a hypothetical model of memory and language representation in temporal lobe epilepsy (TLE). The *yellow* ovals represent language systems, *red* rectangles represent verbal episodic memory encoding systems in the MTL, and *blue* rectangles represent nonverbal episodic memory encoding systems in the MTL. (**a**) Typical state in healthy subjects and patients with late-onset epilepsy. Language and verbal memory processes are strongly left-lateralized, placing the patient at high risk for verbal memory decline. (**b**) Chronic left TLE without shift. The left MTL is dysfunctional, causing Wada memory lateralization to the right, but verbal memory has not shifted, leaving the patient at high risk for verbal memory decline. (**c**) Chronic left TLE with shift. Both language and verbal memory functions have shifted partially to the right, lowering the risk for verbal memory decline. Note the partial lack of correspondence, across patient types, between Wada memory asymmetry and level of risk (Adapted from Binder et al. (2008a))

Wada test used by Binder et al.) therefore do not provide a measure of verbal memory lateralization but rather a measure of overall memory lateralization that includes both verbal and nonverbal encoding processes. Together, these two hypotheses suggest that language asymmetry may be more closely correlated with verbal memory lateralization than Wada memory asymmetry (Fig. 10.5). In particular, some patients with left temporal seizures show right-lateralized memory on the Wada test due to a strong nonverbal memory component in the right hemisphere but are nevertheless at high risk for verbal memory decline because their *verbal* memory remains strongly lateralized to the left (Fig. 10.5b).

These data also have direct implications for clinical practice. First, they confirm the utility of fMRI for predicting verbal memory outcome in patients undergoing left ATL resection. The fMRI language LI is a safe, noninvasive measure that improves prediction accuracy relative to other noninvasive measures. The finding that Wada memory lateralization is not a strong predictor of verbal memory outcome and adds no predictive value beyond these noninvasive measures confirms several previous studies that also examined multivariate prediction models (Chelune and Najm 2000; Kirsch et al. 2005; Lacruz et al. 2004; Lineweaver et al. 2006; Stroup et al. 2003). Although Binder et al. found that Wada language asymmetry is a stronger predictor of verbal memory outcome than Wada memory lateralization, even the addition of both Wada tests together did not contribute additional predictive power after inclusion of available noninvasive data (including fMRI). These results call into question the routine use of the Wada test for predicting material-specific verbal memory outcome, particularly if a validated fMRI measure of language lateralization is available. Some practitioners continue to value the Wada test as a means of predicting more severe "global" amnesia, such is known to occur after bilateral MTL damage (Di Gennaro et al. 2006; Guerreiro et al. 2001; Milner et al. 1962; Scoville and Milner 1957). According to this theory, anesthetization of the

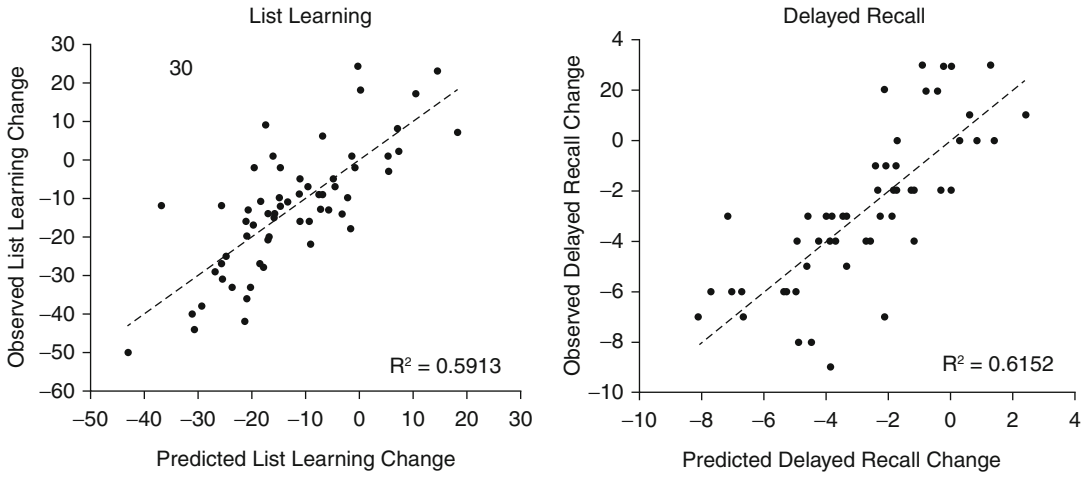

Fig. 10.6 Predicted vs. observed individual memory change scores in 60 left ATL surgery patients on tests of List Learning and Delayed Recall. Predicted list learning change scores were computed from the formula 17.67 − 0.704 (preoperative score) − 0.280 (age at onset) − 12.19 (fMRI LI). Predicted delayed recall change scores were computed from the formula 0.76 − 0.688 (preoperative score) − 0.093 (age at onset) − 2.14 (fMRI LI) (Adapted from Binder et al. (2008a))

to-be-resected MTL is necessary to discover whether the contralateral hemisphere is healthy enough to support memory on its own. Empirical observations, however, provide little support for such an approach. Cases of global amnesia following unilateral temporal lobe resection – especially modern, well-documented cases – appear to be rare in the extreme (Baxendale 1998; Kapur and Prevett 2003; Kubu et al. 2000; Loring et al. 1990a; Novelly and Williamson 1989; Simkins-Bullock 2000). Furthermore, there is ample evidence that contralateral hemisphere "memory failure" on the Wada test suffers from poor test-retest reliability and does not reliably predict amnesia (Kubu et al. 2000; Lee et al. 1995; Loddenkemper et al. 2007; Loring et al. 1990a; Martin and Grote 2002; Novelly and Williamson 1989; Simkins-Bullock 2000). Given the availability of fMRI for predicting material-specific verbal memory outcome, perhaps use of the Wada test should be reserved only for those patients at greatest risk for global amnesia, that is, patients undergoing unilateral ATL resection who have structural or functional evidence of damage to the contralateral MTL. Because it is noninvasive and requires fewer personnel, fMRI is also likely to be considerably less costly than Wada testing.

10.4 Conclusions

Recent studies demonstrate that preoperative fMRI can be used to predict postoperative naming and verbal memory changes in patients undergoing left ATL resection. Most importantly, two studies showed that fMRI significantly improves prediction accuracy when combined with other noninvasive measures (Binder et al. 2008a; Sabsevitz et al. 2003). Thus, fMRI provides patients and practitioners with a tool for making better-informed decisions based on a quantitative assessment of cognitive risk. The quantitative nature of these predictions represents something of a paradigm shift, in that traditional predictive models using the Wada test tended to be implemented as a dichotomous "pass or fail" judgment. The alternative approach followed in many recent studies involves the development of multivariable formulas that compute predicted change scores (Fig. 10.6). These quantitative predictions provide a much more realistic picture of the actual outcomes, which are not dichotomous but vary smoothly along a continuum. Ultimately, of course, the decision whether to undergo surgery is a categorical one, but the categorical nature of the decision does not obviate the need for

precision regarding the factors that enter into the decision. An unemployed patient with frequent seizures may be willing to tolerate a substantial decline in naming or verbal memory, whereas a patient who depends on such cognitive abilities for his livelihood may be willing to risk a small decline but not a large one.

In practice, the use of fMRI for predicting outcome in epilepsy surgery depends critically on the validity of the fMRI protocol and the involvement of clinicians with the necessary clinical expertise. Language fMRI is a complex test of higher brain function, which will produce high-quality results only if high-quality methods are used. Unlike a structural imaging study, the patient is required to perform a specific mental task or tasks during fMRI, must understand fully what to do, and must be monitored for compliance during the study. The task conditions must be designed to reliably and specifically identify the mental processes of interest, based on modern scientific knowledge about these processes rather than on folk psychology or nineteenth-century neurology. These challenges can best be met through close involvement of cognitive scientists in the design of task protocols and by direct involvement of clinicians with expertise in cognitive testing to provide patient instruction and performance assessment during scanning.

Acknowledgments My thanks to Linda Allen, Bill Gross, Thomas Hammeke, Yu Liu, Wade Mueller, Conrad Nievera, Thomas Prieto, Manoj Raghavan, Megan Rozman, David Sabsevitz, Sara Swanson, and other personnel at the Froedtert-MCW Comprehensive Epilepsy Center for assistance with this research, which was also supported by National Institute of Neurological Diseases and Stroke grant R01 NS35929, National Institutes of Health General Clinical Research Center grant M01 RR00058, and the Charles A. Dana Foundation.

References

Adcock JE, Wise RG et al (2003) Quantitative fMRI assessment of the differences in lateralization of language-related brain activation in patients with temporal lobe epilepsy. Neuroimage 18:423–438

Alpherts WC, Vermeulen J et al (2000) The Wada test: prediction of focus lateralization by asymmetric and symmetric recall. Epilepsy Res 39:239–249

Alvarez P, Squire LR (1994) Memory consolidation and the medial temporal lobe: a simple network model. Proc Natl Acad Sci USA 91:7041–7045

Andreasen NC, O'Leary DS et al (1995) Remembering the past: two facets of episodic memory explored with positron emission tomography. Am J Psychiatry 152:1576–1585

Arora J, Pugh K et al (2009) Language lateralization in epilepsy patients: fMRI validated with the Wada procedure. Epilepsia 50:2225–2241

Bahn MM, Lin W et al (1997) Localization of language cortices by functional MR imaging compared with intracarotid amobarbital hemispheric sedation. Am J Radiol 169:575–579

Baldo JV, Dronkers NF (2007) Neural correlates of arithmetic and language comprehension: a common substrate? Neuropsychologia 45:229–235

Bartha L, Brenneis C et al (2003) Medial temporal lobe activation during semantic language processing: fMRI findings in healthy left- and right-handers. Cogn Brain Res 17:339–346

Baxendale S (1998) Amnesia in temporal lobectomy patients: historical perspective and review. Seizure 7:15–24

Baxendale S, Thompson P et al (2006) Predicting memory decline following epilepsy surgery: a multivariate approach. Epilepsia 47:1887–1894

Baxendale S, Thompson P et al (2007) The role of the intracarotid amobarbital procedure in predicting verbal memory decline after temporal lobe resection. Epilepsia 48:546–552

Bell BD, Davies KG et al (2000a) Intracarotid amobarbital procedure and prediction of postoperative memory in patients with left temporal lobe epilepsy and hippocampal sclerosis. Epilepsia 41:992–997

Bell BD, Davies KG et al (2000b) Confrontation naming after anterior temporal lobectomy is related to age of acquisition of the object names. Neuropsychologia 38:83–92

Bell BD, Hermann BP et al (2001) Object naming and semantic knowledge in temporal lobe epilepsy. Neuropsychology 15:434–443

Benke T, Koylu B et al (2006) Language lateralization in temporal lobe epilepsy: a comparison between fMRI and the Wada test. Epilepsia 47:1308–1319

Benson RR, FitzGerald DB et al (1999) Language dominance determined by whole brain functional MRI in patients with brain lesions. Neurology 52: 798–809

Binder JR (2006) fMRI of language systems: methods and applications. In: Faro SH, Mohammed FB (eds) Functional MRI: basic principles and clinical applications. Springer, New York, pp 245–277

Binder JR, Raghavan M (2006) Functional MRI in epilepsy. In: D'Esposito ME (ed) Functional MRI: applications in neurology and psychiatry. Informa Healthcare, London, pp 81–114

Binder JR, Swanson SJ et al (1996) Determination of language dominance using functional MRI: a comparison with the Wada test. Neurology 46:978–984

Binder JR, Frost JA et al (1997) Human brain language areas identified by functional MRI. J Neurosci 17: 353–362

Binder JR, Frost JA et al (1999) Conceptual processing during the conscious resting state: a functional MRI study. J Cogn Neurosci 11:80–93

Binder JR, Bellgowan PSF et al (2005) A comparison of two fMRI protocols for eliciting hippocampal activation. Epilepsia 46:1061–1070

Binder JR, Sabsevitz DS et al (2008a) Use of preoperative functional MRI to predict verbal memory decline after temporal lobe epilepsy surgery. Epilepsia 49:1377–1394

Binder JR, Swanson SJ et al (2008b) A comparison of five fMRI protocols for mapping speech comprehension systems. Epilepsia 49:1980–1997

Binder JR, Desai R et al (2009) Where is the semantic system? A critical review and meta-analysis of 120 functional neuroimaging studies. Cereb Cortex 19:2767–2796

Binder JR, Gross W et al (2010a) Mapping anterior temporal language areas with fMRI: a multi-center normative study. Neuroimage 54:1465–1475

Binder JR, Swanson SJ et al (2010b) A comparison of two fMRI methods for predicting verbal memory decline after left temporal lobectomy: language lateralization vs. hippocampal activation asymmetry. Epilepsia 51:618–626

Bonelli SB, Powell RHW et al (2010) Imaging memory in temporal lobe epilepsy: predicting the effects of temporal lobe resection. Brain 133:1186–1199

Brewer JB, Zhao Z et al (1998) Making memories: brain activity that predicts how well visual experience will be remembered. Science 281:1185–1188

Buckner RL, Wheeler ME et al (2001) Encoding processes during retrieval tasks. J Cogn Neurosci 13:406–415

Buschke H, Fuld PA (1974) Evaluating storage, retention, and retrieval in disordered memory and learning. Neurology 24:1019–1025

Cappelletti M, Butterworth B et al (2001) Spared numerical abilities in a case of semantic dementia. Neuropsychologia 39:1224–1239

Carpenter K, Oxbury JM et al (1996) Memory for objects presented after intracarotid sodium amytal: a sensitive clinical neuropsychological indicator of temporal lobe pathology. Seizure 5:103–108

Carpentier A, Pugh KR et al (2001) Functional MRI of language processing: dependence on input modality and temporal lobe epilepsy. Epilepsia 42:1241–1254

Chelune GC (1995) Hippocampal adequacy versus functional reserve: predicting memory functions following temporal lobectomy. Arch Clin Neuropsychol 10: 413–432

Chelune GJ, Najm IM (2000) Risk factors associated with postsurgical decrements in memory. In: Luders HO, Comair Y (eds) Epilepsy surgery, 2nd edn. Lippincott, Philadelphia, pp 497–504

Chelune GJ, Naugle RI et al (1991) Prediction of cognitive change as a function of preoperative ability level among temporal lobectomy patients at six months follow-up. Neurology 41:399–404

Chelune GJ, Naugle RI et al (1993) Individual change after epilepsy surgery: practice effects and base-rate information. Neuropsychology 7:41–52

Chiaravalloti ND, Glosser G (2001) Material-specific memory changes after anterior temporal lobectomy as predicted by the intracarotid amobarbital test. Epilepsia 42:902–911

Chlebus P, Mikl M et al (2007) fMRI evaluation of hemispheric language dominance using various methods of laterality index calculation. Exp Brain Res 179:365–374

Cohen NJ, Eichenbaum H (1993) Memory, amnesia, and the hippocampal system. MIT Press, Cambridge

Cohen-Gadol AA, Westerveld M et al (2004) Intracarotid amytal memory test and hippocampal magnetic resonance imaging volumetry: validity of the Wada test as an indicator of hippocampal integrity among candidates for epilepsy surgery. J Neurosurg 101:926–931

Constable RT, Carpentier A et al (2000) Investigation of the hippocampal formation using a randomized event-related paradigm and z-shimmed functional MRI. Neuroimage 12:55–62

Craik FIM, Lockhart RS (1972) Levels of processing: a framework for memory research. J Verbal Learn Verbal Behav 11:671–684

Crutch SJ, Warrington EK (2002) Preserved calculation skills in a case of semantic dementia. Cortex 38:389–399

Damasio H, Grabowski TJ et al (1996) A neural basis for lexical retrieval. Nature 380:499–505

Davachi L, Wagner AD (2002) Hippocampal contributions to episodic memory: insights from relational and item-based learning. J Neurophysiol 88:982–990

Davies KG, Bell BD et al (1998a) Naming decline after left anterior temporal lobectomy correlates with pathological status of resected hippocampus. Epilepsia 39:407–419

Davies KG, Bell BD et al (1998b) Prediction of verbal memory loss in individuals after anterior temporal lobectomy. Epilepsia 39:820–828

Deblaere K, Boon PA et al (2004) MRI language dominance assessment in epilepsy patients at 1.0 T: region of interest analysis and comparison with intracarotid amytal testing. Neuroradiology 46:413–420

Desmond JE, Sum JM et al (1995) Functional MRI measurement of language lateralization in Wada-tested patients. Brain 118:1411–1419

Detre JA, Maccotta L et al (1998) Functional MRI lateralization of memory in temporal lobe epilepsy. Neurology 50:926–932

Di Gennaro G, Grammaldo LG et al (2006) Severe amnesia following bilateral medial temporal lobe damage occurring on two distinct occasions. Neurol Sci 27:129–133

Diesfeldt HFA (1993) Progressive decline of semantic memory with preservation of number processing and calculation. Behav Neurol 6:239–242

Eldridge LL, Knowlton BJ et al (2000) Remembering episodes: a selective role for the hippocampus during retrieval. Nat Neurosci 3:1149–1152

Fernandez G, Weyerts H et al (1998) Successful verbal encoding into episodic memory engages the posterior

hippocampus: a parametrically analyzed functional magnetic resonance imaging study. J Neurosci 18: 1841–1847
Fransson P, Merboldt KD et al (2001) Functional MRI with reduced susceptibility artifact: high-resolution mapping of episodic memory encoding. Neuroreport 12:1415–1420
Friederici AD, Meyer M et al (2000) Auditory language comprehension: an event-related fMRI study on the processing of syntactic and lexical information. Brain Lang 74:289–300
Frings L, Wagner K et al (2008) Lateralization of hippocampal activation differs between left and right temporal lobe epilepsy patients and correlates with postsurgical verbal learning decrement. Epilepsy Res 78:161–170
Gabrieli JDE (2001) Functional imaging of episodic memory. In: Cabeza R, Kingstone A (eds) Handbook of functional neuroimaging of cognition. MIT Press, Cambridge, pp 253–291
Gabrieli JDE, Brewer JB et al (1997) Separate neural bases of two fundamental memory processes in human medial temporal lobe. Science 276:264–266
Gaillard WD, Balsamo L et al (2004) fMRI language task panel improves determination of language dominance. Neurology 63:1403–1408
Gleissner U, Helmstaedter C et al (2004) Memory outcome after selective amygdalohippocampectomy in patients with temporal lobe epilepsy: one-year follow-up. Epilepsia 45:960–962
Golby AJ, Poldrack RA et al (2001) Material-specific lateralization in the medial temporal lobe and prefrontal cortex during memory encoding. Brain 124:1841–1854
Greene AJ, Gross WL et al (2006) An fMRI analysis of the human hippocampus: inference, context, and task awareness. J Cogn Neurosci 18:1156–1173
Griffith HR, Perlman SB et al (2000) Preoperative FDG-PET temporal lobe hypometabolism and verbal memory after temporal lobectomy. Neurology 54: 1161–1165
Grunwald T, Lehnertz K et al (1998) Verbal novelty detection within the human hippocampus proper. Proc Natl Acad Sci USA 95:3193–3197
Guerreiro CAM, Jones-Gotman M et al (2001) Severe amnesia in epilepsy: causes, anatomopsychological considerations, and treatment. Epilepsy Behav 2: 224–246
Hamberger MJ, Goodman RR et al (2001) Anatomic dissociation of auditory and visual naming in the lateral temporal cortex. Neurology 56:56–61
Hassabis D, Kumaran D et al (2007) Using imagination to understand the neural basis of episodic memory. J Neurosci 27:14365–14374
Helmstaedter C, Elger CE (1996) Cognitive consequences of two-thirds anterior temporal lobectomy on verbal memory in 144 patients: a three-month follow-up study. Epilepsia 37:171–180
Helmstaedter C, Kurthen M et al (2003) Chronic epilepsy and cognition: a longitudinal study in temporal lobe epilepsy. Ann Neurol 54:425–432
Henke K, Buck A et al (1997) Human hippocampus establishes associations in memory. Hippocampus 7: 249–256
Henke K, Weber B et al (1999) Human hippocampus associates information in memory. Proc Natl Acad Sci USA 96:5884–5889
Hermann BP, Wyler AR et al (1994) Dysnomia after left anterior temporal lobectomy without functional mapping: frequency and correlates. Neurosurgery 35:52–57
Hermann BP, Seidenberg M et al (1995) Relationship of age at onset, chronologic age, and adequacy of preoperative performance to verbal memory change after anterior temporal lobectomy. Epilepsia 36:137–145
Hermann B, Davies K et al (1999a) Visual confrontation naming outcome after standard left anterior temporal lobectomy with sparing versus resection of the superior temporal gyrus: a randomized prospective clinical trial. Epilepsia 40:1070–1076
Hermann BP, Perrine K et al (1999b) Visual confrontation naming following left anterior temporal lobectomy: a comparison of surgical approaches. Neuropsychology 13:3–9
Hertz-Pannier L, Gaillard WD et al (1997) Noninvasive assessment of language dominance in children and adolescents with functional MRI: a preliminary study. Neurology 48:1003–1012
Humphries C, Swinney D et al (2005) Response of anterior temporal cortex to syntactic and prosodic manipulations during sentence processing. Hum Brain Mapp 26:128–138
Humphries C, Binder JR et al (2006) Syntactic and semantic modulation of neural activity during auditory sentence comprehension. J Cogn Neurosci 18:665–679
Hunkin NM, Mayes AR et al (2002) Novelty-related activation within the medial temporal lobes. Neuropsychologia 40:1456–1464
Hwang DY, Golby AJ (2006) The brain basis for episodic memory: insights from functional MRI, intracranial EEG, and patients with epilepsy. Epilepsy Behav 8:115–126
Jeong S-W, Lee SK et al (2005) Prognostic factors for the surgery for mesial temporal lobe epilepsy: longitudinal analysis. Epilepsia 46:1273–1279
Jokeit H, Ebner A et al (1997) Individual prediction of change in delayed recall of prose passages after left-sided anterior temporal lobectomy. Neurology 49:481–487
Jones SE, Mahmoud SY et al (2011) A practical clinical method to quantify language lateralization in fMRI using whole-brain analysis. Neuroimage 54: 2937–2949
Kapur N, Prevett M (2003) Unexpected amnesia: are there lessons to be learned from cases of amnesia following unilateral temporal lobe surgery? Brain 126:2573–2585
Kelley WM, Miezin FM et al (1998) Hemispheric specialization in human dorsal frontal cortex and medial temporal lobe for verbal and nonverbal memory encoding. Neuron 20:927–936
Kensinger EA, Clarke RJ et al (2003) What neural correlates underlie successful encoding and retrieval? A

functional magnetic resonance imaging study using a divided attention paradigm. J Neurosci 23: 2407–2415
Killgore WD, Casasanto DJ et al (2002) Functional activation of the left amygdala and hippocampus during associative encoding. Neuroreport 11:2259–2263
Kirchhoff BA, Wagner AD et al (2000) Prefrontal-temporal circuitry for episodic encoding and subsequent memory. J Neurosci 20:6173–6180
Kirsch HE, Walker JA et al (2005) Limitations of Wada memory asymmetry as a predictor of outcomes after temporal lobectomy. Neurology 65:676–680
Knecht S, Deppe M et al (2000a) Language lateralization in healthy right-handers. Brain 123:74–81
Knecht S, Dräger B et al (2000b) Handedness and hemispheric language dominance in healthy humans. Brain 123:2512–2518
Knecht S, Floel A et al (2002) Degree of language lateralization determines susceptibility to unilateral brain lesions. Nat Neurosci 5:695–699
Kneebone AC, Chelune GJ et al (1995) Intracarotid amobarbital procedure as a predictor of material-specific memory change after anterior temporal lobectomy. Epilepsia 36:857–865
Knight RT (1996) Contribution of the human hippocampal region to novelty detection. Nature 383:256–259
Koylu B, Walser G et al (2008) Functional imaging of semantic memory predicts postoperative episodic memory functions in chronic temporal lobe epilepsy. Brain Res 1223:73–81
Kubu CS, Girvin JP et al (2000) Does the intracarotid amobarbital procedure predict global amnesia after temporal lobectomy? Epilepsia 41:1321–1329
Lacruz ME, Alarcon G et al (2004) Neuropsychological effects associated with temporal lobectomy and amygdalohippocampectomy depending on Wada test failure. J Neurol Neurosurg Psychiatry 75:600–607
Lambon Ralph MA, McClelland J et al (2001) No right to speak? The relationship between object naming and semantic impairment: neuropsychological evidence and a computational model. J Cogn Neurosci 13:341–356
Langfitt JT, Rausch R (1996) Word-finding deficits persist after left anterotemporal lobectomy. Arch Neurol 53:72–76
Langfitt JT, Westerveld M et al (2007) Worsening of quality of life after epilepsy surgery: effect of seizures and memory decline. Neurology 68:1988–1994
Lee GP, Loring DW et al (1995) Intraoperative hippocampal cooling and Wada memory testing in the evaluation of amnesia risk following anterior temporal lobectomy. Arch Neurol 52:857–861
Lee TMC, Yip JTH et al (2002) Memory deficits after resection of left or right anterior temporal lobe in humans: a meta-analytic review. Epilepsia 43: 283–291
Lehéricy S, Cohen L et al (2000) Functional MR evaluation of temporal and frontal language dominance compared with the Wada test. Neurology 54:1625–1633
Li L, Miller EK et al (1993) The representation of stimulus familiarity in anterior inferior temporal cortex. J Neurophysiol 69:1918–1929
Lineweaver TT, Naugle RI et al (2004) Patients' perceptions of memory functioning before and after surgical intervention to treat medically refractory epilepsy. Epilepsia 45:1604–1612
Lineweaver TT, Morris HH et al (2006) Evaluating the contributions of state-of-the-art assessment techniques to predicting memory outcome after unilateral anterior temporal lobectomy. Epilepsia 47:1895–1903
Loddenkemper T, Morris HH et al (2007) Repeated intracarotid amobarbital tests. Epilepsia 48:553–558
Loring DW, Lee GP et al (1990a) The intracarotid amobarbital procedure as a predictor of memory failure following unilateral temporal lobectomy. Neurology 40:605–610
Loring DW, Meador KJ et al (1990b) Cerebral language lateralization: evidence from intracarotid amobarbital testing. Neuropsychologia 28:831–838
Loring DW, Meador KJ et al (1994) Stimulus timing effects on Wada memory testing. Arch Neurol 51: 806–810
Loring DW, Hermann BP et al (1995a) Memory for real objects is superior to line drawing recognition in discrimination of lateralized temporal lobe impairment during the Wada test. J Int Neuropsychol Soc 1:134
Loring DW, Meador KJ et al (1995b) Wada memory asymmetries predict verbal memory decline after anterior temporal lobectomy. Neurology 45:1329–1333
Martin A (1999) Automatic activation of the medial temporal lobe during encoding: lateralized influences of meaning and novelty. Hippocampus 9:62–70
Martin RC, Grote CL (2002) Does the Wada test predict memory decline following epilepsy surgery. Epilepsy Behav 3:4–15
Martin RC, Sawrie SM et al (1998) Individual memory change after anterior temporal lobectomy: a base rate analysis using regression-based outcome methodology. Epilepsia 39:1075–1082
Mazoyer BM, Tzourio N et al (1993) The cortical representation of speech. J Cogn Neurosci 5:467–479
McClelland JL, McNaughton BL et al (1995) Why are there complementary learning systems in the hippocampus and neocortex: insights from the success and failures of connectionist models of learning and memory. Psychol Rev 102:409–457
McIntosh AM, Wilson SJ et al (2001) Seizure outcome after temporal lobectomy: current research practice and findings. Epilepsia 42:1288–1307
Milner B, Branch C et al (1962) Study of short-term memory after intracarotid injection of sodium amytal. Trans Am Neurol Assoc 87:224–226
Morawetz C, Holz P et al (2008) Improved functional mapping of the human amygdala using a standard functional magnetic resonance imaging sequence with simple modifications. Magn Reson Imaging 26:45–53
Mummery CJ, Patterson K et al (2000) A voxel-based morphometry study of semantic dementia: relationship between temporal lobe atrophy and semantic memory. Ann Neurol 47:36–45
Nagata S, Uchimura K et al (2001) Method for quantitatively evaluating the lateralization of linguistic func-

tion using functional MR imaging. Am J Neuroradiol 22:985–991
Novelly RA, Williamson PD (1989) Incidence of false-positive memory impairment in the intracarotid amytal procedure. Epilepsia 30:711
O'Reilly RC, Rudy JW (2001) Conjunctive representations in learning and memory: principles of cortical and hippocampal function. Psychol Rev 108:311–345
Olson IR, Plotzker A et al (2007) The enigmatic temporal pole: a review of findings on social and emotional processing. Brain 130:1718–1731
Otten LJ, Henson RNA et al (2001) Depth of processing effects on neural correlates of memory encoding. Relationship between findings from across- and within-task comparisons. Brain 124:399–412
Paller KA, Wagner AD (2002) Observing the transformation of experience into memory. Trends Cogn Sci 6: 93–102
Parsons MW, Haut MW et al (2006) Anterior medial temporal lobe activation during encoding of words: FMRI methods to optimize sensitivity. Brain Cogn 60:253–261
Patterson K, Nestor PJ et al (2007) Where do you know what you know? The representation of semantic knowledge in the human brain. Nat Rev Neurosci 8: 976–987
Perrine K, Hermann BP et al (1995) The relationship of neuropsychological functioning to quality of life in epilepsy. Arch Neurol 52:997–1003
Pigot S, Milner B (1993) Memory for different aspects of complex visual scenes after unilateral-temporal or frontal-lobe resection. Neuropsychologia 13:1–15
Pillon B, Bazin B et al (1999) Specificity of memory deficits after right or left temporal lobectomy. Cortex 35:561–571
Powell HW, Koepp MJ et al (2005) Material-specific lateralization of memory encoding in the medial temporal lobe: blocked versus event-related design. Neuroimage 48:1512–1525
Powell HWR, Richardson MP et al (2008) Preoperative fMRI predicts memory decline following anterior temporal lobe resection. J Neurol Neurosurg Psychiatry 79:686–693
Prince SE, Daselaar SM et al (2005) Neural correlates of relational memory: successful encoding and retrieval of semantic and perceptual associations. J Neurosci 25:1203–1210
Prince SE, Tsukiura T et al (2007) Distinguishing the neural correlates of episodic memory encoding and semantic memory retrieval. Psychol Sci 18:144–151
Rabin ML, Narayan VM et al (2004) Functional MRI predicts post-surgical memory following temporal lobectomy. Brain 127:2286–2298
Reber PJ, Wong EC et al (2002) Encoding activity in the medial temporal lobe examined with anatomically constrained fMRI analysis. Hippocampus 12: 363–376
Richardson MP, Strange BA et al (2004) Pre-operative verbal memory fMRI predicts post-operative memory decline after left anterior temporal lobe resection. Brain 127:2419–2426
Richardson MP, Strange BA et al (2006) Memory fMRI in left hippocampal sclerosis. Optimizing the approach to predicting postsurgical memory. Neurology 66:699–705
Riches IP, Wilson FAW et al (1991) The effects of visual stimulation and memory on neurones of the hippocampal formation and neighboring parahippocampal gyrus and inferior temporal cortex of the primate. J Neurosci 11:1763–1779
Rogers TT, Hocking J et al (2006) Anterior temporal cortex and semantic memory: reconciling findings from neuropsychology and functional imaging. Cogn Affect Behav Neurosci 6:201–213
Rosen HJ, Gorno-Tempini ML et al (2002) Patterns of brain atrophy in frontotemporal dementia and semantic dementia. Neurology 58:198–208
Ross LA, Olson IR (2010) Social cognition and the anterior temporal lobes. Neuroimage 49:3452–3462
Rugg MD, Otten LJ et al (2002) The neural basis of episodic memory: evidence from functional neuroimaging. Philos Trans R Soc Lond B 357:1097–1110
Rutten G-J, Ramsey N et al (2002) FMRI-determined language lateralization in patients with unilateral or mixed language dominance according to the Wada test. Neuroimage 17:447–460
Sabbah P, Chassoux F et al (2003) Functional MR imaging in assessment of language dominance in epileptic patients. Neuroimage 18:460–467
Sabsevitz DS, Swanson SJ et al (2001) Memory outcome after left anterior temporal lobectomy in patients with expected and reversed Wada memory asymmetry scores. Epilepsia 42:1408–1415
Sabsevitz DS, Swanson SJ et al (2003) Use of preoperative functional neuroimaging to predict language deficits from epilepsy surgery. Neurology 60:1788–1792
Saykin AJ, Stafiniak P et al (1995) Language before and after temporal lobectomy: specificity of acute changes and relation to early risk factors. Epilepsia 36: 1071–1077
Schacter DL, Addis DR (2007) The cognitive neuroscience of constructive memory: remembering the past and imagining the future. Philos Trans R Soc Lond B 362:773–786
Schacter DL, Wagner AD (1999) Medial temporal lobe activations in fMRI and PET studies of episodic encoding and retrieval. Hippocampus 9:7–24
Scoville WB, Milner B (1957) Loss of recent memory after bilateral hippocampal lesions. J Neurol Neurosurg Psychiatry 20:11–21
Seghier ML (2008) Laterality index in functional MRI: methodological issues. Magn Reson Imaging 26:594–601
Simkins-Bullock J (2000) Beyond speech lateralization: a review of the variability, reliability, and validity of the intracarotid amobarbital procedure and its nonlanguage uses in epilepsy surgery candidates. Neuropsychol Rev 10:41–74

Small SA, Nava AS et al (2001) Circuit mechanisms underlying memory encoding and retrieval in the long axis of the hippocampal formation. Nat Neurosci 4:442–449

Sperling RA, Bates JF et al (2001) Encoding novel face-name associations: a functional MRI study. Hum Brain Mapp 14:129–139

Spitsyna G, Warren JE et al (2006) Converging language streams in the human temporal lobe. J Neurosci 26:7328–7336

Spreer J, Arnold S et al (2002) Determination of hemisphere dominance for language: comparison of frontal and temporal fMRI activation with intracarotid amytal testing. Neuroradiology 44:467–474

Springer JA, Binder JR et al (1999) Language dominance in neurologically normal and epilepsy subjects: a functional MRI study. Brain 122:2033–2045

Squire LR (1992) Memory and the hippocampus: a synthesis from findings with rats, monkeys, and humans. Psychol Rev 99:195–231

Stafiniak P, Saykin AJ et al (1990) Acute naming deficits following dominant temporal lobectomy: prediction by age at first risk for seizures. Neurology 40:1509–1512

Stark CE, Squire LR (2001) When zero is not zero: the problem of ambiguous baseline conditions in fMRI. Proc Natl Acad Sci USA 98:12760–12766

Stern CE, Corkin S et al (1996) The hippocampal formation participates in novel picture encoding: evidence from functional magnetic resonance imaging. Proc Natl Acad Sci USA 93:8660–8665

Stroup E, Langfitt JT et al (2003) Predicting verbal memory decline following anterior temporal lobectomy (ATL). Neurology 60:1266–1273

Swanson SJ, Sabsevitz DS et al (2007) Functional magnetic resonance imaging of language in epilepsy. Neuropsychol Rev 17:491–504

Szaflarski JP, Holland SK et al (2008) Comprehensive presurgical functional MRI language evaluation in adult patients with epilepsy. Epilepsy Behav 12: 74–83

Tellez-Zenteno JF, Dhar R et al (2005) Long-term sei-zure outcomes following epilepsy surgery: a systematic review and meta-analysis. Brain 128:1188–1198

Trenerry MR, Jack CRJ et al (1993) MRI hippocampal volumes and memory function before and after temporal lobectomy. Neurology 43:1800–1805

Tulving E, Markowitsch HJ et al (1996) Novelty and familiarity activations in PET studies of memory encoding and retrieval. Cereb Cortex 6:71–79

Uncapher MR, Rugg MD (2005) Encoding and durability of episodic memory: a functional magnetic resonance imaging study. J Neurosci 25:7260–7267

Vandenberghe R, Nobre AC et al (2002) The response of left temporal cortex to sentences. J Cogn Neurosci 14:550–560

Vilberg KL, Rugg MD (2008) Memory retrieval and the parietal cortex: a review of evidence from a dual-process perspective. Neuropsychologia 46: 1787–1799

Vincent JL, Snyder AZ et al (2006) Coherent spontaneous activity identifies a hippocampal-parietal memory network. J Neurophysiol 96:3517–3531

Visser M, Jefferies E et al (2010) Semantic processing in the anterior temporal lobes: a meta-analysis of the functional neuroimaging literature. J Cogn Neurosci 22:1083–1094

Wada J, Rasmussen T (1960) Intracarotid injection of sodium amytal for the lateralization of cerebral speech dominance. J Neurosurg 17:266–282

Wagner AD, Schacter DL et al (1998) Building memories: remembering and forgetting of verbal experiences as predicted by brain activity. Science 281:1188–1191

Wechsler D (1997) Wechsler Memory Scale, 3rd edn. WMS-III Administration and Scoring Manual, vol 3. Psychological Corporation, San Antonio

Weis S, Klaver P et al (2004) Temporal and cerebellar brain regions that support both declarative memory formation and retrieval. Cereb Cortex 14:256–267

Wendel JD, Trenerry MR et al (2001) The relationship between quantitative T2 relaxometry and memory in non-lesional temporal lobe epilepsy. Epilepsia 42:863–869

Wilke M, Schmithorst VJ (2006) A combined bootstrap/histogram analysis approach for computing a lateralization index from neuroimaging data. Neuroimage 33:522–530

Woermann FG, Jokeit H et al (2003) Language lateralization by Wada test and fMRI in 100 patients with epilepsy. Neurology 61:699–701

Worthington C, Vincent DJ et al (1997) Comparison of functional magnetic resonance imaging for language localization and intracarotid speech amytal testing in presurgical evaluation for intractable epilepsy. Stereotact Funct Neurosurg 69:197–201

Xu J, Kemeny S et al (2005) Language in context: emergent features of word, sentence, and narrative comprehension. Neuroimage 25:1002–1015

Yetkin FZ, Swanson S et al (1998) Functional MR of frontal lobe activation: comparison with Wada language results. Am J Neuroradiol 19:1095–1098

Zahn R, Moll J et al (2007) Social concepts are represented in the superior anterior temporal cortex. Proc Natl Acad Sci USA 104:6430–6435

Zeinah MM, Engel SA et al (2003) Dynamics of the hippocampus during encoding and retrieval of face-name pairs. Science 299:577–580

11 Mapping of Recovery from Poststroke Aphasia: Comparison of PET and fMRI

Wolf-Dieter Heiss

11.1 The Principle of Activation Studies

The energy demand of the brain is very high and relies almost entirely on the oxidative metabolism of glucose. Glucose metabolized in neuronal cell bodies mainly supports cellular, vegetative, and housekeeping functions, e.g., axonal transport, biosynthesis of nucleic acids, proteins, and lipids, as well as other energy-consuming processes not related directly to action potentials. Therefore, the energy demand of neuronal cell bodies is relatively low and essentially unaffected by neuronal functional activation (Sokoloff 1999). A larger portion of energy consumption is required for signaling, mainly action potential propagation and postsynaptic ion fluxes; this might account for up to 87 % of the total energy consumed with only 13 % expended in maintaining membrane resting potential (Laughlin and Attwell 2001). As a consequence, the rate of glucose consumption of neuronal cell bodies is essentially unaffected by functional activation, whereas increases in metabolism (and in the coupled regional blood flow) evoked by functional activation are confined to synapse-rich regions, i.e., the neutrophil that contains axonal terminals, dendritic processes, and the astrocytic processes that envelop the synapses (Magistretti 2004). The magnitudes of these increases are linearly related to the frequency of action potentials in the afferent pathways, and increases of metabolism and blood flow in the projection zones occur regardless of whether the pathway is excitatory or inhibitory. Only at the next downstream projection zones, glucose utilization (and, as a consequence, blood supply) is depressed in inhibited neurons and increased in excited neurons.

Mapping of neuronal activity in the brain can be primarily achieved by quantitation of the regional cerebral metabolic rate for glucose (rCMRGlc), as introduced for autoradiographic experimental studies by Sokoloff (Sokoloff 1999) and adapted for positron emission tomography (PET) in humans (Reivich et al. 1979). Functional mapping, as it is widely used now, relies primarily on the hemodynamic response assuming a close association between energy metabolism and blood flow. While it is well documented that increases in blood flow and glucose consumption are closely coupled during neuronal activation, the increase in oxygen consumption is considerably delayed leading to a decreased oxygen extraction fraction (OEF) during activation (Mintun et al. 2001). PET detects and, if required, can quantify changes in CBF and CMRGlc accompanying different activation states of the brain tissue. The regional values of CBF or CMRGlc represent the brain activity due to a specific state, task, or stimulus, in comparison to the resting condition, and color-coded maps can be analyzed or coregistered to morphologic

W.-D. Heiss
Max Planck Institute for Neurological Research,
Gleueler Str. 50, Köln 50931, Germany
e-mail: wdh@nf.mpg.de

S. Ulmer, O. Jansen (eds.), *fMRI – Basics and Clinical Applications*,
DOI 10.1007/978-3-642-34342-1_11,

images. Due to the radioactivity of the necessary tracers, activation studies with PET are limited to a maximum of 12 doses of ^{15}O-labeled tracers, e.g., 12 flow scans, or two doses of ^{18}F-labeled tracers, e.g., two metabolic scans. Especially for studies of glucose consumption, the time to metabolic equilibrium (20–40 min) as well as the time interval between measurements required for isotope decay (HT for ^{18}F 108 min, for ^{15}O 2 min) must be taken into consideration.

Functional magnetic resonance imaging (fMRI) measures signals that depend on the differential magnetic properties of oxygenated and deoxygenated hemoglobin, termed the blood-oxygen-level-dependent (BOLD) signal, which gives an estimate of changes in oxygen availability (Ogawa et al. 1990). This means that mainly the amount of deoxyhemoglobin in small blood vessels is recorded, which depends on the flow of well-oxygenated arterial blood (CBF), on the outflow of O_2 to the tissue ($CMRO_2$) and on the cerebral blood volume (CBV) (Turner et al. 1997). The magnitude of these changes in signal intensity relative to the resting conditions are color-coded to produce fMRI images that map changes in brain function, which can be superimposed on the anatomical image. This results in a spatial resolution of fMRI of 1–3 mm with a temporal resolution of approximately 10 s. As fMRI does not involve ionizing radiation and, thus, is also used without limitations in healthy subjects, allowing more rapid signal acquisition and more flexible experimental setups, it has become the dominant technique for functional imaging. There are some advantages of PET, however – physiologically specific measures, better quantitation, better signal-to-noise ratio, fewer artifacts, and actual activated and reference values – which support its continued use especially in complex clinical situation and in combination with special stimulating technique, as transcranial magnetic stimulation (TMS).

11.2 Language Activation in Healthy Subjects

The capacity to understand and to speak language is strictly lateralized in most subjects to the dominant hemisphere. With a few exceptions, this is the left hemisphere in right-handers, whereas in left-handers, language may be represented in either hemisphere or even bilaterally (Knecht et al. 2002; Thiel et al. 1998). In addition to language dominance, details of the anatomical localization of sensory and motor language areas (Wernicke's and Broca's region) may vary considerably even in normal individuals. A considerable variety of language activation paradigms have been applied for localization of language functions by PET and fMRI (Hickok and Poeppel 2007; Petersen et al. 1988; Price 2000; Wise 2003), producing a vast amount of partly contradictory data (Demonet et al. 1996). For the analysis of aphasia after stroke or due to brain tumors, the application of a simplified scheme may be justified (Fig. 11.1; Price 2000).

The processing of hearing words activates bilaterally the upper temporal gyrus, and the semantic attribution to a meaningful content is achieved in left posterior temporal, temporoparietal, and anterior lower cortical areas. For the production of speech, the activity in the posterior upper temporal sulcus and in the left posterior lower temporal cortex is increased. The activity in the posterior upper temporal sulci is further increased, if words or sequences are repeated or read. In contrast, the left posterior lower temporal cortex in the neighborhood of the middle fusiform semantic area is activated by word fluency. This area is participating in lexical speech production. Independently, planning of articulation activates the left anterior insula and the bordering frontal operculum. Phonologic word retrieval requires the integration of the anterior insula/operculum and the posterior upper temporal sulcus or left posterior lower temporal gyrus. Finally, the bilateral sensomotoric cortex is activated for the motoric control of speech production, and the hearing of the spoken response augments the activation in the upper temporal gyrus.

In the processing of written words, the same areas are involved. Reading selectively activates the posterior fusiform and lingual gyrus, which are also involved in picture naming. For reading, the visual cortex and the posterior upper temporal sulci are activated, which contribute to the functional integration of the language network. According to this model, the function of the Wernicke region is represented in the upper part of the sulcus temporalis, the sulcus temporalis

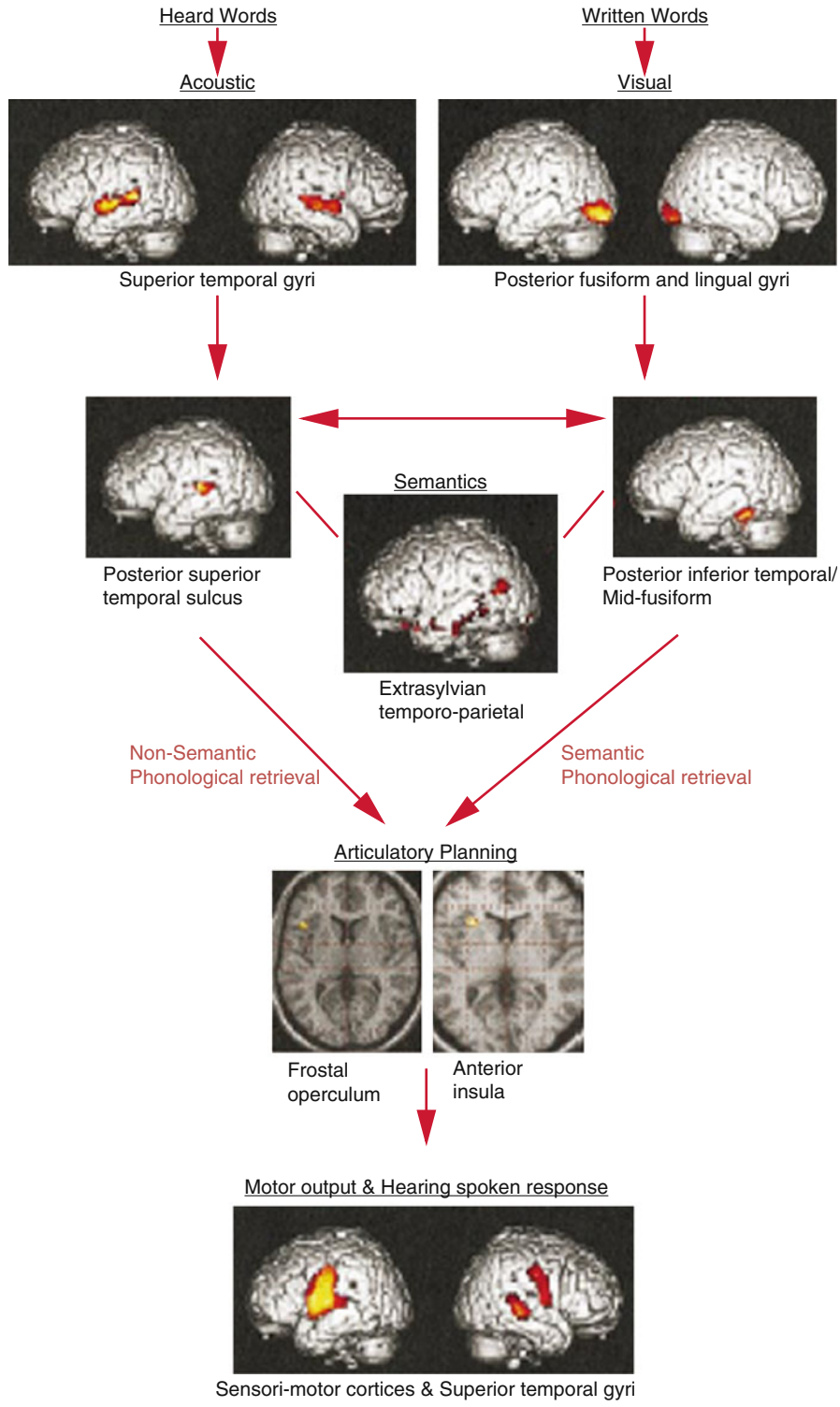

Fig. 11.1 Proposed neurological and cognitive model of language with brain areas activated by different tasks (From Price 2000)

posterior superior; the anterior insula and not the Broca area is responsible for planning articulation; the gyrus angularis is involved in semantic connection and not specific for visualization of words; the meaning of words is located in the left lower and middle temporal gyrus; reading and retrieval of names activate the posterior lower temporal lobe. For these functions – and also for the severity of functional damage – the hierarchy of individual areas within the network and the dominance of left cortical regions are of utmost importance (Heiss and Thiel 2006), which are induced and manifested by collateral and transcallosal inhibition (Karbe et al. 1998; Nudo et al. 1996).

It has to be kept in mind that all usual language functions, which are complex and require integration of several partial functions, activate larger parts of the bilateral network. For instance, the retrieval of substantives and verbs activates large areas in the left dorsomedial prefrontal cortex and the anterior cingulum as well as the supplementary motor area. The processing of meaningful connections activates the left middle temporal gyrus, the left and right temporal pole, as well as the left prefrontal area. Hearing and processing of nouns and generating verbs in relation to nouns involve a network consisting of pars opercularis and triangularis of the left lower frontal gyrus, the posterior part of the temporal sulcus up to the planum temporale, and the anterior part of the left lower temporal gyrus. In this network, even some parts of the cerebellum and of the basal ganglia are integrated (Booth et al. 2007). These complex activation patterns involving widely distributed areas impair the prediction of severity and recovery of speech disturbances caused by infarcts or other localized brain damage.

11.3 Poststroke Aphasia

Aphasia is a severely incapacitating symptom of stroke and is a main cause of functional disturbance. Estimates suggest that more than 20 % of patients suffering a stroke develop aphasia and 10–18 % of survivors are left with a persistent speech deficit (Wade et al. 1986). Most patients with aphasia due to acute nonprogressive brain damage, such as in the case of stroke or head injury, show some degree of recovery of language function during the days, months, or even years following the initial insult. The recuperation is variable, ranging from the hardly noticeable improvement of auditory comprehension of the global aphasia to the apparently complete recovery of the patient with mild fluent aphasia due to small subcortical stroke. It is also well known that improvement can be observed not only in patients submitted to language rehabilitation but also in cases that have not undergone any specific treatment.

11.4 Disturbance of Regional Metabolism and Flow Versus Severity and Persistence of Language Deficit

Studies of glucose metabolism after stroke (Cappa et al. 1997) have shown metabolic disturbances in the ipsilateral hemisphere caused by the lesion and contralateral hemisphere caused by functional deactivation (diaschisis; Feeney and Baron 1986). Most studies have been performed in right-handed individuals with language dominance in the left hemisphere. The left temporo-parietal region, in particular, the angular gyrus, supramarginal gyrus, and lateral and transverse superior temporal gyrus, is most frequently and consistently impaired, and the degree of impairment is related to the severity of aphasia (Karbe et al. 1989; Metter et al. 1990). In contrast, metabolic impairment in subcortical structures is related mainly to language fluency and other behavioral aspects, but not to aphasia severity (Metter et al. 1988). In patients with aphasia attributable to purely subcortical strokes, deactivation of temporo-parietal cortex is regularly found, which is probably responsible for the aphasic symptoms (Kumar et al. 1996).

Recovery of metabolism in both hemispheres was correlated with recovery of aphasia. One specific region crucial for recovery of language perception has been found in the left temporo-parietal cortex (Karbe et al. 1989; Metter et al. 1987) and metabolic disturbance in these areas is related to outcome (Heiss et al. 1993a). Investigations in

the subacute state after stroke showed a highly significant correlation with language performance assessed at follow-up after 2 years (Karbe et al. 1995). The receptive language disorder is correlated with rCMRGlc in the left temporal cortex, and word fluency is correlated with rCMRGlc in the left prefrontal cortex. These results indicate that the functional disturbance as measured by rCMRGlc in speech-relevant brain regions early after stroke is predictive of the eventual outcome of aphasia. However, not only functional deactivation (diaschisis) but also neuronal loss may contribute to metabolic and perfusional changes in the neighborhood of the infarct, and the condition of the surrounding tissue may affect the recovery of individual patients. In this context, it is important to note that early reperfusion to specific areas is able to restore disturbed function, as demonstrated for recovery of naming by reperfusion to the key areas BA37, BA 44/45 (Broca), and BA 22 (Wernicke; Hillis et al. 2006).

11.5 Changes in Activation Patterns Versus Recovery of Language Function

On this basis, it is not surprising that in patients with a poor outcome of poststroke aphasia, metabolism in the hemisphere outside the infarct was significantly less than in those with good language recovery, indicating significant cell loss caused by the ischemic episode outside the ischemic core (Heiss et al. 1993b). In addition, the functionality of the network was reduced in patients with an eventual poor outcome; during task performance, patients with an eventual good recovery predominantly activated structures in the ipsilateral hemisphere. It must be kept in mind that aphasia symptoms – and consequently also activation patterns – improve with restoration of regional blood flow (Jordan and Hillis 2006).

One of the central issues of aphasia research is the question why recovery from aphasia is taking place and what the responsible mechanisms for this recovery are. Converging evidence from clinical studies and neural imaging studies of aphasic patients suggests that primary candidates for recovery in right-handed, left-hemisphere language-dominant patients include undamaged portions of the language network in the left hemisphere and – to a lesser extent – homologous right-hemisphere areas (Rosen et al. 2000). Since the language network is not confined to the dominant hemisphere, the role of the right hemisphere after infarcts in the left hemisphere has been addressed in several studies. Generally, more right-hemispheric activations were seen in the subacute phase of an infarct with language activation than in normals with the same tasks (Ohyama et al. 1996; Price and Crinion 2005; Saur et al. 2006; Weiller et al. 1995). Despite such responses in the right superior temporal gyrus especially in fluent Wernicke's patients (Musso et al. 1999; Weiller et al. 1995) and in the inferior frontal gyrus (Ohyama et al. 1996), efficient restoration of language is usually achieved only if left temporal areas are preserved and can be reintegrated into the functional network (Gainotti 1993; Basso et al. 1989). Only the basic function of mere word repetition appears to be sufficiently supported by sole right-hemisphere activation (Berthier et al. 1991). Based on their study in chronic nonfluent aphasia patients, Belin et al. (1996) suggested that the increased activation within the right hemisphere may be a marker of failed or faulty recovery attempts in the sense of maladaptive plasticity or the breakdown of normal interhemispheric control within the distributed neural network. Language recovery in the months immediately after aphasia onset was associated with regression of functional depression (diaschisis) in structurally unaffected regions, in particular in the right hemisphere (Cappa et al. 1997; Saur et al. 2006). Right-hemispheric activations after left frontal or temporal-parietal damage are not related to the level of recovery (Fernandez et al. 2004), but may reflect transcallosal inhibition as a maladaptive neuronal reorganization rather than functional compensation (Price and Crinion 2005). Despite the brain recruits right-hemispheric regions for speech processing when the left-hemispheric centers are impaired (Raboyeau et al. 2008), outcome studies reveal that this strategy is significantly less effective than repair of the

speech-relevant network in adults (Karbe et al. 1998). The effectiveness of right-hemispheric compensation appears to be higher in childhood than later (Muller et al. 1998). In studies of reorganization of the functional network in the course of aphasia, it is important to take into consideration the specificity of the tasks, the influence of site and extent of lesion, and the effect of treatment focused on a particular language domain on recruitment of different aspects of the language network, especially if compensatory treatment to access limited functional responses would stimulate only required pathways and would do little to stimulate reorganization of the language system (Thompson 2000).

Changes in the activation pattern induced by repeating words in the course after ischemic stroke were related to recovery from poststroke aphasia (Heiss et al. 1999). Repeating words activated blood flow in 10 normal controls by more than 10 % relative to resting condition in both upper temporal gyri, by 5–10 % in planum temporale and Heschl gyrus of both sides and in the lower part of the central gyrus of the left side, and by less than 5 % in the left Broca area. This test procedure was applied to 23 patients with aphasia of different types. Morphological defects were defined on MRI/CT, and the patients were grouped according to the site of the lesion. Activation PET studies were performed in the subacute stage approximately 2 weeks after the stroke and repeated 6 weeks later. On matched MRIs, regions of interest were defined in 14 identified structures of the bilateral language-related network.

The three groups of aphasic patients showed different patterns of activation in the acute and chronic phase, and their improvement was different: Although subcortical and frontal infarcts improved considerably in several tests, temporal infarcts showed only little improvement. These differences in improvement of speech deficits were reflected in different patterns of activation in the course after stroke (Fig. 11.2). The subcortical and frontal groups improved substantially and activated the right inferior frontal gyrus and the right superior temporal gyrus (STG) at baseline and regained regional left STG activation at follow-up. The temporal group improved only in word comprehension; it activated the left Broca area and supplementary motor areas at baseline and the precentral gyrus bilaterally as well as the right STG at follow-up, but could not reactivate the left STG. These differential activation patterns were also obvious when subcortical and frontal infarcts were grouped together according to the extent of improvement: Those with a decrease in Token test errors by more than 50 % could activate the left STG; those with a

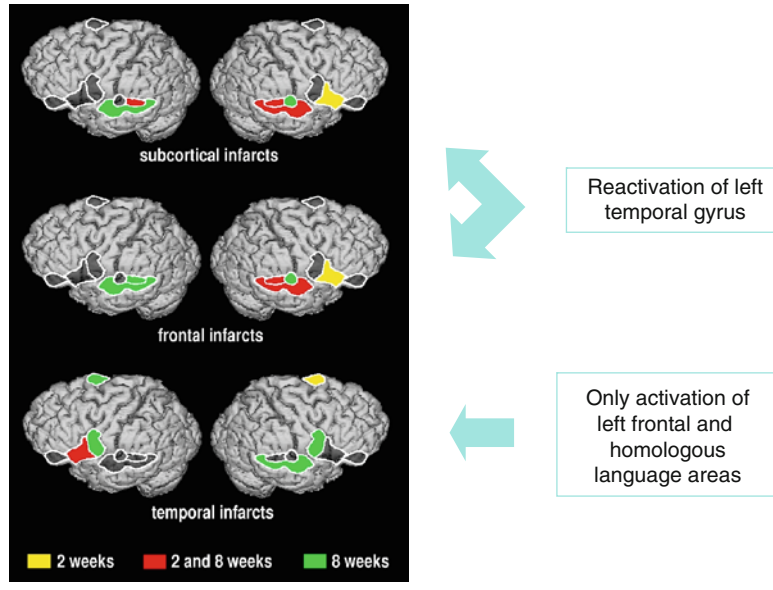

Fig. 11.2 Activation patterns in patients with left-hemispheric stroke 2 and 8 weeks after stroke. In the case of subcortical and frontal infarction, the left temporal areas are reactivated correlating to better recovery of language function (From Heiss et al. 1999)

more unfavorable and unsatisfactory outcome were not able to do this. Similar reactivation patterns were observed in smaller groups of patients (Cao et al. 1999; Warburton et al. 1999). A recent study with repeated fMRI and parallel language testing from the acute to the chronic stage after stroke demonstrated a similar pattern (Saur et al. 2006). All 14 patients recovered clinically as shown by a set of aphasia tests. In the acute phase (mean, 1.8 days poststroke), group analysis showed little early activation of noninfarcted left-hemispheric language structures, while in the subacute phase (12.1 days poststroke), a large increase of activation in the bilateral language network, with a peak in the right Broca homologue, was observed. In the chronic phase (1321 days poststroke), a normalization of activation with reshift to left-hemispheric areas was observed. This reorganization with recruitment of homologue language zones correlated with improvement, the normalization possibly reflected recovery and consolidation of the language system.

11.6 Effect of Treatment in Poststroke Aphasia

Although the effect of physiotherapy on improvement of sensorimotor deficits is unchallenged, the efficiency of speech therapy is still controversial, with several randomized controlled trials yielding no difference in outcome between treated and untreated groups (Ferro et al. 1999; Greener et al. 2001a). Many trials were undertaken to enhance the recovery from aphasia with adjuvant pharmacotherapy, but again, only a few studies demonstrated efficacy: In a double-blind placebo-controlled study, Walker-Batson et al. (2001) observed a significantly increased gain in score in patients treated with dextroamphetamine before speech therapy sessions compared to the placebo group, but the difference was not significant at 6 months' follow-up. Similarly, donepezil improved the effect of speech therapy only temporarily (Berthier et al. 2006). A large Cochrane Review (Greener et al. 2001b) identified piracetam as the only drug with a significant effect on recovery of language, which was also observed in a large multicenter trial (Orgogozo 1998). In order to investigate the question if the effect of piracetam is reflected in altered activation patterns, we performed a study in 24 patients with aphasia after stroke (Kessler et al. 2000). All these patients had speech therapy and were randomly assigned to placebo or 2×2.4 g piracetam. With respect to performance in the aphasia tests, the piracetam group did significantly better especially in subtests reflecting the ability for spontaneous speech, whereas the placebo experienced – as the verum group – improvements in Token test, reading and writing, and comprehension. It was impressive to see that these differences in improvement were also reflected in differences in the achieved activation patterns: In the piracetam group, increase in activation was significantly higher in the left transverse temporal gyrus, the left triangular part of the inferior frontal gyrus, and the left posterior temporal gyrus after the treatment period compared with the initial measures. In the right inferior frontal gyrus, a trend toward a decrease in activation was observed. The placebo group showed an increase in the activation effect only in the left vocalization area, which is the inferior part of the precentral gyrus where the primary motor area of mouth, tongue, and larynx is localized. It might be concluded from the controlled clinical trials and our study of activation patterns that piracetam as an adjuvant to speech therapy improves recovery of various language functions and that this effect is accompanied by task-related flow activation in eloquent areas of the left hemisphere. This again points to the important role of (re)activated areas in the left hemisphere for recovery of language function. Other imaging studies with individualized aphasia treatment in small numbers of patients did not show conclusive changes in fMRI activation patterns (review in Crinion and Leff 2007).

11.7 Combination of Repetitive Transcranial Magnetic Stimulation (rTMS) with Activated Imaging

rTMS is a noninvasive procedure to create electric currents in discrete brain areas (Pascual-Leone et al. 2002) which depending on frequency,

intensity, and duration can lead to transient increases and decreases in excitability of the affected cortex. Low frequencies of rTMS (below 5 Hz) can suppress excitability of the cortex, while higher frequency stimulation (5–20 Hz) leads to an increase in cortical excitability (Kobayashi and Pascual-Leone 2003). As in the motor system (Chen et al. 1997), it can also be applied to identify the various areas involved in language processing and production by a selective disturbance of partial function with low-frequency rTMS. Most frequently, rTMS is used in the so-called lesion mode to interfere with normal brain function. In our studies cited below, rTMS was applied with 4 Hz at resting motor threshold for 10–30 s. These parameter settings were chosen because Wassermann et al. (2002) has shown that 4 Hz is the lowest frequency which consistently interferes with language function and simultaneously minimizes the risk of inducing seizures.

Increases in relative cerebral blood volume (CBV) in contralateral homologous language regions during overt propositional speech fMRI in chronic, nonfluent aphasia patients indicated overactivation of right language homologues (Naeser et al. 2004). This right-hemisphere overactivation may represent a maladaptive strategy, as suggested previously by Belin et al. (1996) and Rosen et al. (2000) in their studies with chronic, nonfluent aphasia patients. This overactivation in the right-hemisphere homologous language areas during overt propositional speech can be interpreted as a result of decreased transcallosal inhibition due to damage of the specialized and lateralized speech areas (Karbe et al. 1998). TMS studies by Martin et al. (2004) and Naeser et al. (2005a) have reported improved picture naming ability in chronic nonfluent aphasia patients following a series of ten 20-min 1 Hz rTMS sessions to suppress a portion of the right pars triangularis area in the right Broca's area. Picture naming ability was significantly improved at 2 months following ten 20-min rTMS sessions (90 % of motor threshold). The authors hypothesized that suppression of the right pars triangularis modulated the bihemispheric neural network for naming, resulting in improved picture naming after the rTMS treatment series.

Both types of inhibition – collateral ipsilateral and transcallosal contralateral – can be demonstrated by simultaneous rTMS and PET activation studies (Thiel et al. 2006b). In six normal male volunteers, the Broca area, as defined by maximal activation during verb generation in the left inferior frontal gyrus, was stimulated by rTMS (4 Hz at resting motor threshold for 30 s) to interfere with normal language function. Interference with language function (positive TMS effect) is usually classified into three types on the behavioral level: (1) No response to the stimulus (e.g., no verb generated to a presented noun), (2) wrong response to the stimulus (e.g., a verb is generated which is not semantically related to the presented noun), and (3) the reaction time latency to the stimulus is changed (e.g., faster response means facilitation, slower response means inhibition). At rest, rTMS decreased blood flow ipsilaterally and contralaterally. During verb generation, rCBF was decreased during rTMS ipsilateral under the coil, but increased ipsilateral outside the coil and in the contralateral homologous area (Fig. 11.3). The effect of rTMS was accompanied by a prolongation of reaction time latencies to verbal stimuli.

The role of activation in the right hemisphere for residual language performance can be investigated by combining rTMS with functional imaging, e.g., PET (Siebner et al. 2001). Such an approach was used in 11 patients with predominantly nonfluent aphasia 2 weeks after left-sided middle cerebral artery infarction (Winhuisen et al. 2005). rTMS stimulation sites were selected according to maximum flow activation within left and right inferior frontal gyrus (IFG). Of these patients, three activated the left and eight the bilateral IFG. rTMS (4 Hz, as described above) resulted in increased reaction time latency or error rate in the word-generation task in five patients with right IFG activation, indicating essential language function. In a verbal fluency task, these patients had a lower performance than patients with effects of rTMS only over the left IFG, suggesting a less effective compensatory potential of right-sided network areas. These results were supported by studies in tumor patients.

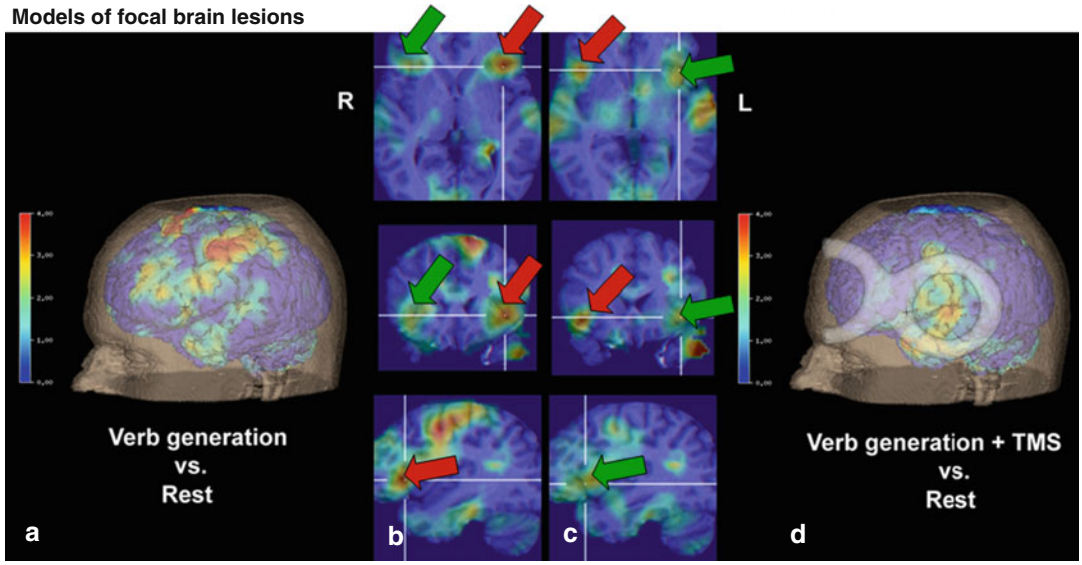

Fig. 11.3 Effect of repetitive transcranial magnetic stimulation on activation pattern by verb generation. Activation pattern (**a**) and coil position (**d**) shown in 3D rendering. Images in 3D (**b**) show activation of left inferior frontal gyrus during verb generation (*red arrows*); images (**c**) clearly show the decreased activation on the left (*green arrow*) and increased activity on the right side (*red arrows*) during rTMS interference (Modified from Thiel et al. 2006b)

As suggested previously (Belin et al. 1996; Rosen et al. 2000), the overactivation of the right-hemisphere homologous areas might represent a maladaptive strategy, and the activated right-hemisphere centers might actually hinder the recovery of the primary centers in the left hemisphere. Several case reports indicate persistent positive effects of repeatedly administered inhibitory rTMS to the right-hemispheric Broca homologue in patients with chronic aphasia (Naeser et al. 2005b, c), but a favorable response was not obtained in all patients (Martin et al. 2009). Low-frequency rTMS over the area that was homologous to the most activated one during word repetition improved performance in another case series (Kakuda et al. 2010) suggesting that transcallosal inhibition of the compensating region should be suppressed irrespective of the hemisphere. As all of these studies lack a control group, a conclusion on the efficacy of this treatment strategy cannot be drawn.

In a randomized, controlled, blinded pilot study, the effect of 1 Hz rTMS over the right-hemispheric Broca homologue in patients with poststroke aphasia in the subacute stage was studied (Weiduschat et al. 2011). In addition to conventional speech therapy, the patients received multiple sessions of rTMS over the right-hemispheric inferior frontal gyrus (intervention group) or over the vertex (control group). PET before and after the 2-week intervention period revealed an activation shift toward the right hemisphere in the control group, which was absent in the intervention group. The intervention group improved significantly in the Aachen Aphasia Test total score. This feasibility study indicated the beneficial effect of inhibition of the development of right-hemispheric overactivation, which was also confirmed clinically in a small controlled study in chronic aphasics (Barwood et al. 2011). However, a larger controlled study is required to finally prove the therapeutic validity.

11.8 Language Function in Brain Tumors

The speed of the development of a brain lesion may have an effect on the functional impairment and on the mechanisms of compensation and

reorganization of the involved networks. In a study on 61 patients with tumors in the dominant left hemisphere (Thiel et al. 2001), a verb-generation paradigm not only increased flow in the left IFG (Brodman 44 and 55), both superior temporal gyri and the cerebellum (the pattern observed in the control group), but additionally in the left frontal medial gyrus (BA 46) and orbital part of the IFG (BA 47), the anterior insula and the left cerebellum. Contrary to the healthy volunteers, two thirds of the right-handed patients showed also an activation of the right IFG, i.e., the area homologous to the Broca area. In 18 % of the patients, a reversed dominance was indicated by a negative laterality index. It was interesting to note that successful resection of a left fronto-temporal tumor improved aphasia and restored left-hemispheric dominance, suggesting the reversibility of the effect of disinhibition by removal of the cause of primary functional damage. In a further study (Thiel et al. 2005), the role of involvement of right IFG in speech performance was tested by disturbing IFG function with rTMS. In all patients, rTMS over left IFG prolonged word-generation latencies, indicating that the left IFG is still essential for performance of this task, as it is in normals. However, in patients but not in controls, significantly longer latencies were also observed during rTMS over the right IFG corresponding to higher right IFG activation. The right IFG therefore can be regarded as essential for language performance because patients and controls activate the IFG only during word generation, e.g., retrieval of verbs and nouns contrasted with a number of control states (Warburton et al. 1996) and TMS over the right interfered with this task in patients as over the left in controls. The lateralization indices, as determined by PET, were significantly lower in patients with right-sided TMS effect than in those without. As described in the article by Thiel et al. (2006a), there was a significant correlation between the laterality index and the performance in a verbal fluency test (FAS, (Lezak et al. 2004)) in the patients without right-positive TMS effect (4 Hz for 20 s, as described above), whereas in patients with a predominant right-positive TMS effect, the performance in the verbal fluency test was comparable with that in controls. This result may indicate that in a few patients with left-hemispheric brain tumors, the slow progression of damage leads to a shift in language function to the right hemisphere, which can compensate for the defect on the left side.

11.9 Hierarchical Organization for Recovery?

The different dynamics of recovery of language function observed in patients after stroke and with tumors in the left hemisphere suggest various mechanisms for compensation of the lesion within the functional network. Despite the limited number of longitudinal studies, the heterogeneity with respect to the type of aphasia in the patients included, and the differences among the activation and stimulation paradigms (Zahn et al. 2006), a hierarchy for effective recovery might be deduced from these data (Fig. 11.4; Heiss and Thiel 2006):

- Best, even complete recovery of function can usually be achieved only by the restoration of the original activation pattern within the network of the dominant hemisphere; this is only feasible after small brain damage, probably only affecting an area of minor importance, permitting functional restitution of the main interconnected components.
- If primary functional centers are damaged, reduction of collateral inhibition leads to activation of areas around the lesion; this intrahemispheric compensation involving secondary centers of the ipsilateral network is the basis for incomplete but often satisfactory improvement of language function.
- If ipsilateral network components are severely damaged, reduction of transcallosal inhibition causes activation of contralateral homotopic areas; this interhemispheric compensation involving homotopic contralesional areas contributes to some improvement in function, which is dependent on the extent of the functional shift between the hemispheres, but usually is not as efficient as intrahemispheric

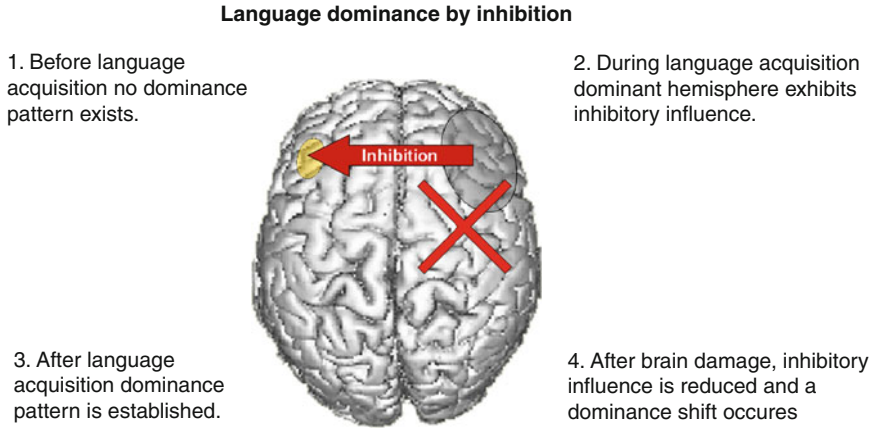

Fig. 11.4 Development of language dominance and changes in hierarchy of areas by lesions. *1* before language acquisition, no dominance pattern exists; *2* during language acquisition, dominant hemisphere exhibits inhibitory influence; *3* after language acquisition, dominance pattern is established; *4* after brain damage, inhibitory influence is reduced and a dominance shift occurs (Courtesy of Thiel)

compensation. However, in some patients with slowly developing brain damage – and perhaps also an a priori not highly lateralized functional network – the language function can be completely shifted to the right hemisphere, and in these cases, speech performance can be preserved or completely recovered despite the damage in the left (previously dominant) hemisphere.

The concept of the difference between the effectiveness of intrahemispheric compensation and interhemispheric compensation may be taken one step further. The blockade of the contralateral intact area by rTMS can be utilized to modulate the inhibitory interactions. In a controlled feasibility study, prevention of right-hemispheric overactivation by rTMS over the Broca homologous area of the right hemisphere was related to improved language performance (Weiduschat et al. 2011). The authors postulated that rTMS decreased excitation in right BA 45 which in turn modulated activity in the distributed, bihemispheric language network. This result suggests that in aphasia patients, contralateral overactivation (likely due to transcallosal disinhibition secondary to dominant, left-hemisphere lesion) may be tempered or suppressed, following a series of slow, 1 Hz rTMS treatments to a posterior portion of the right pars triangularis. The clinical and long-term efficacy of this novel complementary treatment for aphasia, however, needs to be proven in larger clinical trials.

11.10 Conclusions

Specific brain functions, such as language, can be localized by comparing CBF or CMRGlc during performance of a selected task with a "resting" condition. This was originally made possible by PET using FDG. With ^{15}O-water or other ultrashort-lived CBF tracers, multiple replications of conditions in the same subject could be performed. This technique was widely used, especially for the study of higher brain function (cognitive neuroscience) and for evaluating disturbed activation patterns in disease, as in poststroke aphasia. In recent years, fMRI has become the dominating imaging technique in this field because it does not involve ionizing radiation and, therefore, is easily used in normal controls, allowing more rapid signal acquisition and more complex experimental designs. However, PET provides a more physiologically specific signal, a better signal-to-noise ratio, and fewer artifacts in individual acquisitions. PET also provides actual activated and reference regional values, which may show a better correlation with task performance than the difference signal provided by fMRI. Additionally, magnetic stimulations can

be performed during PET examinations. These advantages support its continued use in pathophysiologically complex clinical situations such as stroke and brain tumors, where CBF responses to activation may be altered and may involve unexpected components of a functional network.

References

Attwell D, Laughlin SB (2001) An energy budget for signaling in the grey matter of the brain. J Cereb Blood Flow Metab 21(10):1133–1145

Barwood CH, Murdoch BE et al (2011) Improved language performance subsequent to low-frequency rTMS in patients with chronic non-fluent aphasia post-stroke. Eur J Neurol 18(7):935–943

Basso A, Gardelli M et al (1989) The role of the right hemisphere in recovery from aphasia. Two case studies. Cortex 25:555–566

Belin P, van Eeckhout P et al (1996) Recovery from nonfluent aphasia after melodic intonation therapy: a PET study. Neurology 47(6):1504–1511

Berthier ML, Starkstein SE et al (1991) Transcortical aphasia. Importance of the nonspeech dominant hemisphere in language repetition. Brain 114(Pt 3): 1409–1427

Berthier ML, Green C et al (2006) A randomized, placebo-controlled study of donepezil in poststroke aphasia. Neurology 67:1687–1689

Booth JR, Wood L et al (2007) The role of the basal ganglia and cerebellum in language processing. Brain Res 1133:136–144

Cao Y, Vikingstad EM et al (1999) Cortical language activation in stroke patients recovering from aphasia with functional MRI. Stroke 30:2331–2340

Cappa SF, Perani D et al (1997) A PET follow-up study of recovery after stroke in acute aphasics. Brain Lang 56:55–67

Chen R, Classen J et al (1997) Depression of motor cortex excitability by low-frequency transcranial magnetic stimulation. Neurology 48:1398–1403

Crinion JT, Leff AP (2007) Recovery and treatment of aphasia after stroke: functional imaging studies. Curr Opin Neurol 20:667–673

Demonet JF, Fiez JA et al (1996) PET studies of phonological processing: a critical reply to Poeppel. Brain Lang 55:352–379

Feeney DM, Baron JC (1986) Diaschisis. Stroke 17: 817–830

Fernandez B, Cardebat D et al (2004) Functional MRI follow-up study of language processes in healthy subjects and during recovery in a case of aphasia. Stroke 35:2171–2176

Ferro JM, Mariano G et al (1999) Recovery from aphasia and neglect. Cerebrovasc Dis 9 (Suppl 5):6–22

Gainotti G (1993) The riddle of the right hemisphere's contribution to the recovery of language. Eur J Disord Commun 28:227–246

Greener J, Enderby P et al (2001a) Speech and language therapy for aphasia following stroke (Cochrane Review). The Cochrane Library 3 Oxford: Update Software

Greener J, Enderby P et al (2001b) Pharmacological treatment for aphasia following stroke. Cochrane Database Syst Rev. 2001;(4):CD000424. Review

Heiss WD, Thiel A (2006) A proposed regional hierarchy in recovery of post-stroke aphasia. Brain Lang 98: 118–123

Heiss WD, Emunds HG et al (1993a) Cerebral glucose metabolism as a predictor of rehabilitation after ischemic stroke. Stroke 24:1784–1788

Heiss WD, Kessler J et al (1993b) Cerebral glucose metabolism as a predictor of recovery from aphasia in ischemic stroke. Arch Neurol 50:958–964

Heiss WD, Kessler J et al (1999) Differential capacity of left and right hemispheric areas for compensation of poststroke aphasia. Ann Neurol 45:430–438

Hickok G, Poeppel D (2007) The cortical organization of speech processing. Nat Rev Neurosci 8:393–402

Hillis AE, Kleinman JT et al (2006) Restoring cerebral blood flow reveals neural regions critical for naming. J Neurosci 26:8069–8073

Jordan LC, Hillis AE (2006) Disorders of speech and language: aphasia, apraxia and dysarthria. Curr Opin Neurol 19:580–585

Kakuda W, Abo M et al (2010) Functional MRI-based therapeutic rTMS strategy for aphasic stroke patients: a case series pilot study. Int J Neurosci 120(1): 60–66

Karbe H, Herholz K et al (1989) Regional metabolic correlates of token test results in cortical and subcortical left hemispheric infarction. Neurology 39:1083–1088

Karbe H, Kessler J et al (1995) Long-term prognosis of poststroke aphasia studied with positron emission tomography. Arch Neurol 52:186–190

Karbe H, Thiel A et al (1998) Brain plasticity in post-stroke aphasia: what is the contribution of the right hemisphere? Brain Lang 64:215–230

Kessler J, Thiel A et al (2000) Piracetam improves activated blood flow and facilitates rehabilitation of post-stroke aphasic patients. Stroke 31:2112–2116

Knecht S, Floel A et al (2002) Degree of language lateralization determines susceptibility to unilateral brain lesions. Nat Neurosci 5:695–699

Kobayashi M, Pascual-Leone A (2003) Transcranial magnetic stimulation in neurology. Lancet Neurol 2:145–156

Kumar R, Masih AK et al (1996) Global aphasia due to thalamic hemorrhage: a case report and review of the literature. Arch Phys Med Rehabil 77:1312–1315

Lezak M, Howieson D et al (2004) Neuropsycho-logical assessment. Oxford University Press, Oxford

Magistretti PJ (2004) Brain energy metabolism. In: Byrne JH, Roberts JL (eds) From molecules to networks. Elsevier, Amsterdam: 67–90

Martin PI, Naeser MA et al (2004) Transcranial magnetic stimulation as a complementary treatment for aphasia. Semin Speech Lang 25:181–191

Martin PI, Naeser MA et al (2009) Overt naming fMRI pre- and post-TMS: Two nonfluent aphasia patients, with and without improved naming post-TMS. Brain Lang 111(1):20–35

Metter EJ, Kempler D et al (1987) Cerebellar glucose metabolism in chronic aphasia. Neurology 37:1599–1606

Metter EJ, Riege WH et al (1988) Subcortical structures in aphasia. An analysis based on (18 F)-fluorodeoxyglucose, positron emission tomography, and computed tomography. Arch Neurol 45:1229–1234

Metter EJ, Hanson WR et al (1990) Temporoparietal cortex in aphasia. Evidence from positron emission tomography. Arch Neurol 47:1235–1238

Mintun MA, Lundstrom BN et al (2001) Blood flow and oxygen delivery to human brain during functional activity: theoretical modeling and experimental data. Proc Natl Acad Sci U S A 98:6859–6864

Muller RA, Rothermel RD et al (1998) Brain organization of language after early unilateral lesion: a PET study. Brain Lang 62:422–451

Musso M, Weiller C et al (1999) Training-induced brain plasticity in aphasia. Brain 122(Pt 9):1781–1790

Naeser MA, Martin PI et al (2004) Overt propositional speech in chronic nonfluent aphasia studied with the dynamic susceptibility contrast fMRI method. Neuroimage 22:29–41

Naeser MA, Martin PI et al (2005a) Improved picture naming in chronic aphasia after TMS to part of right Broca's area: an open-protocol study. Brain Lang 93:95–105

Naeser MA, Martin PI et al (2005b) Improved naming after TMS treatments in a chronic, global aphasia patient–case report. Neurocase 11(3):182–193

Naeser MA, Martin PI et al (2005c) Improved picture naming in chronic aphasia after TMS to part of right Broca's area: an open-protocol study. Brain Lang 93(1):95–105

Nudo RJ, Wise BM et al (1996) Neural substrates for the effects of rehabilitative training on motor recovery after ischemic infarct. Science 272:1791–1794

Ogawa S, Lee TM et al (1990) Brain magnetic resonance imaging with contrast dependent on blood oxygenation. Proc Natl Acad Sci U S A 87:9868–9872

Ohyama M, Senda M et al (1996) Role of the nondominant hemisphere and undamaged area during word repetition in poststroke aphasics - a PET activation study. Stroke 27:897–903

Orgogozo JM (1998) Piracetam in the treatment of acute stroke. CNS Drugs 9:41–49

Pascual-Leone A, Davey N et al (2002) Handbook of transcranial magnetic stimula tion. Arnold Press, London

Petersen SE, Fox PT et al (1988) Positron emission tomographic studies of the cortical anatomy of single-word processing. Nature 331:585–589

Price CJ (2000) The anatomy of language: contributions from functional neuroimaging. J Anat 197(Pt 3): 335–359

Price CJ, Crinion J (2005) The latest on functional imaging studies of aphasic stroke. Curr Opin Neurol 18: 429–434

Raboyeau G, De Boissezon X et al (2008) Right hemisphere activation in recovery from aphasia: lesion effect or function recruitment? Neurology 70: 290–298

Reivich M, Kuhl D et al (1979) The (18 F)fluorodeoxyglucose method for the measurement of local cerebral glucose utilization in man. Circ Res 44:127–137

Rosen HJ, Petersen SE et al (2000) Neural correlates of recovery from aphasia after damage to left inferior frontal cortex. Neurology 55:1883–1894

Saur D, Lange R et al (2006) Dynamics of language reorganization after stroke. Brain 129:1371–1384

Siebner HR, Takano B et al (2001) Continuous transcranial magnetic stimulation during positron emission tomography: a suitable tool for imaging regional excitability of the human cortex. Neuroimage 14:883–890

Sokoloff L (1999) Energetics of functional activation in neural tissues. Neurochem Res 24:321–329

Thiel A, Herholz K et al (1998) Localization of language-related cortex with 15O-labeled water PET in patients with gliomas. Neuroimage 7:284–295

Thiel A, Herholz K et al (2001) Plasticity of language networks in patients with brain tumors: a PET activation study. Ann Neurol 50:620–629

Thiel A, Habedank B et al (2005) Essential language function of the right hemisphere in brain tumor patients. Ann Neurol 57:128–131

Thiel A, Habedank B et al (2006a) From the left to the right: how the brain compensates progressive loss of language function. Brain Lang 98:57–65

Thiel A, Schumacher B et al (2006b) Direct demonstration of transcallosal disinhibition in language networks. J Cereb Blood Flow Metab 26:1122–1127

Thompson CK (2000) The neurobiology of language recovery in aphasia. Brain Lang 71:245–248

Turner R, Howseman A et al (1997) Functional imaging with magnetic resonance. In: Frackowiak RSJ, Friston KJ, Frith CD, Dolan RJ, Mazziotta JC (eds) Human brain function. Academic, San Diego, pp 467–486

Wade DT, Hewer RL et al (1986) Aphasia after stroke: natural history and associated deficits. J Neurol Neurosurg Psychiatry 49:11–16

Walker-Batson D, Curtis S et al (2001) A double-blind, pla- cebo-controlled study of the use of amphetamine in the treatment of aphasia. Stroke 32:2093–2098

Warburton E, Wise RJS et al (1996) Noun and verb retrieval by normal subjects studies with PET. Brain 119:159–179

Warburton E, Price CJ et al (1999) Mechanisms of recovery from aphasia: evidence from positron emission tomography studies. J Neurol Neurosurg Psychiatry 66:155–161

Wassermann EM, Pascual-Leone A et al (2002) Safety and side-effects of transcranial magnetic stimulation and repetitive transcranialmagnetic stimulation. In: Handbook of transcranial magnetic stimulation. Arnold Press, London, pp 39–49

Weiduschat N, Thiel A et al (2011) Effects of repetitive transcranial magnetic stimulation in aphasic stroke: a randomized controlled pilot study. Stroke 42(2): 409–415

Weiller C, Isensee C et al (1995) Recovery from Wernicke's aphasia: a positron emission tomographic study. Ann Neurol 37:723–732

Winhuisen L, Thiel A et al (2005) Role of the contralateral inferior frontal gyrus in recovery of language function in poststroke aphasia: a combined repetitive transcranial magnetic stimulation and positron emission tomography study. Stroke 36:1759–1763

Wise RJ (2003) Language systems in normal and aphasic human subjects: functional imaging studies and inferences from animal studies. Br Med Bull 65:95–119

Zahn R, Schwarz M et al (2006) Functional activation studies of word processing in the recovery from aphasia. J Physiol Paris 99:370–385

Functional Magnetic Resonance-Guided Brain Tumor Resection

12

Peter D. Kim, Charles L. Truwit,
and Walter A. Hall

12.1 Introduction

The ultimate goal of brain tumor surgery is maximum tumor removal without the development of a new neurologic deficit. In the treatment of glioblastoma multiforme (GBM), gross total resection (GTR) has been demonstrated in a number of studies to be one of the few attainable factors associated with prolonged survival (Buckner 2003; Jeremic et al. 1994; Lacroix et al. 2001; Vidiri et al. 2006; Ushio et al. 2005). Gross total resection of low-grade gliomas is also supported in the literature and has been demonstrated in several retrospective studies to be associated with a lower risk of tumor recurrence and prolonged patient survival (Claus et al. 2005; Laws et al. 1984; Nicolato et al. 1995; Philippon et al. 1993; Piepmeier et al. 1996). In one reported series where complete radiologic resection was attained in the treatment of low-grade glial tumors, tumor recurrence was not reported (Berger et al. 1994). Additionally, gross total resection has been demonstrated to result in improved postoperative control of seizures (Chang et al. 2008), a major source of disability in these patients. It should be noted, however, that the appropriate treatment of low-grade gliomas is not without controversy (Keles et al. 2001), and there are reported series that have failed to demonstrate a significant correlation between gross total resection and survival (Medbery et al. 1988; Piepmeier 1987). Reported series of high-grade gliomas that have failed to demonstrate a correlation between extent of resection and prognosis have also been published (Kowalczuk et al. 1997; Lai et al. 1993).

There is also a theoretical benefit of maximal tumor resection. The reduction in tumor cells should also allow for maximal benefit of adjuvant therapy and subsequently lengthen the time to tumor recurrence. In patients with GBM, there are genetic changes that occur prior to tumor recurrence (Joki et al. 2001; Speigl-Kreinecker et al. 2002) that may also negatively influence treatment response and thus survival, a finding that provides further rationale for aggressive surgical resection.

Given the increasing body of evidence in the form of retrospective trials and the theoretical advantages of gross total resection as outlined above, we favor a strategy of aggressive resection for the treatment of most gliomas. Recently, a large series of patients with high-grade gliomas were found to have increased survival with gross

P.D. Kim, M.D., Ph.D
Department of Neurosurgery, Gillette Children's Specialty Healthcare, St. Paul Campus, St. Paul, MN, USA

C.L. Truwit
Department of Radiology, University of Minnesota Medical School, Minneapolis, MN, USA

Department of Radiology,
Hennepin County Medical Center,
Minneapolis, MN, USA

W.A. Hall, M.D., MBA (✉)
Department of Neurosurgery, State University of New York Upstate Medical University,
750 East Adams Street, Syracuse, NY 13210, USA
e-mail: hallw@upstate.edu

S. Ulmer, O. Jansen (eds.), *fMRI – Basics and Clinical Applications*,
DOI 10.1007/978-3-642-34342-1_12,

total resection even when stratified for patient age and tumor location near eloquent cortex (Stummer et al. 2008). Surgical resection has also been demonstrated to confer increased survival in patients with single metastatic lesions to the brain (Patchell et al. 1990; Vecht et al. 1993), particularly where the primary source of the tumor is unknown (Nabavi et al. 2001; Weber et al. 1996).

The goal of aggressive tumor removal with the preservation of brain function has led to innovations in imaging that are part of today's surgical armamentarium. Central to the planning and execution of brain tumor surgery is appropriate neuroimaging. The advent of computed tomography (CT) and magnetic resonance imaging (MRI) has revolutionized brain tumor surgery. These modalities were used initially to demonstrate brain anatomy; however, the development of stereotactic techniques added to the accuracy of brain surgery which in turn predated the development of neuronavigation and eventually intraoperative magnetic resonance imaging (ioMRI).

Frameless neuronavigation systems provide surgeons with an unprecedented accuracy in surgical planning. Despite this, a major limitation of this technology is the occurrence of brain shift that results after the resection of any significant amount of tumor (Reinges et al. 2004; Truwit and Hall 2006), the egress of cerebrospinal fluid (CSF; Preul et al. 2004), and the combination of these factors that are further influenced by the effect of gravity on an open surgical field (Nabavi et al. 2001). Computational techniques (Clatz et al. 2005) and methods of validation based on shifting vascular anatomy (Reinertsen et al. 2007) have been used in an attempt to compensate for this effect. Intraoperative imaging circumvents the issue of brain shift and was initially accomplished with computed tomography (Engle and Lunsford 1987); however, ioMRI has been validated as a safe and effective surgical technique that provides near real-time feedback with respect to the extent of tumor resection, the presence of secondary pathology such as an iatrogenic intracerebral hematoma or hydrocephalus, and the location of eloquent structures after brain shift has occurred (Alexander et al. 1997; Berger et al. 1994; Bernays and Laws 1997; Bernstein et al. 2000; Hall et al. 2003; Hall et al. 1998; Kremer et al. 2006; Lam et al. 2001; Nimsky et al. 2004; Schwartz et al. 1999; Trantakis et al. 2003). Many different magnet strengths have been utilized for ioMRI with each magnet and format offering distinct advantages and disadvantages. The first operational system used a 0.5 Tesla (T) magnet with a double coil design (SIGNA SP, General Electric Medical Systems, Milwaukee, WI) in which the surgeon operated between the coils. System field strength has varied from 0.12 T to 3 T, and while low field (up to 0.5 T) systems allow for less rigorous adherence to MRI compatibility, 1.5 T field strength or greater is necessary for advanced MRI techniques that include functional magnetic resonance imaging (fMRI). Although the cost of establishing an operating suite with MRI capabilities is considerable, the use of ioMRI appears to be cost-effective, due to the shorter length of stay in the hospital, improved neurologic outcomes, decreased frequency of tumor recurrence, and longer times to tumor recurrence (Kucharczyk et al. 2001).

Neuronavigation and ioMRI allow the neurosurgeon to identify functional brain tissue with respect to the surgical lesion; however, the determination of eloquent versus non-eloquent areas of brain is dependent upon the surgeon's knowledge of normal anatomy and the ability to interpret accurately the information provided by the MRI. When lesions or planned surgical corridors are in close proximity to presumed eloquent cortex, or the associated white matter fiber tracts, one must consider the displacement of these vital areas that result from mass effect of the lesion. An unacceptably high operative risk for neurological injury may exist in the absence of further definition of the location of eloquent areas. Awake craniotomy with direct cortical stimulation has been well described as a way to maintain neurologic function during high-risk neurosurgical procedures (Jääskeläinen and Randell 2003; Meyer et al. 2001; Picht et al. 2006). This direct surgical technique provides the surgeon with information concerning brain function during the operative procedure but does not allow for the generation of a visual image of the location of

functional areas, nor does it assist with preoperative planning.

The need to identify and locate areas of functional importance and confirm their exact spatial relationships to brain tumors planned for resection has led to the use of functional MRI (fMRI) for intraoperative guidance. The two most commonly used methods of employing fMRI in surgical planning are fMRI in conjunction with neuronavigation and fMRI combined with ioMRI. Additionally, fMRI has been combined with awake craniotomy and electrostimulation techniques (Amiez et al. 2008; Picht et al. 2006).

12.2 Functional MRI Neuronavigation

Functional imaging may be combined with frameless neuronavigation in tumor surgery to allow for the intraoperative localization of both the lesion and areas of brain activation. Blood-oxygenation-level-dependent (BOLD) fMRI (Ogawa et al. 1990) is performed preoperatively. Images are acquired while the patient performs tasks that involve the area of brain that is likely to be at risk during the planned surgery. These data are then coregistered with traditional high-resolution anatomic MRI and appear on the neuronavigation images. Demonstrations of this technique were reported in a small series of patients starting in the late 1990s (Braun et al. 2000; Braun et al. 2001; Kamada et al. 2003; Schulder et al. 1999; Schulder et al. 1997; Signorelli et al. 2003; Fandino et al. 1999; Wilkinson et al. 2003), while validation has been achieved by comparison of fMRI data with the results of direct cortical stimulation at the time of surgery (Braun et al. 2000; O'Shea et al. 2006; Roessler et al. 2005; Schulder et al. 1999; Signorelli et al. 2003). Algorithms for the coregistration of functional areas with structural MRI data have been demonstrated to yield accuracy within a submillimeter median error (Kober et al. 2002).

Neuronavigation combined with fMRI data was used in a series of 15 patients with tumors located in eloquent areas where no patient suffered a postoperative neurologic deficit (Gumprecht et al. 2002); however, in eight of these patients, the tumor was only resected partially. Using a combination of fMRI neuronavigation with direct intraoperative cortical stimulation, Roessler et al. (Roessler et al. 2005) achieved gross total resection in nine of 22 patients, with partial resections in 11 and biopsies in two. Another series examined the use of fMRI neuronavigation in 54 patients with tumors located near the motor strip. Gross total resection was achieved in 45 patients (83%); however, neurologic deterioration was observed in nine (Krishnan et al. 2004). In addition to the traditional mapping of sensorimotor and language functions, neuronavigation with coregistered fMRI data has been used for resection of tumors located near areas involved in short-term memory (Braun et al. 2006). In this series of 14 patients, good surgical results were reported, especially with regards to verbal memory. Two patients with lesions near visual cortex have been surgically treated using fMRI coregistered neuronavigation (Schulder et al. 1999). Functional MRI has also been coregistered with positron emission tomography (PET) data (Braun et al. 2001).

Preservation of functional cortex does not protect against postoperative neurologic deficits when the corresponding deep white matter tracts are surgically damaged. To address this, fMRI data have been coregistered with diffusion tensor imaging (DTI) in order to visualize both functional areas of cortex and their underlying white matter tracts (Kamada et al. 2007).

12.3 Intraoperative Functional MRI

Intraoperative MRI was developed in order to provide the neurosurgeon with near-real-time feedback regarding the extent of tumor resection and the presence of intraoperative hemorrhage. Intraoperative imaging accounts for the effects of brain shift because the imaging data used for guidance are acquired during the surgical procedure and therefore the effects of CSF loss, tissue resection, and gravity are visualized. The main issues in developing ioMRI are magnetic compatibility, timing of intraoperative scans,

maintenance of sterility, and ergonomic design of the operating MRI suite. The latter must allow for the efficient transfer of the patient to and from the scanner and ease of performing the operative procedure. The first ioMRI scanner was low field (0.5 T; Black et al. 1999) and therefore carried a relatively low risk of magnet-related mishaps. As neurosurgeons turned to high-field ioMRI, issues with ferromagnetism of operative tools became a more significant concern. Adaptation of neurosurgical procedures to allow for the presence of the magnet within the operating suite involved definition of the 5 G line, beyond which only MRI-compatible materials may be used. Large surgical series have been reported without significant rates of magnet-related mishaps or increased rates of infection (Hall et al. 2003; Nimsky et al. 2004; Trantakis et al. 2003). Although the first ioMRI system consisted of a double coil design that allowed the surgeon to operate with the patient's head already at the ideal location for image acquisition, we have found that transfer of the patient into and out of the scanner during surgery is easily accomplished. Surgeons may employ slightly different algorithms; however, the basic technical strategy involves obtaining a scan when there is doubt regarding the completeness of the tumor resection and then repeating this process until gross total resection is attained.

12.4 High-Field Functional MRI

Intraoperative images at low field (0.12 T) and midfield (0.5 T) have predictably demonstrated lower image resolution compared to imaging obtained at high field (1.5 T) strength (Nimsky et al. 2004; Nimsky et al. 2006b). Despite the concerns for safety and the proven success of intraoperative high-field MRI at 1.5 T, surgery at 3 T has been performed in order to explore the potential benefits of higher resolution (Trantakis et al. 2003). The improved resolution and signal-to-noise ratio afforded by high-field MRI have led to its use for functional neuronavigation. Feigl et al. (2008) have used real-time 3 T BOLD t-maps coregistered with MRI for neuronavigation for patients with tumors near the motor cortex with success comparable to that seen in a cohort of patients that had previously undergone awake craniotomy.

Our paradigm for fMRI-guided neurosurgery utilizes preoperative high-field (1.5 T or 3 T) fMRI combined with ioMRI at 1.5 T. Intraoperative MRI allows for near-real-time feedback regarding the extent of tumor resection, but the shifted position of functional areas must be mentally extrapolated onto the newly acquired images by the surgeon. Intraoperative fMRI has been used for the resection of tumors located near eloquent cortex. In the remainder of this chapter, we will review our experience with intraoperative fMRI at 1.5 T and 3 T.

12.5 Materials and Methods

12.5.1 The Intraoperative MRI Suite

Surgery was performed at the University of Minnesota Fairview-University Medical Center. The MRI was a short-bore 1.5 T scanner (Gyroscan ACS-NT, Philips Medical Systems, Best, the Netherlands) with strong imaging gradients (23 mT/m, 105 mTm per millisecond) allowing for generation of echo planar imaging that is commonly used in fMRI. The total length of the MRI is 180 cm with an inner bore diameter of 60 cm and a gantry that can extend to 100 cm beyond the flared openings. The operating suite consisted of the scanner and a monitor similar to that used by the technologists to perform scanning. The operating microscope, patient monitors, and anesthesia equipment were all MRI compatible. The magnet was actively shielded with a resulting 5 Gauss (G) line enclosing an area of 7.8 m by 5.0 m. Surgery was performed on an angiography table with a floating tabletop mechanism oriented in-line with the MRI scanner, allowing for patient transfer easily into the MRI. A carbon fiber Malcolm-Rand headframe was used that allowed for the exact reproduction of scan planes between imaging sessions. The ability to obtain high-quality images while maintaining operative access was afforded by a head coil composed of two circular loops arranged as a phased array.

Surgery was performed either at the near end of the room outside the 5G line, or alternatively on the opposite side of the scanner within the 5 G line, where only MRI-compatible instruments were used. The MRI suite was cleaned the day before a surgical procedure and treated as a sterile surgical environment. Pocketless color-coded scrubs were worn within the suite in order to avoid the inadvertent transport of non-MRI-compatible instruments too near to the scanner.

12.6 Functional MRI-Guided Tumor Resection

12.6.1 1.5 T Functional MRI-Guided Resection

Patients underwent fMRI imaging preoperatively. For language, silent speech was used because actual physical vocalization would result in head movement and the subsequent misregistration of the areas of brain activation on the high-resolution MRI obtained for surgical planning. Motor tasks included finger and toe tapping, while list retention was used for short-term memory mapping. Patients were asked to repeat each task multiple times with similar periods of rest between task performances. The fMRI protocol for the 1.5 T scanner was a single-shot EPI scan (TR/TE = 3,000/40 milliseconds; field of view = 210 mm) with a 64×64 image matrix and 7-mm thick slices with 1-mm intersection gap. Acquisition was repeated 72 times over 4 min in sequential fashion. Test accuracy was measured by a wave pattern that was overlaid on a linear graph that indicated when the patient was performing a particular task properly. Areas of BOLD activation were calculated, and these fMRI data were superimposed on high-quality anatomic MRI scans that were displayed on the operating suite viewing monitor.

Intraoperative images were obtained in order to assist in determining the extent of residual disease and whether there was the need for more tumor resection. The choice of imaging sequence was determined by the neurosurgeon in conjunction with the neuroradiologist. T2-weighted images, turbo FLAIR (fluid-attenuated inversion recovery), and HASTE (half-Fourier acquisition single-shot turbo spin echo) images were used most often for intraoperative imaging of low-grade glial tumors (Fig. 12.1). Once the decision to obtain intraoperative imaging was made, all non-MRI-compatible materials were removed from the table and the surgical site was covered with a sterile towel. All operations were performed with the patient under general anesthesia, and therefore, functional scans were not obtained intraoperatively.

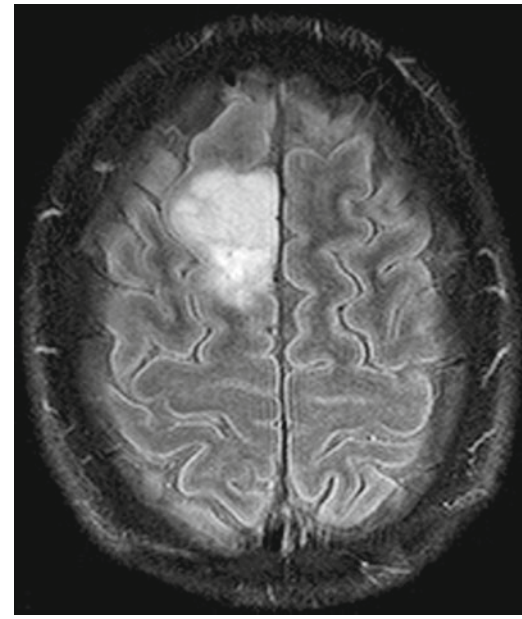

Fig. 12.1 Three Tesla axial turbo FLAIR image demonstrating a right frontal area of increased signal that is consistent with a low-grade glioma. This scan was obtained immediately prior to a brain activation study that was performed to identify the location of functional cortex in proximity to the presumed tumor

Follow-up imaging was obtained 3 months after surgery and subsequently 1–2 times per year. All follow-up films were reviewed by the neuroradiologist to exclude the presence of recurrent tumor.

12.6.2 3 T Functional MRI-Guided Resection

Preoperative mapping of functional areas of the brain was accomplished at 3 T (Fig. 12.2). For

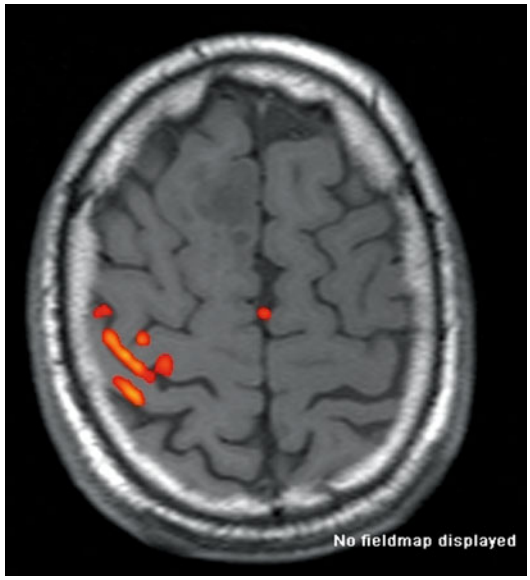

Fig. 12.2 Axial T1-weighted brain activation study performed at 3 T showing the area for finger tapping of the left hand. The tumor that is planned to be surgically resected is just anterior and medial to the cortical area of brain activation. The posterior aspect of the tumor is delineated by a medial and lateral sulcus

preoperative 3 T fMRI studies, one of two scanners was used. One MR system was a short-bore 3 T scanner (Intera, Philips Medical Systems, Best, the Netherlands). The fMRI protocol for this system was a single-shot EPI scan (TR/TE = 3,000/35 ms; field of view = 230 mm) with an 80 × 128 image matrix and 4-mm-thick slices with 1-mm intersection gap. The acquisition was repeated 100 times in a sequential fashion over an imaging interval of 7 min. The other system was the 3 T Siemens scanner (Siemens Medical Solutions, Erlangen, Germany). The fMRI protocol for this system was a single-shot EPI scan (TR/TE = 2,660/30 ms; field of view = 192 mm) with a 64 × 64 image matrix and 3-mm slices with 0.8-mm intersection gap. Acquisition was repeated 60 times in sequential fashion over an interval of 3 min. These data were acquired during repeated performances of toe tapping, finger tapping, or silent speech. Tasks were repeated with periods of rest of similar length intervening. Brain activation (BOLD) imaging data were calculated using Philips software. Intraoperative guidance was still performed with the 1.5 T system as described above. Rigid fixation of the head during intraoperative scans allowed for similar acquisition planes and straightforward identification of the previously identified areas of activation on the intraoperative scans.

12.7 Results

12.7.1 Functional MRI at 1.5 T for the Treatment of Low-Grade Glial Tumors

From 1997 to 2003, 16 patients whose tumors were histologically proven to be low-grade gliomas were operated on using 1.5 T ioMRI guidance after preoperative 1.5 T fMRI was obtained. Fifteen of these patients had operative resection while the last patient underwent ioMRI-guided biopsy because the tumor was determined to be located within the motor cortex. Tumors in this series included oligodendrogliomas ($n = 10$), low-grade astrocytomas ($n = 4$), pleomorphic xanthoastrocytoma ($n = 1$), and dysembryoplastic neuroepithelial tumor ($n = 1$). Mean age at the time of surgery was 31 years, with a range of 10–43 years. Fifteen of the patients in this series presented with seizures; the remaining patient was asymptomatic. No patient had a neurological deficit prior to surgery. Of the 16 patients, 12 were undergoing their first surgical procedure, whereas three patients had previous resection or debulking and one patient had previously undergone biopsy. Locations were right frontal ($n = 5$), left frontal ($n = 6$), left temporal ($n = 3$), and left parietal ($n = 1$). Motor function, speech function, and memory function were localized using fMRI as deemed appropriate by the location of the lesion and planned surgical corridor.

The number and frequency of intraoperative images varied depending on the operative findings; however, all patients had imaging to determine whether the tumor was completely resected and one final scan to exclude the presence of hemorrhage before leaving the operative suite. For the majority of patients, the first scan

obtained after resection revealed some residual tumor that was found to be resected on subsequent imaging after more surgery. In a few cases where the tumor was particularly close to areas of functional imaging, one or more additional intermediate scans were obtained as the resection progressed. In cases where there was doubt about the presence of blood on this scan, another scan was obtained 15–20 min later.

In this series of patients, a gross total resection was achieved in 10 patients (63 %). Of the five patients in whom resection was considered subtotal, residual tumor was left intentionally because it was felt that the lesions were entwined with functional motor cortex in four patients and both language and motor areas in the other patient.

None of the patients in whom complete radiographic resection was achieved had experienced recurrence at last follow-up (mean, 31 months; range, 14–87 months). Of the patients who underwent partial resection, none had evidence of tumor progression at last follow-up (12–20 months). The patient who was treated with radiotherapy as the primary treatment modality had stable disease at their last follow-up at 41 months.

Postoperative morbidity in this series was low. There were no permanent neurological deficits in any patient. One patient experienced a transient hemiparesis that was felt to be related to postoperative edema extending into the motor strip, while another patient exhibited a transient motor apraxia, which was not surprising given the location of the tumor within the supplementary motor area. There were no mishaps involving MRI-incompatible instruments or any other objects within the magnetic field.

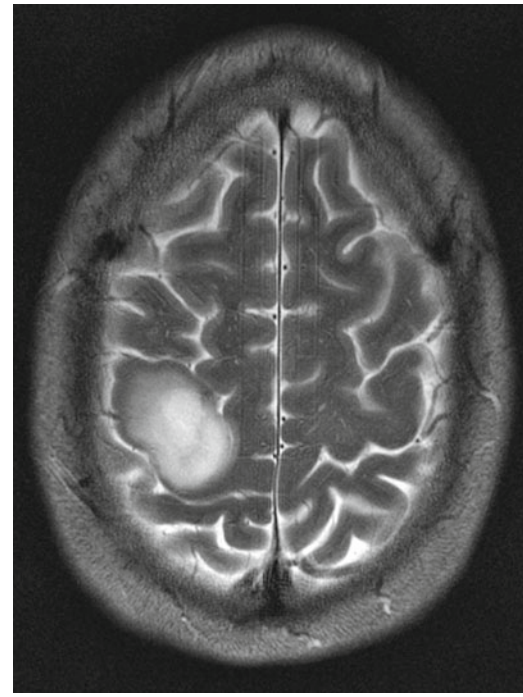

Fig. 12.3 Axial half-Fourier acquisition single-shot turbo spin echo (HASTE) magnetic resonance imaging scan demonstrating a right frontal tumor that was felt to be located within the motor cortex which was confirmed by a brain activation study. This patient underwent a brain biopsy which identified an astrocytoma that was then treated with radiation therapy

12.8 Functional MRI at 3 T

Using fMRI data acquired at 3 T, tumor surgery was performed on 13 patients with primary intracranial tumors located adjacent to eloquent cortex. These tumors included six oligodendrogliomas, three meningiomas, two astrocytomas, and two GBMs. Mean age was 43 years with a median age of 48 years (range, 22–70 years). Tumors were located in the right frontal ($n=5$), left frontal ($n=6$), and left temporal ($n=2$) lobes. Ten of the 13 patients were being operated on for the first time. Twelve of the patients underwent resection with ioMRI guidance after review of fMRI results, while one patient's tumor was within the motor cortex (Figs. 12.3 and 12.4) and therefore a brain biopsy was performed. In the 12 patients whose tumors were resected, a gross total resection was achieved in 10 (Fig. 12.5). The remaining two patients, one with an astrocytoma and the other with a GBM, had partial resections because the fMRI revealed that the tumors were infiltrating into eloquent cortex. Gross total resection was defined either as the removal of all areas of enhancement for high-grade tumors and meningiomas (Figs. 12.6, 12.7, and 12.8) or the removal of the predefined tumor imprint for non-enhancing tumors. There

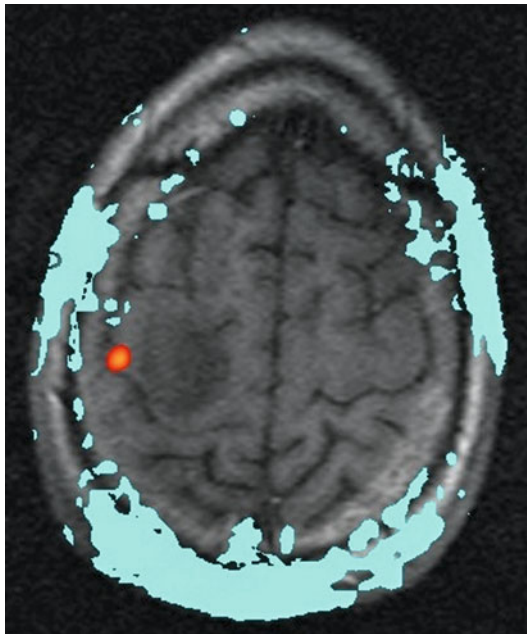

Fig. 12.4 Axial T1-weighted brain activation study performed at 3 T showing the area for finger tapping of the left hand. Because of the proximity of the area of brain activation to the tumor, this patient had a brain biopsy and tumor resection was not attempted

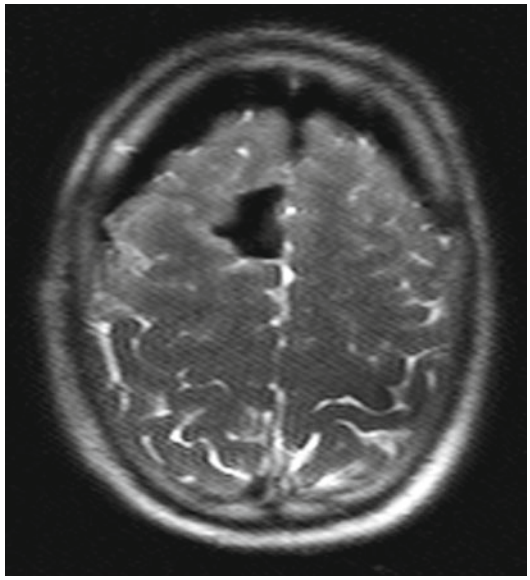

Fig. 12.5 Intraoperative axial half-Fourier acquisition single-shot turbo spin echo (HASTE) magnetic resonance imaging scan demonstrating complete radiographic resection of the tumor footprint. The HASTE imaging technique is used for low-grade gliomas because of its ability to demonstrate clearly residual disease and the rapid acquisition time that is possible during surgery. Note the presence of brain shift of both frontal lobes

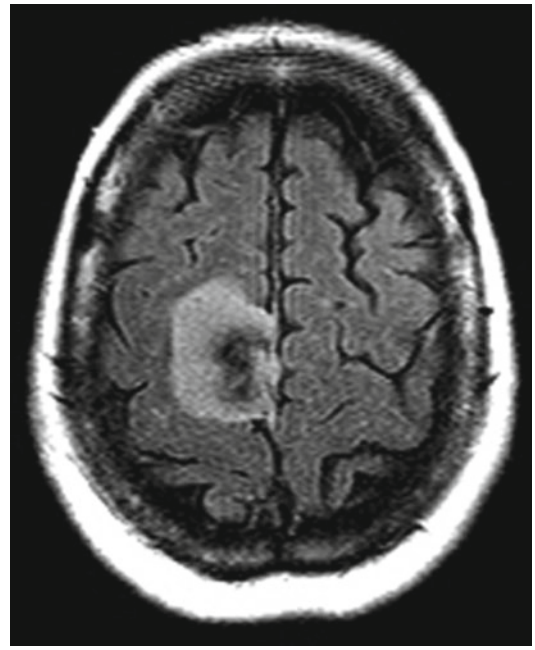

Fig. 12.6 Axial turbo FLAIR magnetic resonance imaging scan demonstrating a right frontal tumor with minimal mass effect or cerebral edema that was found on pathological examination to represent a meningioma

was no postoperative hemorrhage noted in any patient.

The number of intraoperative scans that were obtained during surgery varied widely within this series. A minimum of three scans were generally obtained with one before surgery, one to determine if there was residual tumor, and a final scan before leaving the operative suite to determine if any hemorrhage had occurred during closure. The head position was maintained constant throughout the procedure by use of the headframe, resulting in identical image planes during scanning.

There were no permanent postoperative neurologic deficits seen in this series of patients. Five patients did experience temporary neurologic worsening that included speech apraxia in two patients, motor apraxia in two patients, and combined speech and motor apraxia in one patient. All patients experienced complete resolution of these deficits within 4 weeks of surgery. There were no safety issues that occurred in this series related to the inadvertent transport of ferromagnetic items too near to the magnetic field.

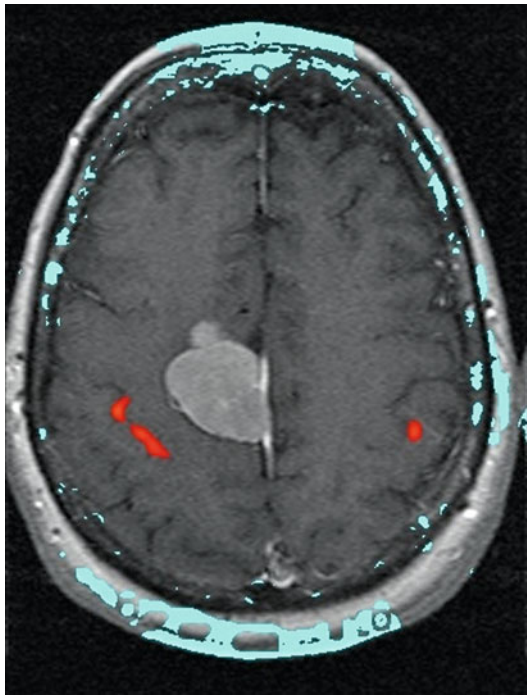

Fig. 12.7 Axial brain activation study performed at 3 T demonstrating the location of the functional area of the cortex for finger tapping of the left hand. The area of activation is just posterior and lateral to the contrast-enhancing tumor on this T1-weighted axial magnetic resonance imaging scan that was found to be a meningioma at surgery

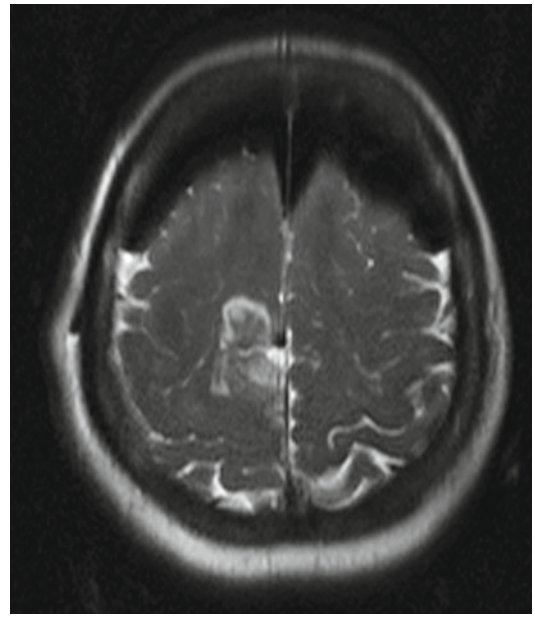

Fig. 12.8 Intraoperative axial turbo FLAIR 1.5 T MRI scan that was obtained after the complete resection of a right frontal tumor. Of note is the pneumocephalus that is present over both frontal lobes and the degree of brain shift that has resulted from the loss of cerebrospinal fluid during surgery

12.9 Discussion

The use of ioMRI at various field strengths has been well described and validated for safety and efficacy in achieving maximal tumor resection in adult and pediatric brain tumor surgery (Alexander et al. 1997; Berger et al. 1994; Bernays and Laws 1997; Bernstein et al. 2000; Black et al. 1999; Hall et al. 2003; Hall et al. 2005; Hall et al. 1998; Kremer et al. 2006; Lam et al. 2001; Martin et al. 1998; Nimsky et al. 2004; Schwartz et al. 1999; Trantakis et al. 2003). The addition of preoperative fMRI provides the neurosurgeon with a clear delineation of the areas of eloquent cortex that must be preserved during tumor resection and, when combined with ioMRI, has allowed for the safe resection of tumors near eloquent cortex that would otherwise require an awake craniotomy or intraoperative cortical stimulation or may even be considered unresectable. A reasonable concern with fMRI is that it defines areas of functionality indirectly, most often due to oxygen consumption during the performance of a task. Differences between functional territories as defined by direct brain mapping and fMRI have been reported (Roux et al. 2003), supporting this concern. Moreover, our speech testing used the commonly accepted paradigm of silent speech to reduce artifact (Friedman et al. 1998; Hinke et al. 1993), although areas of brain activation are not identical to those where true speech is generated (Huang et al. 2002). Awake craniotomy does provide the most direct assessment of functionality of the brain tissue that is being resected; however, in addition to the challenges of anesthesia, it requires direct stimulation with a cooperative patient or loss of function after resection to define eloquent areas. This may result in an irreversible neurological deficit. Most importantly, the lack of permanent postoperative deficits in the 29 patients in our combined series suggests that although indirect, fMRI does yield accurate information on the location of eloquent cortex and allows for the safe resection of tumors lying adjacent to that tissue. Regardless of the technique that is used for localizing tumors, those

that infiltrate directly into functional cortex cannot be safely resected. Because of this limitation, there were patients who still underwent partial resection in both of our series despite the use of fMRI guidance and in other reported series (Nimsky et al. 2006a).

Increasing the field strength of the preoperative fMRI from 1.5 T to 3 T improved the resolution of these images. Although the 1.5 T imaging allowed for safe aggressive resection of the lesions in the first series, the functional data was limited to one axial plane, whereas the 3 T data were visible on multiple slices, allowing for visualization of neurologic function in three dimensions. The success of increasing magnet strength intraoperatively raises the possibility of performing 3 T high-field ioMRI to match preoperative functional imaging at 3 T, which obviously would add clarity to the intraoperative imaging, affording a resolution equal to that of the preoperative functional images. Our experience applying 3 T fMRI preoperative data intraoperatively to guide brain tumor resection at 1.5 T has been sufficient for most surgical decision making; however, intraoperative imaging at 3 T may clearly represent the next degree of sophistication for neurosurgeons working in this field.

Intraoperative scans in our series were obtained to demonstrate brain structure only; therefore, the neurosurgeon was required during surgery to extrapolate the preoperative fMRI data onto the newly acquired ioMRI structural or anatomic scans. While intraoperative fMRI scans would obviate the need for preoperative acquisition, this would also add the time of multiple cycles of anesthesia reversal (for the performance of the intraoperative functional tasks) to the procedure. As with any imaging modality used during surgery, the data does not replace sound surgical judgment and familiarity with the neuroanatomy. Therefore, although our paradigm requires that the surgeon must mentally apply the preoperative fMRI data to newly acquired ioMRI images, this should not compromise the safety or efficacy of this technique.

Functional MRI data may also be coregistered with neuronavigation data as described above, although this has previously been reported to pose the risk of mislocalization (Roux et al. 2001) and still is subject to brain shift as with other frameless stereotactic techniques. Another way to compensate for brain shift that has been reported involves the application of intraoperative high-resolution 3D ultrasound data to registered MRI/fMRI data to allow for the correction of shift (Rasmussen et al. 2007). This is certainly an attractive option, although rigorous validation of computational algorithms is needed.

Diffusion tensor imaging may be used in combination with the above techniques to allow for additional protection to underlying white matter tracts. Diffusion tensor imaging data has been used in combination with direct subcortical stimulation to guide tumor resection near presumed eloquent white matter (Bello et al. 2011). Additionally, software has been developed allowing fMRI data to be used in order to select white matter tracts of particular interest when planning tumor resection (Golby et al. 2011). Intraoperative scans that include acquisition of DTI sequences have been used as well (Prabhu et al. 2011), allowing for true intraoperative acquisition of functional imaging data. In a rare prospective, randomized trial comparing neuronavigation with DTI tractography and traditional structural neuronavigation for tumors near the pyramidal tract, subgroup analysis of 81 high-grade gliomas revealed a significantly higher rate of gross total resection, with a corresponding statistically significant increase in median survival from 14.0 to 21.2 months (Wu et al. 2007).

12.10 Low-Grade Gliomas

Intraoperative MRI has been shown to help facilitate the resection of low-grade gliomas (Martin et al. 1998); however, the lack of clearly defined borders in these infiltrating tumors does increase the risk of damage to adjacent neural structures during image-guided surgery. Because low-grade glial tumors are often infiltrative and there exists controversy regarding the benefits of an aggressive resection of low-grade gliomas, these tumors are often treated without surgery when they occur in close proximity to eloquent cortex. The

infiltrative nature of these lesions may obscure the border between tumor and functional cortex. We have reviewed our experience with resection of low-grade gliomas using ioMRI guidance combined with preoperative fMRI. Our method of combining preoperative fMRI acquired at 1.5 T with 1.5 T ioMRI-guided surgery allowed for complete tumor resection in 10 (63%) patients without neurologic deficit at one month after surgery. Only one patient in this series received adjuvant radiation therapy and all patients enjoyed progression-free survival at last follow-up (median, 25 months). The lack of recurrence or progression of disease is consistent with our belief that maximal resection is the optimal treatment for low-grade gliomas. Furthermore, we interpret the fact that a significant number of the patients in this series exhibited transient postoperative neurologic deficits without permanent sequelae as evidence that ioMRI allowed for the most aggressive resection possible by the neurosurgeon.

12.11 High-Grade Gliomas

High-grade gliomas (HGG) represent the majority of primary intraparenchymal brain tumors in adults and, as mentioned previously, are generally treated with an aggressive surgical approach. Functional MRI neuronavigation as well as ioMRI combined with preoperative fMRI have been used in the treatment of HGG. Because these tumors usually enhance after contrast administration, a radiographic gross total resection can be defined as the removal of the enhancing mass on MRI. High-grade gliomas are generally visible grossly, and the neurosurgeon is often able to determine when gross total resection has been achieved during surgery without imaging. Nevertheless, ioMRI is useful for judging the extent of the tumor resection and confirming whether additional tumor removal is warranted. In our practice, contrast is only given intraoperatively after the apparent removal of most of the grossly abnormal tissue to avoid the diffusion of contrast into the edematous brain around the resection cavity. Although controversy continues as to whether gross total tumor resection extends survival in patients with HGG, the combination of fMRI with ioMRI provides increased protection of eloquent brain structures without the need for an awake craniotomy and cortical stimulation.

12.12 Other Tumors

Although we have focused on gliomas, the strategies outlined in this chapter should be applicable to virtually any lesion near eloquent cortex. The role of aggressive surgical resection is less clear for metastatic brain tumors, and aggressive surgical resection for tumors adjacent to eloquent cortex may be less appealing, especially with the excellent nonsurgical modalities presently available. Within the parameters of a rational approach to surgical resection, however, fMRI-guided neurosurgery likely has a role in a subset of patients with metastatic lesions. Certainly lesions located near eloquent structures will often be symptomatic, and the availability of fMRI-guided resection may be useful in such situations.

Because meningiomas are extra-axial tumors, their surgical resection should pose a lower risk of postoperative neurologic injury. The benefit of radical resection in the treatment of meningiomas is well documented (Simpson 1957). Neuronavigation is often used for planning the surgical resection of meningiomas and may be helpful in achieving complete resection (Keskil et al. 2006). We felt that ioMRI with preoperative functional imaging at 3 T was helpful in three meningiomas in our series that were located near eloquent cortex.

12.13 Conclusions

Functional MRI identifies those areas of cortex that are likely to result in neurologic compromise if resected by the neurosurgeon. Despite the fact that these data are indirectly measured, the use of fMRI has been validated as safe and effective for surgical guidance in the resection of tumors located near areas of functional cortex. We prefer

a paradigm of preoperative high-field fMRI combined with structural ioMRI to guide the removal of tumors that we have described in this chapter. Others have found fMRI useful within the context of coregistered frameless neuronavigation and awake craniotomy.

References

Alexander E 3rd, Moriarty TM et al (1997) The present and future role of intraoperative MRI in neurosurgical procedures. Stereotact Funct Neurosurg 68(1–4 Pt 1): 10–17

Amiez C, Kostopoulos P et al (2008) Preoperative functional magnetic resonance imaging assessment of higher-order cognitive function in patients undergoing surgery for brain tumors. J Neurosurg 108(2):258–268

Bello L, Castellano A et al (2011) Intraoperative use of diffusion tensor imaging fiber tractography and subcortical mapping for resection of gliomas: technical considerations. Neurosurg Focus 28(2):E6

Berger MS, Deliganis AV et al (1994) The effect of extent of resection on recurrence in patients with low grade cerebral hemisphere gliomas. Cancer 74(6): 1784–1791

Bernays RL, Laws ER Jr (1997) Intraoperative diagnostic and interventional magnetic resonance imaging in neurosurgery. Neurosurgery 41(4):999

Bernstein M, Al-Anazi AR et al (2000) Brain tumor surgery with the Toronto open magnetic resonance imaging system: preliminary results for 36 patients and analysis of advantages, disadvantages, and future prospects. Neurosurgery 46(4):900–907

Black PM, Alexander E 3rd et al (1999) Craniotomy for tumor treatment in an intraoperative magnetic resonance imaging unit. Neurosurgery 45(3):423–431

Braun V, Dempf S et al (2000) Functional cranial neuronavigation. Direct integration of fMRI and PET data. J Neuroradiol 27(3):157–163

Braun V, Dempf S et al (2001) Multimodal cranial neuronavigation: direct integration of functional magnetic resonance imaging and positron emission tomography data: technical note. Neurosurgery 48(5):1178–1181

Braun V, Albrecht A et al (2006) Brain tumour surgery in the vicinity of short-term memory representation-–results of neuronavigation using fMRI images. Acta Neurochir (Wien) 148(7):733–739

Buckner JC (2003) Factors influencing survival in high-grade gliomas. Semin Oncol 30(6 Suppl 19):10–14

Chang EF, Potts MB et al (2008) Seizure characteristics and control following resection in 332 patients with low-grade gliomas. J Neurosurg 108(2):227–235

Clatz O, Delingette H et al (2005) Robust nonrigid registration to capture brain shift from intraoperative MRI. IEEE Trans Med Imaging 24(11):1417–1427

Claus EB, Horlacher A et al (2005) Survival rates in patients with low-grade glioma after intraoperative magnetic resonance image guidance. Cancer 103(6): 1227–1233

Engle DJ, Lunsford LD (1987) Brain tumor resection guided by intraoperative computed tomography. J Neurooncol 4(4):361–370

Fandino J, Kollias SS et al (1999) Intraoperative validation of functional magnetic resonance imaging and cortical reorganization patterns in patients with brain tumors involving the primary motor cortex. J Neurosurg 91(2):238–250

Feigl GC, Safavi-Abassi S et al (2008) Real time 3T fMRI data of brain tumour patients for intra-operative localization of primary motor areas. Eur J Surg Oncol 34(6):708–715

Friedman L, Kenny JT et al (1998) Brain activation during silent word generation evaluated with functional MRI. Brain Lang 64(2):231–256

Golby AJ, Kindlmann G et al (2011) Interactive diffusion tensor tractography visualization for neurosurgical planning. Neurosurgery 68(2):496–505

Gumprecht H, Ebel GK et al (2002) Neuronavigation and functional MRI for surgery in patients with lesion in eloquent brain areas. Minim Invasive Neurosurg 45(3):151–153

Hall WA, Martin AJ et al (1998) High-field strength interventional magnetic resonance imaging for pediatric neurosurgery. Pediatr Neurosurg 29(5):253–259

Hall WA, Liu H et al (2003) Influence of 1.5-Tesla intraoperative MR imaging on surgical decision making. Acta Neurochir Suppl 85:29–37

Hall WA, Liu H et al (2005) Functional magnetic resonance imaging-guided resection of low-grade gliomas. Surg Neurol 64(1):20–27

Hinke RM, Hu X et al (1993) Functional magnetic resonance imaging of Broca's area during internal speech. Neuroreport 4(6):675–678

Huang J, Carr TH et al (2002) Comparing cortical activations for silent and overt speech using event-related fMRI. Hum Brain Mapp 15(1):39–53

Jääskeläinen J, Randell T (2003) Awake craniotomy in glioma surgery. Acta Neurochir Suppl 88:31–35

Jeremic B, Grujicic D et al (1994) Influence of extent of surgery and tumor location on treatment outcome of patients with glioblastoma multiforme treated with combined modality approach. J Neurooncol 21(2): 177–185

Joki T, Caroll R et al (2001) Assessment of alterations in gene expression in recurrent malignant glioma after radiotherapy using complementary deoxyribonucleic acid microarrays. Neurosurgery 48(1): 195–202

Kamada K, Houkin K et al (2003) Visualization of the eloquent motor system by integration of MEG, functional, and anisotropic diffusion-weighted MRI in functional neuronavigation. Surg Neurol 59(5): 352–361

Kamada K, Todo T et al (2007) Visualization of the frontotemporal language fibers by tractography combined with functional magnetic resonance imaging and magnetoencephalography. J Neurosurg 106(1):90–98

Keles GE, Lamborn KR et al (2001) Low-grade hemispheric gliomas in adults: a critical review of extent of resection as a factor influencing outcome. J Neurosurg 95(5):735–745

Keskil S, Bademci G et al (2006) Tracing the dural tail with image-guided surgery. Minim Invasive Neurosurg 49(6):357–358

Kober H, Nimsky C et al (2002) Co-registration of function and anatomy in frameless stereotaxy by contour fitting. Stereotact Funct Neurosurg 79(3–4):272–283

Kowalczuk A, Macdonald RL et al (1997) Quantitative imaging study of extent of surgical resection and prognosis of malignant astrocytomas. Neurosurgery 41(5): 1028–1036

Kremer P, Tronnier V et al (2006) Intraoperative MRI for interventional neurosurgical procedures and tumor resection control in children. Childs Nerv Syst 22(7):674–678

Krishnan R, Raabe A et al (2004) Functional magnetic resonance imaging-integrated neuronavigation: correlation between lesion-to-motor cortex distance and outcome. Neurosurgery 55(4):904–914

Kucharczyk J, Hall WA et al (2001) Cost-efficacy of MR-guided neurointerventions. Neuroimaging Clin N Am 11(4):767–772

Lacroix M, Abi-Said D et al (2001) A multivariate analysis of 416 patients with glioblastoma multiforme: prognosis, extent of resection, and survival. J Neurosurg 95(2):190–198

Lai DM, Lin SM et al (1993) Therapy for supratentorial malignant astrocytomas: survival and possible prognostic factors. J Formos Med Assoc 92(3):220–226

Lam CH, Hall WA et al (2001) Intra-operative MRI-guided approaches to the pediatric posterior fossa tumors. Pediatr Neurosurg 34(6):295–300

Laws ER Jr, Taylor WF et al (1984) Neurosurgical management of low-grade astrocytoma of the cerebral hemispheres. J Neurosurg 61(4):665–673

Martin C, Alexander E 3rd et al (1998) Surgical treatment of low-grade gliomas in the intraoperative magnetic resonance imager. Neurosurg Focus 4(4):e8

Medbery CA 3rd, Straus KL et al (1988) Low-grade astrocytomas: treatment results and prognostic variables. Int J Radiat Oncol Biol Phys 15(4):837–841

Meyer FB, Bates LM et al (2001) Awake craniotomy for aggressive resection of primary gliomas located in eloquent brain. Mayo Clin Proc 76(7):677–687

Nabavi A, Black PM et al (2001) Serial intraoperative magnetic resonance imaging of brain shift. Neurosurgery 48(4):787–797

Nicolato A, Gerosa MA et al (1995) Prognostic factors in low-grade supratentorial astrocytomas: a uni-multivariate statistical analysis in 76 surgically treated adult patients. Surg Neurol 44(3):208–221

Nimsky C, Ganslandt O et al (2004) Intraoperative high-field-strength MR imaging: implementation and experience in 200 patients. Radiology 233(1):67–78

Nimsky C, Ganslandt O et al (2006a) Intraoperative high field MRI: anatomical and functional imaging. Acta Neurochir 98(Suppl):87–95

Nimsky C, Ganslandt O et al (2006b) Intraoperative visualization for resection of gliomas: the role of functional neuronavigation and intraoperative 1.5 T MRI. Neurol Res 28(5):482–487

O'Shea JP, Whalen S et al (2006) Integrated image–and function-guided surgery in eloquent cortex: a technique report. Int J Med Robot 2(1):75–83

Ogawa S, Lee TM et al (1990) Brain magnetic resonance imaging with contrast dependent on blood oxygenation. Proc Natl Acad Sci U S A 87(24):9868–9872

Patchell RA, Tibbs PA et al (1990) A randomized trial of surgery in the treatment of single metastases to the brain. N Engl J Med 322(8):494–500

Philippon JH, Clemenceau SH et al (1993) Supratentorial low-grade astrocytomas in adults. Neurosurgery 32(4):554–559

Picht T, Kombos T et al (2006) Multimodal protocol for awake craniotomy in language cortex tumour surgery. Acta Neurochir (Wien) 148(2):127–137

Piepmeier JM (1987) Observations on the current treatment of low-grade astrocytic tumors of the cerebral hemispheres. J Neurosurg 67(2):177–181

Piepmeier J, Christopher S et al (1996) Variations in the natural history and survival of patients with supratentorial low-grade astrocytomas. Neurosurgery38(5):872–878

Prabhu SS, Gasco J et al (2011) Intraoperative magnetic resonance imaging-guided tractography with integrated monopolar subcortical functional mapping for resection of brain tumors. Clinical article. J Neurosurg 114(3):719–726

Preul C, Tittgemeyer M et al (2004) Quantitative assessment of parenchymal and ventricular readjustment to intracranial pressure relief. AJNR Am J Neuroradiol 25(3):377–381

Rasmussen IA Jr, Lindseth F et al (2007) Functional neuronavigation combined with intra-operative 3D ultrasound: initial experiences during surgical resections close to eloquent brain areas and future directions in automatic brain shift compensation of preoperative data. Acta Neurochir (Wien) 149(4):365–378

Reinertsen I, Lindseth F et al (2007) Clinical validation of vessel-based registration for correction of brain-shift. Med Image Anal 11(6):673–684

Reinges MH, Nguyen HH et al (2004) Course of brain shift during microsurgical resection of supratentorial cerebral lesions: limits of conventional neuronavigation. Acta Neurochir (Wien) 146(4):369–377

Roessler K, Donat M et al (2005) Evaluation of preoperative high magnetic field motor functional MRI (3 Tesla) in glioma patients by navigated electrocortical stimulation and postoperative outcome. J Neurol Neurosurg Psychiatry 76(8):1152–1157

Roux FE, Ibarrola D et al (2001) Methodological and technical issues for integrating functional magnetic resonance imaging data in a neuronavigational system. Neurosurgery 49(5):1145–1156

Roux FE, Boulanouar K et al (2003) Language functional magnetic resonance imaging in preoperative assessment of language areas: correlation with direct cortical stimulation. Neurosurgery 52(6):1335–1345

Schulder M, Maldjian JA et al (1997) Functional MRI-guided surgery of intracranial tumors. Stereotact Funct Neurosurg 68(1–4 Pt 1):98–105

Schulder M, Holodny A et al (1999) Functional magnetic resonance image-guided surgery of tumors in or near the primary visual cortex. Stereotact Funct Neurosurg 73(1–4):31–36

Schwartz RB, Hsu L et al (1999) Intraoperative MR imaging guidance for intracranial neurosurgery: experience with the first 200 cases. Radiology 211(2):477–488

Signorelli F, Guyotat J et al (2003) Technical refinements for validating functional MRI-based neuronavigation data by electrical stimulation during cortical language mapping. Minim Invasive Neurosurg 46(5):265–268

Simpson DJ (1957) The recurrence of intracranial meningiomas after surgical treatment. J Neurol Neurosurg Psychiatry 20(1):22–39

Speigl-Kreinecker S, Pirker C et al (2002) Dynamics of chemosensitivity and chromosomal instability in recurrent glioblastoma. Br J Cancer 96:960–969

Stummer W, Reulen HJ et al (2008) Extent of resection and survival in glioblastoma multiforme: identification of and adjustment for bias. Neurosurgery 62(3): 564–576

Trantakis C, Tittgemeyer M et al (2003) Investigation of time-dependency of intracranial brain shift and its relation to the extent of tumor removal using intraoperative MRI. Neurol Res 25(1):9–12

Truwit CL, Hall WA (2006) Intraoperative magnetic resonance imaging-guided neurosurgery at 3-T. Neurosurgery58(4 Suppl 2):ONS-338–ONS-345

Ushio Y, Kochi M et al (2005) Effect of surgical removal on survival and quality of life in patients with supratentorial glioblastoma. Neurol Med Chir (Tokyo) 45(9): 454–460

Vecht CJ, Haaxma-Reiche H et al (1993) Treatment of single brain metastasis: radiotherapy alone or combined with neurosurgery? Ann Neurol 33(6): 583–590

Vidiri A, Carapella CM et al (2006) Early post-operative MRI: correlation with progression-free survival and overall survival time in malignant gliomas. J Exp Clin Cancer Res 25(2):177–182

Weber F, Riedel A et al (1996) The role of adjuvant radiation and multiple resection within the surgical management of brain metastases. Neurosurg Rev 19(1): 23–32

Wilkinson ID, Romanowski CA et al (2003) Motor functional MRI for pre-operative and intraoperative neurosurgical guidance. Br J Radiol 76(902): 98–103

Wu JS, Zhou LF et al (2007) Clinical evaluation and follow up outcome of diffusion tensor imaging-based functional neuronavigation: a prospective controlled study in patients with gliomas involving pyramidal tracts. Neurosurgery 61(5):935–948

Direct Cortical Stimulation and fMRI

13

H. Maximillian Mehdorn, Simone Goebel, and Arya Nabavi

13.1 Introduction

Intracranial space-occupying lesions, particularly glial tumors, may challenge the neurosurgeon who aims at preserving neuronal function as much as possible while removing as much of the lesion as possible. It has been repeatedly questioned whether radical resection of gliomas is the method of choice because of their invasive nature, but it has also been shown recently that patients can benefit from radical resection as much as possible both in primary (Stummer et al. 2006) and recurrent gliomas and in low-grade gliomas (Claus and Black 2006, Sanai and Berger 2008). Radical resection of glial tumors, however, is hampered by the risk of damaging neuronal functions, particularly of speech and motor functions. Therefore, early on in the development of modern neurosurgery, brain tumor surgery under local anesthesia (LA) was suggested in order to reduce the risk of immediate severe and nonreversible postoperative neurological deficit (Berger and Ojemann 1992; Black and Ronner 1987; Ojemann et al. 1989; Ojemann 1988). Most of the patients are initially frightened by the suggestion of undergoing brain tumor surgery under local anesthesia. However, they accept this method when the details are fully explained to them (Danks et al. 1998). Nevertheless, there are limitations, such as patients' inability to cooperate – in the case of very young and very old patients or a tumor located and extending in such a fashion that there is no good way to position the patient with sufficient comfort; patients with reduced cardiopulmonary functions or seizures related to the tumor should be particularly well taken care of. Taking these precautions into account, it has been shown by many centers that it is possible to reduce the risk of a focal neurological deficit while increasing the chance to completely remove a tumor located in eloquent areas (Danks et al. 2000; Duffau 2005a, b; Duffau et al. 2003; Ebeling et al. 1995; Pinsker et al. 2007).

With the advent of magnetic resonance imaging (MRI) and particularly functional MRI (fMRI), this technique is now widely accepted as being able to precisely localize brain functions (Brannen et al. 2001; Naidich et al. 2001), with a high degree of sophistication and reliability (with a 53 % regional specificity (FitzGerald et al. 1997)): even different brain functions requiring complex interactions between various active brain areas. While the latter may be further explored in research projects, some indications for its use in a clinical setting have emerged over the recent years and led to its implementation into routine MRI scanner software. In routine clinical neurosurgical practice, these techniques mainly concern the definition of the dominant hemisphere, the various speech areas and motor cortex. Furthermore, relation between the most

H.M. Mehdorn (✉) • S. Goebel • A. Nabavi
Klinik für Neurochirurgie,
Campus Kiel, Arnold-Heller-Str. 3, Hs 41,
Kiel 24105, Germany
e-mail: mehdorn@nch.uni-kiel.de

S. Ulmer, O. Jansen (eds.), *fMRI – Basics and Clinical Applications*,
DOI 10.1007/978-3-642-34342-1_13,

important areas can be demonstrated by fiber tracking, thus enabling the surgeon to prevent damage to the white matter tracts (Duffau 2005a, b, 2007; Nimsky et al. 2006a, b, c). However, there are certain limitations which may lead one to question the value of these fMRI results in relation to intraoperative application. This chapter should elucidate some of the benefits and pitfalls of both techniques as experienced by the authors in a review of the literature.

13.2 Indications for Direct Cortical Stimulation and/or Functional Magnetic Resonance Imaging (fMRI): Patient Selection

Two factors determine the indication for either direct cortical stimulation (DCS) during surgery under awake conditions or fMRI:

1. The clinical condition of the patient, particularly his presenting symptoms and his neurological status

If the patient's history and presenting symptoms, like temporary speech deficits or focal seizures, suggest a lesion affecting motor or speech areas and the diagnosis of an intrinsic brain tumor in these areas is ascertained, the patient is considered for awake craniotomy using DCS. Special attention should be given to the patient's problems of understanding and his/her capability and willingness to cooperate with the surgeon and the OR team; these factors need to be analyzed preoperatively by the neurosurgical staff members and dedicated neuropsychologists.

These criteria obviously exclude the following patient groups from awake craniotomy: emergency tumor decompressions in comatose patients, small children, and geriatric patients who would be unable to cooperate fully.

In all other patients with tumors in the above-mentioned locations, the method of DCS was the method of choice, before fMRI was available in our institution as well as in others, to determine intraoperatively how much tumor could be removed safely without provoking too big a neurological deficit. In our experience as well in the experience of others, DCS has shown to improve surgical outcome when operating in functionally relevant areas, enhancing both the amount of tumor resection and the preserving function.

Now, since the advancement of MRI technology and introduction of fMRI in the armamentarium of preoperative evaluation, this method needs to be taken into consideration and weighted against the DCS method.

2. Tumor localization and function of brain region

Following the first diagnostic imaging of the tumor which is made in order to grade it in a assumptive manner, its localization, as visualized by preoperative computed tomography (CT) scanning or more appropriately by MRI, is analyzed to determine whether functionally relevant ("eloquent") brain structures including fiber tracts are in vicinity to the tumor and could possibly be harmed during tumor removal. The initial grading should help to define the extent of surgical resection. While resection of a WHO grade III or IV glioma should be attempted with the intent to completely preserve function at the preoperative level for the limited survival time, in grade I or II gliomas, complete resection should be attempted in order to optimize survival times without adjunctive therapy. In these patients, particular workup is required in order to define the spatial relation between the tumor borders and the functionally relevant structures, i.e., speech and motor cortical areas, optical regions, and the fiber tracts, particularly the pyramidal tract and the bundles between the motor and sensory speech areas and also the optical fiber tracts, e.g., the Gratiolet tract.

While fMRI data acquisition can be applied to all patients who tolerate the narrow canal of MRI machines and who understand the need to cooperate while performing the neuropsychological paradigms, the DWI measurements required for representation of fiber bundles demand that a patient lie for some additional time without moving his/her head until the data are acquired.

The fMRI data need to be processed and transferred to the neuronavigation consoles in order to be used for surgical planning.

On the basis of the above-mentioned criteria, the patient is advised to undergo surgery as awake craniotomy.

13.3 Methods

13.3.1 Surgery Under Local Anesthesia: Awake Craniotomy

Details of this technique have been described by our group (Pinsker et al. 2007) and others (Danks et al. 2000; Duffau 2005a, b; Duffau et al. 2003, 1999; Tonn 2007). We have implemented awake craniotomy since 1993 in our department in order to remove as much tumor as possible in or close to eloquent areas while preserving function. Prerequisite for this technique is, in our opinion, a good (neuro-)psychological preparation of the patient. The majority of our brain tumor patients undergo formal preoperative neuropsychological testing by our dedicated neuropsychologists who not only evaluate the aspects of the dominant hemisphere and, in a very sophisticated manner, the neuropsychological deficits but also talk to the patients concerning their individual fears related to the tumor and the upcoming surgery. In the initial phase, we also brought the patients into the operating room and positioned them onto the OR table to make them familiar with the setting; due to time restraints, this is no longer possible, but the patients are well familiarized with this particular type of surgery. Anesthesiologists also play a special role in this setting; they have to take care of the patient during surgery and are essential in keeping a balance between sedation of the patient during some parts of surgery, e.g., craniotomy itself and having him/her awake for testing during tumor removal. Medications used in this regard are propofol and analgesics. Central lining is given to all our patients although this may not be the routine in other centers (Fig. 13.1).

LA is applied to the patient by the neurosurgeon using ropivacaine HCl (Naropin®) 0.75 % for the blocks around the 3-pin headholder. Neuronavigation is used to define the optimal craniotomy site and delineation of the skin incision. Subsequently the line of the skin incision is anesthetized additionally; when a curved incision is required, particular care is paid to apply sufficient anesthesia to the underlying muscles, usually the temporal muscle. After careful aseptic preparation the surgical drapes are placed after having applied a semicircular or rectangular cage-like metal to hold the drapes with sufficient comfort for the patient to whom every single step of draping him/her is explained carefully (Fig. 13.2).

Then surgery is performed as usual while always talking to the patient and explaining all the steps and adding LA as required; particular care is taken while the craniotomy is performed. Until this step and a little bit longer, the patient is also allowed to sleep under anesthesiological supervision and with the help of sedation and/or analgesic short-lasting medication (propofol).

The dura is subsequently opened under the operating microscope and the brain inspected, and, again with the help of the neuronavigation, the brain tumor is localized.

13.3.2 Stimulation

Once the tumor has been outlined with inspection and neuronavigation, the functional mapping is required to define cortical brain areas which are functionally relevant. These areas can be outlined in the fashion as described by Ojemann et al. (Ojemann et al. 1989; Ojemann 1988) and marked by cotton pledgets with numbers on it, or they can be virtually marked with neuronavigation. Results of preoperative fMRI studies defining functionally relevant areas can be implemented during surgery, using particular computer programs, as provided commercially by BrainLAB and other companies, which help to blend them into a particular computer screen adjacent to a surgical microscope or to implement them into light course of the microscope, thus overlaying them virtually onto the surgical field. Both methods are available, presenting the tumor either as outline onto the brain surface or the level of visual acuity or by defining the tumor as 3D volume (Fig. 13.3).

Stimulation itself is performed using the Ojemann stimulator with various settings and eliciting the patient's response to various levels of bipolar stimulation. The motor respective speech disturbances are carefully monitored by

Fig. 13.1 Positioning the awake patient in the 3-pin headholder using local anesthesia. (**a**) Close-up view of the patient. (**b**) During surgery with the neuropsychologist calming and testing the patient

the neuropsychologist attending on the patient during the important phases of surgery, and this way, a mapping of cortical areas which are safe to remove and those whose removal may cause neurological deficits, is ascertained. Particular attention needs to be paid to the vasculature of the cortical surface as it relates to the stimulated areas since one should always remind oneself that the cortical vessels, particularly the arteries, are nearly more important to be preserved than the cortical surface itself which they irrigate.

Once the area which can safely be removed has been defined, the interaction between the surgeon and the patient should not end. Care has to be taken depending on the correlation between the tumor borders and the white matter tracts, e.g., the pyramidal tract (Nimsky et al. 2006a, b, c). Stimulation should therefore be continued while the surgeon is entering the white matter, and combined with neuronavigation, in order to show the spatial correlation between these important structures (Bello et al. 2008; Duffau 2007; Duffau et al. 2002). In our experience, the voltage

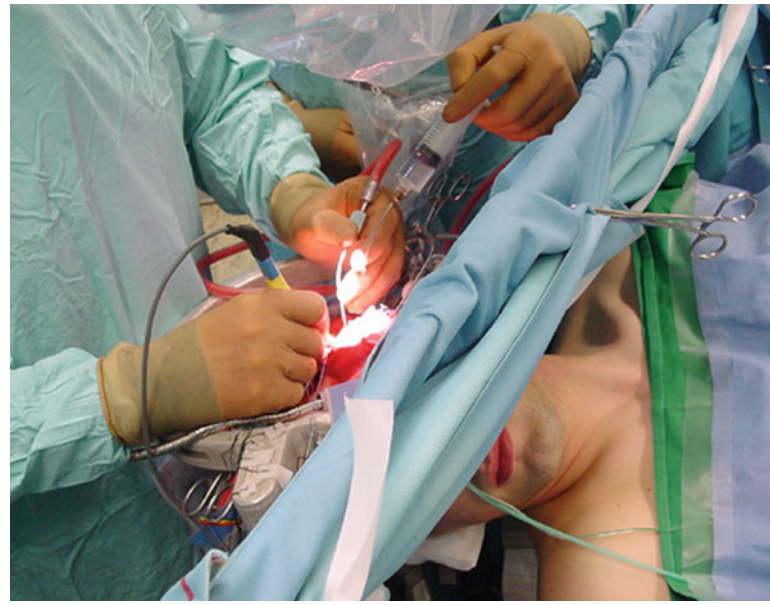

Fig. 13.2 Brain surgery in the awake patient. The patient is operated with standard microneurosurgical equipment while undergoing specific neurophysiologic and neuropsychological testing

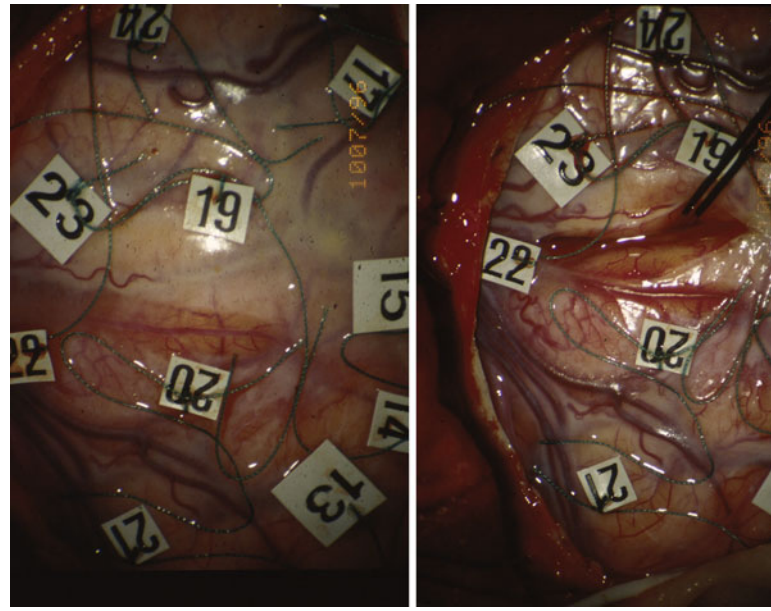

Fig. 13.3 Cortical testing. The tumor encompasses the cortex, clearly visible by the discoloration in the *top* portion of the image. Direct cortical stimulation (DCS) results are registered using numbered cottonoids to map and document the elicited corresponding results. The identified safe access routes are taken for arachnoidal opening, corticotomy, and resection of the tumor. The images show corresponding sites, left before, and right after arachnoid opening and during cortical testing of the sulcal cortical surface with the Ojemann bipolar probe

required to elicit some motor problems in the patient relates well with the distance to the pyramidal tract: the higher the voltage, the longer the distance to the tract. This means that one has to monitor this distance continuously as the tracts may be displaced during surgical removal of the tumor, when compared to their preoperative position.

13.3.3 Intraoperative MRI

The implementation of a high-field MRI machine into a neurosurgical operating room (OR) has facilitated tumor removal further by allowing real-time imaging on a high level of imaging quality. This enables the surgeon to reestablish the true anatomical situation which

changes permanently after opening of the dura due to CSF drainage and manipulation of the brain and during tumor removal (Nabavi et al. 2001; Nimsky et al. 2000). This phenomenon of brain shift is also of high importance concerning the accuracy of fMRI data acquired preoperatively.

13.4 Practical Considerations

In order to optimize the situation for the patient, we have developed a protocol for patients with tumors in or near to eloquent brain areas. Formal neuropsychological testing as an initial step and detailed neuroimaging using MRI (T1 and T2, DWI and DTI, and MPRage for 3D reconstruction and preparation for neuronavigation), fMRI data, and DWI images are performed in order to determine the spatial relationship between tumor and functionally relevant structures, and then the situation is discussed with the patient to see whether awake craniotomy should be suggested. If the patient agrees, he undergoes surgery under LA as usual and under intraoperative high-field MRI control. This allows for reregistration of functionally relevant data and update into the neuronavigation (Nabavi et al. 2003; Nimsky et al. 2006a, b, c). In the recent years, most patients with low- and high-grade gliomas underwent surgery under local anesthesia with intermittent control in the high-field MRI (Mehdorn et al. 2011).

13.5 Results

In a previous paper (Pinsker et al. 2007), we have compared the results of surgery performed between 1998 and 2002 in 80 patients with gliomas located in eloquent areas, using awake craniotomy in 37 primary operations and 18 operations for recurrent gliomas, while using – on the patients' request – general anesthesia in 27 patients. Comparing only patients with tumors located in the motor areas, patients operated using awake craniotomy had a higher rate of complete resection as evaluated by MRI scans within the 48 h post surgery: 20 out of 26 (77 %) as compared to 4 out of 12 (33 %). Worsening of motor functions occurred and lasted more than 3 months in three patients (12 %) following awake craniotomy, while it happened in four patients (33 %) operated under general anesthesia. Since the routine use of preoperative fMRI and fiber tracking and intraoperative high-field MRI, we have the "clinical feeling" that we may be less intense to persuade patients into awake craniotomy, but this feeling needs to be substantiated in a prospective fashion, and the results of this policy are presently evaluated with regard to long-term outcome. Having the possibilities, however, to use elaborate neuropsychological evaluation, intraoperative monitoring, intraoperative MRI scanning, and intraoperative application of local chemotherapy agents, the number of patients coming to us in a predetermined fashion has certainly risen, and such a study may be difficult to evaluate.

Intraoperative guidance by preoperatively acquired data with regard to position of eloquent areas may certainly be helpful (Nimsky et al. 2004; Pinsker et al. 2007) but still the surgeon has to be aware of intraoperative brain deformation, i.e., "brain shift" (Nabavi et al. 2001; Nimsky et al. 2000), and must therefore still use his best surgical judgment while removing tumor tissue in or around eloquent areas. In this regard, intraoperative clinical control plays a substantial role in defining the extent of surgical resection around eloquent areas. A careful comparison of the location of eloquent areas as defined on fMRI studies and the intraoperative definition of these areas will be helpful in determining the clinical value of each of the methods described.

13.6 Perspectives

Further elaboration of preoperative evaluation of patients harboring those life-limiting tumors is warranted in order to further improve quality of life during both treatment and follow-up while enhancing long-term survival. Initial surgery is essential to remove as much tumor as possible and thereby determine long-term results, while second or third surgery often must take compromises to preserve function.

References

Bello L, Gambini A et al (2008) Motor and language DTI fiber tracking combined with intraoperative subcortical mapping for surgical removal of gliomas. Neuroimage 39(1):369–382

Berger MS, Ojemann GA (1992) Intraoperative brain mapping techniques in neurooncology. Stereotact Funct Neurosurg 58(1–4):153–161

Black PM, Ronner SF (1987) Cortical mapping for defining the limits of tumor resection. Neurosurgery 20(6):914–919

Brannen JH, Badie B et al (2001) Reliability of functional MR imaging with word-generation tasks for mapping Broca's area. AJNR Am J Neuroradiol 22(9):1711–1718

Claus EB, Black PM (2006) Survival rates and patterns of care for patients diagnosed with supratentorial low-grade gliomas: data from the SEER program, 1973–2001. Cancer 106(6):1358–1363

Danks RA, Rogers M et al (1998) Patient tolerance of craniotomy performed with the patient under local anesthesia and monitored conscious sedation. Neurosurgery 42(1):28–34; discussion 34–26

Danks RA, Aglio LS et al (2000) Craniotomy under local anesthesia and monitored conscious sedation for the resection of tumors involving eloquent cortex. J Neurooncol 49(2):131–139

Duffau H (2005a) Intraoperative cortico-subcortical stimulations in surgery of low-grade gliomas. Expert Rev Neurother 5(4):473–485

Duffau H (2005b) Lessons from brain mapping in surgery for low-grade glioma: insights into associations between tumour and brain plasticity. Lancet Neurol 4(8):476–486

Duffau H (2007) Contribution of cortical and subcortical electro-stimulation in brain glioma surgery: methodological and functional considerations. Neurophysiol Clin 37(6):373–382

Duffau H, Capelle L et al (1999) Intra-operative direct electrical stimulations of the central nervous system: the salpetriere experience with 60 patients. Acta Neurochir (Wien) 141(11):1157–1167

Duffau H, Capelle L et al (2002) Intraoperative mapping of the subcortical language pathways using direct stimulations. An anatomo-functional study. Brain 125(Pt 1):199–214

Duffau H, Capelle L et al (2003) Usefulness of intraoperative electrical subcortical mapping during surgery for low-grade gliomas located within eloquent brain regions: functional results in a consecutive series of 103 patients. J Neurosurg 98(4):764–778

Ebeling U, Fischer M et al (1995) Surgery of astrocytomas in the motor and premotor cortex under local anesthesia: report of 11 cases. Minim Invasive Neurosurg 38(2):51–59

FitzGerald DB, Cosgrove GR et al (1997) Location of language in the cortex: a comparison between functional MR imaging and electrocortical stimulation. AJNR Am J Neuroradiol 18(8):1529–1539

Mehdorn HM, Schwartz F et al (2011) High-field MRI in glioblastoma surgery: improvement of resection radicality and survival for the patient? Acta Neurochir Suppl 109:103–106

Nabavi A, Black PM et al (2001) Serial intraoperative magnetic resonance imaging of brain shift. Neurosurgery 48(4):787–797; discussion 797–788

Nabavi A, Gering DT et al (2003) Surgical navigation in the open MRI. Acta Neurochir Suppl 85:121–125

Naidich TP, Hof PR et al (2001) The motor cortex: anatomic substrates of function. Neuroimaging Clin N Am 11(2):171–193, vii–viii

Nimsky C, Ganslandt O et al (2000) Quantification of, visualization of, and compensation for brain shift using intraoperative magnetic resonance imaging. Neurosurgery 47(5):1070–1079; discussion 1079–1080

Nimsky C, Ganslandt O et al (2004) Functional neuronavigation and intraoperative MRI. Adv Tech Stand Neurosurg 29:229–263

Nimsky C, Ganslandt O et al (2006a) Intraoperative visualization for resection of gliomas: the role of functional neuronavigation and intraoperative 1.5 T MRI. Neurol Res 28(5):482–487

Nimsky C, Ganslandt O et al (2006b) Implementation of fiber tract navigation. Neurosurgery 58(4 Suppl 2):ONS-292–ONS-303; discussion ONS-303–294

Nimsky C, Ganslandt O et al (2006c) Intraoperative visualization of the pyramidal tract by diffusion–tensor-imaging-based fiber tracking. Neuroimage 30(4):1219–1229

Ojemann GA (1988) Effect of cortical and subcortical stimulation on human language and verbal memory. Res Publ Assoc Res Nerv Ment Dis 66:101–115

Ojemann G, Ojemann J et al (1989) Cortical language localization in left, dominant hemisphere. An electrical stimulation mapping investigation in 117 patients. J Neurosurg 71(3):316–326

Pinsker MO, Nabavi A et al (2007) Neuronavigation and resection of lesions located in eloquent brain areas under local anesthesia and neuropsychological-neurophysiological monitoring. Minim Invasive Neurosurg 50(5):281–284

Sanai N, Berger MS (2008) Glioma extent of resection and its impact on patient outcome. Neurosurgery 62(4):753–764; discussion 264–756

Stummer W, Pichlmeier U et al (2006) Fluorescence-guided surgery with 5-aminolevulinic acid for resection of malignant glioma: a randomised controlled multicentre phase III trial. Lancet Oncol 7(5):392–401

Tonn JC (2007) Awake craniotomy for monitoring of language function: benefits and limits. Acta Neurochir (Wien) 149(12):1197–1198

Imaging Epilepsy and Epileptic Seizures Using fMRI

14

Simon M. Glynn and John A. Detre

14.1 Introduction

Magnetic resonance imaging (MRI) has had an extraordinary impact on the diagnosis and management of epilepsy. The routine use of high-field MRI in clinical epilepsy has also encouraged interest in the potential for functional MRI (fMRI) to image the abnormal brain function that underlies epilepsy. Here, we give a brief overview of epilepsy and the current state of fMRI for the difficult problem of imaging epilepsy and epileptic seizures.

14.2 Background

The term *epilepsy* derives from the Greek *to lay hold of* or *to be seized* and is defined by the tendency to recurrent, spontaneous clinical seizures. Worldwide, epilepsy affects 50 million people and for a quarter of those affected, no combination of standard therapy – primarily medications and surgery – can control their seizures (Sander 2003). Epileptic seizures vary in their forms, from seemingly minor seizures such as brief staring episodes to generalized convulsions, but all seizure types are potentially debilitating regardless of their form. Only in a minority of newly diagnosed persons with epilepsy can a specific etiology for this epileptic activity be determined.

14.3 fMRI in Epilepsy

fMRI is used in epilepsy research as well as in clinical practice in epilepsy centers worldwide. The one universally accepted clinical application for fMRI in epilepsy is to lateralize language function in patients being considered for resective epilepsy surgery. In this application, fMRI provides a safe and repeatable alternative to the more invasive intracarotid amobarbital test, which has been used for this purpose for several decades – although the use of fMRI to lateralize memory function concordant with the intracarotid amobarbital test has been more problematic. This application of fMRI is covered in a separate chapter in this volume and has been the topic of several excellent reviews.

14.4 fMRI and Interictal Phenomena

The second, more ambitious application of fMRI in epilepsy is its use for visualizing the hemodynamic correlates for the abnormal synchronized neuronal activity that underlies epilepsy.

S.M. Glynn (✉)
Department of Neurology, University of Michigan,
University Hospital Floor 1 Room 1B300,
1500 E Medical Center Dr SPC 5036,
Ann Arbor, MI 48109, USA
e-mail: glynn_simon@hotmail.com

J.A. Detre
Center for Brain Injury and Repair,
University of Pennsylvania Medical Center,
3 W Gates Building, 3400 Spruce Street,
Philadelphia, PA 19104, USA

S. Ulmer, O. Jansen (eds.), *fMRI – Basics and Clinical Applications*,
DOI 10.1007/978-3-642-34342-1_14,

A PubMed query performed in 2011 using the MeSH terms (*fMRI* or *functional MRI*) and (*epilepsy* or *seizure*) returned nearly 500 articles. Of these papers, the majority relate to the use of simultaneous EEG and fMRI to localize the epileptogenic focus during interictal recordings (i.e., recorded in the interval between seizures). Using this technique, interictal epileptiform discharges on EEG may be modeled as events in fMRI, and the statistical maximum of the BOLD signal is (usually) asserted to reflect cortical origin of these interictal discharges. In general, the results of these papers have been quite complicated, demonstrating a cortical origin for only a subset of interictal epileptiform discharges but also that these discharges are associated with remarkably extensive (and unexpected) increases and decreases in the BOLD signal. These papers have been the topic of several excellent reviews (see Gotman 2008; or Laufs and Duncan 2007) and will not be reviewed in detail in this chapter. The recent technical advance demonstrating the feasibility of intracranial EEG and fMRI recordings can be expected to dramatically improve our understanding of these dynamics.

14.4.1 Epilepsy as a Network Problem

Two emerging concepts are apparent in the discussion of these spatially extensive and complex BOLD signal correlates for the neural activity in epilepsy. The first is the concept of epilepsy as a network or system-oriented problem (Spencer 2002), as opposed to the concept of an epileptogenic focus or *epileptogenic zone*. This concept of networks is, of course, not new. Methods in EEG for extracting information about the connectivity of different areas of the brain have been developed starting in the 1950s, using the coherence or correlation of EEG signals as a measure of the functional connectivity of spatially distributed brain areas and more recently nonlinear dynamical systems and chaos theory. These methods are important for fMRI because they establish the concept of effective or functional connectivity in the brain (the influence of one neuronal group over another). According to this network concept, the spatially distributed BOLD signal changes well beyond the presumed origin of the epileptic discharge described in these papers are not due to *propagation of discharges*, but reflect the synchronous involvement of distributed neuronal populations, some of which can spontaneously generate interictal discharges that are potentially epileptogenic and others which act as relays for those discharges (Hamandi et al. 2008).

14.4.2 Epilepsy and Functional Connectivity

The second, related concept influencing our recording and interpretation of the BOLD signal in epilepsy has been the observation from functional imaging studies using PET and fMRI that spontaneous (or resting state) brain activity is not random. Instead, spontaneous activity is organized into a set of highly coherent functional networks. At the timescale of fMRI, large-scale neural networks imaged using functional connectivity techniques are largely dependent on anatomic connectivity that reflects the logic of small world networks. These dynamics, in turn, depend critically on *noise* in local or small-scale network dynamics that drives fluctuations in the larger network.

These resting state networks do not map directly to a cognitive process, but they do seem to reflect the functional capacity of the brain, and importantly, these network dynamics seem to be disrupted in disorders that affect cognition. In epilepsy, we can conjecture that the underlying damage or abnormal neuronal function in epilepsy would be expected to lead to *noise* that may drive this larger network out of equilibrium, engaging and disengaging different network configurations. These local dynamics would decrease functional connectivity in resting state networks, reflecting the interictal dysfunction in these networks. In theory, this

network hypothesis has important implications for the concept of interictal dysfunction in epilepsy, as these interictal network dynamics are *always on*. That said, our understanding of these network dynamics is incomplete and the important questions – what is the underlying network, and can this network be modulated to stop seizures – are particularly difficult from a signal processing perspective.

14.5 Imaging Epileptic Seizures

In contrast to interictal EEG-fMRI studies, relatively few papers have been published on the use of fMRI to image epileptic seizures. The obvious reason for this is that seizures are spontaneous, happening without warning (although there are exceptions to this). For this reason, fMRI recordings of clinical seizures are usually merely fortuitous, happening during interictal fMRI studies or, less often, in persons with very frequent seizures or seizures that may be deliberately induced (e.g., hyperventilation-induced absence seizures).

For those fMRI recordings that *do* fortunately image a clinical seizure, there are several methodological issues that complicate fMRI imaging of seizures. First, usually only one clinical seizure will be recorded, and this in turn has implications for the modeling of the hemodynamic response. Second, uncontrolled movement complicates imaging clinical seizures. Obviously, convulsive seizures or seizures characterized by violent movements cannot be imaged in an MRI scanner for safety reasons. But even very small movements of the head seen in myoclonic jerks, absence seizures, or simple focal seizures may be problematic for the interpretation of voxel-based fMRI analyses, as this movement-related noise and *edge-effects* will be correlated to the experimental effect of interest (the clinical seizure) (Lemieux et al. 2007). For these reasons, technical advances in image registration, field-corrected image reconstruction, and techniques to detect activations that are robust to large-amplitude movements during scanning are especially relevant to fMRI imaging in epileptic seizures (see Yeo et al. 2008).

In the next sections we review the papers on fMRI imaging of epileptic seizures. We also describe briefly the different types of clinical epileptic phenomena and their suitability for fMRI imaging, as well as differences in models of neuronal physiology that inform the interpretation of these fMRI data.

14.6 Focal Epilepsies and the Concept of an *Epileptogenic Focus*

The central clinical problem in epilepsy and epileptic seizures may be conceptualized as episodes of abnormal, excessive synchrony in neural networks. These episodes are primarily divided into focal and generalized seizures defined by the absence of clinical or EEG data that would indicate focal onset.

The concept of an *epileptogenic focus* initiating these episodes of abnormal, excessive synchrony is widely accepted in focal seizures. The details of exactly how this epileptogenic focus creates a seizure are complex and controversial (for reviews see McCormick and Contreras 2001; Avanzini and Franceschetti 2003) but in outline may be as follows: In normal brain, bursting pyramidal neurons in the neocortex synapse on nearby excitatory neurons to form recurrent excitatory networks and on GABAergic inhibitory interneurons that modulate this excitatory network. In epileptic brain, failure of these inhibitory dynamics leads to synchronous depolarization and prolonged after-hyperpolarization of large populations of neurons. This phenomenon, termed the *paroxysmal depolarizing shift*, is seen on EEG as an epileptiform spike or sharp wave. Infrequently, for reasons not completely understood, excitatory neurons *outside* the epileptogenic focus start phase locking to the epileptic bursting discharges seen on EEG. This, in turn, starts a cascade of neuronal and extracellular events, the result of which is a clinical seizure.

14.7 Neurovascular Coupling in Focal Epilepsy

Understanding this is important because this outline has consequences for fMRI imaging of focal seizures. These neuronal dynamics result in a supernormal increase in the cerebral metabolic rate of oxygen (CMRO2; Folbergrová et al. 1981). In response, cerebral blood flow and cerebral blood volume, capillary and venous blood oxygen, and BOLD contrast increase dramatically. Indeed, exactly these dynamics were directly observed and described by Penfield in induced epileptic seizures during epilepsy surgery in the 1930s: "… the cerebral arteries pulsate violently.... Their color becomes a bright red and arteries, which were not seen to pulsate before the seizure may now begin to do so visibly. In fact this recovery may go so far that the veins themselves take on an arterial hue" (Penfield 1933).

Several groups using BOLD fMRI in patients with frequent focal seizures have successfully imaged these dynamics. The inferences in these papers are tentative but nonetheless very interesting. First, the amplitude of the BOLD signal increase in focal seizures is large, from 2 % for seizures without clinical accompaniment to increases as large as 40 % in a patient with focal motor seizures (Jackson et al. 1994), compared to the 0.5–1 % increase in BOLD usually seen in cognitive fMRI experiments. This dramatic increase in BOLD signal means that seizures may be identified even in the absence of a clinical or EEG correlate. Indeed, in several papers seizures are identified simply by visually inspecting the BOLD time series for stereotyped signal increases, without the use of spatial statistics or linear regression models (Jackson et al. 1994; Detre et al. 1995; Krings et al. 2000).

The second interesting observation is that this opportunity to directly visualize the dynamics of the BOLD signal then enables mapping the spatial and temporal sequence of a seizure even as this *precedes clinical onset*. This is important for two reasons: First, intracranial EEG recordings directly from the brain usually demonstrate epileptic seizures starting seconds to minutes before clinical onset. Second, clinical onset of a seizure may reflect propagation from the epileptogenic focus and not the ictal onset zone. This is nicely demonstrated in the paper by (Krings et al. 2000) for a single seizure in a patient with a right central tumor and focal motor seizures of the left foot. Visual analysis of the BOLD time series demonstrated an increase in the BOLD signal 65 s preceding clinical onset in the epileptogenic focus adjacent to the tumor but distant from the somatotopic representation for the foot and then followed by a BOLD signal increase in the left foot area coincident with clinical seizure onset.

The third interesting observation relates to the technical development of simultaneous EEG and fMRI. This is important, as it enables fMRI imaging of seizures recorded on EEG that have no obvious clinical correlate (termed electrographic seizures; this also applies to subtle generalized seizures – see next section). This is important for the obvious reason that increases in the BOLD signal are nonspecific and may reflect any number of physiological or technical influences, quite apart from subclinical seizure activity. Conversely, the statistical interpretation of BOLD signal dynamics that correspond to an electrographic seizure on EEG is not straightforward and depends on the dataset. The first paper reporting this technique by (Salek-Haddadi et al. 2002), for example, recorded a single left temporal electrographic seizure of 41 s duration in a patient with frequent simple focal seizures. This electrographic seizure was then modeled as a single neural event using a Fourier basis set to avoid assumptions about the shape of the HRF, and an F contrast was used to test for variance due to the effects of interest (the seizure). The time course for this cluster of time-locked variance on the F map was then extracted and entered into a second model as a single covariate of interest. This demonstrated a BOLD signal increase of 2.5 % over baseline at 6 s following EEG onset in the left anterior temporal lobe (maximum beta value, concordant with the EEG localization) and left inferior parietal cortex (statistical maximum).

In comparison, the second paper reporting this technique by (Kobayashi et al. 2006) recorded

twenty-five brief focal electrographic seizures lasting 2–6 s in a patient with right temporoparietal gray matter nodular heterotopias. Maps of the t-statistic were created using four different hemodynamic response functions (HRFs) with peaks at 3, 5, 7, and 9 s. These t-statistic maps demonstrated widespread and intense activation, including the abnormal right temporoparietal cortex (+10.7 %) but also a clear maximum over the right angular gyrus (+6.1 %) some distance from the inferior temporal localization on EEG. This was interpreted as indicating that the seizures started in the dysplastic cortex but did not generate a visible EEG change.

This last observation that BOLD signal increases may also identify focal seizures without EEG correlate also imposes a very strong constraint on the use of the EEG to model seizures. As an example of this from our laboratory, BOLD fMRI was successfully used in a patient with frequent focal motor seizures of his right face but without EEG correlate. During the fMRI acquisition, no definite clinical seizures were recorded. Nonetheless, visual inspection of these BOLD signal changes demonstrated clear, episodic BOLD signal increases of 3–4 % in the posterior left frontal lobe that were consistent with the localization of focal seizures subsequently recorded on intracranial EEG (Detre et al. 1995). This is important because EEG is frequently normal in focal seizures arising from the medial or basal temporal or interhemispheric neocortex.

14.8 Benign Childhood Focal Epilepsies

Benign childhood focal epilepsies are of special interest in understanding focal seizures. These include the commonest epileptic seizures in children; interestingly, none of these syndromes occur in adults probably due to age-related processes in the developing brain. Most children with these syndromes have an excellent prognosis, often with only one or several seizures. These epilepsy syndromes are nonetheless well suited for EEG-fMRI experiments due to the very high frequency of interictal discharges.

The usefulness of EEG-fMRI for understanding these epilepsy syndromes is demonstrated in a paper by (Archer et al. 2003a) in a child with benign epilepsy with centrotemporal spikes (BECTS, the most frequent of the benign childhood focal epilepsies). This demonstrated the expected increase in BOLD signal in sensorimotor cortex corresponding to the epileptiform discharges on EEG and consistent with the stereotyped facial twitching described in seizures in these BECT patients. More interesting, complex changes in the BOLD signal were also described in the prefrontal cortex and anterior cingulate of the default mode network and consistent with deficits in attention and concentration in these children, echoing the network hypothesis introduced earlier (Archer et al. 2003a, b; Lengler et al. 2007).

A second example of this network hypothesis and the usefulness of EEG-fMRI is the childhood occipital epilepsies, in which the EEG localizes the epileptic activity to the posterior head regions but very often clinically the abnormalities also involve the parietal and temporal areas. In several of these children, EEG-fMRI recordings have been helpful by demonstrating BOLD signal increases and, presumably, neuronal dysfunction in the posterior parietal lobes, distant from the occipital spike focus found using EEG source analysis and, importantly, more consistent with the individual clinical seizures in these children (Leal et al. 2006).

These papers also raise an important technical issue for modeling fMRI experiments in epilepsy. Specifically, (Jacobs et al. 2008) analyzed 64 EEG-fMRI event types in 37 children from 3 months to 18 years old. HRFs calculated for each BOLD event type using a Fourier basis set demonstrated significantly longer peak times of the HRF in the youngest children (0–2 years), suggesting a different coupling between neuronal activity and metabolism or blood flow. Less easy to understand is the observation that even as the t-value increased with frequent spikes in these children, the amplitude of the HRF decreased with spike frequency. These observations, if correct, would indicate that unique HRF models may be required for fMRI with high spiking

rates, a quite common situation in children (Jacobs et al. 2008).

14.9 Generalized Epilepsies

In contrast to focal seizures, generalized seizures are defined by sudden, spontaneous, and transient abnormal hypersynchronization of neuronal activity in both hemispheres simultaneously. Clinically, these are described as spells of impaired consciousness (or *absence*), myoclonic jerks, or tonic-clonic (convulsive) seizures. Of these seizures, absence seizures (or *petit mal*) are the prototype for generalized seizures. Absence seizures are brief spells of staring or unresponsiveness, as a rule less than 30 s in duration. Clinical seizures are frequent, usually (at least) every day, and are easily provoked by hyperventilation in nearly all untreated patients. On EEG, the essential feature is generalized 3–4-Hz spike-wave discharges, involving the entire brain.

14.10 The Concept of Hypersynchrony in Primary Generalized Seizures

Two theoretical lines of reasoning have been proposed for the abrupt onset and termination of the synchronous, generalized spike-wave EEG pattern in absence epilepsy (for reviews see Meeren et al. 2005; Blumenfeld 2005). The first of these is the concept of a *centrencephalic* system located in the brain stem and diencephalon that imposes the 3–4 Hz spike-wave EEG pattern on the cortex via thalamocortical projections (Penfield 1954; Buzsaki 1991). The second line of reasoning proposes that the 3–4 Hz spike-wave EEG pattern is a consequence of diffusely increased cortical excitability. According to this *corticoreticular theory*, cortical neurons respond to normal thalamocortical input by generating spike-wave discharges via cortico-cortical excitation, in the context of impaired GABAergic inhibition (Gloor 1968). Intriguingly, two recent papers suggest – in an animal model of absence epilepsy – that this phenomenon may not require diffusely increased cortical excitability, but may alternatively be initiated by a cortical epileptogenic focus that then activates the thalamocortical network, amplifying and sustaining the discharge (Meeren et al. 2005; Polack et al. 2007).

14.11 Neurovascular Coupling in Generalized Seizures

What are the consequences of this concept of hypersynchrony for fMRI imaging of generalized seizures? First, the temporal resolution of fMRI (indeed, any imaging that uses a hemodynamic signal) is limited by the delayed hemodynamic response to neural activity. This is important; as for this reason fMRI is unlikely to be especially helpful in imaging the fast cortico-cortical and corticothalamic dynamics described in these models of synchronous spike-wave on EEG in absence seizures.

Second, in generalized epilepsy the characteristic feature – at least conceptually – is the transient, abnormal synchronization of neuronal activity and not an increase (or decrease) in neuronal output (action potentials) as seen in focal seizures. For this reason, the expected hemodynamic changes in fMRI experiments of generalized seizures are less obvious than in focal seizures. Indeed, decreases and increases in BOLD signal, as well as no BOLD signal change, have all been described in fMRI experiments of generalized seizures, reflecting this different underlying physiology.

14.12 fMRI Imaging of Generalized Seizures

Spike-wave discharges may be brief (<1 s) or prolonged for as long as 30 s in children with newly diagnosed absence seizures and if brief may not have any obvious clinical correlate. Nonetheless, as a group EEG-fMRI papers describe a remarkably stereotyped fMRI correlate for generalized spike-wave discharges. This consists of a thalamic increase in the BOLD signal as well as decreases in the frontal and parietal cortex as well as posterior cingulate, seemingly irrespective of

the duration and morphology of the spike-wave discharge (Aghakhani et al. 2004; Gotman et al. 2005; Hamandi et al. 2006, Laufs et al. 2006; Moeller et al. 2008). This increased BOLD signal in the thalamus has also been recorded in animal models of absence seizures (Blumenfeld 2005; Tenney et al. 2004). These data would be consistent with the concept introduced in Section 14. 10 that that generalized spike-wave discharges activate a thalamocortical network.

More intriguing, at the cortical level the compelling finding has been a *negative BOLD response* or *deactivation* associated with generalized spike-wave discharges in the frontal, parietal, and posterior cingulate cortex (although these deactivations are variable across subjects and activations are also described). fMRI experiments to examine this unusual phenomenon in selected regions of interest have demonstrated normal coupling between cerebral blood flow (CBF) and BOLD responses and CMRO2 (Hoge et al. 1999; Stefanovic et al. 2005). fMRI experiments over the entire brain using simultaneous BOLD and arterial spin labeling (ASL) perfusion contrast demonstrate that BOLD and CBF are positively correlated during normal EEG activity and also during generalized spike wave, although the value of this correlation varied over the brain (Carmichael et al. 2008; Hamandi et al. 2008). These data indicate that neurovascular coupling is intact and that the negative BOLD signal reflects quite large decreases in CBF (from 11 to 37 %). Decreases in perfusion have also been observed during generalized spike wave using [133Xenon] SPECT (Sperling and Skolnick 1995) and optical imaging techniques (Buchheim et al. 2004).

The proposed rationale for these BOLD deactivations and decreases in CBF depends on the observation that the spatial extent of these negative BOLD signals closely matches the resting state network described by (Raichle et al. 2001) as the so-called *default mode* network of brain activity. Most observers now agree that the *deactivation* or interruption of this resting state network during generalized spike and wave explains absences as an interruption of an organized, baseline neural network (or set of networks) required for normal brain activity. This represents an important conceptual advance in our understanding of absence seizures.

Interestingly, widespread deactivations are also seen in focal seizures (as well as the expected BOLD increases). Currently, there is no agreed interpretation for these BOLD signal decreases that have been described in the opposite hemisphere or at a distance from the BOLD increase (Salek-Haddadi et al. 2002; Federico et al. 2005; Krings et al. 2000). Conceptually, deactivations in focal seizures may reflect GABAergic inhibition, but the relationship of the BOLD signal to inhibition is complex (Logothetis et al. 2001; Arthurs and Boniface 2002; Laurienti 2004). Nor do these deactivations in focal seizures appear to reflect deactivation of default mode networks as proposed above for generalized seizures (Kobayashi et al. 2006).

14.13 Continuous Seizures

Status epilepticus refers to a *continuous seizure* or frequent seizures without return to normal, happening for more than 30 min – in contrast to the vast majority of epileptic seizures that terminate spontaneously in several minutes. In these instances recording the seizure becomes trivial. This is nonetheless at odds with the clinical imperative to use medicines to stop seizures and, with a few exceptions, precludes fMRI imaging. The two potential exceptions to this are (1) generalized absence status epilepticus and (2) focal motor status epilepticus (termed *epilepsy partialis continua*).

14.13.1 Absence Status Epilepticus

Absence status epilepticus is probably the commonest of all continuous seizures and the most likely to be imaged using functional neuroimaging. Typical absence status presents as an impairment of consciousness that may last for hours and occasionally for days before the seizure is recognized, although most patients recognize what is happening. Once recognized, intravenous benzodiazepines

usually stop absence status epilepticus. No papers to date describe the fMRI imaging of absence status epilepticus in humans. In a marmoset model of absence status, EEG-fMRI at 4.7 T of spike-wave discharges for more than 60 min duration demonstrated BOLD increases in the thalamus and sensorimotor cortex (Tenney et al. 2004), resembling the dynamics reviewed earlier for spike-wave discharges in humans. Interestingly, despite the higher field strength and robust clinical phenomena in this model, no significant negative BOLD changes were seen.

14.13.2 Epilepsy Partialis Continua

Epilepsy partialis continua (EPC) is a focal, nonconvulsive form of status epilepticus, presenting as irregular twitching or jerking, often involving the hand or face, for hours or days (and, in some cases, even years). Implicit in this description is the observation that EPC is frequently resistant to antiepileptic medicines. Conversely, this presents unique opportunities to arrange for diagnostic imaging procedures of focal seizures, including fMRI. Lazeyras et al. (2000), for example, used multiple advanced MRI techniques including EEG-fMRI, to image a patient with EPC. This demonstrated an area of increased BOLD signal that was concordant with a new hyperintensity in the occipital region on FLAIR imaging, as well as elevated lactate, decreased N-acetylaspartate (NAA), and elevated choline (Cho) on [(1)H] MR spectroscopy. This NAA level remained reduced even following seizure control, demonstrating irreversible focal neuronal injury from EPC despite the disappearance of the FLAIR signal abnormality.

14.14 Reflex Seizures

In unusual cases of epilepsy, seizures may also be provoked by recognizable stimuli. This may be a simple external stimulus such as flashing lights, startle, or touch or a more elaborate stimulus, for example, reading, performing calculations, eating, or playing Rubik's cube (an example of praxis-induced seizures). These reflex seizures have the obvious advantage for fMRI that events can be induced on demand during image acquisition. The several elegant fMRI experiments in persons with reflex epilepsies demonstrate that fMRI may be useful to localize epileptiform activity in these conditions, as well as advancing our understanding of the mechanisms of seizure onset.

14.14.1 Photosensitive Epilepsy

In this epilepsy syndrome, persons with generalized epilepsy demonstrate a photoparoxysmal (or photoconvulsive) response on EEG in response to flash stimulation. In the only fMRI experiment to date to study this response, EEG-fMRI and [(1)H] MRS were performed in 16 persons with generalized epilepsy, including 9 persons with photosensitive epilepsy, and 12 normal subjects (Hill et al. 1999). Prominent visual cortex activation was seen in all normals and persons with epilepsy during flash stimulation. Photoparoxysmal spike-wave activity on EEG was evoked in only 3/9 epileptics; no BOLD correlate was seen for this photoparoxysmal response. Interestingly, irrespective of the presence of a spike-wave response to the photic stimulation, photosensitive persons demonstrated a larger area of visual cortex activation with photic stimulation than normal as well as a marked undershoot in the BOLD signal following the end of photic stimulation. MRS performed without photic stimulation demonstrated a slight but significant increase in lactate levels in the visual cortex in photosensitive persons, compared to generalized epilepsy or controls. These intriguing findings would support the hypothesis of increased cortical hyperexcitability introduced earlier, at least for the subset of persons with IGE and photosensitivity, reflected in increased vascular reactivity and BOLD signal in the visual cortex.

14.14.2 Reading Epilepsy

Reading epilepsy is an unusual epilepsy characterized by myoclonic movements of the mouth

and throat in persons when they read, especially if aloud. Archer et al. (2003b) identified two individuals with reading epilepsy who agreed to EEG-fMRI imaging of their clinical seizures. The subjects were instructed to read silently for 30 s; this was then compared to visual fixation. In both subjects, reading recruited normal visual and language areas. In one of these subjects, interictal epileptiform discharges on EEG-fMRI demonstrated increased BOLD signal in the left precentral gyrus, concordant with the activation pattern seen in reading in the left middle frontal gyrus. Interestingly, the left central sulcal patterns in both subjects appeared abnormal, leading to the intriguing hypothesis that reading-induced seizures may start as a focal seizure in the left dorsolateral prefrontal cortex that is recruited in reading.

14.14.3 Writing Epilepsy

Abreu et al. (2005) described this condition in a 33-year-old right-handed person in whom seizures started as dystonic posturing and then myoclonic jerks of the right hand 1 min after starting to write that would lateralize to the left hemisphere. Paradoxically, EEG during these seizures demonstrated generalized spike-wave discharges that were maximal over the right (not left) centroparietal head regions. SPECT imaging during a seizure also was discordant, demonstrating increased cerebral perfusion over right frontoparietal cortex. Interestingly, fMRI performed (without EEG) using a writing paradigm demonstrated extensive, intense, abnormal left frontal (supplementary motor area) activation induced by writing that then suddenly terminated with the onset of myoclonic jerking. More intriguingly, the spatial and temporal sequence of this BOLD signal preceding clinical onset of the seizure are consistent with the hypothesis introduced earlier that generalized discharges on EEG (as in this patient) may not require diffusely increased cortical excitability, but may be initiated by a cortical epileptogenic focus – in this instance, in the neuronal networks in the left frontal lobe that subserve writing.

14.14.4 Musicogenic Epilepsy

Musicogenic epilepsy is characterized by focal seizures precipitated by certain types of music or sometimes music played by certain combinations of instruments. However, thinking about, remembering, or playing music may also precipitate a clinical seizure. The stimulus may also be exquisitely specific, for example, in Sutherling's patient; seizures were triggered only by the hymn *Now thank we all our God* played on the organ (Sutherling et al. 1980). Morocz et al. (2003) performed fMRI (but not EEG) on a patient with musicogenic epilepsy triggered by the song *I Believe In You And Me*, performed by Whitney Houston. EEG recordings and ictal SPECT performed previously in this patient had localized seizure onset in the left anterior temporal lobe, even though music function is usually considered to be lateralized to the right hemisphere (at least in nonmusicians). Music was played in a block design, for 39 s per block, for 10 repetitions. A similar but different song, *Somebody Bigger Than You Or I*, from the same album was used as the control condition. The contrast of epileptic music to control music demonstrated BOLD increases in the frontal lobes and especially the right; but no increased BOLD signal in the left temporal lobe. Conversely, using only the five auras elicited by the music as a contrast, BOLD increases were seen in the both the right frontal and left anterior temporal lobes. As the left temporal lobe is not known to play any role in music and was not activated by the epileptogenic music, the authors hypothesized that left anterior temporal lobe onset on in this patient was secondary to the right frontal activation seen on BOLD, perhaps reflecting the emotional processing of music.

14.15 The Future

These uses of fMRI to advance our understanding of epilepsy and to visualize epileptogenic networks in vivo in persons with generalized or focal epilepsy are so compelling that it seems certain development of new fMRI applications in epilepsy will continue. It is of course impossible

to anticipate the direction for fMRI in epilepsy, but it seems certain that experiments in the future will address (at least) two of the topics already introduced, namely, the concept of a preictal state and the dynamics blood flow and oxygenation in focal epileptic activity.

14.15.1 The Concept of a Preictal State

Perhaps the most surprising idea to emerge from fMRI experiments reviewed here is the concept that changes in the BOLD signal may precede the EEG or clinical onset. This concept of a *preictal state* in focal epilepsy has been advanced in several papers using linear (Litt et al. 2001) and nonlinear (Lehnertz and Elger 1995; Elger and Lehnertz 1998) analysis of EEG time series that appear to demonstrate changes in the EEG minutes to hours preceding clinical onset. This idea that hemodynamic changes may define a preictal state has also been investigated in various experiments using different modalities to measure cerebral blood flow. Both increases (Adelson et al. 1999; Makiranta et al. 2005) and decreases (Hoshi and Tamura 1992) in tissue oxygenation have been found tens of seconds before seizure onset. Transcranial doppler studies have demonstrated increases in perfusion 20 min before focal as well as generalized spike-wave seizures (De Simone et al. 1998; Diehl et al. 1998; Weinand et al. 1994). Indirect measurement of CBF in patients with temporal lobe epilepsy has demonstrated significant increases in CBF in the region of the seizure focus 10–12 min preceding onset on intracranial EEG (Weinand et al. 1997). Preictal hyperperfusion in the absence of clinical or EEG change has also been seen on SPECT scans fortuitously obtained minutes prior to seizure onset and during video-EEG monitoring (Baumgartner et al. 1998).

Now, two recent papers on fMRI experiments in epilepsy add to this idea that hemodynamic changes may define a preictal state. The first paper reviewed 143 concurrent EEG-fMRI studies of interictal epileptiform discharges performed at the Montreal Neurological Institute. Of these studies, BOLD changes in nearly half of the datasets preceded interictal epileptiform discharges on EEG used to model the BOLD signal by several seconds.

In the second paper, three persons with frequent frontal lobe seizures on falling asleep recorded their typical seizure in the fMRI scanner (Federico et al. 2005). BOLD changes over the entire brain were first analyzed using a t-contrast to compare a 1 min block immediately preceding seizure onset to a 1-min block beginning several minutes earlier. The time course was then extracted for the ROI defined by the maximal cluster on this t map and for a mirror ROI in the contralateral hemisphere, and these time courses were compared. Each patient showed significant, focal BOLD signal changes (either increased or decreased) up to 20 min over the presumed seizure focus.

Obviously, the interpretation of the hemodynamic changes in these papers is complex. Nonetheless, the concept of a preictal state, if correct, would represent a tremendous advance in our understanding of how seizures happen. This, in turn, is very important clinically because if a preictal state can be detected, then various interventions and devices become possible to intervene and prevent clinical seizures.

14.15.2 Is Perfusion Matched to CMRO2?

The second interesting question for the future concerns the dynamics blood flow and oxygenation in focal epilepsy. It follows from the papers reviewed that the BOLD signal increases during focal seizures, consistent with increases in blood flow and blood oxygenation (and thus a decrease in deoxygenated hemoglobin) and blood volume. It nonetheless is not absolutely clear that this increase in blood flow is adequate to meet the increased CMRO2 in focal seizures. This uncertainty is motivated by recent studies using fast optical techniques in animal models and in humans to image these hemodynamic signals (for a superb review, see Schwartz 2007). Even in normal cognitive experiments, fast optical techniques demonstrate a rapid

decrease in tissue oxygenation and an increase in deoxygenated hemoglobin that precedes the increase in blood flow, termed the *initial dip* of the BOLD response (Frostig et al. 1990). Conversely, in epilepsy fast optical measurements that demonstrate this increase in deoxygenated hemoglobin may persist despite an increase in blood volume and blood flow, during both interictal epileptiform discharges and epileptic seizures (Bahar et al. 2006; Shariff et al. 2006; Suh et al. 2006a, b). Similar data exists from earlier studies using implanted oxygen-sensitive electrodes in humans that recorded a decrease in tissue oxygenation preceding and during focal seizures (Dymond and Crandall 1976). These data, if correct, would indicate that cerebral blood flow and blood oxygen, although increased during focal seizures, may be inadequate for the supernormal increase in CMRO2 seen in focal epilepsy. This, of course, has tremendous implications for our understanding of epilepsy and epileptogenesis.

This conjecture has implications for fMRI as well. If the transient increase in deoxygenated hemoglobin is earlier and more focal than the subsequent increase, then imaging this transient hemodynamic change may be an excellent marker for the epileptic focus. For BOLD contrast fMRI, this means future development of higher resolution magnets and imaging techniques optimized to image this initial dip in hemoglobin oxygenation, as opposed to imaging increases in BOLD contrast, may be the smarter approach.

References

Abreu P, Ribeiro M et al (2005) Writing epilepsy: a neurophysiological, neuropsychological and neuroimaging study. Epilepsy Behav 6(3):463–466

Adelson PD, Nemoto E et al (1999) Noninvasive continuous monitoring of cerebral oxygenation periictally using near infrared spectroscopy: a preliminary report. Epilepsia 40:1484, Äì1489

Aghakhani Y, Bagshaw AP et al (2004) FMRI activation during spike and wave discharges in idiopathic generalized epilepsy. Brain 127(Pt 5):1127–1144

Archer JS, Briellman RS et al (2003a) Benign epilepsy with centro-temporal spikes: spike triggered fMRI shows somato-sensory cortex activity. Epilepsia 44(2):200–204

Archer JS, Briellmann RS et al (2003b) Spike-triggered fMRI in reading epilepsy: involvement of left frontal cortex working memory area. Neurology 60(3): 415–421

Arthurs OJ, Boniface S (2002) How well do we understand the neural origins of the fMRI BOLD signal? Trends Neurosci 25(1):27–31

Avanzini G, Franceschetti S (2003) Cellular biology of epileptogenesis. Lancet Neurol 2(1):33–42

Bahar S, Suh M et al (2006) Intrinsic optical signal imaging of neocortical seizures: the 'epileptic dip'. Neuroreport 17(5):499–503

Baumgartner C, Serles W et al (1998) Preictal SPECT in temporal lobe epilepsy: regional cerebral blood flow is increased prior to electroencephalography-seizure onset. J Nucl Med 39(6):978–982

Blumenfeld H (2005) Cellular and network mechanisms of spike-wave seizures. Epilepsia 46(Suppl 9):21–33

Boor R, Jacobs J et al (2007) Combined spike-related functional MRI and multiple source analysis in the non-invasive spike localization of benign rolandic epilepsy. Clin Neurophysiol 118(4):901–909

Buchheim K, Obrig H et al (2004) Decrease in haemoglobin oxygenation during absence seizures in adult humans. Neurosci Lett 354(2):119–122

Buzsaki G (1991) The thalamic clock: emergent network properties. Neuroscience 41(2–3):351–364

Carmichael DW, Hamandi K et al (2008) An investigation of the relationship between BOLD and perfusion signal changes during epileptic generalised spike wave activity. Magn Reson Imaging 26(7):870–873

De Simone R, Silvestrini M et al (1998) Changes in cerebral blood flow velocities during childhood absence seizures. Pediatr Neurol 18:132, Äì135

Detre JA, Zhang W et al (1994) Tissue specific perfusion imaging using arterial spin labeling. NMR Biomed 7(1–2):75–82

Detre JA, Sirven JI et al (1995) Localization of subclinical ictal activity by functional magnetic resonance imaging: correlation with invasive monitoring. Ann Neurol 38(4):618–624

Di Bonaventura C, Carnfi M et al (2006) Ictal hemodynamic changes in late-onset rasmussen encephalitis. Ann Neurol 59(2):432–433

Diehl B, Knecht S et al (1998) Cerebral hemodynamic response to generalized spike-wave discharges. Epilepsia 39:1284, Äì1289

Dymond AM, Crandall PH (1976) Oxygen availability and blood flow in the temporal lobes during spontaneous epileptic seizures in man. Brain Res 102(1):191–196

Elger CE, Lehnertz K (1998) Seizure prediction by nonlinear time series analysis of brain electrical activity. Eur J Neurosci 10(2):786–789

Espay AJ, Schmithorst VJ et al (2008) Chronic isolated hemifacial spasm as a manifestation of epilepsia partialis continua. Epilepsy Behav 12(2):332–336

Federico P, Abbott DF et al (2005) Functional MRI of the pre-ictal state. Brain 128(Pt 8):1811–1817

Folbergrová J, Ingvar M et al (1981) Metabolic changes in cerebral cortex, hippocampus, and cerebellum during

sustained bicuculline-induced seizures. J Neurochem 37(5):1228–1238
Frostig RD, Lieke EE et al (1990) Cortical functional architecture and local coupling between neuronal activity and the microcirculation revealed by in vivo high-resolution optical imaging of intrinsic signals. Proc Natl Acad Sci U S A 87(16):6082–6086
Garraux G, Hallett M et al (2005) CASL fMRI of subcortico-cortical perfusion changes during memory-guided finger sequences. Neuroimage 25(1):122–132
Gloor P (1968) (ADD)
Gotman J (2008) Epileptic networks studied with EEG-fMRI. Epilepsia 49(Suppl 3):42–51
Gotman J, Grova C et al (2005) Generalized epileptic discharges show thalamocortical activation and suspension of the default state of the brain. Proc Natl Acad Sci U S A 102(42):15236–15240
Greicius MD, Krasnow B et al (2003) Functional connectivity in the resting brain: a network analysis of the default mode hypothesis. Proc Natl Acad Sci U S A 100(1):253–258
Hamandi K et al (2006) EEG-fMRI of idiopathic and secondarily generalized epilepsies. Neuroimage 31(4): 1700–1710
Hamandi K, Laufs H et al (2008) BOLD and perfusion changes during epileptic generalised spike wave activity. Neuroimage 39(2):608–618
Hauser WA, Hesdorffer DC (1990) Epilepsy: frequency, causes and consequences. Demos Vermande, New York
Hauser WA, Annegers JF et al (1991) Prevalence of epilepsy in Rochester, Minnesota: 1940, Äì1980. Epilepsia 32:429, Äì445
Hill RA, Chiappa KH et al (1999) Hemodynamic and metabolic aspects of photosensitive epilepsy revealed by functional magnetic resonance imaging and magnetic resonance spectroscopy. Epilepsia 40(7): 912–920
Hoge RD, Atkinson J et al (1999) Linear coupling between cerebral blood flow and oxygen consumption in activated human cortex. Proc Natl Acad Sci U S A 96(16):9403–9408
Hoshi Y, Tamura M (1992) Cerebral oxygenation state in chemically induced seizures in the rat, Äîstudy by near infrared spectrophotometry. Adv Exp Med Biol 316:137, Äì142
Hwang DY, Golby AJ (2006) The brain basis for episodic memory: insights from functional MRI, intracranial EEG, and patients with epilepsy. Epilepsy Behav 8(1): 115–126
Jackson GD, Connelly A et al (1994) Functional magnetic resonance imaging of focal seizures. Neurology 44(5):850–856
Jacobs J, Hawco C et al (2008) Variability of the hemodynamic response as a function of age and frequency of epileptic discharge in children with epilepsy. Neuroimage 40(2):601–614
Kobayashi E, Hawco CS et al (2006) Widespread and intense BOLD changes during brief focal electrographic seizures. Neurology 66(7):1049–1055
Krings T, Töpper R et al (2000) Hemodynamic changes in simple partial epilepsy: a functional MRI study. Neurology 54(2):524–527
Kurtzke JF (1982) The current neurologic burden of illness and injury in the United States. Neurology 32(11):1207–1214
Laufs H, Duncan JS (2007) Electroencephalography/functional MRI in human epilepsy: what it currently can and cannot do. Curr Opin Neurol 20(4):417–423
Laufs H, Lengler U et al (2006) Linking generalized spike-and-wave discharges and resting state brain activity by using EEG/fMRI in a patient with absence seizures. Epilepsia 47(2):444–448
Laurienti PJ (2004) Deactivations, global signal, and the default mode of brain function. J Cogn Neurosci 16(9):1481–1483, No abstract available
Lazeyras F, Blanke O et al (2000) MRI, (1) H-MRS, and functional MRI during and after prolonged nonconvulsive seizure activity. Neurology 55(11):1677–1682
Leal A, Dias A et al (2006) The BOLD effect of interictal spike activity in childhood occipital lobe epilepsy. Epilepsia 47(9):1536–1542
Lehnertz K, Elger CE (1995) Spatio-temporal dynamics of the primary epileptogenic area in temporal lobe epilepsy characterized by neuronal complexity loss. Electroencephalogr Clin Neurophysiol 95(2):108–117
Lemieux L, Salek-Haddadi A et al (2007) Modelling large motion events in fMRI studies of patients with epilepsy. Magn Reson Imaging 25(6):894–901
Lengler U, Kafadar I et al (2007) FMRI correlates of interictal epileptic activity in patients with idiopathic benign focal epilepsy of childhood. A simultaneous EEG-functional MRI study. Epilepsy Res 75(1): 29–38
Litt B, Esteller R et al (2001) Epileptic seizures may begin hours in advance of clinical onset: a report of five patients. Neuron 30(1):51–64
Logothetis NK, Pauls J et al (2001) Neurophysiological investigation of the basis of the fMRI signal. Nature 412(6843):150–157
Makiranta M, Ruohonen J et al (2005) BOLD signal increase preceeds EEG spike activity, Äìa dynamic penicillin induced focal epilepsy in deep anesthesia. Neuroimage 27:715, Äì724
Mazoyer B, Zago L et al (2001) Cortical networks for working memory and executive functions sustain the conscious resting state in man. Brain Res Bull 54(3):287–298
McCormick DA, Contreras D (2001) On the cellular and network bases of epileptic seizures. Annu Rev Physiol 63:815–846
Meeren H, van Luijtelaar G et al (2005) Evolving concepts on the pathophysiology of absence seizures: the cortical focus theory. Arch Neurol 62(3):371–376
Moeller F et al (2008) Changes in activity of striato-thalamo-cortical network precede generalized spike wave discharges. Neuroimage 39(4):1839–1849
Mórocz IA, Karni A et al (2003) fMRI of triggerable aurae in musicogenic epilepsy. Neurology 60(4): 705–709

Neuroimaging Subcommission of the ILAE (2000) Commission on diagnostic strategies recommendations for functional neuroimaging of persons with epilepsy. Epilepsia 41(10):1350–1356
Penfield W (1933) [ADD]
Penfield W (1954) (ADD)
Polack PO, Guillemain I et al (2007) Deep layer somatosensory cortical neurons initiate spike-and-wave discharges in a genetic model of absence seizures. J Neurosci 27(24):6590–6599
Raichle ME (2003) Functional brain imaging and human brain function. J Neurosci 23(10):3959–3962
Raichle ME, MacLeod AM et al (2001) A default mode of brain function. Proc Natl Acad Sci U S A 98(2):676–682
Salek-Haddadi A, Merschhemke M et al (2002) Simultaneous EEG-correlated ictal fMRI. Neuroimage 16(1):32–40
Sander JW (2003) The epidemiology of epilepsy revisited. Curr Opin Neurol 16:165–170
Schwartz TH (2007) Neurovascular coupling and epilepsy: hemodynamic markers for localizing and predicting seizure onset. Epilepsy Curr 7(4):91–94
Shariff S, Suh M et al (2006) Recent developments in oximetry and perfusion-based mapping techniques and their role in the surgical treatment of neocortical epilepsy. Epilepsy Behav 8(2):363–375
Spencer SS (2002) Neural networks in human epilepsy: evidence of and implications for treatment. Epilepsia 43(3):219–227
Sperling MR, Skolnick BE (1995) Cerebral blood flow during spike-wave discharges. Epilepsia 36(2):156–163
Stefanovic B, Warnking JM et al (2005) Hemodynamic and metabolic responses to activation, deactivation and epileptic discharges. Neuroimage 28(1):205–215
Suh M, Bahar S et al (2006a) Blood volume and hemoglobin oxygenation response following electrical stimulation of human cortex. Neuroimage 31(1):66–75
Suh M, Ma H et al (2006b) Neurovascular coupling and oximetry during epileptic events. Mol Neurobiol 33(3):181–197
Sutherling WW, Hershman LM et al (1980) Seizures induced by playing music. Neurology 30(9):1001–1004
Swanson SJ, Sabsevitz DS et al (2007) Functional magnetic resonance imaging of language in epilepsy. Neuropsychol Rev 17(4):491–504
Tenney JR, Marshall PC et al (2004) FMRI of generalized absence status epilepticus in conscious marmoset monkeys reveals corticothalamic activation. Epilepsia 45(10):1240–1247
Weinand ME, Carter LP et al (1994) Long-term surface cortical cerebral blood flow monitoring in temporal lobe epilepsy. Neurosurgery 35:657, Äì664
Weinand ME, Carter LP et al (1997) Cerebral blood flow and temporal lobe epileptogenicity. J Neurosurg 86(2): 226–232
Wiebe S, Blume WT et al (2001) A randomized, controlled trial of surgery for temporal-lobe epilepsy. N Engl J Med 345:311–318
Wolf RL, Alsop DC et al (2001) Detection of mesial temporal lobe hypoperfusion in patients with temporal lobe epilepsy by use of arterial spin labeled perfusion MR imaging. AJNR Am J Neuroradiol 22(7):1334–1341
Wu R, Bruening R et al (1999) MR measurement of regional relative cerebral blood volume in epilepsy. J Magn Reson Imaging 9:435–440
Yeo DT, Fessler JA et al (2008) Motion robust magnetic susceptibility and field inhomogeneity estimation using regularized image restoration techniques for fMRI. Med Image Comput Comput Assist Interv 11(Pt 1): 991–998
Zyss J, Xie-Brustolin J et al (2007) Epilepsia partialis continua with dystonic hand movement in a patient with a malformation of cortical development. Mov Disord 22(12):1793–1796

Multimodal Brain Mapping in Patients with Early Brain Lesions

15

Martin Staudt

15.1 Introduction

The developing human brain possesses a superior potential of functional reorganization after lesions compared with the adult brain. Because of such reorganizational processes, children with early brain lesions often show abnormally located cortical representations of certain brain functions, e.g. of motor representations (Carr et al. 1993; Staudt et al. 2002a, 2004a) or of language functions (Rasmussen and Milner 1977; Staudt et al. 2002b). Nowadays, these abnormally located representations can be identified non-invasively using techniques such as functional MRI (fMRI), transcranial magnetic stimulation (TMS) or magnetoencephalography (MEG). Thus, these techniques can not only contribute to our general understanding of the processes involved in the reorganization of the developing human brain but can also be used clinically in the presurgical evaluation of children who have to undergo brain surgery, e.g. for the relief of pharmaco-refractory epilepsies originating from their lesions (Hertz-Pannier et al. 2001; Staudt et al. 2001, 2004a, b; Liégeois et al. 2006).

The clinical application of these mapping techniques in this context is particularly challenging: first, most of these patients are children, often with various degrees of cognitive impairments so that their ability to comply with the experimental requirements is often reduced; second, the brain lesions often destroy or distort anatomical landmarks, which can normally be used for the identification of eloquent brain regions; and third, the cortical representations of brain functions may have shifted because of reorganizational processes following lesions acquired during ongoing brain development. This chapter gives typical examples of examinations of children, mostly in the presurgical evaluation before epilepsy surgery, highlighting a number of important aspects.

15.2 Example 1

A 3-year-old boy suffered from therapy-refractory focal seizures originating from a cortical dysplasia (yellow arrows in Fig. 15.1) in the central (Rolandic) region of the right hemisphere. On clinical examination, left hand function was normal. Prior to possible epilepsy surgery, fMRI during a simple active hand motor task (repetitive squeezing of a toy) was used to visualize the spatial relation between the dysplasia and the primary sensorimotor representation of the contralateral hand.

Based on these findings of fMRI activation in the immediate vicinity of the dysplasia, no total resection of the dysplasia was performed.

fMRI can be used even in pre-school children to localize the primary sensorimotor region (S1M1) in the vicinity of epileptogenic lesions.

M. Staudt
Neuropediatric Clinic and Clinic for Neurorehabilitation/ Epilepsy Center for Children and Adolescents, Krankenhausstrasse 20, 83569 Vogtareuth, Germany
e-mail: martin.staudt@med.uni-tuebingen.de

S. Ulmer, O. Jansen (eds.), *fMRI – Basics and Clinical Applications*,
DOI 10.1007/978-3-642-34342-1_15, © Springer-Verlag Berlin Heidelberg 2013

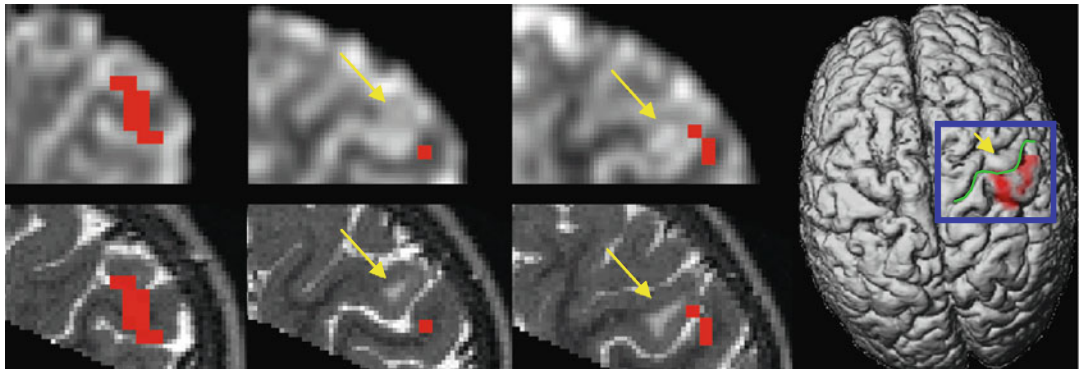

Fig. 15.1 fMRI during active left hand movement in a 3-year-old boy with a focal cortical dysplasia (hyperintense on T2; *yellow arrows*) of the right central (Rolandic) region. The fMRI activation (in *red*) is superimposed directly on the (functional) EPI images (yielding the most reliable topographical localization, since no coregistration is involved; *upper row*) after coregistration, to high-resolution structural T2-weighted images acquired in general anaesthesia during a separate session (*lower row*; Courtesy of Prof. Winkler, Olgahospital Stuttgart) as well as onto a 3D surface reconstruction (*right*). *Green line* = central sulcus; *blue rectangle* = position of the enlarged details on the *left*

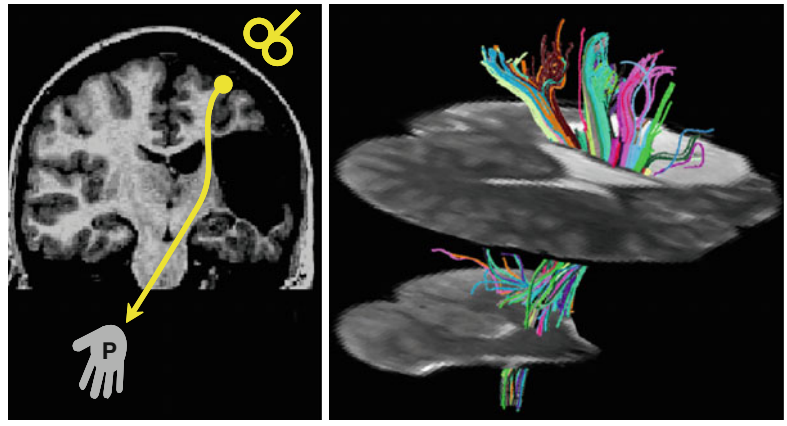

Fig. 15.2 MRI and TMS findings of a 16-year-old girl with congenital hemiparesis due to a large cortico-subcortical infarct. *Left*: coronal T1-weighted image depicting the cystic lesion. TMS (indicated by the *yellow figure-eight-coil symbol*) of the affected hemisphere elicited normal motor-evoked potentials in the paretic hand (P), confirming the presence of preserved crossed cortico-spinal projections (*yellow arrow*). *Right*: MR diffusion tensor tractography (in random colours on unweighted diffusion images; tilted axial planes, anterior-lateral-superior view) visualized numerous fibre trajectories passing through the small bridge of preserved white matter between the cystic lesion and the lateral ventricle (Adapted from Staudt et al. 2006b with permission)

15.3 Example 2

A 16-year-old girl with congenital hemiparesis due to a perinatally acquired cortico-subcortical infarct in the territory of the middle cerebral artery (MCA) showed a striking discrepancy between a large cystic lesion and relatively well-preserved sensorimotor functions (preserved grasp) of the contralateral (paretic) hand (Staudt et al. 2006b). On neurophysiological examination, TMS revealed preserved crossed corticospinal projections from the affected hemisphere to the paretic hand, and MEG identified the first cortical response to repetitive tactile stimulation of the paretic thumb (N20m) in the affected hemisphere, indicating the presence of preserved crossed spino-thalamocortical somatosensory projections. Accordingly, diffusion tensor imaging (DTI) tractography with a seed region positioned in the small bridge of preserved white matter between the enlarged lateral ventricle and the cystic lesion visualized extensive connectivity provided by this area (Fig. 15.2).

Small areas of preserved white matter can provide surprisingly extensive connectivity in patients with early brain lesions. Such projections can be visualized by DTI tractography.

15.4 Example 3

A 20-year-old young man with congenital right hemiparesis due to a large polymicrogyria in the left frontoparietal region shows partially preserved sensorimotor functions (preserved individual finger movements) of the contralateral (paretic) right hand (Staudt et al. 2004b). On neurophysiological examination, TMS revealed preserved crossed corticospinal projections from the affected hemisphere to the paretic hand. Accordingly, fMRI during a simple active hand motor task (repetitive opening/closing of the paretic hand) revealed activation in the polymicrogyric cortex. Thus, both TMS and fMRI demonstrate that, in this patient, the polymicrogyric cortex harbours the primary motor representation of the paretic hand (Fig. 15.3).

Dysgenic cortex (here: polymicrogyria) can fulfil primary motor functions, with normal descending corticospinal motor projections. This can be confirmed by a combination of fMRI and TMS.

15.5 Example 4

A 6-year-old boy with congenital right hemiparesis due to a complex hemispheric malformation suffered from pharmaco-refractory seizures (Staudt et al. 2001). Clinical examination showed preserved individual finger movements in the paretic hand and massive mirror movements during voluntary movements of both the paretic and the non-paretic hand. Prior to epilepsy surgery, fMRI and TMS were performed to identify the primary motor representation of the paretic hand. TMS of the affected hemisphere did not elicit any response, whereas TMS of the contralesional hemisphere elicited bilateral responses with similar latencies. This indicated the presence of fast-conducting ipsilateral corticospinal projections, allowing the contra-lesional hemisphere to exert motor control over the paretic hand. Accordingly, fMRI during a simple active hand motor task (repetitive opening/closing of the paretic hand) revealed activation in the "hand knob" area of the contra-lesional hemisphere,

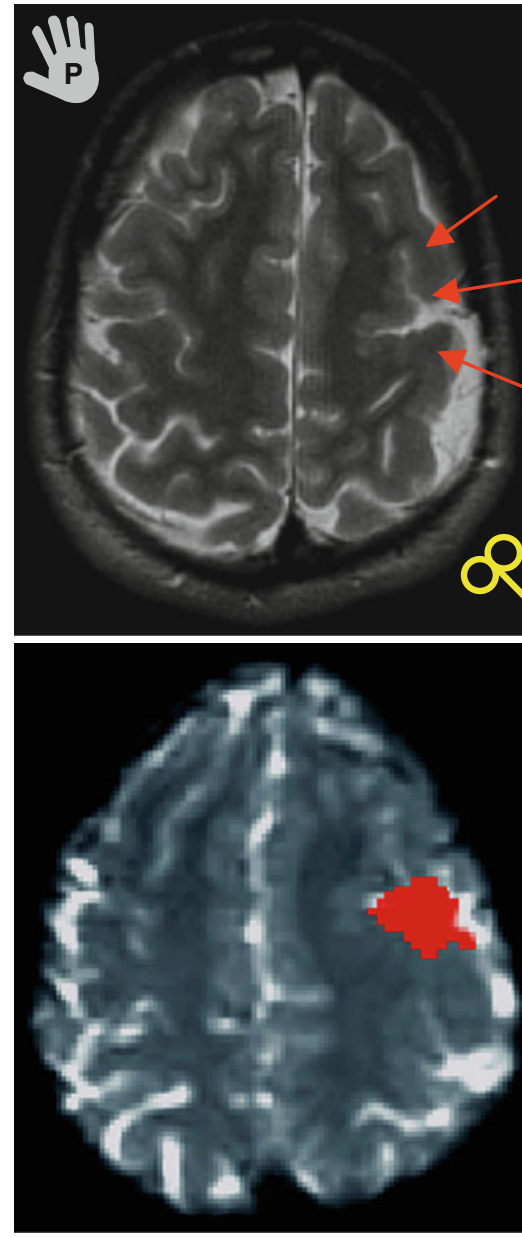

Fig. 15.3 MRI and TMS findings of a 20-year-old man with congenital hemiparesis due to a large polymicrogyria. *Top*: axial T2-weighted image depicting the polymicrogyria in the left frontoparietal region (*red arrows*). TMS (indicated by the *yellow figure-eight-coil symbol*) of the affected hemisphere elicited normal motor-evoked potentials in the paretic hand (P), confirming the presence of preserved crossed corticospinal projections. *Bottom*: fMRI activation (in *red*; superimposed on the functional EPI) during active movement of the paretic hand revealed activation in the polymicrogyria, approximately opposing the Rolandic region in the contra-lesional hemisphere

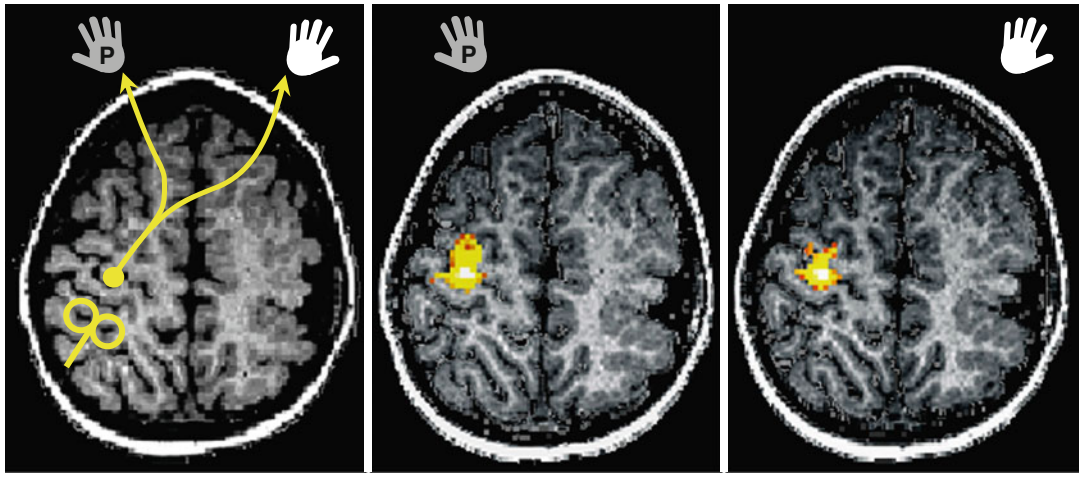

Fig. 15.4 MRI and TMS findings of a 6-year-old boy with congenital hemiparesis due to a complex hemispheric malformation. *Left*: axial T1-weighted image depicting the malformation of almost the entire hemisphere. TMS (indicated by the *yellow figure-eight-coil symbol*) of the contra-lesional hemisphere elicited not only the normal contralateral responses in the non-paretic hand but also ipsilateral motor-evoked potentials in the paretic hand (P), demonstrating the presence of ipsilateral corticospinal projections. fMRI during active movement of the paretic hand (*middle*) revealed activation in the hand knob area of the contra-lesional (ipsilateral) hemisphere, not different from the activation elicited by active movement of the non-paretic hand (*right*)

not different from the fMRI activation elicited by movements of the non-paretic hand. Active grasping was still possible after functional hemispherectomy (Fig. 15.4).

Early brain lesions (malformations but also defective lesions) can induce shifting of the primary motor representation (M1) of the paretic hand to the contra-lesional hemisphere (with ipsilateral corticospinal tracts).

15.6 Example 5

A 19-year-old woman with congenital right hemiparesis due to a large unilateral periventricular brain lesion showed preserved individual finger movements in the paretic hand and massive mirror movements during voluntary movements of both the paretic and the non-paretic hand (Staudt et al. 2006a). As in the patient of Example 4, TMS of the affected hemisphere did not elicit any response, but TMS of the contra-lesional hemisphere elicited bilateral responses with similar latencies. This indicated the presence of ipsilateral corticospinal projections, allowing the contra-lesional hemisphere to exert motor control over the paretic hand. Accordingly, fMRI during a simple active hand motor task (*active* opening/closing of the paretic hand) revealed activation in the "hand knob" area of the contra-lesional hemisphere but also activation in the contralateral Rolandic region, an area from which no motor-evoked potentials could be elicited by TMS. fMRI during *passive* hand movement also elicited activation in the contralateral Rolandic region (i.e. of the affected hemisphere), suggesting preserved somatosensory functions in this region. And indeed, MEG recorded the first cortical response to repetitive tactile stimulation of the paretic thumb (N20m) in the contralateral Rolandic region, confirming this region to harbour the primary somatosensory representation (S1) of the paretic hand. Finally, DTI with a seed region in the dorsal brain stem (tegmentum pontis) visualized ascending spinothalamocortical projections bypassing the lesion on their way to this preserved somatosensory representation of the paretic hand. This observation can be explained by the fact that developing thalamocortical somatosensory projections had not yet reached their cortical target areas by the time of the insult (the early third trimester of

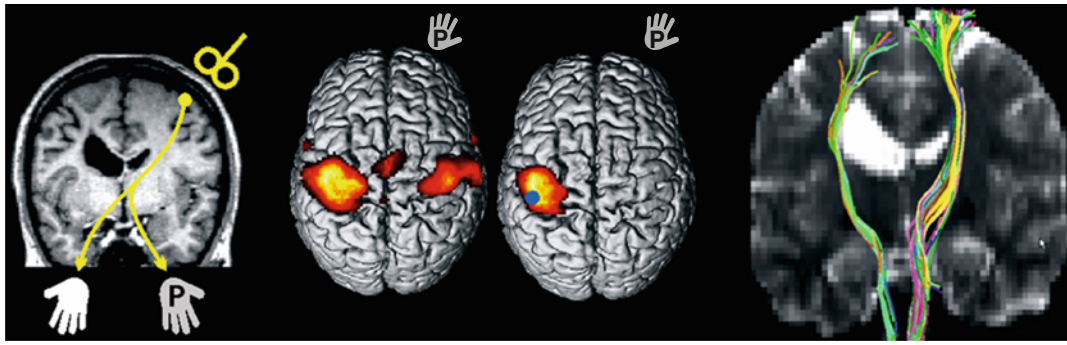

Fig. 15.5 MRI, TMS, fMRI, MEG and DTI tractography findings of a 19-year-old female with congenital hemiparesis due to a unilateral periventricular brain lesion. *Left*: coronal T1-weighted image depicting the periventricular lesion. TMS (indicated by the *yellow figure-eight-coil symbol*) of the contra-lesional hemisphere elicited not only the normal contralateral responses in the non-paretic hand but also ipsilateral motor-evoked potentials in the paretic hand (P), demonstrating the presence of ipsilateral corticospinal projections. *Middle*: fMRI during active (*middle left*) and passive (*middle right*) movement of the paretic hand. The *blue circle* indicates the position of the dipole reconstruction from MEG recording of the first cortical response to tactile stimulation of the paretic thumb. *Right*: diffusion tensor imaging (DTI) tractography of ascending spino-thalamocortical projections, with seed regions in the dorsal brain stem (tegmentum pontis) and in the subcortical Rolandic white matter of both hemispheres (From Staudt et al. 2006a with permission)

pregnancy; Kostovic and Judas 2002) so that these outgrowing fibres could find an alternative route in the preserved tissue, thus forming "axonal bypasses" around the defective areas (Staudt et al. 2006a).

This example and similar cases (Thickbroom et al. 2001; Staudt et al. 2006a) teach important lessons for the application of non-invasive imaging techniques in children with early brain lesions:

1. Different mechanisms are available for reorganization of primary motor and primary somatosensory representations (shifting to the contra-lesional hemisphere for motor functions, forming axonal bypasses around a lesion for somatosensory functions).
2. This can lead to a "hemispheric dissociation" between the primary motor (M1) and the primary somatosensory (S1) representations of a paretic hand.
3. fMRI of passive hand movement alone is not suited to identify the "sensorimotor representation" of a paretic hand (see Fig. 15.5); the reorganization of the primary motor representation in Example 5 would have been missed with the "normal-looking" result for passive hand movement!

15.7 Conclusions

Non-invasive mapping techniques such as fMRI, TMS, MEG and DTI tractography are useful techniques in the presurgical diagnostic workup of children with early brain lesions. These situations often require a combined use of complementary techniques.

The combination of fMRI (during active movements) and TMS is well suited to identify motor representations, with TMS being specific for areas from where corticospinal projections originate and fMRI visualizing the entire sensorimotor network with a high spatial resolution in three dimensions (Thickbroom et al. 2001; Staudt et al. 2002a; 2004a, b). This is important for the identification of (a) the spatial relation between M1 and an epileptogenic lesion (as in Example 1), (b) of a preserved M1 in dysgenic cortex (as in Example 3) and (c) of a reorganization of M1 into the contra-lesional hemisphere (as in Examples 4 and 5). In this respect, patients with a "hemispheric dissociation" between M1 and S1 (Thickbroom et al. 2001; Staudt et al. 2006a) are particularly challenging, since here fMRI of active hand movements typically yields bilateral Rolandic activation.

The combination of fMRI (during passive movements) and MEG is well suited to identify somatosensory representations, with MEG (due to its high temporal resolution) being specific for primary somatosensory representations (e.g. the cortical projection areas of somatosensory fibres) and fMRI visualizing the somatosensory network with a high spatial resolution in three dimensions (Staudt et al. 2006a; Wilke et al. 2008). Similar to the motor system, this combination can identify (a) preserved somatosensory projections in preserved white-matter bridges (as in Example 2), (b) a preserved S1 in Rolandic cortex overlying even large lesions (as in Example 5) and (c) a preserved S1 in dysgenic cortex (no example included here, see Gerloff et al. 2006).

Finally, DTI tractography can visualize preserved projections in the vicinity of a lesion (as in Example 2) or "axonal bypasses" around a lesion (as in Example 5). Because of the uncertainties involved in this new technique, we still recommend to use such information only when additional evidence (e.g. neurophysiological evidence from TMS or MEG) for the existence of such projections is available.

References

Carr LJ, Harrison LM et al (1993) Patterns of central motor reorganization in hemiplegic cerebral palsy. Brain 116:1223–1247

Gerloff C, Braun C et al (2006) Coherent corticomuscular oscillations originate from primary motor cortex: evidence from patients with early brain lesions. Hum Brain Mapp 27:789–798

Hertz-Pannier L, Chiron C et al (2001) Functional imaging in the work-up of childhood epilepsy. Childs Nerv Syst 17:223–228

Kostovic I, Judas M (2002) Correlation between the sequential ingrowth of afferents and transient patterns of cortical lamination in preterm infants. Anat Rec 267:1–6

Liégeois F, Cross JH et al (2006) Role of fMRI in the decision-making process: epilepsy surgery for children. J Magn Reson Imaging 23:933–940

Rasmussen T, Milner B (1977) The role of early left-brain injury in determining lateralization of cerebral speech functions. Ann N Y Acad Sci 30:355–369

Staudt M, Pieper T et al (2001) Functional MRI in a 6-year-old boy with unilateral cortical malformation: concordant representation of both hands in the unaffected hemisphere. Neuropediatrics 32:159–161

Staudt M, Grodd W et al (2002a) Two types of ipsilateral reorganization in congenital hemiparesis: a TMS and fMRI study. Brain 125:2222–2237

Staudt M, Lidzba K et al (2002b) Right-hemispheric organization of language following early left-sided brain lesions: functional MRI topography. Neuroimage 16:954–967

Staudt M, Gerloff C et al (2004a) Reorganization in congenital hemiparesis acquired at different gestational ages. Ann Neurol 56:854–863

Staudt M, Krägeloh-Mann I et al (2004b) Searching for motor functions in dysgenic cortex: a clinical TMS and fMRI study. J Neurosurg 101:69–77

Staudt M, Braun C et al (2006a) Developing somatosensory projections bypass periventricular brain lesions. Neurology 67:522–525

Staudt M, Erb M et al (2006b) Extensive peri-lesional connectivity in congenital hemiparesis. Neurology 66:771

Thickbroom GW, Byrnes ML et al (2001) Differences in sensory and motor cortical organization following brain injury early in life. Ann Neurol 49:320–327

Wilke M, Staudt M et al (2008) Somatosensory system in two types of motor reorganization in congenital hemiparesis: topography & function. Hum Brain Mapp 30:776–788

Special Issues in fMRI Involving Children

16

Lucie Hertz-Pannier and Marion Noulhiane

16.1 Introduction

Anatomo-functional brain imaging methods have considerably developed recently, leading to new advances in *noninvasive* exploration of children with various neurological disorders. In addition, fMRI is a unique method to study healthy children because it does not require any exogenous tracer and has no reported side effects. It thus gives us access to normative data of functional brain development and to the assessment of networks reorganization following focal anatomical or functional abnormality, which is particularly relevant in the child's immature and plastic brain.

In children, like in adults, the main (if not only) clinical application of fMRI is to provide reliable presurgical mapping of eloquent cortices (mostly motor areas and lateralized language areas) and of their relationship with the planned resection (tumor or epilepsy surgery), in order to select patients, tailor resection, and avoid postoperative deficits referring to chapter 15. Staudt in the same book! When combined with clinical, neuropsychological, and neurophysiological data, anatomo-functional MRI techniques offer the possibility of a noninvasive presurgical work-up, therefore reducing the need for invasive techniques and impacting on patient management (Petrella et al. 2006). In that context, all methods implemented must reach a high sensitivity for detecting activated areas at the individual level, and high reproducibility, especially in young children. Thus, most teams use validated tasks amenable to patients with variable abilities, in robust block paradigms, and with individual analyses involving adapted statistical thresholds. Still most needed here are further validation and standardization of the whole process across clinical teams.

Beside this unique clinical application, a number of studies have been performed recently to unravel the neural correlates of various cognitive developmental pathologies (learning disorders, ADHD, autism) and of brain plasticity in children with brain lesions, such as motor plasticity in cerebral palsy, or language plasticity in focal epilepsies. These clinical research studies do involve very different experimental conditions with dedicated and often elaborated paradigms in homogeneous populations of children (patients and controls), which are analyzed as groups to extract differences over the whole groups with increased statistical power, but do not usually provide clinically relevant individual results.

However, the mere comparison between the explosive number of fMRI studies in adults (both cognitive and clinical studies) and the still limited studies in children highlights the intrinsic difficulties of studying children. While all methods and tools have been developed for analyses

L. Hertz-Pannier (✉) • M. Noulhiane
UMR 663, INSERM, Paris Descartes University,
Neurospin, I2BM, DSV, CEA,
Paris, France
e-mail: lucie.hertz-pannier@cea.fr

S. Ulmer, O. Jansen (eds.), *fMRI – Basics and Clinical Applications*,
DOI 10.1007/978-3-642-34342-1_16,

of healthy adult brains, there are numerous specific limitations and constraints pertaining to data acquisition and analysis in the pediatric population that all remain to be solved to make these tools fully adapted to a wide range of clinical pediatric applications. Recently, the possibility of studying brain functional connectivity with fMRI *during rest* (rs-fcMRI for resting-state functional connectivity MRI) has opened new research avenues and makes it possible to overcome a number of those limitations, to assess the development of neuronal networks from birth on, in health and in disease.

16.2 Issues Pertaining to the Developing Brain

Several characteristics of the developing brain are prone to influencing signal in fMRI studies in children, especially in neonates and infants, and are the field of intense research using multimodal imaging with fMRI, DTI, morphometric analyses, and most recently resting-state functional connectivity studies.

16.2.1 Brain Maturation

The main biological characteristics of the developing brain is a succession of progressive and regressive events, with intense synaptic growth from birth on leading to synaptic overproduction and redundancy in the primary school years, and then slow progressive synaptic pruning with stabilization of efficient networks during adolescence and young adulthood (Huttenlocher and Dabholkar 1997). This triphasic process is common to all functional systems but occurs with different time windows in different networks (earlier in primary systems and later into the second decade for associative networks), and is accompanied by changes in glucose consumption and blood flow, according to the known steps of psychomotor development (Chugani et al. 1987; Chiron et al. 1992). At a macroscopic level, these biological events can be seen as local/regional variations of cortical thickness (Faria et al. 2012; Sowell et al. 2003), chapters of both white matter signal and volume and of DTI parameters (decrease in mean and radial diffusivity, increase in fractional anisotropy (Faria et al. 2012)) and finally in global and regional brain growth (Giedd and Rapoport 2010).

Ongoing myelination is accompanied by a longer latency of electrical induction which speeds up rapidly during the first year of life, and more slowly thereafter, during the specification and maturation of functional networks.

16.2.2 Evolution of BOLD Signal According to Age

These combined biological events in immature networks have been associated with changes in oxidative metabolism and vascular reactivity during neuronal firing that may contribute to the negative BOLD response during visual and sensorimotor stimulations described in neonates and infants (Marcar et al. 2004; Morita et al. 2000). Part of this negative response might however also be attributed to sedation, which is commonly used at this age. In a study of nonsedated and sometimes awake 3-month-old infants, using ecological auditory stimuli, we found a hemodynamic response largely comparable to adults (Dehaene-Lambertz et al. 2002). Beyond the first weeks of life, BOLD hemodynamic response is very stable across ages, although with possible increase in amplitude until adulthood (Shapiro et al. 2007), and some variations across tasks (Brauer et al. 2008). Finally, physiological noise is increased in children due to larger cardiovascular and respiratory dynamics, although with no clearly demonstrated effect on BOLD signal.

16.3 Experimental Design of Pediatric fMRI Studies

16.3.1 Paradigm Design

So far, all fMRI clinical applications in children have used "block paradigms" in which the patient performs the tasks repeatedly over the activation and reference periods (usually 20–40 s each),

repeated several times in a single trial. This approach is the most robust and reproducible, because of good statistical power per unit time, and therefore is used when individual assessment is required in clinical applications such as presurgical motor or language mapping. It can also be usefully applied in clinical research programs where children are to be pooled in groups for comparing activation differences according to a clinical marker.

More sophisticated single-event paradigms, which allow monitoring brain response during processing of a single stimulus, may prove very useful in patients, since they avoid using a control task (thus reducing a possible confounding factor); they permit to account for response variability; and they offer extended possibilities of experimental designs (e.g., for memory studies). But their implementation remains difficult in clinical environments (especially in children), due to long acquisition times, lower sensitivity, very large data volumes, and the need for customized analyses.

16.3.2 Choice of Tasks

In children like in adults, the most critical part of fMRI studies resides in the choice of activation and reference tasks, as data analysis most often relies on "cognitive subtraction" (Binder et al. 1995), that is, the resulting activated areas are thought to sustain the cognitive components that are involved in the activated state but *not* in the reference one. For example, the comparison of an auditorily cued semantic decision task and a simple tone discrimination task shows mainly regions involved in semantic processes (Humphries et al. 2006). On the other hand, the comparison of a more global language task (such as sentence generation to a given noun) compared to simple "rest" will show a larger functional network that includes numerous modules of receptive and expressive language (phonemic discrimination, phonological encoding, lexical retrieval, semantic analysis, and syntax, along with verbal working memory and pre-articulatory processing). However, the underlying assumptions of cognitive subtraction may not be fulfilled in all cases because of nonlinearity of many brain processes (interactions may also be studied).

The experimental constraints of fMRI are particularly demanding for children, as tasks paradigms are designed in a very rigid manner, according to a priori models of BOLD contrast time course. In addition, the intrinsically low BOLD contrast/noise ratio requires the repetition of events to gain statistical power. In that context, task complexity is a critical issue, in terms of temporal sequence of both stimuli and responses and of cognitive/attentional demands. According to the research question, the age, and the cognitive level of the subjects, block paradigms with simple tasks may be suited, for example, alternating hand movements with rest for motor mapping. It must be noted that in all cases, tasks can be adapted to the performance level (even in motor paradigms, from complex sequential finger tapping to simple grasp movement, or passive wrist flexion-extension). In cognitive paradigms, explicit tasks are most often used and adapted to subject's abilities and performance. In children, this means using tasks adapted from age-validated neuropsychological tests and appropriately testing them prior to MRI. Implicit tasks can be implemented, especially when there is strong a priori on the localization of signal changes, by the presentation of visual and/or auditory stimuli not requiring any particular response (e.g., Monzalvo et al. 2012). In such paradigms, it is important however to drive the child's attention to the stimuli, usually by the means of a simple additional task (e.g., button press on the detection of a particular visual or auditory stimulus), which also allows to monitor the compliance, but will not be analyzed further.

Strictly passive tasks are also used in particular cases, such as passive movements in patients with motor deficits, or presentation of auditory stimuli in neonates, and asleep infants and toddlers (Dehaene-Lambertz et al. 2002; Redcay et al. 2007). While these tasks may reveal interesting activation often grossly comparable to that of active ones, they obviously do not provide the same level of functional assessment. Sedation can be occasionally used to assess basic functions

for clinical purposes (e.g., auditory stimulation before cochlear implantation (Altman and Bernal 2001)), but with a careful choice of anesthetic drugs and dosages (Heinke and Koelsch 2005).

Multiple tasks are required when testing complex cognitive functions such as language (Wilke et al. 2008) in order to highlight the different processes involved and to increase the robustness of lateralization assessment by combining the different tasks in individual subjects (Rutten et al. 2002). In some instances, lateralization may vary according to the type of task, either as a normal pattern (e.g., left semantic vs. right prosody) or related to mixed language representation secondary to left focal epilepsy or lesion (e.g., with left dominance for expressive language and right dominance for receptive one).

The use of "rest" as reference task is being debated because of the uncertainty regarding what children do while resting. In all cases, giving clues to the child on "rest" instruction (listening to the scanner noise, concentrating on its own breathing…) may help him/her to comply. On the one hand, it has the advantage of simplicity for very young or disabled children that may have difficulties in rapidly alternating different tasks. On the other hand, children may involuntarily not stop the "activation task" (resulting in falsely negative results), and there are no means of controlling ongoing cognitive activity during rest. Some experimenters therefore use very simple tasks as references such as finger tapping or tone listening in children with sufficient mental flexibility.

16.3.3 Control of Task Performance

A precise monitoring of task performance is desirable for fully analyzing and interpreting activation maps, as the latter reflect what has been actually done during scanning. This may be obtained using computer-based paradigms with visual or audio presentation of items, by monitoring responses of the patient pressing on joystick or buttons. In that case, balancing the side of responding hand may be useful to avoid systematic bias in brain activation. However, this right-left shift may complicate the paradigm for young children not fully acquainted with their own right and left side. In language fMRI studies, most tasks are performed silently, producing similar activation as overt ones, but avoiding artifacts due to face movements. Not only this precludes any performance control, but it may also not be amenable to deficient children. Some experimenters have used oral responses (with on line response recording), associated to adapted MR sequences with no image acquisition during the response interval to avoid articulation-related motion artifacts while taking benefit from the delayed hemodynamic response. Nowadays, eye-tracking devices are being increasingly used to monitor eye movements during cognitive tasks, but the experimental setup is very demanding for children and currently remains largely beyond the possibilities of a clinical environment.

16.3.4 Group Studies in Children

In the context of clinical research, it is often desirable to compare two selected groups to unravel a relevant biomarker. Reference data in healthy children can be helpful to understand the spatiotemporal sequence of the development of cognitive systems and to assess brain plasticity in various early pathologies. In the majority of cases, group comparison is thus made with typical children that must be carefully matched to the patient population. However, the criteria for matching pediatric populations are not straightforward, and depend on research goals: while in most studies, the control population is composed by age and gender-matched typical children, this might not prove appropriate in other cases, for example, the study of intellectual deficiencies, where it might be more relevant to use "developmental age" (or associated parameter) as matching criterion. Indeed, gross differences in performance between groups are likely to be accompanied by different strategies and activation patterns, with no particular insight on the specific neural substrates underlying them. In addition, there is very often a recruitment bias in the control population of

published studies, with children with high IQ and/or of high socioeconomic status. One way to alleviate the constraints on group selection is to select "implicit tasks" that do not require active responses (Monzalvo et al. 2012). Still, many other parameters are likely to influence the comparison between two groups with variable cognitive abilities, such as motion artifacts, performance on the reference task, attentional resources, and level of anxiety.

In many developmental studies, the variables of interest strongly depend on age and learning and therefore constitute continuous variables, making it arbitrary to split the population into age groups. Correlation analysis can be performed over the entire group, to demonstrate developmental patterns and their differences between typical and nontypical children (Fair et al. 2008).

Most developmental studies use a cross-sectional design to gather a sample of selected children in a limited period of time, sometimes in multicenter studies (e.g., the NIH pediatric database, http://pediatricmri.nih.gov/nihpd/info/index.html). While having definitive advantages in terms of efficiency, such designs suffer from many confounding factors associated to intersubject variability. The ideal way of studying development is to design longitudinal studies (e.g., Szaflarski et al. 2006), but such designs pose multiple ethical, technical, and methodological questions that make them very challenging, especially when planned on a relatively long term. In particular, the recruitment and follow-up of children over several years, and the maintenance of the methodological setup to keep sequential data comparable despite technical upgrades, are constraints extremely difficult to deal with.

16.3.5 Age Versus Performance

Finally, a critical goal in developmental studies is to disentangle the effects of age and of performance, which are obviously strongly correlated in children. Different approaches can be used (Church et al. 2010), such as the constitution of groups with different ages but similar performances (e.g., Schlaggar et al. 2002), or the post hoc grouping of subjects with equivalent performances. Alternatively, regressing performance variables in the analysis can be helpful if the age regressors are not collinear.

16.4 Technical Issues

As BOLD contrast to noise ratio increases with field strength, the use of higher fields (3 T vs. 1.5 T) increases the sensitivity of functional MRI, despite aggravation of various artifacts (which can be corrected in most cases). This better sensitivity to BOLD contrast can be used to either shorten acquisition time or increase spatial resolution to improve localization of activated clusters, which can be valuable in young children with small heads, all while maintaining adequate signal-to-noise ratio. High-field MR imaging is being considered by the FDA as minimal-risk procedure up to 8 T for adults and children and up to 4 T for neonates below 1 month of age. Nowadays, 3 T fMRI has become standard in babies and children as in adults, including in healthy subjects.

Multichannel coils with parallel imaging have further improved the signal-to-noise ratio, but have made it even more critical to use coils adapted to the head size. In neonates and infants, smaller coils such as knee coils provide better signal and improve the sensitivity of fMRI. MR-compatible incubators are needed to prevent hypothermia in neonates (especially premature babies), but they are expensive and cumbersome. Smaller dedicated 1.5 T MR systems are being designed to be placed in NICU and improve the feasibility of MRI and fMRI in neonates.

One issue often neglected in fMRI is the acoustic noise created by Lorentzian forces secondary to gradient switching in EPI images (in functional imaging as well as in DTI). Not only may noise prevent children to remain still because of anxiety and/or difficulty to sleep, but the risk of acoustic trauma must also not be underestimated, as functional MRI sequences often reach 110-dB levels at peak frequencies. As noise depends upon multiple sequence parameters (type of sequence, spatial and temporal resolutions, parallel imaging), acoustic measurements

should be performed for each sequence, whenever possible. Careful prevention must always be undertaken, including in asleep or sedated infants and children, with a whole variety of devices (earplugs, headphones, foams). Some companies offer hardware options reducing acoustic noise of various sequences by modifying gradients shape and strength.

Temporal resolution of fMRI is mainly dependent upon the shape of the hemodynamic response, which is comparable to adults after the first few months of life (see above). Shortening TR from standard 3–5 to 2–2.5 s provides better sampling of subtle variations of the hemodynamic response and increases statistical power (Beware of acoustic noise!).

Spatial resolution can strongly benefit from higher fields, and it is current standard practice to acquire 3 T EPI data with $3 \times 3 \times 3$-mm^3 voxels. Although this nominal resolution is not clearly reflected in the results due to numerous steps of spatial filtering, it permits better localization of activated clusters in small anatomical regions (e.g., in neonates and infants) by reducing partial volume effects. On the other hand, motion artifacts are more conspicuous and problematic in highly resolved scans.

Finally, "real-time fMRI" may be of particular value in children, as it provides continuous monitoring of the acquisition, by reconstructing and analyzing the images "online," and providing a constant update of the quality of the functional study. This is especially relevant in clinical studies, where paradigms are being kept simple, with reasonable datasets and standard statistical analyses. This might prove a challenge in more sophisticated studies with event-related paradigms, large datasets, and analyses requiring heavy post-processing.

16.5 Feasibility

The constitution of appropriate groups in pediatric clinical research fMRI studies has been partly discussed above. Recruitment of minor subjects (especially when healthy) poses specific ethical questions, requiring to justify the enrolment of children instead of adults in all steps of the research and to ensure full agreement of parents (written consent) and of the child (oral or written consent whenever possible, after providing extended and adapted information). Globally, like in adults, fMRI is recognized worldwide as noninvasive minimal-risk procedure for pediatric studies, even at high field and in neonates and infants, after ruling out the usual contraindications of MRI (intracorporeal ferromagnetic bodies, which are much rarer in children than in adults). Research on healthy fetuses remains not authorized in most countries.

In fMRI activation studies, gaining child's cooperation is critical. However, MR imagers remain very child-unfriendly experimental devices, and strict immobility is mandatory to avoid motion artifacts. Obtaining compliance to the tasks is therefore a challenge in young or deficient children and requires extra time and resources with at best a dedicated visit before the study with the child and the parents. This visit with the experimenter(s) that will perform the fMRI study (such as radiologist, neurologist, or neuropsychologist) is necessary to show the child the imager and explain the tasks, to train him/her to remain still in a mock scanner if available, and to practice the fMRI tasks, but with different stimuli than those used in the fMRI session (to avoid test-retest effects). It also makes it possible to adapt the paradigm in case of deficiency or poor compliance to optimize feasibility of clinical studies, and sometimes to cancel the study, when sufficient compliance cannot be obtained, thus optimizing scanner occupancy.

During scanning, many adaptations can be implemented to improve child's comfort and quietness, such as having the experimenter and the parents in the magnet room, interacting very often to the child through intercom, playing movies during anatomical scans, monitoring child's movements through an MR-compatible camcorder, and providing him/her a feedback along scanning. In all cases is good head immobilization necessary to discourage movements. Providing the child with visual inputs also decreases head motion artifacts (Yuan et al. 2009).

Time issues are critical in fMRI as statistical power depends directly on the number of scan repetitions thus on scanning duration. On the one hand, it is necessary to keep paradigms long enough to get reliable contrast to noise, on the other hand, attentional resources and compliance of children cannot be maintained during too long scans. Higher-field acquisitions (3 T) do contribute to alleviate these constraints. Still, unlike in adults where 20-min runs are commonly acquired, in most children the whole acquisition is preferably segmented in shorter runs of 3–5 min. It is cautious to repeat similar runs during a single session, given the high rate of poor quality data in younger children due to motion or transient incompliance. A whole study must be completed in 20 min in babies or poorly compliant children and in up to 1 h in older school-age children with no significant cognitive or behavioral impairments. Acquisition may also be split in two or more sessions separated by a break, even on separate days, as there are no limitations given the absence of known side effects. In that case, images from different sessions must be coregistered during analysis.

Eventually, cooperation can be obtained for adapted paradigms from children with a developmental age of around 5–6 years and/or IQs around 60, provided there are no behavioral disorders. Passive tasks can be used in sleeping or quiet neonates, infants, and children (either with or without sedation), using receptive language tasks or sensory stimulations.

However, as obtaining cooperation is not possible in younger children, and because sedation cannot be performed in healthy children (for obvious ethical reasons), there is nowadays only a couple of fMRI studies in healthy children between 6 months and 5–6 years (Redcay et al. 2007), since getting natural sleep in such a noisy environment remains a challenge. The emergence of resting-state functional connectivity studies, which require no cooperation from the child, has made it recently possible to get new insights on brain development during early life (see below). Overall, the attrition rate of fMRI studies in children is much higher than in adults, especially in activation studies. It is thus common practice when designing a pediatric study, to plan the inclusion of 10–30 % more children than needed, to account for the risk of failure and/or missing data.

16.6 Data Analysis

Head motion remains a critical limiting factor, especially in uncooperative, young, or debilitated patients, and is more frequent and pronounced in boys than in girls (Yuan et al. 2009). The use of dedicated registration algorithms is most often necessary, but the choice of registration method is rather empirical, depending upon the type and amplitude of movements. Motion parameters can be introduced as regressors of noninterest in the analysis to reduce variance. Some algorithms are based on data interpolation to replace heavily corrupt images; others take into account discarded thus missing data. Overall, the resulting corrected images must be checked carefully, as a significant amount of registered data must eventually be discarded due to insufficient correction, therefore reducing the statistical power of the analysis.

The choice of anatomical template for pediatric group studies is conditioned by the children's age range. Indeed, brain growth and maturation in the first years of life make it inappropriate to use adult templates for normalization and tissue segmentation. Generating dedicated templates (Dehaene-Lambertz et al. 2002; Wilke et al. 2008) provides a common spatial referential to compare children. However, in our experience, it is possible to use adult templates for studies from 6–7 years of age on.

Statistical analysis of pediatric datasets follows the same rules and constraints as in adults and strongly depends upon the goal of the study: in group comparisons, the most frequent goal is to reach high specificity to demonstrate a difference between groups in which individual datasets are analyzed with strictly similar thresholds, often resulting in low sensitivity at the individual level. In pediatric data, analysis must also take into account the frequency of small samples and of missing data within functional runs, given the

high attrition rate. Hemodynamic models adapted for temporal sequences with occasional missing data and nonparametric tests of small samples that may not follow a normal distribution are useful in challenging studies of poorly compliant infants and children (e.g., Dehaene-Lambertz et al. 2006).

Finally, as pediatric studies very often contain continuous variables associated with learning and development (age, performance level, and any associated co-variable), correlation studies are useful to avoid the arbitrary constitution of age groups and to unravel the continuous dynamics of specific learning (Ghetti et al. 2010).

By contrast, in presurgical studies of patients, the main goal is to optimize at the individual level the sensitivity of the detection of activated areas, which may depend upon multiple factors (i.e., age, efficiency, attention, pathology, medications). In such circumstances, testing multiple thresholds and taking into account the performance level is likely to increase the sensitivity of detection of activated networks, especially in children. Overall, in presurgical studies, thresholding and interpretation of activation maps still depend heavily on the expertise of the investigator, especially for datasets containing residual motion artifacts.

16.7 Multimodal Imaging

Multimodality is an exquisite asset of MRI, as comprehensive assessment of brain anatomy, microstructure, function, and biochemistry can be obtained within a single session using different techniques, giving access to structural, functional, and effective brain connectivity during normal and abnormal development. Beyond anatomical imaging for localization of activated clusters, 3D T1 images can be used for morphometric studies of gyration/sulcation development and organization (Dubois et al. 2008) for quantification of gray and white matter volumes (e.g., Giedd et al. 2006). DTI can demonstrate the structural connectivity of involved regions, by tracking the main fascicles (i.e., corticospinal tracts, optic radiations, arcuate and uncinate fasciculi) and monitoring their maturation (Bassi et al. 2008; Dubois et al. 2008). Functional connectivity can be studied in fMRI acquisitions during rest (see below, and Fransson et al. 2009).

16.8 Clinical Research Applications: Studying Plastic Changes of Functional Systems

In the recent years, fMRI has emerged as a unique tool to study the exquisite plasticity of the immature brain, which sustains both normal learning and memory acquisition, and recovery following a focal insult or abnormality with an incomparably better functional outcome as compared to adults with similar condition. As the maturation of functional networks is asynchronous, starting with "lower-level" primary functions such as vision and motricity, and followed by elaborated cognitive functions (i.e., language, memory, executive functions), it can be anticipated that pathological plasticity will strongly depend upon the maturation stage of the involved network, among other parameters.

The general pattern of functional maturation of a specific network has been shown as regional specialization of activated clusters with age, starting from a more widespread activation in earlier ages (Gaillard et al. 2000, 2003), and associating progressive and regressive changes in different regions (Brown et al. 2005). These focal changes are associated with changes in short- and long-range connectivity, as recently discovered by functional connectivity studies (see below).

Importantly, fMRI has also demonstrated that some malformations of cortical development (i.e., heterotopias, polymicrogyrias) may retain functional cortical organization (i.e., vision, motor, language) with a risk of postoperative deficit in case of a resection of the malformed cortex (Liegeois et al. 2004). By contrast, it seems that Taylor-type focal cortical dysplasias do not retain functional activity within the area containing balloon cells (hypersignal on FLAIR or T2 images; Marusic et al. 2002).

16.8.1 Motor Cortex

Plasticity of the primary motor cortex has been probed in several series of adult and pediatric patients with tumors, epilepsy foci, or perinatal lesions located in the central region. These studies have shown consistent activation in regions predicted by the electrophysiological data (Penfield's homonculus), when the lesion was relatively remote from the functional areas. However, plastic changes of the cortical organization could also be demonstrated in cases of lesions within the motor cortex, in excellent agreement with the results of cortical stimulation. Motor plasticity has been extensively studied with fMRI and transcranial magnetic stimulation (TMS) in children with congenital hemiplegia, showing that the central and precentral cortex contralateral to the lesion can take over the impaired function and that the presumed date of the prenatal injury is critical to the development of functional compensation and plasticity (Staudt et al. 2003). Those children with earlier insults (1st trimester) had the best motor recovery, sustained by the persistence of the ipsilateral corticospinal tract. This type of reorganization was however much less observed in children with later lesions (around birth). Overall, these results confirm the good localizing power of motor fMRI in children as well as in adults and its utility in the surgical planning of focal lesions of the central region.

16.8.2 Language

It has been long known that morphological brain asymmetries present from fetal life on are related to speech dominance of the left hemisphere (Dehaene-Lambertz et al. 2006). Recently, fMRI studies in 3-month-old infants showed that the leftward asymmetry of language networks is detectable in early infancy, before oral language development has started (Dehaene-Lambertz et al. 2002, 2010), in agreement with behavioral data in newborns and infants. Longitudinal fMRI studies of healthy children and adolescents have demonstrated that asymmetry is weaker in early childhood (Redcay et al. 2007; Szaflarski et al. 2006) and strengthens over the years toward the adult left dominant pattern, with increasing activation of the frontal lateral cortex (Broca's area) and to a lesser degree of the left posterior temporal region (Wernicke's area) and the angular gyrus (Ressel et al. 2008; Szaflarski et al. 2006) and with differential regional effects of both age and performance (Brown et al. 2005).

In adults with early left hemisphere injury or epilepsy, the capacity of language networks to reorganize either by interhemispheric shift (Rasmussen and Milner 1977) or by intrahemispheric displacement of eloquent areas (Ojemann et al. 1989) is known to depend on many variables such as handedness, type and location of the lesion, age at onset and duration of epilepsy, and baseline of cognitive status. In children, language develops quite similarly in the case of left or right hemispheric lesions, although a slight and transient difference in performances can be disclosed (Vargha-Khadem et al. 1985). Recent data have demonstrated subtle language deficits in children suffering from left hemisphere lesions (MacWhinney et al. 2000) further highlighting the early left hemisphere superiority for language development. The clear deleterious effect of early epilepsy has been demonstrated (Vargha-Khadem and Polkey 1992). However, electrical stimulation in children has shown that developmental lesions and early-onset seizures do not displace language cortex from prenatally determined sites, whereas lesions acquired before the age of 5 years may cause language to relocate to the opposite hemisphere only when language cortex is destroyed (Duchowny and Harvey 1996).

In children with left temporal lobe epilepsy (LTLE), we found that atypical expressive language organization depends on handedness and epilepsy duration and that right-handed children usually retain left dominance, even more so children with mesial TLE, by contrast to adults. These results suggest that early LTLE hampers the normal progression of left hemispheric specialization of expressive, but not receptive, language during childhood, especially in left-handers, supporting the hypothesis of a long-term effect of epilepsy on the organization of language that is

strongly linked with the plasticity of the motor system.

In a series of 100 adults (Woermann et al. 2003), the discordance between invasive gold standard Wada test and fMRI in terms of language dominance remained low (9 % of cases). As the only "gold standard" for testing the function of a specific cortical area would be an unexpected postoperative deficit, which is fortunately rare, it is most often impossible to conclude on language dominance in such cases. In fact, in both tests do results depend on the nature and multiplicity of language tasks and of subject's compliance. Expressive tasks such as sentence or word generation seem to lateralize better and have a better correlation with invasive methods like the Wada test (Lehericy et al. 2000). Even though fMRI assessment of language dominance is now everyday practice in adults, fMRI is not yet fully accepted as a standard of care in pediatric epilepsy because of the limited number of published studies validating the method in children (Hertz-Pannier et al. 1997, 2002; Liegeois et al. 2006).

Presurgical cortical mapping of regions sustaining language functions may be needed when surgery is to be performed in the dominant hemisphere, but these techniques carry significant risks and are difficult to perform. Direct intraoperative cortical stimulation, considered the gold standard in adults, is not feasible in most children. More recently, perioperative stimulation using subdural grids and depth electrodes has been challenged because of its insufficient sensitivity in children. This may result from reorganized language distribution, limited testing capacity, and incomplete myelination leading to higher stimulation thresholds. Concordance between intraoperative stimulations and fMRI has been assessed in both isolated cases and case series in adults and children (de Ribaupierre et al. 2012; FitzGerald et al. 1997; Roux et al. 2003; Ruge et al. 1999; Rutten et al. 2002). Co-localization of fMRI activated regions and significant stimulation sites have been reported within 1–2 cm in several preliminary reports. Overall, in these studies the sensitivity of fMRI varied from 38 to 100 %, and the specificity from 65 to 97 % (de Ribaupierre et al. 2012). However, strict comparison of both techniques remains difficult, since cortical stimulation discloses only limited regions critical to language functions, whereas fMRI does not provide hierarchical information on the numerous activated regions, which may not all be essential to language (low specificity).

Finally, fMRI is a unique tool for longitudinal studies to follow the postoperative reorganization of functional networks. For example, the longitudinal observation of a case of left hemisphere disconnection in a 10-year-old boy suffering from Rasmussen encephalitis demonstrated the late ability of the nondominant hemisphere to take over main language functions in a network mirroring that of the left hemisphere before surgery (Hertz-Pannier et al. 2002).

16.8.3 Reading

Reading may be broken down into two components that are distinct from functional, anatomical, and developmental points of view. First, the visual word form area (VWFA), in the mid-portion of the left occipitotemporal sulcus, encodes the abstract identity of strings of visual letters (Cohen and Dehaene 2004). This system reaches its adult properties by the age of 10, although it is already left lateralized at the time of reading acquisition (Monzalvo et al. 2012). Second, children learn how to translate letter strings into phonological and lexical representations subtended by left perisylvian language areas. An fMRI study of reading has shown a dissociated reorganization of both components in a child with early left inferotemporal epilepsy before reading acquisition, who maintained a left perisylvian language network, with an elective contralateral plasticity of the VWFA allowing to resect the left epileptic focus without creating any postoperative reading deficit (Cohen et al. 2004).

16.8.4 Memory Functions

Nowadays, researches have convincingly demonstrated that temporal lobe epilepsy can cause specific memory deficit in children with distinct patterns of deficiencies according to the lateralization of seizures (Jambaque et al. 1993, 2007;

Kelly et al. 2009; Lehericy et al. 2000; Liegeois et al. 2004, 2006; Lin et al. 2008; Liu et al. 2008; Mabbott and Smith 2003). Children with left temporal lobe epilepsy (LTLE) are mostly impaired on verbal episodic memory, whereas children with right temporal lobe epilepsy (RTLE) are mostly impaired on visuospatial episodic memory. Overall children tend to recover from memory deficits better than adults suggesting that the developing brain may benefit from compensatory cognitive and neurofunctional mechanisms (Jambaque et al. 2007). Whereas fMRI exploration of episodic memory is just emerging in pediatric TLE and preliminary data suggest that a fronto-hippocampo-parietal network may be bilaterally impaired in left TLE, studies in adults with TLE show that mesio-temporal structures are asymmetrically impaired: activations are greater contralaterally to the epilepsy, in good concordance with individual results of the memory Wada test (Detre et al. 1998).

To investigate the role of medial temporal lobe structures in episodic memory, recent fMRI studies have concerned healthy children. These structures, that is, hippocampus and surrounding cortices including entorhinal, perirhinal, parahippocampal, and temporopolar cortices, are known to distinctly contribute to recognition memory in adults (Montaldi and Mayes 2010; Wixted and Squire 2011). Recognition memory network also includes the prefrontal cortex and thalamus, which are both highly connected with the hippocampus and parahippocampal gyrus (Wixted and Squire 2011). Using fMRI, authors have reported discrepant results on age-related changes from childhood to adulthood in these structures (Ghetti et al. 2010; Maril et al. 2010, 2011; Menon et al. 2005) Besides, the structural maturation of medial temporal lobe structures is nonlinear, which leads to distinctly consider hippocampal subregions in developmental studies.

16.9 Resting-State fMRI and Development

As shown above, investigating the maturation of functional networks underlying brain development continues to present unique scientific and methodological challenges. Recent advances in MRI methodology have qualified precise measurements of correlated activity throughout the brain, leading to the first comprehensive descriptions of functional brain networks in humans. In this vein, a growing literature deals with the development of functional networks, from infancy through adolescence, as measured by resting-state functional connectivity MRI (for reviews, see Power et al. 2012; Uddin et al. 2010). This method is now increasingly used to complement traditional task-based fMRI, but its use in developmental studies is still in its infancy.

16.9.1 Functional Connectivity

Functional connectivity is defined as the temporal coherence, or statistical dependence, between measurements of activity in different neurons or neural ensembles. rsfMRI has emerged as a novel framework for investigating the development of large-scale organization of the developing brain by measuring spontaneous, high-amplitude, low-frequency (<0.1 Hz) BOLD signal fluctuations in subjects at rest (i.e., performing no explicit task). These spontaneous fluctuations are posited to organize, coordinate, and maintain functional brain systems (Fox and Raichle 2007; Raichle 2010).

The advantages of using rsfMRI in pediatric and clinical populations are that functional brain organization can be examined independently of task performance, and a full dataset can be collected in as little as 5 min (Van Dijk et al. 2009). Indeed, rsfMRI involves collecting functional imaging data from participants as they lay in the MRI scanner, typically with eyes closed or fixating gaze on a crosshair, without any specific cognitive demand. Because the rsfMRI procedure implies insignificant cognitive load on the participant and requires relatively little time in the scanner compared to task related fMRI studies, data can be collected from low-functioning and very young populations. Functional connectivity measures derived from rsfMRI data are particularly useful in studying age-related variations in the wiring of neural networks (Supekar et al. 2009). For example, Lin et al. (2008)

suggested that sensorimotor networks emerge early in infancy and appear to develop well before visual networks.

16.9.2 Methodological Aspects

Two main methodological approaches are considered here: seed-ROI-based correlation and independent component analysis (ICA), each making significant contributions to the study of intrinsic brain architecture, and they can be used in a complementary method to clarify global and functional properties of the developing brain. Region-of-interest (ROI) seed-based analysis is the most widely used method of analysis of rsf-MRI. This hypothesis-driven approach typically involves choosing one or more ROIs and investigating their whole-brain functional connectivity, often using a regression or correlation model. Unlike ROI-based analysis, independent component analysis (ICA) is a model-free data-driven approach whereby four-dimensional fMRI data is decomposed into a set of independent one-dimensional time series and associated three-dimensional spatial maps, which all describe the temporal and spatial characteristics of the underlying signal or components (Beckmann et al. 2005). ICA is currently a widely used method for analyzing rsfMRI data (Calhoun et al. 2008). Within- and between-subject measures computed from rsfMRI are quite consistent and reproducible (Damoiseaux et al. 2006; Shehzad et al. 2009). However, the methods remain to be fully validated.

Graphs are data structures, which have nodes and edges between the nodes (Bondy and Murty 1976). Graph theoretical metrics such as clustering coefficient, path length, degree, and centrality provide quantitative measures to characterize large-scale networks represented as a graph (Bullmore and Sporns 2009). In a graphical representation of a brain network, a node reflects the functional interactions between two brain regions. Developmental studies are beginning to examine how these network metrics change with age and cognitive skills (Gao et al. 2009; Spreng et al. 2009; Uddin et al. 2007).

16.9.3 Typical Development: From Infancy to Adolescence

Studies investigating functional connectivity in infants, children, and adolescents have revealed consistent findings with respect to the development of long-distance connectivity and regional functional specialization (Uddin et al. 2010). Many of the developmental studies have captured the functional connectivity of the default mode network (DMN) over development. The DMN is so named due to its uniquely high metabolic resting activity (Raichle 2010) and characteristic deactivation during challenging cognitive tasks (Shulman et al. 1997).

Initial developmental studies have shown in neonates five unique resting-state networks in the infant brain that encompassed the primary visual cortex, bilateral sensorimotor areas, bilateral auditory cortex, a network including the precuneus area, lateral parietal cortex, and cerebellum, as well as an anterior network that incorporated the medial and dorsolateral prefrontal cortex. These results suggest that resting-state networks driven by spontaneous signal fluctuations are present already in the infant brain. Further studies have suggested that this intrinsic organization can be demonstrated in awake, asleep, sedated, and event-anesthetized subjects. Beyond infancy, multiple studies agree that by age 7–9, children manifest a similar "small-world" type of functional architecture as adults (Fair et al. 2008; Supekar et al. 2009) although the organizations of individual functional subnetworks as well as their interactions have a protracted developmental course (Supekar et al. 2009).

16.9.4 Neurodevelopmental Disorders: Studies in Children

rsfMRI has been used to investigate potentially altered functional connectivity associated with neurodevelopmental studies, in particular attention-deficit/hyperactivity disorder (ADHD; Cao et al. 2006; Zhu et al. 2008), autism spectrum disorders (e.g., Weng et al. 2010), or other

neurodevelopmental disorders and genetics effects. However, its clinical relevance is still unknown.

In summary, rsfMRI studies contribute to elucidate and reveal key principles of functional brain development, including a shift from diffuse to focal activation patterns, simultaneous pruning of local connectivity, and strengthening of long-range connectivity with age. Nevertheless, most of the studies have been conducted in older children, adolescents, and adults, and thus, to date little is known regarding how global or local network organization changes during the important developmental period from infancy to early childhood. And the clinical impact of this new approach remains to be demonstrated.

16.10 Conclusion

These techniques are constantly evolving and open new avenues to further understand a variety of pathological conditions in infancy and childhood. They also promises to extent the field of clinical applications to the longitudinal evaluation of cognitive rehabilitation methods and the assessment of cognitive side effects of neurotropic drugs and of postoperative plasticity during brain development and maturation. Combined with advances in other related fields such as DTI and morphometric studies, these techniques are likely to profoundly influence the way various neurodevelopmental disorders will be diagnosed and treated in the future.

References

Altman NR, Bernal B (2001) Brain activation in sedated children: auditory and visual functional MR imaging. Radiology 221:56–63

Bassi L, Ricci D et al (2008) Probabilistic diffusion tractography of the optic radiations and visual function in preterm infants at term equivalent age. Brain 131:573–582

Beckmann CF, DeLuca M et al (2005) Investigations into resting-state connectivity using independent component analysis. Philos Trans R Soc Lond B Biol Sci 360:1001–1013

Binder JR, Rao SM et al (1995) Lateralized human brain language systems demonstrated by task subtraction functional magnetic resonance imaging. Arch Neurol 52:593–601

Bondy JA, Murty USR (1976) In: Co. AEP (ed). Graph theory with applications. Elsevier Science Ltd, New York

Brauer J, Neumann J et al (2008) Temporal dynamics of perisylvian activation during language processing in children and adults. Neuroimage 41:1484–1492

Brown TT, Lugar HM et al (2005) Developmental changes in human cerebral functional organization for word generation. Cereb Cortex 15:275–290

Bullmore E, Sporns O (2009) Complex brain networks: graph theoretical analysis of structural and functional systems. Nat Rev Neurosci 10:186–198

Calhoun VD, Kiehl KA et al (2008) Modulation of temporally coherent brain networks estimated using ICA at rest and during cognitive tasks. Hum Brain Mapp 29:828–838

Cao Q, Zang Y et al (2006) Abnormal neural activity in children with attention deficit hyperactivity disorder: a resting-state functional magnetic resonance imaging study. Neuroreport 17:1033–1036

Chiron C, Raynaud C et al (1992) Changes in regional cerebral blood flow during brain maturation in children and adolescents. J Nucl Med 33:696–703

Chugani HT, Phelps ME et al (1987) Positron emission tomography study of human brain functional development. Ann Neurol 22:487–497

Church JA, Petersen SE et al (2010) The "Task B problem" and other considerations in developmental functional neuroimaging. Hum Brain Mapp 31:852–862

Cohen L, Dehaene S (2004) Specialization within the ventral stream: the case for the visual word form area. Neuroimage 22:466–476

Cohen L, Jobert A et al (2004) Distinct unimodal and multimodal regions for word processing in the left temporal cortex. Neuroimage 23:1256–1270

Damoiseaux JS, Rombouts SA et al (2006) Consistent resting-state networks across healthy subjects. Proc Natl Acad Sci USA 103:13848–13853

de Ribaupierre S, Fohlen M et al (2012) Presurgical language mapping in children with epilepsy: clinical usefulness of functional magnetic resonance imaging for the planning of cortical stimulation. Epilepsia 53:67–78

Dehaene-Lambertz G, Dehaene S et al (2002) Functional neuroimaging of speech perception in infants. Science 298:2013–2015

Dehaene-Lambertz G, Hertz-Pannier L et al (2006) Functional organization of perisylvian activation during presentation of sentences in preverbal infants. Proc Natl Acad Sci USA 103:14240–14245

Dehaene-Lambertz G, Montavont A et al (2010) Language or music, mother or Mozart? Structural and environmental influences on infants' language networks. Brain Lang 114:53–65

Detre JA, Maccotta L et al (1998) Functional MRI lateralization of memory in temporal lobe epilepsy. Neurology 50:926–932

Dubois J, Benders M et al (2008) Primary cortical folding in the human newborn: an early marker of later functional development. Brain 131:2028–2041

Duchowny M, Harvey AS (1996) Pediatric epilepsy syndromes: an update and critical review. Epilepsia 37(Suppl 1):S26–S40

Fair DA, Cohen AL et al (2008) The maturing architecture of the brain's default network. Proc Natl Acad Sci USA 105:4028–4032

Faria AV, Zhang J et al (2012) Atlas-based analysis of neurodevelopment from infancy to adulthood using diffusion tensor imaging and applications for automated abnormality detection. Neuroimage 52:415–428

FitzGerald DB, Cosgrove GR et al (1997) Location of language in the cortex: a comparison between functional MR imaging and electrocortical stimulation. AJNR Am J Neuroradiol 18:1529–1539

Fox MD, Raichle ME (2007) Spontaneous fluctuations in brain activity observed with functional magnetic resonance imaging. Nat Rev Neurosci 8:700–711

Fransson P, Skiöld B et al (2009) Spontaneous brain activity in the newborn brain during natural sleep–an fMRI study in infants born at full term. Pediatr Res 66: 301–305

Gaillard WD, Hertz-Pannier L et al (2000) Functional anatomy of cognitive development: fMRI of verbal fluency in children and adults. Neurology 54:180–185

Gaillard WD, Balsamo LM et al (2003) FMRI identifies regional specialization of neural networks for reading in young children. Neurology 60:94–100

Gao W, Zhu H, Giovanello KS et al (2009) Evidence on the emergence of the brain's default network from 2-week-old to 2-year-old healthy pediatric subjects. Proc Natl Acad Sci USA 106:6790–6795

Ghetti S, DeMaster DM et al (2010) Developmental differences in medial temporal lobe function during memory encoding. J Neurosci 30:9548–9556

Giedd JN, Rapoport JL (2010) Structural MRI of pediatric brain development: what have we learned and where are we going? Neuron 67:728–734

Giedd JN, Clasen LS et al (2006) Puberty-related influences on brain development. Mol Cell Endocrinol 254–255:154–162

Heinke W, Koelsch S (2005) The effects of anesthetics on brain activity and cognitive function. Curr Opin Anaesthesiol 18:625–631

Hertz-Pannier L, Gaillard WD et al (1997) Noninvasive assessment of language dominance in children and adolescents with functional MRI: a preliminary study. Neurology 48:1003–1012

Hertz-Pannier L, Chiron C et al (2002) Late plasticity for language in a child's non-dominant hemisphere: a pre- and post-surgery fMRI study. Brain 125: 361–372

Humphries C, Binder JR et al (2006) Syntactic and semantic modulation of neural activity during auditory sentence comprehension. J Cogn Neurosci 18:665–679

Huttenlocher PR, Dabholkar AS (1997) Regional differences in synaptogenesis in human cerebral cortex. J Comp Neurol 387:167–178

Jambaque I, Dellatolas G et al (1993) Verbal and visual memory impairment in children with epilepsy. Neuropsychologia 31:1321–1337

Jambaque I, Dellatolas G et al (2007) Memory functions following surgery for temporal lobe epilepsy in children. Neuropsychologia 45:2850–2862

Kelly AM, Di Martino A et al (2009) Development of anterior cingulate functional connectivity from late childhood to early adulthood. Cereb Cortex 19:640–657

Lehericy S, Cohen L et al (2000) Functional MR evaluation of temporal and frontal language dominance compared with the Wada test. Neurology 54:1625–1633

Liegeois F, Connelly A et al (2004) Language reorganization in children with early-onset lesions of the left hemisphere: an fMRI study. Brain 127:1229–1236

Liegeois F, Cross JH et al (2006) Role of fMRI in the decision-making process: epilepsy surgery for children. J Magn Reson Imaging 23:933–940

Lin W, Zhu Q et al (2008) Functional connectivity MR imaging reveals cortical functional connectivity in the developing brain. AJNR Am J Neuroradiol 29(10): 1883–1889

Liu WC, Flax JF et al (2008) Functional connectivity of the sensorimotor area in naturally sleeping infants. Brain Res 1223:42–49

Mabbott DJ, Smith ML (2003) Memory in children with temporalorextra-temporalexcisions.Neuropsychologia 41:995–1007

MacWhinney B, Feldman H et al (2000) Online measures of basic language skills in children with early focal brain lesions. Brain Lang 71(3):400–431

Marcar VL, Strassle AE et al (2004) The influence of cortical maturation on the BOLD response: an fMRI study of visual cortex in children. Pediatr Res 56:967–974

Maril A, Davis PE et al (2010) Developmental fMRI study of episodic verbal memory encoding in children. Neurology 75:2110–2116

Maril A, Avital R et al (2011) Event congruency and episodic encoding: a developmental fMRI study. Neuropsychologia 49:3036–3045

Marusic P, Najm IM et al (2002) Focal cortical dysplasias in eloquent cortex: functional characteristics and correlation with MRI and histopathologic changes. Epilepsia 43:27–32

Menon V, Boyett-Anderson JM et al (2005) Maturation of medial temporal lobe response and connectivity during memory encoding. Brain Res Cogn Brain Res 25:379–385

Montaldi D, Mayes AR (2010) The role of recollection and familiarity in the functional differentiation of the medial temporal lobes. Hippocampus 20:1291–1314

Monzalvo K, Fluss J et al (2012) Cortical networks for vision and language in dyslexic and normal children of variable socio-economic status. Neuroimage 61: 258–274

Morita T, Kochiyama T et al (2000) Difference in the metabolic response to photic stimulation of the lateral geniculate nucleus and the primary visual cortex of infants: a fMRI study. Neurosci Res 38:63–70

Ojemann G, Ojemann J et al (1989) Cortical language localization in left, dominant hemisphere. An electrical stimulation mapping investigation in 117 patients. J Neurosurg 71:316–326

Petrella JR, Shah LM et al (2006) Preoperative functional MR imaging localization of language and motor areas: effect on therapeutic decision making in patients with potentially resectable brain tumors. Radiology 240:793–802

Power JD, Fair AD et al (2012) The development of human functional brain networks. Neuron 67:735

Raichle ME (2010) Two views of brain function. Trends Cogn Sci 14:180–190

Rasmussen T, Milner B (1977) The role of early left-brain injury in determining lateralization of cerebral speech functions. Ann N Y Acad Sci 299:355–369

Redcay E, Kennedy DP et al (2007) FMRI during natural sleep as a method to study brain function during early childhood. Neuroimage 38:696–707

Ressel V, Wilke M et al (2008) Increases in language lateralization in normal children as observed using magnetoencephalography. Brain Lang 106:167–176

Roux FE, Boulanouar K et al (2003) Language functional magnetic resonance imaging in preoperative assessment of language areas: correlation with direct cortical stimulation. Neurosurgery 52:1335–1345; discussion 1345–7

Ruge MI, Victor J et al (1999) Concordance between functional magnetic resonance imaging and intraoperative language mapping. Stereotact Funct Neurosurg 72:95–102

Rutten GJ, Ramsey NF et al (2002) FMRI-determined language lateralization in patients with unilateral or mixed language dominance according to the Wada test. Neuroimage 17:447–460

Schlaggar BL, Brown TT et al (2002) Functional neuroanatomical differences between adults and school-age children in the processing of single words. Science 296:1476–1479

Shapiro KL, Johnston SJ et al (2007) Increased functional magnetic resonance imaging activity during nonconscious perception in the attentional blink. Neuroreport 18:341–345

Shehzad Z, Kelly AM et al (2009) The resting brain: unconstrained yet reliable. Cereb Cortex 19:2209–2229

Shulman GL, Fiez JA et al (1997) Common blood flow changes across visual tasks: II. Decreases in cerebral cortex. J Cogn Neurosci 9(5):648–663

Sowell ER, Peterson BS et al (2003) Mapping cortical change across the human life span. Nat Neurosci 6:309–315

Spreng RN, Mar RA et al (2009) The common neural basis of autobiographical memory, prospection, navigation, theory of mind, and the default mode: a quantitative meta-analysis. J Cogn Neurosci 21(3): 489–510

Staudt M, Pavlova M et al (2003) Pyramidal tract damage correlates with motor dysfunction in bilateral periventricular leukomalacia (PVL). Neuropediatrics 34: 182–188

Supekar K, Musen M et al (2009) Development of large-scale functional brain networks in children. PLoS Biol 7:e1000157. doi:10.1371/journal.pbio.1000157

Szaflarski JP, Holland SK et al (2006) FMRI study of language lateralization in children and adults. Hum Brain Mapp 27:202–212

Uddin LQ, Iacoboni M et al (2007) The self and social cognition: the role of cortical midline structures and mirror neurons. Trends Cogn Sci 11:153–157

Uddin LQ, Supekar K et al (2010) Typical and atypical development of functional human brain networks: insights from resting-state fMRI. Front syst Neurosci 4:1–12

Van Dijk KR, Hedden T et al (2009) Intrinsic functional connectivity as a tool for human connectomics: theory, properties, and optimization. J Neurophysiol 103(1): 297–321

Vargha-Khadem F, Polkey CE (1992) A review of cognitive outcome after hemidecortication in humans. Adv Exp Med Biol 325:137–151

Vargha-Khadem F, O'Gorman AM et al (1985) Aphasia and handedness in relation to hemispheric side, age at injury and severity of cerebral lesion during childhood. Brain 108:677–696

Weng SJ, Wiggins JL et al (2010) Alterations of resting state functional connectivity in the default network in adolescents with autism spectrum disorders. Brain Res 1313:202–214

Wilke M, Holland SK et al (2008) Template-O-Matic: a toolbox for creating customized pediatric templates. Neuroimage 41:903–913

Wixted JT, Squire LR (2011) The medial temporal lobe and the attributes of memory. Trends Cogn Sci 15: 210–217

Woermann FG, Jokeit H et al (2003) Language lateralization by Wada test and fMRI in 100 patients with epilepsy. Neurology 61:699–701

Yuan W, Altaye M et al (2009) Quantification of head motion in children during various fMRI language tasks. Hum Brain Mapp 30:1481–1489

Zhu CZ, Zang YF et al (2008) Fisher discriminative analysis of resting-state brain function for attention-deficit/hyperactivity disorder. Neuroimage 40:110–120

Modeling Connectivity in Health and Disease: Examples from the Motor System

17

Simon B. Eickhoff and Christian Grefkes

17.1 Principles of Brain Organization

Elucidating the neural correlates underlying dysfunction in neurological or psychiatric disease is one of the major long-term goals in systems neuroscience research. Knowing pathophysiological mechanisms giving rise to complex disorders like schizophrenia or Parkinson's disease will, however, remain futile without understanding physiological brain organization. The human brain, like that of other mammals, is organized according to two fundamental principles: *functional segregation* and *functional integration* (Friston 2002). The former emphasizes that the human brain—and in particular the cerebral cortex—is not a homogenous entity but can be subdivided into regionally distinct *modules* such as cortical areas or subcortical nuclei based on functional or microstructural properties. The idea of *functional integration*, conversely, is based on the observation that no brain region is by itself sufficient to perform any cognitive, sensory, or motor process. Rather, all of these mental capacities or *tasks* have to rely on a dynamic interplay and exchange of information between different regions sustaining different computational processes. Importantly, however, functional integration and functional segregation are not mutually exclusive but rather complementary concepts of brain organization as any interaction will need to take place between specialized regions, each performing a distinct computational sub-process (Friston 2002; Eickhoff et al. 2009).

17.1.1 Specialized Modules in the Brain: The Nodes of Connectivity Models

In particular invasive research in nonhuman primates with electrodes penetrating the cerebral cortex has demonstrated that the regional specialization of the brain, that is, the cognitive or sensory processes that are served by particular location of the cortex, is determined by both the intrinsic (structure) and extrinsic (connectivity) properties of a cortical area (Broca 1863; Brodmann 1909; Eickhoff et al. 2005; Schleicher et al. 2005; Grodzinsky and Santi 2008). In comparison to the fundamental distinction between functional segregation and functional integration

S.B. Eickhoff (✉)
Institute of Clinical Neuroscience and Medical Psychology, Heinrich-Heine-University Düsseldorf, Düsseldorf, Germany

JARA – Translational Brain Medicine, Aachen, Germany

Institute of Neurosciences and Medicine (INM-2), Research Centre Jülich, Jülich, Germany
e-mail: s.eickhoff@fz-juelich.de

C. Grefkes
Neuromodulation & Neurorehabilitation Group, Max Planck Institute for Neurological Research, Cologne, Germany

Department of Neurology, University of Cologne, Cologne, Germany

S. Ulmer, O. Jansen (eds.), *fMRI – Basics and Clinical Applications*,
DOI 10.1007/978-3-642-34342-1_17,

outlined above, this evidence provides a slightly different focus as it suggests that specialization for a particular function or process is not necessarily an intrinsic property of a region independent of its connectivity. Rather, functional specialization of a cortical area is seen as a (potentially necessary) result of both its local anatomical and neurochemical features as well as its distinct pattern of inputs and outputs, that is, connectivity. A module of functional specialization may hence not be completely defined without its (potential) connectivity but is rather provided by the intersection of regionally specific architecture and connectivity patterns. Each cognitive, sensory or motor task, or mental capacity then relies on the coordinated activity and interaction of such modules.

Brain organization and disturbances thereof in neurological and psychiatric disorders might thus only be targeted by considering (i) the anatomical differentiation of the cerebral cortex into microstructurally distinct areas; (ii) the specific response properties or, more general, the pattern of recruitment of brain regions during the performance of various mental operations; and finally (iii) interaction with other brain regions. Research in nonhuman primates has a long tradition for such integrated analysis of regional brain organization (Kobbert et al. 2000; Le et al. 1986; Behrens et al. 2003; Friston 1994). Here, functional properties of a microstructurally distinct area (e.g., as determined by cytoarchitectonic, myeloarchitectonic, or receptorarchitectonic criteria) may be probed by recording single cells or local field potentials (LFPs). Axonal connectivity of the very same location may be revealed by injecting a tracing dye that is transported to interconnected brain regions. All of these techniques, however, ultimately entail sacrificing the examined animal and hence are not feasible in *human*s. Recent advances in neuroimaging techniques, however, have enabled not only the integration of structural and functional data on the organization of the human cerebral cortex but in particular also the modeling of functional interactions, thereby allowing a mechanistic insight into the dynamic interplay between cortical regions.

17.2 Structure-Function Relationships in the Brain

17.2.1 Regional Functional Specialization

Functional neuroimaging approaches such as positron emission tomography (PET) and functional magnetic resonance imaging (fMRI) are well established for the in vivo investigation of functional specialization in the human brain (Biswal et al. 1995; Fox and Raichle 2007; Greicius et al. 2003; Sporns et al. 2004; Buckner 2010). Based on the measurement of local changes in cerebral blood flow, glucose, or oxygen metabolism, these techniques allow the localization of regionally specific neural activation underlying a certain motor, sensory, or cognitive task. Although spatial precision in group activation studies is influenced by factors such as interindividual variability, averaging effects, and imperfect spatial normalization (Eickhoff et al. 2009), group fMRI studies enable localizing specific response patterns and testing hypotheses about, for example, a functional differentiation between two regions or a dichotomy between the neural correlates of two processes in the range of a centimeter or less.

17.2.2 Regional Structural Specialization

The structural examination of the human brain, in particular the histological mapping of the cerebral cortex, has a long tradition in neuroscience (Brodmann 1909). These analyses rely on the investigation of human postmortem tissue, where cell bodies, myelinated fibers, or the presence of specific molecules may be visualized using cell staining, radioactive labeling, or in situ hybridization. More recently, high-field imaging methods also opened the possibility of assessing the microstructural properties of the human brain in vivo (Stephan et al. 2007a). However, currently, no in vivo imaging approach seems capable of providing a microstructural account of the human brain as precise as histological postmortem data.

Therefore, combining functional imaging and histological maps has been proposed for an integrated description of regional segregation (Eickhoff et al. 2005). The currently prevalent approach for analyzing the correspondence between structure and function in the human brain is thus to perform both analyses separately (evidently in two groups of subjects) and then to integrate the obtained data by means of probabilistic brain atlases (Friston et al. 2003; Kiebel et al. 2006; Stephan et al. 2008). These atlases may be generated on the basis of automated analyses of histological sections in micrometer resolution (Schleicher et al. 2005), which are then warped to a common reference brain, for example, the MNI brain, to describe the location and variability of cortical areas on the group level in standard space. In contrast to classical anatomical brain atlases that present the observer-dependent parcellation of one or a few brains as drawings or schematic surface views, probabilistic atlases thus allow the direct and quantitative assessment of structure-function correlations (Fig. 17.1; Eickhoff et al. 2005).

17.2.3 Regional Structure-Function Relationships

Advances in the mapping of regional specialization enable a description of the mental processes that recruit a specific, structurally defined area and have provided plenty of evidence that anatomical borders indeed constrain functional specialization (Friston et al. 2003). However, such a *localization approach* is not sufficient to describe brain function, as a single region may be *specialized* for a broad range of mental operations. For example, the inferior frontal gyrus hosts a distinct cytoarchitectonic area which Korbinian Brodmann coined *area 44* (Brodmann 1909). Pierre-Paul Broca already noticed that this part of the brain is strongly engaged in language production (Broca 1863). A number of neuroimaging studies, however, clearly showed that this region is not language specific but recruited by a broad range of tasks ranging from speech to working memory and motor production (Grodzinsky and Santi 2008). Does this contradict the fundamental idea of functional specialization? Not necessarily, when assuming that BA 44 is specialized toward a particular computational process rather to sustain any particular (psychologically defined) mental operations. These basic computations, however, which may be sequencing or temporospatial updating like, would then be integral parts of many different task-specific recruited networks. Hence, a network perspective seems to be much closer to the neurobiology underlying human brain function under both physiological and pathological conditions.

17.3 The Elusive Concept of Brain Connectivity

In spite of the pivotal role of connectivity analyses for the understanding of human brain organization, the concept of brain connectivity in itself has remained somewhat enigmatic. First, there is no such thing as *the* connectivity of a particular brain region. Rather, several conceptually different aspects of brain connectivity may be distinguished. In the following, we will provide a short outline of the major concepts and approaches, their strength and drawback, and then focus on explicit network modeling as an approach to a mechanical understanding of the context-dependent interactions in health and disease.

17.4 Anatomical Connectivity

Anatomical connectivity in the strict sense denotes the presence of axonal connections between neurons in different brain regions. Several years ago, knowledge on the anatomical connectivity of the human brain was mostly based on postmortem dissection techniques or on extrapolations from invasive tract-tracing studies in nonhuman primates (Kobbert et al. 2000). The advent of diffusion-weighted imaging (DWI) and tractography approaches has more recently also enabled the in vivo explorations of anatomical connectivity in the human brain. DWI is based on the fact that in a

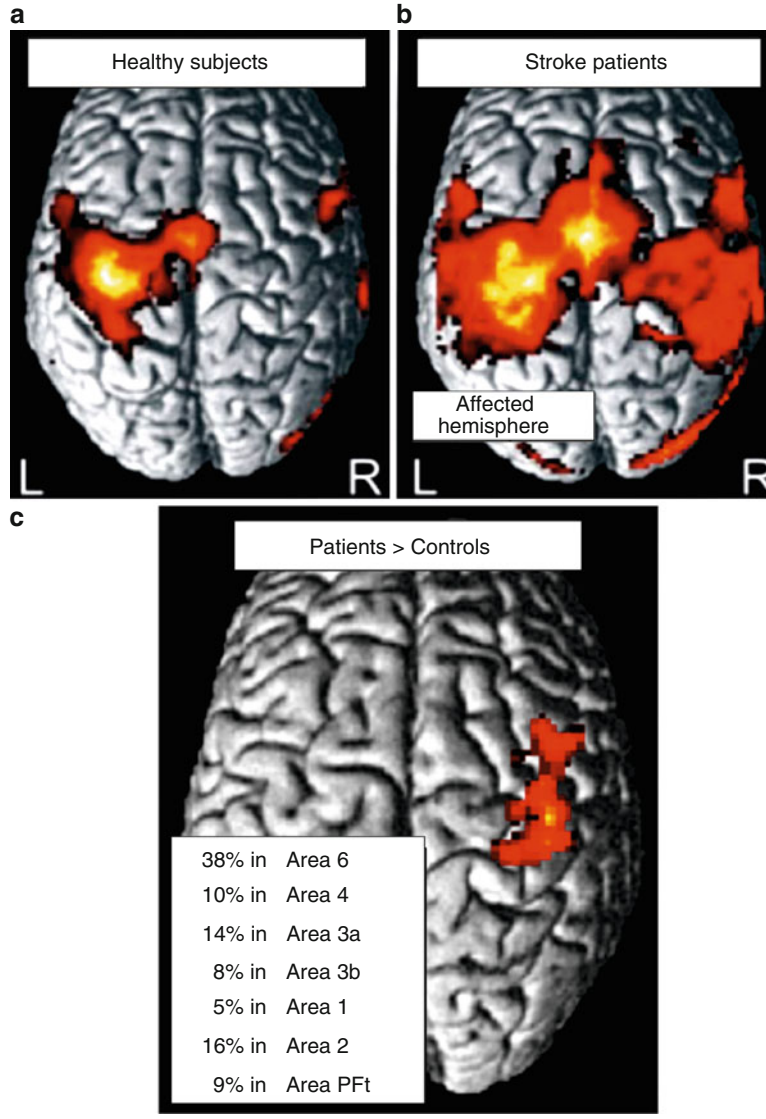

Fig. 17.1 Blood oxygenation level-dependent (BOLD) activity during a simple motor task. (**a**) In healthy subjects, rhythmic fist closures of the right hand activate a left-lateralized network of areas in frontal and parietal cortex. (**b**) BOLD activity in patients with motor deficits of the right hand is more widespread and also found in the unaffected (here right) hemisphere. (**c**) Using a probabilistic cytoarchitectonic atlas, enhanced activity can be localized in distinct cortical areas such as BA 6 (premotor cortex), BA 4 (primary motor cortex), primary somatosensory cortex (BA 3a and 3b) and higher-order somatosensory areas (BA1, BA2, and PFt) (Adopted from Grefkes et al. 2008b)

structured tissue such as a fiber bundle, water does not diffuse isotropic but rather primarily along the direction of the fiber. By employing MR sequences sensitive to random motion of water molecules along a diffusion-encoding direction in a pulsed field gradient (Le et al. 1986), it becomes possible to characterize the diffusion characteristics and hence the fiber orientation in each voxel. From the fiber orientation directions in each voxel in combination with measures about diffusion uncertainty, it is possible to infer the course of a particular fiber tract in the brain. Such *tractography* (Fig. 17.2) may be deterministic (following the principal diffusion direction at each voxel) or probabilistic (by repeated sampling of the possible diffusion directions in each voxel as reflected by the uncertainty on orientation distributions; Behrens et al. 2003). Although it should be noted that such approaches only delineate fiber tracts running from one region to another (rather than axonal connections between neurons in these regions), anatomical connectivity as revealed by diffusion imaging represents the structural scaffold, on which any functional interaction may be realized. It also represents a truly independent aspect of interregional integration and brain networks that is

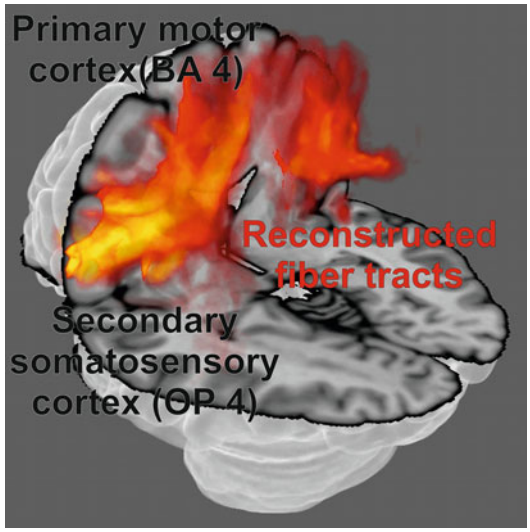

Fig. 17.2 Illustration of the fiber tracts running from area OP 4 of the secondary somatosensory cortex to the primary motor cortex, as delineated by probabilistic tractography based on diffusion-weighted imaging of 17 healthy subjects. Note that due to interindividual variability but also uncertainty about the fiber orientation in each voxel, there is a considerable variance in the data as demonstrated by the fact that only few voxels have high probabilities of belonging to this particular tract (coded in *bright yellow*)

not confounded by using the same source of data as investigations into functional specialization. Anatomical connectivity studies, however, do not allow any inference on information transfer and dynamics within the hereby defined networks.

17.5 Functional Connectivity

Functional connectivity is rather broadly defined as the temporal coincidence of spatially distant neurophysiological events (Friston 1994). That is, areas are presumed to be functionally coupled and hence components of the same network if their properties are consistently correlated. This definition already stresses a key aspect that must be considered when dealing with functional connectivity, that is, its correlative nature. Importantly, functional connectivity thus does not imply any causal relationship or a direct connection between functionally coupled areas. Rather, correlated activity in two regions may be mediated via additional structures relaying information from the first area to the second, including cortical-subcortical loops involving, for example, the basal ganglia or the cerebellum, or a third area may induce correlated activation in two regions not having any direct interaction. An example for the latter situation would be the feed-forward of stimulus-driven activity in sensory areas that is forwarded to parietal sensory areas for perceptual analysis and, in parallel, to premotor cortex for response preparation.

17.5.1 Resting-State Functional Connectivity

To date functional connectivity in neuroimaging is mainly analyzed by assessing coherent low-frequency fluctuations in resting-state fMRI time series (Biswal et al. 1995). Given the richness of fMRI data, which usually consists of several hundred time points of voxel-wise data across the brain, this approach has the perspective to yield information on functional connectivity at the level of the entire brain. Resting-state fMRI time series are obtained while the subjects are scanned lying in the scanner without any imposed task. Given that raw MRI signal time courses are noisy due to scanner or motion-induced effects, there is an important need to reduce spurious correlations by multiple processing steps such as spatial and temporal filtering as well as removal of signal contributions from motion, physiological noise, and global signal fluctuations. A large number of different studies have used data-driven approaches, in particular, independent component analysis (ICA; Fox and Raichle 2007), to delineate large-scale systems of coherent MRI signal changes providing evidence for the existence of several distinct components (i.e., functional networks) in fMRI datasets obtained during a task-free, *resting* state in particular at lower frequencies (<0.1 Hz; Greicius et al. 2003). Most of these *resting-state networks* (RSNs) closely resemble networks that are commonly engaged in task-based fMRI studies (Fox and Raichle 2007). The relationship of these components to task-related networks, however, warrants further examination as intuitive associations may be

premature (Rehme et al. 2013). There is also an ongoing debate on the physiological basis of such correlations. They have been suggested to arise from intrinsic activity events constrained by anatomical connections between the respective areas (Sporns et al. 2004), that is, anatomical connectivity. Other RSNs, however, are poorly explained by anatomical connections and it remains unresolved what drives fluctuations of sufficient magnitude to propagate along anatomical connections (Buckner 2010). This has motivated a modified view, which de-empathizes the *resting* aspect by assuming that the brain is never at *rest* (Fox and Raichle 2007). Rather, the *resting* state should reflect ongoing activity composed of a vast variety of mental functions such as bodily perception, memories, emotions, and explicit cognitive thoughts, including inner speech (Eickhoff and Grefkes 2011). That is, when lying in an MRI scanner without a specific task, subjects are not resting but rather performing all sorts of mental operations in succession or parallel. The correlation in the MR signal-time course between two regions should thus reflect the degree to which these jointly participate in the various mental networks (Laird et al. 2011a). *Resting-state* activity would hence consist of a, more or less random, sampling of all the different task-related networks that the brain is capable of. It has hence been proposed to refrain from the term *resting state* in favor of *endogenous*, *task-free functional connectivity* or *functional connectivity in the absence of a structured task set*.

17.5.2 Task-Based Functional Connectivity

The notion of functional connectivity in the absence of an structured task easily leads to the complementary aspect of *task-based* or *task-dependent* functional connectivity which may be inferred from correlation analysis between time series from different brain regions while performing a particular task (Rehme et al. 2013). In this case, however, inference is limited to the task at hand or, more precisely, the particular experiment rather than addressing the core question about "which other regions does a particular area work with?" In other words, if a particular area is activated, which other brain regions are also co-activated more likely than chance? An answer to this question has emerged from the advent of large-scale databases on functional neuroimaging results (Fig 17.3), which enabled new approaches to task-based functional connectivity analysis (Eickhoff et al. 2010). Such resources, like the BrainMap database (http://brainmap.org/; Logothetis 2000; Friston et al. 2003), contain a summary of the results of several thousands of functional neuroimaging experiments. Given the high standardization when reporting neuroimaging data and the ubiquitous adherence to standard coordinate systems, the results reported in these studies can be readily integrated to assess co-activation probabilities. In practice, functional connectivity of a seed region is established by retrieving all experiments from a database that feature at least one focus of activation within this seed region of interest (Eickhoff et al. 2010; Laird et al. 2009a, 2009b). Coordinate-based meta-analysis is then performed over all activation foci reported in these experiments to test for significant convergence, which (outside the seed itself) reflects above-chance co-activation. In doing so, *meta-analytic connectivity mapping* (MACM) closely follows the definition of functional connectivity by testing for coincidences of neurophysiological events (Laird et al. 2011). In MACM, however, unit of observation is not a specific point in an acquired (e.g., resting-state fMRI) time series but a particular neuroimaging experiment. Thus, functional connectivity is not expressed as coherent fluctuation across time but rather as coherent activation across experiments (Eickhoff and Grefkes 2011; Fig. 17.4).

The fact that functional connectivity analyses are fundamentally correlative in nature represents both their major strength and mostly severe drawback. As noted above, a correlation between neuroimaging signals on any scale does not imply a direct interaction. Moreover, given the absence of a specific model on the nature of the interactions, functional connectivity analyses tend to be rather susceptible to various physiological confounds or epiphenomena. On the other hand, the fact that only minimal assumptions need to be made for

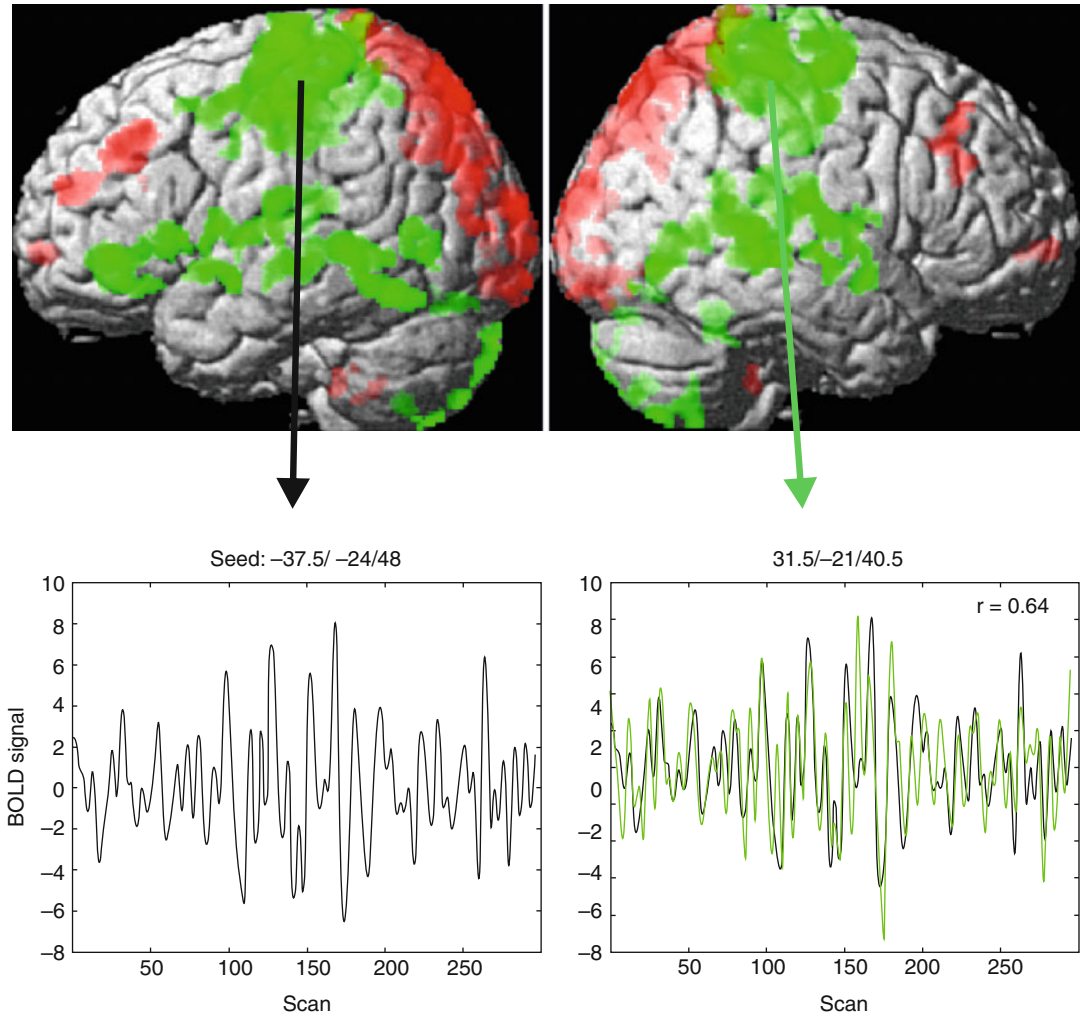

Fig. 17.3 Demonstration of resting-state functional connectivity analysis, seeding from the left primary motor cortex. Following spatial (realignment, spatial normalization, smoothing) and temporal (confound removal, bandpass filtering for the range of 0.001–0.008 Hz) preprocessing, the fMRI time series of the seed is extracted as displayed in the *lower left*. Subsequently, the similarly time series of all other voxels in the brain are correlated with the seed's time series. Significant correlations are shown in *green*, significant anti-correlations in *red*. The significantly correlated time series of the right motor cortex is displayed (*green*) on the seed time series (*black*) in the *lower right panel*

functional connectivity analyses also renders them a particularly unbiased and robust approach toward the mapping of interacting networks.

17.6 Effective Connectivity

Effective connectivity in the brain is defined as the causal influence one area exerts over another (Friston 1994), thus providing an approach toward to understanding how different brain regions affect another. Importantly, in contrast to the correlative nature of functional connectivity analyses, effective connectivity measurements are based on explicit models, how influences between brain regions are mediated. Model parameters are then fitted using the measured fMRI signal.

In spite of the considerable differences between methods and concepts for effective

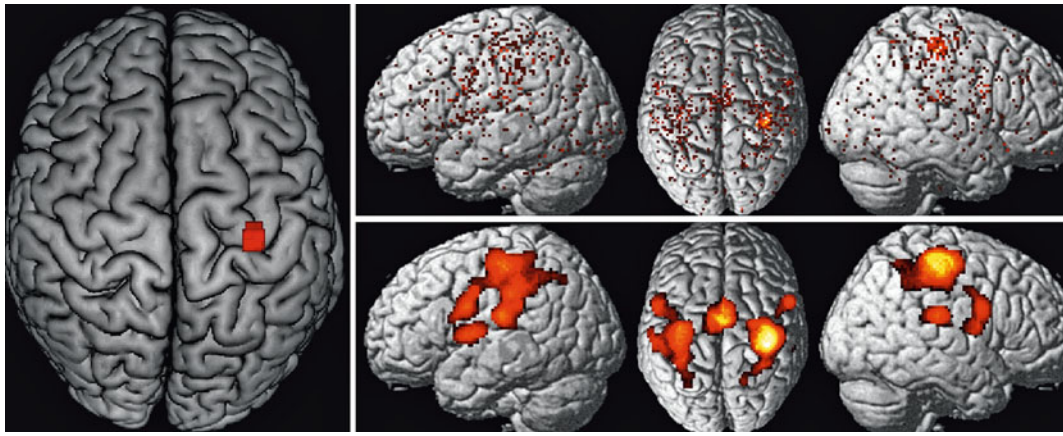

Fig. 17.4 Task-based functional connectivity of the right primary motor cortex. The *left panel* illustrates the location of the seed region on the MNI single subject template. Subsequently, the BrainMap database was filtered to identify all those experiments that featured at least one activation within this region of interest. The location of all foci of activation reported in the thus identified experiments is shown in the *upper-right panel*. By performing a quantitative meta-analysis over the identified experiments, locations where the reported foci significantly converge and which thus show significant above-chance co-activation likelihood with the seed may be identified

connectivity modeling, all approaches allow inference on directed influences. This has led to the common custom of representing effective connectivity analyses as directed graphs, where nodes represent the individual brain regions that were either included in the analysis or inferred from it (Bullmore and Sporns 2009). The directed edges of the graph then express the causal influences of one region on another, that is, effective connectivity. The dependency on an explicit model of interactions between areas is the major advantage of effective connectivity analyses. Since models reflect hypotheses about functional integration in the brain, the comparison of different models allows the comparison of competing hypotheses. Models of effective connectivity are thus hypothesis-driven investigations of how data are propagated and processed in and between different areas of the brain. However, the reliance on the explicit and implicit assumptions going into a particular model and its parameter estimation scheme has also been voiced as the most fundamental limitation of effective connectivity modeling. In particular, while model- and hypothesis-based analyses enable a mechanistic assessment of interaction processes, any inference drawn from these analyses crucially depends on the validity of the modeling assumptions. Moreover, estimating effective connectivity from fMRI time presents a major challenge, since fMRI measurements do not reflect any neuronal signal directly but rather after its convolution with a hemodynamic response function (HRF; Logothetis 2000). Inference hence has to be based on a constrained approximation or inference of neuronal responses based on the measured time series rather than on the hemodynamic observation (David et al. 2008).

Above these fundamental aspects that must be considered for all approaches for assessing effective connectivity, there are also major lines of conceptual and practical distinctions between them. Some methods such as psycho-physiological interactions (PPI) or Granger causality mapping (GCM) enable spatial inference (Friston et al. 1997; Roebroeck et al. 2005). That is, given a particular seed region or a set of seed regions, areas showing functional connectivity with these, either by influencing the seed or being influenced by it, may be delineated. Other approaches, for example, dynamic causal modelling (DCM) or structural equation modeling (SEM), do not aim at localizing effects but rather model the interactions within a predefined network or regions (Friston et al. 2003; McIntosh and Gonzalez-Lima 1994; Stephan

2004). Models of effective connectivity also differ in whether external perturbations of a system are explicitly incorporated in a model, assumed to be stochastic, or in equilibrium. Examples for the former would be PPIs and DCM; the probably prime example for the latter is SEM. Finally, modeling schemes may also differ with respect to the level of hemodynamic modeling involved (David et al. 2008; Stephan et al. 2007b; Penny et al. 2004).

17.6.1 Dynamic Causal Modelling

In contrast to other methods, which are rooted in non-brain imaging applications, dynamic causal modelling (DCM) represents an approach to effective connectivity modeling that has been specifically designed for the analysis of fMRI time series (Friston et al. 2003). Given this conceptual specificity and the fact that it represents by far the most common approach to fMRI-based effective connectivity analysis, we will hence here focus on the theory and application of DCM while referring the reader to specialized literature on other approaches (Stephan et al. 2007a; Kiebel et al. 2006).

The key concept behind DCM is to consider the brain as a nonlinear dynamic system in which external perturbations (inputs, which consist of the experimental manipulations) cause changes in neuronal activity or interregional coupling strength, that is, connectivity. The ensuing changes in neuronal activity states, which are explicitly modeled in DCM, in turn then cause changes in the blood oxygen level-dependent (BOLD) signal observable with fMRI. That is, DCM considers a hidden level of neuronal dynamics (neuronal states) which are driven by the experimental inputs (sensory stimulation or contextual influences such as task settings). These dynamics are explicitly modeled by a set of differential equations but, however, cannot be directly observed, that is, measured by fMRI. Rather, these neuronal dynamics give rise to externally assessable outputs such as BOLD signal changes though the hemodynamic response that they evoke. In DCM, the effective connectivity within the assessed dynamic neuronal system is, therefore, expressed in terms of coupling between unobservable brain states (e.g., the modeled neuronal activity in the different regions comprised in the model), rather than being inferred directly from the measured time series. It must be noted that the neuronal states, which are central to DCM as it is their dynamics and interactions that are at the heart of the model, do not directly correspond to a particular physiological quantity (Friston et al. 2003). Consequently, they do not represent multi-unit activity, spike rates, or local field potentials. Rather they represent the population dynamic of the represented area in an abstract form. The neuronal state of region k at a particular time t is given by $z_{k(t)}$. Aggregating the neuronal states of all modeled regions at a particular time then provides the neuronal state vector $z_{(t)}$, which describes the state of the entire system considered for a particular point in time. Key to the modeling is now to explain the change in the neuronal state variable of each region, which means the dynamic of activity as a function of (i) the influences other areas exert over it (ii) the modulations of these influences brought upon by the experimental manipulations, and (iii) the direct driving input of the latter. This is implemented by a set of differential equations that reflect the change of the neuronal state vector z over time as a function of its current state (via the exerted effective connectivity) and the experimental perturbations that act on the neuronal system. For the purpose of the model, experimental factors are represented by a set of input functions u, with u_j corresponding to the time course (denoting presence or absence) of the jth condition or manipulation. In the standard form of DCM for fMRI, changes in neuronal states over time are represented in the following equation forming the generative model of the neuronal level (Stephan et al. 2008):

$$\frac{dx}{dt} = \left(A + \sum_{j=1}^{m} u_j B^{(j)} + xD \right) x + Cu$$

In this formulation of effective connectivity architecture, the endogenous connectivity matrix

A (square matrix, whose size reflects the number of regions) represents the task- or process-independent component of interregional interactions, that is, the propagation of neuronal activity from one area to another expressed as the change of neuronal state as a function of the current state of the system. The task-dependent modulations in matrix B represent the changes in coupling strength brought upon by a particular stimulus or task. More specifically, $B^{(j)}$ (of the same size as A) reflects the additive effect that is present when the respective context u_j is present. If the respective context is not present, as reflected by a value of 0 in the input function, the term $i_j B^{(j)}$ becomes zero and only the remaining components of the effective connectivity model become expressed. Nonlinear effects are modeled in D which represents the modulatory influence of a particular region on the coupling strength between two other regions (i.e., gating). That is, the change of neuronal states is modeled as a nonlinear (multiplicative) interaction between the activity in two other regions such that the current state of region A only influences the change in the neuronal state of region B (exerting effective connectivity) when activity is also present in region C. Finally, the driving inputs C reflect direct effects of experimental conditions, again separated according to the individual input functions $u_{(j)}$ on the different regions. These driving inputs are particularly relevant, as they inject activity into the system, which is then propagated between the different regions and returns back to baseline level due to negative self-coupling, that is, dampening of activity, within each region. In that context, it must be noted that while the driving inputs mostly reflect sensory stimuli, they are not limited to those. Rather, activity could also enter a particular *higher-order* brain region, like the SMA or the DLPFC, in a given endogenously driven context in the same manner that it could enter a sensory area in the case of an external, for example, visual stimulus.

The modeled neuronal dynamics are then linked to the observable changes in the BOLD response via a biophysically validated hemodynamic forward model translating neuronal states into predicted measurements (Friston et al. 2003). While this approach entails two separate layers of modeling, the neuronal and the hemodynamic, each of which has its own sets of parameters to be estimated, it has two major advantages. First, DCM allows building mechanistic models of neuronal dynamics, interactions, and causal effects at the neuronal level, which evidently is of primary interest. Second, by not de-convolving the observed MRI time series by a canonical hemodynamic response function but rather estimating the regionally specific HRF from the acquired data (under biological constraints), it may accommodate moderate deviations of the hemodynamic effects from their canonical form. The latter is in particular relevant in the application to clinical populations such as patient post-stroke, which may show generalized vascular changes that could impact the form of hemodynamic responses. In the conceptual framework of DCM, effective connectivity within a given brain network is inferred from the coupling parameters computed for the hidden neuronal states as detailed above. In this context, effects are deemed causal in the sense of control theory, describing how dynamics in one neuronal population cause dynamics in another and how such interactions are modulated by contextual manipulations. That is, rather than computing a measure of connectivity from the actual data, DCM fits a model of neuronal states; their interactions and evoked hemodynamics to the measured fMRI time series and effective connectivity in the modeled system are then given by the estimated parameters of the neuronal model.

17.6.1.1 Model Estimation

Estimation of the (in particular neuronal) model parameters and hence inference on effective connectivity is based on perturbing the system through experimental manipulation, for example, by engaging subjects with different tasks while measuring the evoked effects on the BOLD time series of the regions included in the model. The parameters of the model that best translate the input functions based on the experimental design into the measured time series may be estimated by Bayesian inversion. For the hemodynamic parameters, the use of a Bayesian framework has

the major advantage that it allows to incorporate prior knowledge about biophysically plausible ranges for the different parameters controlling the hemodynamic response such as vessel stiffness or transit time (Friston et al. 2003; Stephan et al. 2007a). For the neuronal parameters, in turn, shrinkage priors are employed, that is, the a priori expected effective connectivity for any connection in the model is zero. The precision of these shrinkage priors then determines how much the model is allowed to adapt the parameters to fit the observed data and plays a major role in ensuring model stability. In particular, the larger the model, that is, the more areas it contains, the higher the danger of activity *spiraling up* and the model becoming instable (Friston et al. 2003). Consequently, the precision of the shrinkage prior increases with model size, making the model more conservative as now the prior expectation of zero, that is, no connectivity, has a higher influence on the posterior parameter estimates.

17.6.1.2 Model Comparison

Bayesian model inversion does not only provide estimates (posterior densities) for the model parameters but also an approximation to the log evidence of the model for the observed data. This log evidence can be used to compare alternative DCMs of the same data, that is, to decide between alternative hypotheses on the architecture of the neuronal interactions underlying an observed pattern of activation (Penny et al. 2004). This formal approach to comparing different hypothesis on the model structure has been conceptualized as one of the major advantages of DCM over other approaches to effective connectivity.

17.6.1.3 Deterministic and Stochastic Models

As noted above, perturbation is especially important in the classical formulation of DCM (Friston et al. 2003), as here the modeled neuronal network is considered completely deterministic and only driven by external inputs without which it would remain idle. Without such driving input, however, the system would stay and remain at rest. More recent developments, however, have added stochastic behavior and may thus alleviate the strong dependency of DCM analyses on the experimental manipulation and the assumption that neural population dynamics may be correctly captured from the modeled inputs (Daunizeau et al. 2009). In spite of these revisions, the mainstay of DCM analyses is still the modeling of task-specific contextual influences aiming at an interpretation of functional neuroimaging data in terms of the underlying connectivity patterns. As such, the model and its parameters obviously are strongly conditioned on the performed experimental task and its particular setup. DCM thus primarily represents as a tool providing an additional layer of insight into the causes of regionally specific activation patterns rather than revealing information about functional connectivity patterns that go beyond the particular experiment. In other words, DCM represents the most confirmative modeling approach currently available for effective connectivity modeling in healthy subjects and patients. However, it must be remembered that confirmatory models of connectivity like DCM strongly depend on a priori assumptions, for example, on the included regions, the assessed model space and finally the assumptions underlying the modeling approach itself such as the form of the hemodynamic priors.

17.6.1.4 Application: Modeling Effective Connectivity in the Motor System

Models of effective connectivity like DCM can be used to explain activation patterns observed in conventional fMRI analyses. As shown in Fig. 17.1, simple unilateral hand movements elicit a typical lateralized activation pattern with highest BOLD activity in contralateral primary motor cortex (M1). Patients with motor deficits due to a brain lesion resulting from stroke show several changes in neural activity during movements of the affected hand, especially in the unaffected hemisphere. Applying DCM to the dataset of healthy subjects reveals that neural coupling among key motor areas is symmetrically organized (Fig. 17.5a). Estimating the constant part of connectivity, that is, coupling irrespective of moving the left or right hand (DCM A matrix), reveals that motor areas such

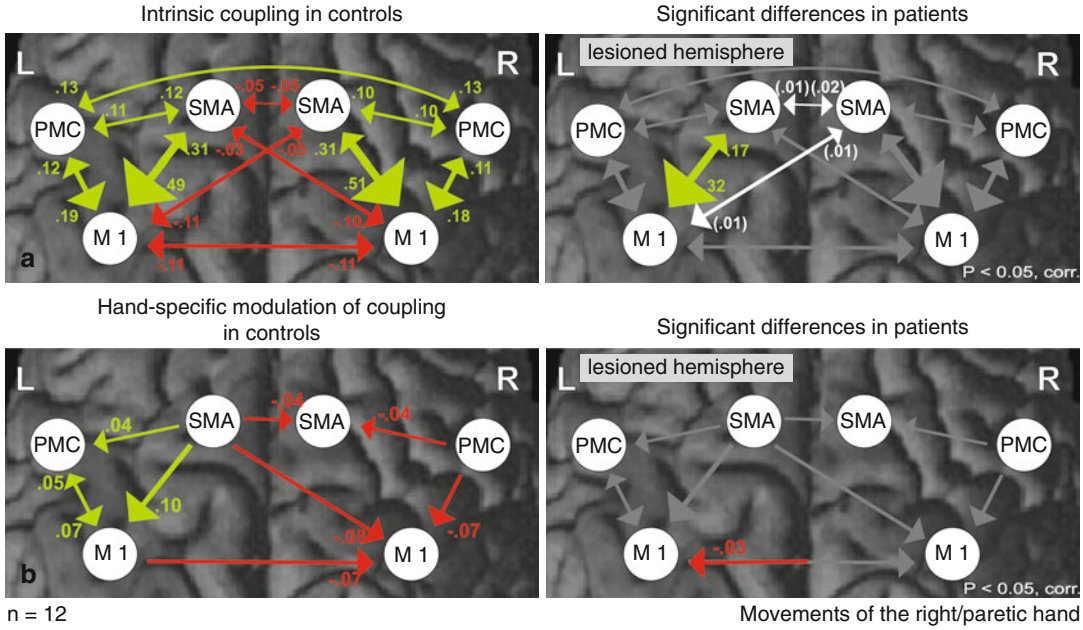

Fig. 17.5 Connectivity among motor regions in healthy subjects and patients with hemiparesis caused by subcortical stroke. Coupling parameters (rate constants in 1/s) indicate connection strength, which is also coded in the size and color of the *arrows* representing effective connectivity. Positive (*green*) values represent facilitatory, negative (*red*) values inhibitory influences on neuronal activity. The greater the absolute value, the more predominant the effect one area has over another. (**a**) Neural coupling in healthy subjects: In healthy subjects, the intrinsic coupling of motor areas is well balanced within and across hemispheres, while movements of the right hand induce a hemispheric-specific modulation of interregional coupling. (**b**) Significant changes of coupling parameters in stroke patients. *Gray arrows* denote no significant difference to healthy control subjects, while *white arrows* indicate a loss of coupling in the patient group. Patients with subcortical stroke show a significant reduction in intrinsic SMA-M1 coupling in the lesioned hemisphere and a decoupling of ipsilesional areas from contralesional SMA (*white arrows*). Movements of the paretic hand are associated with a pathological inhibition of ipsilesional M1 exerted by contralesional M1, which does not occur in healthy subjects and correlate with the motor deficit of the paretic hand (adapted from Grefkes et al. 2008b, with permission)

as the supplementary motor area (SMA), lateral premotor cortex (PMC), and primary motor cortex (M1) show a strong positive coupling with each other, especially between SMA and M1 (Grefkes et al. 2008a). The interhemispheric coupling parameters between left and right M1 are negative, suggesting mutual inhibition in the absence of a particular hand movement (Fig. 17.5a). In contrast, moving the left or the right hand induces a side-specific modulation of interregional connectivity. Neural coupling is strongly enhanced in the hemisphere contralateral to the moving hand, while ipsilateral areas, especially ipsilateral M1, are inhibited (Fig. 17.5b). Patients suffering from stroke-induced motor deficits in the subacute phase (i.e., in the first few weeks and months poststroke) show several changes in this pattern of "normal" cortical connectivity within and across hemispheres (Grefkes et al. 2008b). Especially endogenous (i.e., movement-independent) coupling between ipsilesional SMA and ipsilesional M1 is significantly reduced compared to healthy control subjects (Fig. 17.5a, right panel). Importantly, the amount of *hypoconnectivity* between SMA and M1 correlates with the individual motor deficit, suggesting that reduced motor performance may—at least to some extent—be caused by ineffective processing between ipsilesional SMA and M1. Likewise, the negative coupling with contralesional SMA is significantly reduced in the group of stroke patients (Fig. 17.5a, right panel). As these disturbances in effective connectivity are independent from which hand was

moved by the patients, they might explain the finding that the unaffected hand of stroke patients often shows subtle motor deficits when compared to healthy control subjects (Nowak et al. 2007). Apart from changes in movement-independent coupling, the DCM analysis also revealed significant changes in the modulation of interregional coupling evoked by moving the paretic or non-paretic hand. While in healthy subjects contralateral M1 exerts an inhibitory influence on M1 activity ipsilateral to the moving hand, stroke patients show an additional inhibitory influence on ipsilesional M1 originating from contralesional M1, which is not present in healthy subjects or when patients move their unaffected hand (Fig. 17.5b, right panel). Importantly, the strength of this pathological inhibition from contralesional M1 correlates with the motor impairment of the paretic hand (Grefkes et al. 2008b). This means that especially in patients with stronger motor deficits, ipsilesional M1 activity is negatively influenced by contralesional M1 which exerts a detrimental effect upon motor performance of the paretic hand. Reducing contralesional M1 excitability by means of repetitive transcranial magnetic stimulation (rTMS) is associated with a significant reduction of pathological coupling between contralesional and ipsilesional M1 compared to an rTMS control stimulation site (Grefkes et al. 2010). In addition, intrinsic neural coupling between ipsilesional SMA and ipsilesional M1 is significantly enhanced after rTMS applied over contralesional M1, and the increase in coupling correlates with the increase in motor performance of the paretic hand (Grefkes et al. 2010). Hence, a focal stimulation by means of TMS does not only alter connectivity of the region stimulated but also of areas distant to the stimulation site. This also implies that behavioral effects evolving after stimulation are based on a remodeling of the whole network rather than being caused by excitability changes of a single motor region. In particular, a more effective integration of ipsilesional M1 into the motor network architecture might constitute a key factor for improving motor performance of stroke patients by means of rTMS (Grefkes et al. 2010).

17.7 Conclusion

A connectivity-based approach of analyzing functional imaging data allows hypothesis-driven investigations of the interactions among brain regions under physiological and pathological conditions. In contrast to *classical* voxel-wise analyses of fMRI data aimed at localizing neural activity, models of connectivity make use of a network perspective in which the change of neural activity of a given brain region is explained by interactions with other brain regions. In this context, it is important to underline that there is no such thing as *the* connectivity in the brain, but rather several different characteristics may be assessed. Structural, task-based and task-independent functional as well as effective connectivity all focus on different properties and aspects of network properties and may hence inform our knowledge on the physiological and pathological organization of the human brain.

References

Behrens TE, Woolrich MW et al (2003) Characterization and propagation of uncertainty in diffusion-weighted MR imaging. Magn Reson Med 50:1077–1088

Biswal B, Yetkin FZ et al (1995) Functional connectivity in the motor cortex of resting human brain using echo-planar MRI. Magn Reson Med 34:537–541

Broca P (1863) Localisations des fonctions cérébrales. Bull Soc d'Anthropologie 4:200–208

Brodmann K (1909) Vergleichende Lokalisationslehre der Großhirnrinde. Barth, Leipzig

Buckner RL (2010) Human functional connectivity: new tools, unresolved questions. Proc Natl Acad Sci USA 107:10769–10770

Bullmore E, Sporns O (2009) Complex brain networks: graph theoretical analysis of structural and functional systems. Nat Rev Neurosci 10:186–198

Daunizeau J, David O et al (2009) Dynamic causal modelling: a critical review of the biophysical and statistical foundations. Neuroimage 58(2):312–322

David O, Guillemain I et al (2008) Identifying neural drivers with functional MRI: an electrophysiological validation. PLoS Biol 6:2683–2697

Eickhoff SB, Grefkes C (2011) Approaches for the integrated analysis of structure, function and connectivity of the human brain. Clin EEG Neurosci 42: 107–121

Eickhoff SB, Stephan KE et al (2005) A new SPM toolbox for combining probabilistic cytoarchitectonic

maps and functional imaging data. Neuroimage 25:1325–1335
Eickhoff SB, Laird AR et al (2009) Coordinate-based activation likelihood estimation meta-analysis of neuroimaging data: a random-effects approach based on empirical estimates of spatial uncertainty. Hum Brain Mapp 30:2907–2926
Eickhoff SB, Jbabdi S et al (2010) Anatomical and functional connectivity of cytoarchitectonic areas within the human parietal operculum. J Neurosci 30(18): 6409–6421
Fox MD, Raichle ME (2007) Spontaneous fluctuations in brain activity observed with functional magnetic resonance imaging. Nat Rev Neurosci 8:700–711
Friston KJ (1994) Functional and effective connectivity in neuroimaging: a synthesis. Hum Brain Mapp 2(1–2): 56–78
Friston KJ, Buechel C et al (1997) Psychophysiological and modulatory interactions in neuroimaging. Neuroimage 6:218–229
Friston K (2002) Beyond phrenology: what can neuroimaging tell us about distributed circuitry? Annu Rev Neurosci 25:221–250
Friston KJ, Harrison L et al (2003) Dynamic causal modelling. Neuroimage 19:1273–1302
Grefkes C, Eickhoff SB et al (2008a) Dynamic intra- and interhemispheric interactions during unilateral and bilateral hand movements assessed with fMRI and DCM. Neuroimage 41:1382–1394
Grefkes C, Nowak DA et al (2008b) Cortical connectivity after subcortical stroke assessed with functional magnetic resonance imaging. Ann Neurol 63:236–246
Grefkes C, Nowak DA et al (2010) Modulating cortical connectivity in stroke patients by rTMS assessed with fMRI and dynamic causal modeling. Neuroimage 50:233–242
Greicius MD, Krasnow B et al (2003) Functional connectivity in the resting brain: a network analysis of the default mode hypothesis. Proc Natl Acad Sci USA 100:253–258
Grodzinsky Y, Santi A (2008) The battle for Broca's region. Trends Cogn Sci 12:474–480
Kiebel SJ, David O et al (2006) Dynamic causal modelling of evoked responses in EEG/MEG with lead field parameterization. Neuroimage 30:1273–1284
Kobbert C, Apps R et al (2000) Current concepts in neuroanatomical tracing. Prog Neurobiol 62:327–351
Laird AR, Eickhoff SB et al (2009a) ALE meta-analysis workflows via the brainmap database: progress towards a probabilistic functional brain atlas. Front Neuroinformatics 3:23
Laird AR, Eickhoff SB et al (2009b) Investigating the functional heterogeneity of the default mode network using coordinate-based meta-analytic modeling. J Neurosci 29:14496–14505
Laird AR, Fox PM et al (2011a) Behavioral interpretations of intrinsic connectivity networks. J Cogn Neurosci 23:4022–4037
Laird AR, Eickhoff S et al (2011b) The BrainMap strategy for standardization, sharing, and meta-analysis of neuroimaging data. BMC Res Notes 4:349
Le BD, Breton E et al (1986) MR imaging of intravoxel incoherent motions: application to diffusion and perfusion in neurologic disorders. Radiology 161: 401–407
Logothetis N (2000) Can current fMRI techniques reveal the micro-architecture of cortex? Nat Neurosci 3:413–414
McIntosh AR, Gonzalez-Lima F (1994) Structural equation modeling and its application to network analysis in functional brain imaging. Hum Brain Mapp 2:2–22
Nowak DA, Grefkes C et al (2007) Dexterity is impaired at both hands following unilateral subcortical middle cerebral artery stroke. Eur J Neurosci 25:3173–3184
Penny WD, Stephan KE et al (2004) Comparing dynamic causal models. Neuroimage 22:1157–1172
Penny WD, Stephan KE et al (2004) Modelling functional integration: a comparison of structural equation and dynamic causal models. Neuroimage 23(Suppl 1):S264–S274
Rehme AK, Eickhoff SB et al (2013) State-dependent differences between functional and effective connectivity of the human cortical motor system. Neuroimage 67:237–246
Roebroeck A, Formisano E et al (2005) Mapping directed influence over the brain using Granger causality and fMRI. Neuroimage 25:230–242
Schleicher A, Palomero-Gallagher N et al (2005) Quantitative architectural analysis: a new approach to cortical mapping. Anat Embryol (Berl) 210(5-6):373–386
Sporns O, Chialvo DR et al (2004) Organization, development and function of complex brain networks. Trends Cogn Sci 8:418–425
Stephan KE (2004) On the role of general system theory for functional neuroimaging. J Anat 205:443–470
Stephan KE, Harrison LM et al (2007a) Dynamic causal models of neural system dynamics:current state and future extensions. J Biosci 32:129–144
Stephan KE, Weiskopf N et al (2007b) Comparing hemodynamic models with DCM. Neuroimage 38:387–401
Stephan KE, Kasper L et al (2008) Nonlinear dynamic causal models for fMRI. Neuroimage 42(2):649–662

fMRI in Parkinson's Disease

18

Hartwig R. Siebner and Damian M. Herz

Abbreviations

ACC	Anterior cingulate cortex
BA	Brodmann area
BG	Basal ganglia
BOLD	Blood-oxygenation-level-dependent
CMA	Cingulate motor area
COMT	Catechol O-methyltransferase
DCM	Dynamic causal modeling
DLPFC	Dorsolateral prefrontal cortex
fMRI	Functional magnetic resonance imaging
GPe	External globus pallidus
GPi	Internal globus pallidus
ICD	Impulse control disorder
IFG	Inferior frontal gyrus
IPC	Inferior parietal cortex
M1	Primary motor cortex
MFG	Middle frontal gyrus
MFC	Middle frontal cortex
OFC	Orbitofrontal cortex
PD	Parkinson's disease
PET	Positron-emission tomography
PFC	Prefrontal cortex
PM	Premotor cortex
PPI	Psychophysiological interaction
Pre-SMA	Pre-supplementary motor area
RS-fMRI	Resting-state functional magnetic resonance imaging
SEM	Structural equation modeling
SMA	Supplementary motor area
SNc	Substantia nigra pars compacta
SNr	Substantia nigra pars reticulata
SPECT	Single-photon emission computed tomography
STN	Subthalamic nucleus
VTA	Ventral tegmental area

H.R. Siebner, M.D. (✉) • D.M. Herz, M.D.
Danish Research Centre for Magnetic Resonance,
Center for Functional and Diagnostic Imaging,
Copenhagen University Hospital Hvidovre,
Hvidovre, Denmark
e-mail: hartwig.siebner@drcmr.dk; damianh@drcmr.dk

18.1 Clinical Features and Pathophysiology of Parkinson's Disease

Parkinson's disease (PD) is a progressive neurodegenerative disorder of unknown cause characterized by four cardinal features: slowness of movement (akinesia), rigidity, tremor at rest, and postural instability (Lang and Lozano 1998a, b).

However, non-motor features are common and involve disorders of cognitive, autonomic, and sensory function (Jankovic 2008). Motor impairment in PD has been linked to degeneration of dopaminergic neurons in substantia nigra pars compacta (SNc), leading to abnormal neural processing in the loops connecting cortex and basal ganglia (BG). These loops are thought to subserve action selection, i.e., execution of a selected movement while competing motor programs are inhibited (Mink 1996). This function is implemented by three distinct pathways in the BG

S. Ulmer, O. Jansen (eds.), *fMRI – Basics and Clinical Applications*,
DOI 10.1007/978-3-642-34342-1_18,

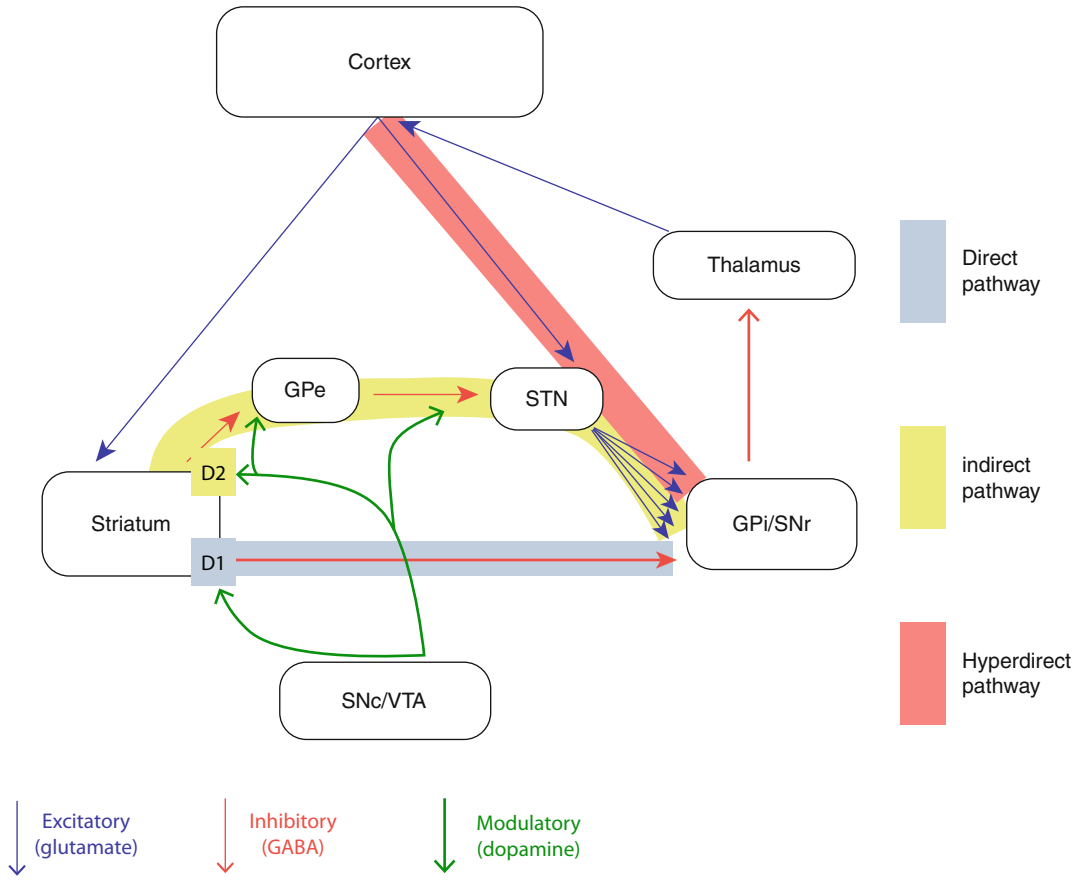

Fig. 18.1 A simplified model of cortico-subcortical pathways. Efferent connections from the cortex are processed in the BG and projected back to the cortex via the thalamus in closed feedback loops. The direct pathway connects the striatum, comprising putamen and caudate nucleus, with the internal globus pallidus (*GPi*)/substantia nigra pars reticulata (*SNr*). Since this connection as well as the connection between *GPi/SNr* and thalamus both are inhibitory, activation of the direct pathway leads to a disinhibition of thalamocortical connections. On the other hand, activation of the indirect pathway leads to a disinhibition of the *STN* via the external globus pallidus (*GPe*). The *STN* has diverging excitatory efferent connections to *GPi/SNr*, which consecutively leads to an inhibition of thalamocortical connections. Dopaminergic innervation of the striatum leads to an activation of the direct pathway via *D1* receptors and an inhibition of the indirect pathway via *D2* receptors and has therefore an excitatory influence on movements. In case of motor loops, dopamine modulates mainly connections from substantia nigra pars compacta (*SNc*) to dorsal striatum while modulating connections from ventral tegmental area (*VTA*) to ventral striatum in case of limbic loops. The hyperdirect pathway consists of a connection from the cortex to subthalamic nucleus (*STN*) bypassing the striatum. This connection can exert a fast global stop signal over the motor system. For simplicity reasons feedback connections within the BG are omitted

(see Fig. 18.1 for a simplified model). According to this model, activation of the direct pathway leads to a focused disinhibition of thalamocortical connections, while the indirect pathway broadly inhibits surrounding connections (Albin et al. 1989; Delong 1990). Additionally, a hyperdirect pathway connecting cortex and the subthalamic nucleus (STN) can serve as a global stop signal for any movement (Nambu et al. 2000). Activation of the hyperdirect pathway can cancel previous or impulsive movements. Consecutive activation of the direct and indirect pathway facilitates the execution of the selected movement while inhibiting competing motor programs. Since dopamine activates the direct pathway via D1 receptors and inhibits the indirect pathway

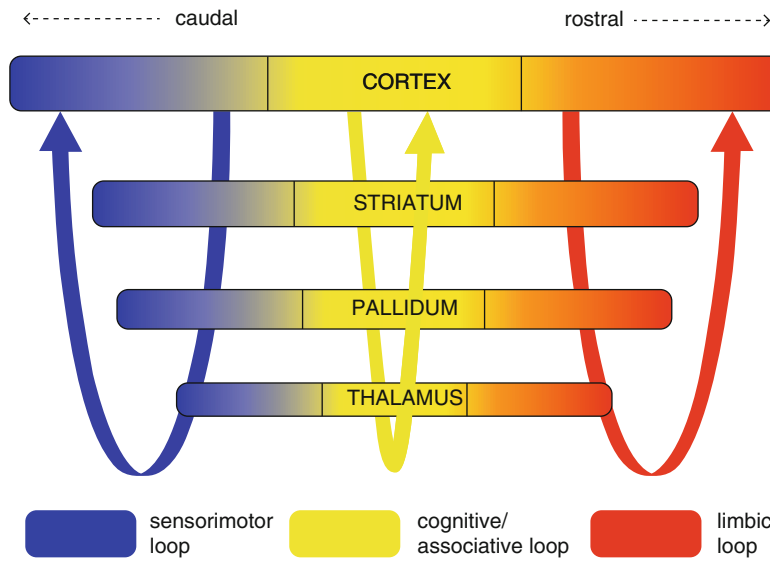

Fig. 18.2 Spatially and functionally distinct cortico-subcortical feedback loops. Each of the loops has its origin in the cortex and is processed via the input (*striatum*) and output structure of the BG (*pallidum*) to the thalamus and back to the cortex. This organization is thought to underlie action selection and reinforcement (Redgrave et al. 2008)

via D2 receptors, dopamine depletion can lead to an increased inhibition of thalamocortical connections via the indirect pathway and thereby cause akinesia. Although this original model is very helpful to explain this cardinal motor feature in PD, it has limitations. Therefore, complex properties such as changes in synaptic plasticity and nonlinear oscillatory coupling are implemented in current models (Brown 2007; Calabresi et al. 2007), which are beyond the scope of this book chapter.

Importantly, it needs to be recalled that the cortico-basal ganglia-thalamo-cortical loops do not merely involve motor networks but consist of additional loops which subserve cognitive or limbic functions (Fig. 18.2; Alexander et al. 1986). Neurodegeneration in PD affects more prominently the caudally localized sensorimotor basal ganglia loops, while the more rostrally localized associative and limbic loops are relatively spared (Rinne et al. 2001).

18.2 Neuroimaging in Parkinson's Disease

Functional neuroimaging techniques, such as positron-emission tomography (PET), single-photon emission computed tomography (SPECT), and functional magnetic resonance imaging (fMRI), have been widely used to study function and dysfunction of neural networks. Early neuroimaging studies of patients with PD mainly involved PET measurements of regional cerebral blood flow (e.g., Jahanshahi et al. 1995; Playford et al. 1992). With the exception of PD patients treated with deep brain stimulation, fMRI has largely replaced PET as the imaging method of choice to study disease-related changes in neural activity and connectivity. In contrast to PET, fMRI does not involve exposure to radiation, which restricts the number of blood flow measurements with PET. Further, fMRI is widely available and has better spatial and temporal resolution, the latter allowing for analysis of event-related activity. This makes PET and fMRI valuable complementary tools for studying changes in neural networks in PD. In the following sections we will mainly focus on studies using fMRI. We report a selection of studies that were conducted at rest as well as during motor tasks and non-motor tasks. Additionally, we included a section about preclinical compensation of dopaminergic degeneration, an exciting new research field studying asymptomatic carriers of PD-related mutations. An overview of the selected publications is given in Table 18.1.

Table 18.1 Selected publications studying patients with PD during rest, motor paradigms, and non-motor paradigms as well as studies of asymptomatic carriers of PD-related mutations

Authors	Year	*n*	OFF/ON	Paradigm	Main findings in patients with Parkinson's disease
Resting-state fMRI studies					
Baudrexel et al.	2011	31	OFF	Resting state	Increased connectivity between M1 and STN during rest
Helmich et al.	2010	41	OFF	Resting state	Reduced spatial segregation of connections between the cortex and putamen
Skidmore et al.	2011a, b	15	OFF	Resting state	Decreased activity in SMA, PFC, right MFG, and left cerebellum and increased activity in right cerebellum. Based on this activity pattern, PD patients can be distinguished from controls with 92 % sensitivity and 87 % specificity
Skidmore et al.	2011a, b	15	OFF	Resting state	The apathy score of PD patients is best predicted by activity in left SMA, right OFC, and right MFC, while depression score is best predicted by right subgenual cingulate activity and disease severity by right putamen activity
Activation fMRI during motor tasks					
Buhmann et al.	2003	8 (drug-naive)	OFF/ON	Simple paced finger opposition task	Decreased activity in SMA and M1 in the OFF state. L-Dopa increases activity in SMA and M1
Haslinger et al.	2001	8	OFF/ON	Paced single joystick movements in a freely chosen direction	Decreased activity in Pre-SMA and increased activity in M1 and lateral PM in the OFF state. L-Dopa increases activity in SMA and decreases activity in M1, lateral PM, and SPC
Rowe et al.	2002	12	OFF	Simple paced overlearned motor sequence task, with and without an additional attentional task	Increased SMA activity during a simple task but less attention-related augmentation of SMA activity due to an impaired connectivity between PFC and both SMA and lateral PM
Rowe et al.	2010	16	OFF/ON	Simple visually paced finger-tapping task	In the ON state selection of action is associated with enhanced coupling between PFC and Pre-SMA. In the OFF state action selection is linked to coupling between PFC and lateral PM
Sabatini et al.	2000	6	OFF	Complex sequential motor task	Decreased activity in Pre-SMA and right DLPFC, and increased activity in M1, lateral PM, IPC, SMA, and ACC
Williams-Gray et al.	2008	29 (high- and low-COMT-activity genotype)	ON	Cognitive task probing the ability to form attentional "sets"	PD patients with low-COMT-activity genotype fail to form an attentional "set." This is associated with an underactivation across frontoparietal attentional networks
Wu et al.	2010	15	OFF	Unimanual, bimanual in-phase and bimanual anti-phase movements	Decreased activity in SMA and BG and increased activity in M1, PM, IFG, precuneus, and cerebellum during anti-phase movements. SMA has decreased connectivity to BG and dorsolateral PFC and increased connectivity to M1, PC, precuneus, and cerebellum
Wu et al.	2011	18	OFF/ON	Self-initiated tapping task	PD patients in the OFF state show a decreased connectivity between BG and cortical areas (M1, Pre-SMA, PM) as well as the cerebellum. In contrast, connections between cortico-cerebellar regions are strengthened

Activation fMRI studies of non-motor functions					
Lewis et al.	2003	21 (cognitively impaired and unimpaired)	ON	Working-memory task	Impairment in working memory is associated with decreased activity in the striatum and PFC
MacDonald et al.	2011	20	OFF/ON	Simple selection task	L-Dopa enhances interference control but impairs encoding and facilitation of consistent stimulus-stimulus relations
Marklund et al.	2009	20 (drug-naive)	OFF	Working-memory (2-back) task	PD patients show a transient (phasic) underactivation in caudate nuclei, putamen, and globus pallidus and sustained (tonic) underactivation in anterior putamen
Rowe et al.	2008	19	OFF/ON	Bimodality continuous performance task	Lateral PFC and caudate nucleus activation show a nonlinear U-shaped relationship to motor disease severity. L-Dopa leads to a shift in this U-shaped function, indicating differential neurodegeneration in distinct connections between cortex and BG
Voon et al.	2010	22 (with and without impulse control disorder)	OFF/ON	Probabilistic learning task	Dopamine agonists increase the rate of learning from gain outcomes in susceptible PD patients and lead to an increased prediction error in the striatum
Voon et al.	2011	28 (with and without impulse control disorder)	OFF/ON	Risk-taking task	Patients with impulse control disorders make more risky choices and show decreased activation in OFC and ACC. Dopamine agonists enhance sensitivity to risk along with decreased activation in the ventral striatum. The opposite is observed in patients without impulse control disorders
Genetically informed fMRI studies					
Buhmann et al.	2005	12 (asymptomatic carriers of a Parkin mutation)	–	Internally selected and externally determined finger movements	Asymptomatic Parkin-mutation carriers show increased activity in right rostral CMA and left dorsal PM during internally selected movements
van Nuenen et al.	2009	22 (asymptomatic carriers of a Parkin or a Pink1 mutation)	–	Simple sequences of three thumb-to-finger opposition movements	In contrast to healthy controls, asymptomatic Parkin- and Pink1-mutation carriers show activation of Pre-SMA and right rostral dorsal PM during simple movements

Studies are listed in alphabetical order in each section

Abbreviations: *M1* primary motor cortex, *SMA* supplementary motor area, *Pre-SMA* pre-supplementary motor area, *PM* premotor cortex, *PFC* prefrontal cortex, *DLPFC* dorsolateral prefrontal cortex, *IFG* inferior frontal gyrus, *MFG* middle frontal gyrus, *MFC* middle frontal cortex, *OFC* orbitofrontal cortex, *ACC* anterior cingulate cortex, *CMA* cingulate motor area, *SPC* superior parietal cortex, *IPC* inferior parietal cortex, *BG* basal ganglia, *STN* subthalamic nucleus

18.2.1 Functional Connectivity Assessed with Resting-State fMRI

Resting-state fMRI (RS-fMRI) measures spontaneous low-frequency (<0.1 Hz) fluctuations in the blood-oxygen-level-dependent (BOLD) signal in the whole brain while participants are at rest. These regional BOLD signal fluctuations are temporally correlated within functional brain networks and thus provide an index of functional connectivity (Biswal et al. 1995; Fox and Raichle 2007). RS-fMRI is particularly suited for functional connectivity studies of the motor system in PD patients with motor disability. Since RS-fMRI does not require patients to engage in a motor task, the connectivity patterns are not confounded by task performance.

Skidmore et al. (Skidmore et al. 2011a) used RS-fMRI to investigate whether 14 patients with PD in the OFF state (i.e., at least 12 h after withdrawal from dopaminergic medication) could be distinguished from healthy controls based on the observed resting-state activity patterns. The amplitude of the low-frequency BOLD signal fluctuations at rest was used as an index of brain activity level in the resting state. PD patients showed decreased activity in supplementary motor area (SMA), prefrontal cortex (PFC), right middle frontal gyrus (MFG), and the left cerebellum as well as increased activity in the right cerebellum. Based on this distributed pattern of activity changes, it was possible to distinguish between PD patients and healthy controls with 92 % sensitivity and 87 % specificity. The same group showed that the resting-state activity pattern in specific brain regions correlated with the presence of apathy or depression in PD (Skidmore et al. 2011b). Apathy was best predicted by the amplitude of the low-frequency fluctuations at rest in the left SMA, right orbitofrontal cortex (OFC), and right MFG, whereas depression was associated with the amplitude of resting-state activity in the right subgenual cingulate. Disease severity was reflected by the amplitude of resting-state low-frequency fluctuations in the right putamen. These results suggest that RS-fMRI might play an important role as a biomarker for PD in the future.

RS-fMRI can also be used to study the connectivity profile of a single, predefined region of interest. Baudrexel and colleagues studied functional connectivity of the subthalamic nucleus (STN) in 31 patients with early-stage PD in the OFF state (Baudrexel et al. 2011). Compared to healthy controls patients had an increased connectivity between STN and cortical motor and premotor cortical areas, which complements similar results from previous electrophysiological studies (Gradinaru et al. 2009; Lalo et al. 2008). In another study, 41 PD patients in the OFF state showed decreased connectivity between inferior parietal cortex (IPC) and posterior putamen and an increased connectivity between IPC and anterior putamen relative to healthy controls (Helmich et al. 2010). This pattern deviates from the normal connectivity profiles of the putamen (Di Martino et al. 2008) and might indicate decreased spatial segregation between corticostriatal loops leading to impaired sensorimotor integration.

18.2.2 Functional MRI Studies of Motor Control

Several fMRI studies have revealed an abnormal activation pattern of executive motor areas when patients with PD perform manual motor tasks (e.g., Buhmann et al. 2003; Haslinger et al. 2001; Helmich et al. 2009; Palmer et al. 2009; Rowe et al. 2002, 2010; Sabatini et al. 2000; Wu et al. 2010, 2011). In an early study, Sabatini and coworkers (Sabatini et al. 2000) used a complex sequential motor task to investigate changes in cortical activity in six PD patients in the OFF state compared to six unmedicated, healthy controls. During the motor task, participants had to perform sequential finger-to-thumb opposition movements as well as opening and clenching of the wrist in a specified order. In PD patients, this cognitively demanding task was associated with hypoactivation in pre-supplementary motor area (Pre-SMA) and dorsolateral prefrontal cortex (DLPFC), in accordance with previous studies using PET (Jahanshahi et al. 1995; Playford et al. 1992). Additionally, hyperactivation in a range of cortical areas, such as the primary motor cortex

(M1) and lateral premotor cortex (PM), was observed. The authors interpreted this as a compensatory mechanism for the underactivation of Pre-SMA and PFC. A following study by Haslinger et al. (Haslinger et al. 2001) included an OFF as well as an ON condition after intake of 200 mg levodopa in eight PD patients. The authors performed fMRI during auditory-paced single joystick movements in a freely chosen directory (four grades of freedom) in an event-related design. The study revealed reduced activation of the Pre-SMA along with an increased activation of M1 and lateral PM in the OFF condition, in accordance with the results of Sabatini et al. After intake of levodopa, patients showed an activation pattern similar to healthy controls, comprising increased activation in the mesial PM and decreased activation in M1, lateral PM, and superior parietal cortex compared to the OFF condition. In contrast, Buhmann et al. found results incongruent to the two aforementioned studies (Buhmann et al. 2003). The authors scanned eight drug-naive patients before and repeatedly every 20 min after intake of 300 mg of fast-release levodopa. The paradigm consisted of a simple auditory-paced finger opposition task at a frequency of 0.33 Hz. While M1 and SMA were hypoactive in the OFF condition, levodopa led to an increase in M1 and SMA activity, which was highly correlated with motor performance. In contrast to Sabatini et al. and Haslinger et al., who proposed that increased activity of M1 in the OFF state might represent a compensational mechanism, Buhmann and colleagues attributed the deficient activation of M1 in unmedicated de novo PD patients to the degeneration of dopaminergic neurons in SNc leading to decreased excitatory input from BG to cortical motor areas (see also Sect. 18.1).

While early fMRI studies were concerned with differences in activation in single neural regions, recent studies focused on changes in functional integration, analyzing the alterations in the connectivity patterns among brain regions forming functional neural networks (Rowe 2010). One fMRI study investigated the underlying pathophysiology of impaired performance of bimanual movements in PD (Wu et al. 2010). PD patients in the OFF state were impaired during the performance of bimanual anti-phase movements, which was associated with decreased activity in SMA and BG and increased activity in multiple areas such as M1, lateral PM, and cerebellum. Using the psychophysiological interaction (PPI) method (Friston et al. 1997), connectivity analysis revealed decreased influence of the SMA to prefrontal regions and BG which was paralleled by an increased coupling with M1, cerebellum, parietal areas, and precuneus. The same group found similar results in 18 PD patients during a self-initiated unimanual tapping task (Wu et al. 2011). In that study, PD patients in the OFF condition showed decreased connectivity from BG to cortical motor areas, such as M1, PM, and Pre-SMA as well as the cerebellum, and an increased connectivity between cortical motor areas and the cerebellum. The increased cortico-cortical and cortico-cerebellar connectivity might compensate for impaired coupling between executive motor areas and BG and explain the observed hyperactivation in M1 in progressed PD (Haslinger et al. 2001; Sabatini et al. 2000). Using a different type of connectivity analysis, dynamic causal modeling (DCM; Friston et al. 2003), Rowe et al. assessed cortico-cortical connectivity during a simple visually paced finger-tapping task in 16 patients with PD both OFF and ON medication (Rowe et al. 2010). In medicated patients as well as healthy controls, action selection was associated with increased coupling between PFC and Pre-SMA. In contrast, patients OFF medication showed enhanced coupling between PFC and lateral PM.

An important factor that determines the cortical activity patterns during motor tasks is the amount of attention that is assigned to the task. Rowe et al. (Rowe et al. 2002) addressed this issue using a simple paced overlearned sequence task in 12 PD patients in the OFF condition. While patients showed a greater than normal activation in SMA during the simple motor task, they failed to augment SMA activity when they were asked to actively attend to their actions. Connectivity analysis based on structural equation modeling (SEM; Buchel and Friston 1997) revealed that in contrast to healthy controls, patients did not

increase effective connectivity between PFC and both lateral PM and SMA when they were asked to attend their actions. This finding indicates that a disconnection between prefrontal attentional networks and frontoparietal motor networks might underlie the commonly observed underactivation in SMA. Interestingly, attentional control in PD patients critically depends on their catechol O-methyltransferase (COMT) genotype. Williams-Gray and colleagues (Williams-Gray et al. 2008) studied 16 patients with high-activity COMT genotypes (val/val) and 13 patients with low-activity COMT genotypes (met/met) with a sophisticated paradigm probing the ability to form an attentional "set" in the ON condition. Patients with low-activity COMT genotypes failed to show a normal approach of shifting attention, which was associated with an underactivation across frontoparietal attentional networks.

Taken together, fMRI studies of the motor system in PD have given important insights into the pathophysiology underlying motor impairment and revealed potential compensatory mechanisms. Recent advances in network analyses have been used to assess abnormal task-related connectivity patterns in PD and highlight the importance of attentional networks in modulating motor loops.

18.2.3 Functional MRI Studies of Non-motor Functions

Even in early stages of the disease, PD impairs neurological functions beyond the motor system (Foltynie et al. 2004; Williams-Gray et al. 2007). Cognitive impairment in PD is commonly described as a disorder of frontal executive function that comprises attentional control, such as working memory, set-switching, and planning, as well as control of reward-related behavior and risk-taking (Owen et al. 1992). The nature of cognitive deficits in PD patients is rather complex, since they depend on disease severity, medication, and genotype (Rowe et al. 2008; Williams-Gray et al. 2008). The optimal dopamine level differs for the motor, cognitive, and limbic loops and is commonly described as an inverted-U-shaped relationship between dopaminergic state and function (Fig. 18.3). However, the optimal dose of levodopa replacement is usually based on motor improvement and can therefore lead to a suboptimal level of dopamine in non-motor loops (Cools and D'esposito 2011).

To investigate the neural underpinnings of impaired working memory in PD, Lewis and coworkers studied 21 PD patients with and without cognitive deficits in the ON state using a working-memory paradigm (Lewis et al. 2003). They could show that impairments in working memory were associated with decreased activity in local sites in the BG and frontal lobe. Since this hypoactivation was not seen in PD patients without cognitive deficits, the authors concluded that cognitive deficits in PD are linked to cortico-subcortical loops distinct to loops responsible for motor impairment. Marklund et al. (Marklund et al. 2009) performed fMRI during a 2-back working-memory task in 20 untreated de novo PD patients to assess distinct processes of working memory. The 2-back task required participants to indicate whether a presented word matched the one presented two times earlier. The study design enabled the authors to dissociate transient (event-related) brain responses from sustained (epoch-related) responses. The results suggested that working-memory dysfunction in early PD is mainly caused by dysregulated phasic dopamine responses in the caudate, even though initial signs of tonic control impairment were also observed.

An important theme of recent neuroimaging research was to clarify how dopaminergic medication impacts on different brain functions in PD (Rowe et al. 2008). To elucidate the effect of dopamine on different cortico-subcortical loops, MacDonald et al. used a selection paradigm in 20 PD patients before and after intake of levodopa (MacDonald et al. 2011). During the behavioral experiment, patients had to encode stimulus-stimulus relations, which is thought to be processed in the ventral striatum, and control interference, which is thought to be mediated by the dorsal striatum. While dopamine replacement enhanced dorsal striatum function (interference control), it impaired function mediated by the

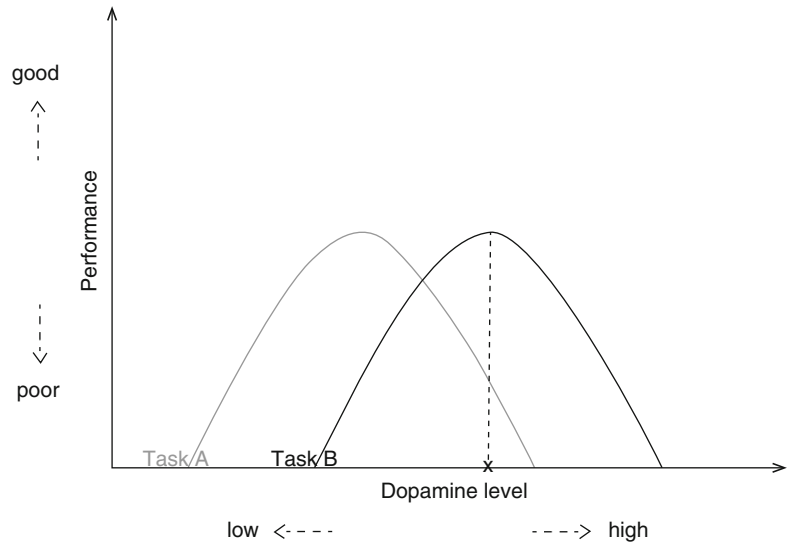

Fig. 18.3 Different optimal dopamine levels for different tasks/functions schematically. While a given dopamine level X optimizes performance on *task B*, it impairs performance on *task A*, which has a lower optimal dopamine level. Such dopamine-dependent differences in performance can be observed in paradigms probing different neural system (e.g., motor vs. cognitive) or different aspects of cognitive control (e.g., stability vs. flexibility)

ventral striatum (encoding of stimulus-stimulus relations). Differential effects of dopamine replacement on functional brain networks in PD had also been demonstrated in 19 PD patients performing a bimodality continuous performance task in which letters were shown at one of eight radial locations (Rowe et al. 2008). Here, a target trial was defined either by the position or type of letter. Subjects were instructed to indicate whether a trial was a target trial and were given a monetary bonus if three sequential targets within a given dimension were detected successfully. Thus, to receive the reward participants had to identify the relevant stimulus dimension (spatial or verbal) and detect the according target trials. PD patients were able to successfully solve the task but showed interindividual differences in neural activation depending on disease severity as reflected by motor impairment. Both lateral PFC and caudate nucleus showed a nonlinear U-shaped relationship between motor impairment and task-related neural activity. Patients with the most and the least motor impairment showed higher task-related activity, whereas patients with medium disease severity showed lower task-related activity. Dopamine replacement led to a lateral shift of this relationship, improving motor impairment but not cognitive function.

Another interesting finding was that activation in the anterior cingulate cortex (ACC) during reward expectation decreased with motor impairment, while ACC activation after an actual reward increased with motor impairment. Rowe et al. discuss that this might signify a change in goal-oriented behavior from expected to actual rewards. Changes in reward-related behavior have important clinical implications. Impulse control disorders (ICD), such as pathological gambling or compulsive shopping, are frequently observed in PD patients and are associated with the use of dopamine agonists (Weintraub et al. 2006). However, the mechanisms underlying impaired control of reward-related behavior and risk-taking by dopamine agonists are not entirely understood. To address this question, Voon and coworkers studied 22 PD patients with and without excessive gambling and shopping behavior using a probabilistic learning task (Voon et al. 2010). In this task participants had to learn if a symbol was associated with reward or loss. A third condition included neutral trials. Unpredicted, surprising outcomes, for instance, when a symbol that only has a 20 % reward probability leads to an actual reward, give rise to a prediction error signal in the ventral striatum that updates the internal representations of reward predictions (Rushworth and Behrens 2008). Patients with ICDs showed an increased striatal prediction error signal in the gain condition after intake of dopamine agonists, signaling a better

than expected outcome. It was argued that this dysregulation might bias PD patients with ICDs toward compulsive reward-seeking behaviors.

The same group investigated if dopamine agonists impair risk control (Voon et al. 2011). They studied 28 PD patients with and without ICDs using a risk-taking paradigm in an OFF and an ON condition. Participants could make a safe or a risky gamble choice starting with either a balanced (gain condition) or negative amount (loss condition). Patients with ICDs made more risky choices in the gain condition associated with decreased activity in OFC and ACC. PD patients with ICDs showed an increased sensitivity to risk, i.e., were biased toward increased risk-taking, after intake of dopamine agonists. This alteration in risk control was associated with decreased activity in the ventral striatum. The authors conclude that PD patients with ICDs show a change in attitude to risky situations, and that the effect of dopamine agonists critically depends on the underlying vulnerability.

Taken together, studies investigating non-motor functions in PD have shown that alterations in networks involved in attentional control occur already in early disease stages. Dopaminergic therapy has differential effects on neural functions depending on the task (e.g., motor and cognitive) and disease severity. Additionally, dopamine agonist can alter the control of reward-related behavior and risk-taking by affecting the regulation of dopaminergic signaling in the striatum and thereby lead to serious side effects such as ICDs.

18.2.4 Preclinical Compensation

Mutations in the Parkin and PINK1 gene are among the most common recessively inherited genes that can cause familial forms of PD (Gasser 2007). Non-manifesting heterozygous carriers of Parkin and PINK1 mutations show a subclinical nigrostriatal dopaminergic degeneration (Hilker et al. 2001; Khan et al. 2005) and give the unique opportunity to study preclinical compensational mechanisms of dopaminergic dysfunction. Importantly, asymptomatic carriers do not show motor impairment, allowing for assessment of motor-related neural activity without a behavioral confound. Buhmann et al. (Buhmann et al. 2005) studied 12 non-manifesting carriers of a Parkin mutation during unimanual simple finger-to-thumb opposition movements. The movements were visually paced at a frequency of 0.33 Hz, and the finger that had to be used was either internally or externally cued. Non-manifesting mutation carriers showed a stronger activation of rostral cingulate motor area (CMA) and left dorsal PM during internally cued compared to externally cued movements. Connectivity analysis using PPI additionally revealed an increased effective connectivity between rostral CMA and the dopamine-deficient left posterior putamen during internally cued movements in Parkin-mutation carriers. A consecutive study by van Nuenen and colleagues included 9 PINK1-mutation carriers and 13 Parkin-mutation carriers (Van Nuenen et al. 2009). Participants had to perform visually cued simple sequences of three unimanual thumb-to-finger opposition movements. In contrast to healthy controls, both PINK1- and Parkin-mutation carriers showed an increased activation of Pre-SMA and the right dorsal PM during the motor task.

These two studies show that a preclinical nigrostriatal dopaminergic degeneration leads to a compensatory increase in activity of motor cortical areas within task-specific networks. Such compensatory mechanisms could explain why patients with sporadic PD first become symptomatic several years after the neurodegeneration of dopaminergic striatonigral neurons has started. The results additionally indicate that it might be possible to detect PD using fMRI even before motor symptoms manifest. This genetically informed approach could be easily extended to other patient groups carrying mutations in other genes associated with PD. An alternative strategy is to perform fMRI studies in populations with clinical signs such as anosmia or REM sleep disorder that might precede the motor manifestation of PD and, thus, are associated with an increased risk to develop PD during later life (Savica et al. 2010).

18.3 Perspectives

Studies using fMRI have given important insights into abnormal neural networks underlying motor and non-motor symptoms in PD. An important fact one has to bear in mind when interpreting these results is that the reported studies almost entirely included patients with akinetic-rigid PD, since tremor heavily interferes with data acquisition. Sophisticated devices, such as online monitoring and correction of movements, would allow for studying this large group of PD patients. Additionally, using pharmacologically modulated fMRI, dynamic changes in neural activity can be assessed by scanning patients during a period from the absence until emergence of involuntary movements. Such studies are necessary to improve our knowledge of pathophysiological changes underlying hyperkinetic movement disorders. Network analyses of resting-state as well as task-related fMRI have been shown to be sensitive to changes caused by PD. Longitudinal studies could help to better understand the effect of progressive neurodegeneration on neural networks and to relate activity patterns to emerging symptoms or side effects. Such studies could render possible to detect patients vulnerable to side effects and used to tailor therapy to the underlying pathology of the individual patient.

References

Albin RL, Young AB et al (1989) The functional anatomy of basal ganglia disorders. Trends Neurosci 12: 366–375

Alexander GE, Delong MR et al (1986) Parallel organization of functionally segregated circuits linking basal ganglia and cortex. Annu Rev Neurosci 9:357–381

Baudrexel S, Witte T et al (2011) Resting state fMRI reveals increased subthalamic nucleus-motor cortex connectivity in Parkinson's disease. Neuroimage 55:1728–1738

Biswal B, Yetkin FZ et al (1995) Functional connectivity in the motor cortex of resting human brain using echo-planar MRI. Magn Reson Med 34:537–541

Brown P (2007) Abnormal oscillatory synchronisation in the motor system leads to impaired movement. Curr Opin Neurobiol 17:656–664

Buchel C, Friston KJ (1997) Modulation of connectivity in visual pathways by attention: cortical interactions evaluated with structural equation modelling and fMRI. Cereb Cortex 7:768–778

Buhmann C, Glauche V et al (2003) Pharmacologically modulated fMRI – cortical responsiveness to levodopa in drug-naive hemiparkinsonian patients. Brain 126: 451–461

Buhmann C, Binkofski F et al (2005) Motor reorganization in asymptomatic carriers of a single mutant Parkin allele: a human model for presymptomatic parkinsonism. Brain 128:2281–2290

Calabresi P, Picconi B et al (2007) Dopamine-mediated regulation of corticostriatal synaptic plasticity. Trends Neurosci 30:211–219

Cools R, D'esposito M (2011) Inverted-U-shaped dopamine actions on human working memory and cognitive control. Biol Psychiatry 69:e113–e125

Delong MR (1990) Primate models of movement disorders of basal ganglia origin. Trends Neurosci 13:281–285

Di Martino A, Scheres A et al (2008) Functional connectivity of human striatum: a resting state FMRI study. Cereb Cortex 18:2735–2747

Foltynie T, Brayne CE et al (2004) The cognitive ability of an incident cohort of Parkinson's patients in the UK. The CamPaIGN study. Brain 127:550–560

Fox MD, Raichle ME (2007) Spontaneous fluctuations in brain activity observed with functional magnetic resonance imaging. Nat Rev Neurosci 8:700–711

Friston KJ, Buechel C et al (1997) Psychophysiological and modulatory interactions in neuroimaging. Neuroimage 6:218–229

Friston KJ, Harrison L et al (2003) Dynamic causal modelling. Neuroimage 19:1273–1302

Gasser T (2007) Update on the genetics of Parkinson's disease. Mov Disord 22(Suppl 17):S343–S350

Gradinaru V, Mogri M et al (2009) Optical deconstruction of parkinsonian neural circuitry. Science 324:354–359

Haslinger B, Erhard P et al (2001) Event-related functional magnetic resonance imaging in Parkinson's disease before and after levodopa. Brain 124:558–570

Helmich RC, Aarts E et al (2009) Increased dependence of action selection on recent motor history in Parkinson's disease. J Neurosci 29:6105–6113

Helmich RC, Derikx LC et al (2010) Spatial remapping of cortico-striatal connectivity in Parkinson's disease. Cereb Cortex 20:1175–1186

Hilker R, Klein C et al (2001) Positron emission tomographic analysis of the nigrostriatal dopaminergic system in familial parkinsonism associated with mutations in the parkin gene. Ann Neurol 49:367–376

Jahanshahi M, Jenkins IH et al (1995) Self-initiated versus externally triggered movements. I. An investigation using measurement of regional cerebral blood flow with PET and movement-related potentials in normal and Parkinson's disease subjects. Brain 118(Pt 4):913–933

Jankovic J (2008) Parkinson's disease: clinical features and diagnosis. J Neurol Neurosurg Psychiatry 79:368–376

Khan NL, Scherfler C et al (2005) Dopaminergic dysfunction in unrelated, asymptomatic carriers of a single parkin mutation. Neurology 64:134–136

Lalo E, Thobois S et al (2008) Patterns of bidirectional communication between cortex and basal ganglia during movement in patients with Parkinson disease. J Neurosci 28:3008–3016

Lang AE, Lozano AM (1998a) Parkinson's disease. Second of two parts. N Engl J Med 339:1130–1143

Lang AE, Lozano AM (1998b) Parkinson's disease. First of two parts. N Engl J Med 339:1044–1053

Lewis SJ, Dove A et al (2003) Cognitive impairments in early Parkinson's disease are accompanied by reductions in activity in frontostriatal neural circuitry. J Neurosci 23:6351–6356

MacDonald PA, MacDonald AA et al (2011) The effect of dopamine therapy on ventral and dorsal striatum-mediated cognition in Parkinson's disease: support from functional MRI. Brain 134:1447–1463

Marklund P, Larsson A et al (2009) Temporal dynamics of basal ganglia under-recruitment in Parkinson's disease: transient caudate abnormalities during updating of working memory. Brain 132:336–346

Mink JW (1996) The basal ganglia: focused selection and inhibition of competing motor programs. Prog Neurobiol 50:381–425

Nambu A, Tokuno H et al (2000) Excitatory cortical inputs to pallidal neurons via the subthalamic nucleus in the monkey. J Neurophysiol 84:289–300

Owen AM, James M et al (1992) Fronto-striatal cognitive deficits at different stages of Parkinson's disease. Brain 115(Pt 6):1727–1751

Palmer SJ, Eigenraam L et al (2009) Levodopa-sensitive, dynamic changes in effective connectivity during simultaneous movements in Parkinson's disease. Neuroscience 158:693–704

Playford ED, Jenkins IH et al (1992) Impaired mesial frontal and putamen activation in Parkinson's disease: a positron emission tomography study. Ann Neurol 32: 151–161

Redgrave P, Gurney K et al (2008) What is reinforced by phasic dopamine signals? Brain Res Rev 58: 322–339

Rinne OJ, Nurmi E et al (2001) [(18)F]FDOPA and [(18)F] CFT are both sensitive PET markers to detect presynaptic dopaminergic hypofunction in early Parkinson's disease. Synapse 40:193–200

Rowe JB (2010) Connectivity analysis is essential to understand neurological disorders. Front Syst Neurosci 4:144

Rowe J, Stephan KE et al (2002) Attention to action in Parkinson's disease: impaired effective connectivity among frontal cortical regions. Brain 125:276–289

Rowe JB, Hughes L et al (2008) Parkinson's disease and dopaminergic therapy–differential effects on movement, reward and cognition. Brain 131:2094–2105

Rowe JB, Hughes LE et al (2010) Dynamic causal modelling of effective connectivity from fMRI: are results reproducible and sensitive to Parkinson's disease and its treatment? Neuroimage 52:1015–1026

Rushworth MF, Behrens TE (2008) Choice, uncertainty and value in prefrontal and cingulate cortex. Nat Neurosci 11:389–397

Sabatini U, Boulanouar K et al (2000) Cortical motor reorganization in akinetic patients with Parkinson's disease: a functional MRI study. Brain 123(Pt 2):394–403

Savica R, Rocca WA et al (2010) When does Parkinson disease start? Arch Neurol 67:798–801

Skidmore FM, Yang M et al (2011a) Apathy, depression, and motor symptoms have distinct and separable resting activity patterns in idiopathic Parkinson disease. Neuroimage (in press)

Skidmore FM, Yang M et al (2011b) Reliability analysis of the resting state can sensitively and specifically identify the presence of Parkinson disease. Neuroimage (in press)

Van Nuenen BF, Weiss MM et al (2009) Heterozygous carriers of a Parkin or PINK1 mutation share a common functional endophenotype. Neurology 72:1041–1047

Voon V, Pessiglione M et al (2010) Mechanisms underlying dopamine-mediated reward bias in compulsive behaviors. Neuron 65:135–142

Voon V, Gao J et al (2011) Dopamine agonists and risk: impulse control disorders in Parkinson's disease. Brain 134:1438–1446

Weintraub D, Siderowf AD et al (2006) Association of dopamine agonist use with impulse control disorders in Parkinson disease. Arch Neurol 63:969–973

Williams-Gray CH, Foltynie T et al (2007) Evolution of cognitive dysfunction in an incident Parkinson's disease cohort. Brain 130:1787–1798

Williams-Gray CH, Hampshire A et al (2008) Attentional control in Parkinson's disease is dependent on COMT val 158 met genotype. Brain 131:397–408

Wu T, Wang L et al (2010) Neural correlates of bimanual anti-phase and in-phase movements in Parkinson's disease. Brain 133:2394–2409

Wu T, Wang L et al (2011) Effective connectivity of brain networks during self-initiated movement in Parkinson's disease. Neuroimage 55:204–215

19 The Perirhinal, Entorhinal, and Parahippocampal Cortices and Hippocampus: An Overview of Functional Anatomy and Protocol for Their Segmentation in MR Images

Sasa L. Kivisaari, Alphonse Probst, and Kirsten I. Taylor

Abbreviations

A	Anterior
Ab	Angular bundle (PHg white matter)
aCf	Anterior calcarine fissure
al	Alveus
Am	Amygdala
bG	Band of Giacomini
cf	Crus of the fornix
Cs	Collateral sulcus
di	Hippocampal digitations
ERc	Entorhinal cortex
Fg	Fusiform gyrus
fi	Fimbria
gA	Gyrus ambiens
gS	Gyrus of Schwalbe
HB	Hippocampal body
Hf	Hippocampal fissure
HH	Hippocampal head
Hs	Hippocampal sulcus
HT	Hippocampal tail
I	Inferior
ILg	Intralimbic gyrus
Is	Isthmus
ITg	Inferotemporal gyrus
L	Laterial
Lg	Lingual gyrus
li-gm	Limen insulae gray matter
li-wm	Limen insulae white matter
M	Medial
Mb	Mammillary body
MTL	Medial temporal lobe
OTs	Occipitotemporal sulcus
P	Posterior
Pu	Pulvinar
PHc	Parahippocampal cortex
PHg	Parahippocampal gyrus
PRc	Perirhinal cortex
qgc	Quadrigeminal cistern
Rs	Rhinal sulcus
S	Superior
SAs	Semiannular sulcus
SLg	Semilunar gyrus
Sp	Splenium
su	Subiculum
TLV	Temporal horn of lateral ventricle
TP	Temporal pole

S.L. Kivisaari, Ph.D. (✉)
Department of Geriatrics,
Memory Clinic, University Hospital Basel,
Schanzenstrasse 55, CH-4031, Basel, Switzerland
e-mail: skivisaari@uhbs.ch

A. Probst, M.D.
Department of Geriatrics,
Memory Clinic, University Hospital Basel,
Schanzenstrasse 55, CH-4031, Basel, Switzerland

Department of Neuropathology,
University Hospital Basel,
Schönbeinstrasse 40, CH-4031, Basel, Switzerland
e-mail: aprobst@uhbs.ch

K.I. Taylor, Ph.D.
Department of Geriatrics,
Memory Clinic, University Hospital Basel,
Schanzenstrasse 55, CH-4031, Basel, Switzerland

Department of Experimental Psychology,
Centre for Speech Language and the Brain,
University of Cambridge,
Downing Street, Cambridge, CB2 3EB, UK
e-mail: ktaylor@uhbs.ch

S. Ulmer, O. Jansen (eds.), *fMRI – Basics and Clinical Applications*,
DOI 10.1007/978-3-642-34342-1_19,

TR	Transentorhinal cortex
U	Uncus
Ug	Uncinate gyrus
un	Uncal notch

19.1 Introduction

Medial temporal lobe (MTL) damage severely disrupts our ability to form new memories (Scoville and Milner 1957). Indeed, memory dysfunction is the hallmark of Alzheimer's disease (AD; e.g., Salmon 2011), a progressive neurodegenerative disorder which begins in and most prominently affects the MTL region (Braak and Braak 1991). Accordingly, the classical model of memory claims that the MTL functions as a single system subserving memory formation, and not other kinds of cognitive processes (Squire and Zola-Morgan 1988; Squire and Zola 1998; Squire and Wixted 2011).

Converging evidence from animal and human cognitive neuroscience research suggests a more differentiated picture, one of functional diversity in the MTL subregions (e.g., Lee et al. 2005; Davachi 2006). Thus, in addition to supporting the formation of memories, each MTL subregion may also perform other specific functions. A first section briefly describes the putative specialized functional roles of the MTL subregions, namely, the perirhinal cortex (PRc; Broadmann areas [BA] 35/36), entorhinal cortex (ERc; BA 28/34), the posteriorly situated parahippocampal cortex (PHc; BA 36; also known as posterior parahippocampal cortex), and the hippocampus proper, highlighting recent findings from animal and human cognitive neuroscience research.

The functional neuroanatomy of the MTL, including but not limited to the domain of memory, has implications for the clinical interpretation of circumscribed MTL lesions as well as the interpretation of functional impairments in patients with neurodegenerative disorders, most notably AD. A second section therefore describes the neuropsychology of the early AD syndrome including amnestic mild cognitive impairment (aMCI; Winblad et al. 2004).

The prerequisite for advancements in this important area of research is the valid and reliable identification of these regions on structural brain imaging scans. Indeed, many of the controversies in current human neuropsychological research may stem from inadequate control of lesion extent and location, as noted by Squire and Wixted: "The importance of thorough neuroanatomical measurement in neuropsychological studies of memory cannot be overstated. Many current disagreements about the facts and ideas emerging from neuropsychological research on human memory can be traced to concerns about the locus and extent of lesions. […] There is no substitute for thorough, quantitative descriptions of damage based on magnetic resonance imaging, as well as (where possible) detailed neurohistological description of the postmortem brain" (Squire and Wixted 2011, p. 268). The identification of MTL subregions is challenging because of the uncertainty or obscurity of anatomical landmarks, a difficulty compounded by the fact that some MTL gyri and sulci are interindividually highly variable. A third section therefore describes the gross anatomy of the MTL and, building upon previous seminal work of especially Insausti and colleagues (Insausti et al. 1998), presents a method for delineating the PRc, ERc, PHc, and the hippocampus proper on structural MR images (see also Watson et al. 1992; Insausti et al. 1998; Pruessner et al. 2000; Van Hoesen et al. 2000; Vogt et al. 2006; Malykhin et al. 2007; Taylor and Probst 2008; Van Hoesen 1995).

19.2 Functional Neuroanatomy of the MTL

The MTL has been irrevocably linked with the formation of long-term memory traces since Scoville and Milner's (Scoville and Milner 1957) description of the patient H.M., who became severely amnesic following an experimental bilateral MTL resection to treat his intractable epilepsy. H.M.'s surgical lesion included the intraventricular portions of the bilateral hippocampi (see Fig. 19.7), the amygdalae, and the medial temporal poles and extended laterally to the ERc, with relative sparing of the PRc and PHc (Corkin et al. 1997). Following the procedure, H.M. suffered from a persistent and profound

anterograde amnesia, that is, an inability to remember events occurring after the operation, and a temporally graded retrograde amnesia, that is, difficulty remembering events that occurred within the 11 years preceding the MTL resection. He also suffered from partial anosmia, a lack of initiative and emotional bluntness (Corkin 1984). Strikingly, H.M.'s intellectual functions were relatively preserved, as were other forms of memory such as perceptual and motor skill learning, priming, habit formation, working memory, and memories for facts, events, and verbal semantic memories remote from his surgery (Corkin 1984). These functions enabled him to perform normally in many tasks including his avid crossword puzzle hobby (Skotko et al. 2008).

Cases such as H.M. were remarkable on many fronts. Most importantly, they demonstrated that memory indeed had a circumscribed anatomic basis in the MTL (*cf.* Lashley 1929).[1] It became clear that the type of memory typically affected in the MTL amnesia syndrome was the acquisition of declarative memories, that is, explicit memories of events from an individual's autobiography (episodic memory) and for facts and world knowledge (semantic memory), all of which are available to conscious awareness. The case of H.M. also sparked intensive work on rodents and nonhuman primates. The strategy used in this research was to ablate cytoarchitectonically distinct regions of the MTL and measure ensuing memory performance, research which critically relied on the delayed (non) matching-to-sample recognition memory paradigm.[2] This work led to the development of an animal model of amnesia where bilateral lesions of the hippocampus, parahippocampal gyrus, and amygdala were associated with severe recognition memory impairments with otherwise apparently preserved cognitive functions (Mahut et al. 1982; Mishkin 1978). More specific ablation studies refined these early results by demonstrating that lesions restricted to the hippocampus (Mahut et al. 1982; Zola-Morgan et al. 1989a; but see also Murray and Mishkin 1998) or to the parahippocampal gyrus (Zola-Morgan et al. 1989c; Meunier et al. 1993), but not amygdala (Zola-Morgan et al. 1989b) or mammillary bodies (Aggleton and Mishkin 1985), were sufficient to produce a severe recognition memory disorder. Moreover, the effects of lesions to different subregions appeared to be additive, and the most severe recognition memory impairment was measured following PRc lesions (Meunier et al. 1993; Zola-Morgan et al. 1989b). Drawing on these seminal experiments, Squire and colleagues developed the classical, single-process model of human memory functioning, which posited that the MTL subregions represent a single memory system in which each area is critical for forming declarative memories but do not participate in other cognitive functions (Zola-Morgan et al. 1986; Squire and Zola-Morgan 1988; Squire and Zola 1998; Squire and Wixted 2011). This classical, single-process model of MTL function has remained highly influential.

The field of MTL research has since burgeoned and now uses multimodal imaging methods with increasingly more detailed cognitive paradigms to study multidimensional aspects of MTL functioning. This work has led many authors to reconceptualize the MTL as a group of functionally specialized subregions (Mishkin et al. 1997; Aggleton and Brown 1999; Lavenex and Amaral 2000; Davachi 2006; Henke 2010; Montaldi and Mayes 2010; Ranganath 2010), with different models emphasizing different aspects of functional specialization. For example, the two-process model argues for specialized memory functions within the MTL, with the PRc supporting context-free item familiarity (i.e., a feeling of knowing that an item was previously encountered) and the hippocampus and PHc explicit, context-rich item recollection (Aggleton and Brown 1999, 2006; Brown and

[1]Later research demonstrated that profound memory impairments were also associated with damage to diencephalic regions such as mammillary bodies or mediodorsal nucleus of the thalamus (Squire and Zola-Morgan 1988; Victor et al. 1989), although the nature of the memory impairment differed from amnesia following MTL damage.

[2]In these experiments, an animal is presented with a sample stimulus during a learning phase. After a delay, the sample stimulus is presented again together with a novel stimulus. Intact recognition memory is demonstrated by the animal displacing either the sample object (delayed matching-to-sample) or the novel object (delayed nonmatching-to-sample).

Aggleton 2001; Yonelinas 2002; Montaldi and Mayes 2010). Other authors highlight functional-neuroanatomical relationships specific to object and spatial information processing (e.g., Davachi 2006; Lee et al. 2008) or item and relational information processing (e.g., Eichenbaum et al. 1999; Davachi and Wagner 2002; Davachi 2006; Henke 2010). Common to these models is the idea that while the entire network of highly interconnected subregions is typically engaged during declarative memory formation, each subregion may be specialized for processing a unique aspect of the event or concept (for reviews, see, e.g., Aggleton and Brown 1999, 2006; Eichenbaum et al. 1999, 2007; Squire et al. 2004; Moscovitch et al. 2005; Henson 2005; Davachi 2006; Henke 2010; Montaldi and Mayes 2010, 2011; Kravitz et al. 2011).

Many researchers of MTL function rely on an anatomically driven connectivity approach based on nonhuman primate data (Mishkin et al. 1983; Lavenex and Amaral 2000) to generate novel hypotheses of human MTL function. Nonhuman primate MTL connectivity demonstrates that each subregion receives information from different sensory and polymodal cortices and integrates the information it receives in intrinsic associational connections, in a hierarchical system from the PRc and PHc to the ERc, and from the ERc to the hippocampus (Mishkin et al. 1983, 1997; Lavenex and Amaral 2000). The first basic premise of this account is that each MTL subregion is specialized to process the information it receives and integrates in intrinsic associational connections (Lavenex and Amaral 2000, 2004). The second basic premise is that each processing level – from PRc/PHc to ERc, and from ERc to the hippocampus – is characterized by an increasing amount of convergence of information and a higher level of associativity of the coded representation (a "hierarchy of associativity"; Lavenex and Amaral 2000). Below we outline the functional neuroanatomy of the PRc, PHc, ERc, and hippocampus based on this approach.

The *perirhinal cortex* receives prominent afferents from the ventral visual object-processing stream (the "what" stream) and less dense inputs from other unimodal and polymodal sensory systems, the orbitofrontal cortex, insula, and cingulate cortex (Suzuki and Amaral 1994a). Tracing studies have also demonstrated a rich network of intrinsic associational connections within the PRc, which presumably bind this multimodal information together (Lavenex et al. 2004). In line with this connectivity pattern, numerous animal lesions studies have demonstrated that the PRc plays an essential role in visual object recognition memory (Meunier et al. 1993; Zola-Morgan et al. 1989c) and multimodal object memory (e.g., by forming flavor-visual and tactile-visual associations; see Murray and Richmond 2001; Murray et al. 1998 for overviews). Bussey, Saksida, Murray and colleagues suggested that the PRc represents the apex of the ventral occipitaltemporal visual processing pathway, which computes increasingly more complex combinations of visual features from posterior to anterior sites. Thus, the PRc may be enanged during demanding visual perceptual task, e.g. discriminating between objects who share many features with one another (Bussey and Saksida 2002; Bussey et al. 2005).

Research on human PRc functioning has been hampered by the paucity of naturally occurring lesions restricted to this region, although PRc damage does occur in the context of more widespread lesions. Moreover, fMRI studies are confronted with signal dropout around the PRc due to nearby air-tissue interfaces which induce susceptibility artifacts in gradient-echo sequences (Cusack et al. 2005; Schmidt et al. 2005; Bellgowan et al. 2006; Schwarzbauer et al. 2010). Nonetheless, converging evidence from human functional imaging and patient studies broadly support the nonhuman primate findings described above. In fMRI studies, PRc activity in healthy controls has been associated with memorizing individual items (Davachi and Wagner 2002), changes in object identity (Pihlajamäki et al. 2004; Köhler et al. 2005; O'Neil et al. 2009), fine-grained analyses of visual objects (Tyler et al. 2004), the recognition of ambiguous visual objects (Moss et al. 2005), demanding visual discrimination tasks (Barense et al. 2005), and the integration of object features from different sensory modalities (Taylor et al. 2006). In

the same vein, patients with brain damage in the parahippocampal gyrus including the PRc were impaired in discriminating highly similar, complex visual stimuli (Barense et al. 2007, 2010; Moss et al. 2005) and integrating crossmodal object features (Taylor et al. 2009, 2011a), even in the absence of memory demands. Finally, difficulties in visual object recognition memory were observed in patients with aMCI (Barbeau et al. 2004), commonly considered a possible AD prodrome with putative PRc pathology (Braak and Braak 1991).

The nature of information integrated in the PRc – multimodal and potentially non-sensory motivational features (Liu et al. 2000) associated with individual objects – has led some authors to suggest that the PRc codes for semantic object memories, that is, our knowledge about individual objects (Murray and Richmond 2001). For example, despite H.M.'s profound amnesia, he was able to acquire fragments of conceptual information, a feat attributed to his relatively intact PRc (*cf.* Corkin et al. 1997). When presented with the names of people who became famous after his MTL resection, H.M. was able to correctly distinguish these names from unfamiliar foil names, showing only a mild impairment relative to control participants (O'Kane et al. 2004). In an influential study, Vargha-Khadem and colleagues (1997) studied four patients with selective hippocampal damage acquired at an early age, who were nonetheless able to acquire normal levels of language comprehension and perform relatively well in school, that is, acquire semantic-like knowledge. Thus, although these individuals were significantly impaired at encoding the events in their lives, they were able to acquire world knowledge (semantic memories), an ability attributed to the intact parahippocampal gyrus (Mishkin et al. 1997; Vargha-Khadem et al. 1997).

MRI studies in humans provide additional support for the role of the PRc in processing the meaning of individual objects: fMRI studies showed that PRc activity was related to the meaning of object stimuli (Moss et al. 2005; Taylor et al. 2006; see also Wang et al. 2010), while voxel-based correlation studies (Hirni et al. 2011; Taylor et al. 2011b) and a cortical thickness study (Kivisaari et al. 2012) demonstrated significant relationships between gray matter integrity in the MTL, including the PRc and performance on semantic object tasks. Semantic object processing in the PRc may also manifest itself as the feeling of familiarity about having previously encountered an object in the absence of recall about specific contextual details (two-process models; see Eichenbaum et al. 2007; Montaldi and Mayes 2010 for reviews). Taken together, these findings suggest that the PRc integrates the visual and multimodal information it receives to support complex visual discriminations (Bussey et al. 2002, 2005) and to form visual and multimodal memories of meaningful objects, that is, semantic object memories.

The *parahippocampal cortex* lies posterior to the PRc and receives afferent projections primarily from the dorsal ("where") processing system in the posterior parietal cortex (Suzuki and Amaral 1994a). This "parieto-medial temporal pathway" has been implicated in visuospatial processing (Kravitz et al. 2011). It begins in the posterior inferior parietal lobule and sends direct connections to the PHc and hippocampus as well as indirect connections via the posterior cingulate and retrosplenial cortices to the PHc and same hippocampal fields. Thus, the PHc is attributed a central role in processing visuospatial and landmark information. Accordingly, in nonhuman primate studies, PHc damage has been linked with the impaired recognition of novel object locations and object-place associations (Alvarado and Bachevalier 2005a; Bachevalier and Nemanic 2008).

Findings from human functional imaging studies suggest that also the human PHc processes spatial and navigational information (Köhler et al. 2002, 2005; Buffalo et al. 2006; Staresina et al. 2011). For example, Pihlajamäki et al. (Pihlajamäki et al. 2004) demonstrated heightened PHc (and posterior hippocampal) activation when participants processed novel spatial arrangements of familiar objects, in contrast with the processing of novel objects in the same spatial arrangement. Evidence for a role of the PHc in landmark processing in healthy participants was provided

by Maguire and colleagues (1998), who found heightened PHc metabolism when participants navigated in virtual environments with salient objects and textures compared to when they navigated in empty environments. Similarly, Burgess and colleagues (Burgess et al. 2001) showed increased BOLD activation in the PHc when participants recalled landmarks from memory and in the absence of spatial scene information. Moreover, Epstein and Kanwisher (Epstein and Kanwisher 1998) observed that posterior parts of the bilateral parahippocampal gyri extending into the lingual gyri were preferentially activated when participants observed real or artificial visual scenes, with attenuated activity during the viewing of objects, faces, or scrambled scenes. These relationships prompted Kanwisher and colleagues to label an area in the posterior PHc displaying these characteristics as the parahippocampal place area (PPA; Epstein and Kanwisher 1998; Epstein et al. 1999; see also Grill-Spector and Malach 2004). These studies suggest that PHc processes both perceptual and mnemonic features of its preferred stimuli, that is, the spatial arrangement of objects or landmarks, which underpin our ability to navigate in the environment.

Other authors have suggested that the PHc processes not just spatial landmark or scenic stimuli and memories but more abstract information related to these stimuli (Diana et al. 2007). For example, BOLD activity in the PHc was stronger in response to strongly semantically related object-scene pairs (e.g., a driving wheel inside a car) compared to weakly semantically related object-scene pairs (e.g., a purse on a table; Bar et al. 2008). Bar and colleagues also found heightened PHc activity in response to objects which were strongly associated with a particular environment (e.g., a roulette wheel or beach chair as opposed to a cherry or basket), in the absence of an explicit spatial stimulus (Bar and Aminoff 2003). The sensitivity of the PHc to the meaningfulness of the visuospatial stimuli resembles the PRc's ability to code for the meaning of its preferred stimulus, that is, objects (see above).

Damage to the human PHc results in a pattern of deficits consistent with the functional imaging studies reported above, specifically, in the syndrome of topographical disorientation. Two variants of topographical disorientation are recognized: landmark agnosia and anterograde topographic disorientation (Paterson and Zancwill 1945; Whiteley and Warrington 1978; De Renzi 1982; Barrash 1998). Damage to the posterior PHc is associated with landmark agnosia, in which patients are unable to recognize famous or familiar environmental stimuli such as buildings, statues, or scenes (Epstein et al. 1999; Takahashi et al. 2002). These agnostic impairments lead to difficulties navigating the environment despite normal topographical memory and spatial processing ability (Aguirre and D'Esposito 1999). Patients with anterograde topographic disorientation (also known as topographical amnesia; De Renzi et al. 1977) following unilateral or bilateral PHc lesions have difficulties forming representations of new environments, with otherwise intact visuospatial functioning (Barrash 1998; Barrash et al. 2000; Bohbot et al. 2000). These patients are therefore also unable to orient and navigate in new environments but may successfully navigate in premorbidly familiar environments. Thus, these findings further support the view that the PHc is primarily involved in the perceptual and mnemonic processing of scenes, that is, the visuospatial arrangement of landmarks, and potentially their meaning, functions which enable orientation and navigation in the world.

The PRc and PHc send afferents to the *entorhinal cortex*, which receives less dense inputs from the amygdala, olfactory structures (e.g., piriform cortex, olfactory bulb), insula, frontal cortex, basal forebrain, thalamus, basal ganglia, and brainstem (Insausti et al. 1987; Suzuki and Amaral 1994b; Canto et al. 2008). A striking feature of the PRc and PHc afferents in the rodent and nonhuman primate ERc is the topographical segregation of their terminations: the anterolateral aspects of the nonhuman primate ERc receive highly integrated visual information via the PRc (Suzuki and Amaral 1994a, b), whereas the posteromedial aspects of the ERc receive information primarily from the parieto-medial temporal visuospatial pathway via the PHc (Suzuki and Amaral 1994a, b; Canto et al. 2008; Kravitz et al. 2011).

Notably, in rodents and nonhuman primates, the segregation of inputs is largely preserved in the intrinsic connectivity of the ERc (Dolorfo and Amaral 1998; Chrobak and Amaral 2007).

The afferent and intrinsic pattern of ERc connectivity suggests a relative segregation of object and spatial information processing in the anterolateral and posteromedial ERc, respectively. While largely unexplored in nonhuman and human primates, rodent research partly supports this functional-neuroanatomic division of labor. For example, cells in the rodent ERc receiving prominent visuospatial inputs show high spatial tuning, whereas cells in other ERc regions are only weakly modulated by spatial changes (Fyhn et al. 2004). Furthermore, lesions specifically in this spatially tuned area in the rodent ERc have been associated with spatial, navigational impairments (Steffenach et al. 2005). Perhaps most strikingly, a subgroup of cells in this region shows a high degree of spatial sensitivity when rats run freely in an open environment: these "grid cells" fire regularly as the rat traverses vertices of an imaginary grid of tessellated triangles mapped onto allocentric physical space (Hafting et al. 2005).[3] The dynamics of the population of grid cells may support "path integration," that is, the ability to determine one's current position relative to a starting point based on self-generated movement, as opposed to environmental cues (Witter and Moser 2006; Hasselmo and Brandon 2008). A potential segregation of ERc function has not yet been explicitly tested in primates (but see Suzuki et al. 1997).

[3]It is tempting to hypothesize similar grid cell properties for human ERc neurons. To our knowledge, a single human fMRI study has found evidence consistent with this hypothesis. Doeller and colleagues (Doeller et al. 2010) found that BOLD activity in the human ERc had a sixfold sinusoidal relationship with "running" direction in a circular-shaped virtual environment. This pattern of activation corresponds to the symmetry of grid cell firing in rodent ERc and putatively reflects whether the participants ran in alignment or misalignment with the grid axes. The ERc was activated as part of a larger network showing these properties, which included the posterior and medial parietal, lateral temporal, and medial prefrontal cortices (Doeller et al. 2010; see also Jacobs et al. 2010).

A specific role of the anterolateral ERc in object processing, as implied by its prominent PRc inputs, has not been definitively established. However, the entire ERc has been strongly implicated in object recognition memory. Animal lesion studies show that object recognition impairments, albeit mild, can follow selective ERc lesions (Leonard et al. 1995; Meunier et al. 1993), and that concomittant lesions of the PRc and ERc exacerbate the object recognition impairments found with selective PRc lesions (Meunier et al. 1993). A functional imaging study with healthy human participants demonstrated greater ERc activation during rote learning of words compared to the relational processing of words, supporting the role of human ERc in processing of single items (Davachi and Wagner 2002). Given the resolution of common fMRI studies, and the additional effects of Gaussian smoothing enabling group analyses, future human studies addressing this question will require high-resolution fMRI (Carr et al. 2010) in conjunction with refined behavioral tasks.

The most striking impairment following damage to the entire human ERc is episodic memory dysfunction (Eustache et al. 2001; Di Paola et al. 2007; Coutureau and Di Scala 2009). These lesions typically extend beyond the ERc into the hippocampus, such that it is not known whether isolated ERc lesions are sufficient to impair episodic memory functioning. Rather than focusing on the types of information processed or integrated in the ERc, recent studies of episodic memory functioning and the ERc focus on the electrophysiological properties of its neurons, which provide key information about how episodic memories are formed in downstream hippocampus. Specifically, in computational models, persistent firing upon depolarization and the oscillations of the dendritic membrane potential of some ERc neurons may give rise to cyclical and graded firing patterns which support information binding in downstream hippocampus (Hasselmo and Brandon 2008; Wallenstein et al. 1998; see also Fyhn et al. 2007; Lipton and Eichenbaum 2008). In summary, the ERc appears to be involved in both object and spatial processing, although evidence for the anatomical segregation of these

processes within the human ERc remains elusive. More evidence from lesion studies exists to suggest that ERc, together with the hippocampus, is critical for the formation of episodic memories, that is, the binding together of contextual and associative information with an object or scene. The ERc's specialized role in episodic memory formation may be reflected not only in the information content delivered by its afferent connections but also by the electrophysiological properties of its neurons.

The perforant pathway connects the ERc with the *hippocampus proper*, with primary projections to the dentate gyrus and weaker projections to the CA1 and CA3 subfields and the subiculum (Witter 2007). Nonhuman primate studies demonstrate that the pathway between the ERc and dentate gyrus has two main components: one set of connections links anterolateral ERc (which receives its primary input from the visual object-processing system via the PRc) with the intermediate and posterior parts of the hippocampus, and a second set links posteromedial ERc (the primary termination of PHc efferents coding spatial information) primarily with the posterior hippocampus (e.g., Witter and Amaral 1991; Witter 2007; see also Dolorfo and Amaral 1998). The most anterior parts of the hippocampus receive afferents from forebrain structures such as the amygdala and hypothalamus via the ERc and have been hypothesized potentially mediate endocrinological functions including stress-related physiological responses (Moser and Moser 1998).

Evidence of an anterior-posterior gradient of functional specialization implied by this connectivity pattern has indeed been demonstrated in several animal and human studies. Activation in the anterior extent of the hippocampal body has been demonstrated in response to judging object novelty (Pihlajamäki et al. 2004), and during a cross-modal object-processing task (e.g., Taylor et al. 2006). Similarly, lesions including the anterior hippocampi are associated with object-processing impairments (Barense et al. 2005; Acres et al. 2009; Taylor et al. 2009). Conversely, research on rats suggests relative specialization of the rodent homologue of posterior hippocampus to spatial processing. For example, the highly spatially tuned "place cells" (for reviews, see Eichenbaum et al. 1999; Burgess et al. 2002) are more prevalent in the rodent homologue of posterior compared to anterior primate hippocampus (Jung et al. 1994).[4] Correspondingly, lesions of the rodent homologue of the posterior hippocampus disrupt spatial learning (Colombo et al. 1998; for a review, see Moser and Moser 1998). Although subsequent research has failed to demonstrate place-like cells in the primate hippocampus, the posterior hippocampus nevertheless appears to contribute to spatial processing in primates (Alvarado and Bachevalier 2005b). For example, in human functional imaging studies, spatial tasks elicited activity in the posterior parts of the human hippocampus (e.g., Pihlajamäki et al. 2004), and a morphometric MR study demonstrated more voluminous posterior hippocampi in London taxi drivers with a highly developed spatial abilities (Maguire et al. 1998).

A higher-order anatomical characteristic of the hippocampus, beyond the hypothesized anterior-posterior gradient of functional specialization, is its location at the top of the MTL processing hierarchy (Lavenex and Amaral 2000). This position confers the ultimate integration ability on the hippocampus, functions presumably supported by intrinsic connectivity both longitudinally and mediolaterally (Witter 2007). Thus, the hippocampus has been suggested to bind multisensory object and spatial, contextual, and associational information together to represent our semantic and episodic memories, also more generally known as "relational memories" (Henke et al. 1997; Eichenbaum et al. 1999; Burgess et al. 2002; Davachi and Wagner 2002; Davachi 2006). In its basic form, these memories bind both spatial or context information from the dorsal stream, transmitted via PHc-ERc connections (Kravitz et al. 2011), together with object information received via PRc-ERc connections (Suzuki and Amaral 1994a).

[4]The original discovery of "place cells" demonstrated that these cells they selectively fired according to the animal's location in the environment (O'Keefe and Dostrovsky 1971), while later studies showed that firing patterns were also modulated by other factors such as motivational factors and environmental cues (Lipton and Eichenbaum 2008; see Eichenbaum et al. 1999 for a review).

Critically, the primate hippocampus additionally integrates higher-order, more abstract information related to objects and episodes together. For example, the nonhuman primate hippocampus was shown to be involved in a transverse patterning task which requires the formation of indirect associations between items (e.g., A is rewarded with B, B is rewarded with C, but A is not rewarded with C or B with A; Alvarado et al. 2002; Alvarado and Bachevalier 2005b). In human functional imaging studies, the hippocampus was activated during the formation of higher-order, semantic associations (Henke et al. 1997, 1999b; Davachi and Wagner 2002), upon presentation of novel spatial organization of objects or novel combination of familiar objects and familiar locations (i.e., Köhler et al. 2005) and object-space relationships (Hannula and Ranganath 2008). These findings are consistent with the clinical sequelae of isolated hippocampal lesions, that is, the classic amnesic syndrome. Such lesions may occur following carbon monoxide poisoning (Zola-Morgan et al. 1986; Vargha-Khadem et al. 1997; Henke et al. 1999a; Gadian et al. 2000), which causes cellular damage in the CA1 subfield of the hippocampus through hypoxic and histotoxic mechanisms (O'Donnell et al. 2000; Gale and Hopkins 2004). Patients with isolated hippocampal lesions display an anterograde amnesia for episodic memories with otherwise relatively normal cognitive functioning, similar to H.M. (see above; Vargha-Khadem et al. 1997; Zola-Morgan et al. 1986), although the magnitude of the impairment may be milder than that following more widespread MTL lesions (Zola-Morgan et al. 1986).

Recent models of hippocampal functioning emphasize its pattern separation and pattern completion abilities (Rolls 2007; Yassa and Stark 2011). Pattern separation is the appreciation of slight differences between sensory input and existing representations, a function which presumably enables the acquisition of distinct and complex representations corresponding to human episodic memories. The dentate gyrus and the CA3 of the hippocampus proper appear to be critically involved in rodent pattern separation (Leutgeb et al. 2007; Rolls 2007; see Yassa and Stark 2011 for a review), and this process is thought to be modulated by neurogenesis in the dentate gyrus (Deng et al. 2010). Tentative evidence for pattern separation functions in the human dentate gyrus and CA3 was provided by a high-resolution fMRI study by Bakker and colleagues (Bakker et al. 2008). These investigators presented participants with pictures of objects that were either novel, repeated, or slightly modified pictures of the repeated objects (lures). An area encompassing the DG and CA3 showed enhanced patterns of activity to novel and lure objects and weaker responses to object repetitions, suggesting that human DG and CA3 detect subtle differences between sensory input and existing representations. The process of pattern separation is hypothesized to be balanced by pattern completion, that is, the ability to recollect an existing representation on the basis of an incomplete set of cues (O'Reilly and McClelland 1994). This process is thought to be supported by ERc afferents bypassing the dentate gyrus, which may introduce the cue to CA3 to reactivate an existing representation, as well as auto-associative recurrent connectivity in CA3 (Leutgeb et al. 2007; Rolls 2007; Yassa and Stark 2011). The complementary processes of pattern separation and pattern completion may give rise to the capacity of human memory to treat highly similar episodes, such as events in the office on last Monday and Tuesday, as distinct from one another (pattern separation) while enabling the retrieval of a memory based on incomplete information, for example, remembering what took place on Monday based on knowing that a chocolate cake was available during the coffee break (pattern completion).

Taken together, animal and human studies demonstrate that the hippocampus, together with the ERc, binds information across spatial and temporal intervals, ultimately giving rise to complex, multicomponential semantic and episodic memories. These processes take place extremely rapidly and may even proceed in the absence of conscious awareness (Henke 2010). Pattern separation and completion processes in the hippocampus may represent fundamental processes supporting memory formation and retrieval, enabling the prerequisite disambiguation of experienced phenomena and successful retrieval based on fragmentary cues, respectively.

19.3 Alzheimer's Disease and Other Dementias Associated with the MTL

AD is a debilitating neurodegenerative condition which globally affects 3.9 % of the individuals over 60 years of age (Qiu et al. 2009). Since the risk of developing AD is strongly linked with increasing age, and given our increasing life expectancies, the prevalence of AD is expected to exponentially increase in the upcoming decades, tripling between 2010 and 2050 (Alzheimer's Association 2011). The clinical diagnosis of probable AD requires the presence of a memory impairment in addition to an impairment in one other domain of cognitive functioning (i.e., language, praxis, gnosis, and executive functions), which are severe enough to affect everyday functioning (American Psychiatric Association 1994). The definite diagnosis of AD is made upon autopsy, where it is characterized by two neuropathological hallmarks: the accumulation of amyloid β-peptide (Aβ) as plaques in the extracellular space in widespread regions of the brain and the formation of insoluble aggregates of hyperphosphorylated isoforms of microtubule-associated tau-proteins (Mattson 2004; Ewers et al. 2011). These abnormal isoforms of tau form neurofibrillary tangles in the nerve cells.

The distribution of neurofibrillary tangle deposition typically follows a sequential progression in the cerebral cortex (Braak and Braak 1991). Correspondingly, the stage of neurofibrillary pathology correlates with cognitive dysfunction, whereas the relationship between Aβ plaques and cognition is less clear (Ghoshal et al. 2002; Guillozet et al. 2003). Neurofibrillary tangles first affect the transentorhinal cortex (TR) of the PRc, from where they spread to the ERc and hippocampus proper, and then to the neocortex (Braak and Braak 1985, 1991). Notable exceptions to this pattern exist, for example, a rare "frontal variant" of AD in which the frontal cortex is heavily affected by neurofibrillary tangles potentially early in the course of the disease (Taylor et al. 2008), and posterior cortical atrophy, where neurofibrillary tangles and plaques predominantly accumulate in the parietal and occipital cortices in most cases (Crutch et al. 2012). Typically, however, reduced volumes (Juottonen et al. 1998) and cortical thinning are observed in the PRc and ERc early in the course of disease (Dickerson et al. 2009), and these changes appear to be related to the accumulation of neurofibrillary tangles and consequent neuronal loss (Silbert et al. 2003). MTL atrophy is accompanied by a progressive episodic memory impairment characterized by poor learning and rapid forgetting, as well as semantic memory impairments (Taylor and Monsch 2007; Salmon and Bondi 2009; Salmon 2011). Cortical thinning throughout the neocortex can be observed at later stages of the disease (Lerch et al. 2005) and is associated with progressive impairments in other cognitive domains such as language and visuospatial processing.

The predicted exponential increase in the incidence of AD (Qiu et al. 2009) has refocused dementia research more strongly on identifying the earliest possible markers of neurofibrillary pathology. The discovery of early or "preclinical" markers would enable the initiation of therapies at a point in the disease process when they are expected to be maximally beneficial. One strand of research investigates the utility of fMRI imaging of memory functioning for the early detection of AD. These studies demonstrate that AD patients show decreased activation in the hippocampus during episodic memory tasks relative to controls (Rombouts et al. 2000; Machulda et al. 2003; for a review, see Dickerson and Sperling 2008). However, patients with aMCI, a putative prodromal stage of AD, tend to show the opposite effect, that is, increased MTL BOLD responses during memory tasks compared to normal control participants (Dickerson et al. 2004). In a similar vein, increased functional activity in the MTL was observed in healthy participants carrying one or two apoE ε4 alleles associated with an increased risk for AD (Bondi et al. 2005). Heightened MTL activity in preclinical stages and reduced MTL activity in early AD may reflect compensatory hyperactivation in the early stages of the disease and a breakdown of these compensatory mechanisms as the disease progresses (see, e.g., Dickerson et al. 2004). Thus, the development of preclinical BOLD markers of

AD faces the challenging task of discriminating normal from pathologically enhanced or pathologically reduced levels of MTL activity, that is, of defining what "normal" BOLD responses during memory formation are.

A potentially fruitful approach to the identification of very early AD is to combine knowledge about the spatiotemporal sequence of neurofibrillary tangle formation and MTL functional specialization described above (Barbeau et al. 2004; Taylor and Probst 2008). Specifically, since the tau pathology associated with the cognitive dysfunction in AD typically begins in the PRc (Braak and Braak 1991), PRc dysfunction as revealed by neuropsychological testing may signal very early and still preclinical AD changes. Preliminary evidence from cross-sectional studies provides proof of this principle: crossmodal integration and complex perceptual and semantic analyses of individual objects, functions associated with the PRc (see above), are indeed impaired in individuals with amnestic MCI and early AD, and these impairments were shown to be related to the integrity of the PRc as estimated by voxel-based morphometry, cortical thickness, and fractional anisotropy MR measures (Hirni et al. 2011; Kivisaari et al. 2012; Taylor et al. 2011b). We note that the neuropsychological changes associated with PRc dysfunction may be subtle in nature, that is, not necessarily detectable in daily life (viz., episodic memory impairments), but demonstrable upon directed neuropsychological testing. Future interdisciplinary research combining neuropsychological and imaging with genetic and cerebrospinal fluid measures will undoubtedly reveal more specific and valid preclinical markers of AD which will be of great utility in the upcoming decades.

19.4 Anatomy of the MTL

The accurate identification of the MTL subregions is the prerequisite for understanding and studying their functional relevance. Below we provide an overview of the gross anatomy of the MTL and a segmentation protocol for the reliable identification of these regions on anatomic MR scans. This parcellation scheme is based primarily on cytoarchitecture (Insausti et al. 1998; Suzuki and Amaral 2003a; Blaizot et al. 2010), myeloarchitecture (Hopf 1956), and patterns of white matter connectivity (Suzuki and Amaral 1994a; Saleem et al. 2007; Zilles and Amunts 2009).

19.4.1 Overview of the Gyral and Sulcal Characteristics of the MTL

The MTL region is characterized by three major gyri – the uncus (U, Fig. 19.1), the parahippocampal gyrus (PHg, Figs. 19.1 and 19.2), and the fusiform gyrus (Fg, Fig. 19.2) – and two major sulci: the hippocampal fissure (Hf, Fig. 19.2), which is located superior to the parahippocampal gyrus, and the collateral sulcus (Cs, Figs. 19.1 and 19.2), which separates the parahippocampal gyrus from the fusiform gyrus (Fg, Fig. 19.2). Together, these gyral and sulcal landmarks are key to identifying the hippocampus proper, ERc, PRc, and PHc.

The uncus is the most medial and superior gyrus in the MTL, and its characteristic bulges are visible on a surface view (Fig. 19.1). From anterior to posterior sections, these bulges correspond to the gyrus ambiens (gA, Figs. 19.1 and 19.2; part of the ERc), the uncinate gyrus (Ug, Fig. 19.1), and the intralimbic gyrus (ILg, Figs. 19.1, 19.2, 19.6, and 19.7), where the band of Giacomini (bG, Fig. 19.1) separates the uncinate from the intralimbic gyrus. The posterior apex of the intralimbic gyrus represents an important anatomical landmark for the separation of the ERc/PRc from the PHc (see below). The uncal notch (un; Figs. 19.1 and 19.2) is an indentation formed mechanically by the free edge of the tentorium cerebelli (Van Hoesen et al. 2000). The parahippocampal gyrus containing most of the ERc, PRc, and PHc lies inferolateral to the uncus (PHg, Figs. 19.1 and 19.2). The parahippocampal gyrus is bordered inferolaterally by the fusiform gyrus. The temporal pole (TP, Fig. 19.2) represents the anterior extreme of the entire MTL, and it typically contains one or

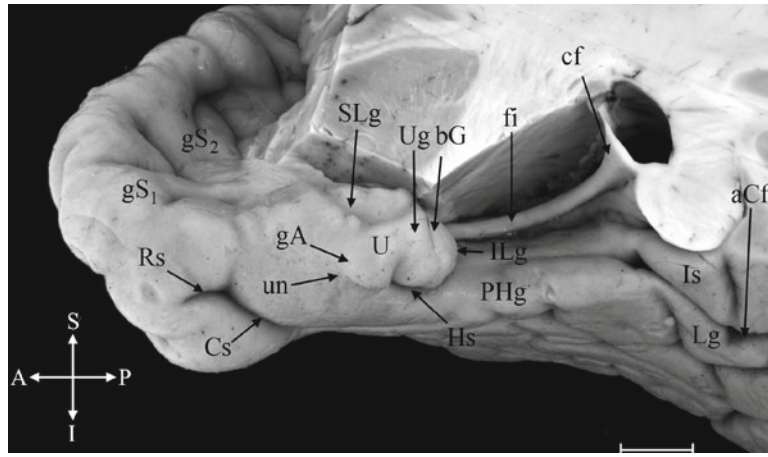

Fig. 19.1 A superomedial view of the right MTL. *Abbreviations*: *aCf* anterior calcarine fissure, *bG* band of Giacomini, *Cs* collateral sulcus, *cf* crus of the fornix, *fi* fimbria, *gA* gyrus ambiens, *gS* gyrus of Schwalbe (this brain has two gyri of Schwalbe, indicated by subscripts), *Hs* hippocampal sulcus, *ILg* intralimbic gyrus, *Is* isthmus, *Lg* lingual gyrus, *PHg* parahippocampal gyrus, *Rs* rhinal sulcus, *SLg* semilunar gyrus, *U* uncus *Ug* uncinate gyrus, and *un* uncal notch. The temporal lobe is viewed from slightly oblique angle medially. Crosshairs indicate *S* superior, *A* anterior, *I* inferior, and *P* posterior. The bar represents circa 1 cm

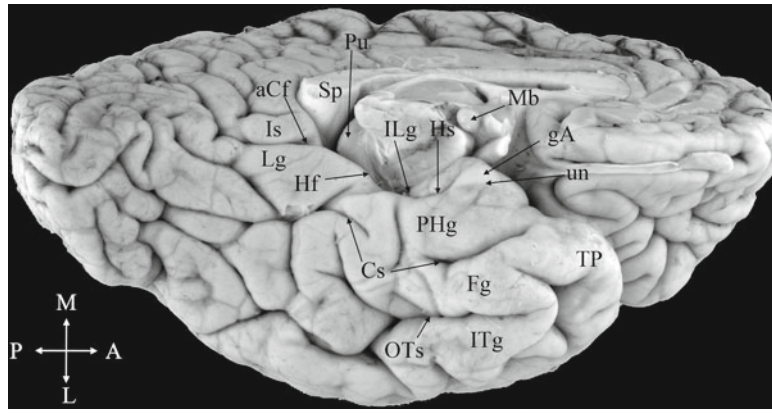

Fig. 19.2 An inferior view of the left cerebral hemisphere. In this brain, the collateral sulcus has an interrupted trajectory. *Abbreviations*: *aCf* anterior calcarine fissure, *Cs* collateral sulcus, *Fg* fusiform gyrus, *gA* gyrus ambiens, *Hf* hippocampal fissure, *Hs* hippocampal sulcus, *ILg* intralimbic gyrus, *Is* isthmus, *ITg* inferotemporal gyrus, *Lg* lingual gyrus, *Mb* mamillary body, *OTs* occipitotemporal sulcus, *Pu* pulvinar, *PHg* parahippocampal gyrus, *Sp* splenium of the corpus callosum, *TP* temporal pole, and *un* uncal notch. The approximate anatomical directions are indicated by crosshairs (*M* medial, *A* anterior, *L* lateral, *P* posterior)

two gyri of Schwalbe on its superior surface (gS, Figs. 19.1 and 19.3).

The hippocampal sulcus (Hs, Fig. 19.1; also known as the uncal sulcus) separates the uncus from the adjacent parahippocampal gyrus (Insausti and Amaral 2004). It starts as a shallow sulcus and deepens progressively at more posterior levels. Posterior to the apex of the intralimbic gyrus, that is, after the uncus ends, the hippocampal sulcus continues as the hippocampal fissure (Fig. 19.2). At more lateral and anterior levels, the rhinal sulcus (Rs, Fig. 19.1) separates the parahippocampal gyrus from the temporal pole (Hanke 1997). The collateral sulcus replaces the rhinal sulcus at more posterior levels, where it separates the parahippocampal gyrus from the

fusiform gyrus (Fig. 19.2). The rhinal and collateral sulci are anatomically variable across individuals, for example, the collateral sulcus may be deep or shallow, may bifurcate, or may be interrupted along its anterior-posterior extent. The occipitotemporal sulcus (OTs; Fig. 19.2) is the most lateral sulcus on the ventral surface of the temporal lobe (Fig. 19.2) and separates the fusiform gyrus from the inferior temporal gyrus (ITg, Fig. 19.2; Van Hoesen et al. 2000). At its most posterior levels, the parahippocampal gyrus is longitudinally divided into two gyri by the anterior calcarine fissure (aCf; Figs. 19.1, 19.2, and 19.9i): the superior part forms the isthmus of the retrosplenial cortex (Is, Fig. 19.1), while the inferior part forms the lingual gyrus (Lg; Figs. 19.1 and 19.9i).

19.4.2 A Segmentation Protocol for the MTL

A protocol for identifying the anatomical borders of the MTL substructures is described below. The protocol begins with the most anterior and lateral structure – the PRc – and continues medially to the ERc, posteriorly to the PHc before describing the most medial structure, the hippocampus proper. All landmarks are based on anatomical studies of the MTL in humans and nonhuman primates (e.g., von Economo and Koskinas 1925; Hopf 1956; Watson et al. 1992; Insausti et al. 1998; Pruessner et al. 2000, 2002; Malykhin et al. 2007; Taylor and Probst 2008) and were selected such that they can be readily identified on structural MR images. All landmarks refer to coronal views of volumes of 1 cubic mm resolution reoriented along the AC-PC axis, and assume that the contrast is set to optimize the differentiation of gray from white matter.

19.4.2.1 Borders of the Perirhinal Cortex

The PRc lies folded inside the collateral sulcus such that only a small part is visible from the cortical surface (Fig. 19.4). The PRc is bordered anteriorly by the temporal pole, posteriorly by the PHc, medially mainly by the ERc, and laterally by the fusiform gyrus. The medial portion of the PRc, that is, the TR, is a cytoarchitectonically distinct transition region between the PRc and ERc and notable as the site of incipient cortical neurofibrillary pathology in AD (Fig. 19.4; Braak and Braak 1985). The anteriorly situated temporal pole is a heterogenous cortex which shares some commonalities with the PRc (Suzuki and Amaral 2003a; Blaizot et al. 2010). According to some authors, the PRc extends into temporopolar cortex (Suzuki and Amaral 2003a; Insausti et al. 1998; Ding et al. 2009; but see also Brodmann 1909; von Bonin and Bailey 1947). However, since the precise extension of the PRc into the temporal pole and the corresponding anatomical borders are under debate (*cf.* Insausti et al. 1998*;* Ding et al. 2009*;* Ding and Van Hoesen 2010), the tempopolar cortex is excluded from this protocol.

The PRc is one of the most challenging structures to identify, in part because the boundaries of this structure have been redefined over time (Suzuki and Amaral 2003b) and in part because of the variability of its key anatomical landmark – the collateral sulcus (Hanke 1997; Pruessner et al. 2002). The medial and posterior PRc landmarks described below apply to the whole PRc including the TR, its medial extent. After a description of the anatomical borders of the PRc, the anatomical borders of the TR are defined. All landmarks take into account the dependence of the PRc and TR location on the shape and depth of the collateral sulcus (Insausti et al. 1998; Taylor and Probst 2008).

Perirhinal Cortex

Anterior Border

A cytoarchitectonic study of the human MTL demonstrated that the anterior portion of the PRc wraps around the anterior end of the ERc (Insausti et al. 1998). The anterior border of the PRc is located circa 24 mm posterior to the apex of the temporal pole or a few millimeters anterior to the most anterior appearance of gray matter of the limen insulae (i.e., frontotemporal junction; Fig. 19.8b; Insausti et al. 1998). Since the length of the temporal pole is more variable than the appearance of the limen insulae gray

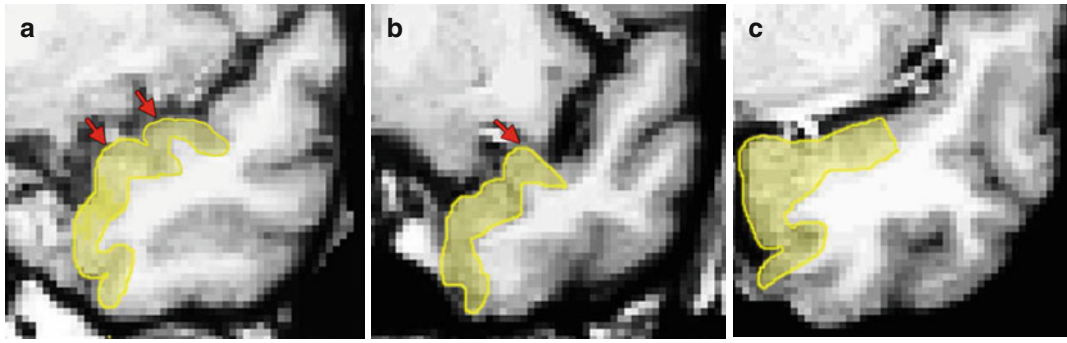

Fig. 19.3 Native space coronal slices of the right hemisphere temporal pole area 1–2 mm anterior to the limen insulae. The figure illustrates the three variants of the gyri of Schwalbe (*red arrows*) and corresponding locations of the PRc (*yellow outlines*): (**a**) a case with two gyri of Schwalbe, (**b**) a case with one gyrus of Schwalbe, and (**c**) a case whose superior aspect of the temporal pole is relatively flat, indicating no gyri of Schwalbe

matter, the anterior PRc border is defined as 2 mm anterior to the most anterior coronal slice containing gray matter in the limen insulae, which corresponds to approximately $y=9$ in MNI coordinates (Fig. 19.8a). The collateral sulcus is typically visible at this level. As noted above, the cytoarchitectonic similarities between the temporopolar region and the PRc indicate that this border may underestimate the true anterior extent of the PRc; however, the resolution of this issue requires additional research (see, e.g., Insausti et al. 1998; Suzuki and Amaral 2003b).

Superolateral/Medial Border

At levels anterior to the limen insulae, the superolateral border is defined with respect to the number and position of the gyri of Schwalbe, which are considered part of the PRc (see Figs. 19.1, 19.3, and 19.8a). In the presence of two gyri of Schwalbe, each laterally bordered by a temporopolar sulcus (prevalence ca. 80 %; Insausti et al. 1998), the superolateral border is the fundus of the most lateral temporopolar sulcus (Figs. 19.3a and 19.8a). When there is one gyrus of Schwalbe (prevalence ca. 12 %; Insausti et al. 1998), the superolateral border of the PRc is defined as the fundus of the temporopolar sulcus (see Fig. 19.3b). If the gyrus of Schwalbe is not visible (prevalence ca. 8 %; Insausti et al. 1998), the superolateral border is defined as the midpoint between the medial and lateral corners of the superior surface of the temporal pole (Fig. 19.3c; Insausti et al. 1998).

At the level of the gray matter of the limen insulae and posterior to this landmark, the medial border of the PRc is the shoulder of the medial bank of the collateral sulcus (Fig. 19.8b–p; Insausti et al. 1998; Taylor and Probst 2008). This also serves as the medial border of the entire TR (see below). If the collateral sulcus is not yet present, or is discontinuous, the medial PRc border is estimated by approximating the angle of the trajectory of the shoulder of the medial bank of the collateral sulcus from more posterior slices.[5] If the collateral sulcus is bifurcated, the criteria described above are applied to the most medial sulcus (Taylor and Probst 2008). Posteriorly, the PRc wraps medially around the ERc and extends 2–4 mm posterior to the last slice containing the apex of the intralimbic gyrus (i.e., the posterior border of the ERc). At this level, the medial border of the PRc extends to the most medial aspect of the parahippocampal gyrus (*cf.* medial ERc border below).

[5]The protocol assumes that in cases where the collateral sulcus cannot be visualized or is discontinuous, the lateral and medial PRc borders are determined on coronal slices anterior and posterior to the interrupted section, and that imaginary lines are drawn from these anterior and posterior levels to connect the lateral borders and the medial borders of the PRc.

Lateral Border

The lateral border of the PRc depends on the length and shape of the collateral sulcus (Insausti et al. 1998). If the collateral sulcus is of regular depth between 1- and 1.5-cm deep (82 % of cases from Insausti et al. 1998), the lateral boundary is the shoulder of the lateral bank of the collateral sulcus (Fig. 19.4a). If the collateral sulcus is shallow, that is, less than 1 cm deep (16 % of cases; Insausti et al. 1998), the lateral border is the midpoint of the fusiform gyrus. We note that this criterion is not applied to the most anterior sections where the collateral sulcus begins to appear; in these anterior sections, the criteria for the regular collateral sulcus are applied or the border is estimated from more posterior slices with an obvious collateral sulcus (*cf.* (Insausti et al. 1998), Fig. 19.5). Finally, if the collateral sulcus is deeper than 1.5 cm (2 % of cases), the lateral border is the midpoint between the fundus and the shoulder of the lateral bank of the collateral sulcus (Fig. 19.4b).

Posterior Border

As in its anterior aspect, the PRc wraps around the posterior end of the ERc forming a border averaging 3-mm wide (range, 2–4 mm; Insausti et al. 1998; see also Krimer et al. 1997). The posterior border is therefore set at 3 mm posterior to the last coronal slice still containing the apex of the intralimbic gyrus, that is, the posterior border of the ERc (e.g., if the last coronal slice containing the intralimbic gyrus is MNI $y=-18$, the last posterior slice with the PRc is MNI $y=-21$, see Fig. 19.8n–o).

Transentorhinal Area

Anterior Border

The medial aspect of the PRc, the TR, is defined as an area of transition between the ERc and PRc (Braak and Braak 1985). Therefore, its anterior border is defined as the first slice where the ERc is present, that is, 2 mm posterior to the first anterior slice where the white matter of the limen insulae is visible (Fig. 19.8d; see Sect. 19.4.2.2).

Medial Border

The medial border of the TR is identical to the medial border of the PRc described above, that is, the shoulder of the medial bank of the collateral sulcus (Insausti et al. 1998; Taylor and Probst 2008; Fig. 19.4 and 19.8d–n).

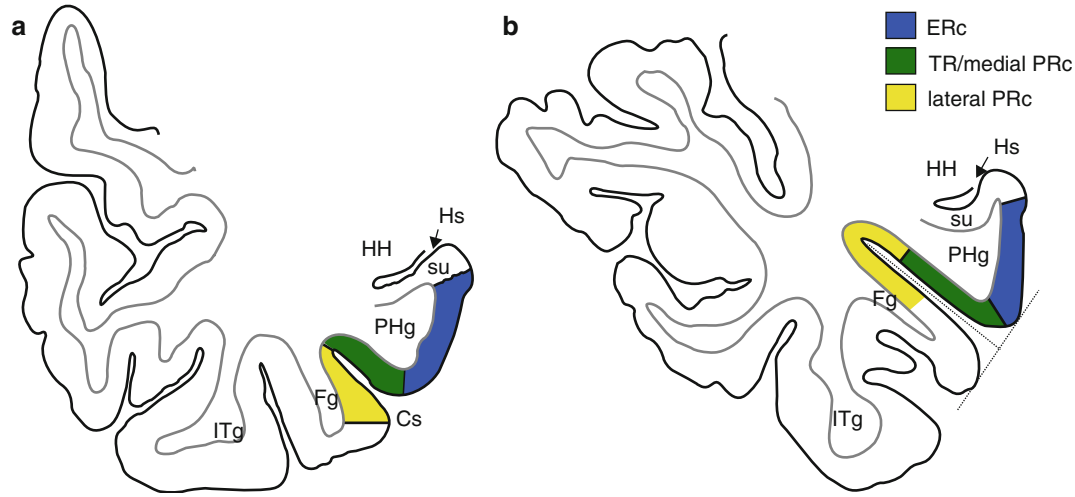

Fig. 19.4 Coronal view of the medial temporal lobe at the level of the hippocampal sulcus (similar coronal level as Fig. 19.8k). The locations of the PRc and TR depend on the depth of the collateral sulcus (*Cs*; see text): (**a**) borders when the collateral sulcus is of regular depth (i.e., 1–1.5 cm) and (**b**) when the collateral sulcus is deep (i.e., > 1.5 cm). *Abbreviations*: *Fg* fusiform gyrus, *HH* hippocampal head, *Hs* hippocampal sulcus, *ITg* inferotemporal gyrus, *PHg* parahippocampal gyrus, *su* subiculum of the hippocampus

Lateral Border

If the depth of the collateral sulcus equals or is less than 1.5 cm, the lateral border of the TR is defined as the fundus of the collateral sulcus (Fig. 19.4a; Taylor and Probst 2008). If the collateral sulcus is deeper than 1.5 cm, the lateral border is the midpoint between (i) the shoulder of the medial bank of the collateral sulcus and (ii) the midpoint of the lateral bank of the collateral sulcus (Fig. 19.4b; Insausti et al. 1998; Taylor and Probst 2008). If the collateral sulcus is bifurcated, these criteria are applied to the most medial sulcus (Taylor and Probst 2008).

Posterior Border

The posterior border of the TR is identical to the posterior border of the ERc, that is, 1 mm posterior to the last slice containing the apex of the intralimbic gyrus (see below).

19.4.2.2 Borders of the Entorhinal Cortex

The ERc is the largest cortical field on the parahippocampal gyrus and is entirely visible from the medial surface view. Macroscopically, the anterior portion of the ERc is characterized by small bumps on the cortical surface called *verrucae hippocampi* (Klingler 1948). The ERc encompasses the gyrus ambiens at anterior levels (Figs. 19.1, 19.2, 19.5, and 19.8g–h). The gyrus ambiens is superomedially neighbored by the semiannular sulcus, beyond which lies the semilunar gyrus of the periamygdaloid cortex. At more posterior levels, the subiculum of the hippocampus proper neighbors the ERc superomedially. The PRc surrounds the anterior, inferior, and lateral sides of the ERc (Insausti et al. 1998).

Anterior Border

Cytoarchitectonic studies have demonstrated that the PRc surrounds the anterior end of the ERc (Insausti et al. 1998). However, because the oblique orientation of the anterior end of the ERc is difficult to delineate, a conservative anterior border is defined corresponding to the most anterior coronal slice with the full extent of the ERc (but see Insausti et al. 1998). This level corresponds approximately to a coronal slice 2 mm posterior to the first anterior slice where the white matter of the limen insulae is visible. Note that because of this conservative border, a segment of the MTL is left uncategorized (Fig. 19.8b–c).

Medial Border

At anterior levels, the medial border of the ERc is the semiannular sulcus (Fig. 19.5). However, because this sulcus is very shallow and seldom identifiable on MR images, the medial border of the anterior ERc is defined here as the midpoint (i.e., medial apex) of the gyrus ambiens (Figs. 19.5b, 19.8d–h). If the gyrus ambiens is not visible, the medial border is the shoulder (i.e., medial apex) of the superomedial bank of the parahippocampal gyrus (see Fig. 19.5c, 19.8i–n).

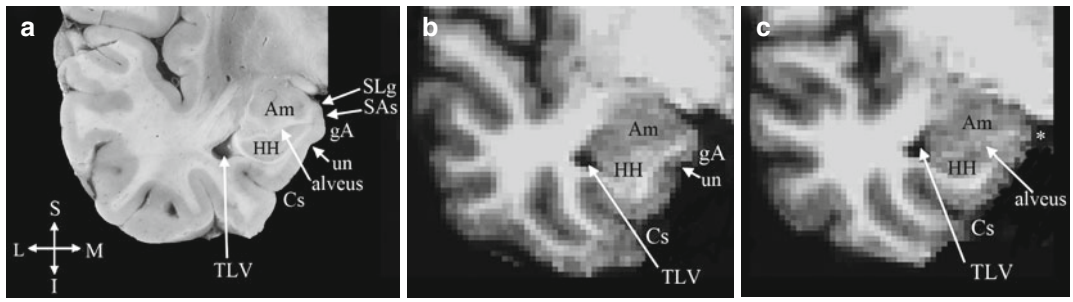

Fig. 19.5 Sections of the temporal lobe at the level of the uncus (approximate MNI $y=-5$): (**a**) a histological section and (**b**) an MRI slice at a similar coronal level where the gyrus ambiens (*gA*) and uncal notch (*un*) are visible. (**c**) An MRI slice at a similar coronal level where the gA and un are not visible. In these instances, the medial apex of the parahippocampal gyrus (*asterisk*) is defined as the medial ERc border. *Abbreviations*: *Am* amygdala, *Cs* collateral sulcus, *gA* gyrus ambiens, *HH* hippocampal head, *SAs* semiannular sulcus, *SLg* semilunar gyrus and *TLV* temporal horn of the lateral ventricle, *un* uncal notch. Anatomical directions: *S* superior, *M* medial, *I* inferior, *L* lateral

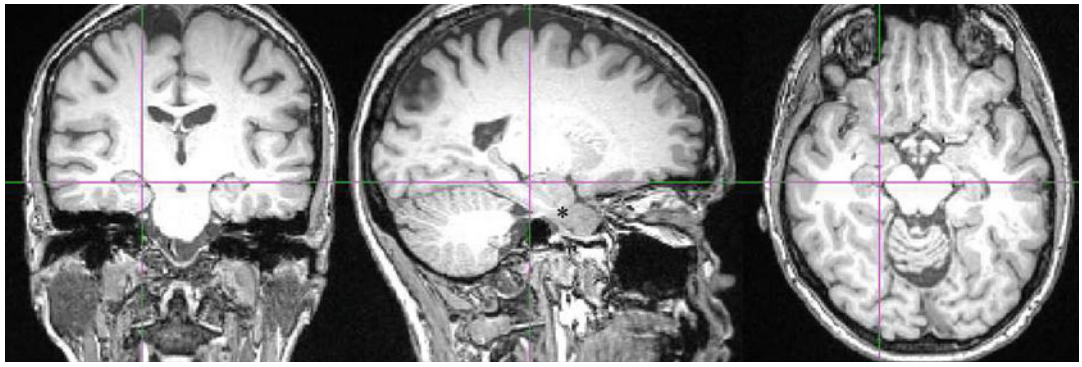

Fig. 19.6 Coronal, sagittal, and axial views of one participant with the crosshair position indicating the location of the apex of the intralimbic gyrus. The *asterisk* in the sagittal view indicates the cone-shaped crossing of the alveus and parahippocampal gyrus white matter, which marks the anterior limit of the hippocampal head

The medial ERc border moves slightly inferiorly when the hippocampal sulcus emerges (Fig. 19.8h–i). However, because this transition is difficult to detect on MR images, an arbitrary landmark is defined as 1 mm anterior to first anterior slice where the hippocampal sulcus can be visualized (see Fig. 19.8j). At this and more posterior levels, the most medial extent of the parahippocampal gyrus, that is, its medial apex, is the medial border of the ERc.

Lateral Border

The lateral border of the ERc is identical to the medial border of the PRc/TR (see above and Figs. 19.4 and 19.8d–n; Taylor and Probst 2008; Krimer et al. 1997).

Posterior Border

The posterior border of the ERc is defined as 1 mm posterior to the last slice containing the apex of the intralimbic gyrus (Fig. 19.6; note that the apex is located in between slices Fig. 19.8n,o, i.e., $y=-18$, which is not shown).

19.4.2.3 Borders of the Parahippocampal Cortex

The PHc is located in the posterior portion of the parahippocampal gyrus posterior to the PRc and ERc (Van Hoesen 1982; Sewards 2011). However, disagreement exists regarding the precise cytoarchitectonic features of the PHc, and, correspondingly, the anatomical boundaries of the PHc are inconsistently defined in the literature (see, e.g., von Economo and Koskinas 1925; Hopf 1956; Saleem et al. 2007; Thangavel et al. 2008). Here, we draw upon the conceptualizations of the PHc as a proisocortical region, that is, a transitional zone between allocortex and neocortex, and as the posterior continuation of the PRc and ERc (Suzuki and Amaral 2003a; Saleem et al. 2007). Thus, the definition of the lateral border of the PHc described below is consistent with Hopf (Hopf 1956; see also Sewards 2011) and corresponds closely to anatomical descriptions in nonhuman primates (Suzuki and Amaral 2003a; Saleem et al. 2007).

As noted above, the PHc is defined as the posterior continuation of the PRc and ERc, located inferolateral to the subiculum of the hippocampal body and tail. Posteriorly, the anterior calcarine fissure divides the PHc longitudinally into the inferiorly situated lingual gyrus and the superiorly situated isthmus of the retrosplenial cortex (Figs. 19.1, 19.2, and 19.9j). The PHc occupies parts of the lingual gyrus and merges without clear anatomical landmarks with the infra- and retrosplenial cortices (Vogt et al. 2006). For this reason, the posterior limit of the PHc is conservatively restricted to levels anterior to the emergence of the calcarine fissure.

Anterior Border

The anterior boundary of the PHc is defined as the first slice after the posterior border of PRc, that is, 4 mm posterior to the last slice containing the apex of the intralimbic gyrus (Fig. 19.9a).

Medial Border

The subiculum of the hippocampus proper neighbors the PHc medially (*cf.* Fig. 19.4). Thus, the medial border is the medial apex of the parahippocampal gyrus (Fig. 19.9a–g).

Lateral Border

According to studies on nonhuman primates (Suzuki and Amaral 2003a; Saleem et al. 2007) and the myeloarchitectonic study by Hopf (Hopf 1956; see Sewards 2011), the PHc represents the posterior extension of the PRc and ERc (but see von Economo and Koskinas 1925). Thus, the lateral border of the PHc is adjusted according to the depth of the collateral sulcus in the same manner as for the lateral border of the PRc (see section "Perirhinal Cortex"; Figs. 19.4 and 19.9a–g).

Posterior Border

The posterior end of the PHc is funnel-shaped and progressively merges with the retrosplenial region. According to Vogt and colleagues (2006), the PHc extends posteriorly several millimeters past the posterior limit of the splenium. However, because the medial and lateral PHc borders at these posterior levels are unclear, a conservative posterior border is defined as the first posterior slice where the pulvinar is no longer visible (Figs. 19.2 and 19.9f–g). Anterior to this level, the lateral and medial landmarks described above can be used.

19.4.2.4 Borders of the Hippocampus Proper

This chapter focuses on the retrocommissural part of the hippocampus proper, extending from the inferior and medial side of the amygdala at the uncinate gyrus to an area posterior and inferior to the splenium of the corpus callosum (Fig. 19.7). This part of the hippocampus is entirely situated inferior to the corpus callosum and appears as a C-shaped structure when viewed from above (Fig. 19.7). Posterior to the apex of the uncus, the hippocampus proper arches laterally around the upper midbrain and curves medially and superiorly, continuing as a thin strip of gray matter of vestigial hippocampus (*indusium griseum*) on the superior surface of the corpus callosum (supracommissural hippocampus) before descending at anterior levels to the subcallosal area (precommissural hippocampus). The supra- and precommissural hippocampi are excluded from this segmentation.

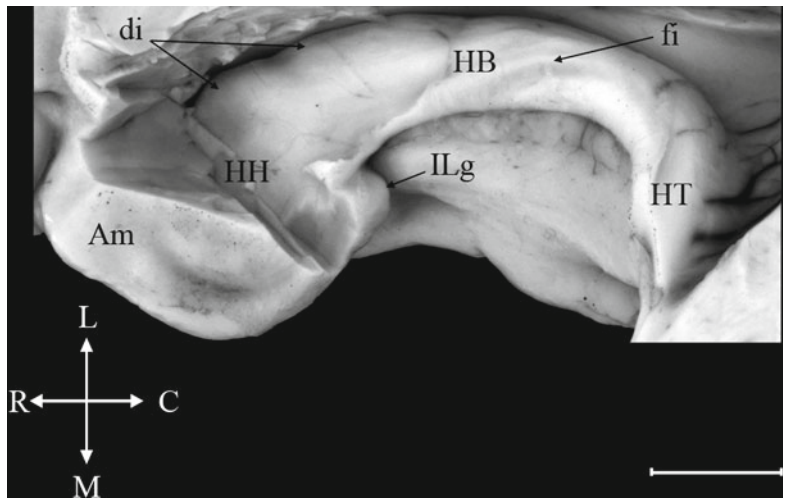

Fig. 19.7 Superior view of the C-shaped hippocampal formation on the right hemisphere after removing the roof of the temporal horn and parts of the amygdala. This view thereby reveals the intra- and extraventricular aspects of the hippocampal formation. *Abbreviations*: *Am* amygdala, *di* hippocampal digitations, *fi* fimbria, *HB* hippocampal body, *HH* hippocampal head, *HT* hippocampal tail, and *ILg* intralimbic gyrus. *Anatomical directions*: *L* lateral, *P* posterior, *M* medial, and *A* anterior. The bar represents circa 1 cm

The alveus is made of the fibers emanating from the pyramidal cells of the hippocampus. It covers the Ammon's horn superiorly and laterally (Fig. 19.5), and its fibers converge to form the fimbria, oriented roughly along the longitudinal axis of the hippocampus (Duvernoy 1998). The fimbria is continuous with a prominent, flattened white matter tract, the crus of the fornix (Figs. 19.1 and 19.9g–i), which begins at posterior levels of the hippocampus and curves superomedially below the corpus callosum. These white matter tracts likewise are excluded from the segmentation (Hogan et al. 2000; Pantel et al. 2000, but see also Pruessner et al. 2000; Malykhin et al. 2007).

Because different anterior to posterior areas of the hippocampus exhibit different patterns of connectivity (Witter and Amaral 1991), which presumably corresponds to functional specialization along its longitudinal axis (see Sect. 19.2.; Colombo et al. 1998; Moser and Moser 1998; Giovanello et al. 2004), we describe anatomical landmarks for the hippocampal head, body, and tail separately (see also Watson et al. 1992; Pantel et al. 2000; Pruessner et al. 2000; Maller et al. 2006; Malykhin et al. 2007). Anatomical tracing typically starts at the anterior border of the hippocampal body and continues to the posterior end of the hippocampal tail. The most anterior aspect, the hippocampal head, lies adjacent to the amygdala and is the most challenging hippocampal structure to trace. This protocol therefore starts with the body of the hippocampus and then discusses the tail and finally the head of the hippocampus.

Hippocampal Body

The hippocampal body consists of subfields CA1-3 and the subiculum which is located on the superior bank of the parahippocampal gyrus. The fimbria is located on the superomedial side of the hippocampus and has a slightly curved trajectory toward the hippocampal tail, where it leaves the hippocampus and continues its path superomedially as the crus of the fornix (Fig. 19.1). For a graphical illustration of the segmentation of the hippocampal body, see Figs. 19.8o–p and 19.9a–f.

Anterior Border

The anterior border of the hippocampal body is defined as one slice posterior to the posterior apex of the intralimbic gyrus (i.e., the last slice containing the intralimbic gyrus; Fig. 19.8n; Malykhin et al. 2007).

Medial Border

The subiculum of the hippocampus proper extends to the medial apex of the parahippocampal gyrus, which represents the medial border of the hippocampus proper (Figs. 19.8o–p and 19.9a–f; Watson et al. 1992).

Lateral Border

The body of the hippocampus extends laterally to the temporal horn of the lateral ventricle (Figs. 19.8o–p and 19.9a–f; Pantel et al. 2000; Pruessner et al. 2000; Malykhin et al. 2007).

Inferior Border

Inferiorly and inferomedially, the body of the hippocampus is bordered by the white matter of the angular bundle of the parahippocampal gyrus (Figs. 19.8o–p and 19.9a–f; Pantel et al. 2000; Malykhin et al. 2007).

Superior Border

The temporal horn of the lateral ventricle forms the superior boundary of the hippocampal body. Care should be taken to exclude the white matter of the fimbria (Hogan et al. 2000; Pantel et al. 2000 but see also Pruessner et al. 2000; Malykhin et al. 2007). Sagittal views may aid the visualization of the continuous border between the hippocampus proper and the cerebrospinal fluid of the lateral ventricle. Care must also be taken to exclude the voluminous choroid plexus, which fills the temporal horn of the lateral ventricle on the superior aspect of the hippocampus.

Posterior Border

The posterior border of the body of the hippocampus is one slice posterior to the first coronal slice where the crus of the fornix is clearly separated from the wall of the lateral ventricle or where its full profile is visible in columnar form, even if it is still attached to the lateral

ventricle (Fig. 19.9f; Maller et al. 2006; Malykhin et al. 2007).

Hippocampal Tail

The tail of the hippocampus proper funnels slightly and turns medially before steeply ascending around the splenium of the corpus callosum (Fig. 19.7). The CA1 subfield occupies a progressively more medial position and forms the gyrus of Andreas Retzius on the surface of the parahippocampal gyrus, while the CA3 subfield forms the gyrus fasciolaris on the superior aspect of the hippocampal fissure (Duvernoy 1998). The location of the hippocampal tail is illustrated in Fig. 19.9f–k.

Anterior Border

The anterior border of the hippocampal tail is defined as the first slice posterior to the posterior limit of the hippocampal body (Fig. 19.9f; Maller et al. 2006; Malykhin et al. 2007).

Medial Border

The isthmus is located on the medial aspect of the hippocampus in an area which had been occupied by the subiculum at more anterior levels (Fig. 19.9i). To ensure the exclusion of the isthmus, an arbitrary medial border for the hippocampal tail is defined: an oblique, straight line drawn from the inside inferolateral corner of the angular bundle along the white matter of the parahippocampal gyrus to the quadrigeminal cistern (see Fig. 19.9f–i). The hippocampal tail is defined as the gray matter superolateral to this line.

Lateral Border

The lateral border of the hippocampal tail is the white matter of the ascending crus of the fornix and the temporal horn of the lateral ventricle (Fig. 19.9f–i; Pantel et al. 2000; Maller et al. 2006).

Superior Border

The tail of the hippocampus proper is superiorly bordered by the crus of the fornix and the white matter of the splenium of the corpus callosum (Fig. 19.9g–j). The pulvinar should be carefully avoided; toward this end, the sagittal plane is helpful in distinguishing the gray matter of the hippocampal tail from the gray matter of the thalamus (Pantel et al. 2000; Malykhin et al. 2007).

Inferior Border

The inferior border is the white matter of the parahippocampal gyrus (Pantel et al. 2000; Malykhin et al. 2007).

Posterior Border

The posterior portion of the hippocampal tail appears as an ovoid-shaped mass of gray matter (Fig. 19.9g–k). The complete disappearance of this shape marks the posterior limit of the hippocampal formation (Fig. 19.9i–j).

Hippocampal Head

The hippocampal head (CA1-3, dentate gyrus, subiculum) abutting the temporal horn of the lateral ventricle bends medially and again posteriorly to become part of the uncus (Insausti and Amaral 2004). Anteriorly, the head of the hippocampus is located inferior to the amygdala (Fig. 19.7), which occupies a progressively larger superolateral area of the hippocampal-amygdaloid complex at more anterior levels (Fig. 19.8e–i). Segmentation begins at posterior levels.

Posterior Border

The posterior border of the hippocampal head is the apex of the intralimbic gyrus, that is, the last slice containing this structure (Figs. 19.6 and 19.8n–o; Duvernoy 1998; Malykhin et al. 2007). This point may best be identified by navigating through sagittal slices.

Medial Border

At posterior levels, the hippocampal head is segmented up to the most medial apex of the parahippocampal gyrus (Fig. 19.8i–n), whereas at anterior levels, the medial border is limited by the white matter of the parahippocampal gyrus (Fig. 19.8h). The transition between the two landmarks takes place 1 slice anterior to the most

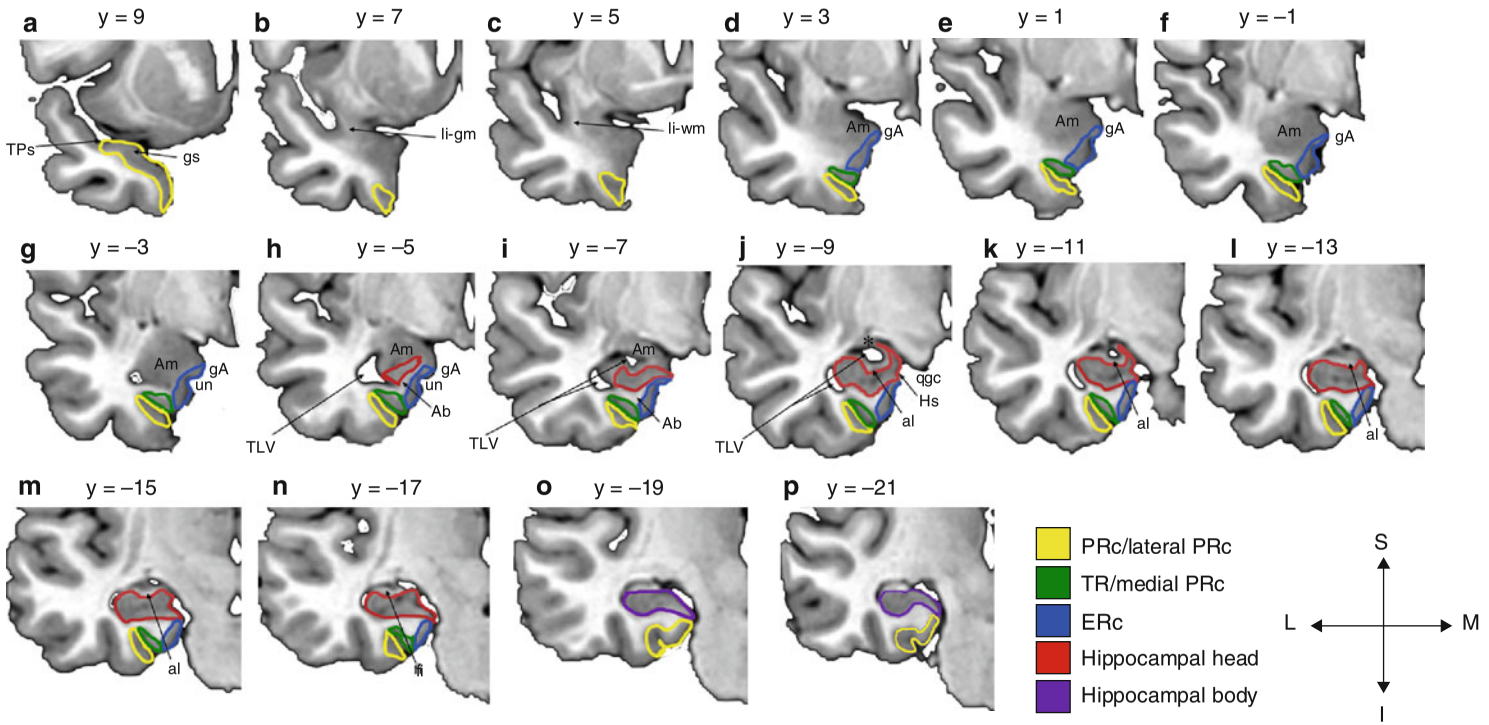

Fig. 19.8 Coronal sections of the temporal lobe at anterior to posterior levels every 2 mm. The coronal level is identified in MNI coordinates. The asterisk represents the most anterior slice where the TLV is continuous with the quadrigeminal cistern (i.e., where ventricular slit is present). The structures are drawn on an MriCron template (http://www.mccauslandcenter.sc.edu/mricro/mricron/). Note that a part of the medial surface in (**b**, **c**) is unsegmented due to the unreliability of tracing the oblique anterior end of the ERc (see text). The fimbria begins only at the level of posterior hippocampal head. *Abbreviations*: *Ab* angular bundle (parahippocampal gyrus white matter), *al* alveus, *Am* amygdala, *fi* fimbria, *gA* gyrus ambiens, *Hs* hippocampal sulcus, *ILg* intralimbic gyrus (the apex is located at $y=-18$), *qgc* quadrigeminal cistern, li-*gm* limen insulae gray matter, *li-wm* limen insulae white matter, *TLV* temporal horn of the lateral ventricle, and *un* uncal notch. Anatomical directions: *S* superior, *M* medial, *I* inferior, and *L* lateral

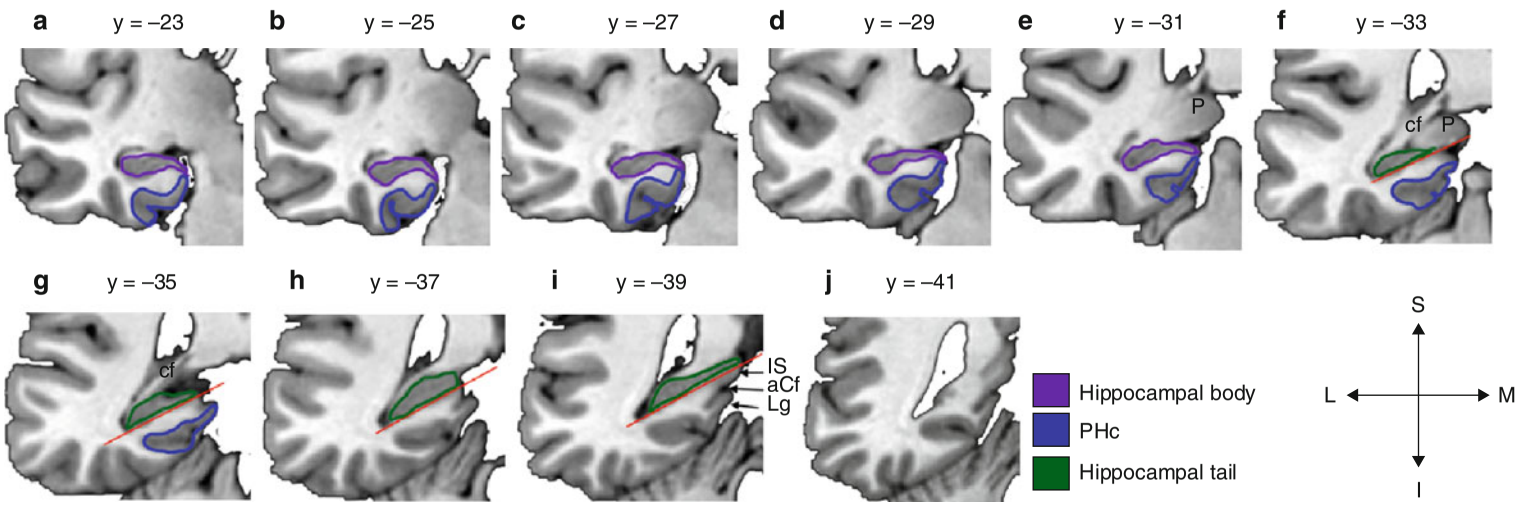

Fig. 19.9 Coronal sections of the temporal lobe at anterior to posterior levels every 2 mm. The numbers represent different coronal levels in MNI (*y*) coordinates. The structures are drawn on an MriCron template (http://www.mccauslandcenter.sc.edu/mricro/mricron/). The red line illustrates the arbitrary border used as the inferomedial limit of the hippocampal tail. *Abbreviations*: *aCf* anterior calcarine fissure, *cf* crus of the fornix, *Is* isthmus, *Lg* lingual gyrus, and *P* pulvinar. Anatomical directions: *S* superior, *M* medial, *I* inferior, and *L* lateral

anterior slice where the uncal sulcus is last visible, corresponding approximately to the level where the semilunar gyrus and anterior cortical nucleus of the amygdala appear.

Lateral Border

The lateral border is the medial wall of the temporal horn of the lateral ventricle (Pantel et al. 2000; Pruessner et al. 2000). If the white matter of the alveus is visible next to the wall of the lateral ventricle, it is excluded (Hogan et al. 2000; Pantel et al. 2000).

Superior Border

At posterior levels, the superior border can be identified as the temporal horn of the lateral ventricle or the white matter of the alveus if visible (Fig. 19.8j–n). At more anterior levels where the amygdala is no longer separated from the hippocampus by a ventricular slit (transition approximately at Fig. 19.8j), the hippocampus is delimited from the amygdala using the white matter of the alveus surrounding the superior aspect of the hippocampal head (Watson et al. 1992). If the alveus is not visible, especially at the most anterior levels, the location of the alveus and thus superior border is estimated from sagittal slices, where the alveus is usually easier to identify. The uncal recess of the inferior horn of the lateral ventricle may additionally aid delineation of the superomedial border of the hippocampal head (Watson et al. 1992; Hogan et al. 2000; Pruessner et al. 2000).

Inferior Border

The hippocampal head is inferiorly bordered by the white matter of the parahippocampal gyrus (Malykhin et al. 2007; Pruessner et al. 2000).

Anterior Border

The anterior border is defined as the most anterior corner of the conical profile formed by the parahippocampal gyrus white matter and the alveus, as visualized on sagittal views (see Fig. 19.6; Pantel et al. 2000; Pruessner et al. 2000). When this point is selected on the sagittal slice, the view is changed to coronal, where the medial, lateral, superior, and inferior borders can be identified.

19.5 Summary

This chapter skimmed the surface of research on the functional neuroanatomy of the MTL. The most influential model of MTL functioning today emphasizes the role of the entire MTL in the formation of conscious memories. This view is supported by numerous patient findings as well as the dense interconnectivity within the MTL, enabling the subregions to work in concert, acting as a unified region. Animal and more recently human neuroscientific research, using ever more sophisticated methods and neuropsychological paradigms, indicates additional levels of processing in the MTL beyond declarative memory formation. Hierarchical, connectivity-based approaches provide a framework within which to study these multidimensional aspects of cognitive functioning in which each MTL subregion is also functionally specialized for a particular kind of information processing. This work not only furthers our basic understanding of the functional neuroanatomy of this complex system but also has obvious clinical implications for patients with acquired brain damage and neurodegenerative disorders, most notably AD. Thus, concerted activity among all MTL structures appears to take place in parallel with functionally specialized processing in each substructure, enabling successful memory encoding and retrieval of complex events, concepts, and scenes.

The prerequisite for advancements in MTL research is the use of well-defined and reliable anatomic landmarks, such as those reported in this chapter. Moreover, the use of different methodologies, tasks, and populations is essential to increase our understanding of human MTL function. Case or patient studies remain a cornerstone in MTL research, providing valuable information about the functions that are lost as a consequence of different kinds and locations of brain damage (e.g., Squire and Wixted 2011). However, this approach is limited by the fact that lesions typically encompass more than one cytoarchitectonic area, that is, that selective lesions of PRc, ERc, or PHc are rare. Thus, voxel-based volumetric methods (e.g., Tyler et al. 2005; Ashburner 2007) and surface-based methods offer increasingly reliable anatomical precision in patient studies (Dale et al. 1999;

Fischl et al. 1999; Klein et al. 2010; Kivisaari et al., 2012). FMRI in healthy individuals, in particular high-resolution imaging, has become increasingly important as it provides high spatial information on the systems normally engaged during a particular task (e.g., Henson 2005), although it does not provide information about whether the activated regions are *necessary* for the particular function. Finally, resting state fMRI and diffusion-tensor imaging, among others, can increase our knowledge about the functional and structural connectivity of these areas in vivo, respectively, which is fundamental to our understanding of how the MTL areas work as a network and interact with other brain areas (e.g., Wang et al. 2006; Catani and Thiebaut de Schotten 2008). Converging evidence from diverse neuroscientific approaches using valid anatomic guidelines is expected to significantly increase our functional-neuroanatomic understanding of the MTL.

Acknowledgments The authors thank Daniela Hirni for comments and helpful discussions. The authors also thank photographer Martin Portmann and the Departments of Neuropathology and Neuroradiology, University Hospital Basel, for providing the post-mortem and MRI brain data, respectively. This research was supported by a Swiss National Science Foundation Ambizione Fellowship (KIT), a grant from the Alzheimer's Association of Both Basels (KIT), the Finnish Concordia Fund (SLK), the Finnish Cultural Foundation (SLK), and the Swiss Federal Comission for Scholarships for Foreign Students (Berne) (SLK).

References

Acres K, Taylor KI et al (2009) Complementary hemispheric asymmetries in object naming and recognition: a voxel-based correlational study. Neuropsychologia 47:1836–1843

Aggleton JP, Brown MW (1999) Episodic memory, amnesia, and the hippocampal-anterior thalamic axis. Behav Brain Sci 22:425–489

Aggleton JP, Brown MW (2006) Interleaving brain systems for episodic and recognition memory. Trends Cogn Sci 10:455–463

Aggleton JP, Mishkin M (1985) Mamillary-body lesions and visual recognition in monkeys. Exp Brain Res 58:190–197

Aguirre GK, D'Esposito M (1999) Topographical disorientation: a synthesis and taxonomy. Brain 122: 1613–1628

Alvarado MC, Bachevalier J (2005a) Comparison of the effects of damage to the perirhinal and parahippocampal cortex on transverse patterning and location memory in rhesus macaques. J Neurosci 25:1599–1609

Alvarado MC, Bachevalier J (2005b) Selective neurotoxic damage to the hippocampal formation impairs performance of the transverse patterning and location memory tasks in rhesus macaques. Hippocampus 15: 118–131

Alvarado MC, Wright AA et al (2002) Object and spatial relational memory in adult rhesus monkeys is impaired by neonatal lesions of the hippocampal formation but not the amygdaloid complex. Hippocampus 12: 421–433

Alzheimer's Association (2011) 2011 Alzheimer's disease facts and figures. Alzheimers Dement 7:208–244

American Psychiatric Association (1994) Diagnostic and statistical manual of mental disorders, 4th edn. American Psychiatric Association, Washington, D.C

Ashburner J (2007) A fast diffeomorphic image registration algorithm. Neuroimage 38:95–113

Bachevalier J, Nemanic S (2008) Memory for spatial location and object-place associations are differently processed by the hippocampal formation, parahippocampal areas TH/TF and perirhinal cortex. Hippocampus 18:64–80

Bakker A, Kirwan CB et al (2008) Pattern separation in the human hippocampal CA3 and dentate gyrus. Science 319:1640–1642

Bar M, Aminoff E (2003) Cortical analysis of visual context. Neuron 38:347–358

Bar M, Aminoff E et al (2008) Scenes unseen: the parahippocampal cortex intrinsically subserves contextual associations, not scenes or places per se. J Neurosci 28:8539–8544

Barbeau E, Didic M et al (2004) Evaluation of visual recognition memory in MCI patients. Neurology 62:1317–1322

Barense MD, Bussey TJ et al (2005) Functional specialization in the human medial temporal lobe. J Neurosci 25:10239–10246

Barense MD, Gaffan D et al (2007) The human medial temporal lobe processes online representations of complex objects. Neuropsychologia 45:2963–2974

Barense MD, Henson RNA et al (2010) Medial temporal lobe activity during complex discrimination of faces, objects, and scenes: effects of viewpoint. Hippocampus 20:389–401

Barrash J (1998) A historical review of topographical disorientation and its neuroanatomical correlates. J Clin Exp Neuropsychol 20:807–827

Barrash J, Damasio H et al (2000) The neuroanatomical correlates of route learning impairment. Neuropsychologia 38:820–836

Bellgowan PSF, Bandettini PA et al (2006) Improved BOLD detection in the medial temporal region using parallel imaging and voxel volume reduction. Neuroimage 29:1244–1251

Blaizot X, Mansilla F et al (2010) The human parahippocampal region: I. Temporal pole cytoarchitectonic and MRI correlation. Cereb Cortex 20:2198–2212

Bohbot VD, Allen JJB et al (2000) Memory deficits characterized by patterns of lesions to the hippocampus and parahippocampal cortex. Ann N Y Acad Sci 911:355–368

Bondi MW, Houston WS et al (2005) FMRI evidence of compensatory mechanisms in older adults at genetic risk for Alzheimer disease. Neurology 64:501–508

Braak H, Braak E (1985) On areas of transition between entorhinal allocortex and temporal isocortex in the human brain. Normal morphology and lamina-specific pathology in Alzheimer's disease. Acta Neuropathol 68:325–332

Braak H, Braak E (1991) Neuropathological stageing of Alzheimer-related changes. Acta Neuropathol 82: 239–259

Brodmann K (1909) Vergleichende Lokalisationlehre der Grosshirnrinde. Barth, Leipzig

Brown MW, Aggleton JP (2001) Recognition memory: what are the roles of the perirhinal cortex and hippocampus? Nat Rev Neurosci 2:51–61

Buffalo EA, Bellgowan PSF et al (2006) Distinct roles for medial temporal lobe structures in memory for objects and their locations. Learn Mem 13:638–643

Burgess N, Maguire EA et al (2001) A temporoparietal and prefrontal network for retrieving the spatial context of lifelike events. Neuroimage 14:439–453

Burgess N, Maguire EA et al (2002) The human hippocampus and spatial and episodic memory. Neuron 35:625–641

Bussey TJ, Saksida LM (2002) The organization of visual object representations: a connectionist model of effects of lesions in perirhinal cortex. Eur J Neurosci 15:355–364

Bussey TJ, Saksida LM et al (2002) Perirhinal cortex resolves feature ambiguity in complex visual discriminations. Eur J Neurosci 15(2):365–374

Bussey TJ, Saksida LM et al (2005) The perceptual-mnemonic/feature conjunction model of perirhinal cortex function. Q J Exp Psychol B 58:269–282

Canto CB, Wouterlood FG et al (2008) What does anatomical organization of entorhinal cortex tell us? Neural Plast 2008:1–18

Carr VA, Rissman J et al (2010) Imaging the human medial temporal lobe with high-resolution fMRI. Neuron 65:298–308

Catani M, Thiebaut de Schotten M (2008) A diffusion tensor imaging tractography atlas for virtual in vivo dissections. Cortex 44:1105–1132

Chrobak JJ, Amaral DG (2007) Entorhinal cortex of the monkey: VII. Intrinsic connections. J Comp Neurol 500:612–633

Colombo M, Fernandez T et al (1998) Functional differentiation along the anterior-posterior axis of the hippocampus in monkeys. J Neurophysiol 80: 1002–1005

Corkin S (1984) Lasting consequences of bilateral medial temporal lobectomy: clinical course and experimental findings in H.M. Semin Neurol 4:249–259

Corkin S, Amaral DG et al (1997) H. M'.s medial temporal lobe lesion: findings from magnetic resonance imaging. J Neurosci 17:3964–3979

Coutureau E, Di Scala G (2009) Entorhinal cortex and cognition. Prog Neuropsychopharmacol Biol Psychiatry 33:753–761

Crutch SJ, Lehmann M et al (2012) Posterior cortical atrophy. Lancet Neurol 11:170–178

Cusack R, Russell B et al (2005) An evaluation of the use of passive shimming to improve frontal sensitivity in fMRI. Neuroimage 24:82–91

Dale AM, Fischl B et al (1999) Cortical surface-based analysis – I. Segmentation and surface reconstruction. Neuroimage 9:179–194

Davachi L (2006) Item, context and relational episodic encoding in humans. Curr Opin Neurobiol 16: 693–700

Davachi L, Wagner AD (2002) Hippocampal contributions to episodic encoding: insights from relational and item-based learning. J Neurophysiol 88:982–990

De Renzi E (1982) Disorders of space exploration and cognition. Wiley, New York

De Renzi E, Faglioni P et al (1977) Topographical amnesia. J Neurol Neurosurg Psychiatry 40:498–505

Deng W, Aimone JB et al (2010) New neurons and new memories: how does adult hippocampal neurogenesis affect learning and memory? Nat Rev Neurosci 11:339–350

Di Paola M, Macaluso E et al (2007) Episodic memory impairment in patients with Alzheimer's disease is correlated with entorhinal cortex atrophy a voxel-based morphometry study. J Neurol 254:774–781

Diana RA, Yonelinas AP et al (2007) Imaging recollection and familiarity in the medial temporal lobe: a three-component model. Trends Cogn Sci 11:379–386

Dickerson BC, Sperling RA (2008) Functional abnormalities of the medial temporal lobe memory system in mild cognitive impairment and Alzheimer's disease: insights from functional MRI studies. Neuropsychologia 46:1624–1635

Dickerson BC, Salat DH et al (2004) Medial temporal lobe function and structure in mild cognitive impairment. Ann Neurol 56:27–35

Dickerson BC, Feczko E et al (2009) Differential effects of aging and Alzheimer's disease on medial temporal lobe cortical thickness and surface area. Neurobiol Aging 30(3):432–440

Ding S-L, Van Hoesen GW (2010) Borders, extent, and topography of human perirhinal cortex as revealed using multiple modern neuroanatomical and pathological markers. Hum Brain Mapp 31:1359–1379

Ding S-L, Van Hoesen GW et al (2009) Parcellation of human temporal polar cortex: a combined analysis of multiple cytoarchitectonic, chemoarchitectonic, and pathological markers. J Comp Neurol 514:595–623

Doeller CF, Barry C et al (2010) Evidence for grid cells in a human memory network. Nature 463:657–661

Dolorfo CL, Amaral DG (1998) Entorhinal cortex of the rat: topographic organization of the cells of origin of the perforant path projection to the dentate gyrus. J Comp Neurol 398:25–48

Duvernoy HM (1998) The human hippocampus, 2nd edn. Springer, Belin

Eichenbaum H, Dudchenko P et al (1999) The hippocampus, memory and place cells: is it spatial memory or a memory space? Neuron 23:209–226

Eichenbaum H, Yonelinas AP et al (2007) The medial temporal lobe and recognition memory. Annu Rev Neurosci 30:123–152

Epstein R, Kanwisher N (1998) A cortical representation of the local visual environment. Nature 392:598–601

Epstein R, Harris A et al (1999) The parahippocampal place area: recognition, navigation, or encoding? Neuron 23:115–125

Eustache F, Desgranges B et al (2001) Entorhinal cortex disruption causes memory deficit in early Alzheimer's disease as shown by PET. Neuroreport 12:683–685

Ewers M, Sperling RA et al (2011) Neuroimaging markers for the prediction and early diagnosis of Alzheimer's disease dementia. Trends Neurosci 34:430–442

Fischl B, Sereno MI et al (1999) Cortical surface-based analysis – II: inflation, flattening, and a surface-based coordinate system. Neuroimage 9:195–207

Fyhn M, Molden S et al (2004) Spatial representation in the entorhinal cortex. Science 305:1258–1264

Fyhn M, Hafting T et al (2007) Hippocampal remapping and grid realignment in entorhinal cortex. Nature 446:190–194

Gadian DG, Aicardi J et al (2000) Developmental amnesia associated with early hypoxic–ischaemic injury. Brain 123:499–507

Gale SD, Hopkins RO (2004) Effects of hypoxia on the brain: neuroimaging and neuropsychological findings following carbon monoxide poisoning and obstructive sleep apnea. J Int Neuropsychol Soc 10:60–71

Ghoshal N, García-Sierra F et al (2002) Tau conformational changes correspond to impairments of episodic memory in mild cognitive impairment and Alzheimer's disease. Exp Neurol 177:475–493

Giovanello KS, Schnyer DM et al (2004) A critical role for the anterior hippocampus in relational memory: evidence from an fMRI study comparing associative and item recognition. Hippocampus 14:5–8

Grill-Spector K, Malach R (2004) The human visual cortex. Annu Rev Neurosci 27:649–677

Guillozet AL, Weintraub S et al (2003) Neurofibrillary tangles, amyloid, and memory in aging and mild cognitive impairment. Arch Neurol 60:729–736

Hafting T, Fyhn M et al (2005) Microstructure of a spatial map in the entorhinal cortex. Nature 436:801–806

Hanke J (1997) Sulcal pattern of the anterior parahippocampal gyrus in the human adult. Ann Anat 179:335–339

Hannula DE, Ranganath C (2008) Medial temporal lobe activity predicts successful relational memory binding. J Neurosci 28:116–124

Hasselmo ME, Brandon MP (2008) Linking cellular mechanisms to behavior: entorhinal persistent spiking and membrane potential oscillations may underlie path integration, grid cell firing, and episodic memory. Neural Plast 2008:1–12

Henke K (2010) A model for memory systems based on processing modes rather than consciousness. Nat Rev Neurosci 11:523–532

Henke K, Buck A et al (1997) Human hippocampus establishes associations in memory. Hippocampus 7:249–256

Henke K, Kroll NEA et al (1999a) Memory lost and regained following bilateral hippocampal damage. J Cogn Neurosci 11:682–697

Henke K, Weber B et al (1999b) Human hippocampus associates information in memory. Proc Natl Acad Sci USA 96:5884–5889

Henson R (2005) A mini-review of fMRI studies of human medial temporal lobe activity associated with recognition memory. Q J Exp Psychol B 58:340–360

Hirni D, Monsch AU et al (2011) Relative association of perirhinal and entorhinal cortex integrity with semantic and episodic memory performance: implications for early detection of Alzheimer's disease. In: 288.0 Neuroscience Meeting Planner. Society for Neuroscience, Washington, D.C.

Hogan RE, Mark KE et al (2000) Mesial temporal sclerosis and temporal lobe epilepsy: MR imaging deformation-based segmentation of the hippocampus in five patients. Radiology 216:291–297

Hopf A (1956) Über die Verteilung myeloarchitektonischer Merkmale in der Stirnhirnrinde beim Menschen. J Hirnforsch 2:311–333

Insausti R, Amaral DG (2004) Hippocampal formation. In: Paxinos G, Mai JK (eds) The human nervous system. Elsevier, Amsterdam, pp 871–914

Insausti R, Amaral DG et al (1987) The entorhinal cortex of the monkey: II. Cortical afferents. J Comp Neurol 264:356–395

Insausti R, Juottonen K et al (1998) MR volumetric analysis of the human entorhinal, perirhinal, and temporopolar cortices. AJNR Am J Neuroradiol 19:659–671

Jacobs J, Kahana MJ et al (2010) A sense of direction in human entorhinal cortex. Proc Natl Acad Sci USA 107:6487–6492

Juottonen K, Laakso MP et al (1998) Volumes of the entorhinal and perirhinal cortices in Alzheimer's disease. Neurobiology of Aging 19(1):15–22

Jung MW, Wiener SI et al (1994) Comparison of spatial firing characteristics of units in dorsal and ventral hippocampus of the rat. J Neurosci 14:7347–7356

Kivisaari SL, Tyler LK et al (2012) Medial perirhinal cortex disambiguates confusable objects. Brain 135:3757–3769

Klein A, Ghosh SS et al (2010) Evaluation of volume-based and surface-based brain image registration methods. Neuroimage 51:214–220

Klingler J (1948) Die makroskopische Anatomie der Ammonsformation. Kommissionsverlag von Gebrüder Fretz A.G., Zürich

Köhler S, Crane J et al (2002) Differential contributions of the parahippocampal place area and the anterior hippocampus to human memory for scenes. Hippocampus 12:718–723

Köhler S, Danckert S et al (2005) Novelty responses to relational and non-relational information in the hippocampus and the parahippocampal region: a comparison based on event-related fMRI. Hippocampus 15:763–774

Kravitz DJ, Saleem KS et al (2011) A new neural framework for visuospatial processing. Nat Rev Neurosci 12:217–230
Krimer LS, Hyde TM et al (1997) The entorhinal cortex: an examination of cyto- and myeloarchitectonic organization in humans. Cereb Cortex 7:722–731
Lashley KS (1929) Brain mechanisms and intelligence: a quantitative study of injuries to the brain. University of Chicago Press, Chicago
Lavenex P, Amaral DG (2000) Hippocampal-neocortical interaction: a hierarchy of associativity. Hippocampus 10:420–430
Lavenex P, Suzuki WA et al (2004) Perirhinal and parahippocampal cortices of the macaque monkey: intrinsic projections and interconnections. J Comp Neurol 472:371–394
Lee ACH, Barense MD et al (2005) The contribution of the human medial temporal lobe to perception: bridging the gap between animal and human studies. Q J Exp Psychol B 58:300–325
Lee ACH, Scahill VL et al (2008) Activating the medial temporal lobe during oddity judgment for faces and scenes. Cereb Cortex 18:683–696
Leonard BW, Amaral DG et al (1995) Transient memory impairment in monkeys with bilateral lesions of the entorhinal cortex. J Neurosci 15:5637–5659
Lerch JP, Pruessner JC et al (2005) Focal decline of cortical thickness in Alzheimer's disease identified by computational neuroanatomy. Cereb Cortex 15:995–1001
Leutgeb JK, Leutgeb S et al (2007) Pattern separation in the dentate gyrus and CA3 of the hippocampus. Science 315:961–966
Lipton PA, Eichenbaum H (2008) Complementary roles of hippocampus and medial entorhinal cortex in episodic memory. Neural Plast 2008:1–8
Liu Z, Murray EA et al (2000) Learning motivational significance of visual cues for reward schedules requires rhinal cortex. Nat Neurosci 3:1307–1315
Machulda MM, Ward HA et al (2003) Comparison of memory fMRI response among normal, MCI, and Alzheimer's patients. Neurology 61:500–506
Maguire EA, Frith CD et al (1998) Knowing where things are: parahippocampal involvement in encoding object locations in virtual large-scale space. J Cogn Neurosci 10:61–76
Mahut H, Zola-Morgan S et al (1982) Hippocampal resections impair associative learning and recognition memory in the monkey. J Neurosci 2:1214–1220
Maller JJ, Réglade-Meslin C et al (2006) Sex and symmetry differences in hippocampal volumetrics: before and beyond the opening of the crus of the fornix. Hippocampus 16:80–90
Malykhin NV, Bouchard TP et al (2007) Three-dimensional volumetric analysis and reconstruction of amygdala and hippocampal head, body and tail. Psychiatry Res 155:155–165
Mattson MP (2004) Pathways towards and away from Alzheimer's disease. Nature 430:631–639
Meunier M, Bachevalier J et al (1993) Effects on visual recognition of combined and separate ablations of the entorhinal and perirhinal cortex in rhesus monkeys. J Neurosci 13:5418–5432
Mishkin M (1978) Memory in monkeys severely impaired by combined but not by separate removal of amygdala and hippocampus. Nature 273:297–298
Mishkin M, Ungerleider LG et al (1983) Object vision and spatial vision: two cortical pathways. Trends Neurosci 6:414–417
Mishkin M, Suzuki WA et al (1997) Hierarchical organization of cognitive memory. Philos Trans R Soc Lond B Boil Sci 352:1461–1467
Montaldi D, Mayes AR (2010) The role of recollection and familiarity in the functional differentiation of the medial temporal lobes. Hippocampus 20:1291–1314
Montaldi D, Mayes AR (2011) Familiarity, recollection and medial temporal lobe function: an unresolved issue. Trends Cogn Sci 15:339–340
Moscovitch M, Rosenbaum RS et al (2005) Functional neuroanatomy of remote episodic, semantic and spatial memory: a unified account based on multiple trace theory. J Anat 207:35–66
Moser M-B, Moser EI (1998) Functional differentiation in the hippocampus. Hippocampus 8:608–619
Moss HE, Rodd JM et al (2005) Anteromedial temporal cortex supports fine-grained differentiation among objects. Cereb Cortex 15:616–627
Murray EA, Mishkin M (1998) Object recognition and location memory in monkeys with excitotoxic lesions of the amygdala and hippocampus. J Neurosci 18:6568–6582
Murray EA, Richmond BJ (2001) Role of perirhinal cortex in object perception, memory, and associations. Curr Opin Neurobiol 11:188–193
Murray EA, Malkova L et al (1998) Crossmodal associations, intramodal associations, and object identification in macaque monkeys. In: Milner AD (ed) Comparative neuropsychology. Oxford University Press, Oxford, pp 51–69
O'Donnell P, Buxton PJ et al (2000) The magnetic resonance imaging appearances of the brain in acute carbon monoxide poisoning. Clin Radiol 55:273–280
O'Kane G, Kensinger EA et al (2004) Evidence for semantic learning in profound amnesia: an investigation with patient H.M. Hippocampus 14:417–425
O'Keefe J, Dostrovsky J (1971) The hippocampus as a spatial map: preliminary evidence from unit activity in the freely-moving rat. Brain Res 34:171–175
O'Neil EB, Cate AD et al (2009) Perirhinal cortex contributes to accuracy in recognition memory and perceptual discriminations. J Neurosci 29:8329–8334
O'Reilly RC, McClelland JL (1994) Hippocampal conjunctive encoding, storage, and recall: avoiding a trade-off. Hippocampus 4:661–682
Pantel J, O'Leary DS et al (2000) A new method for the in vivo volumetric measurement of the human hippocampus with high neuroanatomical accuracy. Hippocampus 10:752–758
Paterson A, Zancwill OL (1945) A case of topographical disorientation associated with a unilateral cerebral lesion. Brain 68:188–212
Pihlajamäki M, Tanila H et al (2004) Visual presentation of novel objects and new spatial arrangements of objects

differentially activates the medial temporal lobe subareas in humans. Eur J Neurosci 19:1939–1949
Pruessner JC, Li LM et al (2000) Volumetry of hippocampus and amygdala with high-resolution MRI and three-dimensional analysis software: minimizing the discrepancies between laboratories. Cereb Cortex 10:433–442
Pruessner JC, Köhler S et al (2002) Volumetry of temporopolar, perirhinal, entorhinal and parahippocampal cortex from high-resolution MR images: considering the variability of the collateral sulcus. Cereb Cortex 12:1342–1353
Qiu C, Kivipelto M et al (2009) Epidemiology of Alzheimer's disease: occurrence, determinants, and strategies toward intervention. Dialogues Clin Neurosci 11:111–128
Ranganath C (2010) A unified framework for the functional organization of the medial temporal lobes and the phenomenology of episodic memory. Hippocampus 20:1263–1290
Rolls ET (2007) An attractor network in the hippocampus: theory and neurophysiology. Learn Mem 14: 714–731
Rombouts SARB, Barkhof F et al (2000) Functional MR imaging in Alzheimer's disease during memory encoding. AJNR Am J Neuroradiol 21:1869–1875
Saleem KS, Price JL et al (2007) Cytoarchitectonic and chemoarchitectonic subdivisions of the perirhinal and parahippocampal cortices in macaque monkeys. J Comp Neurol 500:973–1006
Salmon DP (2011) Neuropsychological features of mild cognitive impairment and preclinical Alzheimer's disease. Curr Top Behav Neurosci 179:34–41
Salmon DP, Bondi MW (2009) Neuropsychological assessment of dementia. Annu Rev Psychol 60: 257–282
Schmidt CF, Degonda N et al (2005) Sensitivity-encoded (SENSE) echo planar fMRI at 3T in the medial temporal lobe. Neuroimage 25:625–641
Schwarzbauer C, Mildner T et al (2010) Dual echo EPI – the method of choice for fMRI in the presence of magnetic field inhomogeneities? Neuroimage 49:316–326
Scoville WB, Milner B (1957) Loss of recent memory after bilateral hippocampal lesions. J Neurol Neurosurg Psychiatry 20:11–21
Sewards TV (2011) Adolf Hopf's 1954 myeloarchitectonic parcellation of the human temporal lobe: a review and assessment. Brain Res Bull 86:298–313
Silbert LC, Quinn JF et al (2003) Changes in premorbid brain volume predict Alzheimer's disease pathology. Neurology 61:487–492
Skotko BG, Rubin DC et al (2008) H.M'.s personal crossword puzzles: understanding memory and language. Memory 16:89–96
Squire LR, Wixted JT (2011) The cognitive neuroscience of human memory since H.M. Annu Rev Neurosci 34:259–288
Squire LR, Zola SM (1998) Episodic memory, semantic memory and amnesia. Hippocampus 8:205–211
Squire LR, Zola-Morgan S (1988) Memory: brain systems and behavior. Trends Neurosci 11:170–175
Squire LR, Stark CEL et al (2004) The medial temporal lobe. Annu Rev Neurosci 27:279–306
Staresina BP, Duncan KD et al (2011) Perirhinal and parahippocampal cortices differentially contribute to later recollection of object- and scene-related event details. J Neurosci 31:8739–8747
Steffenach H-A, Witter M et al (2005) Spatial memory in the rat requires the dorsolateral band of the entorhinal cortex. Neuron 45(2): 301–313
Suzuki WA, Amaral DG (1994a) Perirhinal and parahippocampal cortices of the macaque monkey: cortical afferents. J Comp Neurol 350:497–533
Suzuki WA, Amaral DG (1994b) Topographic organization of the reciprocal connections between the monkey entorhinal cortex and the perirhinal and parahippocampal cortices. J Neurosci 14:1856–1877
Suzuki WA, Amaral DG (2003a) Perirhinal and parahippocampal cortices of the macaque monkey: cytoarchitectonic and chemoarchitectonic organization. J Comp Neurol 463:67–91
Suzuki WA, Amaral DG (2003b) Where are the perirhinal and parahippocampal cortices? A historical overview of the nomenclature and boundaries applied to the primate medial temporal lobe. Neuroscience 120: 893–906
Suzuki WA, Miller EK et al (1997) Object and place memory in the macaque entorhinal cortex. J Neurophysiol 78:1062–1081
Takahashi S, Yonezawa H et al (2002) Selective reduction of diffusion anisotropy in white matter of Alzheimer disease brains measured by 3.0 Tesla magnetic resonance imaging. Neurosci Lett 332:45–48
Taylor KI, Monsch AU (2007) The neuropsychology of Alzheimer's disease. In: Richter RW, Richter BZ (eds) Alzheimer's disease? The basics. A physician's guide to the practical management. The Humana Press Inc., Totowa
Taylor KI, Probst A (2008) Anatomic localization of the transentorhinal region of the perirhinal cortex. Neurobiol Aging 29:1591–1596
Taylor KI, Moss HE et al (2006) Binding crossmodal object features in perirhinal cortex. Proc Natl Acad Sci USA 103:8239–8244
Taylor KI, Probst A et al (2008) Clinical course of neuropathologically confirmed frontal-variant Alzheimer's disease. Nat Clin Pract Neurol 4:226–232
Taylor KI, Stamatakis EA et al (2009) Crossmodal integration of object features: voxel-based correlations in brain-damaged patients. Brain 132:671–683
Taylor KI, Devereux BJ et al (2011a) Conceptual structure: towards an integrated neuro-cognitive account. Lang Cogn Proc 26:1368–1401
Taylor KI, Kivisaari S et al (2011b) Crossmodal integration of audiovisual objects is related to anteromedial temporal lobe integrity in patients with very early Alzheimer's disease. In: 287.20 Neuroscience Meeting Planner. Society for Neuroscience, Washington, D.C

Thangavel R, Van Hoesen GW et al (2008) Posterior parahippocampal gyrus pathology in Alzheimer's disease. Neuroscience 154:667–676

Tyler LK, Stamatakis EA et al (2004) Processing objects at different levels of specificity. Journal of Cognitive Neuroscience 16(3):351–362

Tyler LK, Marslen-Wilson W et al (2005) Dissociating neuro-cognitive component processes: voxel-based correlational methodology. Neuropsychologia 43:771–778

Van Hoesen GW (1982) The parahippocampal gyrus: new observations regarding its cortical connections in the monkey. Trends Neurosci 5:345–350

Van Hoesen GW (1995) Anatomy of the medial temporal lobe. Magn Reson Imaging 13:1047–1055

Van Hoesen GW, Augustinak JC et al (2000) The parahippocampal gyrus in Alzheimer's disease: clinical and preclinical neuroanatomical correlates. Ann N Y Acad Sci 911:254–274

Vargha-Khadem F, Gadian DG et al (1997) Differential effects of early hippocampal pathology on episodic and semantic memory. Science 277:376–380

Victor M, Adams RD et al (1989) The Wernicke-Korsakoff syndrome and related neurologic disorders due to alcoholism and malnutrition, 2nd edn. F.A. Davis Co, Philadelphia

Vogt BA, Vogt L et al (2006) Cytology and functionally correlated circuits of human posterior cingulate areas. Neuroimage 29:452–466

von Bonin G, Bailey P (1947) The neocortex of *Macaca mulatta*. University of Illinois Press, Urbana

von Economo C, Koskinas GN (1925) Die Cytoarchitecktonik der Grosshirnrinde des erwachsenen Menschen. Springer, Berlin

Wallenstein GV, Hasselmo ME et al (1998) The hippocampus as an associator of discontiguous events. Trends Neurosci 21:317–323

Wang L, Zang Y et al (2006) Changes in hippocampal connectivity in the early stages of Alzheimer's disease: evidence from resting state fMRI. Neuroimage 31:496–504

Wang W-C, Lazzara MM et al (2010) The medial temporal lobe supports conceptual implicit memory. Neuron 68:835–842

Watson C, Andermann F et al (1992) Anatomic basis of amygdaloid and hippocampal volume measurement by magnetic resonance imaging. Neurology 42:1743–1750

Whiteley AM, Warrington EK (1978) Selective impairment of topographical memory: a single case study. J Neurol Neurosurg Psychiatry 41:575–578

Winblad B, Palmer K et al (2004) Mild cognitive impairment - beyond controversies, towards a consensus: report of the International Working Group on Mild Cognitive Impairment. J Intern Med 256:240–246

Witter MP (2007) The perforant path: projections from the entorhinal cortex to the dentate gyrus. In: Scharfman HE (ed) The dentate gyrus: a comprehensive guide to structure, function, and clinical implications. Elsevier, Boston, pp 43–61

Witter MP, Amaral DG (1991) Entorhinal cortex of the monkey: V. Projections to the dentate gyrus, hippocampus, and subicular complex. J Comp Neurol 307:437–459

Witter MP, Moser EI (2006) Spatial representation and the architecture of the entorhinal cortex. Trends Neurosci 29:671–678

Yassa MA, Stark CEL (2011) Pattern separation in the hippocampus. Trends Neurosci 34:515–525

Yonelinas AP (2002) The nature of recollection and familiarity: a review of 30 years of research. J Mem Lang 46:441–517

Zilles K, Amunts K (2009) Receptor mapping: architecture of the human cerebral cortex. Curr Opin Neurol 22:331–339

Zola-Morgan S, Squire LR et al (1986) Human amnesia and the medial temporal region: enduring memory impairment following a bilateral lesion limited to field CA1 of the hippocampus. J Neurosci 6:2950–2967

Zola-Morgan S, Squire LR et al (1989a) Lesions of the hippocampal formation but not lesions of the fornix or the mammillary nuclei produce long-lasting memory impairment in monkeys. J Neurosci 9:898–913

Zola-Morgan S, Squire LR et al (1989b) Lesions of the amygdala that spare adjacent cortical regions do not impair memory or exacerbate the impairment following lesions of the hippocampal formation. J Neurosci 9:1922–1936

Zola-Morgan S, Squire LR et al (1989c) Lesions of perirhinal and parahippocampal cortex that spare the amygdala and hippocampal formation produce severe memory impairment. J Neurosci 9:4355–4370

Simultaneous EEG and fMRI Recordings (EEG-fMRI)

20

Friederike Moeller, Michael Siniatchkin, and Jean Gotman

Abbreviations

AAS	Averaged artefact subtraction
BOLD	Blood oxygenation level dependent
EEG	Electroencephalography
fMRI	Functional magnetic resonance imaging
GSW	Generalised spike-wave discharges
HRF	Hemodynamic response function
IGE	Idiopathic generalised epilepsy

F. Moeller (✉)
University Hospital of Pediatric Neurology,
Christian-Albrechts-University of Kiel,
Schwanenweg 20, 24105 Kiel, Germany
e-mail: f.moeller@pedneuro.uni-kiel.de

M. Siniatchkin
University Hospital of Child and Adolescent Psychiatry,
Johann Wolfgang Goethe-University of Frankfurt,
Deutschordenstraße 50, 60528
Frankfurt am Main, Germany
e-mail: michael.siniatchkin@kgu.de

J. Gotman
Montreal Neurological Institute, McGill University,
3801 University Street, H3A 2B4
Montreal, Québec, Canada
e-mail: jean.gotman@mcgill.ca

20.1 Introduction

Scalp EEG is an important tool for the investigation of patients with epilepsy. It can help to diagnose and classify epilepsy and localise the source of epileptic activity. However, a disadvantage of EEG is its low spatial resolution and the weakness to detect epileptic activity from deep brain structures. In contrast, fMRI is characterised by a good spatial resolution and is equally sensitive to signals of deep and superficial brain structures. By combining EEG with fMRI, it is possible to detect BOLD signal changes associated with spikes detected on the scalp EEG, even if deep brain structures are involved.

In the past years, EEG-fMRI studies have been used to delineate the epileptogenic zone noninvasively. Furthermore, EEG-fMRI studies have contributed to the understanding of pathophysiological mechanisms of epilepsy. In this chapter, the methodological background is described and an overview about EEG-fMRI studies in the field of focal and generalised epilepsy and paediatric epilepsy is given. The chapter concludes with EEG-fMRI studies on spontaneous brain activity in healthy subjects.

20.2 Methods

It is challenging to record an EEG in an MRI environment of changing electromagnetic fields which interfere with the EEG. In 1993, Ives and colleagues demonstrated that it is possible to record

S. Ulmer, O. Jansen (eds.), *fMRI – Basics and Clinical Applications*,
DOI 10.1007/978-3-642-34342-1_20,

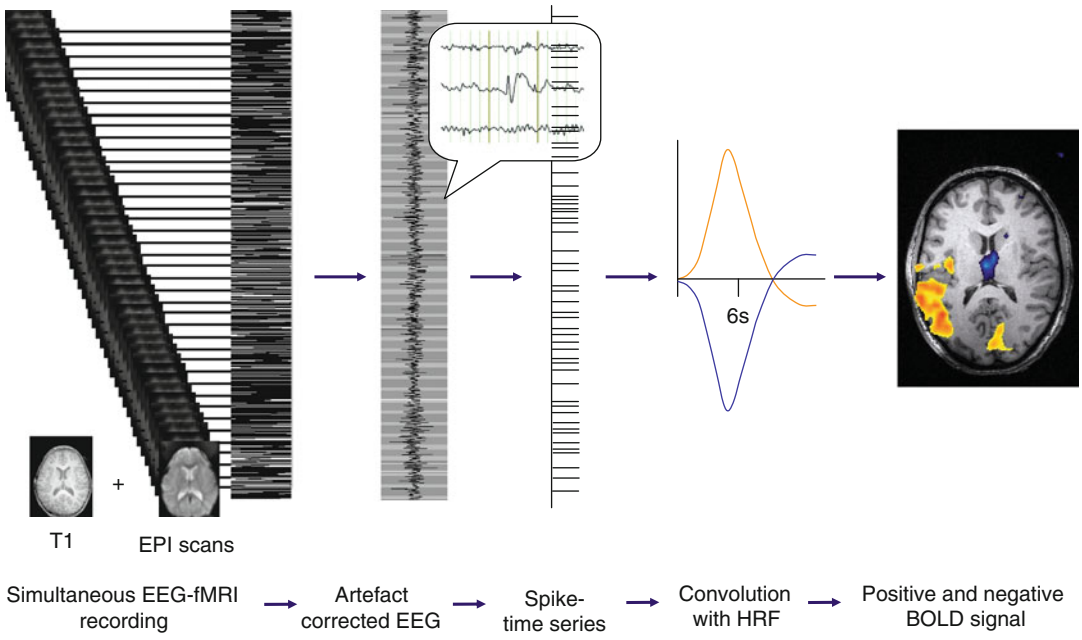

Fig. 20.1 Schematic representation of different steps of an EEG-fMRI investigation: simultaneous recording of EEG and functional MRI, artefact correction of the EEG, identification of the events (e.g. spikes) in the corrected EEG, building a spike-related model, convolution of the model with the hemodynamic response function (here: canonical hemodynamic response function) and detection of spike-related BOLD signal changes

an EEG during an fMRI investigation (Ives et al. 1993). The first EEG-fMRI recordings were performed in a spike-triggered manner: If epileptic activity was observed in the EEG, the fMRI acquisition was started. This way, the images were acquired approximately 4 s after the event, obscuring the EEG with gradient artefacts during the scanning. This approach is possible since the hemodynamic response function peaks several seconds after an event (Krakow et al. 1999; Seeck et al. 1998). However, the correct identification of the spikes during the scanning by an experienced observer is necessary and the time course of the spike-associated BOLD signal changes is not detected. Since the EEG is obscured by gradient artefacts during the scanning, it cannot be excluded that spikes occurred during the acquisition. The development of gradient artefact correction algorithms made it possible to record the EEG continuously during the fMRI investigation (Allen et al. 2000; Hoffmann et al. 2000; Lemieux et al. 2001) which is the standard method used in EEG-fMRI studies today. The scanning time for EEG-fMRI studies varies from 20 min in children up to 90 min in adults.

20.2.1 How to Do It?

Figure 20.1 summarises the different steps of an EEG-fMRI investigation. In order to record the EEG inside the scanner, the following points need to be considered.

20.2.1.1 Equipment

An MRI-compatible recording system is needed. The electrodes and wires need to be nonmagnetic, which is the case for Ag/AgCl or gold electrodes. It is possible to use whole-head caps or single electrodes. Using caps reduces the time needed to attach electrodes which is an important factor if working with children.

Loops in the wires or movement of the wires could cause heating or artefacts and should be avoided. Foam pads and vacuum pillows can be used to help secure the EEG leads, minimise motion and improve patient comfort. The wires are connected to an MRI-compatible high-input impedance amplifier which is placed inside the scanner room either directly behind the head coil (e.g. MR-compatible EEG recording system "BrainAmp-MR" by Brain Products Co., Munich,

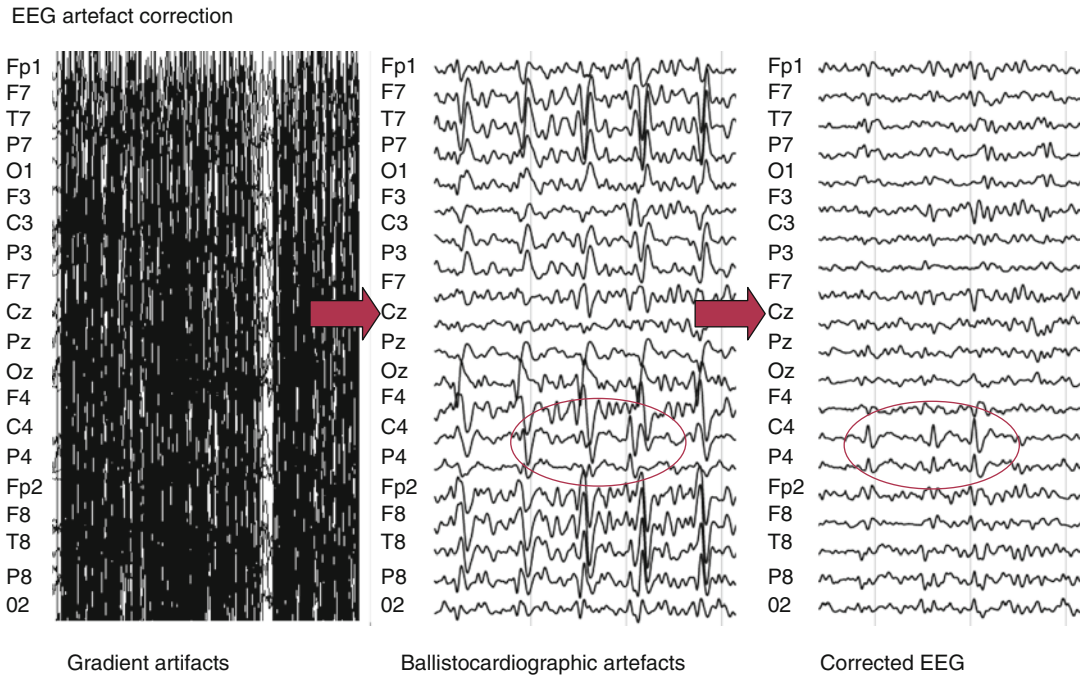

Fig. 20.2 Artefact correction of the EEG recorded during the fMRI recording. Examples of the same segment of the EEG without artefact correction, after gradient artefact correction and after removal of the ballistocardiographic artefacts are shown

Germany) or beside the subject (MR-system Electrical Geodesics, EGI Co., Memphis, USA) in most cases. The data is transmitted via a fibre optic cable to a computer located outside the scanner room. In some cases, MR-compatible caps are used and connected via a long cable with an EEG system placed outside the scanner room (MagLink system, Neuroscan/Compumedics Co.).

20.2.1.2 Artefact Correction

During the scanning, the rapidly changing magnetic field induces a strong current which results in a high-amplitude gradient artefact in simultaneous EEG recordings. These artefacts can be removed after the scanning by artefact correction software so that the EEG is free from artefacts and events can be identified. The most commonly applied artefact correction uses an averaged artefact subtraction (AAS) method described by Allen and colleagues (Allen et al. 2000). This method estimates the gradient artefact and subtracts it from each frame. For this step, a high sampling rate (several kHz) is needed to fully capture the shape of the gradient artefact. Furthermore, the scanner (10 MHz sampling rate) can be synchronised with the EEG amplifier (5 kHz sampling rate) to ensure identical sampling of the artefact for each frame, which optimises the artefact correction. The EEG data is corrected relative to the gradient artefact onset, which is indicated by a trigger received from the MR system and recorded with the EEG. In Kiel and Montreal, the BrainVision Analyzer software (Brain Products Co., Munich, Germany) is used for artefact correction. Corrected EEG data are filtered using a high-pass filter at 0.03 Hz and a low-pass filter at 75 Hz and down sampled to 250 Hz.

In addition to gradient artefacts, many EEG data sets are affected by heartbeat synchronous artefacts. These so-called pulse or ballistocardiographic artefacts are caused by subtle pulse synchronous movements of the head and can be removed by the same AAS method (Allen et al. 1998) or independent component analysis-based procedures (Bénar et al. 2003; Srivastava et al. 2005). Figure 20.2 illustrates the different steps for artefact correction of the EEG.

To enable visual inspection of the EEG during the EEG-fMRI recording, an online correction of gradient artefacts is possible.

20.2.2 Statistical Analysis

The preprocessing of the fMRI images does not differ from a standard fMRI analysis and includes realignment, smoothing and normalisation in the case of group analyses. Since many analyses are based on individual single subject analysis, normalisation is omitted in many studies on focal epilepsy. The classical analysis uses the event-related general linear model-based approach. For building the statistical model, the artefact-corrected EEG is reviewed and all events (e.g. spikes) are marked. The timing of each event is then used to build time series for the statistical analysis. In the standard analysis, the timing of the events is convolved with the standard hemodynamic response function which is derived from a response to brief auditory stimuli and peaks approximately 5 s after the event (Glover 1999). Statistical maps are computed, showing voxels significantly correlated with the marked event in the EEG (Friston et al. 1996). However, taking a standard HRF does not take into account that shape and latency of the HRF might vary with age, different brain regions or altered response in epilepsy. Several studies have shown that the EEG-fMRI results can be improved if a more flexible HRF is applied. A more variable shape of the HRF can be achieved by including the derivative of the HRF in addition to the standard HRF (Hamandi et al. 2006) or by estimating non canonical HRFs (Lemieux et al. 2007; van Houdt et al. 2010). In Montreal, a set of four HRFs with peaks at 3, 5, 7 and 9 s is used to capture BOLD responses with different latencies (Bagshaw et al. 2004). More methodological refinements are mentioned in the Sect. 20.3.1.

20.3 EEG-fMRI in Focal Epilepsy

20.3.1 Interictal Activity

The development of EEG-fMRI was clinically motivated to localise the region presumably generating focal interictal spikes. Patients are usually selected on the basis of having frequent spikes in the routine EEG. However, since spikes occur spontaneously, it cannot be guaranteed that spikes occur during the EEG-fMRI investigation. In two early large case series, spikes were detected in 50 % of the patients and the associated BOLD signal changes were concordant with electroclinical data in approximately 50 % of the patients showing spikes during the investigation (Al-Asmi et al. 2003; Salek-Haddadi et al. 2006). Methodological refinement, e.g. the use of multiple HRFs or fitting of individual HRFs, increases the sensitivity of BOLD signal detection (Bagshaw et al. 2004; Lu et al. 2007). Scanning at 3 T rather than at 1.5 T as in the early studies also improves sensitivity (Gholipour et al. 2011; Pittau et al. 2012). In many EEG-fMRI studies, only few spikes were recorded during the EEG-fMRI investigation leading to inconclusive results. Instead of marking spikes in the scanner EEG, Groullier et al. built scalp voltage maps of averaged spike recorded during clinical long-term monitoring and computed the correlation of this map with the intra-MR topography at each EEG time frame. In 12 patients (~65 %) with previously inconclusive studies, BOLD changes concordant with intracranial EEG or the resection area were detected. This voltage map-based analysis also yielded conclusive results when no clear spike in the scanner EEG was detected (Grouiller et al. 2011). A recent study showed that by modelling sleep-specific activity in epilepsy patients, the sensitivity of the detection of spike-related BOLD signal changes could be increased (Moehring et al. 2011).

20.3.1.1 Does the Spike-Associated BOLD Signal Represent the Spike Generator?

To answer this question, BOLD signal changes were compared to intracranial EEG recordings preformed after the EEG-fMRI investigation. In a study by Bénar et al. active electrodes on the intracranial EEG recordings were close to the areas of spike-associated BOLD response (Bénar et al. 2006). Furthermore, there are several cases in EEG-fMRI studies in focal epilepsy in which the concordance between spike-associated BOLD signal changes and the seizure onset determined by intracranially recorded seizures were detected

(Bagshaw et al. 2004; Laufs et al. 2006a; Grova et al. 2008; Tyvaert et al. 2008a). While these studies compared EEG-fMRI results and intracranial recordings which were recorded on different days, it is now possible to perform an EEG-fMRI recording in patients with intracranial electrodes. One study showed BOLD response close to the electrodes from which spikes were recorded (Vulliemoz et al. 2011). However, not only BOLD signal changes in the presumed epileptogenic zone but also in remote areas were frequently detected in both single subject analyses and group analyses (Kobayashi et al. 2006a, 2009; Laufs et al. 2007). These remote BOLD signal changes may be remote effects of the epileptic spikes. Combined source analysis and EEG-fMRI studies suggests that distant BOLD signal changes might be explained by propagated epileptic activity (Vulliemoz et al. 2009; Groening et al. 2009).

In most studies, both positive and negative BOLD responses were observed. While positive BOLD responses reflect increased neuronal activity compared to baseline (Logothetis et al. 2001), negative BOLD responses have been shown to reflect suppressed neuronal activity (Devor et al. 2007). Spike-associated BOLD deactivation might be caused by remote inhibition (Gotman et al. 2005; Laufs et al. 2007).

20.3.1.2 Can EEG-fMRI Be Used as a Noninvasive Tool in Presurgical Evaluation?

A study in patients with medically intractable epilepsy suggested that EEG-fMRI may add useful information in the preoperative workup (Zijlmans et al. 2007). In patients with nonlesional frontal lobe epilepsy, a concordance between positive BOLD signal changes and postoperative pathological analysis or other imaging modalities was found (Moeller et al. 2009a). An example of the comparison between EEG-fMRI results and methods of the presurgical evaluation in a patient with focal epilepsy is depicted in Fig. 20.3. A postsurgical study showed that a surgical removal including the areas of positive BOLD response was associated with a good postsurgical outcome (Thornton et al. 2010). If a method is used for clinical purposes, it has to yield reproducible results. A recent study by Gholipour and colleagues has shown a good reproducibility of EEG-fMRI results, supporting its validity for clinical use; the study also showed that EEG-fMRI scans performed at 3 T were more sensitive than those performed at 1.5 T (Gholipour et al. 2011). A recent study evaluated the new localising information generated by EEG-fMRI compared to traditional EEG and found that this occurred in a large proportion of patients (Pittau et al. 2012). It is important that results be interpreted carefully since EEG-fMRI does not only show areas of the presumed epileptogenic zone but also areas that might be indirectly influenced by the spikes, also in distant areas. If EEG-fMRI results are considered in the context of other investigations of the presurgical evaluation, they can contribute to a better understanding of the epileptic zone in a specific patient.

20.3.1.3 Beyond the Focus

Several recent studies go beyond the analysis of the epileptogenic zone by investigating the functional connectivity of patients with mesial temporal lobe epilepsy. Functional connectivity studies measure how different brain areas are interconnected during resting state of the brain (for details, please read the chapter on resting state fluctuations in this book). Studies of patients with mesial temporal lobe epilepsy show that the functional connectivity in the diseased hippocampus as well as in default mode areas is decreased, indicating that this localisation-related epilepsy is also a network disease (Bettus et al. 2009; Pereira et al. 2010; Liao et al. 2011; Zhang et al. 2010).

20.3.2 Seizures

It is challenging to record seizures inside the scanner. The occurrence of a seizure cannot be predicted, and it is very rare that a seizure is captured during the short time of EEG-fMRI recording. If a seizure is recorded, it is often accompanied by head movements that make the data analysis difficult. To avoid seizure-induced motion problems, Federico and colleagues analysed the BOLD signal prior to the beginning of the clinical seizure in three patients with focal

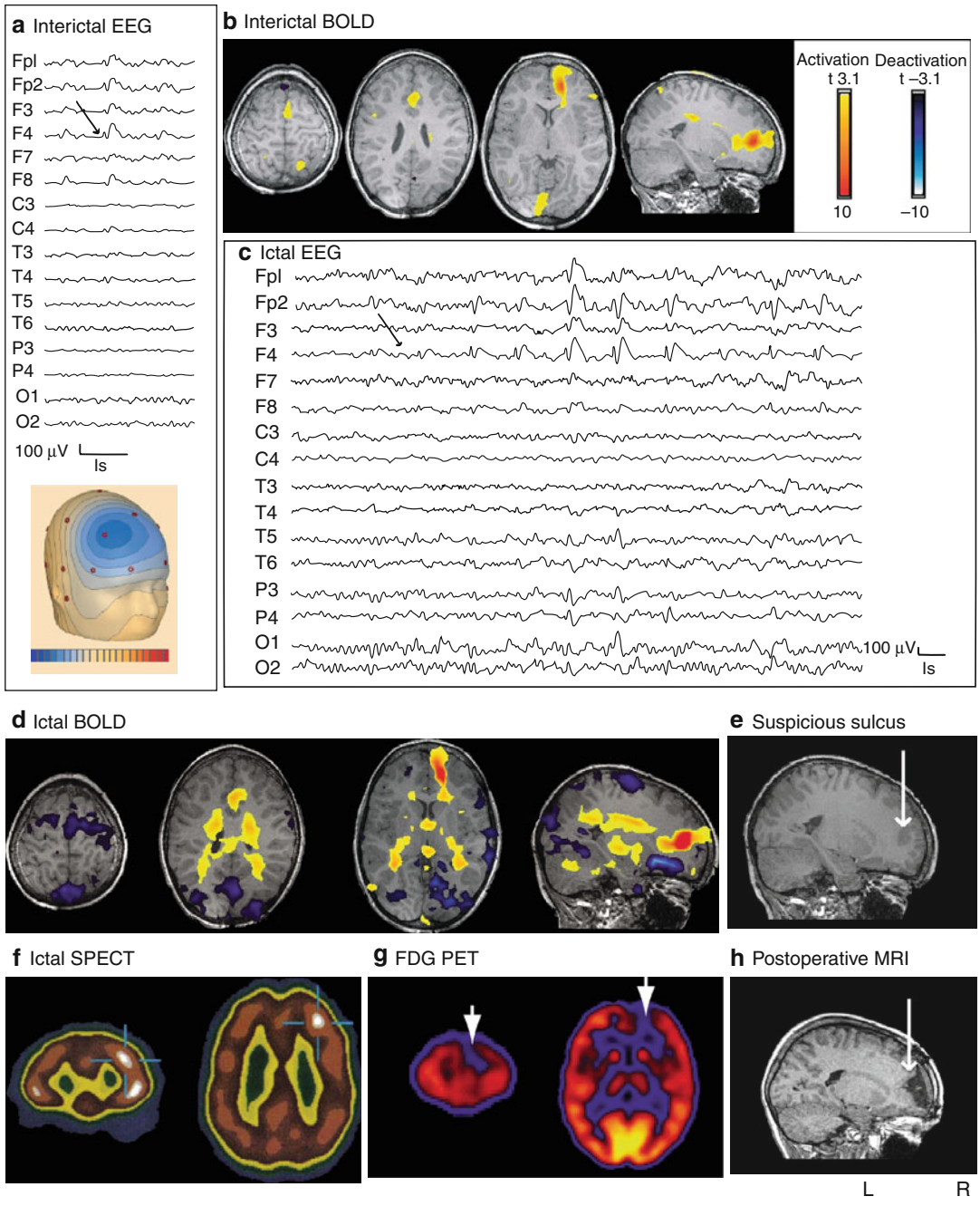

Fig. 20.3 Comparison between EEG-fMRI and methods of the presurgical evaluation in a patient with focal epilepsy. (**a**) Interictal EEG (average montage): focus F4 (*black arrow*). (**b**) Interictal fMRI: positive BOLD response frontopolar; no negative BOLD response. (**c**) Ictal EEG: rhythmic spike and wave F4 (*black arrow*). (**d**) Ictal fMRI: positive BOLD response frontopolar, negative BOLD response: frontal and posterior cingulate. (**e**) MRI: suspicious deep right middle frontal sulcus (*white arrow*). (**f**) Ictal SPECT: hyperperfusion frontal right. (**g**) FDG-PET: hypometabolism frontal right (*white arrows*). (**h**) postoperative MRI (*white arrow* indicates resected area) (Taken from Moeller et al. 2009a)

epilepsy and found BOLD signal changes in the pre-ictal state (Federico et al. 2005). However, over the years, several seizures without associated head movements were recorded. These studies were analysed in a block design and showed extensive seizure-associated BOLD signal changes which also included the presumed seizure onset zone (Salek-Haddadi et al. 2002; Kobayashi et al. 2006b). In a study on malformation of cortical development, interictal and ictal BOLD signal changes differed in some patients (Tyvaert et al. 2008a). By new techniques, the dynamics of seizure-associated BOLD signal changes can also be analysed. In studies where a sequential analysis of the BOLD signal or an independent component analysis was applied, the regions of seizure onset and propagation could be mapped (Tyvaert et al. 2009; Donaire et al. 2009; LeVan et al. 2010).

20.4 EEG-fMRI in Idiopathic Generalised Epilepsy (IGE)

While in focal epilepsy the main aim is to identify the brain area of spike generation, in patients with IGE the aim is to identify networks to better understand the pathophysiological background of these epilepsies. IGE is characterised by EEG with generalised spike-wave discharges (GSW) typically arising from normal background activity. Animal models of IGE show that thalamocortical loops play an important role in the generation of GSW (Gloor 1968; Meeren et al. 2002; Slaght et al. 2004; Timofeev and Steriade 2004; Paz et al. 2005). Early EEG-fMRI studies investigated adult patients with idiopathic generalised epilepsy who showed short GSW paroxysms in the EEG (Aghakhani et al. 2004; Gotman et al. 2005; Hamandi et al. 2006). These studies confirmed that the thalamus is activated during GSW, but also showed a deactivation in default mode areas (Raichle and Mintun 2006). The GSW-associated decrease in BOLD signal in default mode areas may indicate a disturbance of this physiological resting activity (Gotman et al. 2005). While these studies were performed on adult patients with long-standing medically treated epilepsy, Moeller and colleagues investigated absences in drug-naïve children with newly diagnosed epilepsy and confirmed a thalamic activation along with deactivation in default mode areas and the caudate nucleus (Moeller et al. 2008a). But how are absences initiated? Animal studies in genetic models of absence epilepsy strongly suggest that GSW are triggered in a restricted region of the somatosensory cortex (Meeren et al. 2002; Klein et al. 2004; Manning et al. 2004; Polack et al. 2007). A sliding window analysis of human absences showed that default mode areas and the caudate nucleus were involved significantly earlier than the thalamus. Early patient-specific BOLD signal changes could mirror a cortical focus (Moeller et al. 2010a). An example of a sliding window analysis of absences can be found in Fig. 20.4.

There are inconsistent results regarding the question whether BOLD signal changes might occur prior to GSW: while preceding BOLD signal changes are reported in some adult patients with GSW, children with polyspike-wave paroxysms and a group analysis of absences (Hawco et al. 2007; Moeller et al. 2008b; Bai et al. 2010), no preceding BOLD signal changes are detected in other studies (Moeller et al. 2008a, 2011a). Early parietal BOLD signal changes prior to absences (Carney et al. 2010) support the hypothesis that changes in activity within the default mode areas could facilitate the occurrence of GSW (Vaudano et al. 2009). One might assume that conflicting results may be explained by different analyses techniques and different groups of patients.

20.4.1 Absences and Cognitive Impairment

EEG-fMRI studies with simultaneous testing during absences suggest that absences that are associated with a stronger cognitive impairment are associated with more widespread BOLD signal changes than absences with no or mild cognitive impairment (Berman et al. 2010). However, in a case report in a girl with long-lasting GSW paroxysms without concomitant cognitive impairment, the same networks were activated as in absences with clinical manifestation (Moeller et al. 2010b).

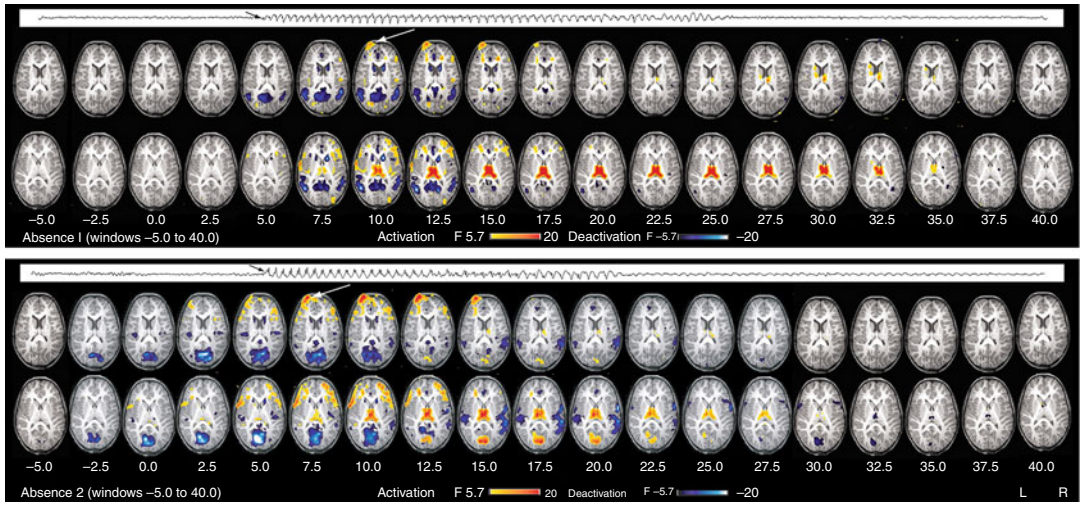

Fig. 20.4 Sliding window analysis for two absences of the same patient (windows −5 to 40 s). The duration of the absence is indicated by one EEG channel (Fp2 with average reference); the onset is indicated by a *black arrow*. Please note that the EEG onset of the absence is shifted 5 s to account for the hemodynamic delay of the BOLD response and allow a direct comparison of absence duration and associated BOLD signal changes. First activation consistent for both absences was found in the left frontopolar cortex (*white arrows*). In the first absence, this activation started 10 s after the onset; for the second, it started 5 s after onset. The thalamic activation started 7.5 s after onset in both, deactivation in the caudate nucleus 5 s after onset and deactivation in default mode areas 5 s after onset in the first and 2.5 s before onset in the second. BOLD signal changes in the thalamus and default mode areas exceeded the duration of the absence by several windows. In the second absence, thalamic activation was followed by thalamic deactivation (Taken from Moeller et al. 2010a)

20.4.2 Absences and Functional Connectivity

As mentioned before, GSW are characterised by a thalamocortical interaction. But are there also pathological thalamocortical interactions in periods free from GSW discharges? A functional connectivity study did not show pathological connectivity in areas that are known to interact during GSW. This confirms the paroxysmal character of GSW discharges (Moeller et al. 2011b). However, networks that are not directly involved in the generation of GSW seem to be altered: children with absence epilepsy showed decreased connectivity in areas of the attention network. This finding might explain impaired interictal attention in these children (Killory et al. 2011).

20.4.3 EEG-fMRI Studies in Generalised Photoparoxysmal Responses

Photoparoxysmal response (PPR) is an electroencephalographic trait characterised by the occurrence of epileptiform discharges in response to visual stimulation. Studying this trait helps to learn about mechanisms of epileptogenicity. An EEG-fMRI study showed an involvement of the parietal and frontal cortex but not the thalamus in most of the subjects during generalised PPR (Moeller et al. 2009b). In contrast to spontaneous GSW in which a thalamic involvement is commonly found, PPR seems to be mainly a cortical phenomenon. However, in a patient in whom photic stimulation evoked a generalised seizure, an excessive increase in BOLD signal in the visual cortex together with thalamic increase in BOLD signal was detected (Moeller et al. 2009c).

20.5 Paediatric EEG-fMRI Studies

Childhood epilepsies differ from adult epilepsies regarding aetiology, pathogenesis, seizure semiology and EEG patterns and prognosis (Roger et al. 2005). The immature brain is more prone to develop seizures, and epileptic discharges are

more frequent and less localised in children than in adults (Holmes 1997). The clinical manifestations are also age-correlated and can vary within patients throughout their maturation process (Ben-Ari 2006). The following section will give an overview about differences in HRFs observed in children and EEG-fMRI studies in different paediatric epilepsy syndromes. Paediatric EEG-fMRI studies in IGE are discussed in the Sect. 20.4.

20.5.1 Modelling Spike-Related BOLD Changes in Children

Jacobs and colleagues underlined the impact of age on the spike-related BOLD changes and demonstrated that children with focal lesional epilepsy show deactivations more frequently than activations in the epileptogenic zone compared to adults; the shape of the HRF especially differed in young children (Jacobs et al. 2007, 2008). Modelling spike-related BOLD signal changes in children might be even more complex since BOLD signal changes which precede the spike can be found in paediatric patients (Jacobs et al. 2009). These preceding BOLD signal changes were more localised than later BOLD signal changes (Jacobs et al. 2009). The question of why BOLD signal changes might precede the spike detected on the scalp EEG is still unanswered. Preceding BOLD signal changes might be explained by synchronised discharges detectable with depth electrodes but not visible on the scalp EEG (Pittau et al. 2011) in some patients only.

20.5.2 Benign Epilepsy with Centrotemporal Spikes (BECTS)

Early applications of EEG-fMRI in children were carried out in cases with benign focal epilepsies. Benign focal epilepsies represent a group of epileptic disorders that are related to well-localised focal EEG patterns of centrotemporal spikes (Dalla Bernardina et al. 2005). Seizures in BECTS typically begin with paraesthesia or jerking in the mouth, face and hand, usually with a preserved level of consciousness, supporting their origin in the sensorimotor cortex. EEG-fMRI studies in patients with BECTS showed spike-related BOLD signal changes in the sensorimotor cortex (Archer et al. 2003; Boor et al. 2003, 2007; Lengler et al. 2007; Siniatchkin et al. 2007a) whereas distant BOLD signal changes were interpreted as propagated activity as shown by source analysis (Boor et al. 2007). In other benign epilepsies (benign occipital lobe epilepsies), Leal and colleagues (Leal et al. 2006, 2007) found an activation pattern in different cortical occipital and parietal areas corresponding well to the localisation of interictal epileptiform discharges.

20.5.3 Epileptic Encephalopathies

West syndrome is a prototype of severe epileptic encephalopathies of infancy, consisting of tonic spasms, psychomotor developmental delay and the characteristic electroencephalographic pattern of hypsarrhythmia. The EEG features are characterised by a multifocal spike and sharp wave activity and high-voltage slow wave activity (Dulac 2001; Hrachovy and Frost 2003). In an EEG-fMRI study, Siniatchkin and colleagues showed that interictal spikes were associated with positive BOLD changes in the cerebral cortex (especially in occipital areas) whereas high-amplitude slow wave activity in hypsarrhythmia was commonly associated with BOLD signal changes in brainstem, putamen, thalamus and different cortical areas (Siniatchkin et al. 2007b). Thereby, the study confirmed PET studies which had shown metabolic changes in cortex, putamen and brainstem in West syndrome patients (Chugani et al. 1992; Chiron et al. 1993; Metsähonkala et al. 2002).

West syndrome often evolves into *Lennox-Gastaut syndrome*, an epileptic encephalopathy characterised by different types of seizures (tonic, tonic-clonic and atonic seizures as well as atypical absences), typical EEG changes (slow spike-wave complexes ranging from 1 to 2.5/s, runs of rapid spikes and polyspikes) and accompanying mental retardation (Arzimanoglou et al. 2009). An EEG-fMRI study in children with Lennox-Gastaut syndrome showed activation of brainstem and thalamus associated with epileptiform

discharges pointing to common pathogenetic pathways of West syndrome and Lennox-Gastaut syndrome (Siniatchkin et al. 2007b, 2011).

Epileptic encephalopathy with *continuous spike and waves during slow sleep* is an age-related disorder characterised by the presence of interictal epileptiform discharges during at least >85 % of sleep and cognitive deficits associated with this EEG pattern. An EEG-fMRI study showed that despite aetiological heterogeneity, patients with continuous spike and waves during slow sleep were characterised by activation of a similar neuronal network: perisylvian region, insula and cingulate gyrus. A comparison with the electrical source analysis results suggested that the activations corresponded to both initiation and propagation pathways. Deactivations in structures of the default mode network are consistent with the concept of epileptiform activity impacting on normal brain function by inducing repetitive interruptions of neurophysiological function (Siniatchkin et al. 2010).

20.6 Physiological Brain Activity

The technique of EEG-fMRI was developed by epileptologists as a new tool to detect spike-associated networks noninvasively. Later, EEG-fMRI was also applied to study physiological rhythms in healthy subjects and provided new insights into neuronal networks underlying physiological brain activity. Neuronal oscillations at different frequencies (such as alpha, gamma, theta and delta frequencies) have been analysed in EEG-fMRI studies (for review, see Laufs 2008). Alpha rhythms were positively correlated with thalamic BOLD signal but negatively correlated with parieto-occipital BOLD signal (Moosmann et al. 2003). Associated with the desynchronisation of alpha activity, a fronto-parietal network was detected when the person is vigilant (Laufs et al. 2003; Laufs et al. 2006b; Mantini et al. 2007). If the alpha desynchronisation was associated with an increase in theta activity, a correlate for drowsiness, occipital BOLD signal changes were detected (Laufs et al. 2006b). Beta power was positively correlated with areas of the default mode network (Laufs et al. 2003). Sleep spindles were shown to be associated with an activation in the thalamus and in some patients in the putamen (Schabus et al. 2007; Tyvaert et al. 2008b). Slow wave sleep is associated with BOLD signal changes in brainstem, cerebellum and cortical areas (Dang-Vu et al. 2010).

20.7 Conclusion

Combining EEG and fMRI has opened a new window into the exploration of epileptic discharges, allowing the investigation of the whole brain noninvasively. It has become a clinical tool in the localisation of the epileptic focus and has uncovered unexpected mechanisms in generalised epileptic discharges. A recent study showed that it might be possible to detect epileptic activity in the fMRI data without the help of an EEG: based on a wavelet model of the fMRI data, Lopes and colleagues could detect similar results compared to an EEG-based fMRI analysis (Lopes et al. 2012). Another recent approach uses altered functional connectivity as a predictor for the surgical outcome of epilepsy (Negishi et al. 2011). Further studies based on altered networks in epilepsy are under way.

References

Aghakhani Y, Bagshaw AP et al (2004) fMRI activation during spike and wave discharges in idiopathic generalized epilepsy. Brain 127:1127–1144

Al-Asmi A, Benar CG et al (2003) fMRI activation in continuous and spike-triggered EEG-fMRI studies of epileptic spikes. Epilepsia 44:1328–1339

Allen PJ, Polizzi G et al (1998) Identification of EEG events in the MR scanner: the problem of pulse artifact and a method for its subtraction. Neuroimage 8: 229–239

Allen PJ, Josephs O et al (2000) A method for removing imaging artifact from continuous EEG recorded during functional MRI. Neuroimage 12:230–239

Archer JS, Briellman RS et al (2003) Benign epilepsy with Centro-temporal spikes: spike triggered fMRI shows somato-sensory cortex activity. Epilepsia 44: 200–204

Arzimanoglou A, French J et al (2009) Lennox-Gastaut syndrome: a consensus approach on diagnosis, assessment, management, and trial methodology. Lancet Neurol 8:82–93

Bagshaw AP, Aghakhani Y et al (2004) EEG-fMRI of focal epileptic spikes: analysis with multiple haemodynamic functions and comparison with gadolinium-enhanced MR angiograms. Hum Brain Mapp 22: 179–192

Bai X, Vestal M, Berman R et al (2010) Dynamic time course of typical childhood absence seizures: EEG, behavior, and functional magnetic resonance imaging. J Neurosci 30:5884–5893

Bénar C, Aghakhani Y et al (2003) Quality of EEG in simultaneous EEG-fMRI for epilepsy. Clin Neurophysiol 114:569–580

Bénar CG, Grova C et al (2006) EEG-fMRI of epileptic spikes: concordance with EEG source localization and intracranial EEG. Neuroimage 30:1161–1170

Ben-Ari Y (2006) Basic developmental rules and their implication for epilepsy in the immature brain. Epileptic Disord 8:91–102

Berman R, Negishi M et al (2010) Simultaneous EEG, fMRI, and behavior in typical childhood absence seizures. Epilepsia 51:2011–2022

Bettus G, Guedj E et al (2009) Decreased basal fMRI functional connectivity in epileptogenic networks and contralateral compensatory mechanisms. Hum Brain Mapp 30:1580–1591

Boor S, Vucurevic G et al (2003) EEG-related functional MRI in benign childhood epilepsy with centrotemporal spikes. Epilepsia 44:688–692

Boor R, Jacobs J et al (2007) Combined spike-related functional MRI and multiple source analysis in the non-invasive spike localization of benign rolandic epilepsy. Clin Neurophysiol 118(4):901–909

Carney PW, Masterton RA et al (2010) The core network in absence epilepsy. Differences in cortical and thalamic BOLD response. Neurology 75:904–911

Chiron C, Dulac O et al (1993) Study of regional cerebral blood flow in West syndrome. Epilepsia 34:707–715

Chugani HT, Shewmon DA et al (1992) Infantile spasms: II. Lenticular nuclei and brain stem activation on positron emission tomography. Ann Neurol 31:212–219

Dalla Bernardina B, Sgro V et al (2005) Epilepsy with centro-temporal spikes and related syndromes. In: Roger J, Bureau M, Dravet C, Genton P, Tassinari CA, Wolf P (eds) Epileptic syndromes in infancy, childhood and adolescence. John Libbey Eurotext Ltd, Montrouge, pp 203–226

Dang-Vu TT, Schabus M et al (2010) Functional neuroimaging insights into the physiology of human sleep. Sleep 33:1589–1603, Review

Devor A, Tian P et al (2007) Suppressed neuronal activity and concurrent arteriolar vasoconstriction may explain negative blood oxygenation level-dependent signal. J Neurosci 27:4452–4459

Donaire A, Bargallo N et al (2009) Identifying the structures involved in seizure generation using sequential analysis of ictal-fMRI data. Neuroimage 47:173–183

Dulac O (2001) What is West syndrome? Brain Dev 23:447–452

Federico P, Abbott DF et al (2005) Functional MRI of the pre-ictal state. Brain 128:1811–1817

Friston KJ, Williams S et al (1996) Movement-related effects in fMRI time-series. Magn Reson Med 35:346–355

Gholipour T, Moeller F et al (2011) Reproducibility of interictal EEG-fMRI results in epilepsy patients. Epilepsia 52:433–434

Gloor P (1968) Generalized cortico-reticular epilepsies, some considerations on the pathophysiology of generalized bilaterally synchronous spike and wave discharge. Epilepsia 9:249–263

Glover GH (1999) Deconvolution of impulse response in event-related BOLD fMRI. Neuroimage 9:416–419

Gotman J, Grova C et al (2005) Generalized epileptic discharges show thalamocortical activation and suspension of the default state of the brain. Proc Natl Acad Sci USA 102:15236–15240

Groening K, Brodbeck V et al (2009) Combination of EEG-fMRI and EEG source analysis improves interpretation of spike-associated activation networks in paediatric pharmacoresistant focal epilepsies. Neuroimage 46:827–833

Grouiller F, Thornton RC et al (2011) With or without spikes: localization of focal epileptic activity by simultaneous electroencephalography and functional magnetic resonance imaging. Brain 134:2867–2886

Grova C, Daunizeau J et al (2008) Concordance between distributed EEG source localization and simultaneous EEG-fMRI studies of epileptic spikes. Neuroimage 39:755–774

Hamandi K, Salek-Haddadi A et al (2006) EEG-fMRI of idiopathic and secondary generalized epilepsies. Neuroimage 31:1700–1710

Hawco CS, Bagshaw AP et al (2007) BOLD changes occur prior to epileptic spikes seen on scalp EEG. Neuroimage 35:1450–1458

Hoffmann A, Jäger L et al (2000) Electroencephalography during functional echo-planar imaging: detection of epileptic spikes using post-processing methods. Magn Reson Med 44:791–798

Holmes GL (1997) Epilepsy in the developing brain: lessons from the laboratory and clinic. Epilepsia 38:12–30

Hrachovy RA, Frost JD (2003) Infantile epileptic encephalopathy with hypsarrhythmia. J Clin Neurophysiol 20:408–425

Ives JR, Warach S et al (1993) Monitoring the patient's EEG during echo planar MRI. Electroencephalogr Clin Neurophysiol 87:417–420

Jacobs J, Kobayashi E et al (2007) Hemodynamic responses to interictal epileptiform discharges in children with symptomatic epilepsy. Epilepsia 48: 2068–2078

Jacobs J, Hawco C et al (2008) Variability of the hemodynamic response function with age in children with epilepsy. Neuroimage 40:601–614

Jacobs J, Levan P et al (2009) Hemodynamic changes preceding the interictal EEG spike in patients with focal epilepsy investigated using simultaneous EEG-fMRI. Neuroimage 45:1220–1231

Killory BD, Bai X et al (2011) Impaired attention and network connectivity in childhood absence epilepsy. Neuroimage 56:2209–2217

Klein JP, Khera DS et al (2004) Dysregulation of sodium channel expression in cortical neurons in a rodent model of absence epilepsy. Brain Res 1000:102–109

Kobayashi E, Bagshaw AP et al (2006a) Temporal and extratemporal BOLD responses to temporal lobe interictal spikes. Epilepsia 47:343–354

Kobayashi E, Hawco CS et al (2006b) Widespread and intense BOLD changes during brief focal electrographic seizures. Neurology 66:1049–1055

Kobayashi E, Grova C et al (2009) Structures involved at the time of temporal lobe spikes revealed by interindividual group analysis ofEEG/fMRI data. Epilepsia 50:2549–2556

Krakow K, Woermann FG et al (1999) EEG-triggered functional MRI of interictal epileptiform activity in patients with partial seizures. Brain 122:1679–1688

Laufs H (2008) Endogenous brain oscillations and related networks detected by surface EEG-combined fMRI. Hum Brain Mapp 29:762–769, Review

Laufs H, Krakow K et al (2003) Electroencephalographic signatures of attentional and cognitive default modes in spontaneous brain activity fluctuations at rest. Proc Natl Acad Sci USA 100:11053–11058

Laufs H, Hamandi K et al (2006a) EEG-fMRI mapping of asymmetrical delta activity in a patient with refractory epilepsy is concordant with the epileptogenic region determined by intracranial EEG. Magn Reson Imaging 24:367–371

Laufs H, Holt JL et al (2006b) Where the BOLD signal goes when alpha EEG leaves. Neuroimage 314: 1408–1418

Laufs H, Hamandi K et al (2007) Temporal lobe interictal epileptic discharges affect cerebral activity in "default mode" brain regions. Hum Brain Mapp 28: 1023–1032

Leal A, Dias A et al (2006) The BOLD effect of interictal spike activity in childhood occipital lobe epilepsy. Epilepsia 47:1536–1542

Leal A, Nunes S et al (2007) Brain mapping of epileptic activity in a case of idiopathic occipital lobe epilepsy (Panayiotopoulos Syndrome). Epilepsia 48:1179–1183

Lemieux L, Salek-Haddadi A et al (2001) Event-related fMRIwithsimultaneousandcontinuousEEG:description of the method and initial case report. Neuroimage 14:780–787

Lemieux L, Salek-Haddadi A et al (2007) Modelling large motion events in fMRI studies of patients with epilepsy. Magn Reson Imaging 25:894–901

Lengler U, Kafadar I et al (2007) fMRI correlates of interictal epileptic activity in patients with idiopathic benign focal epilepsy of childhood. A simultaneous EEG-functional MRI study. Epilepsy Res 75:29–38

LeVan P, Tyvaert L et al (2010) Independent component analysis reveals dynamic ictal BOLD responses in EEG-fMRI data from focal epilepsy patients. Neuroimage 149:366–378

Liao W, Zhang Z et al (2011) Default mode network abnormalities in mesial temporal lobe epilepsy: a study combining fMRI and DTI. Hum Brain Mapp 32:883–895

Logothetis NK, Pauls J et al (2001) Neurophysiological investigation of the basis of the fMRI signal. Nature 412:150–157

Lopes R, Lina JM et al (2012) Detection of epileptic activity in fMRI without recording the EEG. Neuroimage 60(3):1867–1879

Lu Y, Grova C et al (2007) Using voxel-specific hemodynamic response function in EEG-fMRI data analysis: an estimation and detection model. Neuroimage 34:195–203

Manning JP, Richards DA et al (2004) Cortical-area specific block of genetically determined absence seizures by ethosuximide. Neuroscience 123:5–9

Mantini D, Perrucci MG et al (2007) Electrophysiological signatures of resting state networks in the human brain. Proc Natl Acad Sci USA 104:13170–13175

Meeren HK, Pijn JP et al (2002) Cortical focus drives widespread corticothalamic networks during spontaneous absence seizures in rats. J Neurosci 22: 1480–1495

Metsähonkala L, Gaily E et al (2002) Focal and global cortical hypometabolism in patients with newly diagnosed infantile spasms. Neurology 58:1646–1651

Moehring J, Coropceanu D et al (2011) Improving sensitivity of EEG-fMRI studies in epilepsy:the role of sleep-specific activity. Neurosci Lett 505(2):211–215

Moeller F, Siebner H et al (2008a) EEG-fMRI in children with untreated childhood absence epilepsy. Epilepsia 49:1510–1519

Moeller F, Siebner H et al (2008b) Changes in activity of striato-thalamo-cortical network precede generalized spike wave discharges. Neuroimage 39:1839–1849

Moeller F, Tyvaert L et al (2009a) EEG-fMRI: adding to standard evaluations of patients with nonlesional frontal lobe epilepsy. Neurology 73:2023–2030

Moeller F, Siebner HR et al (2009b) FMRI activation during spike and wave discharges evoked by photic stimulation. Neuroimage 48:682–695

Moeller F, Siebner HR et al (2009c) Mapping brain activity on the verge of a photically induced generalized tonic-clonic seizure. Epilepsia 50:1632–1637

Moeller F, Levan P et al (2010a) Absence seizures: individual patterns revealed by EEG-fMRI. Epilepsia 51:2000–2010

Moeller F, Muhle H et al (2010b) EEG-fMRI study of generalized spike and wave discharges without transitory cognitive impairment. Epilepsy Behav 18:313–316

Moeller F, Levan P et al (2011a) Independent component analysis (ICA) of generalized spike wave discharges in fMRI: comparison with general linear model-based EEG-fMRI. Hum Brain Mapp 2:209–217

Moeller F, Maneshi M et al (2011b) Functional connectivity in patients with idiopathic generalized epilepsy. Epilepsia 52:515–522

Moosmann M, Ritter P et al (2003) Correlates of alpha rhythm in functional magnetic resonance imaging and near infrared spectroscopy. Neuroimage 20:145–158

Negishi M, Martuzzi R et al (2011) Functional MRI connectivity as a predictor of the surgical outcome of epilepsy. Epilepsia 52:1733–1740

Paz JT, Deniau JM et al (2005) Rhythmic bursting in the cortico-subthalamo-pallidal network during spontaneous genetically determined spike and wave discharges. J Neurosci 25:2092–2101

Pereira FR, Alessio A et al (2010) Asymmetrical hippocampal connectivity in mesial temporal lobe epilepsy: evidence from resting state fMRI. BMC Neurosci 11:66

Pittau F, Levan P et al (2011) Changes preceding interictal epileptic EEG abnormalities: comparison between EEG/fMRI and intracerebral EEG. Epilepsia 52: 1120–1129

Pittau F, Dubeau F et al (2012) Contribution of EEG/fMRI to the definition of the epileptic focus. Neurology 78(19):1479–1487

Polack PO, Guillemain I et al (2007) Deep layer somatosensory cortical neurons initiate spike-and-wave discharges in a genetic model of absence seizures. J Neurosci 27:6590–6599

Raichle ME, Mintun MA (2006) Brain work and brain imaging. Annu Rev Neurosci 29:449–476

Roger J, Bureau M et al (2005) Epileptic syndromes in infancy, childhood and adolescence. John Libbey Eurotext Ltd, Montrouge

Salek-Haddadi A, Merschhemke M et al (2002) SimultaneousEEG-correlated ictal fMRI. Neuroimage 16:32–40

Salek-Haddadi A, Diehl B et al (2006) Hemodynamic correlates of epileptiform discharges: an EEG-fMRI study of 63 patients with focal epilepsy. Brain Res 1088:148–166

Schabus M, Dang-Vu TT et al (2007) Hemodynamic cerebral correlates of sleep spindles during human non-rapid eye movement sleep. Proc Natl Acad Sci USA 104:13164–13169

Seeck M, Lazeyras F et al (1998) Non-invasive epileptic focus localization using EEG-triggered functional MRI and electromagnetic tomography. Electroencephalogr Clin Neurophysiol 106:508–512

Siniatchkin M, Moeller F et al (2007a) Spatial filters and automated spike detection based on brain topographies improve sensitivity of EEG-fMRI studies in focal epilepsy. Neuroimage 37:834–843

Siniatchkin M, van Baalen A et al (2007b) Different neuronal networks are associated with spikes and slow activity in hypsarrhythmia. Epilepsia 48:2312–2321

Siniatchkin M, Groening K et al (2010) Neuronal networks in children with continuous spikes and waves during slow sleep. Brain 133:2798–2813

Siniatchkin M, Coropceanu D et al (2011) EEG-fMRI reveals activation of brainstem and thalamus in patients with Lennox-Gastaut syndrome. Epilepsia 52(4): 766–774

Slaght SJ, Paz T et al (2004) On the activity of the corticostriatal networks during spike-and-wave discharges in a genetic model of absence epilepsy. J Neurosci 24: 6816–6825

Srivastava G, Grottaz-Herbette S et al (2005) ICA-based procedures for removing ballistocardiogram artifacts from EEG data acquired in the MRI scanner. Neuroimage 24:50–60

Thornton R, Laufs H et al (2010) EEG correlated functional MRI and postoperative outcome in focal epilepsy. J Neurol Neurosurg Psychiatry 81:922–927

Timofeev I, Steriade M (2004) Neocortical seizures: initiation, development and cessation. Neuroscience 123: 299–336

Tyvaert L, Hawco C et al (2008a) Different structures involved during ictal and interictal epileptic activity in malformations of cortical development: an EEG-fMRI study. Brain 131:2042–2060

Tyvaert L, Levan P et al (2008b) Effects of fluctuating physiological rhythms during prolonged EEG-fMRI studies. Clin Neurophysiol 12:2762–2774

Tyvaert L, Levan P et al (2009) Noninvasive dynamic imaging of seizures in epileptic patients. Hum Brain Mapp 30:3993–4011

van Houdt PJ, de Munck JC et al (2010) Comparison of analytical strategies for EEG-correlated fMRI data in patients with epilepsy. Magn Reson Imaging 28: 1078–1086

Vaudano AE, Laufs H et al (2009) Causal hierarchy within the thalamo-cortical network in spike and wave discharges. PLoS One 4:e6475

Vulliemoz S, Thornton R et al (2009) The spatio-temporal mapping of epileptic networks: combination of EEG-fMRI and EEG source imaging. Neuroimage 46: 834–843

Vulliemoz S, Carmichael DW et al (2011) Simultaneous intracranial EEG and fMRI of interictal epileptic discharges in humans. Neuroimage 54:182–190

Zhang Z, Lu G et al (2010) Altered spontaneous neuronal activity of the default-mode network in mesial temporal lobe epilepsy. Brain Res 1323:152–160

Zijlmans M, Huiskamp G et al (2007) EEG-fMRI in the preoperative work-up for epilepsy surgery. Brain 130:2343–2353

Combining Transcranial Magnetic Stimulation with (f)MRI

21

Gesa Hartwigsen, Tanja Kassuba,
and Hartwig R. Siebner

21.1 Introduction

Transcranial magnetic stimulation (TMS) is a non-invasive and painless tool for the electrical stimulation of the human cortex (Barker et al. 1985). TMS depolarizes cortical neurons and can evoke measurable electrophysiological and behavioral effects. TMS is usually applied to one cortical area but can also be given to two or more areas (i.e., multisite TMS). Single or paired stimuli and short stimulus trains (i.e., high-frequency bursts) provide a means of transiently disrupting ongoing neuronal processing in the stimulated cortex. Repetitive TMS (rTMS) refers to the application of prolonged trains of stimuli, which are either given continuously as long trains at a constant rate (continuous rTMS) or intermittently as repetitive bursts (i.e., intermittent or burst-like rTMS). rTMS can modify the excitability of the cerebral cortex at the stimulated site and also at remote interconnected brain regions, beyond the time of stimulation. Its neuromodulatory effects make rTMS a valuable tool to study the functional plasticity of neuronal networks and may be used therapeutically in patients with neurological and psychiatric disorders.

G. Hartwigsen (✉)
Biological Psychology, Institute of Psychology,
Christian-Albrechts-University,
Olshausenstrasse 62, Kiel 24098, Germany
e-mail: hartwigsen@psychologie.uni-kiel.de

T. Kassuba
Department of Psychology,
Center for the Study of Brain,
Mind & Behavior, Princeton University,
Green Hall, 08544 Princeton, NJ, USA

H.R. Siebner
Danish Research Center for Magnetic Resonance,
Center for Functional and Diagnostic Imaging,
Copenhagen University Hospital Hvidovre,
Kettegaard Allé 30 DK-2650 Hvidovre, Denmark

21.1.1 How Does TMS Excite Cortical Neurons?

TMS causes inductive (electro-magneto-electric) stimulation of neuronal axons. A brief, high-current pulse is produced in a stimulating coil. The time-varying electrical field produces a time-varying magnetic field with lines of flux oriented perpendicularly to the plane of the coil. The pulsed magnetic field is not attenuated by the skull and induces an electric field in the superficial brain tissue (i.e., cortex), which runs parallel to the plane of the coil but has a direction that is opposite to the electric field in the coil. Hence, the pulsed magnetic field is only used as a means to generate an electric field in the brain that is suprathreshold for exciting cortical axons.

How does the time-varying electrical field induced in the cortex excite neurons? The electrical field induced in the neuronal tissue drives transmembraneous ionic currents. The most relevant parameter is the rate of change of the electric field along the nerve. Depending on the gradient and the orientation of the electric field gradient relative to the course of the axon, the pulsed electrical field may generate an outward current and

S. Ulmer, O. Jansen (eds.), *fMRI – Basics and Clinical Applications*,
DOI 10.1007/978-3-642-34342-1_21, © Springer-Verlag Berlin Heidelberg 2013

local depolarization at distinct sites of neuronal axons. If the outward current causes sufficient membrane depolarization, this will trigger an action potential. This action potential propagates along the axon and may cause a transsynaptic excitation of postsynaptic neurons. Crucial for an efficient depolarization of an axon is the spatial gradient of the induced electric field in relation to the orientation of the axon. At the cellular level, the events that lead to neuronal excitation are still poorly understood. For instance, the relevance of cellular and gyral shapes, the gray matter boundaries, the local variations in tissue conductivity, and the role of background neuronal activity for neuronal stimulation are largely unknown (for recent reviews, see Miniussi et al. 2010; Sandrini et al. 2011; Siebner et al. 2009b).

The majority of studies have investigated the physiological mechanisms of TMS in the human primary motor cortex (M1) because its effects can be quantified by recording the TMS-evoked motor potential (MEP). For other brain regions, such direct quantification is difficult to obtain. Therefore, researchers have used neuroimaging techniques such as positron emission tomography (PET), electroencephalography (EEG), or functional magnetic resonance imaging (fMRI) to map TMS-evoked changes in regional neuronal activity throughout the brain (Bestmann et al. 2003b; Ilmoniemi et al. 1997; Lee et al. 2003; Massimini et al. 2005; Siebner et al. 2003). These studies have revealed that the TMS-induced changes in regional neuronal activity are not restricted to the stimulated cortex but give rise to functional changes in connected cortical areas, including subcortical brain regions (Bestmann et al. 2003b; Lee et al. 2003; Siebner et al. 2003).

Regarding fMRI, a critical question is whether the blood-oxygen-level-dependent (BOLD) signal really captures the TMS-induced changes in regional neuronal activity. Allen et al. (2007) combined optical imaging with electrophysiological recordings of neuronal activity in cat visual cortex to show that TMS-induced changes in neural activity are readily reflected by cerebral hemodynamics. Further, the quantitative coupling between TMS-evoked neural activity and cerebral hemodynamics was present over a range of stimulation parameters. These results demonstrate the usefulness of combined TMS-fMRI studies in humans showing that TMS-induced neural changes are "faithfully reflected in hemodynamic signals" (Allen et al. 2007).

21.1.2 Some Physical Aspects of Transcranial Magnetic Stimulation

The induced magnetic and electric field decreases rapidly with increasing distance from the coil. The maximal depth of penetration depends on the shape and size of the coil, the employed stimulation intensity, and the responsiveness of the targeted tissue. The decrease with distance is more rapid for small coils than for large ones. The coil should be placed tangentially on the skin to minimize the coil-cortex distance. Commercially used coils reach a penetration depth of approximately 2–6 cm. This implies that only cortical neuronal tissue is within the range of TMS while deep cerebral gray matter nuclei cannot be stimulated directly with TMS.

In general, TMS does not produce a focal stimulation of neuronal tissue at a small predictable site. The geometry of the coil is an important factor in determining the magnitude and spatial extent of cortical stimulation. The two most commonly used coil shapes are circular (i.e., referred to as round coil) and figure-of-eight (referred to as figure-of-eight-shaped coil or butterfly coil). The circular coil induces a concentric circular electric field. If the coil is placed with its entire surface tangentially to the skin, neuronal structures in the tissue underlying the circular coil will be activated. It should be noted that neuronal stimulation is minimal in the brain tissue underlying the center of the coil when the flat surface of the circular coil is placed on the scalp tangentially to the skin (Weyh and Siebner 2007). The other coil design has a figure-of-eight configuration. Figure-of-eight coils consist of two circular coils placed side by side and are wired such that the current from the stimulator passes in opposite directions in each. This produces a relatively clear defined maximum of the induced current where the two coils approach each other (i.e., in the geometrical center of the

coil). With a spatial resolution of approximately 1–1.5 cm, the figure-of-eight coil is substantially more focal than the circular coil. This explains why the figure-of-eight coil is preferred to the round coil when TMS is used to map cortical functions (Walsh and Rushworth 1999). It needs to be borne in mind that commercially available stimulation devices may differ in terms of coil design. This may alter the characteristics of neuronal stimulation, including the heating properties during rTMS and the hardware design (Lang et al. 2006; Weyh et al. 2005).

21.1.3 Clinical and Neuroscientific Applications of TMS

TMS can be used in several ways to study human brain function. Single-pulse or paired-pulse TMS can be applied to probe the excitability of intracortical inhibitory and facilitatory circuits in the motor and visual cortex. Since the action potentials induced by TMS spread along preexisting axonal connections, TMS-induced neuronal excitation is not limited to the stimulated cortex but leads to a transsynaptic spread of excitation to interconnected cortical areas. This renders TMS a very powerful means of studying functional and effective connectivity in the intact human brain (Kobayashi and Pascual-Leone 2003). For instance, TMS has been extensively used to probe corticocortical and corticospinal connectivity in the motor system. In clinical neurology, TMS is commonly used as a routine evaluation of the excitability and conductivity of corticospinal pathways.

TMS can induce a transient dysfunction in the stimulated cortex (i.e., a "virtual lesion"). When being applied in its "virtual lesion" mode during an experimental task, TMS may produce measurable changes in task performance. These changes in behavior can be used to make inferences about the importance of the stimulated brain area for a specific cognitive, sensory or motor function (Walsh and Cowey 2000; Walsh and Rushworth 1999; see Siebner et al. 2009b for a review). Various rTMS protocols are being increasingly used by clinicians and neuroscientists to induce lasting changes in the status of the human brain (Siebner and Rothwell 2003). Conventional rTMS protocols consist of a continuous series of pulses with constant repetition rates. In the "continuous mode" of rTMS, stimulation rates of around 1 Hz are referred to as *low-frequency rTMS* and stimulation rates between 5 and 50 Hz as *high-frequency rTMS*. Most studies regarding the motor cortex suggest inhibitory effects of low-frequency rTMS and facilitatory effects of high-frequency rTMS (Berardelli et al. 1998; Chen et al. 1997a; Pascual-Leone et al. 1998). Recent protocols use more complex temporal stimulation patterns such as double-pulse rTMS (Thickbroom et al. 2006), quadro-pulse rTMS (Hamada et al. 2007), or theta burst stimulation (TBS) which gives short, high-frequent *bursts* of pulses every 0.2 s (Huang et al. 2005). Ongoing research addresses the question whether the neuromodulatory effects of these rTMS protocols may have a therapeutic application in neurological and psychiatric disorders (Wassermann and Lisanby 2001).

TMS can be applied while subjects perform an experimental task (*online TMS*) or shortly before they perform the task (*offline TMS*). Offline TMS usually involves an rTMS protocol that induces a lasting alteration of cortical excitability, while online TMS may consist of single pulses or short high-frequency trains that are given at distinct points in time during task performance. Both approaches allow the testing of the functional relevance of the targeted brain area by measuring the acute (*online TMS*) or conditioning (*offline TMS*) effects of TMS on electrophysiological measures (e.g., the MEP amplitude), behavioral measures (e.g., response latencies or error rate), or more directly on regional brain activity using brain mapping techniques such as EEG, PET, or fMRI (Siebner et al. 2009a). While conventional paradigms apply uni-site TMS over a single cortical area, more recent studies have also started to include multisite TMS over two or more areas simultaneously (Hartwigsen et al. 2010a, b).

21.1.4 Adverse Effects and Safety Precautions

TMS has the capability of producing adverse effects, especially if rTMS is used. These side effects are extensively discussed in a recent review

(Wassermann 2008). The most relevant adverse effect is the induction of epileptic seizures. Since rTMS induces stronger and more persistent effects on cortical excitability and function than single-pulse TMS, it bears a higher risk of provoking epileptic seizures even in healthy individuals. Therefore, safety guidelines were established which specify the maximal number of pulses per session, stimulus intensity and frequency that are considered to be safe in terms of seizure induction (Chen et al. 1997b; Rossi et al. 2009; Wassermann 1998). Since the introduction of the safety guidelines, only a few cases of accidental seizures with TMS have been reported worldwide, and none of the individuals who had experienced rTMS-induced seizures has suffered lasting physical sequelae.

The rapid discharge through the coil produces a characteristic clicking sound in the frequency range of 2–7 kHz. The click is caused by mechanical deformation of the coil during the strong magnetic pulses. Peak sound pressure has been reported to be 120–130 dB at a distance of 10 cm from the coil (Starck et al. 1996). Sound levels will be higher when TMS is given inside the MRI bore because of the additional magnetic field generated by the MR scanner. Therefore, individuals who receive rTMS or are examined in the MR scanner should always wear ear plugs (cf. Sect. 21.3.2.1).

21.2 Placement of the Coil Over the Cortical Target Area

Accurate placement of the TMS coil over the cortex area that is to be stimulated with TMS is crucial. The motor response that is evoked by TMS can be used to localize the primary motor cortex. A similar approach can be chosen for TMS of the visual cortex by positioning the coil at the site where TMS most reliably elicits a phosphene. In both instances, TMS produces an overt response which can be used to functionally determine the appropriate site of stimulation. For most remaining cortical areas, no such responses can be elicited and other strategies have to be used to accurately place the coil over the cortical target.

Some researchers use the optimal site to stimulate the primary motor cortex as "anchor point" for the stimulation of pericentral cortical areas such as premotor or somatosensory areas (Gerschlager et al. 2001; Koch et al. 2006; Lee and van Donkelaar 2006). However, this method is not sufficiently accurate for targeting more distant areas such as the dorsolateral prefrontal cortex (Bohning et al. 2003b).

The international 10–20 system for the placement of EEG electrodes (Jasper 1958) is often used for positioning of the TMS coil. The 10–20 system offers a grid of electrode sites located on the scalp that is derived from standard cranial landmarks, i.e., the inion, nasion, or preauricular points. This method assumes a consistent correlation between scalp locations and underlying brain structures across subjects. Greater accuracy can be obtained by acquiring structural MR images of the brain together with capsules containing a high-contrast marker attached to the head (Terao et al. 1998). The placement of the coil can then be referenced to the position of the marker.

Neuronavigated TMS guided by frameless stereotaxy represents the method of choice as it allows both, exact placement and monitoring of the coil throughout the TMS experiment (Denslow et al. 2005a; Herwig et al. 2003a; Neggers et al. 2004; Sack et al. 2006; Schonfeldt-Lecuona et al. 2005). Optical (infrared-based) and acoustic (ultrasound-based) devices are available for neuronavigation. These systems use passive (reflecting) or active (emitting) markers which are attached to the subject's head and to the TMS coil (Ettinger et al. 1998). Sparing et al. (2008) compared different methods for the placement of the TMS coil over the primary motor cortex in terms of accuracy. The least accurate results were obtained when the 10–20 EEG system or function-guided procedures were used, although there was a great variation among different electrode positions as some can be located more reliably than others. In that study, fMRI-guided neuronavigated stimulation yielded the highest spatial accuracy in the range of a few millimeters. Other studies have confirmed these results (Denslow et al. 2005a; Herwig et al. 2003b; Schonfeldt-Lecuona et al. 2005).

Neuronavigation requires a T1-weighted, high-resolution image of the subject's brain. The anatomical images have to be transferred into three-dimensional space. Optionally, individual

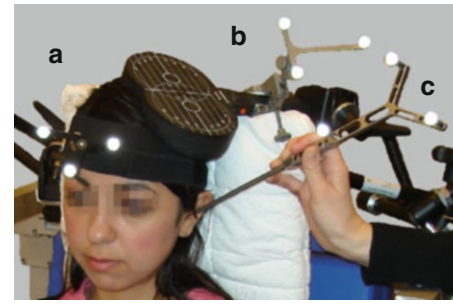

Fig. 21.1 Neuronavigated TMS guided by frameless stereotaxy. A tracker with three passive spheres is attached to the headband of the subject (**a**), to the TMS coil (**b**), and fixed on a pointer (**c**). These dynamic reference systems provide online information about the location of the head and the coil in space. A camera system (**d**) detects the position of the dynamic reference systems and displays this information on a computer screen using navigation software for visual localization of the coil

fMRI activation maps can be overlaid on the structural images. Predefined anatomical landmarks are marked on the individual structural MRI with special neuronavigation software. Usually, the nasion, the nibs of the tragus of both ears, and the internal angle of the eyes are used. A headband is then strapped around the subject's head. A tracker with at least three passive spheres or ultrasound reflecting transmitters is firmly attached to the headband, indicating the position of the subject's head. Another tracker is fixed onto the TMS coil. These dynamic reference systems provide online information about the location of the head and the coil in space. A camera system detects the position of the dynamic reference systems and displays this information on a computer screen using navigation software for visual localization of the coil (see Fig. 21.1).

The subject's head and the structural MR scans are coregistered by touching the predefined landmarks on the subject's face using a pointer equipped with trackers. An accurate coregistration procedure is crucial to exact placement of the coil. The position of the coil is visualized in real time on a computer screen relative to the individual three-dimensional anatomy of the brain. The exact position of the cortical target area can be defined either anatomically based on the gyral anatomy or functionally on the

basis of activation maps that have been obtained with fMRI. In addition to the individual activation map, one can also use the stereotactic coordinates of a peak activation that has been identified in a group of subjects. In this instance, the coordinates from standardized space (MNI, Talairach) have to be transformed to the subject's "native" space.

21.3 Combinations of fMRI with TMS

21.3.1 Why Combine TMS with fMRI?

fMRI provides a sensitive means of identifying brain regions where regional neuronal activity correlates with behavior. Due to its correlative nature, fMRI-based activation maps cannot establish whether such activation makes a relevant contribution to the behavior. By temporarily disrupting ongoing neural activity, TMS permits to make causal inferences regarding the contribution of the stimulated cortex to a specific brain function. Since single-pulse TMS offers a high temporal resolution, it can also be used to identify the period during which the stimulated area makes a critical contribution to the experimental task. Thus, combined TMS and fMRI gives access to noninvasive measuring of stimulation effects on the brain with a high spatial (fMRI: spatial resolution in the millimeter range) and temporal (single-pulse TMS: temporal resolution in the order of milliseconds) resolution.

The temporal relationship between TMS and fMRI defines which question can be addressed using a combined TMS-fMRI approach. TMS can be given in the MR scanner during fMRI data acquisition (online approach) to investigate the immediate effects of TMS on brain activity and behavior. Alternatively, TMS and fMRI may be separated in space and time (offline approach). In this case, TMS is given outside the MRI suite before or after fMRI (see Fig. 21.2).

21.3.2 TMS in the MR Scanner During fMRI (Online TMS-fMRI Approach)

TMS during fMRI (interleaved TMS-fMRI) enables the researcher to probe the immediate impact of TMS on regional neuronal activity across the whole brain. By applying TMS during different functional states of the brain, the online TMS-fMRI approach can explore how the TMS influences on neuronal activity in the stimulated and distant areas vary with task demands.

21.3.2.1 Methodological Issues

Although the prerequisites to apply TMS during fMRI were already introduced by Bohning et al. (Bohning et al. 1997, 1998, 1999) approximately 10 years ago, interleaved TMS-fMRI failed to become a routine procedure yet. At present, most of the studies that used interleaved TMS-fMRI were carried out by three research groups in Charleston (North Carolina, USA), Göttingen (Germany), and London (UK; for details, see Table 21.1). A simple implementation of TMS in the MRI environment is precluded by problems originating from the application of magnetic pulses in the static magnetic field of the MR scanner and in the presence of magnetic field gradients required for image acquisition (Baudewig et al. 2001). Therefore, nonferromagnetic coils have to be used which are mechanically strengthened to prevent coils from breaking during fMRI. Subjects have to wear ear plugs and headphones because mechanical interactions between the TMS-evoked local magnetic field and the static magnetic field of the MR scanner result in a louder click when the coil is discharged inside the scanner. The presence of the MR-compatible TMS coil may cause geometric image distortions (Baudewig et al. 2000; Bestmann et al. 2003a). These can be reduced by a shorter readout time of echoplanar imaging (EPI) sequences, the use of stronger imaging gradients, and parallel imaging.

The ferromagnetic stimulation device must be placed at sufficient distance from the magnetic field of the MR scanner, outside the scanner room, or in a radio-frequency-shielded cabinet inside the scanner room. This requires a longer cable to connect the coil with the stimulator.

MR-compatible TMS coil holders help to ensure accurate placement of the coil inside the scanner. Yet spatial limitations imposed by the MR head coil may restrict the access to some cortical areas, especially in the basal, frontal, and temporal lobe. TMS also evokes twitches of cranial muscles and somatosensory and auditory

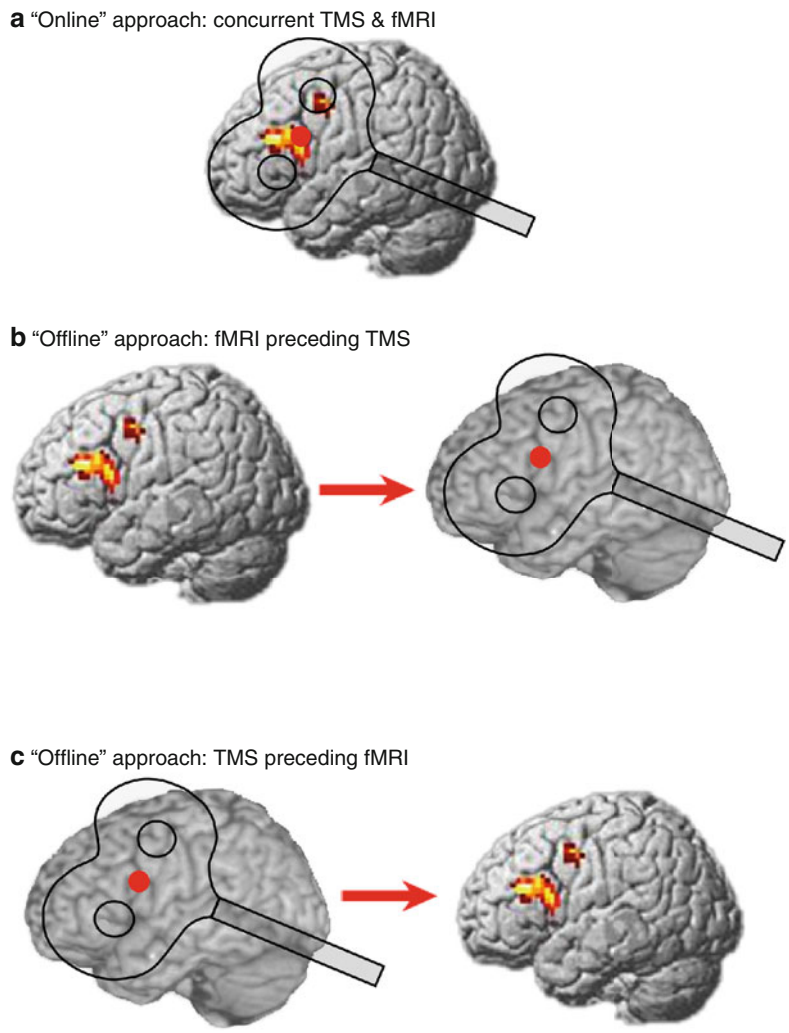

Fig. 21.2 Relative timing of TMS and fMRI determines the application of combined TMS-fMRI. TMS and fMRI can be performed interleaved (i.e., "online" approach) to investigate immediate effects of TMS on brain functions (**a**). In the "offline" approach, fMRI precedes or follows TMS. fMRI preceding TMS is usually used to identify appropriate sites for focal TMS (**b**), while TMS preceding fMRI can be used to probe the lasting effects of TMS conditioning on brain functions (**c**)

stimulation which may cause discomfort and movement artifacts and contribute to functional brain activation. Nonspecific auditory and somatosensory stimulation as well as the unpleasantness of TMS complicate the interpretation of TMS-induced brain activation by causing BOLD signal changes in subcortical and cortical areas involved in sensory or affective processing (Bestmann et al. 2005). It is therefore advisable to include a control condition which matches the auditory and somatosensory stimulation but does not cause transcranial cortical stimulation. Alternatively, the same TMS protocol might be applied to a control area in a separate fMRI session.

Dynamic artifacts pose a major problem to concurrent TMS during fMRI. Radio-frequency (RF) noise can markedly reduce the signal-to-noise ratio of MR images. TMS stimulators may themselves produce RF noise, and the antenna-like properties of the TMS coil cable can additionally guide RF noise into the scanner which can be reduced by customized RF filters. Leakage currents that originate from the high-voltage capacitors of the TMS stimulator may induce additional image distortions and artifacts. Of note, these leakage currents change with the intensity of TMS and can give rise to intensity-dependent BOLD signal changes. Remote-controlled high-voltage relay-diode systems reduce leakage currents flowing between the stimulator and the TMS coil and can thus be used to resolve this problem (Bestmann et al. 2007).

Table 21.1 Studies using interleaved TMS-fMRI in healthy volunteers

Target area	Task	TMS-fMRI protocol (frequency; %MT; total no. of pulses per train/session)	Reference
Left M1	Rest	0.83 Hz; 110; 20/session	Bohning et al. (1998)
Left M1	Rest	1 Hz; 80/110; 18/session	Bohning et al. (1999)
Left M1	Rest/finger movements	1 Hz; 110; 21/train	Bohning et al. (2000a)
Left M1	Rest	SP; 120; 15/session	Bohning et al. (2000b)
Left M1	Rest/finger movements	10 Hz; 110; 10/train	Baudewig et al. (2001)
Left PMd		10 Hz; 90/110;10/train	
Left PFC	Rest	1 Hz; 80/100/120; 21/train	Nahas et al. (2001)
Left M1/S1	Rest	4 Hz; 90/110/110 AMT; 40/train	Bestmann et al. (2003b)
Left M1	Rest	1 Hz; 110; *not reported*	Bohning et al. (2003a)
Left M1	Rest	1 Hz; 120; 1,2,4,8,16,24/train	Bohning et al. (2003c)
Left M1	Rest	4 Hz; 150; 4/train	Kemna and Gembris 2003
Left M1	Rest	1 Hz; 110; 21/train	McConnell et al. (2003)
Left M1	Rest	3.1 Hz; 90/110 AMT; 30/session	Bestmann et al. (2004)
Left M1/S1	Rest/finger movements	1 Hz; 110; 21/train	Denslow et al. (2004)
Left PFC	Rest	1 Hz; 100; 21/session	Li et al. (2004a)[a]
Left M1	Rest	1 Hz; 110/120; *not reported*	Li et al. (2004b)
Left PFC			
Left PMd	Rest/finger movements	3 Hz; 90/110 AMT; *not reported*	Bestmann et al. (2005)
Left M1	Rest/finger movements	1 Hz; 110; 21/train	Denslow et al. (2005a)
Left M1	Rest	1 Hz; 110; 21/train	Denslow et al. (2005b)
Left M1	Rest	SP; ~90;98/102;110 SoM; 20; 40/session	Bestmann et al. (2006)[b]
Right FEF	Rest/visual judgment	9 Hz; 40/55/70/85 TOP;	Ruff et al. (2006)
		10 Hz; 65 TOP; 5/train	
Left PMd	Isometric left hand grips	11 Hz; 70/110; 5/train	Bestmann et al. (2007)
Left/right SPL	Visuospatial tasks	13.3 Hz; 100 TOP; 5/train	Sack et al. (2007)
Right IPS/FEF	Visual task (moving stimuli)	9 Hz; 40/55/70/85 TOP; 5/train	Ruff et al. (2008)

AMT active motor threshold, *FEF* frontal eye field, *IPS* intraparietal sulcus, *M1* primary motor cortex, *PFC* prefrontal cortex, *PMd* dorsal premotor cortex, *RMT* resting motor threshold, *SoM* sense of movement, *SP* single pulse, *TOP* total output

[a]Depressive patients

[b]Amputee patient

The strong magnetic pulses induced by TMS can severely distort MR images depending on TMS coil orientation, TMS pulse intensity, and MR magnetic field strength (Bestmann et al. 2003a; Shastri et al. 1999). Therefore, a direct interference between TMS pulse and EPI excitation pulses should be avoided, and images being perturbed by TMS pulses must be replaced (Bestmann et al. 2008). A feasible solution to this problem is to introduce a sufficiently long temporal gap between TMS pulses and subsequent MR image acquisition (for more technical details, see Baudewig and Bestmann 2007; Bestmann et al. 2008).

21.3.2.2 Applications of Interleaved TMS-fMRI

Several researchers applied TMS over the motor cortex during rest and showed that TMS-induced acute changes in BOLD signal are a dose-dependent fashion (Baudewig et al. 2001; Bestmann et al. 2003a, 2004; Bohning et al. 1998, 1999, 2000b). A single TMS pulse evoked regional increases in BOLD signal which were similar to those evoked by volitionally movements (Bohning et al. 2000b). Such BOLD signal increases were only observed at suprathreshold intensities which evoked a

muscle twitch in the contralateral hand. Hence, it remains unclear whether the observed activation was directly induced by cortical stimulation or resulted from somatosensory feedback activation caused by the TMS-induced movement. However, Bestmann et al. (Bestmann et al. 2005) applied short trains of 3 Hz rTMS over the left premotor cortex which produced an increase in BOLD signal in the stimulated cortex and connected areas. Since the premotor TMS train did not produce overt muscle movements, it was concluded that these BOLD signal changes resulted from cortical stimulation rather than from somatosensory feedback activation.

Interleaved TMS-fMRI studies revealed that TMS can evoke changes in neural activity in connected cortical and subcortical areas (Baudewig et al. 2001; Bestmann et al. 2004, 2005; Bohning et al. 1998, 1999, 2000a; Ruff et al. 2008). These distant BOLD signal changes can occur even in the absence of consistent signal changes in the area that was directly targeted by TMS (Bestmann et al. 2004). This suggests that transsynaptic spread of excitation from the stimulated to connected brain areas makes a major contribution to neuronal stimulation that is induced by TMS in the human brain.

Interleaved TMS-fMRI opens up the possibility to examine how TMS interacts with intrinsic task-related activation and how these TMS-induced changes in task-related activity relate to changes in behavior. In a recent study, parietal rTMS was performed during fMRI to map TMS-induced changes in task-related brain activity that underlies the TMS-induced impairment of visuospatial judgments (Ruff et al. 2008). Concurrent TMS-fMRI was employed, to investigate the influences of a short high-frequency rTMS train over the right frontal eye field (FEF) or intraparietal sulcus, on the BOLD response in occipital activity to visual stimulation. The authors showed that TMS-induced changes in occipital activity critically depend on the actual state of the visual system at the time of TMS. Increased activity over visual area V5/MT + was only found if moving stimuli were concurrently presented. Conversely, visual areas V1–V4 were specifically activated during the absence of input.

So far, very few interleaved TMS-fMRI studies have been carried out in patients. In a case study, Bestmann et al. (Bestmann et al. 2006) investigated TMS-induced activity changes in distinct cortical areas of an amputee. At an intermediate stimulus intensity, TMS over the motor hand representation contralateral to amputation elicited a phantom sensation of a movement in half of the trials without producing overt activity in remaining muscles. The authors compared event-related BOLD signal changes in trials with versus without a phantom sensation of movement. Because the settings of TMS were identical, this comparison subtracted out any nonspecific TMS effects on regional neuronal activity. The sensation of a phantom movement was associated with increased activity in primary motor cortex, dorsal premotor cortex, anterior intraparietal sulcus, and caudal supplementary motor area. Based on these results, it was argued that activity in these frontoparietal areas represents the neuronal correlate of the phantom sense of movement (see Fig. 21.3 for details). Concurrent TMS-fMRI may also be of value to study how "therapeutic" rTMS protocols acutely change neuronal activity in functional brain networks. For instance, fMRI has been used to probe the immediate effects of continuous 1 Hz TMS at 100 % MT over the left dorsolateral prefrontal cortex in 14 patients with major depression (Li et al. 2004a).

21.3.3 Offline Combination of TMS and fMRI

21.3.3.1 TMS Following fMRI

There is consensus that fMRI can reliably identify brain regions in which increases in BOLD signal are correlated with the performance of an experimental task. Yet, the correlational nature of fMRI provides no information about the functional contribution of any activated brain region to the task. This question can be addressed using TMS. TMS can be applied over the area of interest to disrupt neuronal processing while participants perform the same experimental task. If the TMS-induced local perturbation affects task performance, this is taken as evidence that the stimulated cortical area is functionally relevant.

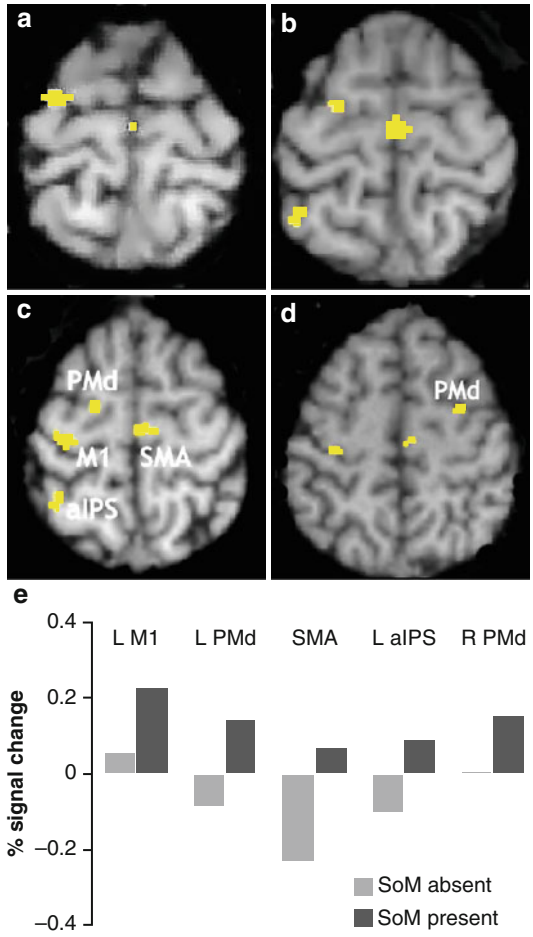

Fig. 21.3 Activity changes for the comparison of trials with versus without SoM reported, at intermediate TMS intensities (SPM(T) thresholded at $T \geq 3$). When a conscious phantom SoM was perceived, activity increases were observed in several motor-related regions, including the left (stimulated) M1, left and right PMd, left anterior intraparietal sulcus (aIPS), and caudal SMA. Note that the intermediate stimulation intensities applied were held constant in this contrast and were below threshold for evoking peripheral muscle responses. The results are displayed on the patient's anatomical T1-weighted MRI: (**a**) transverse section, $z=72$; (**b**) $z=67$; (**c**) $z=62$; (**d**) $z=57$; (**e**) fMRI percent signal change with respect to the session mean in peaks from these five motor-related regions (left M1, left and right PMd, SMA, left aIPS), for trials with or without evoked phantom SoM experienced (Reprinted from Bestmann et al. (2006), with permission from Elsevier)

An elegant illustration of this approach was provided by Cohen and colleagues in a TMS study on blind subjects (Cohen et al. 1997). Previous neuroimaging studies had shown that Braille reading consistently activated visual cortical areas in blind subjects but not in those with sight. To investigate the significance of task-related activation in the occipital cortex, short trains of 10 Hz rTMS were given to several brain regions time-locked to Braille reading. Occipital rTMS induced errors and distorted the tactile perceptions of congenitally blind subjects, but had no effects on tactile performance in normal-sighted. This finding proved that the occipital visual cortex makes a relevant contribution to the processing of tactile input in blind subjects.

More recently, we used a multifocal TMS approach to investigate whether right hemisphere brain regions critically contribute to specific language functions (Hartwigsen et al. 2010a). This study was based on previous fMRI investigations that had shown activation of the supramarginal gyri (SMG) in both hemispheres for phonological word processing. To test the functional relevance of these phonological activation patterns, we applied 10 Hz rTMS trains to left, right, or bilateral SMG while participants performed phonological and semantic word decisions. The results of this study showed that TMS relative to an ineffective sham procedure impaired phonological decisions but did not affect semantic decisions independent of the stimulated hemisphere. Moreover, performance was not worse for dual-site TMS as opposed to uni-site TMS. Together, these findings provide evidence that both hemispheres equally contribute to accurate and efficient phonological decisions in the healthy brain, without any evidence for an acute compensation of a "virtual lesion" induced in the homologous area in the opposite hemisphere.

Functional MRI can be used to functionally localize the optimal site for TMS. In a study by Neggers and colleagues (2007), participants first performed a saccade task during fMRI. In each subject, the individual peak activation in the precentral sulcus was identified and superimposed on the structural image of the subject's brain. Then, frameless stereotaxy was used to place the coil over the fMRI-defined FEF. This fMRI-guided stereotactic approach is likely to be more precise than relying on structural anatomical landmarks because it takes into account the interindividual variability of the functional

representation of the FEF in the precentral cortex. An alternative strategy uses the results of a previous fMRI study that has used the same or a similar experimental task. The stereotactic coordinates of task-related peak activation in the area of interest define the site of stimulation. The individual site of stimulation is determined by using the inverse of the normalization transformation and transforming the coordinates from standard to "individual" space (e.g., Hartwigsen et al. 2010a, b). Considering the high interindividual variability of the therapeutic effects of rTMS in psychiatric and neurological disorders (e.g., Gross et al. 2007; Lefaucheur et al. 2007; Ridding and Rothwell 2007), the use of fMRI-guided TMS which takes into account the functional neuroanatomy of each individual may also increase the efficacy of rTMS as a therapeutic tool.

21.3.3.2 fMRI Following TMS

Another way to combine rTMS and fMRI is to apply rTMS before fMRI. Here rTMS is used to induce an acute reorganization in the human brain (Siebner and Rothwell 2003). After rTMS, fMRI is performed to map the lasting functional impact of rTMS on task-related neuronal activity at a system level (O'Shea et al. 2007; Rounis et al. 2007). Performing fMRI after rTMS outside the scanner does not require specific methodological precautions because rTMS and fMRI are separated in space and time. This *condition-and-map approach* can be used to study the changeability of functional brain networks. Preferably, fMRI should start as quickly as possible after rTMS to capture the transient effects of rTMS (Baudewig and Bestmann 2007). The conditioning effects of rTMS on regional neuronal activity can be detected by comparing task-related activation before and after rTMS. It is important to control unspecific changes in task-related activity that are simply due to the repetition of the experimental task in the MR scanner. This can be achieved by introducing a second session during which sham rTMS is given to the cortical target area. Sham rTMS should match real rTMS in terms of auditory and somatosensory stimulation but without inducing transcranial stimulation of the cortex. Alternatively, the same effective rTMS protocol might be applied to a second (control) area. A change in the pattern of activation after rTMS but not after control rTMS indicates a true reorganization in response to rTMS conditioning. The task specificity of functional reorganization can be shown by having participants perform a control task during the same fMRI session.

The condition-and-map approach has mostly been applied to study functional plasticity in healthy volunteers (see Table 21.2). For example, a recent study investigated the modulation and reorganization of networks associated with sensory perception and motor performance after subthreshold high-frequency (10 Hz, 90 % resting motor threshold) rTMS of the right primary motor hand area (Yoo et al. 2008). Using a sham-controlled within-subject design, BOLD signal change during a sequential finger motor task and noxious tactile stimulation of the left hand were assessed before and after real and sham rTMS. Compared to sham rTMS, real rTMS led to increased activation in the motor network which was associated with enhanced motor performance. On the other hand, real rTMS caused deactivation in the sensory network which correlated with an increase in tactile sensory threshold. In another study, fMRI used in healthy right-handers to probe short-term reorganization in right PMd after 1 Hz rTMS induced a lasting disruption of neuronal processing in the dominant left PMd specialized for action selection (O'Shea et al. 2007). 1 Hz rTMS specifically increased activity in right PMd and connected medial premotor areas during action selection without affecting behavior. Based on additional experiments, it was claimed that this increase in activity reflects compensatory short-term reorganization that helps to preserve behavior after the "neuronal challenge" induced by rTMS.

To date patients have been rarely studied with the offline combination of rTMS and fMRI (Cardoso et al. 2008; Fitzgerald et al. 2007; Nowak et al. 2008). However, a large number of condition-and-map studies used offline rTMS followed by PET in patients with neurological and psychiatric disorders such as tinnitus (Richter et al. 2006; Smith et al. 2007), depression (Kuroda et al. 2006; Peschina et al. 2001; Speer et al. 2000),

Table 21.2 Studies performing fMRI after a conditioning session of rTMS

Target area	Task during fMRI	TMS protocol (frequency; %RMT; total no. of pulses/ session)	Reference
Left S1	Rest	5 Hz; 90; 2,500	Tegenthoff et al. (2005)
Left IFG	Semantic object classification	10 Hz; 110; 300	Wig et al. (2005)
Left S1	Tactile frequency discrimination	5 Hz; 90; 1,250	Pleger et al. (2006)
Right vs. Left DLPFC	Cued choice reaction	5 Hz; 90 AMT; 1,800	Rounis et al. (2006)
Left PFC	Face-name memory	5 Hz; 80; 500	Sole-Padulles et al. (2006)[a]
Right PFC	Tower of London	1 Hz; 110; 720 vs. 10 Hz; 100; 1,500	Fitzgerald et al. (2007)[b]
Left PMd, Left SM	Action selection	1 Hz; 90 AMT; 900	O'Shea et al. (2007)
Left DLPFC	Emotional stimuli	5 Hz; 120; 3,750	Cardoso et al. (2008)[c]
Right FEF	Saccade-fixation	30 Hz TBS; 80; 600	Hubl et al. (2008)
Contrales. M1	Hand grip movements	1 Hz; 100; 600	Nowak et al. (2008)[d]
Right M1	Sequential finger motor task, noxious tactile stimuli	10 Hz; 90; 1,000	Yoo et al. (2008)

AMT active motor threshold, *DLPFC* dorsolateral prefrontal cortex, *FEF* frontal eye field, *IFG* inferior frontal gyrus, *M1* primary motor cortex, *PFC* prefrontal cortex, *PMd* dorsal premotor cortex, *RMT* resting motor threshold, *S1* primary somatosensory cortex, *SM* sensorimotor cortex, *TBS* theta burst stimulation
[a]Elderly subjects with memory complaints
[b]Patients with treatment-resistant depression
[c]Depressive patients with Parkinson's disease
[d]Stroke patients

schizophrenia (Langguth et al. 2006), dystonia (Siebner et al. 2003), or Parkinson's disease (Strafella et al. 2005). These studies have shown that the condition-and-map approach is important to advance our understanding of the therapeutic effects of rTMS as well as the underlying pathological brain mechanisms and should encourage investigators to perform fMRI after rTMS in patients.

21.4 Conclusion

TMS can be used concurrently with fMRI (online approach), or it can be given before or after fMRI (offline approach). While online TMS during fMRI is technically demanding and requires specific safety precautions, the offline TMS before or after fMRI approach outside the MR scanner can be easily performed. The relative timing between TMS and fMRI defines the scientific and clinical questions that can be tackled with the combined TMS-fMRI approach. This approach provides unique opportunities to explore the dynamic aspects of functional neuronal networks in space and time, and how these functional interactions are affected by disease. It also bears great potential for studying the physiological impact of TMS on the human brain. This knowledge will be crucial to the increased efficacy of TMS as a therapeutic tool.

References

Allen EA, Pasley BN et al (2007) Transcranial magnetic stimulation elicits coupled neural and hemodynamic consequences. Science 317:1918–1921

Barker AT, Jalinous R et al (1985) Non-invasive magnetic stimulation of human motor cortex. Lancet 1:1106–1107

Baudewig J, Bestmann S (2007) Transkranielle Magnetstimulation und funktionelle Magnetresonanztomographie [Transcranial magnetic stimulation and functional magnetic resonance tomography]. In: Siebner HR, Ziemann U (eds) Das TMS-Buch [the TMS book]. Springer, Heidelberg

Baudewig J, Paulus W et al (2000) Artifacts caused by transcranial magnetic stimulation coils and EEG

electrodes in T(2)*-weighted echo-planar imaging. Magn Reson Imaging 18:479–484
Baudewig J, Siebner HR et al (2001) Functional MRI of cortical activations induced by transcranial magnetic stimulation (TMS). Neuroreport 12:3543–3548
Berardelli A, Inghilleri M et al (1998) Facilitation of muscle evoked responses after repetitive cortical stimulation in man. Exp Brain Res 122:79–84
Bestmann S, Baudewig J et al (2003a) On the synchronization of transcranial magnetic stimulation and functional echo-planar imaging. J Magn Reson Imaging 17: 309–316
Bestmann S, Baudewig J et al (2003b) Subthreshold high-frequency TMS of human primary motor cortex modulates interconnected frontal motor areas as detected by inter-leaved fMRI-TMS. Neuroimage 20: 1685–1696
Bestmann S, Baudewig J et al (2004) Functional MRI of the immediate impact of transcranial magnetic stimulation on cortical and subcortical motor circuits. Eur J Neurosci 19:1950–1962
Bestmann S, Baudewig J et al (2005) BOLD MRI responses to repetitive TMS over human dorsal premotor cortex. Neuroimage 28:22–29
Bestmann S, Oliviero A et al (2006) Cortical correlates of TMS-induced phantom hand movements revealed with concurrent TMS-fMRI. Neuropsychologia 44: 2959–2971
Bestmann S, Swayne O et al (2007) Dorsal pre-motor cortex exerts state-dependent causal influences on activity in contralateral primary motor and dorsal premotor cortex. Cereb Cortex 18(6):1281–1291
Bestmann J, Ruff CC et al (2008) Concurrent TMS and functional magnetic resonance imaging: methods and current advances. In: Wassermann EM, Epstein CM, Ziemann U (eds) The Oxford handbook of transcranial stimulation. Oxford University Press, New York
Bohning DE, Pecheny AP et al (1997) Mapping transcranial magnetic stimulation (TMS) fields in vivo with MRI. Neuroreport 8:2535–2538
Bohning DE, Shastri A et al (1998) Echoplanar BOLD fMRI of brain activation induced by concurrent transcranial magnetic stimulation. Invest Radiol 33:336–340
Bohning DE, Shastri A et al (1999) A combined TMS/fMRI study of intensity-dependent TMS over motor cortex. Biol Psychiatry 45:385–394
Bohning DE, Shastri A et al (2000a) Motor cortex brain activity induced by 1-Hz transcranial magnetic stimulation is similar in location and level to that for volitional movement. Invest Radiol 35:676–683
Bohning DE, Shastri A et al (2000b) BOLD-f MRI response to single-pulse transcranial magnetic stimulation (TMS). J Magn Reson Imaging 11:569–574
Bohning DE, Denslow S et al (2003a) Interleaving fMRI and rTMS. Suppl Clin Neurophysiol 56:42–54
Bohning DE, Denslow S et al (2003b) A TMS coil positioning/holding system for MR image-guided TMS interleaved with fMRI. Clin Neurophysiol 114:2210–2219
Bohning DE, Shastri A et al (2003c) BOLD-fMRI response vs. transcranial magnetic stimulation (TMS) pulse-train length: testing for linearity. J Magn Reson Imaging 17:279–290
Cardoso EF, Fregni F et al (2008) rTMS treatment for depression in Parkinson's disease increases BOLD responses in the left prefrontal cortex. Int J Neuropsychopharmacol 11:173–183
Chen R, Classen J et al (1997a) Depression of motor cortex excitability by low-frequency transcranial magnetic stimulation. Neurology 48:1398–1403
Chen R, Gerloff C et al (1997b) Safety of different inter-train intervals for repetitive transcranial magnetic stimulation and recommendations for safe ranges of stimulation parameters. Electroencephalogr Clin Neurophysiol 105:415–421
Cohen LG, Celnik P et al (1997) Functional relevance of cross-modal plasticity in blind humans. Nature 389:180–183
Denslow S, Lomarev M et al (2004) A high resolution assessment of the repeatability of relative location and intensity of transcranial magnetic stimulation-induced and volitionally induced blood oxygen level-dependent response in the motor cortex. Cogn Behav Neurol 17:163–173
Denslow S, Bohning DE et al (2005a) An increased precision comparison of TMS-induced motor cortex BOLD fMRI response for image-guided versus function-guided coil placement. Cogn Behav Neurol 18:119–126
Denslow S, Lomarev M et al (2005b) Cortical and subcortical brain effects of transcranial magnetic stimulation (TMS)-induced movement: an interleaved TMS/functional magnetic resonance imaging study. Biol Psychiatry 57:752–760
Ettinger GJ, Leventon ME et al (1998) Experimentation with a transcranial magnetic stimulation system for functional brain mapping. Med Image Anal 2:133–142
Fitzgerald PB, Sritharan A et al (2007) A functional magnetic resonance imaging study of the effects of low frequency right prefrontal transcranial magnetic stimulation in depression. J Clin Psychopharmacol 27:488–492
Gerschlager W, Siebner HR et al (2001) Decreased corticospinal excitability after subthreshold 1 Hz rTMS over lateral premotor cortex. Neurology 57:449–455
Gross M, Nakamura L et al (2007) Has repetitive transcranial magnetic stimulation (rTMS) treatment for depression improved? A systematic review and meta-analysis comparing the recent vs. the earlier rTMS studies. Acta Psychiatr Scand 116:165–173
Hamada M, Hanajima R et al (2007) Quadropulse stimulation is more effective than paired-pulse stimulation for plasticity induction of the human motor cortex. Clin Neurophysiol 118:2672–2682
Hartwigsen G, Baumgaertner A et al (2010a) Phonological decisions require both the left and right supramarginal gyri. Proc Nat Acad Sci USA 107:16494–16499
Hartwigsen G, Price CJ et al (2010b) The right posterior inferior frontal gyrus contributes to phonological word decisions in the healthy brain: evidence from dual-site TMS. Neuropsychologia 48:3155–3163

Herwig U, Abler B et al (2003a) Verbal storage in a premotor-parietal network: evidence from fMRI-guided magnetic stimulation. Neuroimage 20:1032–1041

Herwig U, Satrapi P et al (2003b) Using the international 10–20 EEG system for positioning of transcranial magnetic stimulation. Brain Topogr 16:95–99

Huang YZ, Edwards MJ et al (2005) Theta burst stimulation of the human motor cortex. Neuron 45:201–206

Hubl D, Nyffeler T et al (2008) Time course of blood oxygenation level-dependent signal response after theta burst transcranial magnetic stimulation of the frontal eye field. Neuroscience 151:921–928

Ilmoniemi RJ, Virtanen J et al (1997) Neuronal responses to magnetic stimulation reveal cortical reactivity and connectivity. Neuroreport 8:3537–3540

Jasper HH (1958) The ten-twenty electrode system of the International Federation. Electroencephalogr Clin Neurophysiol 10:367–380

Kemna LJ, Gembris D (2003) Repetitive transcranial magnetic stimulation induces different responses in different cortical areas: a functional magnetic resonance study in humans. Neurosci Lett 336:85–88

Kobayashi M, Pascual-Leone A (2003) Transcranial magnetic stimulation in neurology. Lancet Neurol 2: 145–156

Koch G, Franca M, Albrecht UV et al (2006) Effects of paired pulse TMS of primary somatosensory cortex on perception of a peripheral electrical stimulus. Exp Brain Res 172:416–424

Kuroda Y, Motohashi N et al (2006) Effects of repetitive transcranial magnetic stimulation on [11C]raclopride binding and cognitive function in patients with depression. J Affect Disord 95:35–42

Lang N, Harms J et al (2006) Stimulus intensity and coil characteristics influence the efficacy of rTMS to suppress cortical excitability. Clin Neurophysiol 117:2292–2301

Langguth B, Eichhammer P et al (2006) Neuronavigated transcranial magnetic stimulation and auditory hallucinations in a schizophrenic patient: monitoring of neurobiological effects. Schizophr Res 84:185–186

Lee JH, van Donkelaar P (2006) The human dorsal premotor cortex generates on-line error corrections during sensorimotor adaptation. J Neurosci 26:3330–3334

Lee L, Siebner HR et al (2003) Acute remapping within the motor system induced by low-frequency repetitive transcranial magnetic stimulation. J Neurosci 23:5308–5318

Lefaucheur JP, Brugieres P et al (2007) The value of navigation-guided rTMS for the treatment of depression: an illustrative case. Neurophysiol Clin 37:265–271

Li X, Nahas Z et al (2004a) Acute left prefrontal transcranial magnetic stimulation in depressed patients is associated with immediately increased activity in prefrontal cortical as well as subcortical regions. Biol Psychiatry 55:882–890

Li X, Teneback CC et al (2004b) Interleaved transcranial magnetic stimulation/functional MRI confirms that lamotrigine inhibits cortical excitability in healthy young men. Neuropsychopharmacology 29:1395–1407

Massimini M, Ferrarelli F et al (2005) Breakdown of cortical effective connectivity during sleep. Science 309:2228–2232

McConnell KA, Bohning DE et al (2003) BOLD fMRI response to direct stimulation (transcranial magnetic stimulation) of the motor cortex shows no decline with age. J Neural Transm 110:495–507

Miniussi C, Ruzzoli M et al (2010) The mechanism of transcranial magnetic stimulation in cognition. Cortex 46:128–130

Nahas Z, Lomarev M et al (2001) Unilateral left prefrontal transcranial magnetic stimulation (TMS) produces intensity-dependent bilateral effects as measured by interleaved BOLD fMRI. Biol Psychiatry 50:712–720

Neggers SF, Langerak TR et al (2004) A stereotactic method for image-guided transcranial magnetic stimulation validated with fMRI and motor-evoked potentials. Neuroimage 21:1805–1817

Neggers SF, Huijbers W et al (2007) TMS pulses on the frontal eye fields break coupling between visuospatial attention and eye movements. J Neurophysiol 98:2765–2778

Nowak DA, Grefkes C et al (2008) Effects of low-frequency repetitive transcranial magnetic stimulation of the contralesional primary motor cortex on movement kinematics and neural activity in subcortical stroke. Arch Neurol 65:741–747

O'Shea J, Johansen-Berg H et al (2007) Functionally specific reorganization in human premotor cortex. Neuron 54:479–490

Pascual-Leone A, Tormos JM et al (1998) Study and modulation of human cortical excitability with transcranial magnetic stimulation. J Clin Neurophysiol 15:333–343

Peschina W, Conca A et al (2001) Low frequency rTMS as an add-on antidepressive strategy: heterogeneous impact on 99 mTc-HMPAO and 18F-FDG uptake as measured simultaneously with the double isotope SPECT technique. Pilot study. Nucl Med Commun 22:867–873

Pleger B, Blankenburg F et al (2006) Repetitive transcranial magnetic stimulation-induced changes in sensorimotor coupling parallel improvements of somatosensation in humans. J Neurosci 26:1945–1952

Richter GT, Mennemeier M et al (2006) Repetitive transcranial magnetic stimulation for tinnitus: a case study. Laryngoscope 116:1867–1872

Ridding MC, Rothwell JC (2007) Is there a future for therapeutic use of transcranial magnetic stimulation? Nat Rev Neurosci 8:559–567

Rossi S, Hallett M et al (2009) Safety, ethical considerations, and application guidelines for the use of transcranial magnetic stimulation in clinical practice and research. Clin Neurophysiol 120(12):2008–2039

Rounis E, Stephan KE et al (2006) Acute changes in frontoparietal activity after repetitive transcranial magnetic stimulation over the dorsolateral prefrontal cortex in a cued reaction time task. J Neurosci 26:9629–9638

Rounis E, Yarrow K et al (2007) Effects of rTMS conditioning over the frontoparietal network on motor versus visual attention. J Cogn Neurosci 19:513–524

Ruff CC, Blankenburg F et al (2006) Concurrent TMS-fMRI and psychophysics reveal frontal influences on human retinotopic visual cortex. Curr Biol 16:1479–1488

Ruff CC, Bestmann S et al (2008) Distinct causal influences of parietal versus frontal areas on human visual cortex: evidence from concurrent TMS-fMRI. Cereb Cortex 18:817–827

Sack AT, Kohler A et al (2006) The temporal characteristics of motion processing in hMT/V5+: combining fMRI and neuronavigated TMS. Neuroimage 29:1326–1335

Sack AT, Kohler A et al (2007) Imaging the brain activity changes underlying impaired visuospatial judgments: simultaneous FMRI, TMS, and behavioral studies. Cereb Cortex 17:2841–2852

Sandrini M, Umilta C et al (2011) The use of transcranial magnetic stimulation in cognitive neuroscience: a new synthesis of methodological issues. Neurosci Biobehav Rev 35:516–536

Schonfeldt-Lecuona C, Thielscher A et al (2005) Accuracy of stereotaxic positioning of transcranial magnetic stimulation. Brain Topogr 17:253–259

Shastri A, George MS et al (1999) Performance of a system for interleaving transcranial magnetic stimulation with steady state magnetic resonance imaging. Electroencephalogr Clin Neurophysiol Suppl 51:55–64

Siebner HR, Rothwell J (2003) Transcranial magnetic stimulation: new insights into representational cortical plasticity. Exp Brain Res 148:1–16

Siebner HR, Filipovic SR et al (2003) Patients with focal arm dystonia have increased sensitivity to slow-frequency repetitive TMS of the dorsal premotor cortex. Brain 126:2710–2725

Siebner HR, Bergmann TO et al (2009a) Consensus paper: combining transcranial stimulation with neuroimaging. Brain Stimul 2:58–80

Siebner HR, Hartwigsen G et al (2009b) How does transcranial magnetic stimulation modify neuronal activity in the brain? Implications for studies of cognition. Cortex 45:1035–1042

Smith JA, Mennemeier M et al (2007) Repetitive transcranial magnetic stimulation for tinnitus: a pilot study. Laryngoscope 117:529–534

Sole-Padulles C, Bartres-Faz D et al (2006) Repetitive transcranial magnetic stimulation effects on brain function and cognition among elders with memory dysfunction. Cereb Cortex 16:1487–1493

Sparing R, Buelte D et al (2008) Transcranial magnetic stimulation and the challenge of coil placement: a comparison of conventional and stereotaxic neuronavigational strategies. Hum Brain Mapp 29:82–96

Speer AM, Kimbrell TA et al (2000) Opposite effects of high and low frequency rTMS on regional brain activity in depressed patients. Biol Psychiatry 48:1133–1141

Starck J, Rimpilainen I et al (1996) The noise level in magnetic stimulation. Scand Audiol 25:223–226

Strafella AP, Ko JH et al (2005) Corticostriatal functional interactions in Parkinson's disease: a rTMS/[11C] raclopride PET study. Eur J Neurosci 22:2946–2952

Tegenthoff M, Ragert P et al (2005) Improvement of tactile discrimination performance and enlargement of cortical somatosensory maps after 5 Hz rTMS. PLoS Biol 3:e362

Terao Y, Ugawa Y et al (1998) Localizing the site of magnetic brain stimulation by functional MRI. Exp Brain Res 121:145–152

Thickbroom GW, Byrnes ML et al (2006) Repetitive paired-pulse TMS at I-wave periodicity markedly increases corticospinal excitability: a new technique for modulating synaptic plasticity. Clin Neurophysiol 117:61–66

Walsh V, Cowey A (2000) Transcranial magnetic stimulation and cognitive neuroscience. Nat Rev Neurosci 1:73–79

Walsh V, Rushworth M (1999) A primer of magnetic stimulation as a tool for neuropsychology. Neuropsychologia 37:125–135

Wassermann EM (1998) Risk and safety of repetitive transcranial magnetic stimulation: report and suggested guidelines from the International Workshop on the Safety of Repetitive Transcranial Magnetic Stimulation, 5–7 June, 1996. Electroencephalogr Clin Neurophysiol 108:1–16

Wassermann EM (2008) The motor-evoked potential in health and disease. In: Wassermann EM, Epstein CM, Ziemann U (eds) The oxford handbook of transcranial stimulation. Oxford University Press, New York

Wassermann EM, Lisanby SH (2001) Therapeutic application of repetitive transcranial magnetic stimulation: a review. Clin Neurophysiol 112:1367–1377

Weyh T, Siebner HR (2007) Hirnstimulation – Technische Grundlagen [stimulation of the brain – technical basics]. In: Siebner HR, Ziemann U (eds) Das TMS-Buch [the TMS book]. Springer, Heidelberg

Weyh T, Wendicke K et al (2005) Marked differences in the thermal characteristics of figure-of-eight shaped coils used for repetitive transcranial magnetic stimulation. Clin Neurophysiol 116:1477–1486

Wig GS, Grafton ST et al (2005) Reductions in neural activity underlie behavioral components of repetition priming. Nat Neurosci 8:1228–1233

Yoo WK, You SH et al (2008) High frequency rTMS modulation of the sensorimotor networks: behavioral changes and fMRI correlates. Neuroimage 39:1886–1895

Clinical Magnetoencephalography and fMRI

22

Steven M. Stufflebeam

22.1 Introduction

Over the past two decades, numerous studies have demonstrated that functional magnetic resonance imaging (fMRI) conveniently maps brain activity, both at rest and during a task. The spatial resolution of fMRI in clinical scanners can exceed 1 mm in plane resolution. The temporal resolution, however, is limited to around 1 s or perhaps a few hundred milliseconds depending on the technique and the paradigm used. Today, in the clinical and research setting, MEG directly measures neuromagnetic activity at a high temporal resolution and supplements or replaces the spatial information provided by fMRI.

For purposes of identifying eloquent cortex, typically evoked activity from somatosensory, motor, auditory, visual, and language stimulation is recorded with MEG. During an MEG examination, the weak magnetic fields generated by neuronal currents in the brain are recorded. By measuring the magnetic field at several sites over the head, the most probable brain sources are estimated. The technique is best suited for measuring the activity in the fissural cortex of the cerebral hemispheres. Such areas are generally positioned so that they are difficult to measure even with invasive intracranial recordings. Thus, MEG detects brain activity that would be difficult to measure even in an operating room environment (Hämäläinen and Hari 2002). This chapter reviews the history of clinical MEG, introduces basic concepts about biophysics and analysis unique to MEG and electroencephalography (EEG), and compares and contrasts its clinical use with fMRI.

22.2 Clinical MEG Instrumentation

In 1968, David Cohen recorded the first magnetoencephalogram using a room-temperature copper coil as a detector, at the University of Illinois (Cohen 1968). After moving to the Massachusetts Institute of Technology, he built a more elaborate shielded room. At about the same time, James Zimmerman and colleagues developed the superconducting quantum interference device (SQUID), which uses the Josephson junction, to measure tiny magnetic fields. It requires cooling to liquid helium temperatures and has a sensitivity that is several hundred times that of a copper coil. Zimmerman brought this detector to Cohen's room, and this combination of shielding and detector allowed the first clear measurements of the body's magnetic fields. After they had measured the heart, Cohen recorded the first MEG measured with a SQUID (Cohen 1972). The initial measurements of magnetic brain activity were done by physicists who used a single magnetometer.

S.M. Stufflebeam
Department of Radiology,
Harvard Medical School/Massachusetts Institute of Technology, Athinoula A. Martinos Center for Biomedical Imaging, Massachusetts General Hospital, 149 Thirteenth Street – 2301, Charlestown, MA 02129, USA
e-mail: sms@nmr.mgh.harvard.edu

S. Ulmer, O. Jansen (eds.), *fMRI – Basics and Clinical Applications*,
DOI 10.1007/978-3-642-34342-1_22,

Most MEG devices now have hundreds of channels that can provide whole-head coverage. This makes it possible to map activity throughout the cerebral cortex, or beyond, and is critical for detecting propagating or widespread epileptic activity. Because of interference from extraneous magnetic fields, all MEG measurements must be performed in a magnetically shielded room, which typically consists of two layers of aluminum and multiple layers of ferromagnetic shielding.

22.3 Magnetoencephalography and Electroencephalography Basic Biophysics

MEG and EEG both measure electric currents in the brain. There are critical differences between MEG and EEG that make them complementary. Importantly, MEG preferentially detects activity in superficial, nonradial areas of cortex, that is, the fissural cortex of the cerebral hemispheres. This is particularly advantageous if the area of activity is in the walls of the sulci, such as in the somatosensory or the auditory areas. Much of the neural activity measured by MEG is related to postsynaptic activity in the pyramidal cells of the cerebral cortex. It measures the neural activity directly, as contrasted with BOLD fMRI, which measures neural activity indirectly via the hemodynamic response. MEG localizes neural activity more accurately than EEG because magnetic fields are less perturbed than electrical potentials by overlying brain structures: scalp, skull, cerebrospinal fluid, meninges, and vascular structures. Recently, the advancements in the statistical combination of structural MRI, fMRI, and MEG have taken a great stride forward by yielding the maximum benefit from each technique into a single image (Dale and Halgren 2001; Dale et al. 2000).

The calculation of the magnetic field is more straightforward than that of the electric field because of the symmetries and conductivity distribution of the human head. As the EEG electrodes are in direct contact with the head, they measure the extracellular volume currents. All currents, both intracellular and extracellular, generate magnetic fields, but, because of the near spherical shape of the head, one can calculate the resultant magnetic fields due to primary currents without taking into account the conductivity layers of the head.

22.4 Analysis of MEG

In order to intelligently interpret the results of a clinical MEG measurement, the data is examined in both the sensor space and in the brain (source space). The basic measurement with MEG is magnetic field strength as a function of time. In order to improve the signal-to-noise ratio of measured signals, it is often necessary to average several (typically around 100 trials) responses from an identical stimulus. This tends to average the extraneous activity to around zero in the evoked response, thus effectively improving the overall signal-to-noise ratio.

22.4.1 Source Modeling

Source modeling is necessary to determine the neural origin of the measured magnetic fields. The mathematical approach to this problem is known as the inverse problem. Generally, the inverse solution is nonunique and ill posed. If proper assumptions are made, however, the solution becomes solvable.

22.4.1.1 Equivalent Current Dipole

In order to make the inverse solution tractable, one can approximate that the activity from primary sensory or motor cortex originates as a single equivalent current dipole (ECD). This is physiologically plausible, given that a limited patch of cortex is synchronously activated and that the sensors are at least a few centimeters from the source. The ECD provides spatial information, magnitude (current dipole moment), and direction. It is typically computed using a standard iterative least-square algorithm (Marquardt 1963), which can also provide a measure of dipole parameter confidence, as well as the

best-fitting parameters such as goodness-of-fit (GOF) measure (Hämäläinen et al. 1993). Thus, by assuming a single source, the inverse problem has a unique solution. This works particularly well for primary sensory areas, for focal epilepsies, and for higher cognitive areas that have a focal source. Further advances in the ECD approach, for both EEG and MEG, have made it possible to find multiple ECDs with a multidipole approach, such as that developed by Hari and colleagues for somatosensory activation (Hari et al. 1993). One approach to investigate temporal changes in different areas of the brain is known as the time-varying dipole model. In this model, a series of dipoles are modeled such that the locations are fixed, but allowing the amplitudes to vary over time. This ECD approach works quite well for sequentially or simultaneously activated cortical sources, although the fine spatial details are lost due to the fact that the measurements are obtained at least 3 cm from the sources (Hämäläinen et al. 1993).

22.4.1.2 Distributed Solutions

If a large area of cortex is activated, the single ECD solution may be misleading. In practice, this may be suspected when a dipole localizes too deep to be physiologically plausible, that is, in the deep white matter. In such cases, distributed solutions such as the minimum norm estimate (MNE) or the minimum current solution (MCE) maybe more accurate. Although numerous other inverse solutions exist (Mosher et al. 1999; Mosher and Leahy 1998), this review concentrates on MNE and MCE.

22.4.1.3 Minimum Norm Estimate (MNE)

Originally pioneered by Hämäläinen (Hämäläinen and Ilmoniemi 1984) and recently improved by Dale and colleagues (Dale and Halgren 2001; Dale et al. 2000), MNE is now available in commercial software packages. The basis of the MNE is that a leadfield describes the contribution to the surface magnetic field from a series of dipoles in the brain. Although computationally expensive, the leadfield can be expressed as a matrix computed from a realistic head model from a head MRI.

The MNE does have some important limitations that must be kept in mind especially when they are used clinically: a depth bias and the difficulty in determining the extent of activation. In its most elementary expression, the source variance is assumed to be equal throughout the volume, and the MNE solution is biased toward the most superficial currents. One approach to lessen this effect is to use a cortical constraint obtained from the anatomic MRIs (Dale and Sereno 1993). In addition to a depth bias, determining the extent of the sources is also problematic. Simulations (Dale and Sereno 1993) show that the point-spread function of estimates is a function of location. Further, the spread depends on the assumed source variance. In order to further compensate for the superficial bias of current estimates and also give a more accurate estimation of the extent of activation, Dale has suggested producing a statistical parametric map (SPM) by normalizing the estimate MNE by source noise (Dale et al. 2000). Simulations have determined that the point-spread function is then a much lesser function of location (Liu et al. 2002). Additionally, the SPM can be used for hypothesis testing of the spatial extent of estimated activity in individuals across stimulus conditions, or between groups of subjects.

22.4.2 Combination with Other Imaging Technologies

In order to improve the spatial localization capabilities of MEG, the inverse solution can be combined with the spatial information provided from other sources, such as fMRI, positron emission tomography (PET), or optical imaging. As noted above, the spatial information from anatomic MRI can be used to restrict the solution to the cortical surface. For example, Dale and Halgren (2001) report the ability to create spatiotemporal "movies" of the processing of the brain during reading, by statistically combining the information from fMRI and MEG done with identical stimulus conditions, performed on different sessions (see Fig. 22.1). It might thus be possible to use such a technique to locate and quantify complex language and cognitive tasks presurgically.

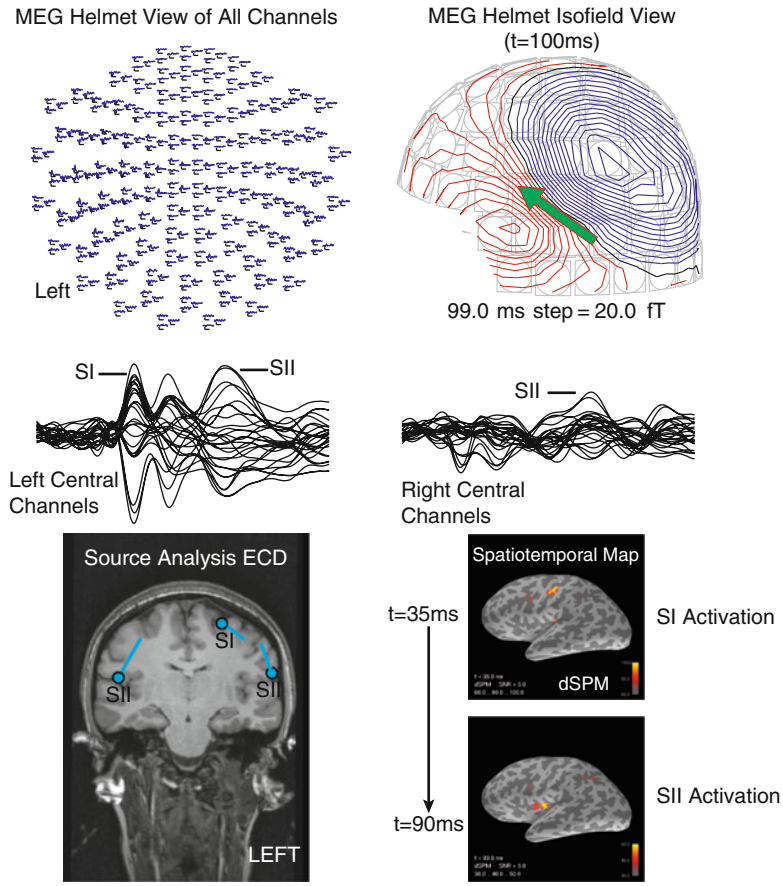

Fig. 22.1 Somatosensory-evoked field using MEG in an epilepsy patient. *Upper left* shows all 306 channels in a helmet view during electrical stimulation of the right median nerve. *Upper right* shows the isofield map of the current dipole (*green arrow*) over the SII area of the somatosensory cortex. *Middle panels* show enlargement of the channels over the somatosensory cortex of the right and left sides. *Lower left* shows the equivalent current dipole (ECD) of the contralateral SI and bilateral SII estimates superimposed on a T1-weighted MRI. *Lower right* shows two time frames (35-ms and 90-ms poststimulation of the right median nerve) demonstrating the activity location and magnitude (F-statistic) of SI (*upper*) and SII (*lower*). This activity can be converted to a millisecond resolution "movie" of the cortical current activity after a stimulus

22.5 Presurgical Mapping

22.5.1 Somatosensory Mapping

Using a tactile stimulator, the somatosensory cortex homunculus can be easily mapped by successively stimulating finger digits, foot digits, and lip using MEG. Alternatively, an electrical nerve stimulator can be used to map the median, tibial nerve, and lip representative areas. If an electrical nerve stimulator is used, the electrodes are placed, and the intensity set, such that thumb twitching or toe twitching is elicited. Typically, 100 repeated stimuli are required to obtain adequate signal-to-noise ratio. Both the primary (SI) and secondary (SII) somatosensory cortices are detectable with MEG (see Fig. 22.2).

After recording the evoked magnetic fields, the primary somatosensory cortex is typically localized with an ECD (Hari 1991; Hari and Forss 1999). If the median nerve electrical stimulation technique is used, the N20 m – the first "fast" component of the evoked magnetic field – is easily obtained in nearly all patients, including ones under deep anesthesia or in a coma (Hoshiyama et al. 1996; Kakigi 1994). The N20 m generator is located in the anterior wall of the somatosensory gyrus (area 3b), with a nonradial orientation, which is ideal for detection with MEG (Hari 1991; Hari et al. 1993; Hari and Forss 1999; Hoshiyama et al. 1996). It is a preconscious field that bypasses the thalamus and, due to a high signal-to-noise ratio, has a very repeatable localization, usually within a few millimeters of the hand area of the somatosensory cortex.

MEG identification of the central sulcus has been validated by several groups using intraoperative measurements (Beisteiner et al. 1995; Inoue et al. 1999; Kober et al. 2001a; Schiffbauer et al. 2001). Firsching et al. (Firsching et al. 1992,

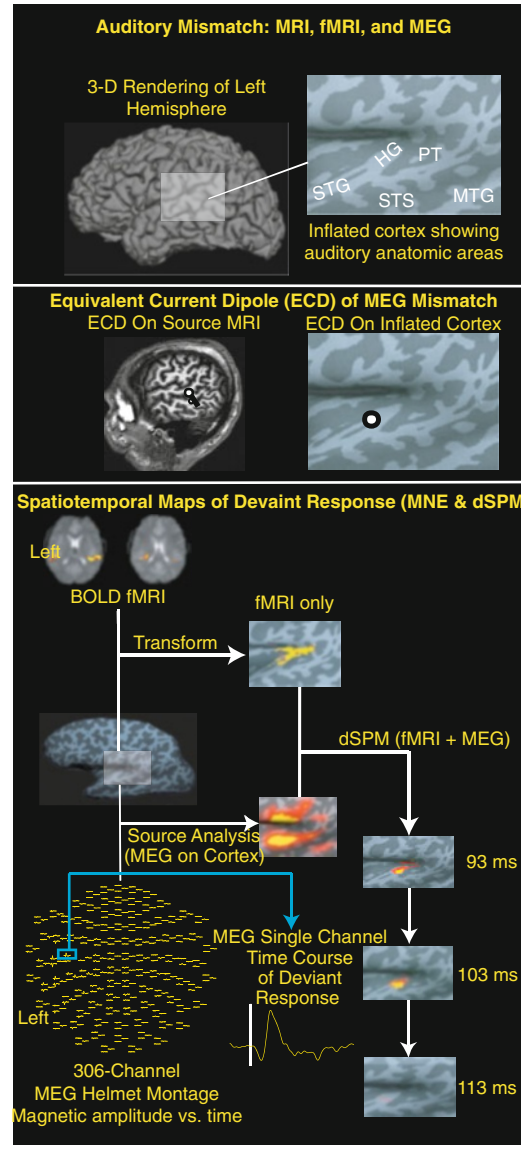

Fig. 22.2 Auditory mismatch response preliminary data using multiple imaging technologies in a control subject. Stimuli were narrowband standard tones (220 Hz center, 1/8 octave widths) and deviants (3 octaves above standard, with 1/8 octave width) presented rarely (5 %). Labeled areas are Heschl's gyrus (*HG*), planum temporale (*PT*), superior temporal gyrus (*STG*), superior temporal sulcus (*STS*), and middle temporal gyrus (*MTG*). The *next panel* shows a focal source analysis technique, the equivalent current dipole (*ECD*) method, which is traditionally used for MEG source estimation. *On the left* is a sagittal MRI with the ECD source estimate location with the black bar indicating the dipole direction. *On the right*, the dipole representing the peak in the magnetic mismatch response (*MMNm*) is registered onto the inflated cortex. Notice that in this case, the dipole is near the anterior portion of Heschl's gyrus. The *third panel* illustrates how the actual pilot data from fMRI, MEG data, and the inflated cortex data are combined to create a "movie" or spatiotemporal map. The fMRI data is superimposed on source EPI BOLD MRI images, which is then transformed onto the inflated cortex. The *lower panel* illustrates how the activity from the 306 channels of MEG data is transformed using the minimum norm estimate (*MNE*), a distributed source estimate method, onto the inflated cortical source. Note that only the auditory areas in the rectangular region over the STG are shown for the fMRI, MNE, and dSPM panels. Next, the fMRI data and the MNE results are combined into a spatiotemporal movie, or dSPM. With this pilot data from a healthy subject, some activity of the mismatch response is seen at 93 ms, which peaks at approximately 103 ms, and is diminished by 113 ms

2002) recently reported that in 30 patients, ECD localization of the tactile neuromagnetic response localized in the somatosensory cortex and was in agreement with phase reversal measurements at the time of surgery, without exception. Recent reports of noninvasive multimodal technologies – MEG, fMRI, and others – have noted that when combined, they enhance the reliability of identification of the central sulcus. Some have suggested that using a functional risk profile (FRP) based on MEG findings improves surgical decision-making (Hund et al. 1997). It should be kept in mind that brain tumor patients with known sensory or motor deficits often have diminished evoked fields (Hund et al. 1997).

22.5.2 Motor Mapping

As noted above, many functional imaging techniques, such as fMRI and PET, can accurately identify the central sulcus (Bittar et al. 1999). However, isolating pure motor activity with fMRI is difficult due to inevitable activation of the adjacent somatosensory cortex or other components of the motor system. MEG, however, can be used

to isolate pure motor activity. In practice, it requires precise timing of the onset of motor movement in order to produce an averaged evoked field. This can be achieved by a self-paced button press, or by the use of a trigger, a photo-optic switch. Activity that peaks between 20 and 50 ms before the onset of movement reflects activity in the primary motor cortex (Lewine and Orrison 1995).

Alternatively, the motor cortex can be mapped by performing a coherence analysis of the activity over the motor cortex with the electromyogram (EMG) waveform, as suggested by Makela et al. (Makela et al. 2001). By placing bipolar electrodes over the first interosseous muscle and instructing the patient to press the thumb against the index finger, the coherence of the MEG-EMG yields a spectrum with a peak near 20 Hz, most concentrated in the MEG sensors over the motor cortex. This coherence calculation isolates the primary motor cortex response from the rest of the motor system (Makela et al. 2001). MEG can be combined with neuronavigational systems in the neurosurgical suite to guide neurosurgeons of motor cortex (Ganslandt et al. 1999; Rezai et al. 1996, 1997). More recently, MEG has been reported to be useful in identifying the entire motor network, activated during the planning and the act of motor movement, including supplementary cortex (Erdler et al. 2000, 2001) and premotor cortex (Gross et al. 2000, 2001).

22.5.3 Auditory Cortex

MEG localizes the middle (50–200 ms) and late components (>400 ms) of the auditory response. Localization of the primary auditory cortex can be used as surgical reference, especially when using a neuronavigational system (Jannin et al. 2000, 2002). More importantly, the later components of the auditory-evoked response can be used to map higher-level functioning such as language processing. The N1 m peak is the largest and most robust, displaying a strong dipolar response, which localizes to the posterior superior temporal gyrus in or near the primary auditory cortex (see Fig. 22.1). The auditory cortex has multiple tonotopic maps, and some report the ability to use the neuromagnetic response from a series of tone pips at various frequencies (i.e., 100 Hz, 200 Hz, 500 Hz, 1 kHz, 5 kHz) to define a dominant tonotopic organization (Pantev et al. 1995).

22.5.4 Visual Cortex

In patients with tumors lying near visual eloquent areas, mapping of the visual cortex is possible. The primary visual cortex can be mapped by a simple ECD of the first visual-evoked peak from a strong visual stimulus, such as a checkerboard flash. Mapping of the visual areas is theoretically difficult with ECD mapping due to synchronously active sources. In practice, however, it does yield valid results (Hatanaka et al. 1997; Nakasato et al. 1996; Nakasato and Yoshimoto 2000). Mapping of the magnetic equivalent of visual-evoked potentials N75, P100, and N145 components is robust with large visual stimuli with phase reversal techniques and can be performed to detect visual field deficits (Hatanaka et al. 1997; Nakasato et al. 1996; Nakasato and Yoshimoto 2000). During a visual language task, it is often possible to fit ECDs to dipole locations, so that it does not necessarily have to be a separate stimulation which can save time during the MEG measurement.

22.5.5 Language Mapping

In patients with brain tumors in the perisylvian region, as well as in patients with epilepsy, lateralization and localization of language processing are critical. Although fMRI has become standard at some institutions, the intracarotid injection of amobarbital, known as the Wada test, is still considered the gold standard for a presurgical determination of hemispheric dominance. Still, the Wada test has been criticized because of potential cross-flow to the contralateral hemisphere and the lack of testing of territory supplied by the posterior circulation. There are several reports of MEG being used in determining both

hemispheric dominance for language, as well as regional language mapping of individual language areas (Breier et al. 1999a, b; Castillo et al. 2001; Floel et al. 2001; Simos et al. 1999a, b, 2001; Szymanski et al. 1999, 2001). MEG of language areas holds the promise of providing a noninvasive method of mapping language areas, with the goal of prolonging survival and making possible more extensive resections of brain tumors, yet preserving language function, in order to increase the survival. Such a test could reduce the need for invasive Wada tests and stimulation-based intraoperative mapping techniques.

22.5.5.1 Functional Language Paradigms

Determining hemispheric dominance or regional language processing in a brain tumor patient requires choosing the task that best activates the desired stream of language processing. Specific language processes include phonological, lexical, and syntactic processing. In addition, memory storage and retrieval occurs concurrently. Supporting processes include attention, motor planning (speech), and basic visual or auditory processing. Semantic decision tasks are probably the most popular tasks used in MEG as they require a response from the patient, such as a forced binary decision, allowing one to monitor the quality of the patient's responses. Otherwise, covert responses are desirable, as overt (spoken) responses can lead to unacceptable motion artifacts. Still, some passive sensory paradigms requiring no patient response have been reported in the literature to be successful (see below).

22.5.5.2 Hemispheric Dominance for Language

Determination of the language-dominant hemisphere is critical in the presurgical workup of tumors or other lesions near language-processing areas. MEG accurately determines the hemisphere dominant of language, analogous to determining the dominant hemisphere with an intracarotid amobarbital test (IAP). The most common methods fall into two broad categories: (1) sequential equivalent current dipole mapping and (2) distributed solutions.

Wada and Rasmussen determined that over 93 % of patients are left language dominant and that over 96 % of right-handed patients are so, as well, although more recent studies indicate that many patients have more bilateral representation of language than the original studies (Beisteiner et al. 1995). In left-handed patients, only about 70 % demonstrate left hemispheric dominance for language, with about 15 % of patients demonstrating bilateral language lateralization.

Recently, sequential dipole fitting has been proposed to determine language dominance. First proposed by Papanicolaou et al. (Papanicolaou et al. 1999), statistical criteria based on the ECD are used for determining the best dipoles in a sequential equivalent current dipole fit. The stimuli may consist of auditory and/or visual words. The results concur with Wada test results (Simos et al. 1998; Breier et al. 1999a; Papanicolaou et al. 2004, 2006; Merrifield et al. 2007; Kamada et al. 2007; Passaro et al. 2011) and electrical stimulation mapping (Panagiotis 1999). Szymanski et al. (Szymanski et al. 2001) reported using simple phonetic stimuli, such as the vowel sounds /a/ and /u/, for determining the language hemispheric dominance by summing the number of selective dipoles in the late auditory magnetic field on each hemisphere and calculating a lateralization index. Multiple groups report a strong correlation with both intraoperative mapping techniques and the results of the Wada test (Simos et al. 1999a; Szymanski et al. 2001).

Kober et al. (2001b) propose using a spatial filter, continuous localization by spatial filtering (CLSF), to determine language hemispheric dominance which can image simultaneously active sources. CLSF requires parcellating the brain into approximately 6,000 "vowels" and calculating the current produced in each "vowel." Bowyer et al. (Bowyer et al. 2005) analyzed the MEG data with MR-FOCUSS (Multi-Resolution FOCal Underdetermined System Solution) and demonstrated that the laterality determined by this method was highly consistent with the IAP results. McDonald et al. (McDonald et al. 2009) reported spatiotemporal source analysis of MEG using dSPM (dynamic statistical parametric mapping) provided the detailed time course of

activation associated with language processing in both epileptic patients and healthy controls.

22.5.5.3 Spatiotemporal Regional Language Mapping

MEG can localize, with a high temporal resolution, both receptive (auditory and visual) and productive brain areas, either alone or in combination with fMRI. There are number studies of the language system activation under a variety of passive and task-activated language paradigms, usually done for the purposes of understanding how the brain processes language. This has led to a revolution in mapping brain function and understanding how the brain processes information. However, the practical needs for the presurgical workup of brain tumor patients and the needs of basic neuroscience are fundamentally different in several respects. First, the neurosurgical application requires precise localization in the individual patient, while the neuroscientist can average the response over several subjects in order to increase the signal-to-noise ratio of small activations. Second, the neurosurgeon usually requires mapping the *essential language areas*, not just the participating areas. Essential language areas are those that, when removed, result in a language deficit. *Participating* areas are activated during language paradigms but do not result in a postoperative language deficit after resection, either because there are areas of redundant processing or because other areas learn to take over the same function. Currently, there is no way to distinguish essential areas from participating areas with noninvasive imaging, and this is a major goal of clinical functional imaging. Combining the fMRI, DTI tractography, and MEG source, analysis can be used to guide neurosurgery.

By simply applying a source localization procedure, the same techniques described for determining hemispheric dominance can be used for regional language mapping. The mapping of ECDs of the late auditory-evoked fields can be used for both posterior temporal and frontal operculum mapping (Papanicolaou et al. 1999; Breier et al. 2001). Temporal maps of activation have similar profiles as determined by invasive electrocorticography (ECoG). The latency of Wernicke's area is typically between 210 and 420 ms, and Broca's area between 400 and 1,100 ms, depending on the individual subject and the particular language paradigm. Generally, the peak activation of Wernicke's area precedes Broca's area, although occasionally, other temporal profiles have been reported (Kober et al. 2001b). Interestingly, MEG maps the posterior language areas (Wernicke's area) best and is less sensitive for the anterior frontal areas (Broca's area).

22.6 Spontaneous Activity: Epileptic Spike Localization

Localization of seizure activity can be performed both within the context of a low-grade brain tumor or as part of the workup of surgical epilepsy. Although interictal activity is most easily captured with MEG, ictal activity is also being detected and localized with whole-head MEG systems – particularly if the instrument is located in a hospital where antiepileptic medicines can be tapered and stopped. The most effective workup of epilepsy with MEG is with a whole-head system and is usually performed with simultaneously recorded EEG. A standard EEG electrode array, which has no magnetic material, is convenient and provides a way of producing a standard EEG classification of ictal or interictal activity. Higher-density caps are also available if EEG source localization is contemplated.

22.7 MEG and fMRI: What Is the Difference?

The precise relationship between the evoked neuromagnetic response and the BOLD signal is complex and incompletely understood. One might, for example, assume that increased signal in MEG or EEG would be positively correlated with an increase in fMRI BOLD, but this is not always the case. The electromagnetic response is a weighted sum of the postsynaptic potentials in the brain occurring on a millisecond scale, yet the BOLD signal is a hemodynamic response resulting from a convolution over several seconds of the temporal mean of cortical activity. Thus, the precise relationship is still under activity investigation by

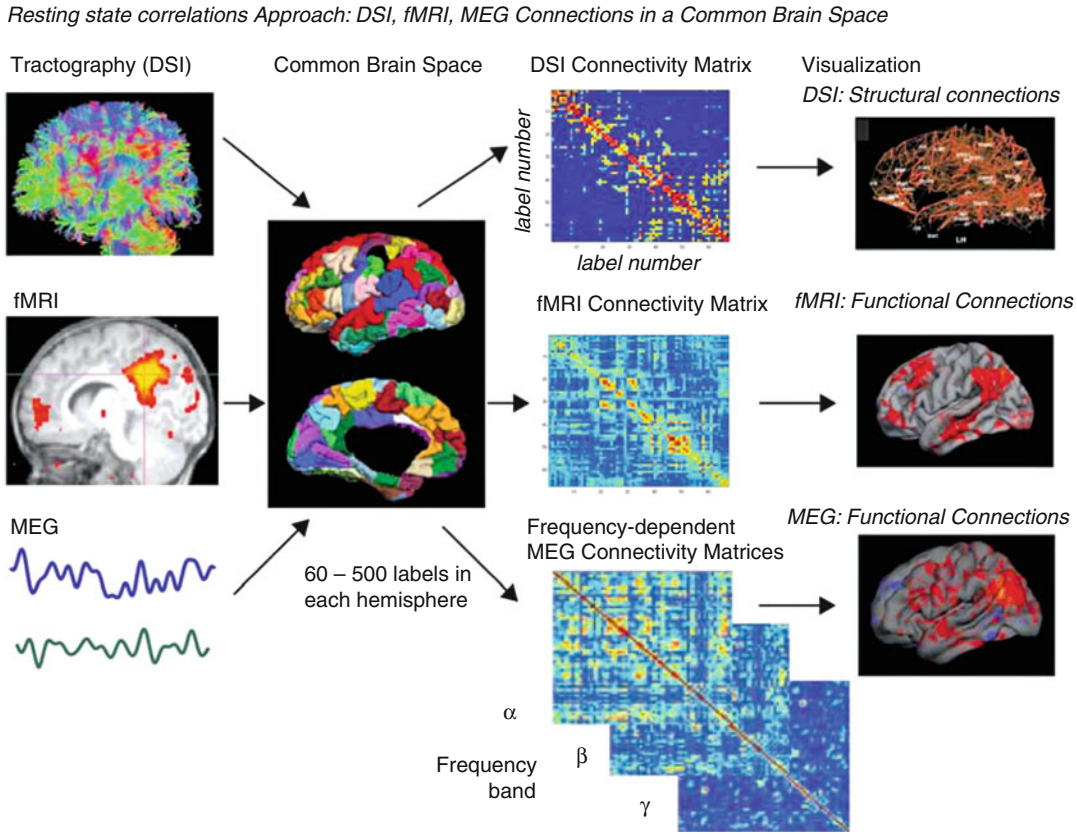

Fig. 22.3 The human brain connectome. Combining structural MRI from diffusion tractography (here as DSI), resting-state functional connectivity MRI, and resting-state MEG. The brain can be divided into a number of subregions, in this case using cortical parcellations of the gyral patterns using FreeSurfer (Fischl et al. 2004), as shown in the second column. The functional and structural connectivity can be compared using the correlation matrices (*third column*) based on the cortical parcellations (Hagmann et al. 2008). For MEG, the spectral envelopes at various frequency bands that were used for the correlation analysis from activity were the same cortical parcellations found with an MNE source analysis. In this subject, there was a similarity between the spatial patterns of correlation at the upper beta/lower gamma band envelopes and the functional connectivity MRI and DSI (*leftmost column*)

a number of groups. Interestingly, fMRI appears to be related to changes in the neural firing rate, which decreases with increased inhibition.

The relationship of functional connectivity using fMRI and MEG has also recently been investigated (Hillebrand 2012). The functional connectivity found with MEG is more complex than found with resting-state fMRI (Brookes et al. 2011). The resting-state networks are frequency dependent (Hillebrand 2012; Stam and Reijneveld 2007), and the functional connectivity analysis may be applied to spectral envelopes of the signal (Liu et al. 2010; de Pasquale et al. 2010; Ghuman et al. 2011). The analysis of resting-state MEG has been shown to be clinically important, such as identifying epileptic cortex (Douw et al. 2010) and cognition level (Douw et al. 2011) or finding eloquent cortex infiltrated by brain tumors (Martino et al. 2011). The combination of the high temporal information in MEG and the spatial resolution fMRI can be combined with structural information, such as DTI or diffusion spectral imaging (DSI), to identify the human brain connectome (Fig. 22.3).

An advantage of fMRI is that it easily and conveniently detects multiple areas activated during a particular sensory or motor task. For example, during motor activation, the supplementary and

premotor areas are activated in addition to the primary motor cortex. MEG also detects premotor activity, but the signal from the supplementary motor is weaker. Therefore, fMRI can image activity in some regions that are problematic with MEG. MEG can, however, detect the activity exclusively from the primary motor cortex with the use of EMG-MEG coherence, as described above. BOLD activity is not subject to spatial cancellation effects as surface MEG and EEG are (Ahlfors and Simpson 2004). Another advantage of fMRI over MEG is that it does not require increasingly sophisticated models to solve the inverse problem (Hämäläinen and Hari 2002).

A disadvantage of fMRI is that, especially at lower field strengths (3.0 T and below), significant activity detection is due to large draining veins, which can be at some distance from the cortical sites, leading to confusion in the localization of central sulcus (Ugurbil et al. 2003). MEG is useful in cases of a compromise to the hemodynamic compensatory mechanisms, such as arteriovenous malformations and, importantly, tumors (Roberts et al. 2000). This is especially true if the functional cortex is located within the radiologically defined extent of the tumor, such as those of a slow-growing, low-grade nature. This has been emphasized in a study by Inoue et al. (Inoue et al. 1999) who found two examples where the tumor and edema mass effect led to the disruption of normal hemodynamic response that caused an incorrect localization. Holodny et al. (Holodny et al. 1999, 2000) found decreased BOLD activation of the motor and somatosensory cortices adjacent to brain tumors, despite normal neurological function. Thus, abnormal vascular supply may decrease the hemodynamic response measured by fMRI. MEG, on the other hand, is a direct measure of neural activity and is immune to the constraints imposed by the vascular system (Roberts et al. 2000).

22.8 Conclusion

MEG/EEG and fMRI have excellent temporal and spatial resolution. Clinically, they can be used together to accurately map eloquent cortex and epileptic cortex in both healthy and diseased populations.

References

Ahlfors SP, Simpson GV (2004) Geometrical interpretation of fmri-guided MEG/EEG inverse estimates. Neuroimage 22(1):323–332

Beisteiner R, Gomiscek G et al (1995) Comparing localization of conventional functional magnetic resonance imaging and magnetoencephalography. Eur J Neurosci 7(5):1121–1124

Bittar RG, Olivier A et al (1999) Presurgical motor and somatosensory cortex mapping with functional magnetic resonance imaging and positron emission tomography. J Neurosurg 91(6):915–921

Bowyer SM, Moran JE et al (2005) Language laterality determined by MEG mapping with MR-FOCUSS. Epilepsy Behav 6:235–241

Breier JI, Simos PG et al (1999a) Lateralization of cerebral activation in auditory verbal and non-verbal memory tasks using magnetoencephalography. Brain Topogr 12(2):89–97

Breier JI, Simos PG et al (1999b) Language dominance determined by magnetic source imaging: a comparison with the Wada procedure. Neurology 53(5): 938–945

Breier JI, Simos PG et al (2001) Language dominance in children as deter- mined by magnetic source imaging and the intracarotid amobarbital procedure: a comparison. J Child Neurol 16(2):124–130

Brookes MJ, Hale JR et al (2011) Measuring functional connectivity using MEG: methodology and comparison with fcMRI. Neuroimage 56(3):1082–1104

Castillo EM, Simos PG et al (2001) Mapping of expressive language cortex using magnetic source imaging. Neurocase 7(5):419–422

Cohen D (1968) Magnetic field measurements of human alpha rhythm. Science 161:784–786

Cohen D (1972) Magnetoencephalography: detection of the brain's electrical activity with a superconducting magnetometer. Science 175(22):664–666

Dale AM, Halgren E (2001) Spatiotemporal mapping of brain activity by integration of multiple imaging modalities. Curr Opin Neurobiol 11(2):202–208

Dale AM, Sereno MI (1993) Improved localization of cortical activity by combining EEG and MEG with MRI cortical surface reconstruction: a linear approach. J Cogn Neurosci 5(2):162–176

Dale AM, Liu AK et al (2000) Dynamic statistical parametric mapping: combining fMRI and MEG for high-resolution imaging of cortical activity. Neuron 26:55–67

de Pasquale F, Della Penna S et al (2010) Temporal dynamics of spontaneous MEG activity in brain networks. Proc Natl Acad Sci USA. 107(13):6040–6045

Douw L, Schoonheim MM et al (2010) Epilepsy is related to theta band brain connectivity and network topology in brain tumor patients. BMC Neurosci 11:103

Douw L, Beisteiner R et al (2011) Cognition is related to resting-state small-world network topology: an magnetoencephalographic study. Neuroscience 175:169–177

Erdler M, Windischberger C et al (2000) Supplementary motor area activation pre- ceding voluntary movement is detectable with a whole-scalp magnetoencephalography system. Neuroimage 11(6 Pt 1):697–707

Erdler M, Windischberger C et al (2001) Dissociation of supplementary motor area and primary motor cortex in human subjects when comparing index and little finger movements with functional magnetic resonance imaging. Neurosci Lett 313(1–2):5–8

Firsching R, Klug N et al (1992) Lesions of the sensorimotor region: somatosensory evoked potentials and ultrasound guided surgery. Acta Neurochir (Wien) 118(3–4):87–90

Firsching R, Bondar I et al (2002) Practicability of magnetoencephalography-guided neuronavigation. Neurosurg Rev 25(1–2):73–78

Fischl B, van der Kouwe A et al (2004) Cerebral Cortex 14:11–22

Floel A, Knecht S et al (2001) Language and spatial attention can lateralize to the same hemisphere in healthy humans. Neurology 57(6):1018–1024

Ganslandt O, Fahlbusch R et al (1999) Functional neuronavigation with magnetoencephalography: outcome in 50 patients with lesions around the motor cortex. J Neurosurg 91(1):73–79

Ghuman AS, McDaniel JR et al (2011) A wavelet-based method for measuring the oscillatory dynamics of resting-state functional connectivity in MEG. Neuroimage 56(1):69–77

Gross J, Tass PA et al (2000) Cortico-muscular synchronization during isometric muscle contraction in humans as revealed by magnetoencephalography. J Physiol 527(Pt 3):623–631

Gross J, Kujala J et al (2001) Dynamic imaging of coherent sources: studying neural interactions in the human brain. Proc Natl Acad Sci USA 98(2): 694–699

Hagmann P, Cammoun L et al (2008) Mapping the structural core of human cerebral cortex. PLoS Biol 6(7)

Hämäläinen M, Hari R (2002) Magnetoencephalography. In: Toga AW, Mazziotta JC (eds) Brain mapping: the methods. Academic, Amsterdam, p xvii, 877

Hämäläinen MS, Ilmoniemi RJ (1984) Interpreting measured magnetic fields of the brain: estimates of current distributions. Technical Report TKK-F-A559. Helsinki University of Technology, Helsinki

Hämäläinen M, Hari R et al (1993) Magnetoencephalography – theory, instrumentation, and application to noninvasive studies of the working human brain. Rev Mod Phys 65:413–497

Hari R (1991) On brain's magnetic responses to sensory stimuli. J Clin Neurophysiol 8(2):157–169

Hari R, Forss N (1999) Magnetoencephalography in the study of human somatosensory cortical processing. Philos Trans R Soc Lond B Biol Sci 354(1387): 1145–1154

Hari R, Hämäläinen H et al (1990) Separate finger representations at the human second somatosensory cortex. Neuroscience 37(1):245–249

Hari R, Karhu J et al (1993) Functional organization of the human first and second somatosensory cortices: a neuromagnetic study. Eur J Neurosci 5(6):724–734

Hatanaka K, Nakasato N et al (1997) Striate cortical generators of the N75, P100 and N145 components localized by pattern reversal visual evoked magnetic fields. Tohoku J Exp Med 182(1):9–14

Hillebrand A (2012) Frequency-dependent functional connectivity within resting-state networks: an atlas-based MEG beamformer solution. Neuroimage 59(4): 3909–3921

Holodny AI, Nusbaum AO et al (1999) Correlation between the degree of contrast enhancement and the volume of peritumoral edema in meningiomas and malignant gliomas. Neuroradiology 41(11):820–825

Holodny AI, Schulder M et al (2000) The effect of brain tumors on BOLD functional MR imaging activation in the adjacent motor cortex: implications for image-guided neurosurgery. AJNR Am J Neuroradiol 21(8):1415–1422

Hoshiyama M, Kakigi R et al (1996) Somatosensory evoked magnetic fields following stimulation of the lip in humans. Electroencephalogr Clin Neurophysiol 100(2):96–104

Hund M, Rezai AR et al (1997) Magnetoencephalographic mapping: basic of a new functional risk profile in the selection of patients with cortical brain lesions. Neurosurgery 40(5):936–942; discussion 942–943

Inoue T, Shimizu H et al (1999) Accuracy and limitation of functional magnetic resonance imaging for identification of the central sulcus: comparison with magnetoencephalography in patients with brain tumors. Neuroimage 10(6):738–748

Jannin P, Fleig OJ et al (2000) A data fusion environment for multimodal and multi-informational neuronavigation. Comput Aided Surg 5(1):1–10

Jannin P, Morandi X et al (2002) Integration of sulcal and functional information for multimodal neuronavigation. J Neurosurg 96(4):713–723

Kakigi R (1994) Somatosensory evoked magnetic fields following median nerve stimulation. Neurosci Res 20(2):165–174

Kamada K, Sawamura Y et al (2007) Expressive and receptive language areas determined by a non-invasive reliable method using functional magnetic resonance imaging and magnetoencephalography. Neurosurgery 60:296–305

Kober H, Nimsky C et al (2001a) Correlation of sensorimotor activation with functional magnetic resonance imaging and magnetoencephalography in presurgical functional imaging: a spatial analysis. Neuroimage 14(5):1214–1228

Kober H, Möller M et al (2001b) New approach to localize speech relevant brain areas and hemispheric dominance using spatially filtered magnetoencephalography. Hum Brain Mapp 14(4):236–250

Lewine JD, Orrison WW Jr (1995) Magnetic source imaging: basic principles and applications in neuroradiology. Acad Radiol 2(5):436–440

Liu AK, Dale AM et al (2002) Monte Carlo simulation studies of EEG and MEG localization accuracy. Hum Brain Mapp 16(1):47–62

Liu Z, Fukunaga M et al (2010) Large-scale spontaneous fluctuations and correlations in brain electrical activity observed with magnetoencephalography. Neuroimage 51(1):102–111

Makela JP, Kirveskari E et al (2001) Three-dimensional integration of brain anatomy and function to facilitate intraoperative navigation around the sensorimotor strip. Hum Brain Mapp 12(3):180–192

Marquardt DW (1963) An algorithm for least-squares estimation of nonlinear parameters SIAM. J Soc Ind Appl Math 11(2):431–441

Martino J, Honma SM et al (2011) Resting functional connectivity in patients with brain tumors in eloquent areas. Ann Neurol 69(3):521–532

McDonald CR, Thesen T et al (2009) Distributed source modeling of language with magnetoencephalography: application to patients with intractable epilepsy. Epilepsia 50:2256–2266

Merrifield WS, Simos PG et al (2007) Hemispheric lavvnguage dominance in magnetoencephalography: sensitivity, specificity, and data reduction techniques. Epilepsy Behav 10:120–128

Mosher JC, Leahy RM (1998) Recursive MUSIC: a framework for EEG and MEG source localization. IEEE Trans Biomed Eng 45(11):1342–1354

Mosher JC, Leahy RM et al (1999) EEG and MEG: forward solutions for inverse methods. IEEE Trans Biomed Eng 46(3):245–259

Nakasato N, Yoshimoto T (2000) Somatosensory, auditory, and visual evoked magnetic fields in patients with brain diseases. J Clin Neurophysiol 17(2):201–211

Nakasato N, Seki K et al (1996) Clinical application of visual evoked fields using an MRI-linked whole head MEG system. Front Med Biol Eng 7(4):275–283

Panagiotis B (1999) Grand mal seizures with liver toxicity in a case of clozapine treatment. J Neuropsychiatry Clin Neurosci 11(1):117–118

Pantev C, Bertrand O et al (1995) Specific tonotopic organizations of different areas of the human auditory cortex revealed by simultaneous magnetic and electric recordings. Electroencephalogr Clin Neurophysiol 94:26–40

Papanicolaou AC, Simos PG et al (1999) Magnetoencephalographic mapping of the language-specific cortex. J Neurosurg 90(1):85–93

Papanicolaou AC, Simos PG et al (2004) Magnetoencephalography: a noninvasive alternative to the Wada procedure. J Neurosurg 100:867–876

Papanicolaou AC, Pazo-Alvarez P et al (2006) Functional neuroimaging with MEG: normative language profiles. Neuroimage 33:326–342

Passaro AD, Rezaie R et al (2011) Optimizing estimation of hemispheric dominance for language using magnetic source imaging. Brain Res 1416:44–50

Rezai AR, Hund M et al (1996) The interactive use of magnetoencephalography in stereotactic image-guided neurosurgery. Neurosurgery 39(1):92–102

Rezai AR, Mogilner AY et al (1997) Integration of functional brain mapping in image-guided neurosurgery. Acta Neurochir Suppl 68:85–89

Roberts TP, Ferrari P et al (2000) Presurgical mapping with magnetic source imaging: comparisons with intraoperative findings. Brain Tumor Pathol 17(2):57–64

Schiffbauer H, Ferrari P et al (2001) Functional activity within brain tumors: a magnetic source imaging study. Neurosurgery 49(6):1313–1320; discussion 1320–1321

Simos PG, Breier JI et al (1998) Assessment of functional cerebral laterality for language using magnetoencephalography. J Clin Neurophysiol 15:364–372

Simos PG, Breier JI et al (1999a) Atypical temporal lobe language representation: MEG and intraoperative stimulation mapping correlation. Neuroreport 10(1):139–142

Simos PG, Papanicolaou AC et al (1999b) Localization of language-specific cortex by using magnetic source imaging and electrical stimulation mapping. J Neurosurg 91(5):787–796

Simos PG, Castillo EM et al (2001) Mapping of receptive language cortex in bilingual volunteers by using magnetic source imaging. J Neurosurg 95(1):76–81

Stam CJ, Reijneveld JC (2007) Graph theoretical analysis of complex networks in the brain. Nonlinear Biomed Phys 1(1):3

Szymanski MD, Rowley HA et al (1999) A hemispherically asymmetrical MEG response to vowels. Neuroreport 10(12):2481–2486

Szymanski MD, Perry DW et al (2001) Magnetic source imaging of late evoked field responses to vowels: toward an assessment of hemispheric dominance for language. J Neurosurg 94(3):445–453

Ugurbil K, Toth L et al (2003) How accurate is magnetic resonance imaging of brain function? Trends Neurosci 26(2):108–114

Incidental Findings in Neuroimaging Research: Ethical Considerations

23

Stephan Ulmer, Thomas C. Booth, Guy Widdershoven, Olav Jansen, Gunther Fesl, Rüdiger von Kummer, and Stella Reiter-Theil

23.1 Introduction

Neuroimaging – especially functional MR imaging (fMRI) – opens the door to non-invasively map cortical processing and to understand how our brain works. fMRI evolved from basic (Ogawa et al. 1990, 1993; Kwong et al. 1992) and clinical applications in the 1990s (Yousry et al. 1995) to become a powerful and ubiquitous tool in neurocognitive research. Because fMRI can be used to answer clinical questions, the more research conducted, the greater the potential for clinical translation and subsequent patient benefit. This book focuses on the clinical applications of fMRI; however, prior to any routine clinical use, there is a need to test its reliability in healthy controls. The focus of this chapter is on ethical questions raised by incidental findings (IF) in fMRI in healthy volunteers and the conclusions to be drawn. Considering ethical issues are important in patient care but should be taken even more serious in healthy volunteers. Ethical

S. Ulmer (✉)
Medizinisch Radiologisches Institut (MRI) Zürich, (Bahnhofsplatz/Bethanien/Stadelhofen), Bahnhofsplatz 3, Zürich 8001, Switzerland

Institut für Neuroradiologie, Universitätsklinikum Schleswig-Holstein, Schittenhelmstrasse 10, Kiel 24105, Germany
e-mail: ulmer@email.com

T.C. Booth
Cancer Research UK, Cambridge Research Institute Li Ka Shing Centre, Robinson Way Cambridge CB2 0RE, UK

Department of Biochemistry, University of Cambridge, 80 Tennis Court Road, Cambridge CB2 1GA, UK
e-mail: tombooth@doctors.org.uk

G. Widdershoven
Netherlands School of Primary Care Research (CaRe), VU Medical Center, 7057, Amsterdam 1007 MB, The Netherlands
e-mail: g.widdershoven@vumc.nl

O. Jansen
Institut für Neuroradiologie, Universitätsklinikum Schleswig-Holstein, Schittenhelmstrasse 10, Kiel 24105, Germany
e-mail: o.jansen@neurorad.uni-kiel.de

G. Fesl
Abteilung für Neuroradiologie, Klinikum Grosshadern, Ludwig-Maximilians-Universität München, Marchioninistrasse 15, München 81377, Germany
e-mail: gunther.fesl@med.uni-muenchen.de

R. von Kummer
Abteilung Neuroradiologie, Universitätsklinikum Carl Gustav Carus, Fetscherstr. 74, Dresden 01307, Germany
e-mail: ruediger.vonkummer@uniklinikum-dresden.de

S. Reiter-Theil
Clinical Ethics University Hospital Basel / Psychiatric Hospitals of the University Basel
Schanzenstrasse 13, CH-4056 Basel, Switzerland
e-mail: s.reiter-theil@unibas.ch

S. Ulmer, O. Jansen (eds.), *fMRI – Basics and Clinical Applications*,
DOI 10.1007/978-3-642-34342-1_23, © Springer-Verlag Berlin Heidelberg 2013

issues relevant to fMRI concern how requirements of voluntary participation and privacy are handled by the researchers (Carli et al. 2012), how harm is prevented, and whether appropriate information and decisional aids are offered to the subjects or patients before obtaining informed consent (Reiter-Theil and Stingelin Giles 2007). Because an IF can have a major impact on the subject's life, the management pertaining to such a discovery should be analysed thoroughly (Ulmer et al. 2009).

23.2 Incidental Finding Prevalence

An IF is defined as a previously undetected abnormality of potential clinical relevance that is unrelated to the purpose of the examination (Illes et al. 2006). Within the last decade, IF were increasingly recognised as a new problem to deal within neuroimaging research (Garnett et al. 2011). The wider use of neuroimaging in research results in a higher prevalence of IF (Booth et al. 2012), and recent publications have emphasised the need for improved management (Woodward and Toms 2009; Ulmer et al. 2009; Hartwigsen et al. 2010). IF are frequent; the prevalence of recognisable and clinically significant neuropathologies ranges between 2 % and 9 % in the general population. All 'deviations from normal' (i.e. clinically significant, insignificant and indeterminate findings) are even more frequent (Katzman et al. 1999; Weber and Knopf 2006; Vernooij et al. 2007; Brown and Hasso 2008; Illes and Chin 2008; Hartwigsen et al. 2010; Ulmer et al. 2012). The prevalence of IF can be considerably higher in certain populations, i.e the elderly (e.g. Alphs et al. 2006; Gupta and Belay 2008). In a recent meta-analysis (Morris et al. 2009) of 16 studies with a total of 19,559 people, IF were found in only 2.7 % of the cases. This study, however, clearly underestimates their actual prevalence as findings such as small white matter lesions, lacunar infarcts or microhaemorrhages were excluded. It is noteworthy that MR image resolution varied between studies; furthermore, in some studies, scans were not read by neuroradiologists; thus, a considerable amount of IF might have been missed.

23.3 Consequences Arising from Incidental Findings

An IF may impact on the subject's life in a multitude of ways. Tumours (ranging between 0.2 % and 1.6 % in the general population) or vascular abnormalities (ranging from 0.5 to 1.8 %; Katzman et al. 1999; Weber and Knopf 2006; Vernooij et al. 2007) may require immediate neurosurgical, endovascular or medical therapy or, at the very least, require follow-up (Morris et al. 2009; Illes and Chin 2008; Hartwigsen et al. 2010). Other findings may herald the onset of disease (such as multiple sclerosis) even in the absence of clinical symptoms at the time of diagnosis (Okuda et al. 2009; Ulmer et al. 2012). Many findings may require medical treatment and have a profound impact on the subject's life, especially in planning a family, choosing a career, obtaining insurance and engaging in recreational activities. A volunteer who is informed that he/she has brain abnormality may decide to change some aspects of his/her daily routine and also formulate new goals in life.

Besides the consequences of discovering an IF for the individual, there may be implications for the wider community. For example, many brain lesions can cause clinical symptoms such as seizures which can put the surrounding population at substantial risk (e.g. from a subsequent motor vehicle accident). Detection of such lesions is clearly of societal benefit – indeed disclosure of an IF in this scenario is mandatory according to the World Medical Association, which represents approximately 80 national medical associations despite the usual right of a subject 'not to know' (see below; World Medical Association 2008).

There are also financial implications. Some lesions never become symptomatic, yet follow-up imaging of such lesions often incurs considerable costs for the individual, the state or insurance companies depending on the national health-care system (Machaalany et al. 2009). On the other hand, early identification of an IF might be of unequivocal benefit to the patient if the condition is treatable and early diagnosis improves outcome. Prevention, as well as a reduction, of the risk of death or long-term disability may even reduce overall health costs.

23.4 Consent

Although it is widely agreed amongst researchers that consent should be obtained from the volunteer prior to neuroimaging research, in practice, the information provided at the time differs widely between research groups. In the UK, for example, over 10 % of participants are not apprised of contingency plans, potential benefits and harms should any IF be found, despite an expectation from the National Research Ethics Service (2007; Booth et al. 2012). Radiologists are more likely than non-radiologists to discuss potential implications of IF which likely reflect greater familiarity with common IF and the issues that they raise. About 20 % of researchers discuss whether any IF are likely to be treatable, which is an European 'Additional Protocol' requirement (Council of Europe Steering Committee on Bioethics 2004). This practice is, not surprisingly, more common amongst medical (i.e. medically qualified) than nonmedical researchers. The WHO/UNESCO also recommend discussion prior to consent of 'the extent of the investigator's responsibility to provide medical services to the participant' should an IF be discovered (The Council for International Organizations of Medical Sciences (CIOMS) 2002). This ethical guideline is followed by 42 % of researchers in the UK. Practice also differs between countries. For example, just over one-third of UK researchers warn volunteers that reanalysis of the data in the future may lead to recontact after the study has finished. This compares to only 4 % in the USA (Lawrenz and Sobotka 2008), despite the recommendation that such information is routinely given (Wolf et al. 2008). In the UK, medical researchers are more likely than nonmedical researchers to discuss recontact, which may again reflect differences in perception of the wider implications and limits of researchers' responsibilities.

23.5 Detection of Incidental Findings

Even if an unexpected finding may be of no clinical concern to the volunteer, the research data may be confounded, for example, if an arachnoid cyst is discovered during an fMRI study. In this example, normalising brains (e.g. to the Montreal Neurological Institute (MNI) space) may lead to incorrect topographical localisation of functional areas. For most fMRI research groups, anatomical images consist of high-resolution T_1-weighted sequences (such as a MPRage or SPGR) which are used for an overlay. Nonetheless, although these sequences differentiate grey and white matter well, they are likely to be inadequate for clinical screening purposes where additional T_2-weighted sequences (TSE or FLAIR), contrast agents and additional orthogonal acquisitions may be required.

In neuroimaging research, there is no universally agreed approach to acquiring and reporting scans in anticipation of IF (Booth et al. 2010). In terms of reporting strategies, UK and US studies show wide variation amongst researchers (Booth et al. 2012; Illes et al. 2004). This ranges from no radiological review of images to 'reactive' strategies (where radiological advice is sought only if an abnormality is noticed by a researcher or radiographer) to 'proactive' (all images are reviewed by a radiologist) and 'very proactive' (where additional anatomical imaging is performed routinely to better identify and characterise any IF) reporting (Ulmer et al. 2009; Booth et al. 2010). There may also be variation as to whether a specialist radiologist reports a study (e.g. a neuroradiologist reviewing a brain MRI) as opposed to a non-specialist.

'Proactive' radiological review of research images is likely to provide more sensitive and specific detection of significant IF (Royal and Peterson 2008). Furthermore, the IF prevalence meta-analysis mentioned above (Morris et al. 2009) demonstrates that the detection of IF almost doubles if a 'very proactive' strategy is adopted. In the UK, the 'reactive' strategy is the most common reporting method (26 %), although few researchers (16 %) consider this ideal practice (defined as without funding or time constraints; Booth et al. 2012). On the other hand, the most popular ideal reporting strategy is 'proactive' reporting by specialist radiologists (29 %) but is the current practice for only 14 % of researchers. Medical researchers, especially radiologists, tend towards more 'proactive' reporting strategies compared with nonmedical investigators.

The reasons for researchers not undertaking 'proactive' reporting may reflect no or little access to a radiological opinion, cost limitations, limited awareness of the frequency and implications of IF and opinions as to the extent of responsibility of the researcher with regard to detection of such abnormalities (Royal and Peterson 2008). Additionally, policies of 'reactive' reporting are sometimes justified on the grounds that detection of IF lies outside the remit of the research study (Miller et al. 2008).

23.6 Disclosure of Incidental Findings

There are few publications relating to disclosure of IF. Regardless of the reporting method, research groups must decide how to manage an IF once it is discovered. In the same UK study mentioned above, IF disclosure management is shown to vary and be influenced by the background of the principal investigator. Here, researchers most commonly disclose IF to volunteers when judged 'relevant' (47 %), and a similar percentage considers this ideal (46 %). Face-to-face disclosure is the most common method of communication (41 %) and is thought by many to be ideal (70 %). Disclosure is performed most commonly by the volunteer's family practitioner (43 %), which is also thought to be ideal practice by one-third of the responders (32 %).

Nonmedical researchers are more likely never to disclose IF to the volunteer. The two common reasons given for this are that non-clinicians process the images, which makes subsequent disclosure appear inappropriate, and that disclosure is harmful and causes stress to the volunteer.

Those who have been researchers for a shorter period of time are more likely to disclose IF 'routinely' to the volunteer than those who have been researchers for a longer period, but more experienced investigators are more likely than less experienced researchers to disclose IF to the volunteer if this is felt to be 'relevant'. Medical researchers are more likely to use a research team physician to disclose IFs than nonmedical researchers, as are radiologists compared with non-radiologists. Nonmedical researchers are more likely to use the volunteer's own family practitioner but also feel this is ideal practice.

Neuroimaging studies, however, are not designed to screen for IF. In research, there is rarely a traditional physician-patient relationship, and in many research groups, there are no neuroradiologists reading brain MRI scans. Furthermore, additional high-resolution anatomical MR imaging is not performed to reduce scanning time and cost, yet adequate image resolution is required to enable the detection of IF.

23.7 Ethical Considerations

Ethical standards for conducting research with human beings were formulated several decades ago in the Declaration of Helsinki in 1975 as well as in the Belmont Report in 1979 which relied on earlier documents such as the Nuremberg Code from 1947 (Declaration of Helsinki 1975; The National Commission for the Protection of Human Subjects of Biomedical and Behavioral Research 1979; Tröhler and Reiter-Theil 1998). Basic principles of research ethics include the respect of the volunteers and their autonomy, avoiding harm (non-maleficence), promoting the well-being of subjects participating in research studies (beneficence) and fairness (Beauchamp and Childress 2009).

There is a variety of ethical arguments in favour of different management strategies. On one hand, the aim in research is not to detect IF, and therefore it can be argued that this is not the researcher's responsibility. On the other hand, if an IF could be detected easily by the researcher and if that could help to avoid harm to the volunteer in the future, it could be considered the researcher's responsibility not to miss it.

The ability of detecting IF obviously varies amongst professional groups performing research, largely dependent upon the training of the researcher in reading and interpreting MR images. Because a lesion not detected by a doctoral student is more likely to be detected by a radiologist, the question arises as to who should perform or read the scan.

We hold the view that, if resources allow it, an acceptable image quality should be used during imaging and that trained neuroradiologists should read the scans. Potentially this reduces the likelihood of missing IF and allows the clinical significance of such lesions to be determined by fuller characterisation. This might have a major impact on the subject's life, and although evidence is lacking, the net effect is likely to be one of beneficence. For example, this approach may allow treatable pathologies to be detected early before they may become symptomatic and cause problems for the individual (respecting the individual voluntarily participating in research) or others.

One basic question is whether IF should be communicated to the volunteers at all. Kirschen et al. (Kirschen et al. 2006) published data from a survey on subjects' expectations regarding the detection and management of IF in neuroimaging research which suggests that IF should be communicated to the volunteers. In that study, 54 % of the subjects expected abnormalities to be detected should they be present and >90 % preferred IF to be communicated to them. This was despite the researchers obtaining written informed consent without mention of disclosure of findings. Furthermore, subjects of research studies expect that their images are read by a trained person regardless of the information given during the process of consent. The authors underline that clarity about procedures for handling IF is essential to ensure that the subjects' expectations are consistent with, or adjusted to, the purpose of the study.

The PI's responsibility does not end with detecting IF. Indeed, it becomes more complex after that. Once IF are detected, a standardised management protocol needs to be followed to take care of any further diagnostic tests or treatment that may result from these findings (Illes et al. 2006; Gupta and Belay 2008; Ulmer et al. 2009; Hartwigsen et al. 2010). Cooperation between research groups and clinicians has been suggested (Ulmer et al. 2009; Hartwigsen et al. 2010) including an outpatient service to take care of these volunteers. Consistent with the ethical principle of respecting the autonomy of the volunteers, if such management was to be offered, each subject could decide whether they prefer to use this service or their primary care physician or want to ignore such findings altogether or until they become symptomatic. In our local (Germany) experience, however, all volunteers used the outpatient service. Respecting the autonomy of a research participant is important should volunteers not want to be told of any unexpected scan findings. In these cases, the principal investigator (PI) may face a dilemma when detecting an IF: on the one hand, the wishes of the individual subject 'not to know' should be respected; on the other hand, it could be argued that it is problematic if researchers acquire information relevant for future health which they are not allowed to share with the volunteer. Furthermore, the IF may put the community at risk as discussed above. A possible solution is to exclude volunteers who explicitly state they do not want any information about IF to be disclosed to them.

In genetics, there are also published papers dealing with similar principles. Most research studies are not carried out under the Clinical Laboratory Improvement Amendments (CLIA)-certified laboratory testing guidelines of quality assurance (Clinical Laboratory Improvement Amendments, CLIA; http://www.cms.hhs.gov/CLIA), and often researchers are not clinically certified to evaluate the clinical significance of genetic or genomic IF (Van Ness 2008). In 2004, the National Heart, Lung, and Blood Institute (NHLBI) of the US National Institutes of Health developed a set of recommendations where genetic results should be reported to the research participant depending on whether there was a significant risk of disease and whether the disease would have important health implications (i.e. fatal consequences or substantial morbidity); moreover, the recommendations suggested that this should be made explicit in the study design and Institutional Review Board (IRB) approval (National Heart, Lung, and Blood Institute 2004). Furthermore, only CLIA-certified tests should be reported as clinically valid. Knoppers et al. (Knoppers et al. 2006) concluded that at the international level, an ethical duty exists to return individual genetic research results to the subject after proof of validity, significance and benefit. Even where these criteria are met, the right of the

research participant 'not to know' also has to be taken into consideration. In 1991, the Council for International Organizations of Medical Sciences (CIOMS) International Guidelines for Ethical Review of Epidemiological Studies maintain that being informed of findings 'that pertain to their health' is one of the 'reasonable' benefits of participation for 'communities, groups and individuals' in research (The Council for International Organizations of Medical Sciences (CIOMS) 1991). A similar position was also expressed by the Council of Europe (Council of Europe. http://www.coe.int/T/E/Legal_affairs/Legal_cooperation/Bioethics/Activities/Biomedical_research/Protocol_Biomedical_research.pdf and http://conventions.coe.int/treaty/en/Treaties/Html/164.htm).

At-risk family members also should be considered in the discussion as to whether there is a need or requirement for disclosure of IF (Knoppers et al. 2006).

An international recommendation on handling theses complex issues has yet to be produced. Researchers should be aware of the problem of IF; in the absence of general guidelines, they have to come up with local and individual solutions to ensure responsible management of their volunteers even in the absence of international recommendations. However, there are useful sources of information available from various imaging centres, for example, in the appendix of a UK summary of an international meeting on IF (Royal College of Radiologists (RCR) 2011).

23.8 Recommendations

The management of IF varies between institutions and countries (Booth et al. 2010). International or European guidelines would – as in other fields – be prudent but are not yet established. In our opinion, volunteers who enable research to be performed should be offered the following:

- Initially informed consent will be obtained from the participant, which should include information about the possibility of detecting IF with a thorough explanation as to what the consequences might be. The exact requirements of informed consent depend on national regulations, but it might be pragmatic to explain to the participant that IF, if discovered, have to be documented from this point forward, and that they may require immediate treatment and further imaging or follow-up exams. Furthermore, IF might have a major impact on the individual's life and therefore should be disclosed to the participant.
- If the person performing the research is not medically qualified, a medical professional should be incorporated into the team in order to obtain informed consent from the volunteer. Although dependent on the nation's health-care system, it appears sensible for any subsequent costs of discovering an IF – if not covered by the volunteer's insurance company– to be underwritten by the research institution. As discussed above, the right 'not to know' can be problematic. A possible solution is to exclude volunteers who explicitly state that they do not want to know any information about IF. It remains a matter of debate what scans, if any, should be obtained in addition to those required for the research. Additional T_2-weighted sequences and additional orthogonal acquisitions appear judicious.

  If no neuroradiologist is part of the research group, it would be sensible for the scanning protocol to be discussed with an external expert. We do not recommend intravenous contrast agent as this is intrusive to the volunteer. As in standard clinical practice, the neuroradiologist reading the scans should take responsibility for detecting abnormalities. There are several options to compensate for costs that arise from professional reading of these images, the suitability of which depends on the local institution (Booth et al. 2010; Hartwigsen et al. 2010). As discussed above, in our opinion, professional reading of the images is an ethical requirement, not only to enable detection of IF but also to depict deviations from normal that might hamper further post-processing of the data, that is, for the topographical location of functional areas.
- In our opinion, further steps need to be in place should an IF be discovered. These include a medical professional being able to

explain the consequences of the IF. Questions from the volunteer, who might have become a patient, should be answered professionally. An outpatient service, taking care of further steps including additional screening or treatment, has proven to be useful (Hartwigsen et al. 2010; Ulmer et al. 2009, 2012). Some patients prefer to see their primary care physician, so this option should also be available. Again, costs that might arise could be covered either by the volunteers' insurance or a dedicated institutional insurance policy for volunteers in general.

References

Alphs HH, Schwartz BS et al (2006) Findings on brain MRI from research studies of occupational exposure to known neurotoxicants. AJR Am J Roentgenol 187:1043–1047

Beauchamp TL, Childress JF (eds) (2009) Principles of biomedical ethics, 6th edn. Oxford University Press, Oxford. ISBN ISBN-13: 978-0-19-533570-5

Booth TC, Jackson A et al (2010) Incidental findings discovered in 'healthy' volunteers during research imaging; legal and ethical lessons from UK and overseas. Br J Radiol 83:456–465

Booth TC, Jackson A et al (2012) Management of incidental findings during imaging research in 'healthy' volunteers; current UK practice. Br J Radiol 85: 11–21

Brown DA, Hasso AN (2008) Toward a uniform policy for handling incidental findings in neuroimaging research. AJNR Am J Neuroradiol 29:1425–1427

Carli V, Hadlaczky G et al (2012) Maintaining confidentiality in prospective studies: anonymous repeated measurements via email procedure (ARME). J Med Ethics 38:127–129

Clinical Laboratory Improvement Amendments, CLIA; Centers for Medicare and Medicaid Services. Clinical Laboratory Improvement Amendments. http://www.cms.hhs.gov/CLIA

Council of Europe. http://www.coe.int/T/E/Legal_affairs/Legal_cooperation/Bioethics/Activities/Biomedical_research/Protocol_Biomedical_research.pdf and http://conventions.coe.int/treaty/en/Treaties/Html/164.htm

Council of Europe Steering Committee on Bioethics (2004) Additional protocol to the convention on human rights and biomedicine concerning biomedical research. http://conventions.coe.int

Declaration of Helsinki (1975) WMA declaration of Helsinki – ethical principles for medical research involving human subjects. www.wma.net/en/30publications/10policies/b3/

Garnett A, Whiteley L et al (2011) Neuroethics and fMRI: mapping a fledgling relationship. PLoS One 6:e18537

Gupta SN, Belay B (2008) Intracranial incidental findings on brain MR images in a pediatric neurology practice: a retrospective study. J Neurol Sci 264:34–37

Hartwigsen G, Siebner HR et al (2010) Incidental findings are frequent in young healthy individuals undergoing magnetic resonance imaging in brain research imaging studies: a prospective single-center study. J Comput Assist Tomogr 34:596–600

Illes J, Chin VN (2008) Bridging philosophical and practical implications of incidental findings in brain research. J Law Med Ethics 36(298–304):212

Illes J, Kirschen MP et al (2004) Discovery and disclosure of incidental findings in neuroimaging research. J Magn Reson Imaging 20:743–747

Illes J, Kirschen MP et al (2006) Ethics. Incidental findings in brain imaging research. Science 311:783–784

Katzman GL, Dagher AP et al (1999) Incidental findings on brain magnetic resonance imaging from 1000 asymptomatic volunteers. JAMA 282:36–39

Kirschen MP, Jaworska A et al (2006) Subjects' expectations in neuroimaging research. J Magn Reson Imaging 23:205–209

Knoppers BM, Joly Y et al (2006) The emergence of an ethical duty to disclose genetic research results: international perspectives. Eur J Hum Genet 14: 1170–1178

Kwong KK, Belliveau JW et al (1992) Dynamic magnetic resonance imaging of human brain activity during primary sensory stimulation. Proc Natl Acad Sci USA 89:5675–5679

Lawrenz F, Sobotka S (2008) Empirical analysis of current approaches to incidental findings. J Law Med Ethics 36:249–255

Machaalany J, Yam Y et al (2009) Potential clinical and economic consequences of noncardiac incidental findings on cardiac computed tomography. J Am Coll Cardiol 54:1533–1541

Miller FG, Mello MM et al (2008) Incidental findings in human research: what do investigators owe research participants? J Law Med Ethics 36:271–279

Morris Z, Whiteley WN et al (2009) Incidental findings on brain magnetic resonance imaging: systematic review and meta-analysis. BMJ 339:b3016

National Heart, Lung, and Blood Institute (NHLBI) of the US National Institutes of Health (2004) http://www.nhlbi.nih.gov/meetings/workshops/gene-results.htm

National Research Ethics Service (2007) National Patient Safety Agency information sheets and consent forms. Guidance for researchers and reviewers. http://www.nres.npsa.nhs.uk/EasySiteWeb/GatewayLink.aspx?alld

Ogawa S, Lee TM et al (1990) Brain magnetic resonance imaging with contrast dependent on blood oxygenation. Proc Natl Acad Sci USA 87:9868.9872

Ogawa S, Menon RS et al (1993) Functional brain mapping by blood oxygenation level-dependent contrast magnetic resonance imaging. A comparison of signal characteristics with a biophysical model. Biophys J 64:803–812

Okuda DT, Mowry EM et al (2009) Incidental MRI anomalies suggestive of multiple sclerosis: the radiologically isolated syndrome. Neurology 72:800–805

Reiter-Theil S, Stingelin Giles N (2007) Ethical aspects of screening and preventive diagnosis with radiological imaging. In: Reiser MF, van Kaick G, Fink C, Schoenberg SO (eds) Screening and preventive diagnosis with radiological imaging. Springer, Berlin, pp 137–146

Royal College of Radiologists (RCR) (2011) Management of incidental findings detected during research imaging. www.rcr.ac.uk/docs/radiology/pdf/BFCR(11)8_Ethics.pdf

Royal JM, Peterson BS (2008) The risks and benefits of searching for incidental findings in MRI research scans. J Law Med Ethics 36:305–314

The Council for International Organizations of Medical Sciences (CIOMS) (1991) International Guidelines for Ethical Review of Epidemiological, European Federation of the International Epidemiologist Association (IEA). http://www.dundee.ac.uk/iea/GoodPract.htm

The Council for International Organizations of Medical Sciences (CIOMS) (2002) International ethical guidelines for biomedical research involving human subjects. http://www.cioms.ch

The National Commission for the Protection of Human Subjects of Biomedical and Behavioral Research (1979) Belmont report. http://ohsr.od.nih.gov/guidelines/belmont.html

Tröhler U, Reiter-Theil S (eds) (1998) Ethics codes in medicine: foundations and achievements 1947–1997. Ashgate, Aldershot

Ulmer S, Jensen UR et al (2009) Impact of incidental findings on neuroimaging research using functional MR imaging. AJNR Am J Neuroradiol 30(4):E55

Ulmer S, Stippich C et al (2012) Incidence and responsible management of incidental findings (IF) in neuroimaging research. Nervenheilkunde 31(4): 246–249

Van Ness B (2008) Genomic research and incidental findings. J Law Med Ethics 36(2):292–297, 212

Vernooij MW, Ikram MA et al (2007) Incidental findings on brain MRI in the general population. N Engl J Med 357:1821–1828

Weber F, Knopf H (2006) Incidental findings in magnetic resonance imaging of the brains of healthy young men. J Neurol Sci 240:81–84

Wolf SM, Lawrenz FP et al (2008) Managing incidental findings in human subjects research: analysis and recommendations. J Law Med Ethics 36:219–248

Woodward CI, Toms AP (2009) Incidental findings in "normal" volunteers. Clin Radiol 64:951–953

World Medical Association (2008) World Medical Association declaration on the Rights of the Patient, 2008. http://www.wma.net

Yousry TA, Schmid UD et al (1995) Topography of the cortical motor hand area: prospective study with functional MR imaging and direct cortical mapping at surgery. Radiology 195:23–29

Index

S. Ulmer, O. Jansen (eds.), *fMRI – Basics and Clinical Applications*,
DOI 10.1007/978-3-642-34342-1, © Springer-Verlag Berlin Heidelberg 2013